OPTICAL AND ELECTRICAL INSTABILITIES IN AMORPHOUS SEMICONDUCTORS

Janos P. Hajto, MSc., Ph.D.

Doctor of Science

University of Edinburgh

1993

CONTENTS

	Page
ACKNOWLEDGEMENTS	(i)
DECLARATION	(ii)
ABSTRACT	(iii)
LIST OF PUBLICATIONS	(iv)
PUBLICATIONS	1-432

ACKNOWLEDGEMENTS

I would like to thank the many people with whom I have collaborated over the years and without whose co-operation this thesis could not have been produced.

I have had the privilege to work with academic collegues covering a number of areas of research. I would like to express my sincere thanks to Dr. Istvan Kosa-Somogyi (Ph.D. Supervisor), Professor A.E. Owen, Professor W.E. Spear, late Professor P.G. LeComber, Dr. A.J. Snell, Dr. M.J. Rose, Dr. I. Janossy, Dr. Norbert Kroo, Dr. G. Zentai, Dr. J. Gazso, Dr. M. Fustoss-Wegner, Dr. W.K. Choi, Dr. S. Reynolds, and Dr. S.M. Gage.

I am also most grateful to my wife Eva and my children Zsuzsa and Agnes for their support and encouragement.

DECLARATION

(a) Most of the papers published with my colleagues has been originated and supervised myself. Some papers published with my colleagues have been on research in which I have played at least an equal role in supervising the research and preparing the results for publication.

(b) The published works included herein have not been submitted, in whole or in part, for any degree or diploma.

(c) The publishers of the works included herein have given permission for photocopies included in this thesis.

ABSTRACT

Studies have been carried out in the following areas:

(1) Laser-induced crystallization

The laser-induced crystallization of amorphous chalcogenide thin films has been studied, especially the kinetics and thermodinamics characterising the process.

(2) Optical bistability and oscillatory phenomena

The laser-amorphous semiconductor interaction has been studied especially c.w. laser induced optical bistabilities and oscillatory phenomena in transmittance and reflectance. Theoretical models of thermally induced optical bistability and oscillation have also been described.

(3) Optical anisotropy

The effect of linearly polarised c.w. laser light in inducing birefringence and dichroism in amorphous semiconductors has been studied. The kinetics of reorientation has also been investigated. A quantitative theory of optical anisotropy and reorientation has been described.

(4) Current instabilities and electrical switching

The effects of electrically induced current instabilities especially digital and analogue memory switching have been studied. A theoretical model has been described in terms of filament formation and tunneling conduction in metal-amorphous silicon-metal structures.

(5) Step-like current-voltage characteristics

Unusual step-like current-voltage characteristics in electroformed metal-amorphous semiconductor- metal structures have been studied over a range of temperatures from 4.2 K to 400 K and theoretical models proposed.

LIST OF PUBLICATIONS

1. J.Hajto and G.Acs — 1
Laser induced Set-Reset processes in chalcogenide thin films
Proc. of Int.Conf. on "Amorphous Semiconductors 74", Rheinhardsbrunn
(1974) 437-440

2. J.Hajto and G.Radnoczi, — 6
The structure of laser irradiated chalcogenide films
Reports of KFKI, Hungarian Academy of Sciences, Budapest,
KFKI 24 (1974) 1-7

3. J.Hajto and T.Kemeny, — 14
Thermodynamic data on chalcogenide glasses
Journal of Thermal Analysis, 9/1 (1976) 53-58

4. J.Gazso, J.Hajto and G.Zentai, — 20
Kinetics of optical memory switching in chalcogenide thin films
Reports of KFKI, Hungarian Academy of Sciences, Budapest
KFKI 4 (1976) 1-19

5. G.Zentai and J.Hajto, — 42
AC measurements on As-Se-Te samples
Proc. of Int. Conf. on "Amorphous Semiconductors 77", Balatonfured
Hungary, ed. by I.Kosa Somogyi, Budapest (1977) 227-231

6. J.Hajto and G.Zentai — 47
Kinetics of laser induced crystallization on As-Se-Te films
Proc. of Int. Conf. on "Amorphous Semiconductors 77", Balatonfured
Hungary ed. by I.Kosa Somogyi, Budapest (1977) 371-375

7. J.Hajto and T.Kemeny, 52
Thermodynamic properties of As-Se-Te chalcogenide glasses
Proc. of Int.Conf. on "Amorphous Semiconductors 77", Balatonfured
Hungary ed. by I.Kosa Somogyi, Budapest (1977) 493-497

8. J.Hajto and L.Pogany, 57
Electron microscopical investigation of $GeSe_2$ chalcogenide films
after laser induced oscillation
Reports of KFKI, Hungarian Academy of Sciences, Budapest
KFKI 42 (1977) 1-6

9. J.Hajto, J.Gazso and G.Zentai, 65
The kinetics of laser induced crystallisation of As-Se-Te films
Proc. of 7th. Int. Conf. on Amorphous and Liquid Semiconductors
ed. by W.E. Spear, Edinburgh UK (1977) 807-811

10. L.Toth, J.Hajto and G.Zentai, 72
Light induced light absorption changes in AsSe
and $GeSe_2$ thin films
Solid State Communications, Vol. 23 (1977) 185-188

11. J.Hajto, G.Zentai and I.Kosa Somogyi, 76
Light induced transmittance oscillation in $GeSe_2$ films
Solid State Communications, Vol. 23 (1977) 401-403

12. J.Gazso and J.Hajto, 79
Self-controlled laser beam chopping effect in $GeSe_2$ thick films
Phys. stat. sol., (a) 45 (1978) 181-186

13. J.Hajto and P.J.S.Ewen, 85
Laser induced birefringence and transmittance oscillations
in As_2S_3 glasses,
Proc. of Amorphous Semiconductors'78 Pardubice, September (1978),
436-439

14. J.Hajto and P.J.S.Ewen, 90

Natural optical activity and related phenomena in As_2S_3 glasses
Phys. stat. sol., (a) 54 (1979) 385-390

15. I.Kosa Somogyi, J.Hajto and G.Zentai, — 96
Doping and absorption edge of amorphous silicon,
Reports of KFKI, Hungarian Academy of Sciences,
Budapest KFKI 67 (1979) 1-10

16. J.Hajto and P.Apai, — 108
Investigation of laser induced light absorption oscillation
Journal of Non-Crystalline Solids, 35-36 (1980) 1085-1090

17. J.Hajto, — 114
Laser induced oscillatory phenomena in amorphous $GeSe_2$ films
Journal de Physique, C4 no4 (1980) 63-70

18. J.Hajto and M.Fustoss Wegner, — 121
Oscillations of light absorption and photocurrent in a-$GeSe_2$
films,
Proc. of Int. Conf. on Amorphous Semiconductors 80' Kishinev USSR
(1980)

19. J.Hajto and M.Fustoss-Wegner, — 128
Laser induced oscillatory phenomena in amorphous $GeSe_2$ films
Journal de Physique, C4 no10 (1981) 313-316

20. J.Hajto, G.Radnoczi, L.Pogany and E.Hajto, — 132
Electron microscopical investigation of laser irradiated
a-$GeSe_2$ and a-As_2S_3 films
Reports of Central Research Inst. of Physics, Budapest, 96 (1981) 1-23

21. J.Hajto, I.Janossy and G. Forgacs, — 158
Laser induced optical anisotropy in self-supporting
amorphous $GeSe_2$ films
J.Phys. C. Solid State Physics, 15 (1982) 6293-6303

22. J.Hajto, J.Gazso, G.Zentai and I.Kosa Somogyi, — 169
Laser induced crystallisation of a-Si:H thin films
J.Physique-LETTRES, 43 (1982) L-97-L-102

23. A.Kolobov, B.T.Kolomiets, N.Sebastian, M.A.Tagirdzhanov, and J.Hajto, Photostimulated processes in glassy arsenic and germanium chalcogenides Soviet Physics Solid State 24(4) (1982) 603-605 — 175

24. J.Hajto and I.Janossy, Optical bistability observed in amorphous semiconductor films Philosophical Magazine, 47 (1983) 347-366 — 178

25. J.Hajto, I.Janossy and A.Firth, Explanation of the laser induced oscillatory phenomenon in amorphous semiconductor films Philosophical Magazine, 48 (1983) 311-321 — 198

26. A.E.Owen, P.G. Le Comber, W.E. Spear and J.Hajto, Memory switching in amorphous silicon devices Journal of Non-Crystalline Solids 59-60 (1983) 1273-1280 — 209

27. P.G.Le Comber, A.E. Owen, W.A.Spear and J.Hajto, Electronic switching in amorphous silicon junction devices SEMICONDUCTORS and SEMIMETALS, Vol.21 part D Copyright by Academic Press Inc. (1984) 275-289 — 217

28. I.Janossy, A.Jakli and J.Hajto, Photodarkening and laser induced anisotropy in chalcogenide glasses Solid State Communications, 51 (1984) 761-764 — 232

29. J.Hajto and A.E.Owen, Applications of amorphous semiconductor materials in electronics Materials and Design, Vol.5. no5. (1984) 221-227 — 236

30. J.Hajto, I.Janossy and W.K.Choi, Optical bistability and oscillatory phenomena in amorphous semiconductors Journal of Non-Crystalline Solids, 77-78 (1985) 1273-1276 — 243

31. P.G. LeComber, A.E.Owen, W.E.Spear, J.Hajto, A.J.Snell and W.K.Choi, 247
Switching mechanism in amorphous silicon junctions
Journal of Non-Crystalline Solids 77-78 (1985) 1373-1382

32. I.Janossy, J. Hajto and W.K.Choi, 257
Mechanism of laser induced optical anisotropy in chalcogenide glasses
Journal of Non-Crystalline Solids, 90 (1987) 529-532

33. J.Hajto and I.Janossy, 261
Model for the non-linear intensity dependence of photostructural changes in amorphous semiconductors
Journal of Non-Crystalline Solids, 97-98 (1987) 1207-1210

34. W.K.Choi, S.Reynolds, J.Hajto, S.M.Gage, A.E.Owen, and A.E.Snell 264
Pre-Formed J-V and C-V characteristics of a-Si:H p^+ni junctions
Journal of Non-Crystalline Solids 97-98 (1987) 1331-1334

35. E.Hajto, P.J.S.Ewen, R.Belford, J.Hajto and A.E.Owen, 268
Optical properties of spin-coated amorphous chalcogenide thin films,
Journal of Non-Crystalline Solids 97-98 (1987) 1191-1194

36. W.K.Choi, S.Reynolds, J.Hajto, A.E.Owen, P.G.Le Comber and W.A. Spear 272
Transient current instabilities in a-Si:H p^+ni structures
IEE PROCEEDINGS, Vol. 134, Pt.I, No.1, Febr. (1987) 1-6

37. J.Hajto, I.Janossy, W.K.Choi and A.E.Owen, 278
Model of laser induced regular and chaotic oscillations in amorphous semiconductors
Journal of Non-Crystalline Solids 114 (1989) 304-306

38. M.J.Rose, J.Hajto, W.K.Choi, P.G.LeComber, A.J.Snell and A.E.Owen, 281
Amorphous silicon memory devices
Journal of Non-Crystalline Solids 115 (1989) 168-170

39. S.M. Gage, J.Hajto, S.Reynolds, W.K.Choi, M.J.Rose, P.G.LeComber, A.J.Snell and A.E.Owen, — 284
Anomalously high zero bias resistance in metal-amorphous silicon-metal structures
Journal of Non-Cryst Solids 115 (1989) 171-173

40. J.Hajto., M.J.Rose, A.J.Snell, P.G.LeComber, and A.E.Owen, — 287
The programmability of Amorphous Silicon Memory Elements
in Proc. MRS. Soc. Symp., San Francisco, USA, Vol.192 (1990) 405-410

41. J.Hajto, M.J.Rose, P.G.LeComber, A.E.Owen, ans A.J.Snell, — 294
Observation of Quantised Ballistic Transport in Amorphous Silicon Memory Structures
in Proc. MRS. Soc. Symp., San Francisco, USA, Vol.192 (1990) 347-352

42. J.Hajto, A.E.Owen, A.J.Snell, P.G.LeComber, and M.J.Rose, — 301
Analogue Memory and Ballistic Electron Effects in Metal-Amorphous Silicon Structures
Philosophical Magazine B, Vol.63 No.1 (1991) 347-352

43. J.Hajto, A.E.Owen, S.M.Gage, A.J.Snell, P.G.LeComber and M.J.Rose, — 322
Quantized Electron Transport in Amorphous Silicon Memory Structures
Physical Review Letters, Vol.66, No.14 (1991) 1918-1921

44. J.Hajto, M.J.Rose, A.J.Snell, I.S.Osborne, A.E.Owen, and P.G.Lecomber, — 326
Quantised Electron Effects in Metal/a-Si:H/Metal Thin Film Structures
Journal of Non-Crystalline Solids, Vol.137-138 (1991) 499-502

45. A.J.Snell, P.G.LeComber, J.Hajto, M.J.Rose, A.E.Owen, and I.S.Osborne, — 330
Analogue Memory Effects in Metal/a-Si:H/Metal Memory Devices
Journal of Non-Crystalline Solids, Vol.137-138 (1991) 1257-1262

46. M.J.Rose, J.Hajto, P.G.LeComber, A.J.Snell, A.E.Owen and I.S.Osborne, — 336
Amorphous Silicon Analogue Memory Elements
Proceedings of MRS. Soc. Symp. San Fransisco, USA Vol.219 (1991) 525-530

47. A.E.Owen, P.G.LeComber, J.Hajto, M.J.Rose and A.J.Snell, — 342
Switching in amorphous devices,
Int. J.Electronics vol. 73, no.5, 897-906 (1992)

48. J.Hajto, M.Rose, I.S.Osborne, A.J.Snell, P.G.LeComber and A.E.Owen, — 352
Quantisation effects in metal/a-Si:H/metal devices,
Int. J.Electronics, vol. 73, no.5, 911-913 (1992)

49. J.Hajto, A.E.Owen, A.J.Snell, P.G.LeComber and M.J.Rose, — 355
Electronic Switching in Amorphous Semiconductor Thin Films,
Amorphous and Microcrystalline Semiconductor Devices,
Volume II,
Artech House, Editor, J.Kanicki Chapter 14 (1992) 641-701

50. M.J.Rose, A.J.Snell, P.G.LeComber, J.Hajto, A.G.Fitzgerald, and A.E.Owen, — 416
Aspects of non-volatility in a-Si:H memory devices,
Mat.Res.Soc.Symp.Proc. Vol.258, (1992)

51. A.A.Reeder, I.P.Thomas, C.Smith, J.Whittgreffe, D.J.Godfrey, J.Hajto, A.E.Owen, A.J.Snell, A.F.Murray, M.J.Rose, I.S.Osborne and P.G.LeComber, — 422
Application of analogue amorphous silicon memory devices to resistive synapses for neural networks,
Mat.Res.Soc.Sym.Proc. Vol.258, (1992) 1081-1086

52. I.S.Osborne, J.Hajto, M.J.Rose, A.J.Snell, P.G.LeComber and A.E.Owen, — 428
The role of the a-Si:H layer in the metal/a-Si:H/metal memory structures,
Mat.Res.Soc.Symp.Proc. Vol.258, (1992) 1169-1173

Akademie der Wissenschaften der DDR
Zentralinstitut für Elektronenphysik

Tagungsbericht Proceedings

Сборник докладов

II

Conference
Amorphous Semiconductors '74

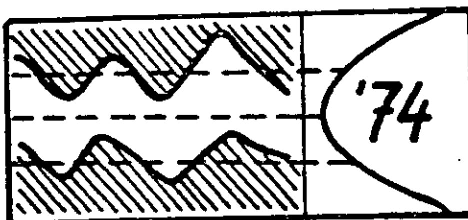

Совещание
Аморфные Полупроводники '74

Reinhardsbrunn, 11.-15. XI. 1974

LASER INDUCED SET-RESET PROCESSES IN CHALCOGENIDE THIN FILMS

J. Hajtó and G. Ács
Central Research Institute for Physics
Budapest, Hungary

Нанесение аморфных и кристаллических точек удалось осуществить посредством коротких импульсов лазера. Электронмикроскопическое исследование пленок показало, что диаметр аморфных точек равняется 0,5 микрон. Значения температуры, полученные из уравнения теплопроводности показали, что нанесение аморфных точек является результатом быстрого охлаждения, происходящего вслед за расплавлением вещества.

1. INTRODUCTION

In this paper we describe the thermal profiles as results of a laser induced melt quench cycle in a film of $Te_{87}Ge_9As_4$ composition. These data are combined with electron-microscopic examination in order to determine the diameters of laser induced areas.

2. EXPERIMENTAL

Thin films of the chalcogenide glasses were prepared by evoporation of three elements As, Te and Ge onto a carbon-collodium cover on a sample grid of a JEM-100 U transmission electron microscope. Film thickness was nominally 670 Å. The film was in crystalline state. Crystallization is due to the thermal treatment of the layers. The light source was a He-Ne gas laser / λ = 6328 Å/. The laser beam was focused on the sample with a 40 power microscope objective lens.

3. RESULTS

3.1 Electron-microscopic examination

It is possible to write crystalline and amorphous spots using 0.4-0.6 μsec pulses from the He-Ne gas laser /laser power = 13.1 mW/. The amorphous spots can be erased both by laser or electron means /Figs. 1 and 2/. Erasure results from the crystallization of the amorphous spot.

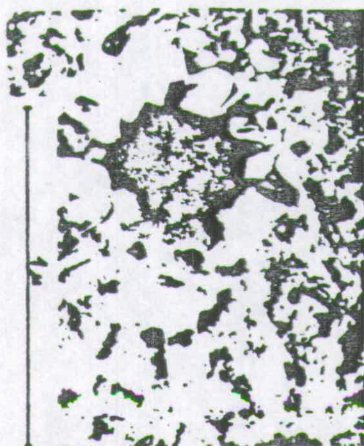

Fig.1 Electron micrograph amorphous spot on $Te_{87}Ge_9As_4$ film

Fig.2 Electron micrograph of the same spot in erased state

3.2 Temperature profile

The temperature profile can be obtained by solving the following differential equation of heat conduction:

$$C_p \cdot \varrho \cdot h \frac{\partial T}{\partial t} = Q(r,t) + \lambda \cdot h \cdot \Delta T \quad (1)$$

where: C_p = specific heat, ϱ = density, λ = thermal conductivity, h = thickness of the film, Q = laser flux density.

Taking the values C_p = 0.09 cal/gr, ϱ = 5.61 g/cm³, h = 760 Å λ = 1 kcal/m°Ch, we found the following results /Figs. 3 and 4/.

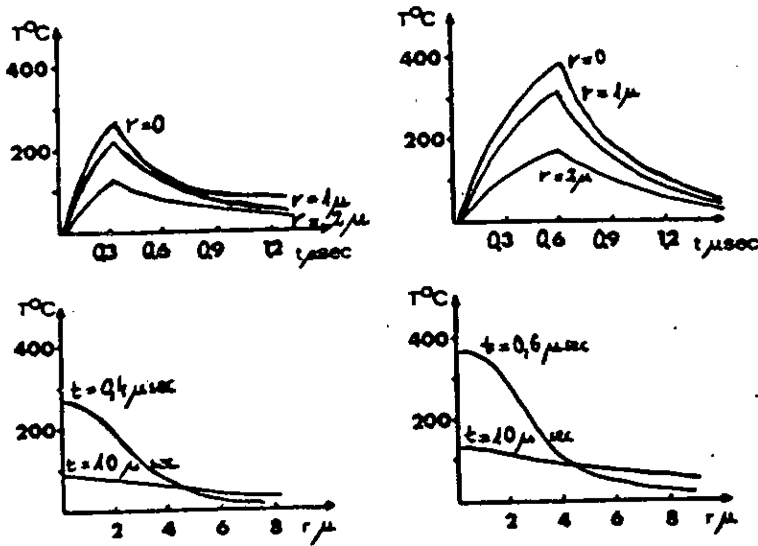

Fig.3a,b. Temperature profiles at various radii from the centre of the spot for a Gaussian laser pulse /a/ 0.4 and /b/ 0.6 μsec duration.

In the case of 0.4 μsec pulse the temperature of illuminated area /2.8 μ diameter/ reaches the crystallization temperature range /T_x = 225°C-375°C/. Using a 0.6 μsec laser pulse the temperature of the illuminated area /0.5 μ diameter/ reaches the melting temperature of the material /T_m = 375°C/. We found the cooling rate value predicted by the equation of heat conduction to be ~150°C/μsec. This rate was sufficiently rapid, For the melted material to remain in the disordered /amorphous/ state.

A summary of our results is shown in Table I.

Laser power [mW]	Pulse duration [μsec]	Diameter of crystalline spots [μ]		Diameter of amorphous spots [μ]	
		Electronmicroscopic observation	From equation of heat conduction	Electronmicroscopic observation	From equation of heat conduction
13.1	0.3	2.6	2.8	-	-
13.1	0.4	2.75	3.0	-	-
13.1	0.52	3.1	3.3	0.4	0.5
13.1	0.6	3.2	3.45	0.5	0.55

4. DISCUSSION

The temperature values predicted by the equation of heat conduction and the electron-microscopic examination show that the laser writing and erasing can be ascribed to the thermally induced reversible amorphous crystalline phase transition of the material. Crystallization occurs only in the irradiated area; amorphization is due to the rapid cooling of the melted substance.

5. REFERENCES

1 J.Feinleib, J.de Neufville, S.C.Moss and S.R.Ovskinsky Appl.Phys.Lett. 18, 254 /1971/

2 P.Chaudhari, S.R.Herd, J. Non Cryst. Solids 8-10, 56 /1972/

3 A.Hamada, T.Kurosu, M.Saito, M.Kikuchi, Appl.Phys.Lett. 20, 1 /1972/

4 R.J. Von Gutfeld, P.Chandhari, J.Appl.Phys. 43, 11 /1972/

KFKI-74-21

THE STRUCTURE OF LASER-IRRADIATED CHALCOGENIDE FILMS

J. Hajtó

Central Research Institute for Physics, Budapest, Hungary
Chemistry Department

and

Gy. Radnóczy

Research Institute for Technical Physics, Budapest, Hungary

ABSTRACT

Optical switching from the crystalline to the amorphous state has been studied in chalcogenide films producing amorphous spots by the help of 60 nsec pulses of a ruby laser. These amorphous written spots can be erased both by laser and electron beams. Electron-microscopic examination of the films has shown that the diameters of the amorphous spots are 0.5 μm. The structural properties of these films depend on their thickness.

РЕЗЮМЕ

Нами были изучены возможности оптического переключения из кристаллической в аморфную фазу на халькогенидной пленке. Нанесение аморфных точек удалось осуществить посредством коротких импульсов лазера; длительность импульса составила $6x10^{-2}$ мксек. Эти точки можно стирать с помощью лазерного или электронного излучения. Электрон-микроскопическое исследование этих пленок показало, что диаметр аморфных точек равняется 0,5 микрон.

KIVONAT

A kristályosból az amorf állapotba történő optikai kapcsolást tanulmányoztuk kalkogenid filmekben. 60 nsec besugárzási idejü rubin lézer segitségével amorf pontokat sikerült létrehozni. Ezek a beirt amorf pontok mind lézer-, mind elektronsugárral törölhetők. A filmek elektronmikroszkópos vizsgálata kimutatta, hogy a foltátmérő 0,5 μm. A filmek szerkezeti tulajdonságai függnek vastagságuktól.

INTRODUCTION

Reversible changes in the reflectivity of amorphous chalcogenide films by laser irradiation have recently been reported [1-8] . It was found, that the optical properties of chalcogenide films were altered by a laser beam to a sufficient extent which makes them attractive for optical memories. The structure of laser written lines have been examined in chalcogenide films [5]. Gutfeld and Chandhari showed [9] that it is also possible to write by amorphizing pulses.

In this paper some of our results on laser writing and erasing in $Te_{85}Ge_{10}As_5$ and $Te_{88}Ge_6As_6$ are described.

SAMPLE PREPARATION

Thin films of the chalcogenide glasses were prepared by evaporation of three elements As, Te and Ge onto a carbon-collodium cover on a sample grid for electron-microscopy measurements /Fig. 1/. The film composition measured by mass-spectrometrical analysis was found to be $Te_{85}Ge_{10}As_5$ and $Te_{88}Ge_6As_6$. Film thicknesses were nominally 210 Å and 670 Å. The morphological changes were photographed with a JEM 100-U transmission electron-microscope. The electron-micrograph and the diffraction pattern of the two films are shown in Figs. 2-3.

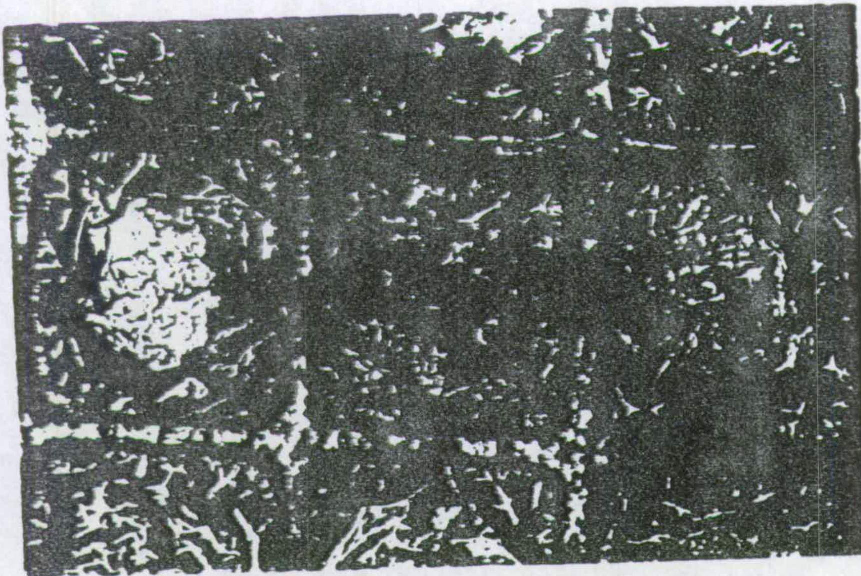

Fig. 1 Microphoto of evaporated film on a sample grid for electron-microscopic measurements.

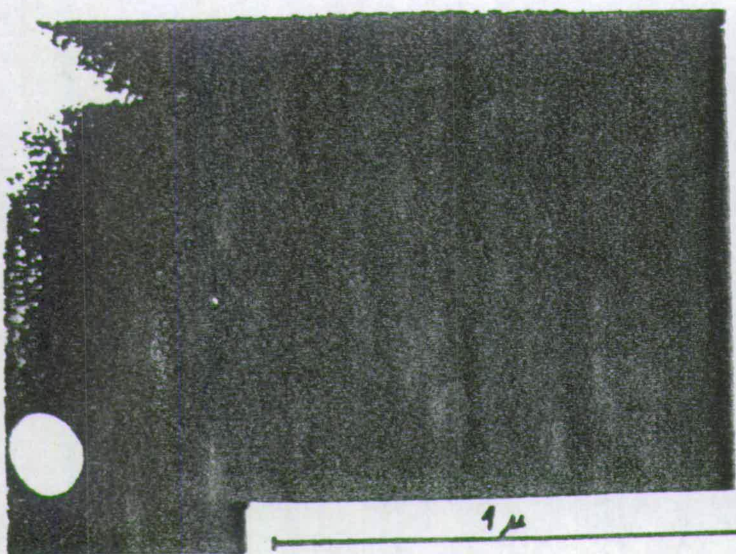

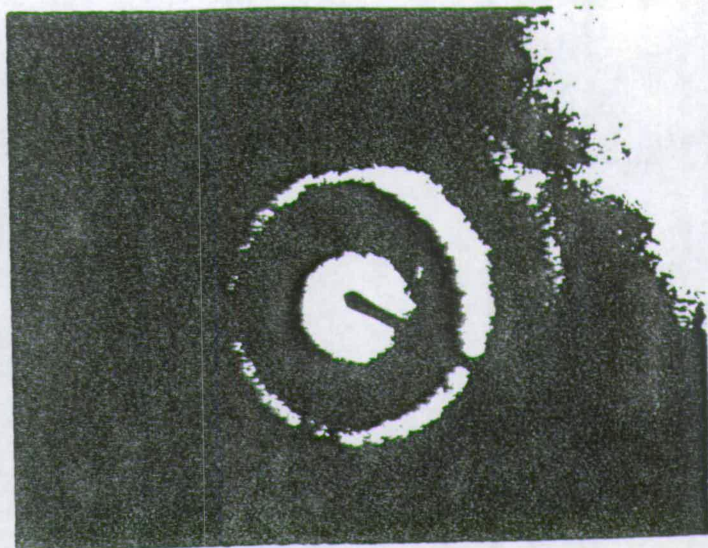

a/ b/

Fig. 2 Electron-micrograph and the diffraction pattern of evaporated 210 Å thick film

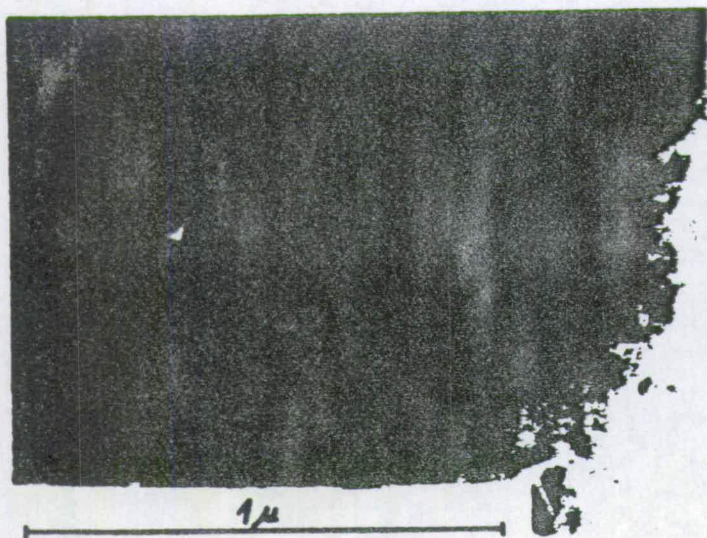

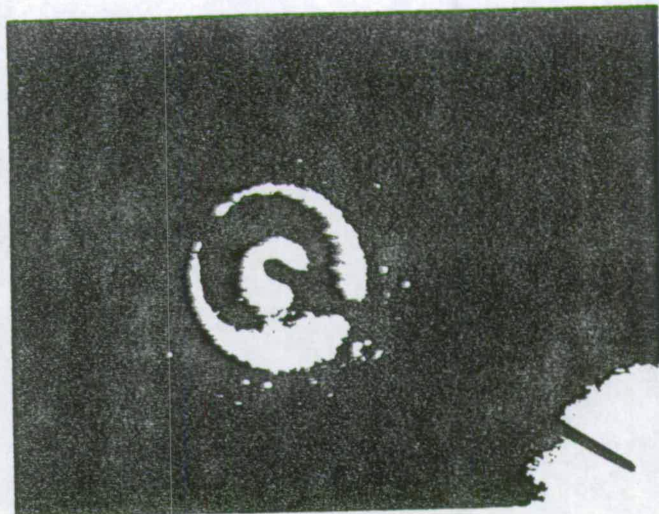

a/ b/

Fig. 3 Electron-micrograph and the diffraction pattern of evaporated 270 Å thick film

The diffraction pattern of the 210 Å films was characteristic for amorphous films but the 670 Å film was in the crystalline state. Crystallization is thought to be due either to the increase of film thicknesses or to the thermal treatment of the layers.

CRYSTALLIZATION EFFECT IN CHALCOGENIDE FILMS

Two lasers were employed in our experiments. The output of a He-Ne gas laser was used for writing in the μsec range and that of a Q-switched ruby laser for the nsec range. The output of each of the lasers was focused into a Leitz microscope.
For a writing time of 3.5 μsec a minimum energy density of about 65 mJ/cm^2 is required. A comparison of the micrographs and the electron-micrographs of written spots shows that the spot is not the result of a phase change, but it is a consequence of the increased reflectivity due to crystallites of bigger sizes /Figs. 4-5/.

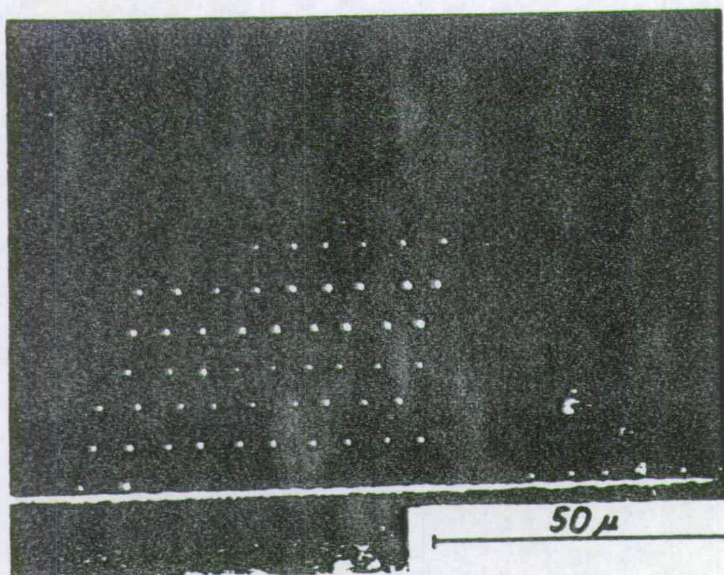

Fig. 4 Micrograph of spots, written by He-Ne laser on $Te_{88}Ge_6As_6$ film

AMORPHIZATION EFFECT IN CRYSTALLINE CHALCOGENIDE FILMS

It is possible to write amorphous spots using 60 nsec pulses from a Q-switched ruby laser. The energy density was 0.25 mJ/μ^2. These amorphous spots can be erased both by laser or electron means /Figs. 7-8/. Erasure is due to the crystallization of the amorphous spot.
It is possible to write amorphous lines using a He-Ne laser. When the power density of the laser was 96 mJ/cm^2 amorphous lines were obtained /Figs. 9-10/, but using only 80 mJ/cm^2, the film was transformed in the higher reflective crystalline state.

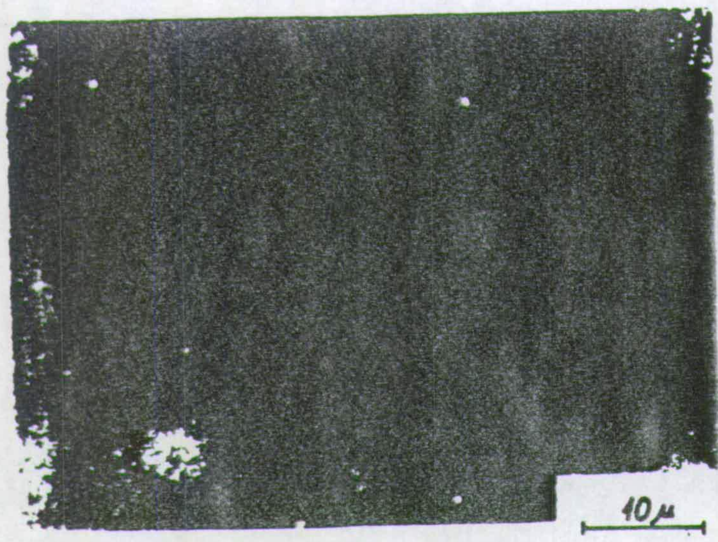

Fig. 5-6 Electron-micrograph of spot, written by He-Ne laser on $Te_{88}Ge_6As_6$ film

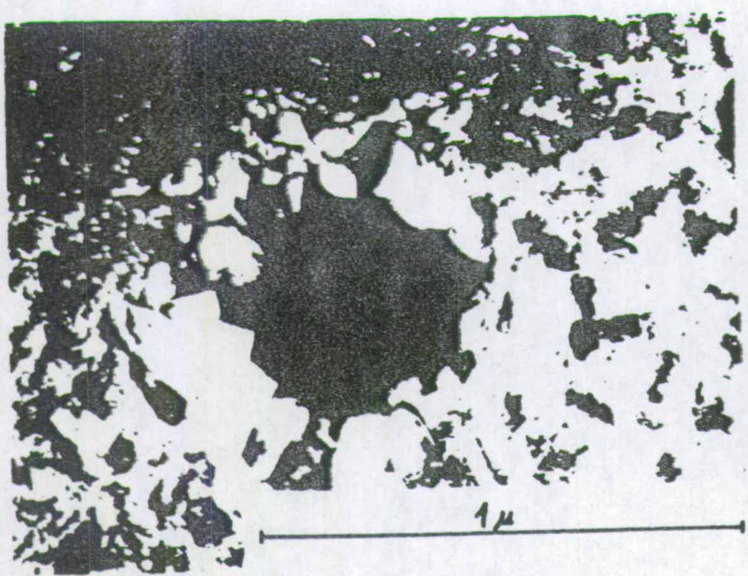

Fig. 7 Electron-micrograph of amorphous spot on $Te_{88}Ge_6As_6$ film

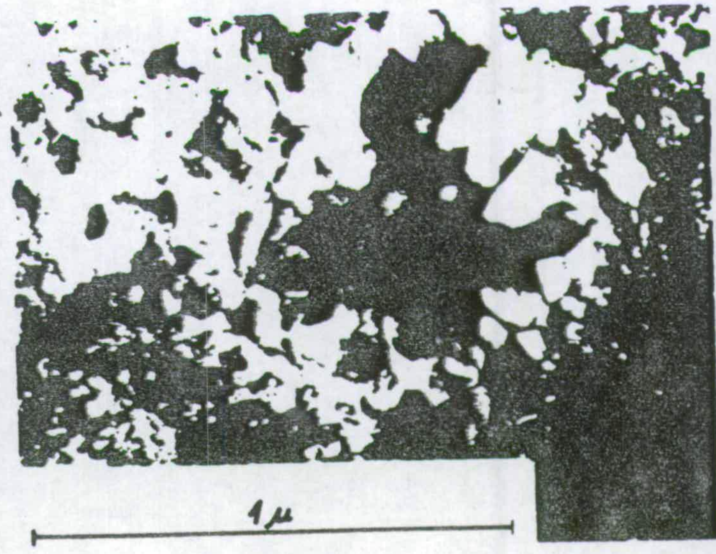

Fig. 8 Electron-micrograph of the same spot as in Fig. 7 in erased state

Fig. 9 *Crystalline and amorphous line produced by laser beam*

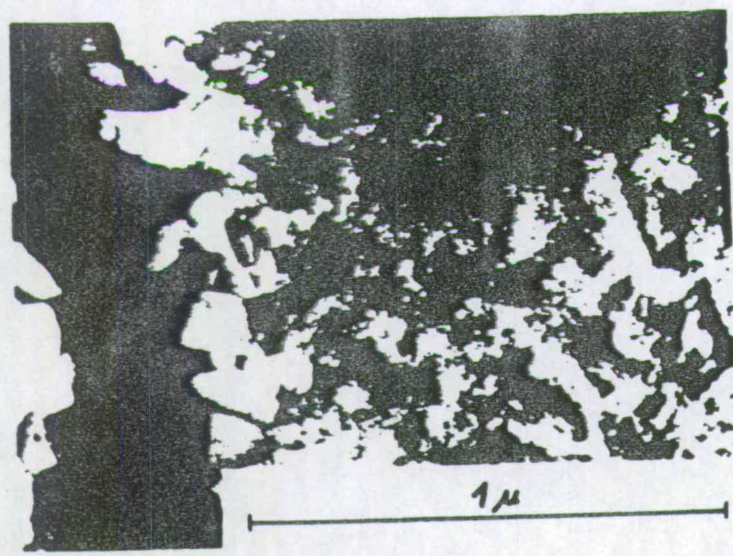

Fig. 10 *Amorphous line produced by laser beam*

DISCUSSION

Reversible optical switching from the crystalline to the amorphous phase has been performed in $Te_{85}Ge_{10}As_5$ and $Te_{88}Ge_6As_6$ films. Amorphous written spots were erased both by laser and electron means. The writing time was 60 nsec at 0.25 nJ/ μ^2 energy density but can be decreased by increasing the energy density. The diameter of amorphous spots is nominally 0.5 µ. Thus a packing density of 10^8 bit/cm^2 can be obtained, i.e. an order of magnitude higher than with crystalline spots, which have a diameter of 1-2 µm [3]. Since 0.5 µm linewidth amorphous lines separated by crystalline zones of the same width can be written in, the resolution is 1000 lines/mm.

REFERENCES

[1] E.I. Ewans, I.H. Elbers and S.R. Ovshinsky, J. Non-Cryst Solids 2, 334 /1970/

[2] I. Feinleib, J. de Neufville, Appl. Phys. Letters 18, 254 /1971/

[3] I. Feinleib, S. Isawa, S.C. Moss, J.P. Neufville, J. Non-Cryst. Solids 8-10, 909 /1972/

[4] I.S. Berkes, S.W. Ing, V.J. Hillegas, J. Appl. Phys., 42, 4908 /1971/

[5] P. Chaudhari, S.R. Herd, J. Non-Cryst. Solids 8-10, 56 /1972/

[6] A. Hamada, T. Kurosu, M. Saito, M. Kikuchi, Appl. Phys. Letters 20, 1 /1972/

[7] T. Iyo, Y. Toysohima, Japan J. Appl. Phys. 11, 117 /1972/

[8] M. Terao, H. Yamamoto, S. Asai, E. Maruyama, Oyo Butsuri Suppl. 41, 68 /1972/

[9] R.J. von Gutfeld, P. Chaudhari, J. Appl. Phys. 43, 11 /1972/

Journal of Thermal Analysis, Vol. 9 (1976) 53–58

THERMODYNAMIC DATA ON CHALCOGENIDE GLASSES

J. HAJTÓ and T. KEMÉNY

Central Research Institute for Physics, Budapest, Hungary

(Received March 15, 1975; in revised form July 10, 1975)

The temperature-dependence of the specific heat near to the glass temperature was investigated for several Te- and As-based chalcogenide glasses, the latent heats of melting and crystallization of the former alloys also being measured. No thermal change could be detected in the transformation of the As-based alloys from the solid to the liquid state.

The present report describes some results of our investigations into the thermal properties of certain chalcogenide glasses. Electrical and optical switching and memory effects have been observed in many amorphous chalcogenides [1–2]. Pearson [3] and Eaton [4] suggested that thermally-induced phase changes were responsible for these phenomena. In glasses of appropriate composition, the amorphous material transforms to the crystalline modification upon being heated to the crystallization temperature. When the melted sample is cooled down, two different phases may be obtained depending on the cooling rate: slow cooling leads to crystallization, whereas if the sample is cooled down rapidly it solidifies in the amorphous state [5–8]. There is, however, a concentration region where even slow cooling produces amorphous material.

We measured the temperature-dependence of the heat capacities of the glassy and the crystalline material near to the glass temperature. In addition, the latent heats of melting and crystallization of the Te-based alloys were measured, and it was observed that these could be cycled repeatedly between the amorphous and the crystalline state.

Experimental

The required amounts of high-purity reactants were weighed out and approximately 2 g of the powder mixture was sealed in an evacuated glass tube. Six chalcogenide alloys of different compositions (see Table 1) were prepared by the usual melt-cool procedure.

The thermal parameters were determined with a Perkin–Elmer type DSC-2 differential scanning calorimeter. The encapsulated samples (~10 mg) were scanned from room temperature to 700 K at 20 K/min. The detailed theory of DSC can be found elsewhere [9–10].

Results and discussion

A list of the transition temperatures observed upon heating at 20 K/min may be found in Table 1.

Table 1

Transition temperatures of chalcogenide glasses

Sample No.	Composition	T_g K	T_{Cr_1}, K	T_{Cr_2}, K	T_{m_1}, K	T_{m_2}, K
1	$Te_{81}Ge_{15}As_4$	403	468	494	647	667
2	$Te_{85}Ge_{15}$	404	445	489	655	680
3	$Te_{75}As_{25}$	360	404	—	636	—
4	$Te_{71}Ge_{15}Sb_2S_2$	386	445	469	633	674
5	$As_{40}Se_{50}Ge_{10}$	510	—	—	—	—
6	$As_{40}Se_{25}S_{25}Ge_{10}$	514	—	—	—	—

The samples can be divided into two different groups. Samples 1 – 4 show three types of thermal change:

a) a sudden increase in the heat capacity at $T = T_g$, the glass temperature T_g depends on the heating rate (Fig. 1);
b) an exotherm at $T = T_{Cr}$, which is interpreted as crystallization;
c) an endotherm at $T = T_m$, which is associated with the melting of the crystalline material.

In Table 2 we have collected the experimental and computed specific heat data near to the glass temperature.

Table 2

Specific heat in cal/g K

Sample No.	$C(T < T_g)$	$C(T > T_g)$	C_{comp}
1	0.055	0.10	0.053
2	0.051	0.07	0.051
3	0.075	0.10	0.054
4	0.054	0.09	0.051
5	0.091	0.12	0.082
6	0.097	0.14	0.092

$C(T < T_g)$ is the measured specific heat just below, and $C(T > T_g)$ just above T_g, while C_{comp} is the specific heat computed on the basis of the Neumann – Kopp rule, assuming that the heat capacity of the alloy can be approximated

T_g can be observed only in the samples quenched from $T > T_m$. When the sample is heated to T_{Cr} it goes through the exotherm, and after this the heat capacity shows no anomaly at $T = T_g$ (see Fig. 1). These facts together confirm that T_g is characteristic of the amorphous state, T_{Cr} is the crystallization and T_m the melting of the sample.

Samples 1, 2 and 4 show two distinct crystallization and two melting peaks (Fig. 2). The interpretation of these peaks is possible by assuming the crystallization of two different phases with different melting temperatures.

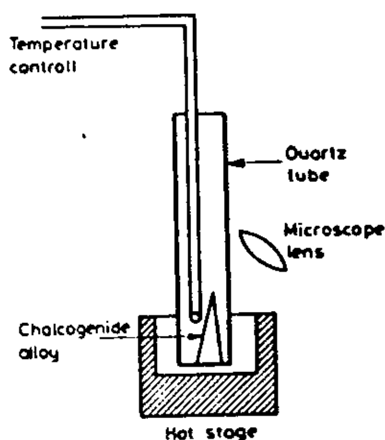

Fig. 3. A simple arrangement for determining the melting of chalcogenide glasses

The first exothermic transformation takes place between 440 and 470 K. This produced X-ray diffraction lines which were characteristic of Te crystallites [11]. The second exothermic transformation takes place between 470 and 500 K. X-ray diffraction identification of the heat-treated samples showed the presence of GeTe crystallites [11].

The latent heats of the transformations may be found in Table 3. The latent heat of crystallization is 2 – 5 times smaller than that of melting.

Table 3

Latent heat ΔH in cal/g

Sample No.	Crystallization	Melting
1	−9.3	17.9
2	−6.3	20.9
3	−5.5	26.1
4	−7.7	19.9

by the addition of the heat capacity of the constituents. The fact that the heat capacity below T_g is nearly equal to the heat capacity of the crystalline material (Fig. 1), which can be approximated to by the Neumann – Kopp rule, shows clearly that the extra degrees of vibrational freedom present in the amorphous state are almost completely frozen below T_g.

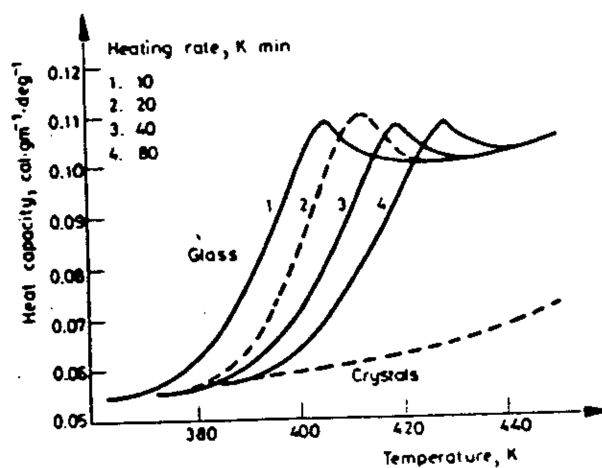

Fig. 1. Heat capacity of glassy and crystalline $Te_{85}Ge_{15}$ *vs.* temperature and heating rate

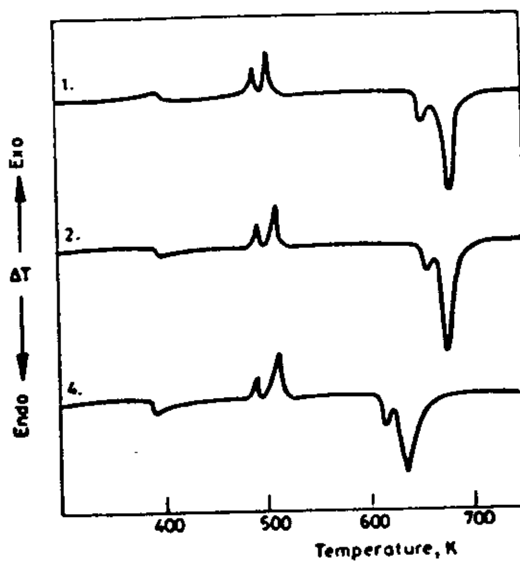

Fig. 2. DSC diagrams of samples 1, 2 and 4

The magnitude of ΔH_{Cr} is dependent on the amount of glass crystallized at T_{Cr} for a given scan rate. Studies by Quinn and Johnson [12] on bulk chalcogenide glasses have shown that crystallization nucleates at the surface, and therefore the surface-to-volume ratio must be important in the process of converting from a non-crystalline to a crystalline state.

We carried out a simple experiment to determine whether the samples melt in the temperature range investigated by us. The experimental setup can be seen in Fig. 3. Visual observation shows that sample 5 begins to melt at 570 K. At 700 K the sample takes on a completely spherical shape, which means that the solid material transformed to the liquid state in the temperature range 570 – 700 K. A similar phenomenon could be observed in the case of sample 6, where the melting interval was estimated as 580 – 720 K.

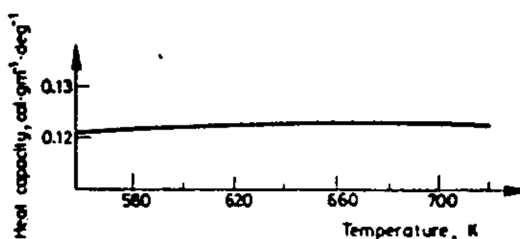

Fig. 4. Heat capacity of glassy $As_{10}Se_{30}Ge_{10}$ *vs.* temperature

Figure 4 proves that the samples show no significant thermal change (latent heat or heat capacity maximum) during melting. If there is any thermal anomaly, the associated energy must be smaller than the sensitivity of our instrument, i.e. less than 10^{-3} times the latent heat of melting observed with the crystalline material.

There is a structural difference between the thermal properties of samples 1 – 4 and samples 5 and 6. The first group can be characterized as "simple molecular

Table 4

Numerical values of the glass-forming tendency

Sample No.	K_{gl}
1	0.36
2	0.20
3	0.19
4	0.31

where $K_{gl} = \dfrac{T_{Cr_1} - T_g}{T_m - T_{Cr_1}}$.

glass forms" [13]. The numerical values of K_{gl} characteristic of the glass-forming tendency [14] are less than 0.4 (see Table 4); the glasses are therefore metastable and easily transform to the crystalline modification upon heating to the crystallization temperature.

Samples 5 and 6 have a high molecular polymer character [15, 16]. The glass is the most stable state of the substance. It is supposed that the temperature-dependence of the viscosity of the polymer glass form results in the absence of crystallization and melting effects.

The relationships between the thermodynamic data and the viscoelastic and dielectric properties are being studied further.

References

1. M. H. Cohen, H. Fritzsche and S. R. Ovshinsky, Phys. Rev. Letters, 22 (1969) 1065.
2. B. G. Bagley and H. E. Bair, J. Non-Crystalline Solids, 2 (1970) 155.
3. A. D. Pearson, Advances in Glass Technology. Plenum Press, New York, 1963, p. 145.
4. D. L. Eaton, J. Am. Ceram. Soc., 47 (1964) 554.
5. H. J. Stocker, Appl. Phys. Letters, 15 (1969) 55.
6. H. Fritzsche and S. R. Ovshinsky, J. Non-Crystalline Solids, 2 (1970) 148.
7. J. Feinleib, J. de Neufville, S. C. Moss and S. R. Ovshinsky, Appl. Phys. Letters, 18 (1971) 254.
8. K. Weiser, R. J. Gambino and J. A. Reihold, Appl. Phys. Letters, 22 (1973) 1.
9. A. P. Gray, Analytical Calorimetry Vol. I, pp. 209–218.
10. M. J. O'Neill, Anal. Chem., 36 (1964) 1238.
11. A. Bienenstock, F. Betts and S. R. Ovshinsky, J. Non-Crystalline Solids, 2 (1970) 347.
12. R. K. Quinn, R. T. Johnson, J. Non-Crystalline Solids, 12 (1973) 213.
13. D. Turnbull, Contempt. Phys., 105 (1969) 488.
14. A. Hruby, Czech J. Phys., 22 (1972) 1187.
15. J. H. Gibbs, J. Chem. Phys., 25 (1956) 185.
16. J. H. Gibbs and E. A. DiMarzio, J. Chem. Phys., 3 (1958) 173.

Résumé — On a étudié au voisinage de la température de la transition vitreuse la variation de chaleur spécifique en fonction de la température pour différents verres à base de chalcogénures de Te et As, en mesurant la chaleur latente de fusion et de cristallisation. Pour les alliages à base d'arsenic on n'a pas détecté de changement thermique après la transformation de l'état solide à l'état liquide.

Zusammenfassung — Die Temperaturabhängigkeit der spezifischen Wärme verschiedener Te- und As-Chalkogenid Gläser wurde in der Nähe der Glastemperatur untersucht, indem die latente Schmelzwärme und die Kristallisation gemessen wurden. Bei den Legierungen auf As-Basis konnte nach dem Übergang von dem festen in den flüssigen Zustand keine thermische Veränderung nachgewiesen werden.

Резюме — Исследована температурная зависимость удельной теплоемкости нескольких халькогенидных стекол на основе Te и As около температуры стеклования. Для первого из двух сплавов была измерена скрытая теплота плавления и кристаллизации. Для халькогенидного стекла на основе As не было обнаружено термического изменения при переходе из твердого в жидкое состояние.

KFKI-76-4

J. GAZSÓ
J. HAJTÓ
G. ZENTAI

KINETICS OF OPTICAL MEMORY SWITCHING IN CHALCOGENIDE THIN FILMS

Hungarian Academy of Sciences

CENTRAL
RESEARCH
INSTITUTE FOR
PHYSICS

BUDAPEST

KFKI-76-4

KINETICS OF OPTICAL MEMORY SWITCHING IN CHALCOGENIDE THIN FILMS

J. Gazsó, J. Hajtó, G. Zentai
Solid State Physics Division
Central Research Institute for Physics
1525 Budapest P.O.B. 49., Hungary

Submitted to Thin Solid Films

ISBN 963 371 103 7

ABSTRACT

Crystallization and reamorphization of As-Te-Ge chalcogenide thin films exposed to a pulsed laser beam have been investigated and direct information about the change in the speed of crystallization and amorphization has been obtained. The relation between time and minimum power needed for crystallization is presented. Microscopic examination of the diameter shows that laser writing and erasing can be ascribed to the thermally induced phase transition of the material. An estimate based on computer simulation of heat conductivity gives a lower limit of 0.1 usec for the writing--in process.

АННОТАЦИЯ

Нами были изучены кристаллизация, аморфизация и скорость фазового перехода халькогенидных пленок с составом As-Te-Ge с помощью лазерных импульсов. Наши были измерены зависимость длительность записи от минимальной мощности лазерового излучения.Електрон-микроскопическое исследование кристаллических точек показало что запись и стирание является результатом термического фазового перехода вещества Длительность записи полученные из уравнения теплопроводности равнялась 0.1 μсек.

KIVONAT

As-Te-Ge összetételü kalkogenid vékonyrétegek lézer impulzusok hatására történő kristályosodását és reamorfizációját tanulmányoztuk és meghatároztuk a fázisátalakulások sebességét. Vizsgáltuk a kristályosodáshoz szükséges minimális lézer teljesitmény és a beirási idő közti összefüggést. A kristályosodott foltok elektronmikroszkópos vizsgálata azt mutatja, hogy a lézeres beirást és törlést a vékonyrétegek hőmérséklet aktiválta fázisátalakulásával lehet magyarázni. A beiró folyamat sebessége a hővezetőképességi modell alapján számolva nem lehet rövidebb mint 0.1 μsec.

1. Introduction

Reversible changes in the reflectivity of Te-based chalcogenide films by laser irradiation have recently been reported /1-5/. It was found that the optical properties were altered by short laser pulses on chalcogenide films using mainly the amorphous or crystalline forms as starting materials. The thermodynamic data of Te-based thin films showed that the heat treated amorphous films contained Te crystals at about 220°C; at higher temperatures of about 260°C, Ge-Te was produced /6-8/. On cooling down the melted sample, two different thermodynamic phases may be obtained depending on the cooling rate and the compositions. However, if the melted material is cooled rapidly to room temperature it solidifies in the amorphous state.

The speed of "photocrystallization" in thin films is of the order of microseconds /9/ according to the speed of the amorphous - crystalline phase transition. The "photo-amorphization" is a faster process than that of the reverse mode /10/ and can take place within nanoseconds at the temperature of the phase transition. To obtain re-amorphized spots at room temperature, the process is controlled by the cooling rate of the material; values of the order of 10^{10} °C/sec have been calculated. A study of the crystallization kinetics has

shown /1/ that it can be reconciled with thermal effects only.

In this paper we summarize our results on laser--writing and erasing in chalcogenide thin films. The investigations on switching time and the data of electron-microscopic examination compared with the results of computer solution are detailed.

2. Sample preparation and experimental technique

Thin films of the chalcogenide alloys were prepared by the co-evaporation of the three elements of As, Te and Ge onto a glass substrate and simultanously onto a carbon collodium cover on a sample grid for electron-microscopic measurements. The film compositions measured by mass-spectrometrial analysis were found to be $Te_{80}Ge_{15}As_5$ and $Te_{88}Ge_6As_6$. Film thicknesses were nominally 210 Å and 670 Å. The morphological changes were photographed with a YEM 100 U transmission electron-microscope. The electron--micrograph and the diffraction pattern of the two films are shown in Fig. 1.

The diffraction pattern of the 210 Å thick film was characteristic for amorphous films but the 670 Å film was in the polycrystalline state. Crystallization takes

place during the thermal treatment of the layer - at about 230°C. This process may occur during the deposition of the film if the sample holder is not cooled. This fact has to be taken into account by the depositing of layers with thicknesses of more than 500 Å.

A modulated He-Ne laser beam / λ = 6328 Å/ was used for writing and erasing /crystallizing and amorphizing/ in amorphous chalcogenide thin films and its light intensity was monitored /Fig. 2/. Simultanously a He-Cd laser beam / λ = 4416 Å/ was threaded through the written spon in order to obtain direct information about the change in the speed of crystallization and amorphization. The change in transmission of the sample was detected by a photomultiplier 14 .

3. Results

Sensitivity dependence

Optical storage media can be classified into two groups 11 depending upon whether the photoresponse involves primarily sensitivity to the exposure energy /photographic media/, or sensitivity to the exposure intensity /threshold materials/. The Te-rich memory alloys generally show the photocrystallization phenomenon which leads to the threshold recording characteristics. Therefore our

first aim was to determine the relation between the laser pulse duration and the minimum power needed for crystallization to set in for the $Te_{88}Ge_6As_6$ thin films.

As Fig. 3 shows, the power - time relation in logarithmic scale is a straight line with a slope of - 1/3 in the μsec region but for higher "t" values as $t > 10^4\ \mu s$ the power limit becomes a constant. This constant value gives the minimum power needed for the onset of crystallization at which stage the heat loss and the heating by the laser are just in equilibrium and the temperature is just above the crystallization limit. This minimum power depends on a series of optical and thermal parameters: e.g. reflectivity and adsorptivity of the specimens at the given wavelength, heat capacities and conductivites, film thickness, etc. The failure of the reciprocity law between the pulse length and the exposure intensity involves that our alloy is none of the two extremes. We were unable to carry our measurements under 0.1 μsec because of the power limit of our He-Ne laser, though from heat conductivitiy considerations 0.1 μsec seems to be a lower limit value for successful crystallization /see Discussion/.

Speed of phase changes

The second aim of our investigation was to measure the speed of the amorphous-crystalline and crystalline-

-amorphous phase changes. The results shown in Figs 4a and b were obtained at a laser power of 13 mW.

Figure 4a shows the change in the light intensity of the He-Cd reading laser beam having gone through the written spot. The dotted line represents the form of the crystallizing pulse the length of which is chosen so that crystallization is completed during the light pulse and no changes take place after it. In this case the speed of "writing" is limited by the duration of the amorphous-crystalline phase transition which was shorter than 0.5 μsec. Figure 4b shows the kinetics of amorphization /"erasing"/ by the same laser power /13 mW/. The melting of the material needs higher energy than does crystallization so we used a longer pulse. The duration of amorphization and crystallization processes were approximately equal at a given laser power. These results are not inconsistent with the results of Gutfeld and Chaudhari 10 : the amorphization process may indeed be more rapid than the crystallization if the exposure intensities are not restricted.

Repeated testing

Writing-erasing cycles with fixed laser power /13 mW/ were carried out on the same spot, which was switched 150 times without any demage. Figure 5 shows the photo-

multiplier signals, plotted by an X-Y recorder. The time scaling is much greater, so the switching pulses themselves cannot be detected, only the changes in transmittivity caused by them. The time needed for crystallization is constant during cycles, but the pulse length, i.e. /energy/ needed for reamorphization increased somewhat during switchings /0.54-0.6 μsec/. This is experimental proof of the fact that the energy needed for reamorphization depends on the degree of crystallization 1 .

There is a sharp limiting value of 0.61 μsec for amorphizing pulses /at 13 mW power/: shorter pulses are not capable of transforming the crystalline spot into the amorphous state totally, but they do increase the remaining part in the crystalline state.

Electron microscopic examination

Electron-microscopic examination was carried out to determine the morphological changes during the writing - erasing cycles.

Pulses of 0.54-0.6 μsec from the He-Ne gas laser were used in the films of 670 Å thickness /polycrystalline ad deposited/. Figure 6a shows the transmission electron micrograph of the yielded structure. As can be

observed, the central region with the diameter of about 0.5 μ is perfectly amorphous; here the material was melted /T > 375°C/. This central region is surrounded by a halo region to the diameter of 1 μ. Here the polycrystalline structure is conserved /225°C < T < 375°C/, but the crystallites are rough. In the light-microscopic observations the amorphous spots are more transparent, and the reflectivity increases with the size of the crystallites. In Figure 6b the same spot is depicted in the "erased" state: in the place of the central amorphous region recrystallization has occurred under the heating influence of the focused electron beam of the electron microscope.

Films deposited from the vapour on room temperature substrates contain defects in high concentration and the numbers of these defects are greatly reduced during high temperature annealing. The most dense films are those which have been annealed at the highest temperature. This effect can be demonstrated by scanning electron microscope observations. In Fig. 7a, the central, hottest region of the laser exposed area is seen to be more concave. The structure corresponds to that shown in Fig. 6b i.e. the whole film is crystalline but the central part is the most dense. In the amorphized state the surface of the concavity has been smoothed /Figs 7b and 6a, respectively/. The data of the X-ray microanalyser showed no change in

the composi... n of the laser irradiated areas; it is true, however, that the resolution of this equipment was not better than 4 μ. On applying too intense pulses, the material melts, evaporates, and flows out /Fig. 7c/.

Temperature behaviour

The radial and temporal temperature profiles of the laser induced areas can be obtained as a first approximation by solving the following differential equation of heat conduction 15

$$c_p \rho h \frac{\partial T}{\partial t} = Q(r,t) + \lambda h \Delta T \qquad /1/$$

where: C_p = specific heat, ρ = density, λ = thermal conductivity, h = thickness of the film, Q = laser flux density whose form is assumed to be Gaussian:

$$Q = Q_0 \frac{1}{\sqrt{2\pi\sigma^2}} e^{-\frac{1}{2}\left(\frac{r}{\sigma}\right)^2} \qquad /2/$$

This analysis ignores the differences in thermal conductivity, reflectivity and absorptivity between the crystalline and the amorphous regions. The problematic effect of latent heat 16 is neglected, too.

From the distribution /2/ it follows that equation /1/ can be used only when the thickness of the film is

many times smaller than the diameter of the laser induced areas. This calculation is for the case of chalcogenide films on a thin carbon collodium layer: heat loss is taken into account only at the circular boundary of the spot. Taking the values $h = 0.067\mu$, $d = 1-3\mu$, $c_p = 0.09$ cal/gr ^oC, $\rho = 5.61$ gr/cm^3, $\lambda = 1$ kcal/m^{o}Ch, we found the following results:

In the case of the 0.4 μsec pulse the temperature of the illuminated area /2.8 μ diameter/ reaches the crystallization temperature range /$T_x = 225^oC-375^oC$/.

Using a 0.6 μsec pulse for reamorphization the temperature in the central region /0.5 μ diameter/ according to the Gaussian form of the laser flux density reaches the melting temperatures of the material /$T_m = 375^oC$/.

We found the cooling rate values predicted by the equation of heat conduction to be of the order of $600^oC/\mu$sec. This rate was sufficiently rapid for the melted material to remain in the disordered /amorphous/ state.

A summary of our results is shown in Table I.

Laser power mW	Pulse duration /us	Diameter of crystalline spots / u/		Diameter of amorphous spots	
		Electron microscopic observation	From equation of heat conduction	Electron microscopic observation	From equation of heat conduction
13.1	0.3	2.6	2.8	-	-
13.1	0.4	2.75	3.0	-	-
13.1	0.52	3.1	3.3	0.4	0.5
13.1	0.6	3.2	3.45	0.5	0.55

The diameter of amorphous spots are 0.4-0.55/u, but during amorphization a crystallization also takes place around the amorphous spots. The diameter of the crystalline region limits the packing density of the material: an order of 10^7 bit/cm² can be reached.

4. Discussion

In contrast to the As_2S_3, As_2Se_3 and related alloys, where photostructural changes appear to be the result of a non-equilibrium distribution of trapped charges created by illumination 11 , the study of the phase changes in the Te-rich thin films shows that the effects in them may be purely thermal in origin. The reciprocity failure seems to be attributed to the sensitivity dependence on the exposure intensity. In the limit of exceedingly short

/5 to 100 nsec/ pulses the sensitivity is stated to be higher /1, 10/; conversely, for long pulse exposures, e.g. 10^{-3} to 10^{-5} sec the sensitivity may be 10 to 10^3 times smaller 9 .

Since there are no generally accepted models or theories of the glass transformation, the following question may arise: does crystallization and revitrification occur via a process glass ↔ liquid ↔ crystal or directly glass ↔ crystal? 12 . Vitrification need not always involve thermodynamic melting as Herd and Chaudhari 13 demonstrated for electron beam exposure of Se at -100°C. In our case, however, for repeated testing on the same spot, there was a narrow range for the right vitrification pulse length: /0.605±0.005/ μsec at 13 mW laser power /Fig. 6/. Longer pulses caused the evaporation of the material /Fig. 5/ so it seems to be certain that amorphizing laser pulses do cause melting /Fig. 8c/.

It follows from the curves of the computer solutions of the heat conductivity that the decay time constant characteristic for the investigated spots with the given sample parameters is of the order of some hundreds of nanoseconds. /In our estimate the loss by thermal radiation which diminishes the decay constant at elevated temperatures was not taken into account./ Crystallization falls

to zero near to the melting point, and it should have its maximal values within the temperature range of 225°C to 325°C /Fig. 3/. Cooling the material in the central region of the spot, i.e. in the case of short ending of the vitrification pulses, the temperature crosses this critical interval during approximately 0.1 μsec /Fig. 8/. It should, however, be mentioned with regard to this estimate that for shorter pulses the attempt to write in may not results in perfect crystallization /at whatever high laser intensities/ due to the thermal parameters of our chalcogenide thin films.

REFERENCES

1 K.Weiser, R.I.Gambino, I.A.Reinhold: Appl.Phys. Letters 22 /1973/ 48

2 J.Feinleib, J.P.de Neufville, S.C.Moss., S.R.Ovshinsky: Appl.Phys.Letters 18 /1971/ 254/

3 M.Terao, H.Yamamoto, S.Asai, E.Maruyama: Prod. 3rd Conf. Solid State Devices, Tokyo /1971/ 68

4 S.Asai and E.Maruyama: Japan Soc.Appl.Phys. Tokyo /1970/ 172

5 J.Feinleib, S.Iwasa, S.C.Moss, J.P. de Neufville, S.R.Ovshinsky: J.Non-Cryst. Solids 8-10 /1972/ 909

6 H.Fritzsche, S.R.Ovshinsky: J.Non-Cryst. Solids 2 /1970/ 147

7 D.L.Eaton: J.Am.Ceram.Soc. 47 /1964/ 554

8 A.D.Pearson, in: Advances in Glass Technology, Plenum Press, New York /1963/ 145

9 A.Hamada, T.Kurosu, M.Saito, M.Kikuchi: Appl.Phys. Letters 20 /1972/ 9

10 R.I.von Gutfeld, P.Chaudhari: J.Appl.Phys. 43 /1972/ 4688

11 J.P. de Neufville, in: Proc. 5th Int.Conf.Amorph. Liquid Semic. /1973/ 1351

12 A.E.Owen, in: Electr.Struct.Prop. of Amorph.Semicond. /ed. P.G.LeComber and J.Mort/ Academic Press, London and New York /1973/ 161

13 S.Herd, P.Chaudhari: J.Appl.Phys. 44 /1973/ 102

14 G.Zentai: Proc. "Amorph.Semicond.'74" /Reinhardsbrunn, GDR/ 441

15 J.Hajtó, G.Ács: Proc. "Amorph.Semicond.'74" /Reinhardsbrunn, GDR/ 437

16 R.J. von Gutfeld: Appl.Phys.Lett. 22 /1973/ 257

FIGURE LEGENDS

Fig. 1. Electron micrograph and the diffraction pattern of evaporated a./ 210 Å and b./ 670 Å thick films

Fig. 2. Measuring arrangement

Fig. 3. Minimum power vs. pulse length

Fig. 4. Kinetics of phase changes
a/ amorphous - crystalline; b/ crystalline - amorphous

Fig. 5. Repeated writing - erasing test on one spot

Fig. 6. Transmission electron micrographs of
a/ an amorphous spot in starting polycrystalline $Te_{88}Ge_6As_6$ film
b/ the recrystallized state via slow electron beam heating
c/ the crystallized spot exposure to laser beam

Fig. 7. Scanning electron micrographs of
a/ crystallized spot
b/ reamorphized spot
c/ burned-out spot

Fig. 8. Temporal temperature behaviour of the chalcogenide film using a simple radial heat flow model for computer simulation
a/ slow crystallization pulse
b/ rapid crystallization pulse
c/ amorphizing pulse

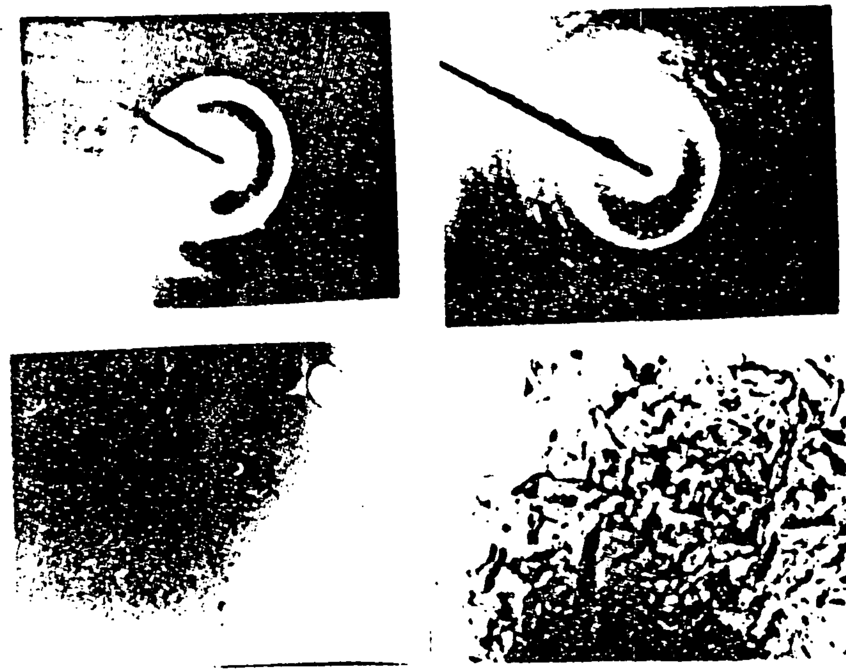

Fig. 1

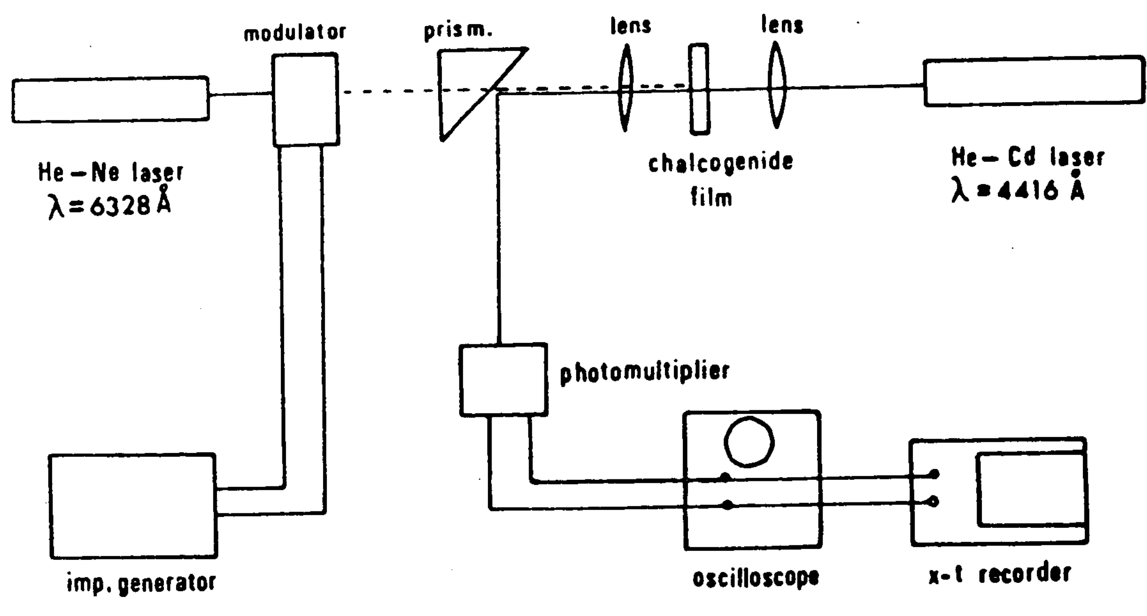

Fig. 2

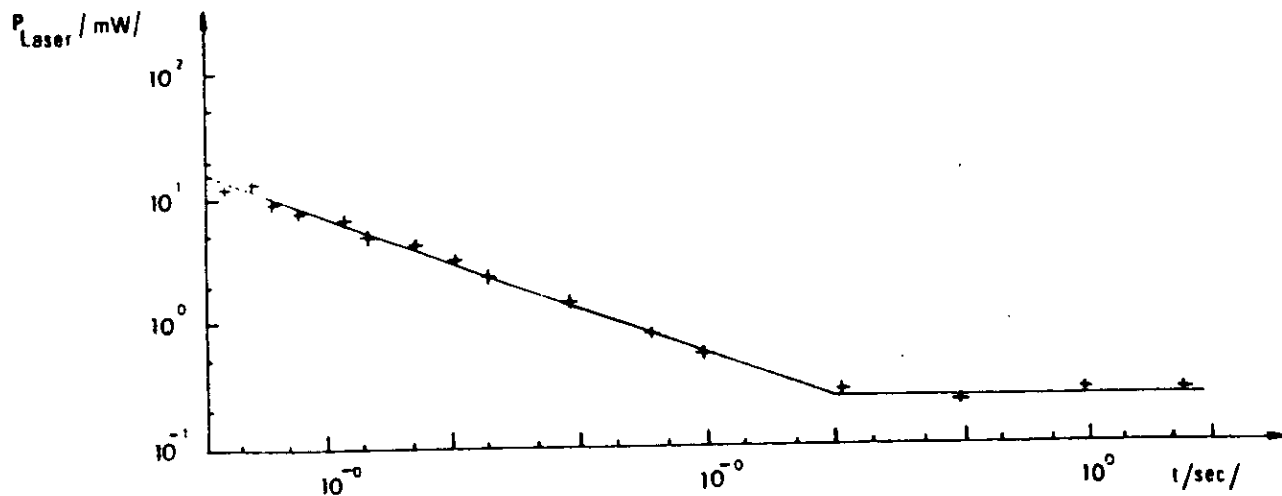

Fig. 3

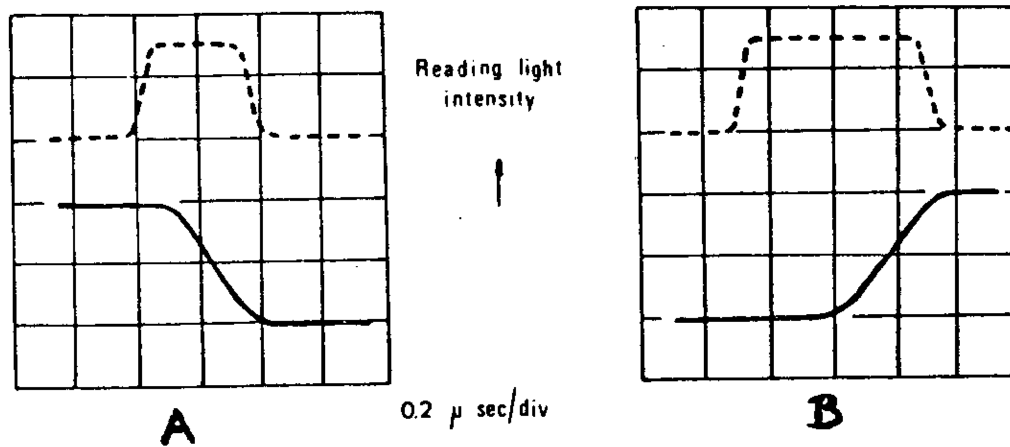

Fig. 4

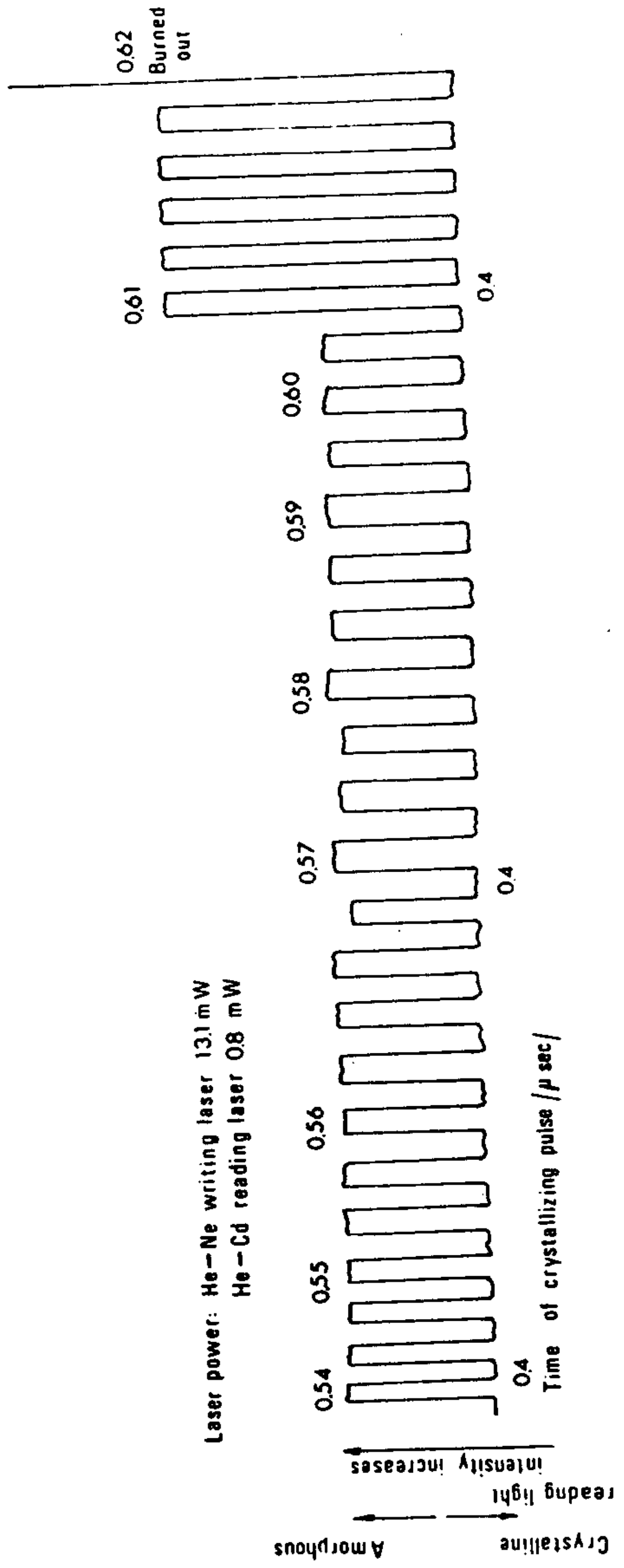

Fig. 5

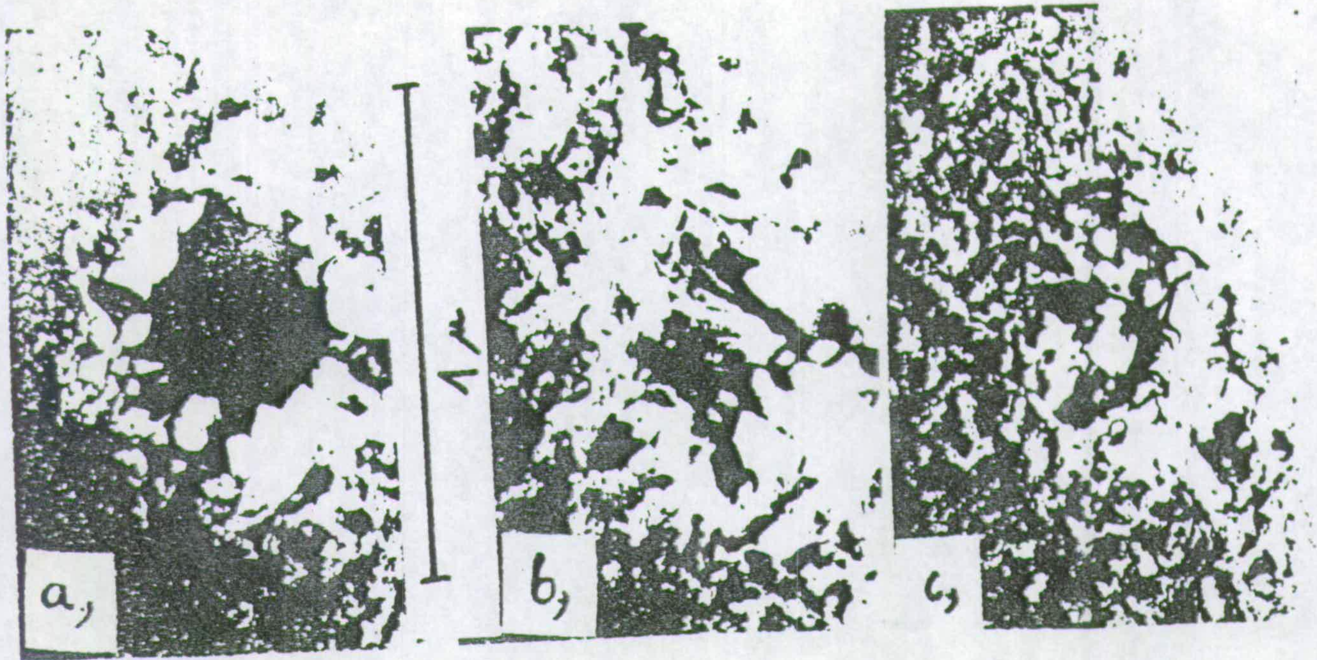

Fig. 6

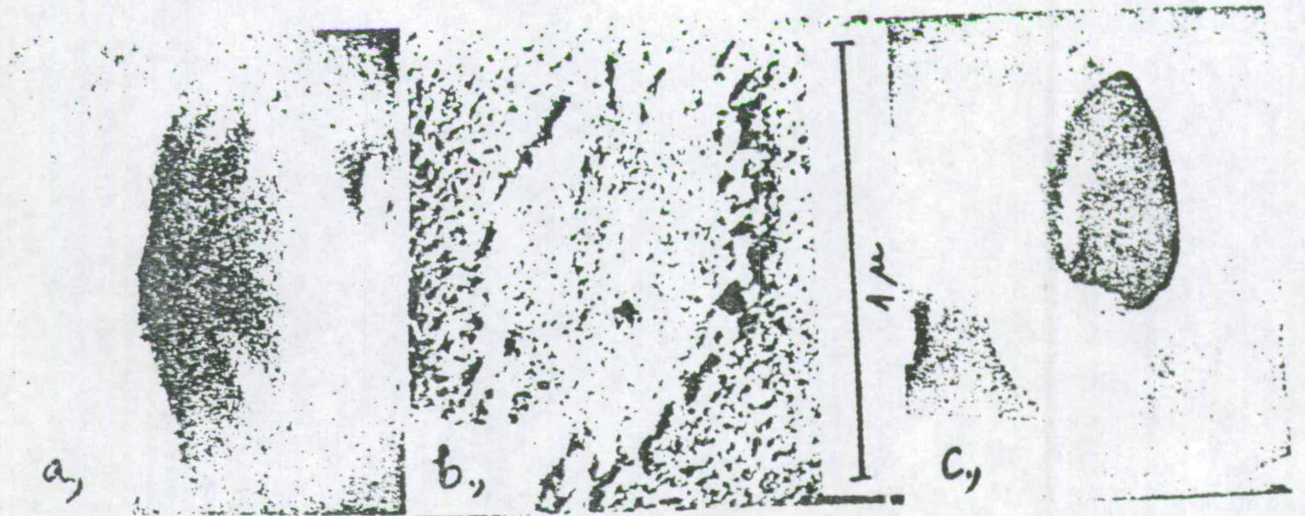

Fig. 7

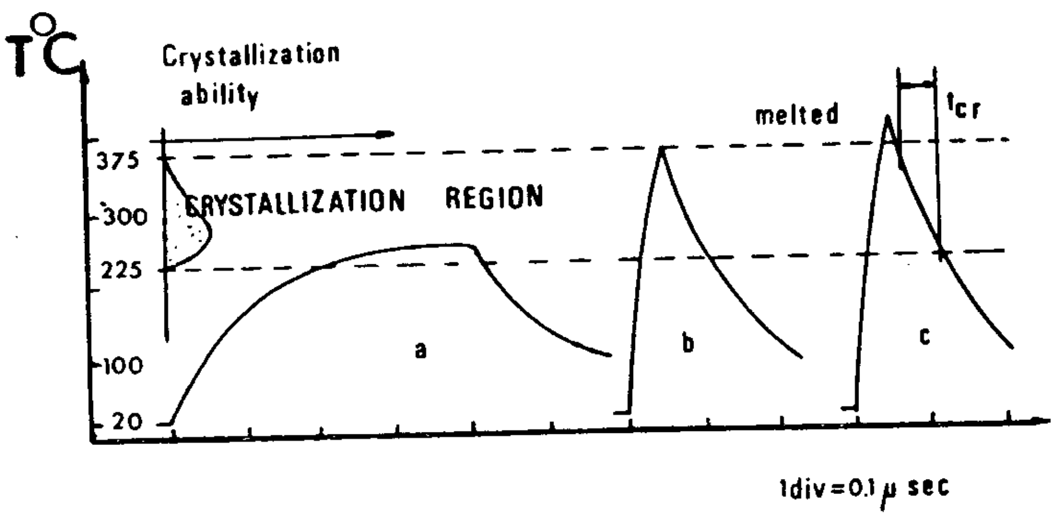

Fig. 8

AC MEASUREMENTS ON As-Se-Te SAMPLES

G.Zentai and J.Hajtó

Central Research Institute for Physics,
H-1525 Budapest, P.O.B. 49., Hungary

INTRODUCTION

Variation of a.c. conductivity and permittivity with frequency and temperature were measured on Te-Se-As compounds in order to clarify the role of Te in the conduction mechanism. The compositions of materials were chosen in connection with our investigations in the field of chalcogenide optical memories.

EXPERIMENTAL

Te, Se and As elements of 99.99% purity were pulverized, mixed, placed in evacuated quartz ampoules kept at 1000 C for 5 hours and quenched in water to obtain their disordered form. Discs were cut from the bulk materials with diameters 5-8 mm and thickness 0.5-1.4 mm. The two faces of the discs were polished. Copper wires were stuck onto the surfaces with silver paste or in another case the two plates were covered by evaporated thick gold layers (2-5μ) and copper rods were connected to the gold surfaces as current leads. During measurements the samples were held in a vacuum. Measurements were made by R-C bridges with variable frequency.

In the case of measurements of frequency dependence the temperatures were constant with an accuracy of ±0.5 C. The samples were measured in parallel RC equivalent in order to determine their permittivity and conductivity.

Samples of the following compositions were used: K1: $Te_{40}Se_{30}As_{30}$; K2: $Te_{50}Se_{25}As_{25}$; K3: $Te_{58}Se_{21}As_{21}$; K4: $As_{20}Se_{80}$.
K1 and K2 were unable to crystallize as verified by DSC measurements. K2 and K3 crystallize above 120°C.

RESULTS

Fig. 1 shows the change of permittivity with frequency. The permittivity at low frequencies has a very high value depending slightly on temperature. It is to be noted that those frequencies at which the permittivity starts to diminish increase with increasing temperature and with the Te content of the samples. For example the half values of the low frequency

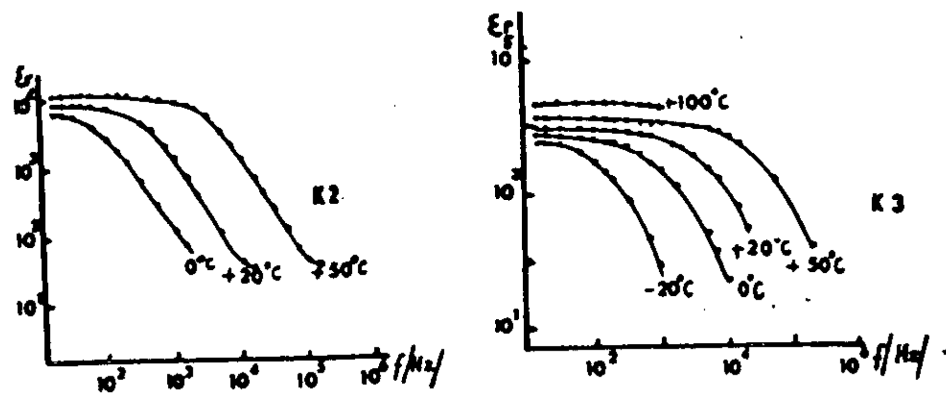

Fig. 1 Frequency dependence of permittivity at different temperatures

permittivities at T=20 C are for K1 ≅150 Hz; for K2 ≅500 Hz and for K3 ≅2 kHz. The permittivity of the samples at low frequencies were all in the order of 10^3-10^4 and slightly increased with increasing Te content.

In the case of crystallizable material (K2; K3) the permittivity shows a very sharp decrease at crystallization temperature and it goes into a negativ value (this is probably due to the inductance of the measuring leads) whilst the conductivity sharply increases (see Fig 2 .)

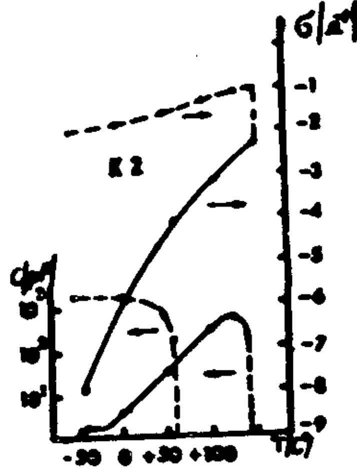

Fig. 2 Temperature dependence of permittivity and conductance in crystallizable material. —— amorphous state; ------ crystalline state; $\omega = 10^4$ rad/sec was constant during this measurement f ≅ 1600 Hz

Lowering the temperature in the crystalline state sample causes the capacitance to appear again and sharply grow up to a high value.

On Fig. 3 the variations of σ with f at constant temperatures are shown. In the frequency range of 10^1-10^5 Hz σ vs. f curves show S like shape and increase with frequency.

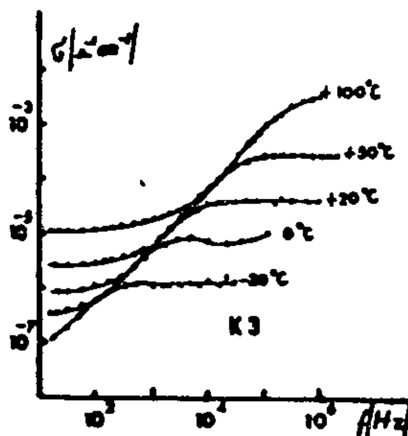

Fig. 3 σ - ω dependence at different temperatures

In the case of K4 ($Se_{20}As_{80}$) sample no frequency or temperature dependence of permittivity was observable; the permittivity was constant from -60 C to +120 C having a value of about 8, but the conductivity grew up significantly with temperature. No special difference was detected between samples having Ag paste type or evaporated gold electrodes. The voltage-current characteristic for DC was ohmic even in the low mV region especially for the gold plated samples.

DISCUSSION

Ac measurements similar to ours were made on thin films by J.Gassó [1], D.B.Dove and Irani [2] on Te-Ge-As compounds and on other compositions as well. It is very interesting, that until now behaviour similar to our observations and similarly high dielectric constant at low frequencies were observable only in samples containing Te. In Ref.[1, 2] only thin samples were investigated, where the electrode area was comparable with the valume of thin film. We used bulk samples where the electrode area was small compared with the volume of amorphous material.

The peculiar frequency dependences found in this study - and also by others [1, 2] - are usually regarded to be caused by the contact effects. We have found the same be-

haviour using different contacting methods and believe that it is due to the amorphous material investigated.

Although frequency dependences are expected to occur in amorphous materials generally, but at much higher frequencies only and there the dielectric constant should increase with increasing frequency in contrary to that observed.

The behaviour of σ and ε is similar to that found in cases where small metal particles are present i.e. in case of tunneling or one dimensional materials. We suggest therefore, that our results can be explained by a model regarding our amorphous materials as consisting of well conducting pieces embedded in an insulating matrix. This theory was first applied to metal strands interrupted by lattice defects [3, 4, 5]. Te clusters or filamentlike species might serve as conductors in our cases. The well conducting parts separated by insulating Se-As layers behave like condensators and the material can be modellized as a capacitor network (Fig. 4).

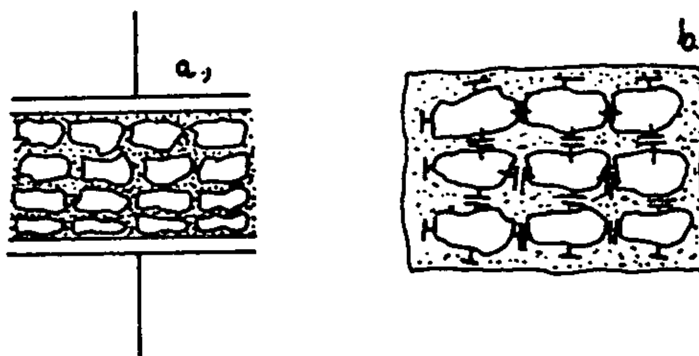

Fig. 4 Condensator network model as explanation of relativly high permittivity

Because a very large amount of little capacitances are connected in series and parallel, summing them between the two electrodes leads to a capacitance with high dielectric constant.

The dielectric constant observable at low frequencies between the two electrodes nearly proportional to the ratio of the well conducting to the insulating parts times the dielectric constant of the insulating parts. The dielectric constant of the insulating parts is of the order of 10 taken from the low temperature measurements of permittivity at relatively high frequencies. Thus the permittivity of the

well conducting parts relative to the insulating ones is of the order 10^2-10^3.

Unfortunately, there is no straightforward distinction between the interfacial and the space charge polarization (see e.g. [6, 7]), thus both electrode effect and the above mentioned "conducting parts interrupted by insulating parts effect" can produce the measured frequency dependence of permittivity and conductivity [7]. But in the interfacial polarization by purely electrode effect such a high temperature dependence of ε as measured in our case, is not expected. It is very important, that in the case of different electrodes such high permittivity can be obtained only by Te containing samples.

Nevertheless more investigation needs to clarify the structure of these material, what mechanism can make metal-like parts in Te containing amorphous materials.

REFERENCES

[1] J.Gazsó: Conference on Amorphous Semiconductors'74. Proceeding II. (1974) 433-436

[2] D.B.Dove and R.F.Irani: Thin Solid Films 34, 77 (1976)

[3] J.Giaever and H.R.Zeller: Phys.Rev.Lett. 20, 1504 (1968)

[4] H.R.Zeller and J.Giaever: Phys.Rev. 181, 789 (1969)

[5] O.Kuse, H.R.Zeller: Phys.Rev.Lett. 27, 1060 (1971)

[6] H.Fröhlich: Theory of Dielectrics, 1949. Clarendon Press London

[7] A. von Hippel: Dielectrics and Waves, 1954. John Wiley and Sons Inc. London

AMORPHOUS SEMICONDUCTORS '76

Kinetics of laser induced crystallization on As-Se-Te thin films

J.Hajtó and G.Zentai

Central Research Institute for Physics
H-1525 Budapest, POB. 49., Hungary

INTRODUCTION

In a large group of chalcogenide thin films, the memory effect is the result of a reversible phase change between a high transparent amorphous and a low transparent crystalline state [1-6].

To clarify the role of light in the process of crystallization, results are reported of laser induced crystallization on As-Se-Te thin films.

RESULTS

1. Change in optical properties

The optical properties of three As-Se-Te thin films were measured in amorphous and laser induced crystalline states (Table I). A He-Ne laser beam of 8.68 mW was used for crystallisation.

Table I.

No.	Composition	Thickness Å	Transmission % at λ = 6328 Å Before illumination	Transmission % at λ = 6328 Å After illumination	Reflexion % at λ = 6328 Å Before illumination	Reflexion % at λ = 6328 Å After illumination
1	$As_{25}Se_{25}Te_{50}$	850	2.72	0.41	44.88	66.77
2	$As_{21}Se_{21}Te_{58}$	850	2.41	0.34	43.15	67.22
3	$As_{19}Se_{19}Te_{62}$	880	2.01	0.50	44.20	56.42

Laser induced crystallisation changes the optical properties of thin films significantly. In every case the crystalline state can be characterised with lower transmission and higher reflexion values than the amorphous one. The considerable change in the optical properties, especially in the transmission, facilitates the study of laser induced crystallisation process.

The sample No.2. had nearly equal glass forming and crystallisation tendency [7] a requirement for reversible optical memory, that it was choosen for a more detailed study.

The decrease of transmission during the laser irradiation was taken as a measure of the crystallisation rate.

$$\frac{T}{T_{am}} = \exp\left(-f\ d\ \Delta\alpha\right) \tag{1}$$

where T_{am}=transmission of the amorphous layer, T=transmission of the layer during crystallization, $\Delta\alpha$ = the difference of the absorption coefficient between the two state, d=thickness of the layer, f=fraction of the crystallized material. The value of $-(1 - T/T_{am})$ is proportional to f.

2. Isothermal crystallisation

Let us suppose that the crystallization of the amorphous layer is a first order process. In this case it can be described by the equation

$$\frac{dx}{dt} = c(1-f) \tag{2}$$

at constant temperature, in which f is the fraction of crystallised material and c is the rate constant. Integration of equation leads to the equation:

$$c = \frac{1}{t}\ln\left[\frac{1}{1-f}\right] \tag{3}$$

By means of the method outlined in 3, the fraction of the crystallized material can be obtained from the measured transmission values.

The temperature of laser irradiated areas was measured by the thermopower of vacuum evaporated Ni-Au thermocouple [8] (Fig 1). We have found that after 40 second the temperature of laser irradiated films becomes a constant value. Because of the duration of the reaction time ($\sim 10^3$sec) we can calculate with constant temperature value at given laser intensity.

Plots of $\ln\left[\frac{1}{1-f}\right]$ values versus t give straight lines. Their slopes are the rate constants of crystallization at given temperature (at given laser flux density) Table II.

Table II. Laser induced crystallisation kinetic data on $As_{21}Se_{21}Te_{58}$ thin film

ϕ [Watt/cm²]	T [°K]	C [1/sec]
13.2	365.5	$4.427\ 10^{-3} \pm 4.4$ %
12.5	362.1	$2.956\ 10^{-3} \pm 7.8$ %
11.8	358.3	$2.265\ 10^{-3} \pm 6.6$ %
11.5	356.9	$1.911\ 10^{-3} \pm 4.0$ %
10.2	350.9	$1.006\ 10^{-3} \pm 2.63$ %

The errors of values c were calculated by least square method.

The temperature dependence of the kinetic rate constant can be fitted by an Arrhenius type equation (Fig 1).

$$C = 5.36\ 10^{12}\ \exp\ \frac{-1.09\ eV}{kT} \qquad (4)$$

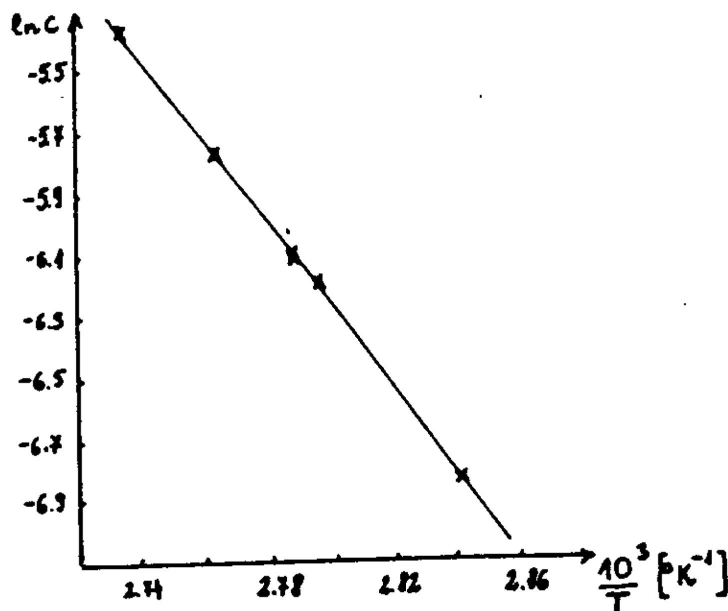

Fig 1 The kinetic rate constant versus the temperature of laser irradiated area on $As_{21}Se_{21}Te_{58}$ thin film

3. Non-isothermal crystallisation

At higher laser intensities the temperature of laser irradiated area increases during the laser irradiation. Because of the difficulty to measure or calculate exactly the temperature of thin films we didn't measured the kinetics at higher laser intensity.

Measuring the rate of transmission change of the film and the diameter of crystalline spots, we calculated the radial crystal grouth dependence on the laser flux density (Fig 2).

The radial crystal growth rate depends significantly on the laser flux density, it can be fitted by an equation

$$u = k\ \phi^5$$

where u = radial crystal growth rate[μ /sec], k=constant,

ϕ = laser flux density [Watt/cm²].

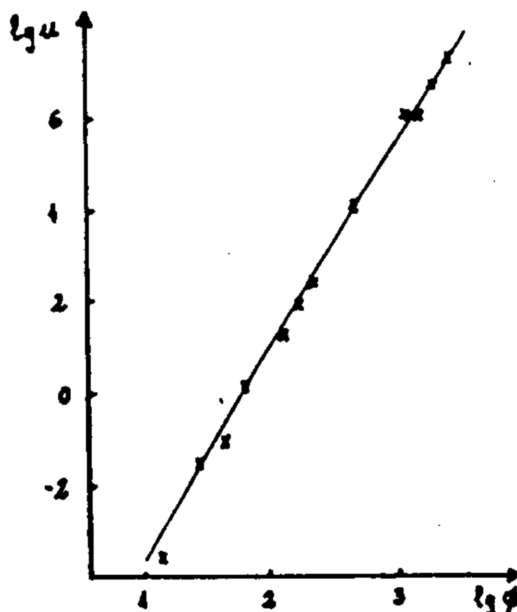

Fig 2 The radial crystal growth rate versus the laser flux density on $As_{21}Se_{21}Te_{58}$ thin film

CONCLUSION

In the As-Se-Te system a rather wide range of optical memory compositions exist. In contrast to the As_2S_3, As_2Se_3 and related alloys, where photostructural changes appear to be the result of a non-equilibrium distribution of trapped charges created by illumination [9], the study of the phase changes of As-Se-Te thin films shows that the effects in them may be purely thermal origin.

The value of c_0 [$5.36\ 10^{12}$/sec] is about the atomic vibration frequency and shows that this process can be applied for rapid optical memories. The amorphous-crystalline--amorphous phase changes can take place during one laser pulse. This result can be explained by a thermal effects. First the laser irradiated area crystallizes, the transmittance decreases and after the melting to the crystalline spot the transmittance increases to the original amorphous value . After the switching off the laser pulse the material cools rapidly, therefore it solidifies in the amorphous phase. In this way the changing of the pulse duration results "writing in" crystallisation or "erasing" amorphisation at the same laser intensity.

REFERENCES

1 K.Weiser, R.J.Gambino, J.A.Reinhold: Appl.Phys.Letters 22, 48 (1973)

2 J.Feinleib, J.P. de Neufville, S.C.Moss, S.R.Ovshinsky: Appl.Phys.Letters 18, 254 (1971)

3 M.Terao, H.Yamamoto, S.Asai, E.Maruyama: Proc. of 3d Conf. Solid State Devices, Tokyo 68 (1971)

4 S.Asai and E.Maruyama: Japan Soc. Appl. Phys. Tokyo 172 (1970)

5 R.J. von Gutfeld and P.Chaudhari: J.Appl.Phys. 43, 4688 (1972)

6 S.Herd, P.Chaudhári: J.Appl.Phys. 44, 102 (1973)

7 J.Hajtó and T.Kemény: Thermodynamic properties of $(AsSe)_{1-x}Te_x$ alloys - This proceeding

8 D.D.Thornburg and C.M.Wayman: J.Appl.Phys. 40, 3007 (1969)

9 J.P. de Neufville: Proc. 5th Int. Conf. Amorph. Liquid Semic. 1351 (1973)

EX BIBL. UNIV. EDINBURGH

AMORPHOUS SEMICONDUCTORS '76

THERMODYNAMIC PROPERTIES OF $(AsSe)_{1-x}Te_x$ CHALCOGENIDE GLASSES

J.Hajtó and T.Kemény

Central Research Institute for Physics,
H-1525 Budapest P.O.B. 49., Hungary

INTRODUCTION

The recent interest in chalcogenide glasses is motivated by their potential applicability for optical data storageing. The physical basis of this application is a reversible transition [1-5] between the crystalline and amorphous states which have very different optical properties. The thermal parameters are very important in order to formulate a clear picture of the crystallization and vitrefication processes. The temperature and concentration dependence of the thermal properties and the viscosity of chalcogenide glasses were measured. The role of the Te in $(AsSe)_{1-x}Te_x$ glasses is discussed.

SAMPLE PREPARATION

Six different compositions were prepared by the standard procedure: the required amount of high purity elements was melted together in an evacuated quartz ampoulle. The melt was kept at 1000°C for 10 hours, and after it was cooled down to room temperature.

VISCOSITY AND DENSITY MEASUREMENTS

The density was measured by picnometric method at room temperature. The results, summarized in Table I. show, that for As-Se-Te glasses, the density is about 5-8% lower than that of the crystalline phase.

Table I.: The density of $(AsSe)_{1-x}Te_x$ alloys

Code No.	X_{Te} at%	ϱ_{cryst} [g/cm³]	ϱ_{glass} [g/cm³]
0	0	-	4.375
1	40	-	4.82
2	50	5.376	5.016
3	58	5.682	5.171
4	62	5.821	5.483
5	66	5.902	5.608

The viscosity of the glasses was determined by the method of Nemilov [6]. Here one measures the velocity of a needle, driven to the material investigated with a given force. The concentration dependence of the viscosity at two,

arbitrarily chosen temperature can be seen in Table II.,
η = Poise

x_{Te}	lg η T=420 K	lg η T=450 K
0	14.1	13.4
1	11.2	9.4
2	8.8	7.3
3	7.3	-

THERMAL PROPERTIES

The thermal behaviour of chalcogenide glasses has been investigated with a Perkin-Elmer DSC-2 differential scanning calorimeter. The temperature calibration of the instrument has been performed at different heating rates with the well known transition points of high purity In, Zn and K_2CrO_4. The energy calibration has been checked with the heat capacity of synthetic sapphire, 6N purity Al and with the melting enthalpy change of In. The different calibrations resulted in the same energy sensitivity within the 2% standard error of our measurement.

We investigated the glass transition, the crystallization and the melting of the $(AsSe)_{1-x}Te_x$ alloy series where the glass forming tendency (see below) decreases with increasing Te content. The alloys with less than 50 atomic% Te content form stable glasses, i.e. they do not show any crystallization. The $(AsSe)_{0.5}Te_5$ alloy can be converted to the glassy state by cooling down from the melt at 80°/min in the calorimeter. The $(AsSe)_{0.42}Te_{58}$ alloy solidifies in the vitreous state after quenching the sealed calorimetric sample holder in water. The $Te_{0.62}$ and $Te_{0.66}$ alloys can be produced in the non-crystalline form only by spraying the melt directly to liquid nitrogen. It means, that the critical cooling rate for glass forming increases with increasing Te content.

The glass transition T_g and crystallization T_{cr} temperatures, measured at 10 K/min heating rate, are plotted in Fig 1.

T_g is represented by the midpoint of the heat capacity curve, and the peak temperature of the crystallization exotherm is taken as T_{cr}.

T_g decreases with increasing Te concentration, and shows negative deviation from linearity. T_{cr} decreases more steeply with Te content than T_g, i.e. $T_{cr}-T_g$ which measures the thermal stability of the glasses, also decreases with increasing Te concentration. The markedly non-linear molar volume dependence calculated from the density data suggests that the atomic volume of Te changes with concentration.

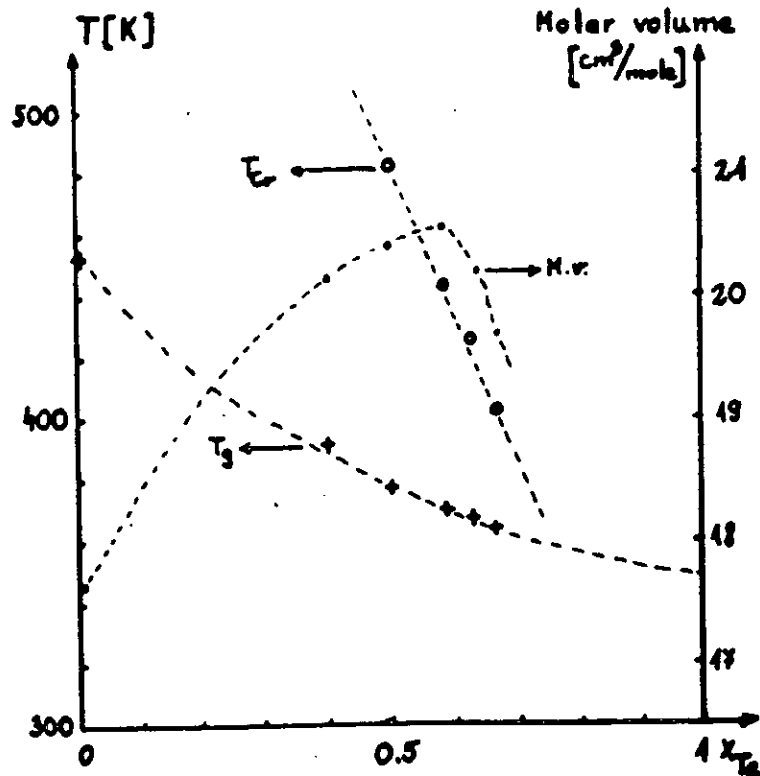

Fig 1. Transition temperatures and molar volumes of $(AsSe)_{1-x}Te_x$ chalcogenide glasses

The thermal stability of the No 0 → No 2 alloys facilitates the detailed investigation of the glass-transition, because crystallization does not interfere. We measured the temperature dependence of the heat capacity at different heating rates $\dot{T}_p$ from 2.5 K/min → 80 K/min. A representative result for No 2 can be seen in Fig 2.

In contrast with the experimental findings of [7] our T_g vs. log $\dot{T}_p$ plot has deviated from linearity, but could be expressed as

$$T_g = T_g^{(o)} + A \, \dot{T}_p^{\,n}$$

where T_g^{o} is approximately T_g 2.5[K/min] - 6 K ±4 K and n 0.3±0.05. The relatively great error of the parameters is not an experimental scatter, it is due almost exclusively to the significant statistical correlation between the two quantities.

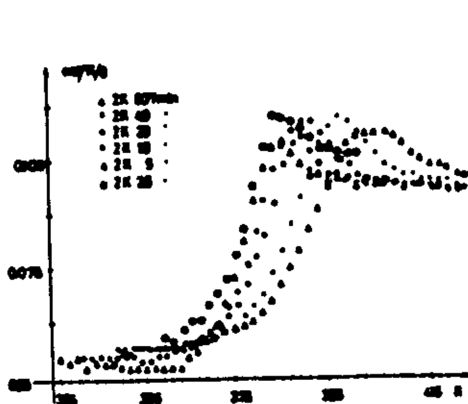

Fig 2. Heat capacity of $(AsSe)_{0.5}Te_{0.5}$ versus the heating rate and temperature

The specific heat below T_g agrees within 5% with the Dulong-Petit limit, i.e. 3R/mole, and increases about 60% at T_g where new translational and rotational degrees of freedom become accessible for the glass.

DISCUSSION

The concentration dependence of the thermal properties and the viscosity in the $(AsSe)_{1-x}Te_x$ alloy series can be explained with the continous destabilisation of the vitreous phase. A similar behaviour has been observed in the binary As-Te system [8] with the admixture of Te. AsSe can be described as a high-molecular polymer type glass with relatively great viscosity even at elevated temperatures. Due to this great viscosity the diffusion probability of a given atom remains very small in the temperature region where the free energy of the glass is greater than that of some hypothetical crystalline modification. It means that the diffusion barrier prevents the system from attaining its thermodynamically stable state of minimal free energy. The diffusion becomes significant only in the high temperature region, where the free energy is dominated by the entropy contribution -TS, i.e. where the glassy state with its higher entropy content has lower free energy than the possible crystalline phases. The admixture of Te weakens the chemical bonding, decreases the glass temperature, reduces the viscosity (Table II.), i.e. decreases the diffusion barrier. The increased diffusion permits the rearrangement of the constituents in the temperature region where a crystalline phase exists with lower free-energy. The crystallisation temperature depends very steeply on the composition (Fig 1), because the viscosity depends exponentially on T_g.

With increasing Te content the viscosity decreases and the alloy can be retained in the glassy state only with fast cooling from the melt, and on heating the sample crystallises

in the vicinity of T_g - which is really observed with our No4 - No5 samples.

The power-law dependence of T_g on heating rate is in fair agreement with the free-volume concept of the glass transition [9]. The theory would predict stepwise change in the heat capacity which is smeared out in real measurements, where at finite heating rate the experimental time scale becomes compatible with the atomic reorganization time scale at T_g. By reducing the heating rate the glass transition should become sharper and the measured T_g-s should converge, which is really observed in our measurements.

REFERENCES

1 M.H.Cohen, H.Fritzsche and S.R.Ovshinsky: Phys.Rev.Lett. 22, 1065 (1969)

2 B.G.Bagley and H.E.Bair: J.Non.Crystalline Solids 2, 155 (1970)

3 A.D.Pearson: Advances in Glass Technology, Plenum Press, New York p.145, (1963)

4 K.Weiser, R.J.Gambino and I.A.Reihold: Appl.Phys.Lett. 22, 1 (1973)

5 H.Fritzsche and S.R.Ovshinsky: J.Non.Crystalline Solids 2, 148 (1970)

6 Nemilov and Petrovsky: Solid State Phys. 36, 222 (1963)

7 M.Lasocka: Materials Science and Engineering 23, 173 (1976)

8 J.Cornet, D.Rossier: J. of Non-Crystalline Solids 12, 61 (1973)

9 D.Turnbull, M.H.Cohen: J. of Chemical Physics 52, 3038 (1970)

KFKI-1977-42

J. HAJTÓ
L. POGÁNY

ELECTRONMICROSCOPICAL INVESTIGATION OF $GeSe_2$ CHALCOGENIDE FILMS AFTER LASER INDUCED OSCILLATION

Hungarian Academy of Sciences

CENTRAL
RESEARCH
INSTITUTE FOR
PHYSICS

BUDAPEST

KFKI-1977-42

ELECTRONMICROSCOPICAL INVESTIGATION OF $GeSe_2$ CHALCOGENIDE FILMS AFTER LASER INDUCED OSCILLATION

J. Hajtó and L. Pogány

Central Research Institute for Physics, Budapest

HU ISSN 0368-5330
ISBN 963 371 260 2

ABSTRACT

The structural changes caused by transmittance oscillation of $GeSe_2$ thin films under the influence of a continuous He-Ne laser beam (λ = 6328 Å) were investigated by scanning electron microscopy. The changes of surface morphology during oscillation show that this process is probably due to a diffusion controlled amorphous-crystalline-amorphous phase change.

АННОТАЦИЯ

Нами были изучены структурные изменения, вызванные осцилляцией оптического пропускания аморфных пленок с составом $GeSe_2$ под влиянием излучения He-Ne лазера / λ= 6328 Å/. Электронно-микроскопическое исследование изменения поверхности пленок показало, что колебание пропускания является результатом фазового перехода вещества диффузией.

KIVONAT

$GeSe_2$ amorf vékonyrétegen folyamatos üzemű He-Ne gázlézer (λ= 6328 Å) által kiváltott transzmisszió oszcilláció okozta szerkezeti változásokat vizsgáltuk pásztázó elektronmikroszkóppal. A folyamat során megfigyelhető felületi változások arra mutatnak, hogy az oszcilláció feltehetőleg egy diffúzió határolt amorf-kristályos-amorf fázisátalakulás eredménye.

INTRODUCTION

In a recent letter [1] we have described the laser induced transmittance oscillation in $GeSe_2$ thin films. It can be maintained only within a certain light intensity range, in our case between 1.4-2.7 kwatt/cm^2. Oscillation is probably caused by differences in the absorption coefficients of the melted and crystalline $GeSe_2$ leading to successive cooling (crystallization) and heating (melting) cycles, if the rate of energy absorption and loss is dose to an equilibrium. Investigating further this new phenomenon we summarize our electron microscopic observations of the samples which had taken part in laser induced oscillation.

SAMPLE PREPARATION AND EXPERIMENTAL TECHNIQUE

$GeSe_2$ films were prepared by evaporating of crystalline grains on water cooled, SnO_2 coated silica substrates in a $2x10^{-5}$ Torr vacuum at 40 Å/sec deposition rate.The Thickness of the films was 6.4 μm as measured by a quartz crystal monitor. X-ray diffraction showed the film to be amorphous.

A continuous He-Ne laser beam (λ= 6328 Å) was used for creating the oscillation effect. The transmittance changes were detected by an appropriate photomultiplier and displayed on an oscilloscope. The morphological changes caused by the laser beam during oscillation were photographed by a Jeol JSM scanning electron microscope.

RESULTS

Although the films were in amorphous state, the surface of them was not homogeneous (Fig. 1). This observation is in good agreement with the grain like structure of the as deposited film as observed earlier [2].

The laser induced transmittance oscillation set in if the laser beam intensity reaches a certain value, and can be maintained within a rather small intensity range. In our case this light intensity range was 1.4-1.7 kwatt/cm^2.

Samples being in one of the two limiting states, i.e. when their transmittances differ most, were examined under a light and electron microscope. After oscillation had started, a few μm wide nucleus appeared in the centre of laser illuminated area, independently of which limiting state it had been in, when oscillation was interrupted. However in polarized light, the central light-colored nuclei behave differently: by rotating the analyzer some of them darken, whilst the others - just like the crystalline halo surrounding each central nucleus - remain unchanged (Fig. 2).

The centres of the halo on the spots frozen in the less transparent state are crystalline, while those of the more transparent state are mostly amorphous with little crystalline grains as verified by scanning electron microscope (Fig. 3).

Two effects can be observed during oscillation. One is a steady change of the morphology of oscillating spot. After some hundered switching a $\sim 1\,\mu$m deap hole is formed at the surface (Fig. 4.a). This hole disappears gradually and transformes into a ring-shaped like structure during oscillatin (Fig. 4.b).

During oscillation a continuous homogenization process takes place on the surface of the oscillating center clearly observable at higher magnification (Fig. 5).

DISCUSSION

An appreciable material transport can be observed during oscillation. This electron microscopical investigations are in good agreement with our explanation of oscillation based on a laser induced thermal processes leading to the associated transmittance changes as observed earlier [1]. The above mentioned homogenization process of $GeSe_2$ layers (see Fig. 5) found also in [2] under the influence of thermal treatment shows that the thermal effect of the laser irradiation plays an important role in the process of laser induced crystallization. The number of oscillation depends on the heat conductivity circumstances of the laser illuminated area, and 10^5-10^6 cycles can be reached at optimal laser intensity. This effect can be used for light controlled modulation of laser irradiation. Good reversibility of the crystallization-melting-crystallization process opens a possibility for a steady--state model of reversible phase changes on chalcogenide thin films.

REFERENCES

[1] J.Hajtó, G.Zentai and I.Kósa Somogyi: Transmittance oscillation on amorphous $GeSe_2$ films. Solid State Communications (in press)

[2] M.Noda and T.Arizumi: Japan J. App. Phys. 15, 1 (1976)

FIGURES

Fig. 1 Electron micrograph of as deposited $GeSe_2$ layer

Fig. 2 Microphoto of the spots being in the a/ less transparent and b/ the more transparent state

Fig. 3 SEM. Pictures of the spots being in the a/ less transparent and b/ more transparent state

Fig. 4 SEM pictures of the spots a/ after one hundred, b/ after ten-thousand oscillation

Fig. 5 SEM pictures of the center of the spots after a/ three-hundred, b/ three thousand, c/ twelf-thousand oscillation

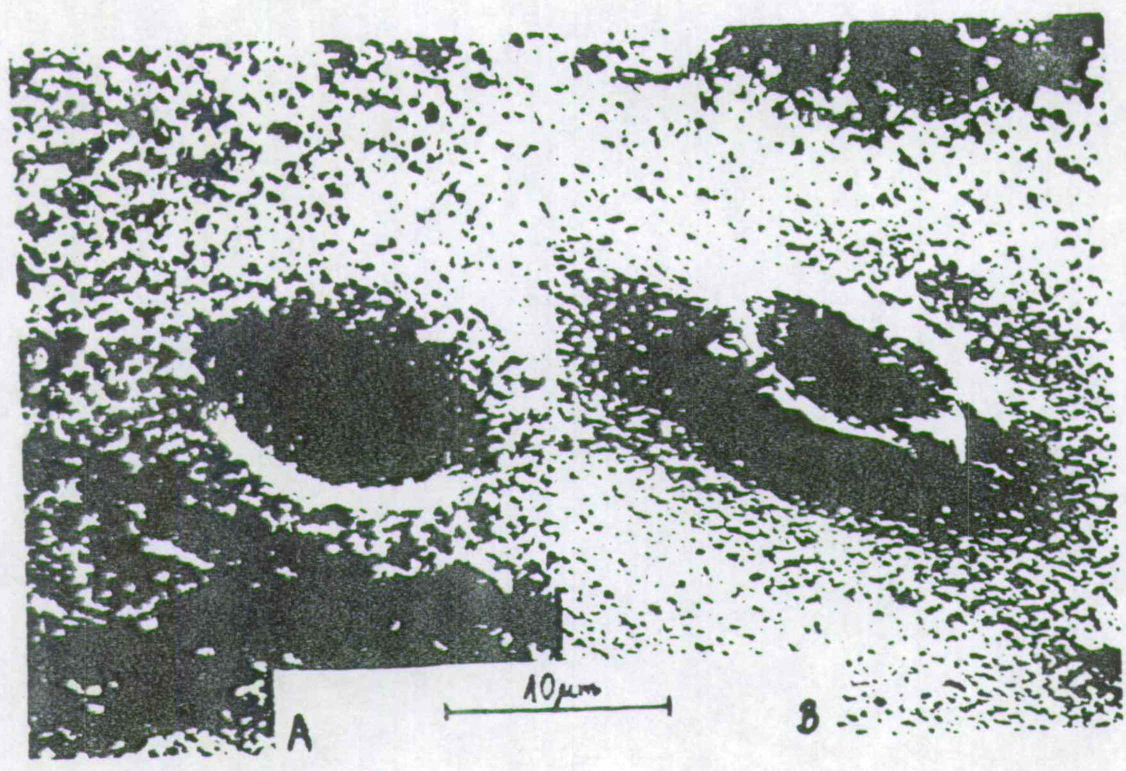

Fig. 4

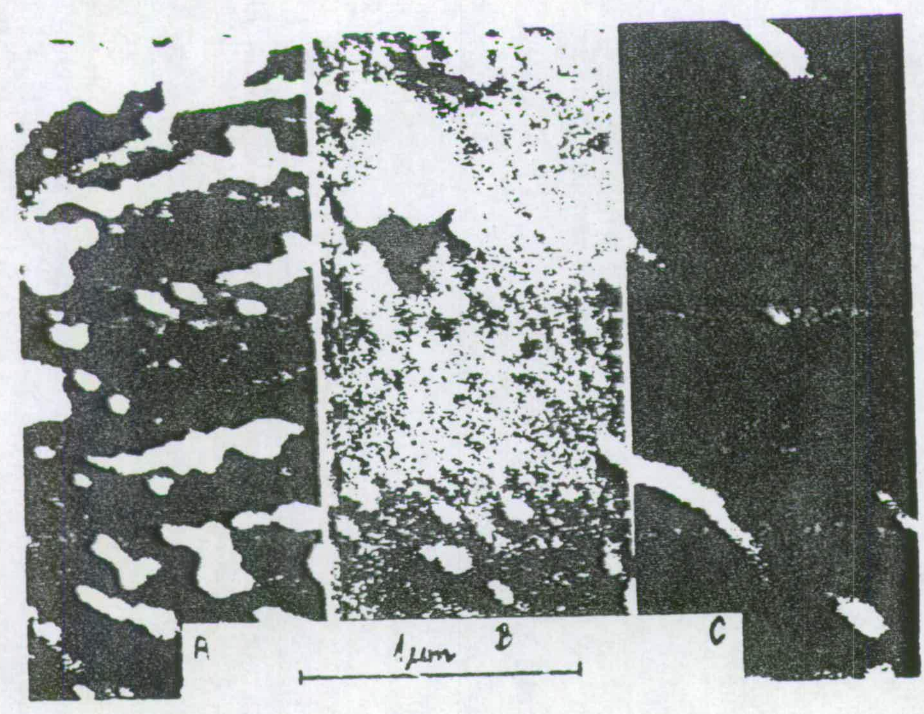

Fig. 5

AMORPHOUS AND LIQUID SEMICONDUCTORS

Proceedings of the Seventh International Conference on Amorphous and Liquid Semiconductors

Edinburgh, June 27 – July 1, 1977

Edited by
W.E. Spear, University of Dundee

Published on behalf of the Conference Committee by the Centre for Industrial Consultancy and Liaison, University of Edinburgh

THE KINETICS OF LASER INDUCED CRYSTALLIZATION OF $Te_x(AsSe)_{1-x}$ FILMS

By J. Hajtó, J. Gazsó and G. Zentai
Central Research Institute for Physics
H-1525 Budapest POB.49. Hungary

Abstract

Thin amorphous films of $Te_x(AsSe)_{1-x}$ (x=0.7; 0.62; 0.5) chalcogenide alloys were studied in respect to their light-enhanced crystallization speeds and dependence on compositions. An analytical formula was derived for the time development of the crystallized spots and the kinetic rate constants of the observed processes could be deduced. Although thermal activation cannot be excluded, photocrystallization is still observable well below the glass-transition temperatures.

1. Introduction

Chalcogenide glasses of the $Te_x(AsSe)_{1-x}$ system are known for the possibility that reversible phase transitions between the amorphous and crystalline states can be induced by intensive light irradiation. As a consequence, optical properties of the respective phases differ markedly which is of primary interest in optical information storage[1-3].

This paper is concerned with laser induced crystallization kinetics. It is suggested that light in the visible range plays a more important role in the increase of the crystallization speeds than just to provide sufficient influx of power for heating up the irradiated volume element. With the help of fairly small sized thin film thermocouples we could establish the temperature increases in the centres of the illuminated spots at different intensities. Compared to purely thermal DSC data[4], where the glass-transition temperature T_g of these glasses was in the range of 100 to 120 C. Crystallization still persisted at relatively low intensities (e.g. 1.5 W/cm^2) when the temperature of the centre of the spot rose to only 56.5 C.

2. Experimental

Three glasses of the $Te_x(AsSe)_{1-x}$ ternary chalcogenide alloy system were used in our experiments. The bulk ingots were obtained by melting together weighed amounts of the constituent elements in evacuated quartz ampoules at 900 C for 24 hours, and then quenched in cold water. Mass-spectroscopical analyses confirmed the composition data given above. Thin films of 800 Å thicknesses were vacuum evaporated onto fused silica holders. X-ray diffraction proved them to be amorphous. To facilitate temperature checks, evaporated Au-Ni thermocouples (size 0.1x0.2 mm^2) were built in under the chalcogenide films.

Two laser beams were used in our measurements, passing through the same spot on the film. A higher output regulated intensity Ar ion laser beam (λ= 5145 Å, P_{max} = 0.7 W, diameter at the spot 3.5 mm) was used for inducing the crystallization. A modest output intensity He-Ne laser

beam (1 mW, λ = 6328 Å, Ø = 3.5 mm) served for detecting the growth of the spot. Since the contrast ratios between the transmission values of the amorphous and crystalline phases are high enough[5] (6.6, 7.1 and 7.3 respectively) a calibration curve of the transmitted light vs spot diameter was measured (fig. 1). For green light the absorption of the chalcogenide film is much higher than for red. A red filter was placed in front of the detector.

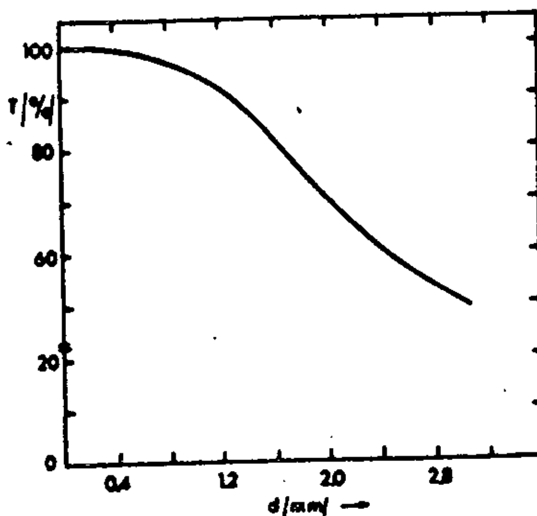

Fig.1. Calibration curve for detected transmitted light vs. measured diameter of crystalline spot.

3. Results

Our conception of the process is in essence a 2-dimensional picture (the 800 Å thickness being so small compared to the planar variables that the film crystallizes through that thickness entirely even before our recordings start). Nucleation and growth commences in the centre of the beam. After the very beginning the growth rate corresponds to the velocity of the boundary wall advancing radially.

We assume that the functional form of the crystal growth rate reflects its dependence on the temperature and the incident light intensity in form of a product. Since the light distribution is $i(x) = I\exp(-x^2)$ in a gas laser beam (x is the normalized radial distance), and in the pre-factor we expect thermal activation:

$$v(x) = B\exp(-\frac{A}{kT})\ I\exp(-x^2) = C\exp(-x^2)$$

Then by virtue of $v = \frac{dx}{dt}$, $dt = dx\exp(+x^2)/C$, expanding into series the exponential and taking the integral;

$$t(x) = C^{-1}(x+\frac{x^3}{3} + \ldots + \frac{x^{2k+1}}{(2k+1)k!} + \ldots) = F(x)/C$$

The shape of log F(x) vs. log x is depicted on fig. 2.

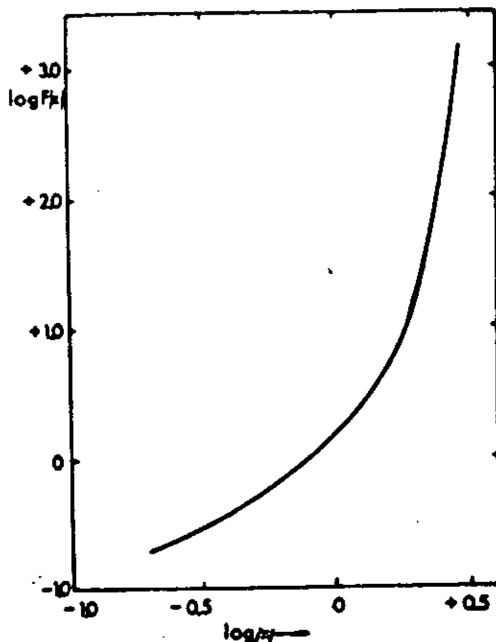

Fig.2. Theoretical relationship in case of a Gaussian intensity distribution between the diameter of crystallized spot and time elapsed.

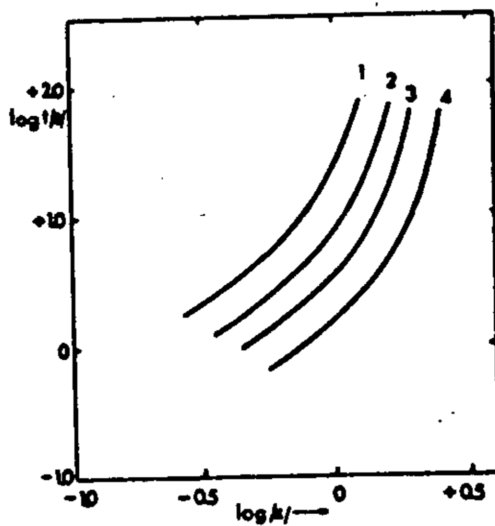

Fig.3. Measured functions of spot diameters vs time elapsed for $Te_{62}(AsSe)_{38}$ (I: 1.916; 2.56; 3.2; 3.83 W/cm^2 for 1, 2, 3, 4, resp.)

Fig.3 shows the measured graphs for one of the compositions. The shape of the empirical curves agrees well with fig. 2, thus confirming the validity of our assumpiton leading to F(x).

Table I. Incident light intensity I and temperature in the centre of the spot

I(W/cm²)	t (C)
1.53	44.6
1.92	56.5
2.56	85
3.2	111
3.83	136.3
4.47	162

Table I. contains the temperatures of the illuminated area, at each input intensity. Since F(x), T and I are all known, the pre-exponential factor B and the activation energy A (Table II) and the crystal growth rates (fig.4) can be calculated.

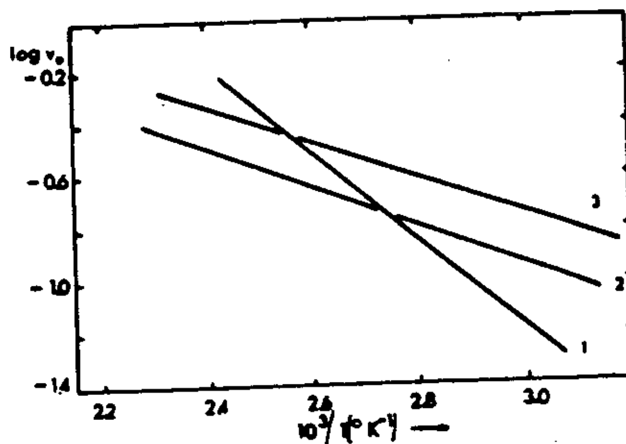

Fig.4. Isothermal growth rates for 1 W/cm² light intensity vs reciprocal temperatures.

1: $Te_{70}(AsSe)_{30}$
2: $Te_{62}(AsSe)_{38}$
3: $Te_{50}(AsSe)_{50}$

Table II. Pre-exponential factors (B) and activation energies (A) for different compositions

Composition	B $\frac{mm}{sec} \cdot cm^2/W$	A (eV)
$Te_{70}(AsSe)_{30}$	17 44	0.29
$Te_{62}(AsSe)_{38}$	4.75	0.11
$Te_{50}(AsSe)_{50}$	8.1	0.11

4. Conclusions

Our findings indicate that on applying light intensities of order 1 W/cm^2 in the visible range, crystallization starts at temperatures (e.g. 50-60°C) where without irradiation no observable changes take place. Although this photoenhanced crystallization does show thermal activation character, yet these energies (A values in Table II) are much smaller than those obtained by DSC (above 1 eV)[6]. The analysis outlined here regarded the growth as isothermal; this may have introduced some possible errors, but our belief is that the thermal gradients along the radii must be negligible. Any explanation aiming at the microphysical role of light in crystallization processes needs further evidence and reconsideration.

References

1. J.Feinleib, J. de Neufville, S.C. Moss and S.R. Ovshinsky, Appl. Phys. Lett. 18, 254 (1971)
2. S.R. Ovshinsky and P.J. Klose, J. Non-Cryst. Solids 8-10, 892 (1972)
3. J.P. de Neufville, in Amorphous and Liquid Semiconductors, ed. by J. Stuke and W. Brenig (Taylor and Francis, London, 1974) p.1351.
4. J. Hajtó, T. Kemény, in Amorphous Semiconductors'76, ed. by I. Kósa Somogyi (Akadémiai Kiadó, Budapest, 1977) p.493.
5. J. Hajtó, G. Zentai, in Amorphous Semiconductors'76, ed. by I. Kósa Somogyi (Akadémiai Kiadó, Budapest, 1977) p.371.
6. J. Hajtó, T. Kemény, to be published in J. Non-Cryst. Solids

Solid State Communications, Vol. 23, pp. 185–188, 1977. Pergamon Press. Printed in Great Britain

LIGHT-INDUCED LIGHT ABSORPTION CHANGES IN AsSe AND $GeSe_2$ THIN FILMS

L. Tóth, J. Hajtó and G. Zentai

Central Research Institute for Physics, 1525 Budapest P.O.B. 49., Hungary

(*Received 29 March 1977 by E.F. Bertaut*)

Reversible transmittance (T) changes for $\lambda = 6328$ Å light were observed in stabilized AsSe and $GeSe_2$ thin films when irradiated by $\lambda = 5145$ Å and $\lambda = 4880$ Å wavelength exciting light pulses. During photodarkening, T reaches a steady state value obeying a $T \propto t^{-1}$ relationship then approaches its starting value exponentially when the light is switched off. Both of these processes develop in a few seconds. The transmittance changes are explained by variations in the absorption coefficients with temperature, controlled by the absorption and loss of energy.

LUMINESCENCE measurements [1–3] and the optical stopping effect [4, 5] have indicated that excitation by light quanta of energy $\hbar\omega > E_g$ produces transitory states in the forbidden gap of chalcogenide semiconductors which absorb radiation of energy corresponding to about $\hbar\omega \sim 1/2E_g$. A model has been proposed by Mott, Davis and Street (MDS) [6–8] in which localized states due to dangling bonds and lattice distortion have either none or two electrons in the ground state. The transitory state corresponds to the singly occupied dangling bond, D^0, which appears only on excitation. Since lattice distortion is involved in the formation and disappearance of the localized states, slow response on excitation is expected; indeed Kikuchi *et al.* [5] measured response times in the range 0.01 – 1 sec.

Measurements described in this letter were performed in order to further investigate the kinetics of light-induced processes in chalcogenide thin films.

AsSe and $GeSe_2$ films were prepared by evaporating glass powders onto water cooled glass substrate in a 2×10^{-5} torr vacuum at rates 20–30 Å sec^{-1}. Samples were 1.85 (AsSe) and 6.4 μm ($GeSe_2$) thick. In our measuring set-up a Spectra-Physics Ar-ion laser at $\lambda = 5145$ Å and $\lambda = 4880$ Å, focussed on a 1.8 mm dia. spot were used for excitation, whilst a He–Ne laser light beam served for the detection of transmittance changes caused by excitation. The intensity of the detecting light beam was kept so low that it could not cause any photodarkening in the chalcogenide thin layer. The intensity of the exciting lasers was varied between 2.5–15 W cm^{-2}, whilst the detecting He–Ne laser power was in the 0.5–2 mW range. An appropriate filter was placed between the sample and the Si photodiode for cutting off light having wavelengths shorter than $\lambda = 6328$ Å. Luminescence light caused by excitation was too weak to be detected in this arrangement by the Si detector.

In order to record the increase of temperature caused by the absorbed light the studied chalcogenide thin film spots were deposited on evaporated Au–Ni thermo-couples, whose thermo e.m.f. was displayed on the storage oscilloscope or recorded potentiometrically.

The transmittance of as deposited AsSe films decreased (photodarkening), while that of the $GeSe_2$ films increased (photo-bleaching), when first illuminated by the exciting light. The extent of these initial stable photodarkening and photobleaching depend on the intensity of exciting light. The transmittance changed exponentially with time during both processes, reaching saturation values corresponding to 80–90% decreases or 20–30% increases, respectively. Such photodarkened and photobleached (stabilized) layers, i.e. layers, irradiated by exciting light until their α for He–Ne laser light has reached a stable value, were used as starting materials for further studies described here in detail, during which *reversible* photodarkening, caused by only 1–2% (AsSe) or 50–60% ($GeSe_2$) decrease of the original transmittance and its disappearance, were taking place.

The change of transmittance with time of such stabilized AsSe films for the red $\lambda = 6328$ Å light when switching on the exciting light follows a $T \propto t^{-1}$ relationship, whilst after switching off, the transmittance recovers its starting value exponentially (Fig. 1), then overshots it slightly. This overshot appears only on AsSe samples and varies with the exciting laser power (Fig. 2). The decrease of transmittance for He–Ne laser light is proportional to the intensity of the exciting blue light (Fig. 2). This behaviour is expected if the build up of the absorbing species has an exponential character, i.e. their recombination rate is proportional to their concentration.

The shape of the transmittance response on the blue light pulse changed somewhat when the sample was plunged in liquid nitrogen; it retained its overall

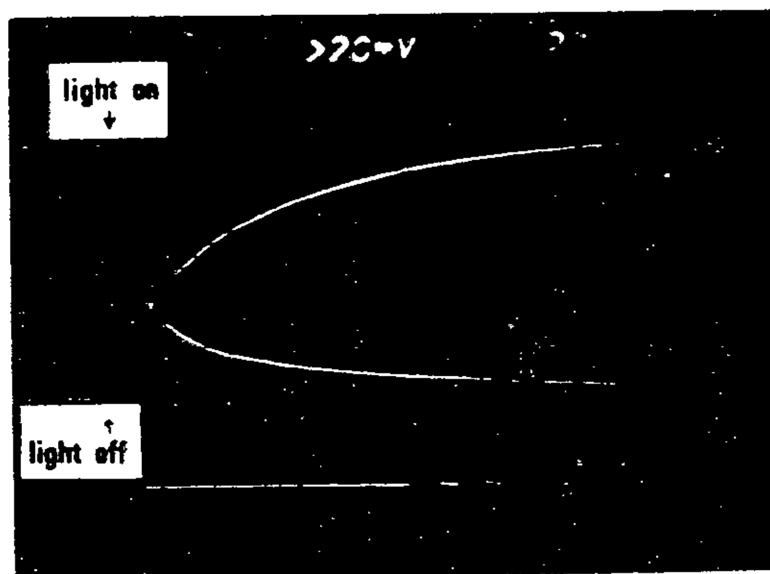

Fig. 1. The change of transmittance for $\lambda = 6328$ wavelength light caused by a $\lambda = 4880$ Å wavelength 14.4 W cm^{-2} intensity laser pulse. AsSe film, $d = 1.85\ \mu m$.

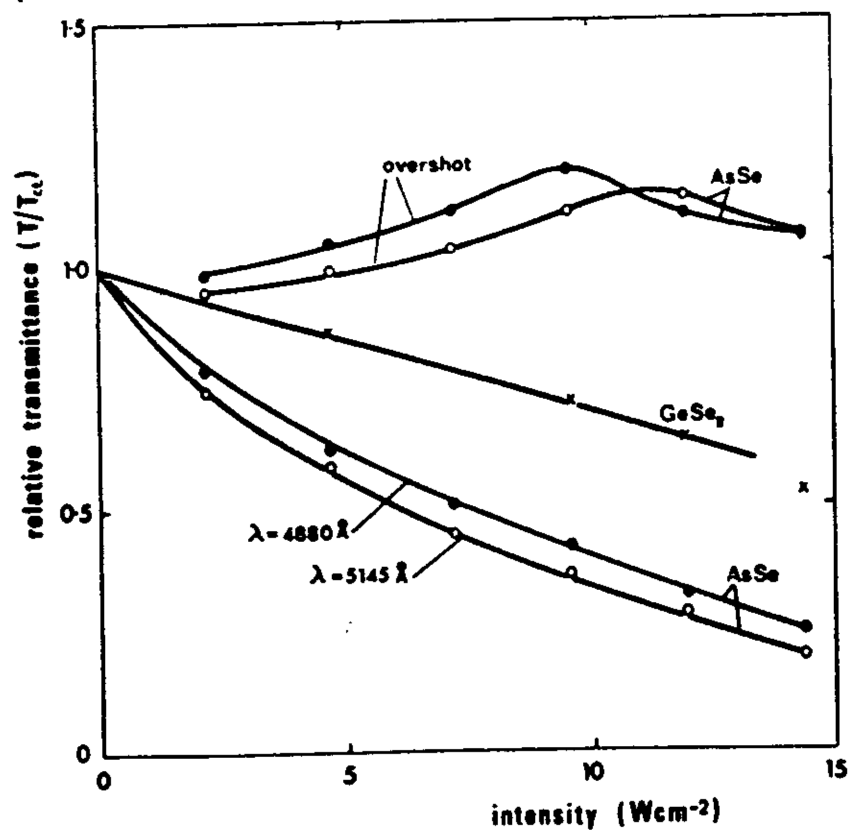

Fig. 2. The variation of relative transmittance and the overshot ($T = 1$ at room temperature) with laser pulse intensity.

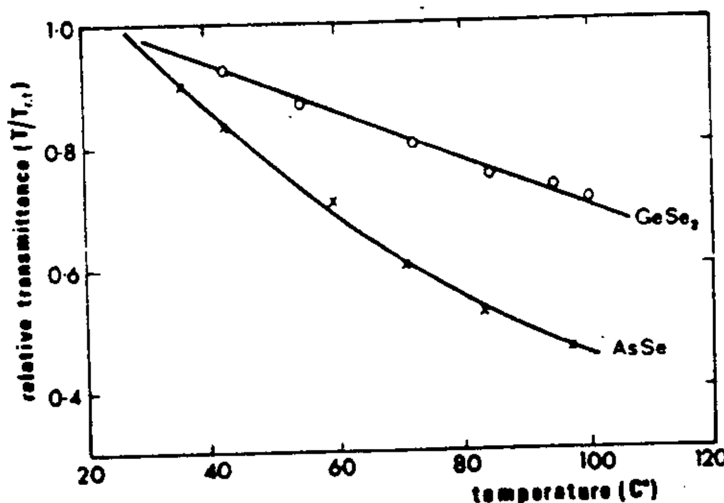

Fig. 3. Relative transmittance for λ = 6328 Å light vs sample temperature for amorphous $GeSe_2$ and AsSe thin films

shape but τ diminished. The depth of modulation, i.e. the change of transmittance at a given laser power, also got considerably smaller.

The measurements performed at 77 K indicate that heat transfer affects the kinetics of transmittance variation. We measured the variation of sample temperature during the exciting light pulse, and after it had been switched off. It has the same overall shape as the transmittance vs time curves shown in Fig. 1, and can be described by an exponential with parameters close to those of the recovery curve in Fig. 1.

Shift of the absorption edge with temperature for certain chalcogenides were reported [9, 10]. To evaluate the magnitude of transmittance changes caused by this effect, transmittance vs temperature curves were obtained for the He–Ne laser light (Fig. 3).

Our data seem to indicate that the transient photodarkening of AsSe and $GeSe_2$ thin films are connected with heat-induced reversible structural changes; the decrease of transmittance is due to the increase of sample temperature causing a red shift of the absorption edge. The somewhat faster response to exciting light pulses of samples held in liquid nitrogen and the smaller modulation depth are probably due to increased heat conduction. No fast components indicating the presence of electronic processes could be indicated by our measuring set-up which were able to trace 10 nsec events. The absorption edge at $\alpha = 1\ cm^{-1}$ for the stabilized AsSe and $GeSe_2$ films are at 1.8 and 2.0 eV, respectively. The temperature-induced red shift (photodarkening) for AsSe is greater than that for $GeSe_2$ (Fig. 3). Because of the absorption edge shifts towards smaller energies, α for the exciting light also increases, resulting in higher temperatures and further red shift. This self-accelerating process leads to a steady state transmittance value determined by the equilibrium of the heating and cooling rates.

Both initial photodarkening and photobleaching as well as reversible transmittance changes seem to justify the supposition of two alternative configurations for the atoms, one of these configurations is obtainable after overcoming an energy barrier. The temperature increase caused by light absorption is effective to some extent in the formation of this transitory state, too. The return to the initial, i.e. stable configuration, is connected with the disappearance of this metastable arrangement.

The photostructural changes described here involve transitory states separated by only ~ 0.1 eV from the band edge and not necessarily involve states deep in the gap. Further measurements to check absorption changes in the whole gap rather than just near the absorption edge are needed to see whether D^0 like states are also involved in these reversible optical changes.

REFERENCES

1. VASSILYEV V.A., PAVLOV S.K. & KOLOMIETS B.T., *Proc. Int. Conf. Amorphous Semiconductors, 1976,* p. 189. Akadémiai Kiadó, Budapest (1977).
2. VASSILYEV V.A., MAMONTOVA T.N. & KOLOMIETS B.T., *Proc. Int. Conf. Amorphous Semiconductors 1976*, p. 171. Akadémiai Kiadó, Budapest (1977).
3. VASSILYEV V.A., KOÓS M. & KÓSA SOMOGYI I., *Solid State Commun.* 22, 663 (1977).

4. MATSUDA A., MIZUNO H., TAKAYAMA T., SAITO M. & KIKUCHI M., *Appl. Phys. Lett.* 24, 314 (1974).
5. KIKUCHI M. & MATSUDA A., *Proc. 6th Int. Conf. Amorphous and Liquid Semiconductors, Electrical Properties*, p. 35. Nauka, Leningrad (1976).
6. STREET R.A., *Adv. Phys.* 25, 397 (1976).
7. STREET R.A. & MOTT N.F., *Phys. Rev. Lett.* 35, 1293 (1975).
8. MOTT N.F., DAVIS E.A. & STREET R.A., *Phil. Mag.* 32, 961 (1975).
9. TANAKA K. & KIKUCHI M., *Amorphous and Liquid Semiconductors Proc. 5th Int. Conf.* p. 339. Taylor and Francis, London (1974).
10. TANAKA K., *Appl. Phys. Lett.* 26, 243 (1975).

Solid State Communications, Vol. 23, pp. 401–403, 1977. Pergamon Press. Printed in Great Britain

LIGHT-INDUCED TRANSMITTANCE OSCILLATION IN $GeSe_2$ THIN FILMS

J. Hajtó, G. Zentai and I. Kósa Somogyi

Central Research Institute for Physics, Budapest, Hungary

(*Received* 22 *April* 1977 *by A. Zawadowski*)

The light-induced light transmittance oscillation observed in $GeSe_2$ thin films can be maintained only within a certain light intensity range, in our case between 1.4 and 2.7 kW cm^{-2}. Oscillation frequency and the transmittance change are controlled by energy absorption and loss; they could be varied from 3–50 Hz and ~ 10–90%, respectively. Oscillation is caused by differences in the absorption coefficients of the melt and the crystalline $GeSe_2$ leading to successive cooling (crystallization) and heating (melting) cycles if the rate of energy absorption and loss are close to equilibrium.

IN A RECENT LETTER [1] we have described the kinetics of light-induced transmittance changes in $GeSe_2$ thin films. On investigating further these light-induced processes we have discovered transmittance oscillation. We describe here our observations and give a tentative explanation based on light-induced thermal processes leading to the associated transmittance changes.

$GeSe_2$ films were prepared by evaporating single-crystalline grains on water cooled SnO_2 coated glass substrates in a ~ 2×10^{-5} torr vacuum at 40 Å sec^{-1} deposition rate. The thickness of the films was 6.4 μm as measured during deposition by a quartz crystal monitor. X-ray diffraction showed the films to be amorphous.

A continuous 30 mW He–Ne laser beam through a power regulating polarizer was focused on the sample by a 45x microscope objective, illuminating a 22 μm diameter spot. The transmittance changes were detected by an appropriate photomultiplier and displayed on an oscilloscope. Occasionally an additional 3 mW He–Ne laser was used for triggering and regulating purposes (see below), when both laser beams were focused on the same spot at the same time.

To set in train the transmittance oscillation the laser beam intensity should be increased until a dark central area appears in the illuminated spot. Oscillation continues if the light intensity is within a certain range. In our set-up with the above described samples this light intensity range was from 1.4–2.7 kW cm^{-2}.

The frequency and amplitude of oscillation markedly depend on the light intensity: an increase in laser power is followed by an increase in transmittance change and a decrease in oscillation frequency (Fig. 1). The dependence of oscillation parameters on the light intensity can be conveniently investigated by focusing two laser beams on the same spot and varying the

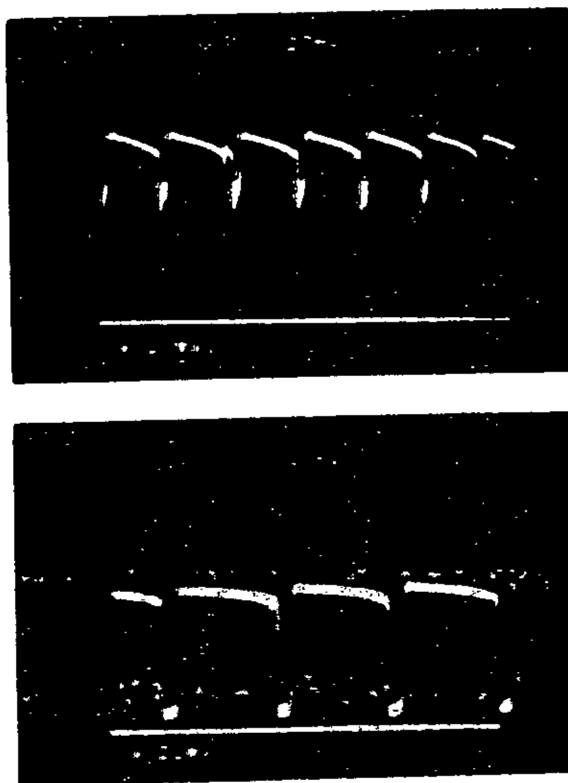

Fig. 1. Shape of transmittance changes at different light intensities: (a) $J = 1.66$ kW cm^{-2} (b) $J = 2.6$ kW cm^{-2}.

intensity of one of them. Oscillation can be triggered, stopped, and its amplitude and frequency varied easily within the intensity range shown in Fig. 2. As can be seen, near threshold light intensity, when $J = 1.39$ kW cm^{-2}, there is a 15.2% transmittance change and an

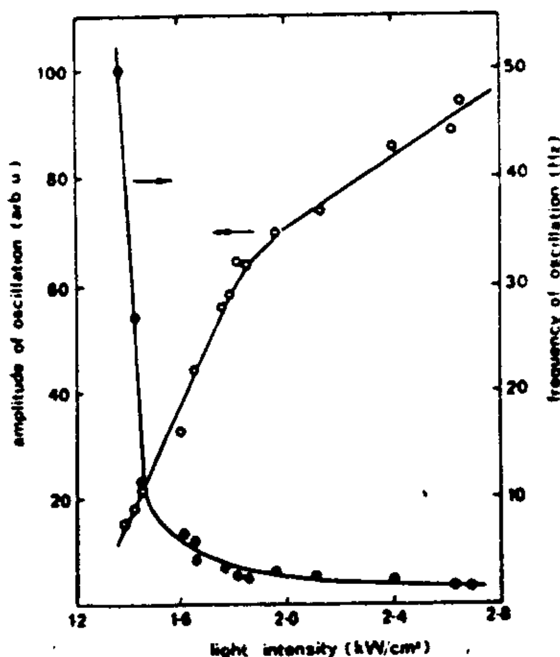

Fig. 2. Variation of transmittance and oscillation frequency with light intensity.

oscillation frequency of 50 Hz, whereas close to the upper limit, where oscillation breaks down at 2.65 kW cm^{-2}, transmittance change of 94.4% and 2.2 Hz were measured.

Samples being in one of the two limiting states, i.e. when their transmittances differ most, were examined under a microscope. The laser beam first photobleaches the sample as observed earlier [1] resulting in a light spot surrounded by the darker as deposited amorphous region. After oscillation had started a clear, few μm wide, nucleus appeared in the centre of this photobleached spot in every sample independently of the limiting state it had been in when oscillation was interrupted. However, in polarized light the central light-coloured nuclei behave differently: by rotating the analyser some of them darken whereas the others – just like the crystalline halo surrounding each central nucleus – remain unchanged (Fig. 3). The centres of the halo on the spots frozen-in in the less transparent state are crystalline, those of the more transparent state are mostly amorphous with tiny crystals in their centre – as verified by scanning electron microscopy

The oscillation of transmittance is due to repetitive crystallization from the melt. To start the process the central part of the illuminated spot should be heated above the melting temperature, T_m, of the film. This melted nucleus is surrounded by a microcrystalline

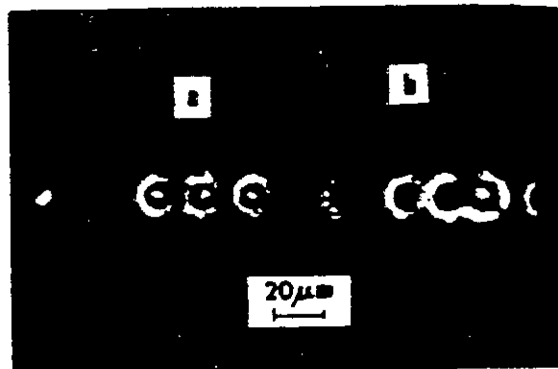

Fig. 3. Microphotos in polarized light of the spots in (a) the less transparent and (b) the more transparent state.

halo, its diameter depending somewhat on the light intensity. Because of greater heat loss at the upper and lower surfaces the hottest point in the amorphous layer is situated and, consequently the crystallization temperature T_{cr} is first reached inside the film. The buried crystallized region, on further absorption of light quanta, melts causing a decrease in the absorption coefficient; the melt cools quickly, the temperature goes through T_{cr} again. A considerable portion of the melt crystallizes, starts to heat up again, and so on. The transmittance of the melt is higher than that of the crystals so the crystallization of the central nucleus is accompanied by a sharp drop in the transmitted light intensity. Differences in the heat conductions of the crystalline and melted regions might also take part in the continuing oscillation.

On repeated cycling and/or higher light intensities the amount of melt and the diameter of the crystalline halo grow, they reach the surface and a visible crater encircled by the crystalline halo appears.

The change of oscillation amplitude and frequency with the light intensity can be explained by variations in the mass of the melt; more melt causes larger transmittance change and needs a longer time to cool. Threshold light intensity is just enough for melting the film while above an upper limit the heat loss cannot prevail over heat absorption so oscillation stops after a few cycles only.

Near the threshold light intensity the oscillation is quite stable: after about 10 thousand cycles neither its amplitude nor its frequency changed appreciably. Taking account of the possible difference in the conductivity of the crystalline and amorphous modifications of $GeSe_2$, these light-induced transmittance oscillations should be accompanied by current oscillations of the same frequency.

Alternating trap filling and trap emptying similar to those described in [2] might take place in our samples, too. Should this be so, the heat effect of charge carriers recombination occurring abruptly when a critical temperature has been reached could play some role in the regulation of the oscillation. However, the direct heating due to laser light absorption is probably overwhelming.

REFERENCES

1. TÓTH L., HAJTÓ J. & ZENTAI G., *Solid State Commun.* **23**, 185 (1977).
2. OHI K. & IESAKA S.: *J. Phys. Soc. Japan* **40**, 1371 (1976).

phys. stat. sol. (a) 45. 181 (1978)

Subject classification: 20.1; 2; 11; 22.7

Central Research Institute for Physics, Budapest[1])

Self-Controlled Laser Beam Chopping Effect in $GeSe_2$ Thick Films

By

J. Gazsó and J. Hajtó

Studying the optical properties of 5 to 10 μm thick $GeSe_2$ glassy films under the influence of focussed, continuous He–Ne laser beams a region of medium intensity (1.4 to 2.7 kW/cm²) is found where a low frequency (3 to 50 Hz) periodic pulsation in the transmitted light signal sets in. A tentative explanation is suggested in terms of internal total reflections due to different metastable and excited states in $GeSe_2$.

Нами были исследованы оптические свойства аморфных пленок с составом $GeSe_2$ толщиной от 5 до 10 μm, изменяющиеся под действием излучения He–Ne лазера. Был получен эффект осциллирования прозрачности в области средней мощности 1,4 до 2,7 kW/cm². Процесс осциллирования можно объяснить появлением различных метастабильных и возбужденных уровней в пленке $GeSe_2$, которые вызывают полное внутреннее отражение.

1. Introduction

The possibility of oscillatory behaviour in the transmittance of glassy $GeSe_2$ films illuminated by a continuous He–Ne laser beam was reported in a recent letter [1]. Until then the transmission of amorphous $GeSe_2$ did not attract particular interest, and optical measurements performed on it were carried out at intensities several orders of magnitude lower than our present range of interest. This paper is not concerned with a comprehensive study of the subject but aims at presenting a possible mechanism of the observations so far.

2. Experimental

$GeSe_2$ films were vacuum-evaporated onto water-cooled transparent substrates. Substrates used were either fused silica or glass or glass coated with 20 μm thick SnO_2 layers. Deposition rates ranged usually from 20 to 40 Å/s, and the thicknesses were measured by a quartz crystal monitor during evaporation. Starting materials were either crystalline $GeSe_2$ or grains of $GeSe_2$ glass prepared by the usual melting-quenching processes. X-ray diffraction confirmed the films to be amorphous. The refractive index ($n = 2.5$) was obtained by Brewster angle ellipsometry [2].

The continuous beam of a 30 mW output power He–Ne laser ($\lambda = 6328$ Å) was focussed on the sample, to a spot diameter of 15 to 20 μm. Incident light intensity could be reduced by a polarizer, and the transmitted light signals were displayed on a storage oscilloscope screen. A magnifying arrangement was established by using microscope objectives and lenses, and the image of the illuminated spot could be projected onto a white sheet, thus making close examination of any change in the light distribution possible.

[1]) P.O.B. 49, H-1525 Budapest, Hungary.

3. Results

3.1 Photobleaching

The changes induced by the laser beam can be of three kinds (see Table 1), depending on the input power density. Starting with modest intensities (0.1 to 1.4 kW/cm²), the

Table 1
Processes caused by laser light of different intensities in 6 μm thick a-GeSe₂ films

intensity (kW/cm²)	response
0.1 to 1.4	photobleaching
1.4 to 2.7	transmittance pulsations
over 2.7	crystallization

first effect of interest is the permanent "photobleaching" of the $GeSe_2$ films, even without focussing. That means, for example, an increase in transmittivity from 30 to 80% in case of a layer of 6.4 μm thickness, while the reflectivity remains at 18%. The transmittivity edge of a-$GeSe_2$ shifts towards shorter wavelengths (Fig. 1, curve 2). Annealing the samples at 200 °C for 30 min produces similar bleaching (Fig. 1, curve 3), so the heating effect caused by the laser irradiation may be partly responsible for the phenomenon (see Section 4.1). The melting point of crystalline $GeSe_2$ is 740 °C [3], while the glass transition temperature is $T_g \approx 410$ °C (from differential scanning calorimetry measurements).

3.2 Transmittance pulsations

To produce pulsations in the transmitted light intensity the incident power density should be increased until a dark centre develops in the middle of the image. This can be distinguished from crystallization since on reducing the intensity it disappears completely, without delay, leaving no sign of any permanent phase changes. On the other hand, the intensity (averaged over the 20 μm spot) should not exceed an upper limit (about 2.7 kW/cm² for 6 μm thick films), otherwise the central region quickly becomes crystalline and thereafter does not show further optical changes.

In the range 1.4 to 2.7 kW/cm² the central dark spot expands radially, driving an adjacent brighter ring outwards. After having reached a critical radius of about 3 μm, the whole image structure collapses suddenly like a bubble. Then the centre becomes brighter; soon it transforms into a ring having a dark inside, and the process repeats itself continually — if adjusted carefully. The corresponding pulses in the transmitted intensity are shown in Fig. 2.

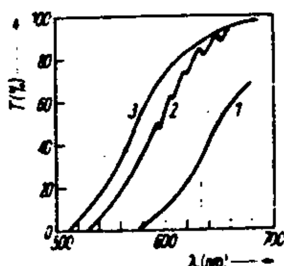

Fig. 1. Transmittivity T vs. wavelength for amorphous $GeSe_2$ films (the mark indicating λ_{He-Ne}). (1) Virgin sample, (2) laser-irradiated, (3) heat-treated

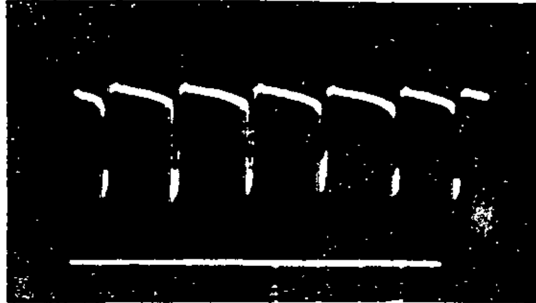

Fig. 2. Transmittance pulsation in an amorphous $GeSe_2$ film under focussed continuous He-Ne laser beam ($I \approx 1.84$ kW/cm²). Ordinate: 10 mV/div.; abscissa: 200 ms/div.

The frequency and the difference between maxima and minima in the transmitted light signals depend on the incident power density [1]. The degree of modulation is not uniform: in the middle of the image the intensity can vary between 10 and 95%, while the maximum change in the total amount of light transmitted is ≈ 35%.

It should be emphasized that if operated well below the upper threshold the material does not deteriorate in any way; it can work for several hours — although the amplitude ratios and pulsation frequencies may show fluctuations. An energy dispersive X-ray microprobe analyser of type Link combined with a Jeol scanning electron microscope showed no difference between the compositions of the oscillating spots after 10000 oscillations and the surrounding original $GeSe_2$ layer, thus no material transport occurs during oscillation.

We tried to induce similar pulsations in $GeSe_2$ by using the green ($\lambda = 5145$ Å) and blue ($\lambda = 4880$ Å) wavelengths of a more powerful (700 mW) Ar-ion laser. Permanent photobleaching was obtained, but no transmittance pulsations occurred. Instead of any oscillatory response, the irradiated spots became darker with increasing intensities and then changed over to a permanent crystalline state.

4. Discussion

4.1 Photobleaching

Our starting point is that, according to [4], amorphous $GeSe_2$ is very similar to the crystalline material with Ge fourfold coordinated by Se atoms and Se twofold coordinated by Ge. The Se atoms are fairly close to each other even in the twofold coordination. In freshly evaporated $GeSe_2$ films, a large number of defect states are expected, mostly neutral Se bonding in single and threefold coordination (Fig. 3a and f). Now it is clear from Fig. 3a that Se_1^0 possesses an unpaired p-electron on a non-bonding

Fig. 3. Energy level occupations in the different electron configurations of Se (subscripts: coordination numbers; superscript: charge states)

orbital ("dangling bond" [5]), which contributes substantially to the observed absorption in the virgin state. According to Street [6] the charged valence alternation pairs of Se_1^- and Se_3^+ (Fig. 3b and g) represent an energetically lower state than the pairs of neutral Se_1^0, Se_3^0 defects. The heat treatment and light excitation at modest intensities serve to overcome energy barriers.

4.2 Pulsations

On raising the incident intensity to above 1.4 kW/cm^2, other processes will dominate. The observed increase in the absorptivity of $GeSe_2$ could be accounted for the generation of unpaired electrons on non-bonding orbitals (see Fig. 3):

$$Se_1^- + h\nu \to Se_1^0 + e \qquad (1)$$

or

$$Se_2^0 + h\nu \to Se_2^+ + e\,, \qquad (2)$$

or by breaking Se–Se bonds (1.9 eV [7]), thus producing two unpaired electrons for each broken bond.

The higher number of dangling bonds raises not only the absorptivity but the refractive index as well [8], since $\varepsilon \approx n^2$ varies as [9]

$$\frac{\varepsilon_{film} - 1}{\varepsilon_{cryst} - 1} = \frac{\varrho_{film}}{\varrho_{cryst}} \frac{1}{(1 - s)^2} \left(\frac{d_{film}}{d_{cryst}}\right)^3, \qquad (3)$$

where s is the fraction of dangling bonds, d the average distance between nearest neighbours, and ϱ the density. In the room temperature equilibrium state, s is close to zero, while under intense irradiation s can reach 0.1 to 0.3. At the same time, the mean distance between nearest neighbours should increase either since the Coulomb attraction between Se_1^-–Se_3^+ pairs vanishes for Se_1^0–Se_3^+ pairs or for the broken Se_2^0–Se_2^0 bonds. Anticipating a 5 to 10% increase in d, the right-hand side of (3) should increase by 1.6 to 3.2 times. Taking $\varepsilon_{cryst} = 6.25$, then n_{film} will lie in the range 3.1 to 4.2.

Thus the first period in the light-induced pulsation process (AB in Fig. 4) is characterized by a gradual increase in both the absorptivity and the refractive index of the film. These changes, however, should still remain fairly homogeneous over the irradiated volume element, at least on a scale of the wavelength used (250 nm inside the film); so they are unresolved by the magnifying set-up. There must be, of course, some thermal gradients along the optical axis, for the substrate provides better heat transport than air at the front surface.

Lower temperatures facilitate recombination; therefore it is the substrate side of the $GeSe_2$ film where small layered regions of recombined material are expected to develop sooner (stage 1 in Fig. 5). Recombined regions are understood as consisting mostly of the same kind of valence alternation pairs as the room temperature ones, thus restoring the refractive index roughly to the original. (There may be some difference due to the elevated temperature.) The increased absorption in the front

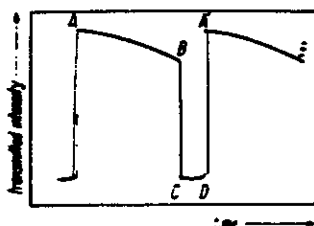

Fig. 4. Characteristic intervals in the pulsing period

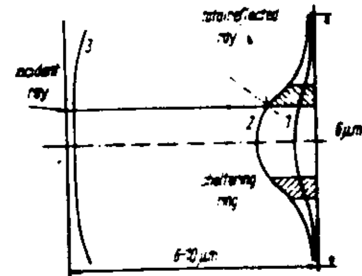

Fig. 5. Geometry of the model proposed (a-$GeSe_2$)

surface region also aids the establishment of a recombination front at the back side, since re-excitation will be less likely there. It seems to be plausible that the boundary advances at the highest rate along the axis, and with increasing curvature the angle of total reflection (37 to 53° for the n_{min} range indicated above) will soon be reached for some rays (stage 2 in Fig. 5 and point B in Fig. 4).

The appearance of a totally reflecting layer introduces a qualitatively new element into the time development of the process. The amount of light transmitted across the central 6 μm diameter spot will be greatly reduced. This explains the sudden drop in the signal (BC in Fig. 4 and Fig. 2). In the usual situation of total reflectance the optical boundary is provided by *permanently* different phases. In our model, on the hand, the origin of the appearance of total reflectance lies in the *induced* changes. Such an optical boundary cannot have a stable position inside a continuum, since:

a) the reflecting layer must have a finite thickness;

b) at the instant as this transition layer structure shifts to any spatial position, the rear is cut off from a substantial part of the intense input power supply, and the absorptivity and the refractive index are bound to drop to the new equilibrium values;

c) by virtue of continuity requirements, the adjacent values have to drop as well;

d) in effect, the maximal gradient spot is shifted towards the front where the incident rays are coming from;

e) the speed of the boundary propagation is determined by the relaxation rates.

The minimum period (CD) lasts about 5 to 50 ms; during that time the boundary layer is assumed to advance along the axis at an average speed of 10^{-1} to 10^{-2} cm/s.

When the moving layer approaches the front face it cannot maintain the high curvature, simply for geometrical reasons. It inevitably levels out (stage 3 in Fig. 5), thus letting the rays hitherto reflected penetrate into the central region (DA′ jump in Fig. 4 and 2). We are back again at the starting point of the next cycle, all the more so since the temperature of the central region has been reduced substantially during the sheltered period.

5. Conclusions

Our model is compatible with a number of observations on glassy $GeSe_2$, and it explains why this particular material and sample configuration is efficient in producing a periodic pulsing effect. Amorphous $GeSe_2$ has $T_g \approx 410$ °C, high enough to resist devitrification under fairly intense light irradiation. Its optical absorption edge varies just around the wavelength of the exciting He-Ne laser. Due to its large Se content, the fraction of dangling bonds can rise considerably, and in the *glassy state* the nearest-neighbour distance has a greater degree of freedom to change according to the dominant charged defect states, than it would have in the crystalline phase. Indeed, the corresponding density fluctuations in the irradiated volume element have been observed by scanning electron microscopy in a-$GeSe_2$ [10]. In principle, other amorphous chalcogenide compounds, having an absorption edge in the visible range, should behave similarly. $GeSe_2$ has the great practical advantage of resisting chemical decomposition and being fairly indifferent to air humidity, which does not apply to $SiSe_2$ or Si_2Te_3, for example. More work is needed in this field to find other substances, or modifiers to $GeSe_2$ raising its sensitivity.

References

[1] J. Hajtó, G. Zentai, and I. Kósa Somogyi, Solid State Commun. **23**, 401 (1977).
[2] F. Abelès, J. Phys. Radium **11**, 310 (1950).
[3] N. Kh. Abrikosov and L. E. Shelimova, Poluprovodnikovie materiali, Izd. Nauka, Moskva 1975 (p. 174).
[4] D. E. Sayers and F. W. Lytle, in: Proc. V. Conf. Amorphous Liquid Semicond., Garmisch-Partenkirchen, 1974, Ed. J. Stuke and W. Brenig, Taylor & Francis, London 1975 (p. 403).
[5] D. Adler, Scientific American **236**, 36 (1977).
[6] R. A. Street, Adv. Phys. **25**, 395 (1976).
[7] L. Pauling, The Nature of Chemical Bonds, 3rd ed., Cornell Univ., Ithaca (N.Y.) 1960 (p. 85).
[8] T. S. Moss, Optical Properties of Semiconductors, Butterworths, London 1959 (pp. 24 and 48).
[9] M. H. Brodsky and P. J. Stiles, Phys. Rev. Letters **25**, 798 (1970).
[10] J. Hajtó and L. Pogány, Rep. Central Res. Inst. Physics, Budapest, KFKI-1977-42.

(Received November 11, 1977)

PROCEEDINGS
of the conference

AMORPHOUS SEMICONDUCTORS ´78

Pardubice, September 1978

II

Institute of Solid State Physics, Czechoslovak Academy of Sciences
Prague

University of Chemical Technology
Pardubice

LASER INDUCED BIREFRINGENCE AND TRANSMITTANCE OSCILLATION IN As_2S_3 GLASSES

J. Hajtó and P. J. S. Ewen+

Central Research Institute for Physics, Budapest, Hungary
+ Department of Electrical Engineering, University of Edinburgh, U.K.

Optical anisotropy and transmittance oscillation have been found under the influence of continuous laser irradiation in As_2S_3 glasses.

The purpose of the present work was to check the optical isotropy of bulk a-As_2S_3 before and after laser irradiation and to determine the origin of any anisotropy observed. The optical isotropy was investigated using polarimetry, transmission and reflection measurements.

The samples were cut from a block of a-As_2S_3 obtained from the American Optical Company (of dimensions 1.5x1.5x0.7 and 2.5x2.5x1.2 cm) and were polished on all six faces. The material was of good optical quality yielding an ellipticity ratio of 27 db or less with polarised radiation from a He-Ne laser (6328 Å).

The light source used in the three types of experiment was either a dye laser (Spectra-Physics Model 375) tunable over the range 5700-6500 Å or a He-Ne laser (Spectra-Physics Model 125) operating at 6328 Å. In the polarimetry measurements a polarisation rotator (Spectra-Physics Model 310-21) was used to vary the plane of polarisation of the incident beam and a polaroid sheet mounted on a divided circle was used to determine the plane of polarisation of the beam emerging from the sample.

When low intensity polarised laser light (0.1-0.5 mW with diameter 0.5 mm) of wavelength 6300-6500 Å was passed through the samples it was found that the plane of polarisation was rotated. The value of the rotation angle θ depended on the incident polarisation relative to the sample: θ was zero for four orthogonal directions and for polarisation at 45° to these directions, θ showed maxima.

The maxima values θ_{max} varied from one region to another. There were two main types of regions, those which gave rise to a larger value for θ_{max} (for a thickness of 1.2 cm θ_{max} was typically 85-90° in these regions) and those for which θ_{max} was small (for a thickness of 1.2 cm θ_{max} was typically 10-12° in these regions). In the border regions between these principal types, intermediate values of θ_{max} were obtained (Fig. 1).

It was found that the rotation angle θ could be altered by increasing the incident laser power density above a few W/cm^2. In the

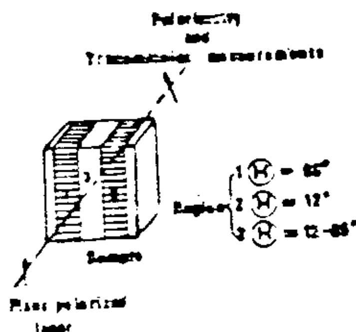

Fig. 1. Experimental arrangement for observation of optical rotation in As_2S_3 sample

case of the regions yielding a smaller value of Θ_{max} $\Theta(t)$ increased during illumination if the incident polarisation was such that $\Theta(0)=0$. In this case $\Theta(t)$ increased steadily but eventually reached a saturation value $\Theta(\infty)$. In Fig. 2 we plotted the values of $\Theta(\infty)$ obtained for various incident power densities: the points can be fitted by a straight line.

Those regions which yielded a large value for Θ_{max} showed the reverse behaviour, $\Theta(t)$ decreased during illumination when the incident polarisation angle was one for which $\Theta(0)=\Theta_{max}$. If the incident polarisation angle was one for which $\Theta(0)=0$ no optical rotation was observed, $\Theta(t)$ remained zero. This is the position, where oscillation in the transmission can be observed (Fig. 3).

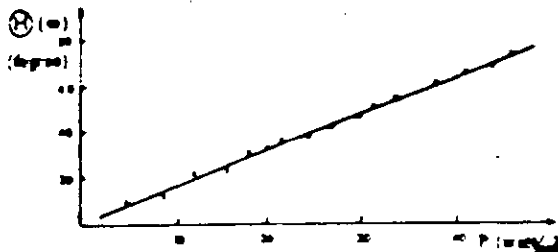

Fig. 2. Laser induced optical rotation in a-As_2S_3 glass, thickness=1.1 cm λ= 6328 Å

Fig. 3. Oscillation of the transmission, under the influence of laser irradiation at a) P = 63.7 watt/cm^2; b) 90.7 watt/cm^2 power density

Laser power density $[watt/cm^2]$	Magnitude of oscillation (Percentage of transmitted light) [%]	Frequency of oscillation $[sec^{-1}]$
60.1	4.1	4.79
63.7	5.4	4.87
70.8	10.6	4.93
80.8	13.5	4.97
90.7	17.1	4.98

Table I. Transmission oscillation in As_2S_3 glass. Laser orientation: non bo- tation state (E ∥ P)

The amount of the transmitted light oscillates between two characteristic values under the influence of continuous laser radiation at the power density of $P = 54-91$ watt/cm^2. The experimental results are collected in Table I.

<u>Discussion</u> - The origin of this optical anisotropy is uncertain. Evans and Young [1] have reported that there is a marked dichroism between light polarised parallel and perpendicular to the c-axis of crystalline As_2S_3 as a result of its layer structure.

X-ray diffraction studies of As_2S_3 glass [2] have shown that the nearest-neighbour and next-nearest neighbour coordinations are the same as in the crystal. Thus the layer structure is expected to be conserved to some extent in a-As_2S_3 therefore may be responsible for the observed optical anisotropy. However, stress and density fluctuations cannot be ruled out as possible causes of the optical anisotropy in glasses [3]. It should be noted that in the present investigation Raman spectra obtained from various regions in the samples [4] indicated that the glass structure was the same throughout them. Also the Raman spectra were in good agreement with the published data for a-As_2S_3 and showed no signs of c-As_2S_3 bonds or of spectra features indicative of phase separated regions. The As_2S_3 molecules are consisting of two dissimilar atoms therefore possess permanent dipole moments. We suppose, that due to the layer structure of the crystal which is conserved to some extent in the glass these dipole moments are not distributed randomly but oriented in certain directions. Therefore the As_2S_3 matrix which is isotropic on the average (with refractive index $n_o+i\varkappa_o$) contains prolate ellipsoids with dimensions $d \ll \lambda$ which are oriented with their major axis perpendicular to the polarisation of the exciting light and which have an anisotropic structure [5]. The refractive index along the ellipsoid is $n_l+i\varkappa_l$ while that transverse to the ellipsoid is $n_t+i\varkappa_t$. The differences between the optical properties of the ellipsoids are small: $n_l-n_o \approx \Delta$, $n_o-n_t \approx \Delta$, $\varkappa_t-\varkappa_o \approx b$, and $\varkappa_o-\varkappa_l \approx b$, where Δ and b are functions of λ. Making use of the approximations of the optics of turbid media

[6-7] one can draw some qualitative conclusions about the optical properties of such a system: It exhibits positive birefingence [8], i.e., $a \gg b$. It exhibits negative dichroism in scattering in the region with $a \gg b$ i.e. the scattering of linearly polarised light along the axes of the ellipsoids is weaker than that transverse to these axes if $n_o - n_t \gg n_1 - n_o$. This conclusion agrees qualitatively with experiment.

The oscillatory behaviour of the transmission is not a unique feature of As_2S_3 glass only. Similar oscillation of the transmission was observed recently in amorphous $GeSe_2$ films too [9]. In both cases the oscillation was induced by a continuous laser irradiation ($h\nu$ = 1.96 eV) in the low absorption region of these materials. At the present time the mechanism responsible for the phenomena is not clear. The observed oscillation of transmission in $GeSe_2$ was explained by a sudden but reversible change in the refractive index (n) of the material [10]. We suppose, that the observed oscillation indicates the existence of metastable states excited by nearly band gap radiation [11]. A more quantitative analysis, especially on a change in polarisation properties of As_2S_3 galsses, is required for obtaining more information on these phenomena.

References

[1] Evans B. L. and Young P. A.: Proc.Roy.Soc.A. 297 (1967), 230
[2] Vaipolin A. A. and Porai-Koshits E. A.: Fizika Tverd.Tela 5 (1963), 246
[3] Isard I. D. Desai S. J. and Munila K.: J.Phys.D. 11 (1978), 433
[4] Hajtó J. and Ewen P. J. S. to be published in Non.Cryst.Solids
[5] Zhdanov V. G. and Malinovski V. K.: Sov.Techn.Phys.Lett. 3 (1977), 9
[6] Van de Bulst H. C.: Light Scattering by Small Particles, Wiley, New York 1957.
[7] Rozenberg G. V.: Usp.Fiz.Nauk. 69 (1959), 57
[8] Cherdyntsev S. V.: Zh.Fiz.Khim. 15 (1941) 419
[9] Hajtó J., Zentai G. and Kósa Somogyi I.: Solid State Comm. 23 (1977) 401
[10] Gazsó J. and Hajtó J.: phys.stat.sol.(a) 45 (1978) 181
[11] Street R. A.: Proc. of VIIth Conf.Amorph.Liq.Semic. Edited by W.E.Spear, Edinburgh, 1977. p.509.

phys. stat. sol. (a) 54, 385 (1979)

Subject classification: 2; 20.1; 22

Central Research Institute for Physics, Budapest[1] *(a) and Department of Electrical Engineering, University of Edinburgh (b)*

Natural Optical Activity and Related Phenomena in As_2S_3 Glasses

By

J. Hajtó (a) and P. J. S. Ewen (b)

Natural optical activity is observed in As_2S_3 glasses. The value of the rotation angle depends on the incident polarisation direction relative to the sample i.e. optical anisotropy is found. The existence of optical activity is due to a structural pecularity of individual asymmetric molecules. To explain the observed anisotropy it is assumed that the layer structure of the crystalline As_2S_3 is conserved to some extent in the glass i.e. a proportion of the total number of molecules are oriented in the corresponding planes.

Нами наблюдалась естественная оптическая активность в As_2S_3-стекле. Величина угла вращения зависела от направления поляризации падающего луча, т.е. была обнаружена оптическая анизотропия. Существование оптической активности является следствием особенностей структуры индивидуальных молекул. Наблюденная оптическая активность обьясняется в предположении, что слоистая структура кристалла As_2S_3 частично остается в стекле, т.е. часть полного числа молекул ориентируется вдоль плоскости соответствующих слоев.

1. Introduction

A variety of photo-induced effects have been observed in amorphous chalcogenide materials, particularly in a-As_2S_3: photodarkening [1 to 3], photopolymerisation [4, 5], photodissociation [6], volume [7] and refractive index [8] changes have all been reported for this glass. Optical isotropy was not considered in these earlier studies but recent results [9] on evaporated a-As_2S_3 films show that illumination of this material leads to its becoming optically anisotropic. In the case of bulk a-As_2S_3 it has been shown that optical anisotropy can be induced by the application of an electric field [10] (electro-optic effect) or a magnetic field [11] (Faraday effect).

An amorphous solid may be optically anisotropic even in the absence of applied fields: birefringence can be produced in glasses by stress, the presence of laminations, structural anisotropy, or the presence of "particles" (e.g. phase-separated regions) smaller in size than the wavelength of the light used in examining the material [12]. The purpose of the present work was to investigate the optical isotropy of bulk a-As_2S_3 before and after illumination and to determine the origin of any anisotropy observed. The optical isotropy was investigated using polarimetry and transmission measurements.

2. Experimental

The samples were cut (of dimensions $1.5 \times 1.5 \times 0.7$ and $2.5 \times 1.5 \times 1.2$ cm^3) from a block of a-As_2S_3 obtained from the American Optical Co. and were polished on all six faces. The material was of good optical quality yielding an ellipticity ratio of 27 dB or less with polarised radiation from a He–Ne laser ($\lambda = 6328$ Å).

[1] P.O.B. 49, H-1525 Budapest, Hungary.

The light sources used in the three types of experiment were either a dye laser (Spectra-Physics Model 375) tunable over the range $\lambda = 5700$ to 6500 Å or a He-Ne laser (Spectra-Physics Model 125) operating at $\lambda = 6328$ Å. In the polarimetry measurements a polarisation rotator (Spectra-Physics Model 310-21) was used to vary the plane of polarisation of the incident beam and a polaroid sheet mounted on a divided circle was used to determine the plane of polarisation of the beam emerging from the sample. The transmission was monitored with a laser power meter (Spectra-Physics Model 404).

In a number of experiments transmission and emergent beam polarisation were monitored simultaneously.

3. Results

3.1 *Optical activity and related oscillation of transmission*

When low-intensity polarised laser beam (0.2 mW power with diameter of 0.5 mm) of wavelength 6300 to 6500 Å was passed through the samples it was found that the plane of polarisation was rotated. The experimental arrangement can be seen in Fig. 1. The value of the optical rotation angle is given as $\varrho = (\gamma - \beta)$ where γ is the angle of the incident polarisation plane relative to plane A fixed to the sample and β is the angle of the emergent light polarisation plane relative to the same reference plane A. The value of the rotation angle depended on γ; ϱ was zero for four orthogonal directions and showed maxima for polarisations at 45° to these directions (Fig. 2).

The maxima values of the optical rotation ϱ_{max} varied from one region to another. There were two main types of regions, those which gave rise to a larger value for ϱ_{max} (for a thickness of 1.2 cm ϱ_{max} was typically 85 to 90° in these regions) and those for which ϱ_{max} was smaller (for a thickness of 1.2 cm ϱ_{max} was typically 10 to 12° in these regions). In the border regions between these principal types intermediate values of ϱ_{max} were obtained (Fig. 1).

It was found that the rotation angle ϱ could be altered by increasing the incident laser power density above a few W/cm². In the case of the regions yielding a smaller value of ϱ_{max}, $\varrho(t)$ (t being the time of light exposure) increased during illumination and reached a saturation value ϱ_∞, if the incident polarisation was such that $\varrho(t)_{t=0} = 0$. In Fig. 3 we plotted the values of ϱ_∞ obtained for various incident power densities; the points can be fitted by a straight line. Those regions which yielded a large value of ϱ_{max} showed the reverse behaviour, $\varrho(t)$ decreased during illumination when the incident polarisation angle was one for which $\varrho(t)_{t=0} = \varrho_{max}$. If the position of the incident beam was the same as before, namely $\varrho(t)_{t=0} = 0$, no optical rotation was observed, $\varrho(t)$ remained zero. This is the position, where oscillation in the transmission can be observed (Fig. 4) and the value of the transmission oscillated between two characteristic values under the influence of continuous laser radiation at a power density of $P = 54$ to 91 W/cm². The experimental results are collected in Table 1.

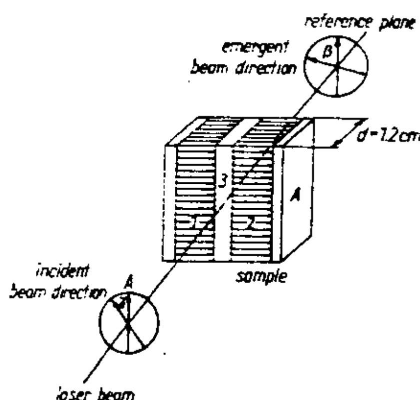

Fig. 1. Experimental arrangement for observation of optical rotation. For region 1: $\varrho \approx 85°$, region 2: $\varrho \approx 12°$, region 3: $\varrho \approx 12°$ to 85°

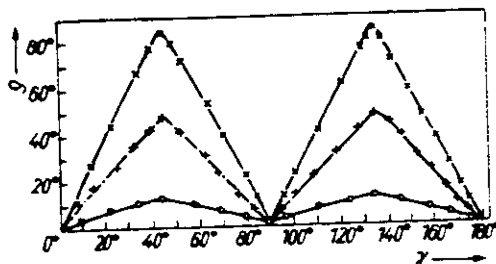

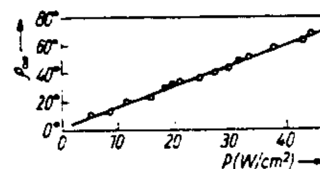

Fig. 2

Fig. 3

Fig. 2. Orientation anisotropy in a-As_2S_3. – x – x region 1, – ○ – ○ – region 2, – – – – – region 3

Fig. 3. Laser-induced optical rotation. d = 1.2 cm, λ = 6328 Å

Table 1

Transmission oscillation in As_2S_3 glass. Laser orientation: non-rotation state

laser power density (W/cm²)	magnitude of oscillation (percentage of transmitted light) (%)	frequency of oscillation (s⁻¹)
60.1	4.1	4.78
63.7	5.4	4.87
70.8	10.6	4.93
80.8	13.5	4.97
90.7	17.1	4.98

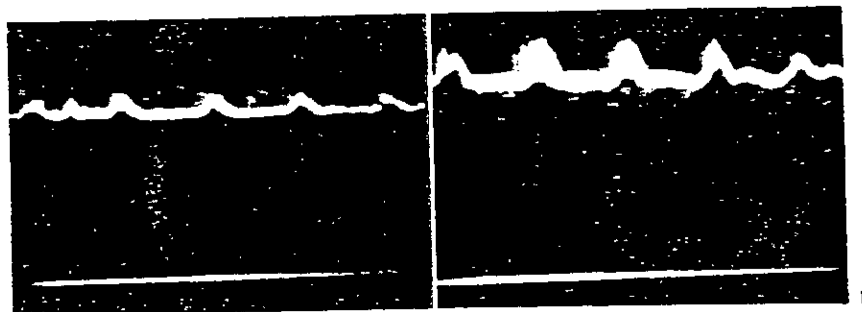

a b

Fig. 4. Oscillation of the transmission under the influence of continuous laser irradiation at a) P = 63.7, b) 90.7 W/cm² power density. Ordinate: transmission, abscissa: time (0.2 s/divis)

3.2 Transmission changes

Numerous reports of photodarkening in sputtered and evaporated films of a-As_2S_3 exist [1 to 3] and it has also been observed in melt-quenched bulk specimens [13]. In the present investigation a decrease in the transmission through the bulk a-As_2S_3 samples as a function of irradiation was always observed, the rate of decrease depended on the incident power density. Typical plots of the fractional change in the transmitted laser intensity $I(t)$, as a function of exposure time, t, are shown in Fig. 5. It is noteworthy that in the present experiments the wavelengths of the light inducing the decrease of the transmission (6300–6500 Å) correspond to $\alpha \approx 1$ cm^{-1}, α being the absorption coefficient of the unilluminated material (Fig. 5).

It was also found that the kinetics of the transmission change depended on the orientation of the sample relative to the plane of polarisation of the incident light.

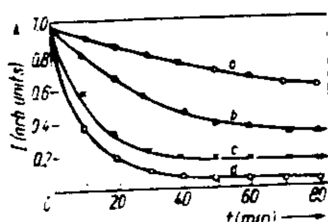

Fig. 5. Changes of the intensity of transmitted light in a-As_2S_3. (a) $P = 10$, (b) 25, (c) 45, (d) 45 W/cm²

Curves a and b of Fig. 5 were obtained for two different orientations of the sample; the frequency and power density of the incident beam were identical in each case and both curves were obtained from a region of the sample for which ϱ_{max} was large. In the case of curve c the sample was oriented so that no rotation of the incident polarisation occurred before illumination (for this orientation no optical induced rotation occurred during illumination), while for curve d the sample was oriented to yield the maximum rotation of the incident polarisation before illumination (a rotation of 75° occurred during this run). Comparison of the two curves shows that the transmission change is faster when it is accompanied by rotation of the incident polarisation.

If in the course of illumination the plane of polarisation of the incident beam was altered, the transmission increased discontinuously and then started to decrease in the usual way. When the polarisation was changed back to the original direction it was found that the transmission for this polarisation was larger than it would have been if the incident polarisation had not altered, i.e. the original transmission change can be partly reversed by changing the plane of polarisation of the incident light. A recovery of 6% in transmittance was observed in some of these experiments. This effect may be of technological importance as it is the basis for a new type of optical memory.

When one of the samples was photographed in ordinary light after it had been illuminated with laser irradiation ($P = 20$ W/cm²) no changes in any optical properties were observable (Fig. 5, curve *a*). However when it was illuminated with polarised light and photographed through an analyser, changes in the laser-irradiated regions were observed; the path of the beam through the sample was clearly visible (Fig. 6b). This confirms that laser-induced changes are taking place inside the sample during irradiation.

To our knowledge this is the first observation of laser-induced polarisation phenomenon in chalcogenide glasses.

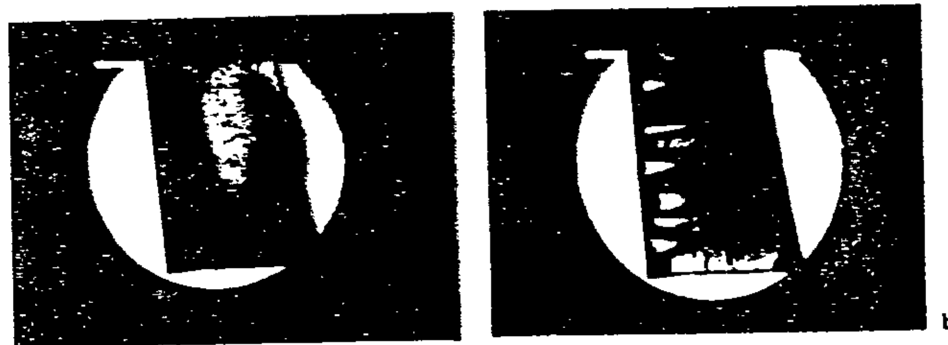

Fig. 6. Laser-induced polarisation phenomenon in As_2S_3 glass

4. Discussion

If an electric field E is applied to a medium having polarisability α, a polarisation P will be induced obeying the relation $P = \alpha E$, where α is a tensor. In our study E is the field associated with an electromagnetic radiation and it can be expressed as $E = E_0 \cos \omega_L t$ where ω_L is the laser frequency. Since the molecular dimension is of the order of Angstroms and the laser wavelength is of the order of thousands of Angstroms the field is constant over many molecular units (Born approximation). Therefore the average polarizability of the sample can be approximated by averaging the product of the volume V, density of the sample, and the polarizability of each molecule ($\alpha(i)$). Further evidence to this is that the value of the molar refraction ($4/3\pi\alpha_P$) determined from the Lorentz-Lorentz equation is in excellent agreement with the measured value for a-As_2S_3 (9.42 and 9.44, respectively) [14].

The observed optical activity is due to a structural peculiarity of individual molecules. The As_2S_3 molecule is asymmetric therefore the polarizability tensor is anisotropic, i.e. the glass contains optically anisotropic elements in molecular scale. In this case the optical activity is a natural consequence of the asymmetric molecular structure. If all the molecular units were distributed randomly according to the classical model of glassy state no anisotropy in the optical activity would be observed. The recent experiments show that this is not the case for the glassy As_2S_3.

Two kinds of optical anisotropy have to be explained: a) where the value of the optical rotation angle depended on γ (see Section 3.1) at a fixed position of the sample (orientation anisotropy), b) where the value of the optical rotation angle changes in different regions of the glass (bulk optical anisotropy).

Ewans and Young reported [15] that there is a marked dichroism between light polarised parallel and perpendicular to the c-axis of crystalline As_2S_3 as a result of its layer structure. X-ray diffraction studies of As_2S_3 glass [16] have shown that the nearest-neighbour and next-nearest-neighbour coordinations are the same as in crystal. Thus the layer structure is expected to be conserved to some extent in a-As_2S_3. Therefore the absorption and propagation of linearly polarised light is strongly affected by the relative orientation of the polarisability tensor (which is tied to the symmetry axis of the molecule) to the polarisation plane of the light. This explains the orientational anisotropy. If the number of plane-oriented molecular units varies in different regions of the glass, the value of the optical rotation angle varies, too. This is the cause of the bulk anisotropy.

To discuss the observed laser-induced polarisation phenomenon in the glass, the chemical bond approach will be helpful. In the present case a structural change in the As–S network might not be expected since the photon energies used in these experiments (1.91 to 1.95 eV) are smaller than the energy required to rupture an As–S bond (2.12 eV). Indeed simultaneous Raman experiments have confirmed that no significant structural change occurs during laser irradiation [17]. Most of the polarisability of As_2S_3 molecules arises from the lone-pair electrons of S atoms [18]. Lone pairs are probably more localized than bonding electrons because of the small nearest-neighbour overlap. Due to the large bond-free solid angle [19] a rearrangement of the lone-pair charge density of S atoms occurs corresponding to the direction of the electric field E (field of applied polarised light). A similar mechanism is possible for group V elements, too, namely for As atoms that are threefold coordinated but the bond-free solid angle is smaller. This rearrangement of the charge density results in energetically more stable state so the light-induced polarisation will be permanent (see Fig. 6).

The linearly polarised light is commonly regarded as a result of the superposition of two circularly polarised waves. The optical activity is produced as an indirect

effect of the difference in velocities of propagation of right and left circularly polarised waves. The angle of optical rotation can be expressed directly in terms of the difference of the two refraction indices [20]

$$\varrho = \frac{\pi d}{\lambda} (n_l - n_r) , \tag{1}$$

where λ is the wavelength of light and d the thickness of sample. Using the measured values of $\lambda = 0.63\ \mu m$ and $\varrho = 80°$ for a thickness of 1.2 cm glass, the calculated difference in the refractive indices is $(n_l - n_r) = 4.7 \times 10^{-6}$, so considerable rotations can be produced in spite of $(n_l - n_r)$ being very small. Or, in other words, a small change in polarisability $(\varepsilon = n^2)$ connected with the charge density rearrangement of lone-pair electrons causes considerable rotation of the polarised light.

The oscillatory behaviour of the transmission is not a unique feature of As_2S_3 glass only. Similar oscillation of the transmission was observed recently in amorphous $GeSe_2$ films, too [21]. In both cases the oscillation was induced by a continuous laser irradiation ($h\nu = 1.96$ eV) in the low-absorption region of these materials. At present time the mechanism responsible for the phenomena is not clear. The observed oscillation of transmission in $GeSe_2$ was explained by a sudden but reversible change in the refractive index (n) of the material [22].

We suppose that the recent observed oscillation indicates the existence of metastable states excited by nearly band gap radiation [23]. A more quantitative analysis, especially on a change in polarisation direction is required for providing more insight into these phenomena.

References

[1] K. Tanaka, Appl. Phys. Letters 26, 243 (1975).
[2] I. P. de Neufville, S. C. Moss, and S. R. Ovshinsky, J. non-crystall. Solids 13, 191 (1974).
[3] T. Igo and Y. Toyoshima, J. non-crystall. Solids 11, 304 (1973).
[4] I. P. de Neufville R. Seguin, S. C. Moss, and S. R. Ovshinsky, Proc. V. Internat. Conf. Amorphous Liquid Semicond., Vol. 2, Ed. J. Stuke and W. Bering, Taylor & Francis, London 1974 (p. 737).
[5] S. A. Solin, Phys. Rev. B 15, 2084 (1977).
[6] Y. S. Berkes, S. W. Ing, and W. J. Hillegas, J. appl. Phys. 42, 4908 (1971).
[7] T. Igo, Y. Noguchi, and H. Nagai, Appl. Phys. Letters 25, 193 (1974).
[8] I. P. de Neufville, R. Seguin, S. C. Moss, and S. R. Ovshinsky, see [4] (p. 740).
[9] V. G. Zhdanov and V. K. Malinovskii, Soviet tech. Phys. Letters 3, 387 (1977).
[10] N. F. Borelli, Phys. Chem. Glasses 12, 93 (1971).
[11] G. Grevendonk, P. Ruymbeek, P. van den Keybus, and A. de Bock, phys. stat. sol. (b) 78, K89 (1976).
[12] I. O. Isard, S. I. Desai, and K. Munila, J. Phys. D. 11, 433 (1978).
[13] H. Hamanaka, K. Tanaka, and S. Iizima, Solid State Commun. 23, 63 (1977).
[14] A. R. Hilton, C. E. Jones, and M. Brau, Phys. Chem. Glasses 7, 105 (1966).
[15] B. L. Ewans and P. A. Young, Proc. Roy. Soc. A297, 230 (1967).
[16] A. A. Vaipolin and E. A. Povai-Koshits, Fiz. tverd. Tela 5, 246 (1963).
[17] J. Hajtó and P. J. S. Ewen, Rep. Centr. Res. Inst. Phys., Budapest, KFKI-1978-97.
[18] M. Kastner, Phys. Rev. Letters 28, 355 (1972).
[19] M. Kastner, Phys. Rev. B 7, 5237 (1973).
[20] E. U. Condon, Rev. mod. Phys. 9, 432 (1937).
[21] J. Hajtó, G. Zentai, and I. Kósa Somogyi, Solid State Commun. 23, 401 (1977).
[22] J. Gazsó and J. Hajtó, phys. stat. sol. (a) 45, 181 (1978).
[23] R. A. Street, Proc. VII. Internat. Conf. Amorphous Liquid Semicond., Edinburgh, Ed. W. E. Spear, Centre Ind. Consultancy and Liaison,, Edinburgh 1977 (p. 509).

(Received March 2, 1979)

KFKI-1979-67

I.S. KÓSA
J. HAJTÓ
G. ZENTAI

DOPING AND ABSORPTION EDGE OF AMORPHOUS SILICON

Hungarian Academy of Sciences

CENTRAL
RESEARCH
INSTITUTE FOR
PHYSICS

BUDAPEST

KFKI-1979-67

DOPING AND ABSORPTION EDGE OF AMORPHOUS SILICON

I.Kósa Somogyi, J.Hajtó and G.Zentai

Central Research Institute for Physics
H-1525 Budapest, P.O.B.49. Hungary

Presented at International Summer School on New Developments in Semiconductor Physics, Szeged, Hungary, 1-6 July 1979.

HU ISSN 0368 5330
ISBN 963 371 590 3

ABSTRACT

Taking amorphous silicon as an example the difficulties encountered in the doping of amorphous semiconductors and possible ways and means to overcome them are described. The main structural and electronic characteristics of amorphous Si:H films produced by glow-discharge technique and those prepared by vacuum evaporation are compared. Factors which might cause the observed differences in the absorption edge of undoped a-Si:H layers are mentioned.

АННОТАЦИЯ

На примере аморфного кремния показаны трудности, возникающие при легировании аморфных полупроводников а также возможные пути их преодоления. Далее дается сравнение главных характеристик микро- и электронной структуры тонких пленок a-Si:H, полученных в тлеющем газовом разряде, с нелегированными пленками, полученными методам вакумного испарения, указываются возможные причины отличия полосы оптического поглощения, наблюдаемые у нелегированных пленок a-Si:H.

KIVONAT

Az amorf szilicium példáján keresztül ismertetjük az amorf félvezető anyagok dopolásának nehézségeit s a nehézségek leküzdésének módjait. Összehansonlitjuk a ködfénykisüléssel előállitott hidrogénezett, illetve vákuumgőzöléssel készitett a-Si:H rétegek mikroszkópikus és elektron szerkezeteinek fontosabb jellemzőit. Rámutatunk a dopolatlan a-Si:H vékonyrétegek optikai elnyelési éle változásának lehetséges okaira.

INTRODUCTION

Amorphous semiconductors have been used widely in the photocopying business but were not considered suitable in other conventional areas (diodes, transistors, etc.) because of doping difficulties. The recent discovery by Spear et al. [1] of the possibility to dope glow discharge produced hydrogenated amorphous silicon directed the attention of many physicists towards this material. If the extensive studies aimed at providing an understanding of the role hydrogen plays in the removal of gap states achieve their ultimate aim and thereby make controlled doping of a-semiconductors a reliable process, these materials may well become competitive in many areas, especially those where large surfaces are needed, e.g. in solar energy convers ion to electricity.

PRINCIPLES OF DOPING

The doping of crystalline materials is based on the bonding constraint the perfect lattice imposes on any atom forming the 3-D network. This perfection in the connection of atoms in tetrahe drally bonded crystalline semiconductors enforces the doping atoms, e.g. B and P, to part with their inherent bonding requirements and forces them to imitate the fourfold coordinated neighbours. Substitutional doping and long range order are thus inherently connected.

The amorphous state cannot exist unless sufficient deviations from the perfect lattice exist in the network. An ideal amorphous random network can be constructed by allowing bond angle variations only, but real amorphous materials always contain energetically more serious defects like empty lattice points, dangling bonds, microscopic voids, etc. In such materials there are no unique bonding requirements beyond those inherent in the atoms, there is no need to copy distant neighbours: only nearest neighbours count. As a result some flexibility in bonding is permitted and the individuality of atoms with a different number of valence electrons is honoured. Quasi 1-D and 2-D (i.e. chain--like and layered) structures and atoms with multiple bonding configurations help the formation of the amorphous structure.

The lack of perfection - an inherent requirement for amorphicity - in contrast to the perfect long range order in crystalline materials make the v- and c-bands in these two phases energetically different. The spread of bond angles and strengths as well as states due to different types of defects result in the well known tailing of the band edges into the forbidden gap and a high density of states in the gap. The tail states overlap, partly ionize and pin the Fermi level somewhere near the middle gap. In pure amorphous Si prepared by vacuum evaporation the density of gap-states is enormous as can be seen from Fig. 1. Because of the high density of gap-states a-Si produced by vacuum evaporation or sputtering cannot be doped sufficiently since the introduction of N_D (cm^{-3}) doping atoms into the network does not supply free charge carriers to the extended states. Instead a redistribution of ionized gap-states takes place followed by only minor shifting of the Fermi level - as shown in Fig. 2.

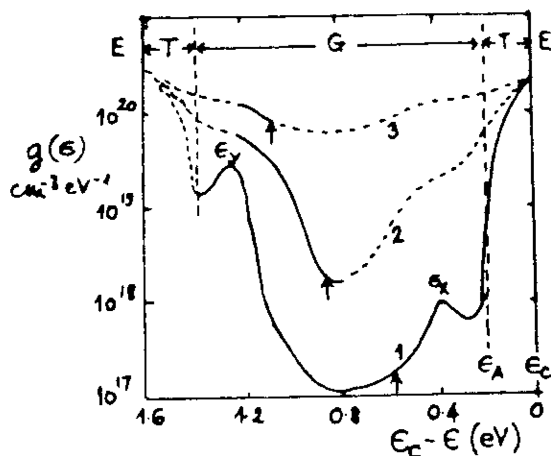

Fig. 1. Density-of-state distribution for a-Si specimens. Curve 1, glow discharge specimen, $T_d \sim 520$ K; curve 2, glow discharge specimen, $T_d \sim 350$ K; curve 3, evaporated specimen. The full lines indicate results obtained from field experiments and the arrow on each curve shows the position of the Fermi level. E, extended states; T, tail states; G, gap states. (From reference [15].)

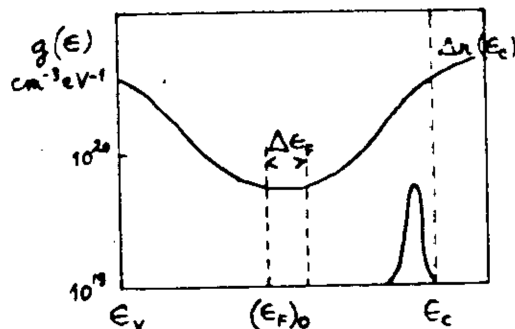

Fig. 2. Density-of-state distribution in an amorphous semiconductor, possibly evaporated (or sputtered) Ge or Si. $(\epsilon_F)_0$ Fermi energy in undoped material; $\Delta\epsilon_F$, shift in the Fermi energy when N_D donors are introduced. (From reference [15].)

For successful doping of amorphous semiconductors one has to

a) get rid of or substantially decrease the number of gap-states inherent in the amorphous structure;
b) create, in a controllable manner, new gap (donor or acceptor) states.

One way of achieving a) would be to make the random network more and more ideal (e.g. by long heat treatment or deposition at substrate temperature T_s below but not too far from T_g, the glass transition temperature). This would shrink the band tails but would not prohibit the satisfaction of bonding requirements of the doping atoms. Ultimately, this method of improving the

perfection of the network would result in recrystallization, with the simultaneous disappearance of the properties amorphous semiconductor are praised for over crystalline ones (e.g. flexibility, smoothness of the surface, etc.).

To achieve a) and also to preserve the amorphous state requires, instead of after-treatments, preventive methods which suppress the formation of unnecessary - from the standpoint of doping - defects, but which nevertheless allow for the formation of those defects necessary for the stabilization of the amorphous network.

Dangling bonds in pure amorphous Si in concentrations of $\sim 10^{20}$ cm^{-3} are the most numerous defects responsible for the gap states. A retrospectively obvious way to their removal is by reacting them with monovalent atoms such as hydrogen. Such a reaction will be effective if the bond formed is stronger than the Si-Si bond so that the bonding and antibonding levels will be situated deep in the v- and c-bands. Additionally, the monovalent atom used for the neutralization of dangling bonds should have a suitably small Van der Waals radius enabling its stress-free building into the lattice. It is also likely that small nomovalent atoms are favourable because - being able to form only one strong bond - they will not bridge two Si atoms and will thus not firmly connect the network. This circumstance allows the formation of structural point-, line-, and layer-like defects which are necessary for the stabilization of the amorphous network. Beyond hydrogen, small halogen atoms seem to be suitable for the neutralization of dangling bonds. Indeed Ovshinsky claims [2] that fluorinated a-Si is better qualified for doping that a-Si:H. Electropositive elements of the first group are monovalent but until now were not used for the neutralization of dangling bonds, although Li, Na, K and Cs were found to be electrically active dopants [3].

After decreasing the dangling bond density to below about 10^{15}-10^{17} cm^{-3} one can expect that the addition of doping atoms in a concentration of one or two orders of magnitude in excess of the above value would appreciably shift the Fermi level and change the electrical properties as well. It is quite natural that because of the above mentioned doping difficulties only a part of the dopants will be in-built in an electrically active form. According to [4] in the case of hydrogenated a-Si, ~ 20 % of B dopant atoms became electrically active.

PREPARATION METHODS

In that the effective doping of a-Si was discovered by Spear his method - the deposition from glow discharge plasma - has been studied most extensively.

Figure 3 illustrates the principle of the experimental method by which thin films of up to several tens of microns in thickness can be formed by decomposing silane, SiH_4. The plasma, generated usually by 10-50 watt generators working in the 1-100 MHz frequency range coupled to the system inductively or capacitively, contains highly excited, chemically very active species: atoms in status nascendi, free radicals and ions and a relatively high concentration ($\sim 10^{10}$ cm^{-3}) of highly energetic electrons of 1-10 eV energy. Different reactions between these unstable species occur when they enter the surface of the growing a-Si:H film making the structure and properties of this material unique among those prepared by other methods. This method is not restricted to the use of SiH_4; other Si-containing gases, e.g. SiF_4, and different diluent gases like Ar, N, etc. have been used recently.

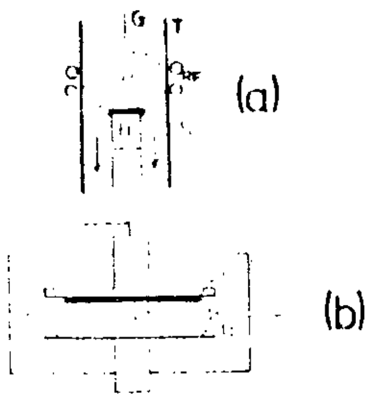

Fig. 3. Diagrams illustrating experimental methods for gas-phase deposition of an a-semiconductor; (a) inductive coupling of the RF, (b) capacitive coupling. (From ref. [15].)

The concentrations and the energies of the active species and their spatial distribution in the plasma depend on a number of variables like the composition of the gas mixture, the rf power level, the substrate temperature, the potential of the growing surface and probably scores of other parameters. The control of these variables is rather difficult thereby justifiying the search for other, simpler means of preparation.

Since the understanding of the role atomic hydrogen plays in removing dangling bonds, other preparation methods supplying H atoms during the deposition process have been attempted. Both reactive sputtering with H_2 in argon and coevaporation of Si with atomic H have been successful and lead to good quality, dopable and photosensitive a-Si:H layers. H^+ ion implantation into Si leaves residual damage in the so treated layer, unfavourably affecting the doping efficiency. The post treatment in H_2 plasma of UHV evaporated high purity a-Si films has produced a-Si:H layers electrically very similar to the gd a-Si:H.

PROPERTIES AND STRUCTURE OF a-Si

The electronic properties of pure and hydrogenated amorphous Si are summarized (from ref. [5]) in Table I.

Table I. Comparison of electronic properties

	Pure	Hydrogenated
Dangling bonds	5×10^{19} cm^{-3}	10^{16} cm^{-3}
States in the gap	10^{19}-10^{20} cm^{-3} eV^{-1}	10^{15}-10^{17} $cm^{-3}eV^{-1}$
Conductivity	Hopping at Fermi level $\exp-(T_0/T)^{1/4}$	Activated to band or band tail $\exp-E/kT$
Optical absoprtion	Tails into infrared	Edge near 1.7 eV
Photoresponse	Nil	Photoconductive, photoluminescent
Doping effects	Not discernible	p- or n-type conductivity changes up to 10^{10} times

New structural features of the gd a-Si:H layers have been revealed quite recently by Brodsky and Kaplan [6] and Knights et al. [7]. It has been shown by IR spectroscopy that SiH, SiH_2, SiH_3 and $(-SiH_2-)_n$ building blocks are embedded in the gd produced films, their relative content varying in a controllable manner with the parameters of the plasma. Electron-microscopic investigation of the films revealed elongated voids of ~40 Å arranged in a kind of network resulting in a columnar structure perpendicular to the surface. This fine sponge like structure could be responsible for the sensitivity of the electrical properties of a-Si films to various gaseous or liquid adsorbates [8]. It can be deduced from the shape of these voids that their appearance is probably closely connected with the formation of short polymer-like $(SiH_2)_n$ chains which are only weakly connected to the surrounding atoms.

It has been shown that not all the dangling bonds on the inner surface of the voids are neutralized by hydrogen atoms: there remains a great number of dangling bonds a part of which by interacting can form weak distorted bonds. The latter, e.g. during post-treatment in H_2 plasma, can react with H atoms. The existence of distorted and weak bonds on the surface of the microvoids is responsible for the discrepancy found between ESR measurements and the results obtained by thermal removal of H atoms. The amount of removed H was found to be two to three orders of magnitude higher than the concentration of ESR active dangling bonds indicating that a one H atom to one dangling bond correspondence cannot hold. The excess H content is taken up by weak and distorted bonds which do not give an ESR signal. Figure 4 is an SEM picture of a gd a-Si:H layer showing its columnar structure.

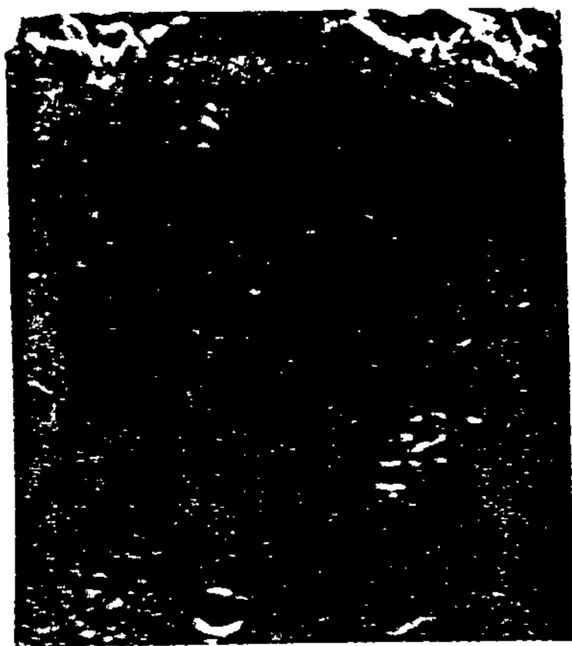

Fig. 4. SEM picture of a gd a-Si:H layer showing its columnar structure

OPTICAL PROPERTIES OF a-Si

The optical absorption edge of amorphous silicon, like that of other amorphous materials, depends on the conditions of sample preparation.

Figure 5 shows the optical absorption coefficient as a function of photon energy for glow discharge produced and vacuum evaporated a-Si layers. The data are compared with the edge of crystalline silicon.

In the crystalline Si the onset of indirect optical transitions is at approximately 1.1 eV at room temperature. This corresponds to the minimum separation between the valence and conduction bands (Fig. 6) (thermal activation energy).

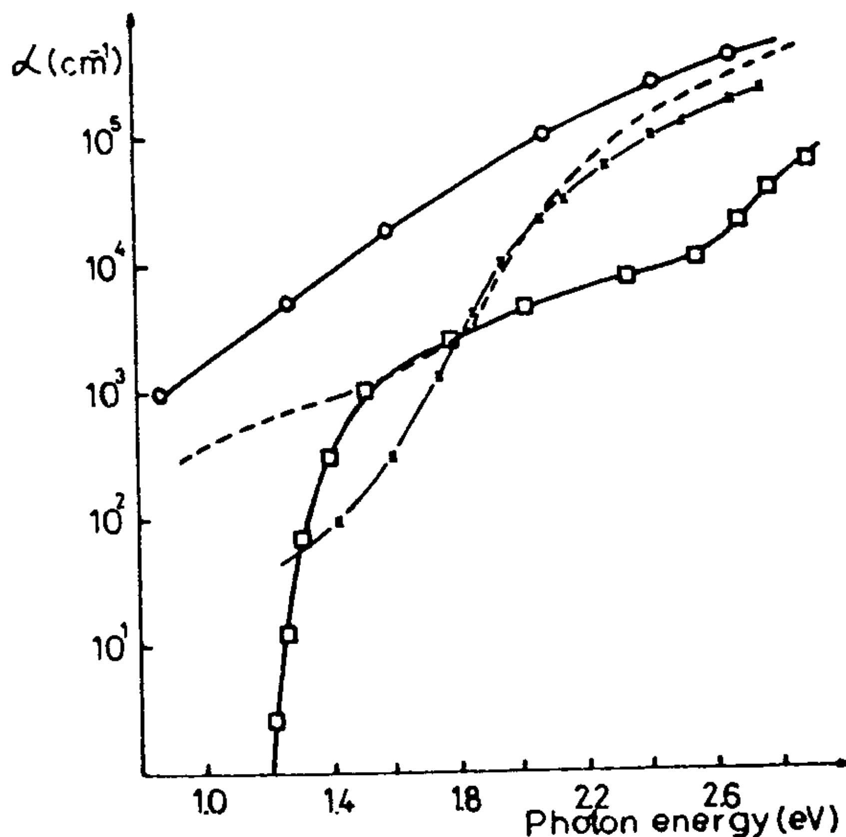

Fig. 5.
The variation of the absorption coefficient as a function of photon energy in amorphous and crystalline Si at room temperature. □ c-Si [8]; o evaporated a-Si [9]; -- glow discharge produced a-Si [10]; x glow discharge produced a-Si (present measurement).

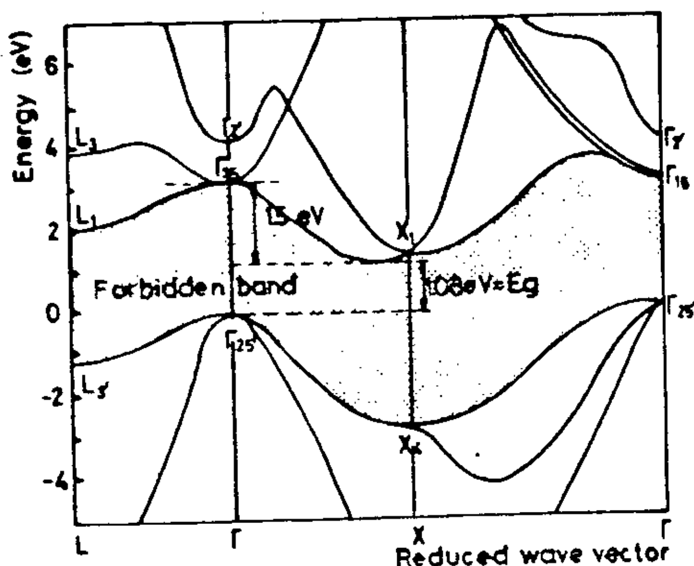

Fig. 6. The energy band structure of crystalline Si [11]

At higher photon energies there is an increase of absorption indicating the threshold of direct optical transitions from Γ_{25} to Γ_{15} at about 2.6 eV.

The high values of α observed for glow discharge produced and for vacuum evaporated amorphous silicon in the range 1 to 2.6 eV give good evidence for a relaxation of the k-conservation rule [13]. There are, however, important differences depending on the conditions of sample preparation. At the lower energy absorption region of the amorphous samples the absorption coefficient rises exponentially with the photo energy [12]:

$$\alpha = \alpha_o \exp(\Gamma \hbar\omega)$$

which is the most characteristic feature of amorphous semiconductors. The slope of the Urbach edge is considerably higher for glow discharge produced films than that of the vacuum evaporated ones. This fact indicates a more ordered chemical bonding for the glow discharge produced films, i.e. the internal field created by charged impurities is smaller according to the Dow and Redfield theory [14].

The absorption is higher in the region from 1 to 1.8 eV for the glow discharge produced films studied by LeComber et al. [10] than for the films produced by us. The difference is probably due to the different hydrogen content of the films which in our case should be higher because we used a 2 % silane 98 % hydrogen mixture instead of pure silane as did LeComber et al. [10].

At the higher absorption region α obeys the relation $\alpha\hbar\omega \sim (\hbar\omega - E_o)^2$ for both the vacuum evaporated and glow discharge produced samples (Fig. 7).

The extrapolated values of α vs $\hbar\omega$ yield the optical energy gap E_o which is considerably less (1.36 eV) for the vacuum evaporated amorphous silicon layers than for the glow discharge produced ones, viz. 1.71 and 1.74 eV, respectively.

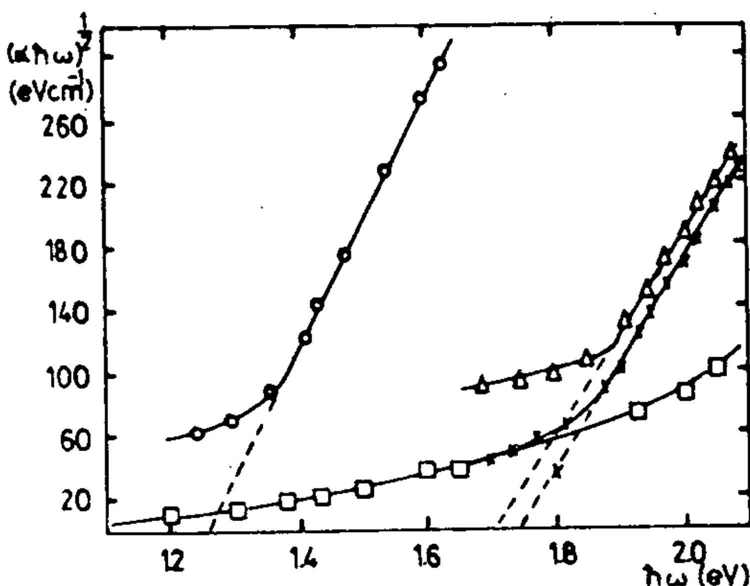

Fig. 7. Plot of $(\alpha\hbar\omega)^{1/2}$ vs photon energy for different Si films (Marking is the same as in Fig. 5.)

The results from absorption coefficient measurements underline the role of hydrogen in (a) reducing the optical density of states in the low absorption region and (b) increasing the optical energy gap in amorphous silicon layers. Further studies are needed to understand the correlations between the factors determining the electronic structure of a-Si:H.

REFERENCES

[1] W.E.Spear and P.G.Lecomber, Solid State Commun. 17, 1193 (1975)

[2] S.R.Ovshinsky, J.Non-Cryst. Solids 32, 17 (1979)

[3] W.E.Spear, P.G.Lecomber, S.Kalbitzer and G.Müller, Phil.Mag. 39, 159 (1979)

[4] P.G.LeComber, W.E.Spear and D.Allan, J.Non-Cryst.Solids 32, 1 (1979)

[5] M.H.Brodsky, Understanding the role of hydrogen in amorphous silicon, Paper presented at American Physical Society Meeting, Chicago. March 24, 1979

[6] M.H.Brodsky and D.Kaplan, J.Non-Cryst.Solids 32, 431 (1979)

[7] J.C.Knights, G.Lucovsky and R.J.Nemanich, J.Non-Cryst.Solids 32, 393 (1979)

[8] W.C.Dash, R.Newman, Phys.Rev. 99, 1151 (1955)

[9] D.Beaglehole and M.Zavetova, J.Non-Cryst. Solids 4, 272 (1970)

[10] P.G.LeComber, R.J.Loveland, W.E.Spear and R.A.Vaughan, in Proc. of Fifth Int. Conf. on Amorphous and Liquid Semiconductors, Garmisch-Paternkirchen, F.R.G., ed. by J.Stuke and W.Brenig, Taylor and Francis, London, p.245, 1974

[11] M.Cardona and F.H.Pollack, Phys.Rev. 142, 530 (1966)

[12] F.Urbach, Phys.Rev. 92, 1324 (1953)

[13] N.F.Mott and E.A.Davis, in Electronic Processes in Non-Cryst. Materials p.242, Clarendon Press, Oxford, 1971

[14] J.D.Dow and D.Redfield, Phys.Rev. B1, 3358 (1970)

[15] W.E.Spear, Advances in Physics 26, 811 (1977)

Journal of Non-Crystalline Solids 35 & 36 (1980) 1085-1090
© North-Holland Publishing Company

INVESTIGATION OF LASER INDUCED LIGHT ABSORPTION OSCILLATION

J. Hajtó and P. Apai

Central Research Institute for Physics
of the Hungarian Academy of Sciences
H-1525 Budapest, P.O.B. 49,
Hungary

Studying the optical properties of the films under the influence of focussed continuous He-Ne laser beams, a region of medium intensity (1.4-2.7 kW/cm^2) is found where a low frequency (3-50 Hz) periodic pulsation in the transmitted and reflected light signal sets in. The analysis of the in situ optical measurements shows that $GeSe_2$ possess optically metastable states existing only under the influence of laser illumination. A model for light induced absorption oscillation is presented based on the metastable self-trapped exciton states of the material.

INTRODUCTION

In a recent letter we described the phenomena of laser induced transmittance oscillation of vacuum evaporated amorphous $GeSe_2$ films (Hajtó (1977)). Oscillation can be observed when the incident light intensity is within a certain range (1.4-2.7 kW/cm^2 for a 6.4 μ thick film for example). The frequency and amplitude of oscillation depend on the light intensity, an increase in the laser power is followed by an increase in the amplitude of transmittance change and a decrease in oscillation frequency. According to the model suggested by Gazsó and Hajtó (1978) the oscillation is connected with the appearance of total internal reflection due to different metastable states of the material. This mechanism requires a simultaneous increase of reflexion or light scattering during the decreasing transmittance period of oscillation process. This paper is concerned with the investigation of optical properties (transmittance, reflectance, scattering) of vacuum evaporated $GeSe_2$ films under the influence of laser irradiation. The measured optical data present an evidence that there are neither increasing light scattering nor increasing reflectance during the decreasing transmittance period of oscillation i.e. real absorption changes occur in this case, therefore we suggest an explanation which is a better approach to the experimentally observed properties of the material.

EXPERIMENTAL

$GeSe_2$ films were vacuum evaporated onto water cooled silica substrates. Deposition rates usually ranged 20-40 Å/sec. The thicknesses were measured by quartz crystal monitor and later checked by Talystep. X-ray diffraction confirmed the layers to be amorphous. The continuous beam of 30 mW output power He-Ne laser (λ = 6328 Å) was focussed on the layers to a spot diameter of 15-20 μ. The incident light intensity could be reduced by a polarizer and the transmitted,reflected

and scattered light signals were displayed on a storage oscilloscope. In this way in situ measurements on the optical data could be performed during the light absorption processes.

RESULTS

The changes induced by the laser irradiation can be of three kinds (see Table I) depending on the input power density. (The crystallization is not discussed in this paper.) The two optical parameters of interest were the absorption coefficient α and the refractive index n as X functions of photon energy.

Intensity (kW/cm^2)	Response
0.1 to 1.4	photobleaching
1.4 to 2.7	transmittance and reflectance pulsations
over 2.7	crystallization

Table I. Processes caused by laser light of different intensities in 6 μ thick a-$GeSe_2$ films.

From $10^2 cm^{-1}$ to $10^4 cm^{-1}$ the optical absorption coefficient varies exponentially with the photon energy as $\alpha = \alpha_0 \exp[\Gamma\hbar\omega]$. (Urbach edge) (Fig.1).

Either illumination or annealing cause a permanent shift of the absorption edge to higher photon energies and an increase in the slope of the edge.

At photon energies above the exponential edge the absorption coefficient α obeys the relation $\alpha\hbar\omega = B(\hbar\omega - E_g)^2$ where E_g is the optical energy gap and B is a constant determined by the extent of the localized tail states. Either illumination or annealing caused an increase both in E_g and B indicating a reduction in the extent of the localized tail states adjacent to the band edge.

In the low absorption region the refractive index n was calculated from the measured reflectance and transmittance data using the method of Brattain and Briggs (1949) where multiple reflexions were taken into account. $n(\omega)$ could be fitted by the Wemple-Di Domenico (1971) dispersion relationship

$$\varepsilon_1(\omega) = n^2(\omega) = 1 + E_d E_o \Big/ \left[E_o^2 - (\hbar\omega)^2\right] \quad (1)$$

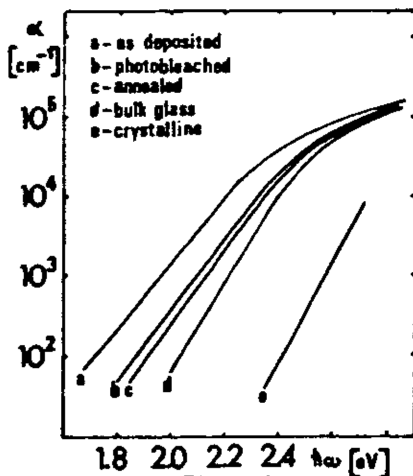

Figure 1
Absorption coefficient of $GeSe_2$ films as a function of photon energy

where E_o and E_d are single oscillator fitting constants which measure the oscillator energy and strength respectively. E_o corresponds for chalcogenide glasses to the mean energy of transitions from valence band (lone-pair) states to conduction band states. E_d measures the strength of interband transitions and is related to the average charge distribution within each unit cell. E_d depends mainly on the coordination number and valency. By plotting $(n^2-1)^{-1}$ versus $(\hbar\omega)^2$ (Fig. 2) and fitting the data by a straight line E_d and E_o can be determined directly from the intercept (E_o/E_d) and the slope $(-1/E_d \cdot E_o)$.

The decrease in n accompanying exposure and annealing of $GeSe_2$

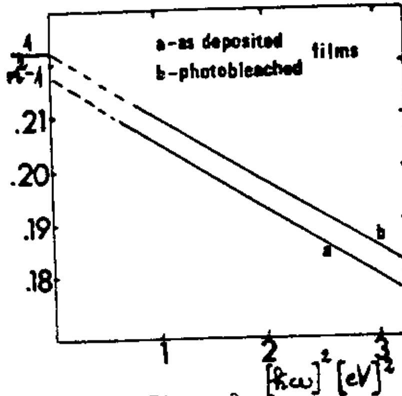

Figure 2
$(n^2-1)^{-1}$ versus $(\hbar\omega)^2$ for $GeSe_2$ films

films is associated more with an increase in E_o than with the small change in E_d (Table II).

Sample	E_o(eV)	E_d(eV)	n	Δn
as deposited	4.92	22.96	2.475	
exposed	5.1	23.0	2.414	-0.061
annealed	5.12	23.0	2.409	-0.066

Table II. Index of refraction (at ω=1.96 eV) and oscillator parameters of $GeSe_2$ films

To produce pulsations in the transmitted and reflected light the incident power density should be increased until a dark centre develops in the middle of the image. This can be distinguished from crystallization since on reducing the intensity it disappears completely, without delay, leaving no sign of permanent phase changes. On the other hand, the intensity (averaged over the 20 μ spot) should not exceed an upper limit (about 2.7 kW/cm^2 for 6 μ thick films) otherwise the central region quickly becomes crystalline and thereafter doesn't show further optical changes.

The transmittance, reflectance and light scattering pulsations measured simultaneously have the same character (Fig. 3 and 4). A decrease of transmittance is accompanied by a simultaneous decrease of the reflectance and of the scattered light independently of the angle of scattering.

Using the expressions of Brattain and Briggs (1949) one can calculate the changes of the absorption coefficient and refraction index of the films from the measured transmittance and reflectance changes during the oscillation periods (Fig. 5). The absorption coefficient

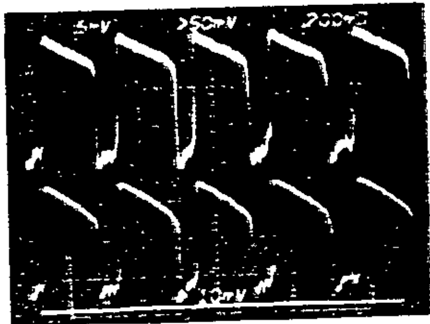

Figure 3
Transmittance and reflectance pulsation in $GeSe_2$ 6 μ thick films under the influence of continuous laser irradiation (P=2.6 kW/cm^2). Ordinate: intensity of transmitted (a) and reflected (b) light, abscissa: time 200 ms/div.

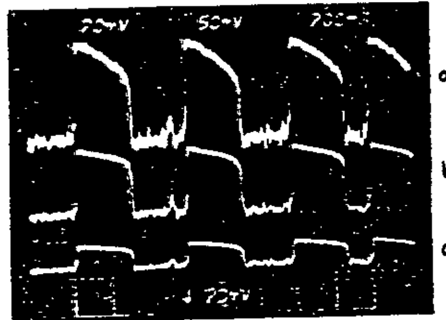

Figure 4
Transmittance and scattered light oscillation in the same sample. a) transmittance; b) large angle scattering; c) small angle scattering

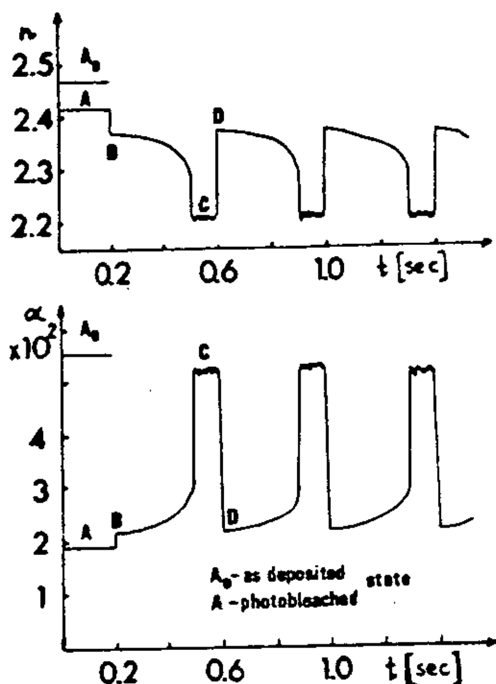

Figure 5
Absorption coefficient and refraction index changes (at $\hbar\omega$=1.96 eV) under the influence of continuous laser illumination of He-Ne laser ($\hbar\omega$=1.96 eV, P=2.6 kW/cm^2)

of the $GeSe_2$ films has two characteristic values during the oscillation period. Both level B(α = 2.4x$10^2$$cm^{-1}$) and level C($\alpha$ = 5.1x$10^2$$cm^{-1}$) (see Fig. 5) are metastable states of the material and exist only under the influence of intensive laser irradiation. When the exciting laser light is switched off the value of the absorption coefficient decreases to that of the stable photobleached state (level A: α = 1.9x$10^2$$cm^{-1}$) independently of the momentary state of oscillation.

The refractive index changes in opposite direction than the absorption coefficient and has a *minimum* value as reaches the maximum indicating that a real absorption change does occur during the oscillation period.

Oscillation can not be induced by using the green (λ= 5145 Å) and blue (λ= 4880 Å) wavelengths of an Ar-ion laser. The irradiated spots became darker with increasing intensities without any sign of oscillation and then changed over to crystalline state.

DISCUSSION

The fact that oscillation phenomena or photobleaching effect can not be achieved in crystalline $GeSe_2$ indicates that the clue to the oscillation lies in some unique properties of the amorphous state.

The energy of laser light used to induce the photobleaching and oscillation is 1.96 eV (λ= 6328 Å), slightly less than the value of optical energy gap of the $GeSe_2$ films (E_g = 2.15 eV). Therefore the assumption that the electrons are mostly excited from the localized tail states of the valence band edge is plausible. In the freshly evaporated $GeSe_2$ films a large number of defect states are expected (Ge-Ge, Ge-Se bonds, dangling bonds (Kastner and Adler (1976)) which conbribute substantionally to the observed absorption edge. Upon illumination or annealing a local rearrangement of these defect states (weaker bonds) occurs forming stronger Ge-Se bonds. The extent of the localized tail states adjacent to the bond edge decreases as a result of the reduction of defect states. Therefore one can observe a shift of the absorption edge to the direction of bulk well annealed glass state (see Fig. 1). The slope of Urbach edge increases upon illumination or annealing indicating the decrease of internal fields created by charged impurities in the material (Dow and Redfield (1970)).

The increase of the mean energy (E_o) (see Table II) of transitions from valence band (lone-pair) states to conduction band states similarly should be attributed to the reduction of the density of localized tail states. This conclusion is supported by the fact that the oscillator strength constant (E_d) have not changed upon illumination indicating that there is no sufficient change in the average coordination or in the charge distribution i.e. only the defect states (existing in concentrations of about 10^{18} cm^{-3}) are involved in the photobleaching process.

It is clear from the measured optical data that a real absorption oscillation occurs at the low absorption region of the Urbach tail in $GeSe_2$ films. We assume that the observed new type of optical phenomenon gives an evidence for the existence of light induced optically induced metastable exciton states. Due to the strong electron-phonon coupling the formation of metastable self trapped exciton states can be expected (Street (1978)). In the model used by Street (1978) two distinct mechanism of optical excitation are possible. One is a transition to the uncoupled exciton state. The second possible transition is to the self trapped exciton state thought to be responsible for the reversible photostructural change that is found in glassy chalcogenides (Street (1977)). Thus the increased absorptivity during the oscillation period (B →C in Fig. 5) could be attributed to the appearence of self-trapped exciton states created by continuous low energy ($\hbar\omega$ = 1.96 eV), high intensity (P = 2.4-2.7 kW/cm^2) illumination. Because of the higher absorptivity, the temperature increases too. At higher temperatures the density of optically induced metastable states decreases because the potential barrier can be overcome by thermal excitation. Complete annealing should be achieved at T_g since this is the temperature at which the defects are in thermal equilibrium (Street (1978)). As a result of thermal release of the self-trapped exciton states the absorptivity decreases (C →D in Fig. 5) therefore the temperature falls down and the process should start again resulting in a continuous oscillation of light absorption.

CONCLUSION

The amorphous $GeSe_2$ is particularly efficient in producing a periodic pulsing effect because due its cross-linked network structure the glass transition temperature (T_g = 360 °C) is high enough to resist devitrification under fairly intense light irradiation and its optical absorption edge varies just around the wavelength of the exciting He-Ne laser. In principle other amorphous chalcogenide glasses having an absorption edge in the visible range and high enough T_g should behave similarly. The phenomenon of the absorption oscillation can be explained by the appearance and thermal release of light induced metastable centers in the material. Although the origin of the recombination centers is not clear yet Se defects peculiar to $GeSe_4$ tetrahedral structure may be operative in the oscillation process.

More work is needed in this field to determine the connection between the localized charged centers and the macroscopic optical properties of the material. We assume that the observed new type of optical phenomenon gives an evidence for the existence of light induced optically metastable exciton states in $GeSe_2$.

REFERENCES

1 Hajtó, J., Zentai, G., Kósa-Somogyi, I., Light induced transmittance oscillation in $GeSe_2$ films, Solid State Commun. 23 (1977) 401-403.

2 Gazsó, J. and Hajtó, J., Self controlled laser beam chopping effect in $GeSe_2$ films, phys.stat.sol.(a) 45 (1978) 181-186.

3 Brattain, W.H. and Briggs, H.B., The optical constants of Ge, Phys. Rev. 75 (1949) 1705-1710.

4 Wemple, S.H. and Di Domenico, H., Behaviour of the electronic dielectric constant in covalent and ionic materials, Phys.Rev.B. 3 (1971) 1338-1351.

5 Kastner, H. and Adler, D., Valence alternation model in lone pair semiconductors, Phys.Rev.Lett. 37 (1976) 1504-1507.

6 Dow, J.D. and Redfield, D., The excitonic absorption edge, Phys.Rev. 1 (1970) 3358-3371.

7 Street, R.A., Recombination in amorphous semiconductors, Phys. Rev. B. 17 (1978) 3984-3995.

8 Street, R.A., Non-radiative recombination in chalcogenides, in: Spear, W.E. (ed), Proc. of 7th Conf. on Amorphous and Liquid Semicond. p.509. (Centre for Industrial Cons. and Liaison, University of Edinburg,1977).

JOURNAL DE PHYSIQUE Colloque C4, supplément au n° 5, Tome 41, mai 1980, page C4-63

LASER INDUCED OSCILLATORY PHENOMENA IN AMORPHOUS $GeSe_2$ FILMS

J. Hajtó

Central Research Institute for Physics H-1525 Budapest, P.O.B. 49, Hungary.

Abstract.- Studying the optical properties of 5μ to 10μ thick $GeSe_2$ glassy films under the influence of focussed, continuous He-Ne laser beams a region of medium intensity (1.4 to 2.7 kW/cm^2) is found where a low frequency (3 to 5 Hz) periodic pulsation in the absorption coefficient sets in. A tentative explanation is suggested in terms of laser induced self-trapped exciton states of the material.

1. Introduction.- The oscillatory behaviour of the transmittance of amorphous $GeSe_2$ films illuminated by a continuous He-Ne laser beam was reported in a recent letter /1/. Oscillation can be observed when the incident light intensity is within a certain range (1.4-2.7 kW/cm^2 for a 6.4 thick film for example). The frequency (3-50 Hz) and amplitude of oscillation depend on the incident light intensity, an increase in the laser power is followed by an increase in the amplitude of the transmittance change and a decrease in oscillation frequency. Two models were presented to explain the observed oscillation which are: a) the effect is due to reversible amorphous-crystalline-amorphous phase changes /1/; b) oscillation is connected with the appearance of total internal reflection due to different metastable and excited states in the material /2/.

Although the physical grounds of the two suggested mechanisms are different, both ~~ones~~ require a simultaneous increase of reflexion or light scattering during the decreasing transmittance period of oscillation. It has been shown in a recent paper /3/ that there are no phase difference in the reflected, transmitted and scattered light signals during the oscillation i.e. the decrease in the transmittance is accompanied by a simultaneous decrease of reflectance and scattered light. Therefore the origin of oscillation has not cleared yet.

This paper is concerned with the investigation of optical properties (transmittance, reflectance and scattering) and temperature of vacuum evaporated $GeSe_2$ under the influence of laser irradiation.

2. Experimental.- $GeSe_2$ films were vacuum evaporated onto water cooled silica substrates. Deposition rates usually ranged from 20 to 40 Å/s, the thicknesses were measured by a quartz crystal monitor during evaporation.

The temperature of the films was measured using vacuum evaporated Au-Ni thermocouples /4/

The continuous beam of a 30 mW output power He-Ne laser (λ = 6328 Å) was focussed on the samples to a spot diameter of 15-20 microns. The incident light intensity could be varied by a polarizer and the transmitted, reflected and scattered light signals were displayed on a storage oscilloscope. In this way in situ measurements on the optical data could be performed during the oscillation.

3. Results.- The changes induced by laser irradiation can be of three kinds (see Table I) depending on the input power density /2/. The crystallization is not discussed in this paper.

Table I. Processes caused by laser light of different intensities in 6μ thick a-$GeSe_2$ films

Intensity (kW/cm^2)	Response
0.001-1.4	Photobleaching
1.4-2.7	Oscillation
over 2.7	Crystallization

3.1. Photobleaching.- Starting with modes intensities the first effect of interest is the "photobleaching" of the films even without focusing of the laser beam. This

means, for example an increase in transmittance from 30 % to 70 % (at λ = 6328 Å) in the case of layer of 6.4 μ thickness. In polarized light the photobleached spots are darker (Fig. 1b) or brighter (Fig. 1c) by rotating the analyzer than photographed in non-polarized light (Fig. 1a). This fact indicates that illumination of the film leads to its becoming optically anisotropic which is to our knowledge the first observation in evaporated chalcogenide films.

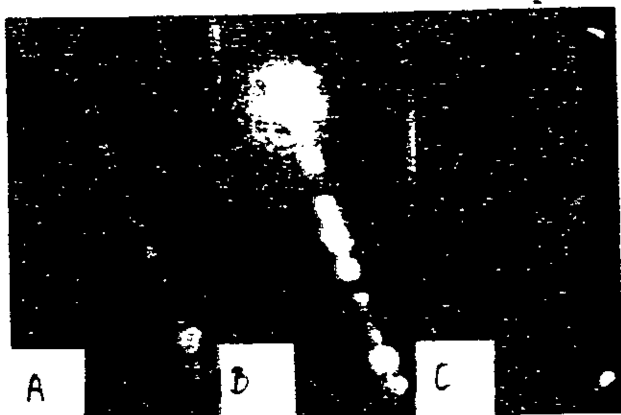

Figure 1. Microphotos of photobleached spots in $GeSe_2$ film.

From $\alpha = 10^2$ cm^{-1} to $\alpha = 10^4$ cm^{-1} the optical absorption coefficient varies exponentially with the photon energy as $\alpha = \alpha_o \exp[\Gamma\hbar\omega]$ (Urbach edge) (Fig. 2). Illumination causes a permanent shift of the Urbach edge to higher photon energies and an increase of the slope of the edge. The shift of the absorption edge of the as deposited films is irreversible and permanent, heat treatment of the layers causes a similar shift. de Neufville as presented a "localized heating" model for the reversible photostructural change observed in chalcogenide films /5/ assuming that the reversible photo induced structural change is characterized by an increase in randomness in atomic configurations and a thermal recovery corresponds to the restoration of the initial short range order. This mechanism is not applicable for the irreversible changes observed in our case, because even at very low incident light intensities (I<1 W/cm²) photobleaching occurs. At intensities below 1 W/cm² the direct heating effect of the beam is negligible as measured by evaporated Au-Ni thermocouples.

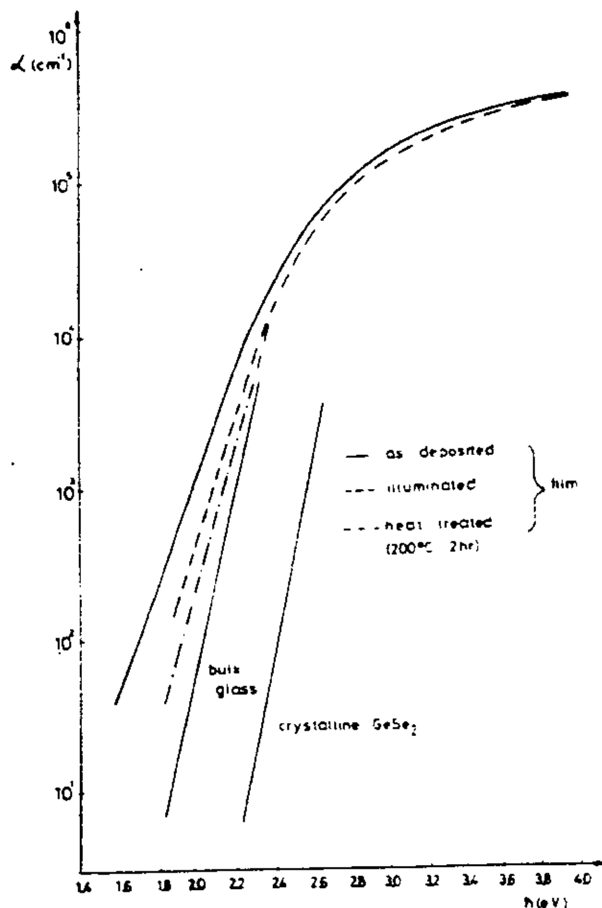

Figure 2. Absorption coefficient versus photon energy of $GeSe_2$ films.

The other optical parameter of interest was the refractive index (n) as a function of photon energy between 1 and 2 eV. In this low absorption portion of the optical spectrum $n^2(\omega) = \varepsilon_1(\omega)$..$n(\omega)$ was calculated from the measured reflexion and transmission data using the method of Brattain and Briggs /6/ where multiple reflexions were taken into account. $n(\omega)$ can be fitted by the Kemple-Di Domenico /7/ dispersion relation-ship.

$$\varepsilon_1(\omega) = n^2(\omega) = 1 + E_d E_o / [E_o^2 - (\hbar\omega)^2]$$

where E_o and E_d are single oscillator fitting constants which measure the oscillator energy and strength respectively. E_o for chalcogenide glasses corresponds to the mean energy of transitions from valence band (lone-pair) states to conduction band states /8/. E_d measures the

strength of interband optical transitions and is related to the charge distribution within each unit cell. E_d primary depends on the coordination number and valency. By plotting $(n^2-1)^{-1}$ versus $(\hbar\omega)^2$ (Fig. 3)

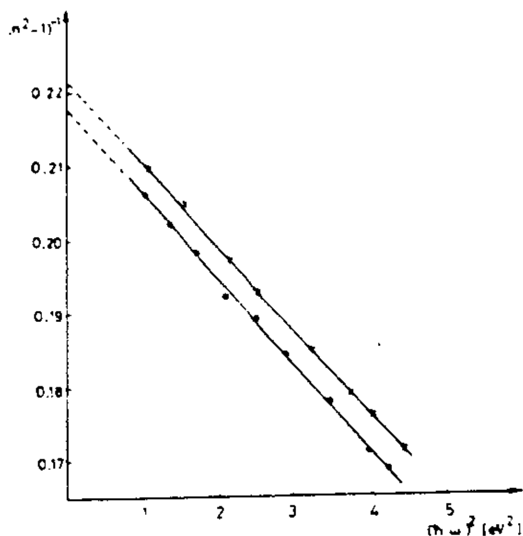

Figure 3. $(n^2-1)^{-1}$ versus $(\hbar\omega)^2$ for $GeSe_2$ films

and fitting the data by a straight line E_d and E_o can be directly determined from the intercept (E_o/E_d) and the slope $(-1/E_d\ E_o)$. It is clear that the decrease in n accompanying exposure and annealing of $GeSe_2$ films is associated with an increase in E_o rather than be a change in E_d (Table II).

Table II. Index of refraction (at $\hbar\omega$ = 1.96 eV) and oscillator parameters of $GeSe_2$ films

Sample	E_o (eV)	E_d (eV)	n	$\Delta n = n_1 - n_2$
1 as deposited	4.91	22.96	2.472	
2 exposed	5.1	23.0	2.451	−0.021
3 annealed	5.12	23.0		

The measured changes on the absorption coefficient and the refractive index indicate a reduction of the disorderness of atomic bounding between the neighrest and second neighrest neighbours due to the evaporation process and therefore a decrease of the extent of the localized tail states adjacent to the band edge (increase in the slope of the absorption edge and in the oscillator energy E_o).

3.2. Self induced oscillation of light absorption.- To produce pulsations in the transmitted and reflected light the incident power density should be increased until a dark centre develops in the middle of the image. This can be distinguished from crystallization since on reducing the intensity it disappears completely, without delay, leaving no sign of permanent phase changes. On the other hand, the intensity (averaged over the 20 μ spot) should not exceed an upper limit (about 2.7 kW/cm^2 for 6 μ thick films) otherwise the central region quickly becomes crystalline and thereafter doesn't show further optical changes.

The transmittance, reflectance and light scattering pulsations measured simultaneously have the same character (Figs. 4-5). A decreasing of transmittance is accompanied by a simultaneous decreasing of the reflectance and a same decrease of the scattered light independently on the angle of scattering.

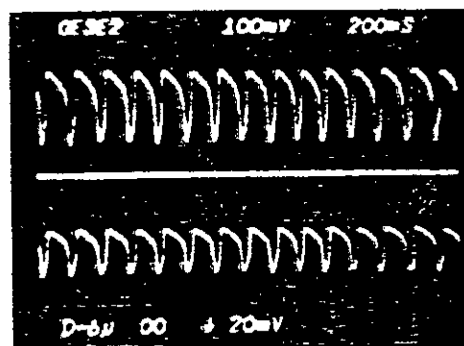

Fig. 4. Transmittance (upper signal) and reflectance (lower signal) pulsations under focussed continuous He-Ne laser beam (I = 1.9 kW/cm^2). Ordinate: intensity of transmittance and reflectance; abscissa: time 200 ms/div.

Using the expressions of Bruttain and Briggs /6/ one can calculate the changes of the absorption coefficient and refraction index of the films from the measured transmittance and reflectance changes during the oscillation periods (Fig. 6). The absorption coefficient of the $GeSe_2$ films has two characteristic values during the oscillation period. Both level B ($\alpha = 2.4 \times 10^2\ cm^{-1}$) and level C ($\alpha = 5.1 \times 10^2\ cm^{-1}$)(see Fig. 6) are metastable

states of the material and exist only under the influence of intensive laser irradiation. The value of the absorption coefficient decrease to the stable photo-bleached state (level A: $\alpha = 1.9 \times 10^2\ cm^{-1}$)

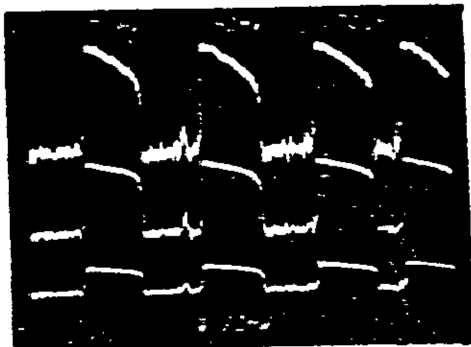

Fig. 5. Transmittance (A), small angle (B) and large angle (C) scattered light pulsations under focussed continuous He-Ne laser beam ($I = 2.5\ kW/cm^2$)

independently of the momentary state of the oscillation when the exciting laser light is switched off. The refractive index changes in opposit direction as the absorption coefficient and has a minimum value as α reaches the maximum indicating that a real absorption change does occur during the oscillation period.

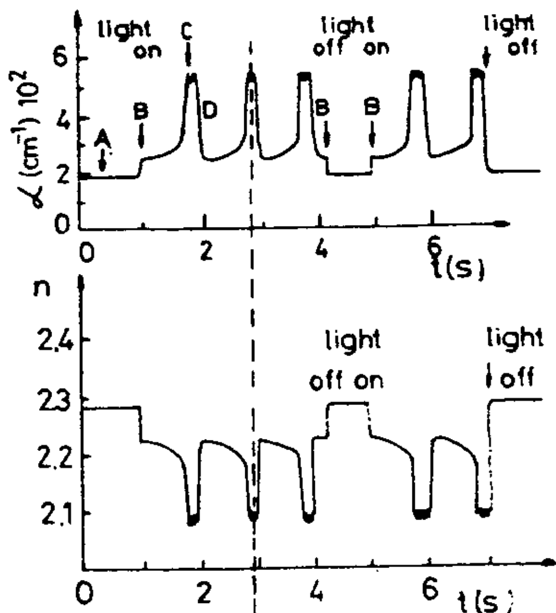

Fig. 6. Oscillations of absorption coefficient and refractive index (at $\hbar\omega = 1.96$ eV) under the influence of continuous laser irradiation ($I = 2.7\ kW/cm^2$)

It is possible to measure the temperature of the $GeSe_2$ films during oscillation using vacuum evaporated thin film Au-Ni thermocouples because the thermocouple transparent enough to detect the transmitted laser beam (Fig. 7).

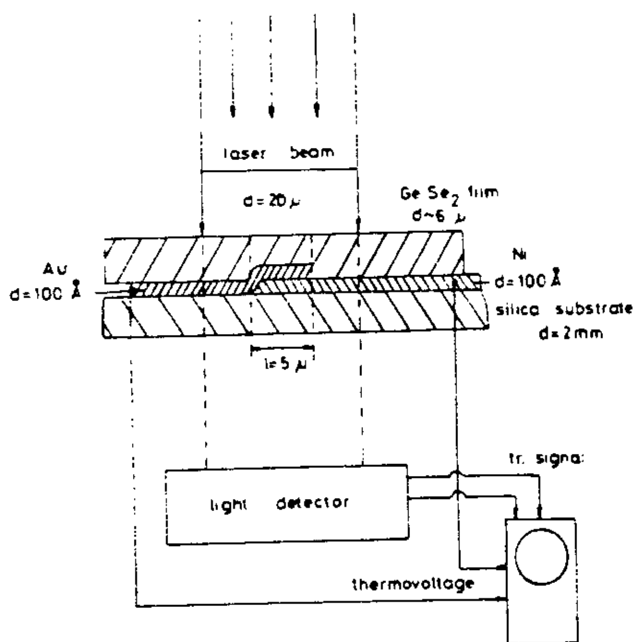

Fig. 7. Experimental arrangement for simultaneous observation of transmittance and temperature oscillation.

The thermovoltage and the transmittance were recorded simultaneously on a storage oscilloscope (Fig. 8). As the transmittance increases the temperature of the $GeSe_2$ film decreases exponentially and the decrease of the transmittance (increasing absorption) is accompanied by a simultaneous exponential increasing of the temperature.

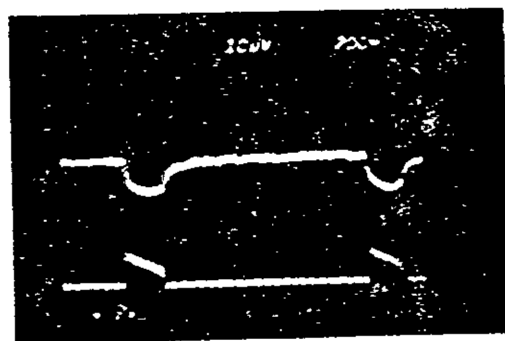

Fig. 8. Transmittance (A) and temperature of $GeSe_2$ film under the influence of laser irradiation ($I = 2.7\ kW/cm^2$)

Oscillation can't be induced using the green (λ = 5145 Å) and blue (λ = 4880 Å) wavelengths of a continuous Ar-ion laser. The irradiated spots become darker with increasing intensities without any sign of oscillation and then changed over to crystalline state.

We tried to induce similar pulsations in 6 μ thick self-supporting films (removing the substrate) at the same experimental conditions. Permanent photobleaching was obtained but no transmittance or reflectance pulsations occurred. Instead of any oscillatory response the transmittance of the films decrease gradually under the influence of continuous laser irradiation (Fig. 9). The duration of steps is depending on the illumination conditions. The steps are shorter (second signal in Fig. 9) when the sample is illuminated again 0.8 s after the first gradual decreasing of the transmittance (first signal in Fig. 9) and are longer when the sample was kept in darkness for 8 s (third signal in Fig. 9).

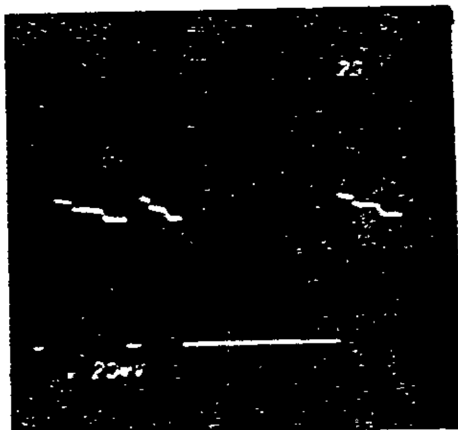

Fig. 9. Step by step decreasing of the transmittance of the $GeSe_2$ film under the influence of continuous laser irradiation (I = 0.5 kW/cm^2)

4. Discussion.- 4.1. Photobleaching.- The energy of laser light ($\hbar\omega$ = 1.96 eV at λ = 6328 Å) used to induce the photobleaching and oscillation is slightly less than the value of optical energy gap of $GeSe_2$ films (E_g = 2.1 eV). Therefore the assumption that the electrons are mostly excited from the localized tail states of the valence band edge is plausible.

In the freshly evaporated $GeSe_2$ films a large number of defect states are expected (Ge-Ge, Se-Se bonds, dangling bonds /9/ which contributes substantionally to the observed absorption edge. Upon illumination or annealing a local rearrangement of these defect states (weaker bonds) occurs forming stronger Ge-Se bonds. The extent of the localized tail states decreases as a result of the reduction of the defect states. Therefore one can observe a shift of the absorption edge to the direction of bulk well annealed glass state (see Fig. 2). The slope of the Urbach edge increases upon illumination or annealing indicating the decrease of internal electric fields created by charged impurities in the material /10/.

The increase of the mean energy (E_o see Table II) of transitions from valence band (lone-pair) states to conduction band states similarly should be attributed to the reduction of the localized tail states. This conclusion is supported by the fact that the oscillator strength constant (E_d) haven't changed upon illumination indicating that there is no sufficient change in the average coordination or in the charge distribution i.e. only the defect states are involved in the photobleaching.

4.2. Absorption oscillation.- It is clear from the measured optical data that a real absorption oscillation occurs at the low absorption region of the Urbach tail in the $GeSe_2$ films.

There are two important features of the oscillation: a) oscillation can't be induced using higher energy light ($\hbar\omega$ = 2.2-2.4 eV); b) there are at least two optically metastable states existing only under the influence of intensive laser irradiation therefore the effect of temperature has to be considered. According to the Onsager model /11/ after photoexcitation the electron and hole will diffuse apart to a distance R determined by the diffusion constant and the thermalization time which is proportional to the excess kinetic energy. The bonding energy between the electron and hole is

$e^2/4\ _oR$. If R is larger than the critical distance R_o where $e^2/4\pi\varepsilon\varepsilon_o$ = kT then the electron and hole will diffuse apart. Because of the energy of excitation used in our experiments ($\hbar\omega$ = 1.96 eV) represents a low energy excitation for the $GeSe_2$ glasses i.e. $R < R_o$ exciton formation occurs. The mobilities in $GeSe_2$ are less than 1 cm^2/volts /12/ thus the charge carriers (excitons) move slowly and spend a comparatively long time at a given site between hops. Due to the strong electron-phonon coupling a metastable self trapped excition is formed. The configurational coordinate diagram for the excition has been described by /13/ and used by /14/ for the explanation of photostructural phenomena in chalcogenides (Fig. 10).

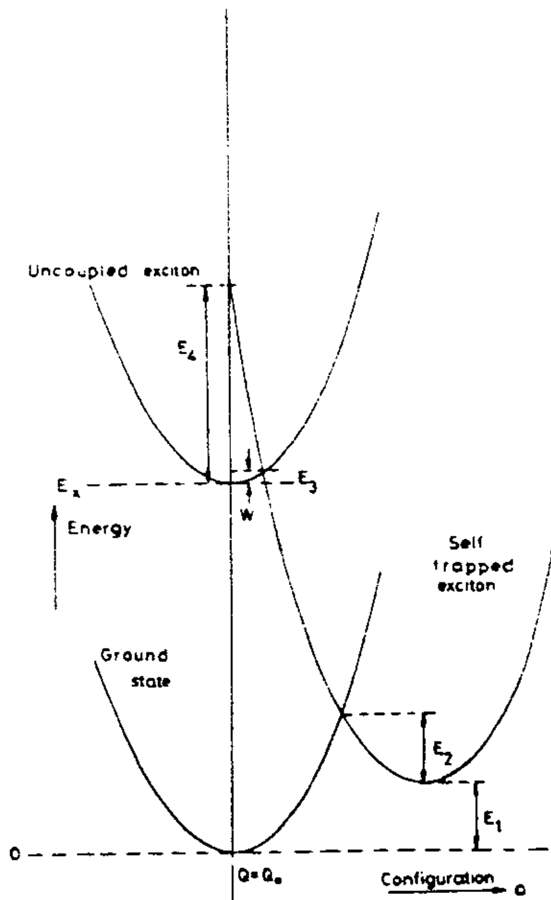

Fig. 10. Configurational coordinate diagram for chalcogenide glasses.

In this model two distinct mechanisms of optical excitations are expected. One is a transition to the uncoupled exciton state and the second is to the self trapped excition state. We assume that the increased absorption during the oscillation could be accounted to the formation of self trapped exciton states generating by high intensity low energy excitation of continuous laser light. Because of the higher absorption, the temperature of the film raises too. At higher temperature the thermal recombination of self trapped charge carriers becomes important. As a result of thermal release of self trapped excited states the absorption decreases again because the energy of ground state lies below the energy level of the self-trapped excition states (see Fig. 10). As the absorption decreases the temperature decreases too (see Fig. 8), the material cools down and the process should start again resulting in a continuous oscillation of light absorption.

The quantitative treatment of the oscillation has not been completed so far, we present this model merely as an interesting example for consideration. This qualitative model is in good accordance with a number of observations an amorphous $GeSe_2$ and it explains why this particular material is efficient in producing a periodic pulsing effect. Amorphous $GeSe_2$ has $T_g \approx 400$ °C high enough to resist crystallization under fairly intense light irradiation. Its optical absorption edge varies just around the wavelength of the exciting He-Ne laser. Due to its large Se content the fraction of dangling bonds can rise considerably and in the glassy state the narest neighbour distance has a greater degreee of freedom to change according to the dominant charged defect states, than it would have in the crystalline phase. Indeed the corresponding density fluctuations in the irradiated volume element have been observed by scanning electron microscopy in a-$GeSe_2$ /15/. In principle, other amorphous chalcogenide compounds, having an absorption edge in the visible range should behave similarly. We believe that the clue of the oscillation is laying on some unique properties of the amorphous state. More work is needed in this field to find other substances or modifiers to $GeSe_2$ raising its sensitivity.

Acknowledgements.- The author wish to thank I. Kósa Somogyi and J. Gazsó for their interest and help in connection with the work and G. Zentai who helped in resolving the experimental difficulties involved in the work.

/1/ Hajtó, J., Zentai, G., and Kósa Somogyi I., Solid State Commun. 23, (1977) 401.

/2/ Gazsó, J., and Hajtó, J., Phys. Status soliditi (a) (1978) 181.

/3/ Hajtó, J., and Apai, P., to be published in the Proc. of 8th Int. Conf. on Amorphous and Liquid Semiconductors, Cambridge, Massachusetts, U.S.A.

/4/ Thornburg, D. D., and Wayman, C. H., Appl. Phys. 40, (1969) 3007.

/5/ de Neufville, J. P., Optical properties of Solids-New Developments, ed. by B. O. Seraphin (North Holland Publ. Co.) 1978.

/6/ Brattain, W. H., and Briggs, H. B., Phys. Rev. 75 (1949) 1705.

/7/ Wemple, S. H., and Di Domenico, M., Phys. Rev. B 3, (1971) 1338.

/8/ Kastner, M., Adler, D., and Fritzsche, H., Phys. Rev. Lett. 37, (1976) 1504.

/9/ Street, R. A., and Mott, N. F., Phys. Rev. Lett. 35, (1975) 1293.

/10/ Dow, I. D., and Redfield, D., Phys. Rev. B 1, (1970) 3358.

/11/ Onsager, L., Phys. Rev. 54, (1938) 554

/12/ Tóth, L., to be published in Phys. Status soliditi (a) 54, (1979).

/13/ Mott, N. F., Davis, E. A., and Street, R. A., Phil. Mag. 32, (1975) 961.

/14/ Street, R. A., in Proc. of 7th Int. Conf. on Amorphous and Liquid Semiconductors, Edinburgh, UK, ed. by W. A. Spear p. 509, 1977.

/15/ Hajtó, J., Pogány, Reports of Central Research Institute for Physics, KFKI-42-1977.

Int.Conf. of "AMORPHOUS SEMICONDUCTORS 80"
KISHINEV USSR (1980)

OSCILLATIONS OF LIGHT ABSORPTION AND PHOTOCURRENT IN a-$GeSe_2$ FILMS

J.Hajtó and M.Füstöss-Wégner

Central Research Institute for Physics
H-1525 Budapest, P.O.B. 49, Hungary

1. INTRODUCTION

The laser induced oscillation of the transmittance of vacuum evaporated amorphous $GeSe_2$ films has been described first in a recent paper [1]. The oscillation of transmittance is accompanied by a simultaneous oscillation of reflectance i.e. real absorption oscillation has been found [2]. A tentative explanation was suggested in terms of laser induced self-trapped exciton states of the material [3]. However the physical grounds of oscillation has not been cleared yet. In this paper we summarize our experimental results of the optical properties and steady state photoconductivity measurements on a-$GeSe_2$ films under the influence of medium intensity continuous laser irradiation.

2. EXPERIMENTAL

$GeSe_2$ films were vacuum evaporated onto silica or mica substrates. Deposition rates usually ranged 20-40 Å/sec. The thicknesses were measured by quartz crystal monitor and later checked by Talystep. X-ray diffraction confirmed the layers to be amorphous. The ϵ_2 spectra of the as deposited and illuminated films were calculated from the measured transmission and reflectivity with the help of the well known formula, where multiple reflections insided the sample are taken into account.

The continuous beam of 30 mW output power He-Ne laser (λ = 6328 Å) was focussed on the layers to a spot diameter of 20-350 μ. The incident light intensity could be reduced by a polarizer and the transmitted light signal was displayed on a storage oscilloscope. The photocurrent measurements were made on surface type samples prepared by vacuum evaporation of coplanar gold electrodes onto mica substrates.

The steady state photocurrent (under continuous laser irradiation) was measured by an electrometer or amplified and displayed on a storage oscilloscope. The RC time constant of the electrical circuit was less than 1 msec. In this way simultaneous measurements of the transmittance and photocurrent pulsations could be performed during the light absorption oscillation.

3. RESULTS

3.1 Steady state photocurrent measurements

The typical plots of photocurrent versus 1/T for the $GeSe_2$ films are shown in Fig. 1. The photocurrent (λ = 6328 Å) varies exponentially with an activation energy E_1 = 0.3–0.5 below 373°K depending on the incident photon flux and with an activation energy E_2 = 0.8 eV above 373°K which doesn't depend on the incident photon flux. In every cases the photocurrent increases linearly with the voltage indicating the lack of space charge limitation and electrode effects.

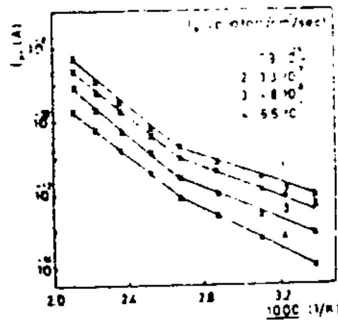

Fig. 1. Temperature dependence of photocurrent in a-$GeSe_2$ films

The photocurrent increases much more rapidly than proportional to the increase of absorption with temperature (Fig. 2) indicating that other temperature dependent quantities (mobility, life-time) have to be taken into account.

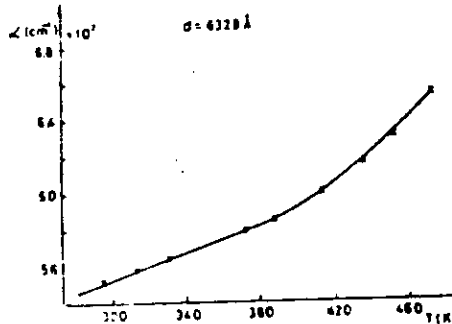

Fig. 2. Temperature dependence of the absorption coefficient in a-$GeSe_2$ film at λ = 6328 Å

3.2 Laser induced changes

The changes induced by the laser irradiation can be of three kinds (see Table I.) depending on the incident laser power density as described earlier [2]. The crystallization is not discussed in this paper.

Table I. Processes caused by laser light of different intensities in 6μ thick a-$GeSe_2$ films

Intensity (kW/cm^2)	Number of photons (photon·cm^{-2}·sec^{-1})	Response
10^{-4}–1.4	$3.21\cdot10^{17}$–$4.5\cdot10^{21}$	Photobleaching
1.4–2.7	$4.5\cdot10^{21}$–$8.68\cdot10^{21}$	Transmittance and photo-current oscillations
over 2.7		Crystallization

3.2.1 Photobleaching

It has already been reported [2] that the optical absorption edge associated with transitions involving electronic states at or near the band edges varies with illumination or annealing. We consider first the region of high enough absorption ($\alpha > 2\cdot10^4$ cm^{-1}) where $\varepsilon_2(h\nu)$ follows the relation

$$\varepsilon_2(h\nu)^2 \propto (h\nu - E_o)^2 \qquad (1)$$

Upon illumination or annealing the value of E_o (optical energy gap) as well as the slope of the edge increases. The corresponding values of E_o are 2.08 eV for as deposited state 2.17 eV for photobleached state and 2.22 eV after annealing of the films respectively.

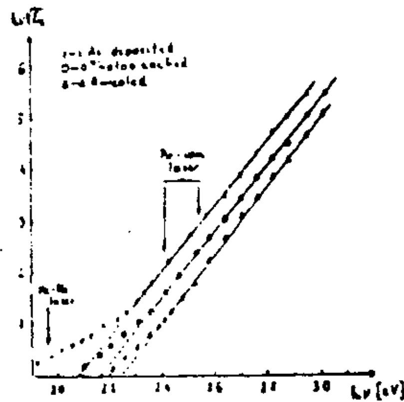

Fig. 3. Optical absorption edge in a-$GeSe_2$ films

At lower energies, for smaller absorption coefficients ($\alpha < 2\cdot10^4$cm^{-1}) ε_2 departs from the behaviour described by Eq.(1) and falls of less rapidly with decreasing energy (absorption tail see Fig. 3). The absorption tail (shaded area) decreased upon illumination or annealing indicating a reduction in disorderness in the as deposited amorphous network.

The fundamental absorption band is shown in Fig. 4. The decrease of the maximum intensity with illumination and annealing is accompanied with a shift of the maximum position (E_g) to higher energies. E_g is expected to vary with modifications of the bonding; it has been predicted that E_g must depend on the bond length d as $d^{-2.5}$ [4]. The measured values of E_g and the calculated average (Ge Se) bond length (d) are summarized in Table II.

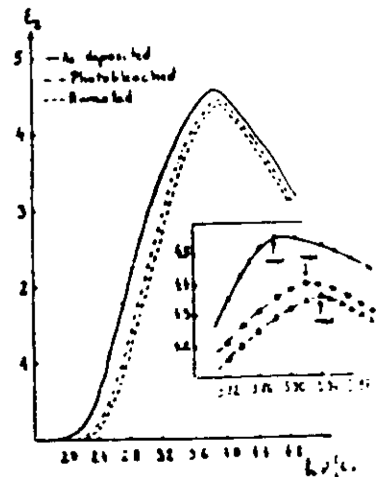

Fig. 4. Imaginary part of the dielectric constant ϵ_2 for a-$GeSe_2$ films

Table II. Characteristic values of E_g and d in a-$GeSe_2$ films

Sample	E_g (eV)	d (Å)
as deposited	3.88	2.34
photobleached	3.92	2.33
annealed	2.94	2.326

3.2.2 Simultaneous transmittance and photocurrent oscillations

To produce pulsations in the transmitted light intensity the incident laser power density should be increased to 1.4 kW/cm^2 ($I = 4.5\cdot10^{21}$ photon$\cdot cm^{-2}\cdot sec^{-1}$) until a dark centre develops in the middle of the irradiated area. This can be distinguished from crystallization since on reducing the intensity it disappears completely, leaving no sign of any permanent phase changes. On the other hand the intensity (averaged over the 20 μm spot) should not exceed an upper limit (about 2.7 kW/cm^2) for 6 μm thick films) otherwise the central region quickly becomes crystalline and thereafter does not show further optical changes.

Fig. 5. Transmittance and photocurrent oscillations in 6 μm thick a-$GeSe_2$ films under the influence of continuous laser irraditaion ($P=2.3$ W/cm^2, $I=7.5\cdot10^{21}$ photon$\cdot cm^{-2}\cdot sec^{-1}$). Ordinate: Intensity of transmitted light (upper signal) and photocurrent (lower signal). Abscissa: time 200 msec/div.

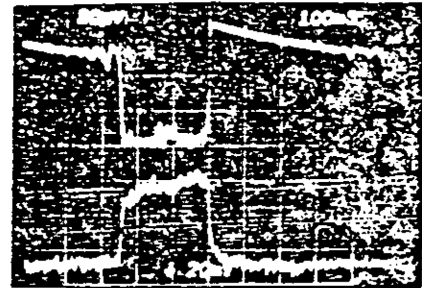

Fig. 6. Transmittance and photocurrent oscillations in the same sample Abscissa time: 100 msec/div.

The oscillation of the transmittance is accompanied with a simultaneous oscillation of the photocurrent signal (Fig. 5). When the transmittance gets lower (higher absorption) the photocurrent rapidly increases to a higher level and when the transmittance gets higher (lower absorption) the photocurrent falls back at the same time to the lower value (Fig. 6).

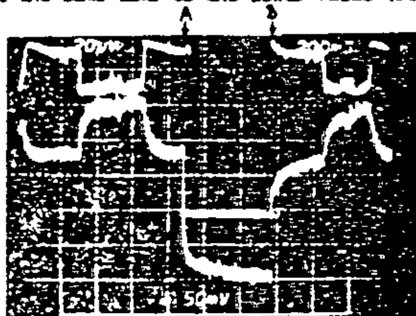

Fig. 7. Oscillations of transmittance (upper signal) and photocurrent (lower signal) versus time (I_0=5.8·10^{21} photon·cm^{-2}·sec^{-1}, P=1.8 kW/cm^2)

When the exciting light is switched off (point A on Fig. 7) the photocurrent decays first rapidly then more slowly to the dark current value. When the exciting light is switched on (point B on Fig. 7) the photocurrent increases continuously to the lower level (corresponding to the lower absorption state) then starts to oscillate simultaneously with the oscillation of the transmittance. We calculated the absorption coefficient for the lower and higher absorption state during the oscillation (see Fig. 7). The optical data are summarized in Table III. together with the measured changes in photocurrent.

Table III. Measured and calculated optical and electrical parameters of a-$GeSe_2$ film during oscillation. (I_0=5.8·10^{21} photon·cm^{-2}sec^{-1}, d=6.02μm, at λ=6328 Å)

Note	T_v %	R %	i_p measured (arb.units)	α (cm^{-1})
Higher absorption state	27	9.97	1.00	1.83·10^3
Lower absorption state	38.55	15.27	0.73	1.04·10^3

The oscillation can be eliminated by heating the films up to 420-450°K which corresponds to an energy ΔE = kT = = 0.036-0.039 eV. Decreasing the temperature of the films below 400°K the oscillation starts again under the influence of continuous laser irradiation.

4. DISCUSSION

The measured photocurrent data give direct information on the electrical properties of $GeSe_2$ films because the photocurrent was proportional to the voltage in agreement with Ohm's law (no space charge limitation) and because the electrodes were not illuminated (surface type cell). The increase of the photocurrent with the decrease of the transmittance (Fig. [illegible]) is in accordance with the temperature dependence of the photoconductivity ([illegible] 1-2). However the rapid increase of the photocurrent can not be explained by a pure thermal effect due to the higher light absorption because the temperature increases exponentially and more slowly than the photocurrent as observed during the simultaneous trans-

mittance oscillation and temperature measurements [3].

The increased photocurrent signal is not in accordance with the proposed self trapped exciton model [2-3]. In this model the increasing absorption during the oscillation can be attributed to the appearance of self trapped excition states. The self trapped excitons (in form of D^+D^- pairs) are localized and neutral Therefore one should not observe an increase in the photocurrent signal (indicating an appearance of excess number of free charge carriers) during the increasing absorption period of the oscillation.

Tanaka [5] has pointed out the importance of the interaction between electron and lattice vibrations producing local structural change in the amorphous network which is more conceivalbe. The light induced increase in fluctuation in Ge-Se bond angle has been directly observed in amorphous sputtered Ge-Se film by Utsugi et al. [6]. Such a bending flexibility may produce bistable local bonding geometries responsible for the oscillation. According to the model proposed by Anderson et al. [7] in any glass system there should be a certain number of atoms (or groups of atoms) which can sit more or less equally well in two equilibrium positions.

The bistable local bonding geometry represents local bistable configurations which give two minima in the potential energy of the system as a function of some appropriate local atomic coordinates.

The energy of laser light used to induced the oscillation in 1.96 eV (λ = 6328 Å) is slightly less than the value of the optical energy gap of the $GeSe_2$ films (E_g = 2.15 eV). Therefore the assumption that, the electrons and holes are mostly excited from the localized tail states of the valence band edge (lone pair electrons) is plausible. Photoexcitation of a valence electron in lone pair state gives rise to a change in the interactions between lone pair electrons on two neighboruing chalcogen atoms and interactions with their local envirorment producing transition from one to the other configuration (local phase change). It explains why one can observe a sudden change in the optical and photocurrent signal during the oscillation. We suppose that the total energy difference between the two metastable configuration is about 0.04 eV according to the temperature dependence of oscillations (see 3.2.2).

Because of the higher absorption the temperature increases too. The mechanism of the recovery process is probably complex either due to the increase temperature, or the increased number of excited chemical bonds. The role of the substrate is also questionable the recent measurements show that the oscillation is not stable using films without substrate [3]. When the system turns back to the lower absorption state the temperature falls down and the process should start again resulting in a continuous oscillation of light absorption and photocurrent.

REFERENCES

1 J.Hajtó, G.Zentai, I.Kósa Somogyi, Solid State Commun. 23, 401 (1977)

2 J.Hajtó and P.Apai, Journal of Non-Cryst.Solids 35-36, 1085 (1980)

3 J.Hajtó, in Proc. of European Physics Study Conf. on Laser Induced Nucleation in Solids Masnuy St. Jean, Belgium, Oct. 9-11. (1979)

4 J.A. Van Vechten, Phys. Rev. 182, 891 (1969)

5 K.Tanaka, Journal of Non-Cryst.Solids 35-36, 1023 (1980)

6 Y.Utsugi and Y.Mizushima, J.Appl.Phys. 49, 3470 (1978)

7 P.W.Anderson, B.I.Halperin, C.H.Varma, Philosophical Magazine 25, 1 (1972)

JOURNAL DE PHYSIQUE
Colloque C4, supplément au n°10, Tome 42, octobre 1981 *page C4-313*

LASER INDUCED OSCILLATORY PHENOMENA IN a-$GeSe_2$ FILMS

J. Hajtó and M. Füstöss-Wégner

Central Research Institute for Physics, H-1525 Budapest, P.O.Box 49, Hungary

Abstract. - Studying the optical and photoelectric properties of 5 μ to 10 μ thick $GeSe_2$ amorphous films under the influence of focussed continuous He-Ne laser beams (just below band gap laser light of wavelength λ = 6328 Å) a region of medium intensity (1.4 to 2.7 kW/cm^2) is found where low frequency (3 to 50 Hz) oscillations in the absorption coefficient and the photocurrent sets in. To date, this seems to be the only amorphous semiconductor in which a constant input evokes and oscillatory response, which is obviously a far from equilibrium phenomenon. The experimental optical data are compared with the micorscopic model of cooperative charge disproportionation of defect centers described by P.Fazekas to explain the first cycle of oscillation which is a sudden switch from the transparent to the dark state. The simultaneous change in photocurrent is also discussed.

1. Introduction. - The oscillatory behaviour of the transmittance and reflectance of amorphous $GeSe_2$ films illuminated by a continuous He-Ne laser beam was reported in several recent communications [1-3]. Oscillation can be observed when the intensity of the focussed laser beam lies in a certain range which is 1.4-2.7 kW/cm^2 for a 6.4 μ thick film for example. The oscillation of the optical properties is accompanied with a simultaneous oscillation of the photocurrents [4]. A microscopic model was suggested by P.Fazekas [5] to describe the first step of the oscillation which is a sudden switch from a transparent to a dark state. It is argued [5] that the evaporated $GeSe_2$ films contain unusually high density of defects, and this gives rise to cooperative behaviour, due to both interdefect Coulomb, and laser induced interactions. The zero temperature phase diagram of a model Hamiltonian was calculated and above a threshold photon density a laser induced, partially charge-ordered phase was ound. The switching to the dark state was interpreted as a transition into this phase. This paper is concerned with the investigation of optical (frequency depencence) and electrooptical (photocurrent measurements) properties of vacuum evaporated $GeSe_2$ films under the influence of continuous laser irradiation. We describe further experimental details of the previously reported oscillation behaviour of the material and compare the results with the qualitative predictions of the Fazekas model.

2. Experimental. - $GeSe_2$ films were vacuum evaporated onto silica or mica substrates were measured by quartz crystal monitor and later checked by Talystep. A continuous beam of 30 mW output power He-Ne laser (λ = 6328 Å) was focussed on the layers to a spot diameter of 20-350 μ. The incident light intensity could be varied by a polarizer, the reflected and transmitted signals were displayed on a storage oscilloscope.The photocurrent measurements were made on surface type samples prepared by vacuum evaporation of coplanar gold electrodes onto mica or glass substrates.

The steady state photocurrent (under continuous laser irradiation) was measured by an electrometer or amplified and displayed on a storage oscilloscope. In this way simultaneous measurements of the transmittance, reflectance, and photocurrent pulsations could be performed during the light absorption oscillation.

To obtain the light absorption spectra during the oscillation, a continuous tunable dye laser was focussed on the same spot as the He-Ne laser. The intensity of the measuring dye laser beam was kept on a low value not to influence the oscillation processes. In this optical arrangement the He-Ne laser was used for high power illumination and the tunable dye laser served as a light source for adsorption measurements. The absorption spectra were calculated from the measured transmission and reflection during the oscillation using the method of Brattain and Briggs [6].

3. Results and discussion.

3/a Light absorption measurements

From $\alpha = 10^2 cm^{-1}$ to $\alpha = 10^4 cm^{-1}$ the optical absorption coefficient varies exponentially with the photon energy according to the equation $\alpha = \alpha_o \exp[\Gamma h\nu]$ (Urbach edge). The smaller value of the slope of the observed exponential adsorption edge ($\Gamma = 8.7 eV^{-1}$ for the as deposited films and $\Gamma = 15.3 eV^{-1}$ for the bulk glass) indicates higher concentration of defects in the as deposited films than in the bulk glass form, i.e. the decrease of the slope of the Urbach edge is due to the increase of internal electric fields created by charged impurities of the material [7].

Absorption oscillation can be observed when the amorphous $GeSe_2$ films are illuminated by a continuous He-Ne laser beam with incident light intensity of 1.4-2.7 kW/cm^2 for a 6.4 μ thick film for example. We measured the changes of absorption edge during the oscillation induced by He-Ne laser at an incident laser power density of 2.7 kW/cm^2. (Maximum laser power density at which oscillation can be observed for 6 μ thick films.) The absorption edge has two characteristic positions during the oscillation. First the edge shifts to lower photonenergies (line 1 in Fig. 1) with a slope ($\Gamma = 5.7 eV^{-1}$) smaller than for the as

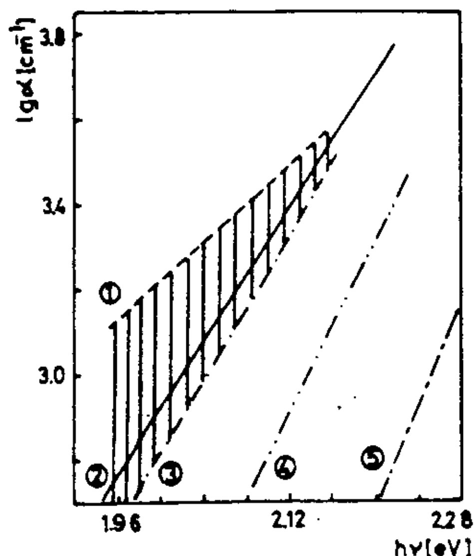

Fig. 1:
Optical absorption edges of a-$GeSe_2$ films.
1 - dark state of oscillation,
2 - as deposited films,
3 - bright state of oscillation
4 - photobleached state,
5 - bulk glass

deposited material and after turns back to higher photonenergies (line 3 in Fig. 1), with a slope ($\Gamma = 9.1 eV^{-1}$ about the same as for the as deposited edges (line 1 and line 3 in Fig. 1) represent metastable states of the material and exist only under the influence of intense He-Ne laser irradiation. The absorption edge shifts to the stable photobleached state (line 4 in Fig. 1) independenty of the momentary state of the oscillation, when the exciting laser is switched off. The "amplitude" of oscillation (shaded area in Fig. 1) becomes more marked as the measureing light energy is lowered from the band gap suggesting

that the relevant optical transitions are between localised states according to the phase transition model [5] for the laser induced switching. Evaporated a-$GeSe_2$ films in contrast to bulk samples are likely contain large defect concentration according to the low value of the slope of the absorption edge, and to the temperature dependence of the steady state photocurrent.

The shifts in the absorption edge can be associated with either changes in the charge state or conecntration of defects [7] or with changes in temperature (according to the temperature dependence of the Urbach tail).

3/b Photocurrent measurements

Temperature dependence of dark current I_d (curve 1) and photocurrent I_{ph} (curves 3,4,5 and 6) for different photoexcitation intensities in $GeSe_2$ films are shown in Fig. 2. The photocurrent measurements were completed by photocurrent-intensity characteristics as it can be seen in Fig. 3.

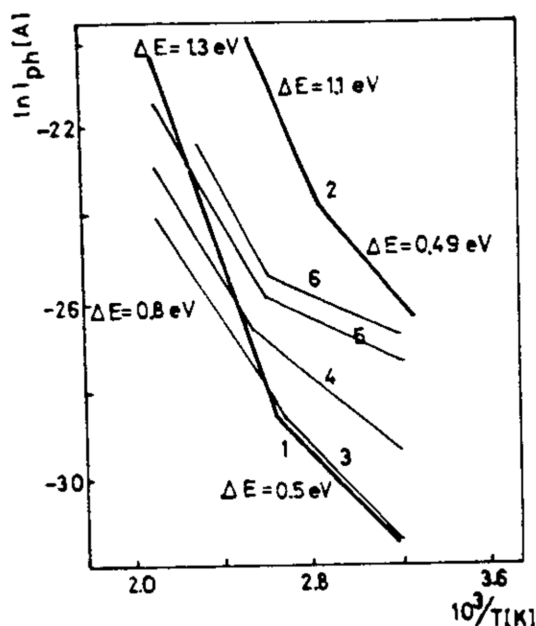

Fig. 2: Temperature dependence of dark and photocurrent in $GeSe_2$ films; dark current in surface type samples (curve 1) dark current in sandwich type samples (curve 2), photocurrents at different light intensities where ΔE varies from 0,5 eV to 0,2 eV at low temperatures [4]

As compared to the general form of temparature and intensity dependence of photocurrent observed for different chalcogenides, these curves show two anomalies. First of all the photocurrent rieses with increasing temperature up to 500 K independently of magnitude of the dark current. Secondly, the photocurrent I_{ph} is proportional to the intensity F at "low"-temperature range and the exponent γ in relation $I_{ph} \sim F^{\gamma}$ is about 0.6 at elevated temperatures.

Above 380 K the mechanism of dark conduction may be a charge carrier transport by carriers excited beyond the mobility edge into extended states. The activation energy for dark current (1.1-1.3 eV) will be the sum of the energy E_1 to form a D^0 centre and of the energy ε required to take a hole from a D^0 centre into the valence band. Below 380 K we can assume hopping conduction according to the "tail" observed in log I_d versus 1/T plot. (The shape of dark current curves were the same whether the surface type (curve 1 in Fig.2) or the sandwich type (curve 2 in Fig. 2) samples were investigated.) The activation energy of charge carrier motion is the energy E_1 (i.e. the energy of a D^0 centre's formation) and an energy W representing the hopping activation energy of charge carriers in the D^0D^-, D^0D^- system.

The photocurrent is controlled, on the one hand, by the recombination for which the rate-determining step is the $2D^0 \rightarrow D^+ + D^-$ relation, and on the other hand, by the drifts mobility which depends on filling of charged centres D^+ and D^-. The drift mobility, which is trap limited above 380 K, is activated with an energy ε and the photocurrent will be proportional to it in this temperature range (ΔE = 0.8 eV). The fact that the recombination with thermally excited charge carriers does not become dominant up to 500 K(γ ~ 0.60) indicates the unusually high concentration of defects D^0 in the films. This is in a good agreement with

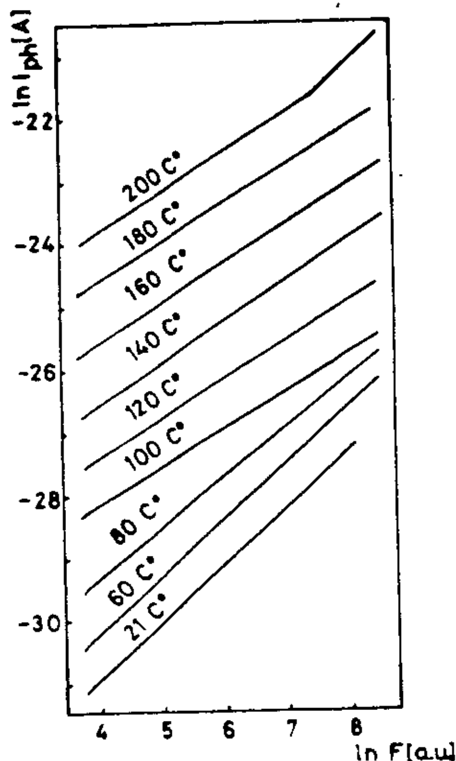

Fig. 3: Photocurrent (I_{ph}) - intensity (F) characteristics at different temperatures

the ESR measurements which show high defect concentrations ($D^0 \sim 5.10^{19}$-$10^{20}/cm^3$) as in as deposited as in photobleached conditions of evaporated $GeSe_2$ layers (M.Erö-Gécs private communications). In the low temperature region a transition to monomolecular recombination kinetics is observed ($\gamma \sim 0.9$) and it seems that the role of the different traps increases too. It can be seen that the slope of lines 3,4,5 and 6 in Fig. 2 varies with the light intensities, i.e. the activation energy depends on the filling of traps. As it was previously established the oscillation of transmittance was accompanied with a simultaneous oscillation of the photocurrent signal. With synchronous measurements of the transmittance, the reflection and the photocurrent we could estimate the change of the absorption (the number of photons absorbed per second in the sample) and the photocurrent when the as deposited sample was photobleached and during the oscillation. While the ratio of absorption in the as deposited state (A_{as}) to the absorption in photobleached one (A_{phb}) is

$\frac{A_{as}}{A_{phb}} = 1.2$, the ratio of adequate photocurrents shows a higher value;

$\frac{I_{as}}{I_{phb}} = 1.7$. During the oscillation the absorption ratio of 1.9 ($\frac{I_d}{I_{tr}} = 1.9$, where I_d the absorption in the dark and I_{tr} in the more transparent state) attend upon a ratio of 2.9 in photocurrents; the change of photocurrent is not proportional to the change of absorption. It seems that the formation of defects D^0 is followed by a change in the recombination process of/and in the charge carrier mobility.

References

[1] Hajtó J., Zentai G., and Kósa Somogyi I., Solid State Communications 23 (1977) 401

[2] Gazsó J., and Hajtó J., Physica Status Solidi (a) 45 (1978) 181

[3] Hajtó J., Journal de Physique C4 no5 Tome 41 page C4-63

[4] Hajtó J., and Füstöss-Wégner M., in Prod. of Int. Conf. on Amorphous Semiconductors, Kishinev, USSR 1980, page 189

[5] Fazekas P., 1980, Presented at the IUPAP-ICTP Symposium on Amorphous Semiconductors, and Trieste preprint IC-117-80-1980

[6] Brattain W. H., and Briggs H. B., Phys. Rev. 75 (1949) 1705

[7] Dow I. D., and Redfield D., Phys. Rev. B. 1 (1970) 3358

KFKI-1981-96

J. HAJTÓ
G. RADNÓCZI
L. POGÁNY
É. HAJTÓ

ELECTRON MICROSCOPICAL INVESTIGATION OF LASER IRRADIATED A-$GeSe_2$ AND A-As_2S_3 THIN FILMS

Hungarian Academy of Sciences

CENTRAL RESEARCH INSTITUTE FOR PHYSICS

BUDAPEST

KFKI-1981-96

ELECTRON MICROSCOPICAL INVESTIGATION OF LASER IRRADIATED a-$GeSe_2$ AND a-As_2S_3 THIN FILMS

J. Hajtó, G. Radnóczi*, L. Pogány, É. Hajtó

Central Research Institute for Physics
H-1525 Budapest 114, P.O.B. 49, Hungary

*Research Institute for Technical Physics,
Budapest, Hungary

Submitted to Journal of Non Crystalline Solids

HU ISSN 0368 5330
ISBN 963 371 821 3

ABSTRACT

The structural changes of vacuum evaporated a-As_2S_3 and a-$GeSe_2$ films caused by cw He-Ne laser irradiation and thermal treatment were investigated by transmission and scanning electron microscopy. The changes of the amorphous networks are in correlation with their different optical responses on laser irradiation and thermal treatment. A tentative model is presented for the photostructural changes in these materials.

АННОТАЦИЯ

Исследовались структурные изменения аморфных пленок с составом As_2S_3 и $GeSe_2$, вызыванные лазерной и термической обработкой. Структурные изменения изучались с помощью электронного микроскопа. Изменения оптических свойств, вызванные лазерной и термической обработкой, можно согласовать с изменением аморфной структуры. Нами была предложена модель фотоструктурных превращений.

KIVONAT

Vákuumpárologtatással készitett amorf As_2S_3 és amorf $GeSe_2$ vékonyrétegek szerkezetében végbemenő változásokat vizsgáltuk. A folyamatos He-Ne lézer és hőkezelés hatására bekövetkezett szerkezeti változásokat transzmissziós és pásztázó elektronmikroszkóp segitségével tanulmányoztuk. A lézersugárzás és hőkezelés okozta optikai változásokat korreláltattuk az amorf szerkezetben bekövetkezett változásokkal. Egy lehetséges modellt javaslunk a fotoszerkezeti átalakulásokra.

1. INTRODUCTION

A variety of photo-induced effects have been observed in amorphous chalcogenide materials, some of them showing photo-structural effects [1-3] or photo-induced chemical changes [4-5] or photo-induced optical anisotropy [6-8].

A lot of attention has recently been paid to photostructural changes in amorphous chalcogenide films in connection with their applications for information storage [9].

Reversible optical transition has been found in thin films of As-Se [3], As-S [1] and As-Se-Ge [2] systems where band gap illumination causes a shift of the optical absorption edge to longer wavelengths (photodarkening) or annealing near the glass-transition temperature (*Tg*) leads to its displacement to shorter wavelengths (bleaching).

In contrast to this, the effects of illumination and annealing were nearly identical in vacuum evaporated $GeSe_2$ films [8]. For both cases bleaching has been found and the virgin state of the films (as deposited) could not be regained by either illumination or annealing. $GeSe_2$ is a particular substance where oscillation of the optical absorption has been found under the influence of continuous laser irradiation [8]. In this paper we concentrated on the problem, why different optical responses can be expected for different types of chalcogenide thin films under the influence of laser irradiation and heat treatment. We studied the amorphous structure by electron microscopy and compared our experimental results with the present models on photo-induced absorption changes [10-13]. Two particular compositions of As_2S_3 and $GeSe_2$ were chosen for investigation because of their significant differencies in optical properties under the influence of illumination and annealing.

2. EXPERIMENTAL

The thin films were prepared by vacuum evaporation from Ta boat at $P = 2 \cdot 10^{-5}$ *Torr*, onto carbon film substrate mounted on a copper mesh and examined by transmission electron microscope type JEM-100 U or scanning electron microscope type JSH-35. For evaporation we used amorphous (As_2S_3) and polycrystalline ($GeSe_2$) materials. The thickness of the films and the evaporation rate were *700 Å* and *8 Å/sec* respectively. The films were irradiated by a continuous He-Ne laser (λ = *0.63 μm*) and the incident laser power density was in the range of $2\text{-}40\ W/cm^2$ using focussed irradiation. Some of the films were annealed for one hour in the temperature range of $150\text{-}220\ ^oC$.

3. RESULTS

3.1 As_2S_3 films

Figure 1 shows the transmirsion electron micrograph and the diffraction patterns of a film in as-deposited state. The film is amorphous and homogeneous, no voids (defects) or fluctuations of the film density could be observed. As a result of cw laser irradiation, a fluctuation in the film density started to develope although there were no detectable changes in the diffraction patterns. The degree of inhomogeneity depended on the incident laser power density (*Fig. 2*). The laser induced changes in the amorphous structure were reversible because the initial homogeneous network could be ragained upon subsequent electron beam irradiation (*Fig. 3*). Thermal erasing of the laser induced inhomogeneous structure was also possible. As a result of annealing (*200 ^oC, 1 hour*), the formation of bubbles could be observed (*Fig. 4*). This was attributed to ordering of the amorphous network [14].

3.2 $GeSe_2$ films

The structure of as-deposited $GeSe_2$ films (*Fig. 5/a*) was different from that of the As_2S_3 films. It exhibited an inhomogeneous columnar structure, similar to that observed in a-Ge [14, 15] and obliquely deposited a-$Se_{(1-x)}Ge_x$ films [16]. The rods were oriented towards the vapour beam direction with an average size of *300 Å*. After laser irradiation or annealing the columnar structure tended to disappear. The number of denser clusters decreased from $\sim 400/\mu m^2$ in the as-deposited state to $\sim 280/\mu m^2$ as a result of illumination (*Fig. 5/b*). The decrease of the number of the rods depended on the incident laser power density. Complete erasing of the rod-like structure was possible using laser power density ($35\ W/cm^2$) below the level necessary for crystallization (*Fig. 6*).

As a result of annealing, smaller brighter spots appeared near the rods indicating an ordering process in the amorphous phase i.e. the defects are concentrating into smaller area (*Fig. 7/a*). The brighter spots are oriented in one direction as compared to the columns i.e. structural anisotropy was observed as a result of heat treatment. The bright spots (point defects) were more apparent with increasing temperature during the annealing (*Fig. 7/b*).

In addition we have observed periodic density fluctuations in the laser irradiated $GeSe_2$ films (*Fig. 8*). The laser irradiation was performed from a cw He-Ne laser that was focussed on the samples giving a Gaussian spot, *40 µm* in diameter. The laser power density ($P = 37\ W/cm^2$) using in this experiments was higher than the level necessary for complete erasing of the columnar structure ($P = 35\ W/cm^2$) but lower than that of the level necessary for crystallization ($40\ W/cm^2$). The period of the density variations was equal with the wavelength of the incident radication (*0.63 µm*) in our experiments. The electron diffraction patterns (inset in *Fig. 8*) of the laser irradiated $GeSe_2$ films differ significantly from that of the as deposited ones (inset in *Fig. 5/a*) indicating that structurally different phases are existing in the amorphous state.

The laser irradiated surface of the same films (*P = 37 W/cm²*) was investigated also by scanning electron microscope. The SEM picture show the presence of parallel surface ripples with distance of *~0.6 μm* (*Fig. 9*). In each case the ripple period was equal to that expected from interference of the incident laser light with a wave scattered from a surface deviation. This assumption is supported by the fact that circular interference fringes could also be observed around a clod-like defect on the surface as a result of laser irradiation (*Fig. 10*).

Similar periodic structure variations and correlated surface ripples have been observed in ion-implanted silicon layers as a result of pulsed laser irradiation [17-18].

Under the influence of electron beam of the transmission electron microscope the as-deposted films could be converted into another amorphous, structurally different network (darker area in *Fig. 11*) as evident from the changes of the electron diffraction patterns.

3.3 Volume changes

In parallel with the above experiments, measurements of thickness were carried out for As_2S_3 and $GeSe_2$ films. The thickness difference of the exposed and the unexposed area was measured by a surface profile recorder (Talystep) as described in detail in [19]. The laser induced changes for As_2S_3 and $GeSe_2$ films are summarized in Table I where the signs of "plus" and "minus" refer to the increase and the decrease of the thickness after irradiation respectively. The As_2S_3 films expanded as a result of irradiation while $GeSe_2$ films shrinked. The fractional change $\Delta d/d$ was the same for different thicknesses indicating that the change should be attributed to volume effect for both materials. Similar volume expansion was observed in evaporated As_2S_3 films by Hamanaka et al. [19]. Volume contraction has been observed for $As_4Se_5Ge_1$ [19] and for $Ge_xSe_{(1-x)}$ [16] films on irradiation with photons of energy higher than the band gap.

4. DISCUSSION

The experimental results indicate that the structure of evaporated amorphous materials shows significant dependence on their composition and the difference in optical response is due to their different amorphous structure in the as-deposited state.

The failure to observe granular or columnar structure in As_2S_3 films by electron microscopy implies that the scale in density variations must be below *50 Å*. The photodarkening in A-As_2S_3 films is due to a structural change in the as-deposited network i.e. density fluctuations have been developed as a result of laser irradiation. Our observation is in good accordance with the models of photodarkening proposed by Tanaka et al. [10] and Kolobov et al. [11]. In these models the photodarkening is related to a disorder in the amorphous network i.e. to fluctuations in bond lengths and bond angle. The recovery process by annealing (thermal belaching) corresponds to a thermal structural relaxation, restoring the initial amorphous network as verified by our investigation (see *Fig. 4*). Nang T. et al. [14] proposed a "random covalent network" model for the photostructural changes in chalcogenide thin films assuming that the antibonding band of the As_2S_3 (responsible for the optical properties of the material) was shifted to lower energies after illumination or annealing which means photodarkening for both cases. This model is not consistent with our experimental observation according to which the responses are different for the illumination (photodarkening) and for the annealing (thermal bleaching). It is also not possible to explain the photodarkening by the creation of homopolar bonds [20] because the optical edge shift has the opposite direction to that of expected on the base of this model. We found that the As_2S_3 film posses metastable structure as a result of laser irradiation and the initial amorphous network could be regained upon annealing or electron beam irradiation. The electron microscopical observations (see *Figs. 2, 3*) show that the photo structural change in As_2S_3 can be related to bulk oriented feature of the amorphous network rather than to the creation of defects [12]. This assumption is also supported by the volume effect measurements (see Table I).

The different response of the $GeSe_2$ thin films upon illumination (photobeaching) is originating from the different as-deposited structure compared to As_2S_3. The columnar structure of $GeSe_2$ films is the result of the special type of chemical bonding of the material. The mechanism of growing of the columnar structure is based on stacking of the configurationally unique double chain $GeSe_2$ rafts [21]. The perfectly stacked rafts grow more rapidly (dendritically) during evaporation forming column centers. As a result of laser irradiation or annealing, the columnar structure is disappearing i.e. the material is continuously transforming to the lowest energetic configuration (planar polymerized corner and edge sharing tetrahedra in the single crystal). This is the reason why the material shows the same response (bleaching) either on irradiation or annealing, because any structure change in this case takes place in the direction of ordering. By structural ordering the optical properties approach the properties of the single crystalline state, that is why bleaching can be observed.

To clarify the structural differencies between the two materials as a result of laser irradiation and annealing we propose a simple model in which the enthalpy of the material is figured versus the structural parameter (R). It is well established that the enthalpy of an amorphous system is greater than that of the stable crystalline state [22]. The structural parameter (R) characterizes the changes in atomic positions (configurational rearrangements [23,24]) that take place when the atoms of the amorphous network are transformed from their ground state (as deposited state) to lower energy positions as a result of laser irradiation or annealing.

In the case of As_2S_3 (*Fig. 12*) the enthalpy of the laser irradiated material is higher (state B in *Fig. 12*) than that of the as-deposited one (state A in *Fig. 12*) due to the anisotropy of the structure in the photodarkened state. So the as-deposited state in As_2S_3 can be considered as a metastable one (a minimum of H at A). Increasing R by thermal vibrations the material transforms from state B to state C, to a new metastable modification, but may return to A (when irradiated by the electron beam

in the microscope) by decreasing *R*. This latter phenomenon was also observed by us (*Fig. 3*).

In the case of $GeSe_2$ (*Fig. 13*) the columnar structure tends to disappear gradually, i.e. the enthalpy of the structure decreases gradually by increasing *R*. It means that the as deposited state (state *A* in *Fig. 13*) can be considered as to be unstable one, frozen in due to quenching during deposition i.e. there is no minimum on *H*(*R*) dependence in this state.

Table I

The changes of the thickness of As_2S_3 and $GeSe_2$ films after laser irradiation

Film	Laser flux watt/cm^2	Thickness d[μm]	Thickness change Δd [Å]	Fraction Δd/d
As_2S_3	2.1	1.1	+ 50	$4.6 \cdot 10^{-3}$
	2.1	2.4	-110	$4.6 \cdot 10^{-3}$
$GeSe_2$	2.4	2.4	-190	$8.0 \cdot 10^{-3}$
	2.4	3.2	-260	$8.1 \cdot 10^{-3}$

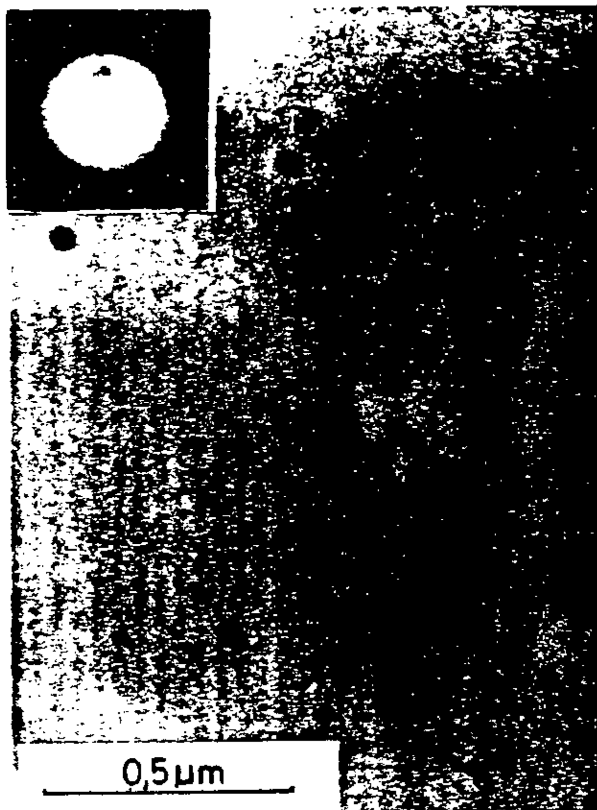

Fig. 1
TEM picture of the As_2S_3 film as evaporated

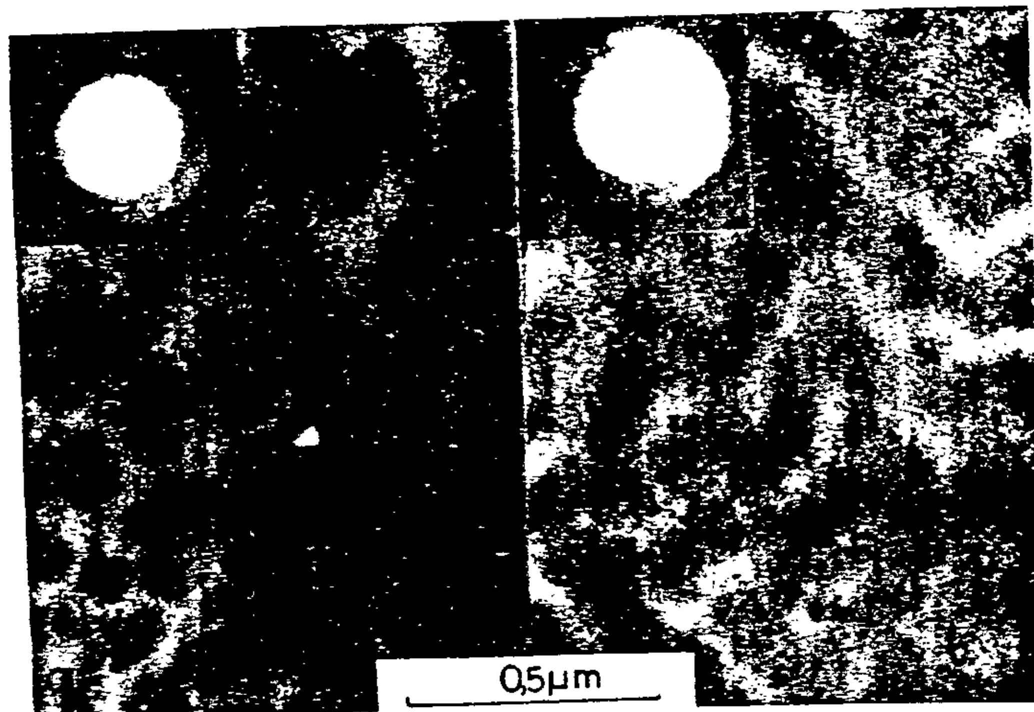

Fig. 2

TEM picture of the laser irradiated As_2S_3 film:
a) $P = 10\ W/cm^2$; b) $P = 15\ W/cm^2$

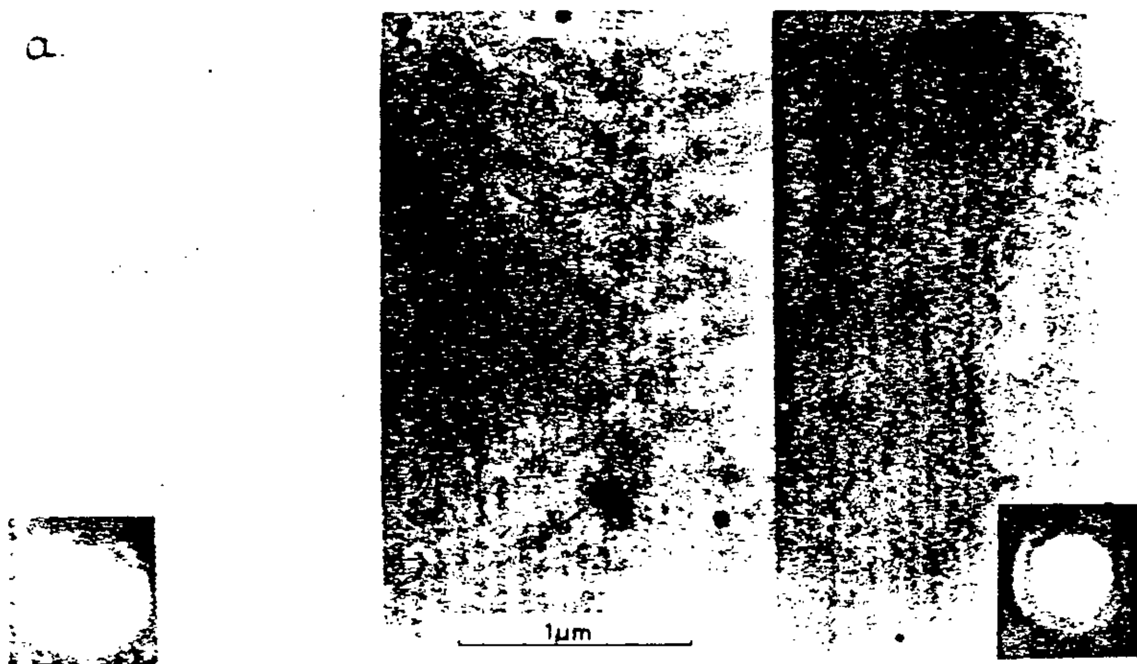

Fig. 3

Step by step erasing of the laser induced inhomogeneous structure (state a) of As_2S_3 film by electron beam; state b) t = 30 s irradiation with the electron beam; c) t = 60 s irradiation with the electron beam

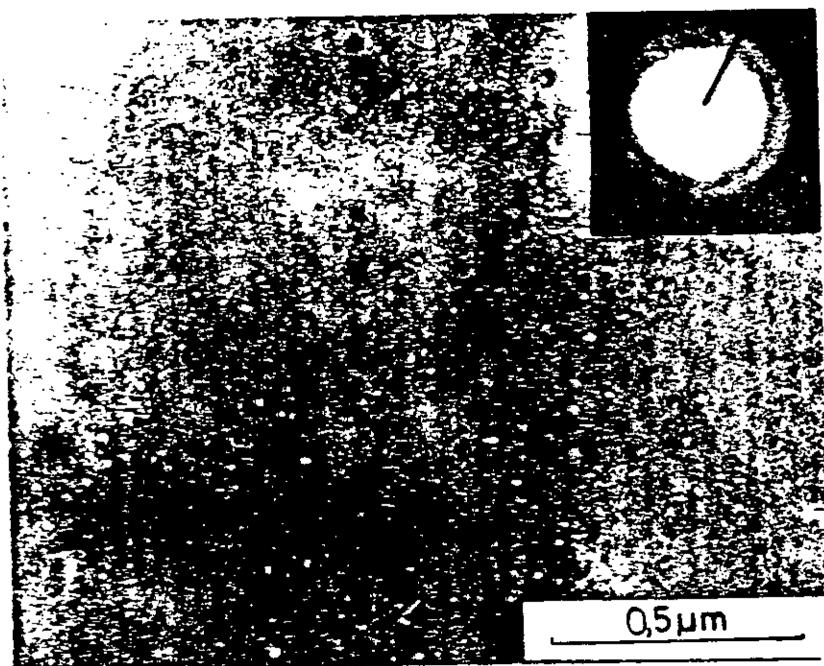

Fig. 4

TEM picture of the laser irradiated area of As_2S_3 film after annealing of the film

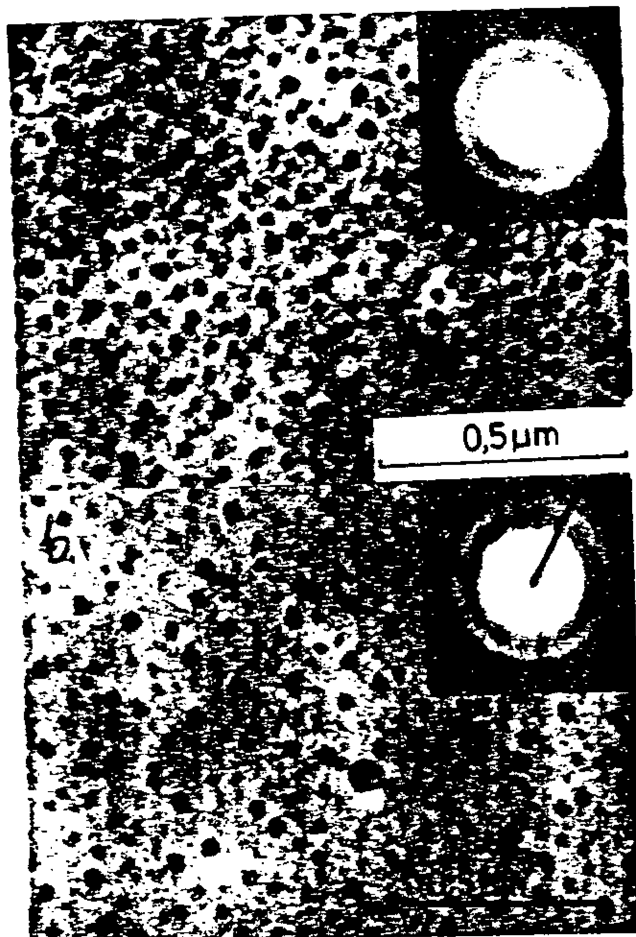

Fig. 5

a) *Inhomogeneous structure of as-deposited a-$GeSe_2$ film;*

b) *Structure after laser irradiation (P = 20 W/cm^2)*

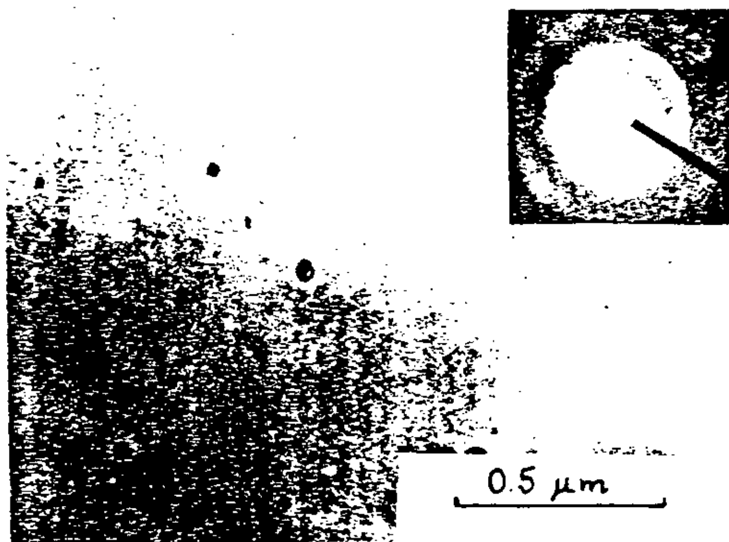

Fig. 6
Structure of the laser irradiated $GeSe_2$ film
($P = 35\ W/cm^2$)

Fig. 7

Electron micrograph of the annealed $GeSe_2$ films

a) t = 60 min at T = 170 °C;
b) t = 60 min at T = 240 °C

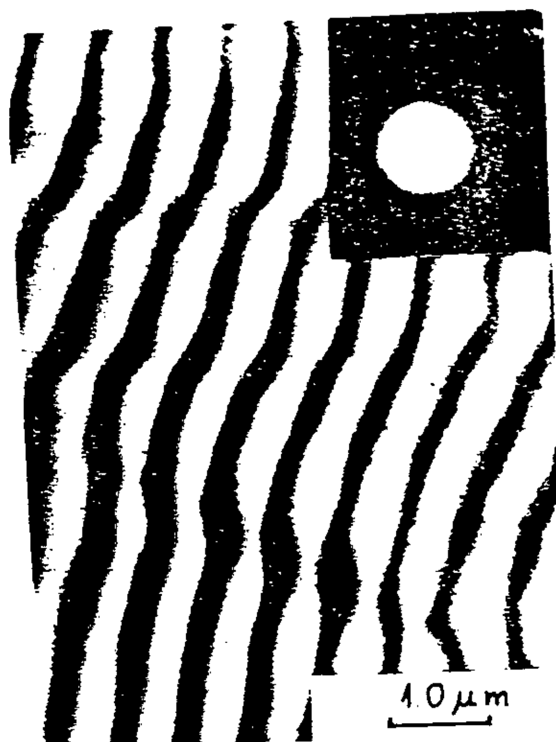

Fig. 8

TEM micrograph of the laser irradiated $GeSe_2$ film (P = 37 W/cm^2)

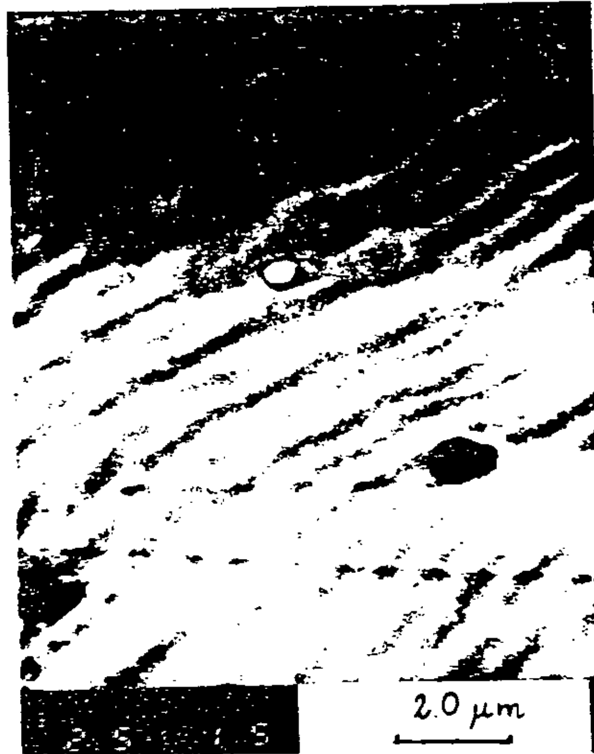

Fig. 3

Surface ripples on the laser irradiated $GeSe_2$ film (P = 37 W/cm^2).

Fig. 10

Circular interference fringes in laser irradiated $GeSe_2$ film photographed by TEM ($\bar{P}$ = 37 W/cm^2)

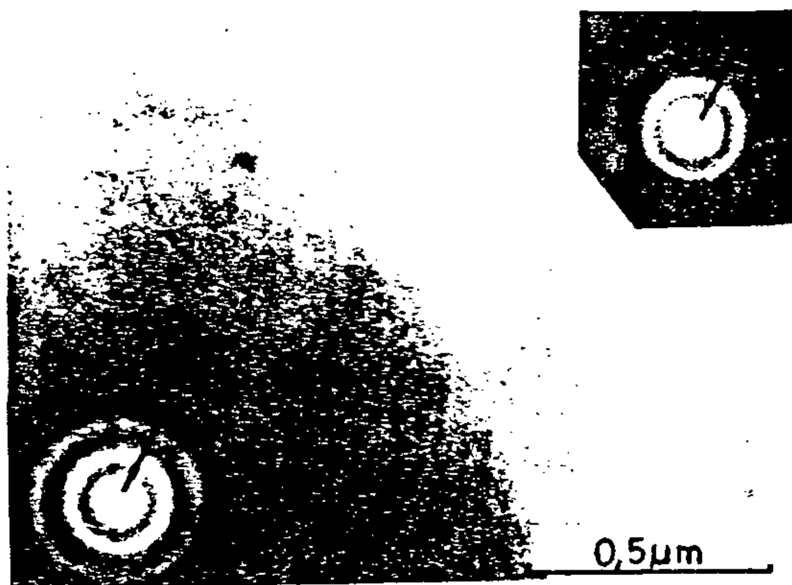

Fig. 11

TEM picture of different amorphous structures induced by the electron beam in $GeSe_2$ film

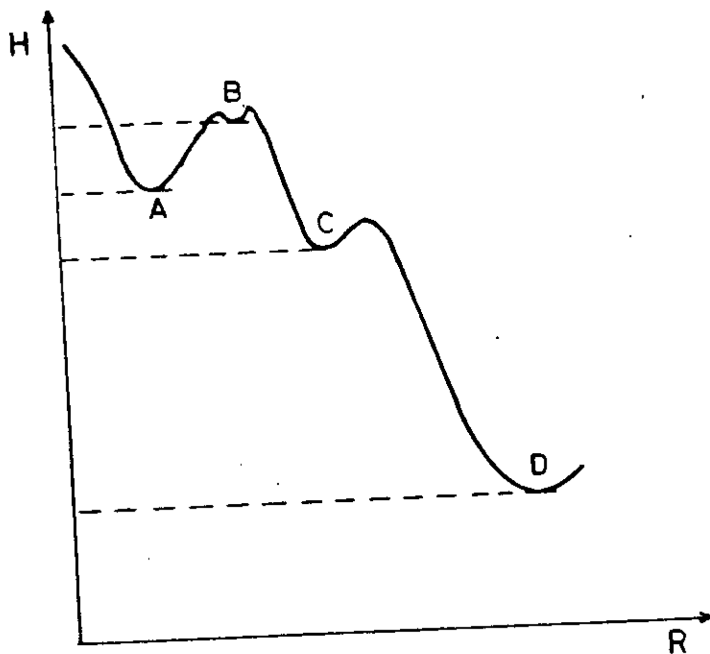

Fig. 12

Enthalpy vs. R in As_2S_3 films

A: as deposited state; B: photodarkened state; C: annealed state; D: crystalline state

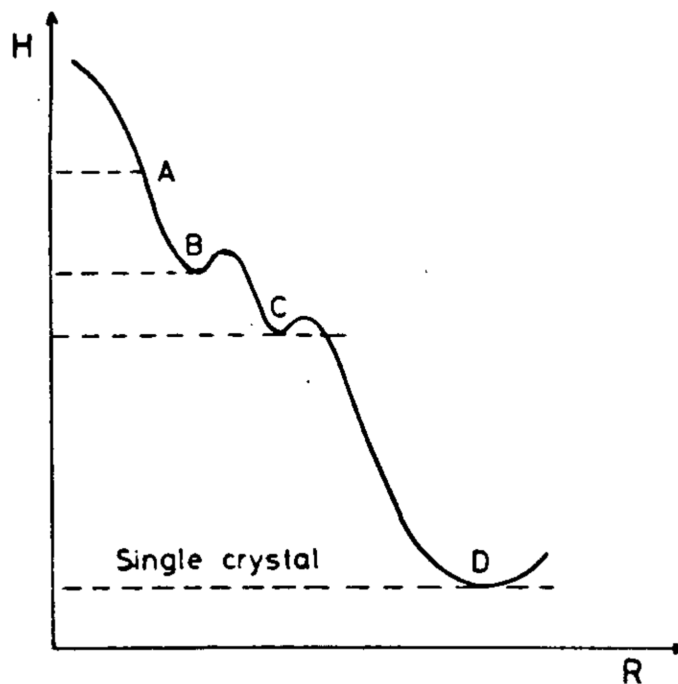

Fig. 13

Enthalpy vs. R in $GeSe_2$ films

A: as deposited state; B: photobleached state; C: annealed state; D: crystalline state

REFERENCES

[1] Tanaka, K., Appl. Physics. Letters 26, 243 (1975)

[2] Igo, T. and Toyoshima, Y., Journal of Non-Cryst. Solids. 11, 304 (1973)

[3] Averyanov, V.L., Kolomiets, B.T., Lyubin, V.M., Taguirdzhanov, M.A., Proc. of the 7th Int. Conf. on Amorphous and Liquid Semicond. ed. by Spear W.E., Edinburgh, p. 802 (1977)

[4] Berkes, Y.S., Ing, S.W. and Hillegas, W.J., J. Appl. Phys. 42, 4908 (1971)

[5] De Neufville, J.P., Moss, S.C. and Ovshinsky, S.R., Journal of Non-Cryst. Solids 13, 191 (1974a)

[6] Zhdanov, V., Kolomiets, B.T., Lyubin, V., Malinovski, V., phys. stat. sol. (a) 52, 621 (1979)

[7] Hajtó, J., Even, P.J.S., phys. stat. sol. (a) 54, 385 (1979)

[8] Hajtó, J., Journal de Physique Col. C4 no.5 41, 63 (1980)

[9] De Neufville, J.P., Optical Properties of Solids New Developments ed. by Seraphin B.O., North Holland Publ. Co. Amsterdam, p. 473 (1976)

[10] Tanaka, K., Hammaka, H., Izima, S., Proc. of the 7th Int. Conf. on Amorphous and Liquid Semicond., ed. by Spear W.E. Edinburgh, p. 787 (1977)

[11] Kolobov, A.V., Kolomiets, B.T., Konstantinov, O.V. and Lyubin, V.M., Journal of Non-Cryst. Solids 45, 335 (1981)

[12] Street, R.A., Proc. of the 7th Int. Conf. on Amorphous and Liquid Semiconductors ed. by Spear W.E., Edinburgh, p. 509 (1977)

[13] Nang, T., Okuda, M., Matsushita, T., Phys. Rev. B19, 947 (1979)

[14] Barna, Á., Barna, P.B., Bodó, Z., Pócza, J.F., Pozsgai, I., and Radnóczi, G., Proc. of 5th Int. Conf. on Amorphous and Liquid Semiconductors, ed. by Stuke J. and Brenig W., Taylor and Francis Ltd. London, p. 109 (1974)

[15] Nakhodkin, N.G. and Shaldervan, A.J., Thin Solid Films 10, 109 (1972)

[16] Singh, B., Rajagopalan, S., Bhat, P.K., Pandya, D.K. and Chopra, K.L., Journal of Non-Cryst. Solids 35-36, 1053 (1980)

[17] Birnbaum, M., J. Appl. Phys. 36, 3688 (1965)

[18] Leamy, H.I., Rozgonyi, G.A. and Sheng, T.T., Appl. Phys. Lett. 32, 535 (1978)

[19] Hamanaka, H., Tanaka, K., Matsuda, A. and Izima, S., Solid State Communications 19, 499 (1976)

[20] Street, R.A., Nemanich, R.J. and Conell, G.A.N., Physical Review B18, 6915 (1978)

[21] Phillips, J.C., Journal of Non-Cryst. Solids 35-36, 1157 (1980)

[22] Bagley, B.G. and Chen, H.S., Materials (American Institute of Physics) (1979) p. 97, Sec. 1.b.

[23] Anderson, P.W., Phys. Rev. Letters 34, 953 (1975)

[24] Mott, N.F., Davis, E.A., Street, R.A., Phil. Mag. 32, 961 (1975)

J. Phys. C: Solid State Phys., 15 (1982) 6293–6303. Printed in Great Britain

Laser-induced optical anisotropy in self-supporting amorphous $GeSe_2$ films

J Hajtó, I Jánossy and G Forgács
Central Research Institute for Physics, H-1525 Budapest, PO Box 49, Hungary

Received 29 March 1982, in final form 25 May 1982

Abstract. A comprehensive study of laser induced optical anisotropy in amorphous $GeSe_2$ films is presented. This anisotropic structure of the amorphous network can be reoriented reversibly by changing the incident-beam polarisation. A model is constructed that accounts for experimental findings, in particular for the logarithmic time development of the laser-induced anisotropy.

1. Introduction

A variety of photo-induced changes have been observed in amorphous chalcogenide films (de Neufville 1976). The best known of these effects are photodarkening and photobleaching which have been intensively studied.

There have also been observations that a linearly polarised laser beam can produce optical anisotropy in chalcogenide glasses and chalcogenide evaporated films (Zhdanov *et al* 1979, Hajtó and Ewen 1979). However the existing experimental results are not sufficient to understand the underlying mechanism that produces the observed optical anisotropy. In this paper we report a comprehensive study of the laser-induced optical anisotropy in self-supporting amorphous $GeSe_2$ films.

The vacuum-evaporated $GeSe_2$ films exhibit interesting non-linear optical effects, e.g. light-induced oscillations of the transmission. These properties were reviewed in a recent paper (Hajtó 1980).

The experiments described here were carried out at the incident-laser-power density range from 3 to 50 W cm^{-2}. In this range of relatively low intensities no oscillation of the optical properties occurs; however a non-linear behaviour of the optical absorption does already appear (the absorption increases with the increase of the laser power density at a fixed wavelength).

The paper is organised as follows: in § 2 we describe the experimental method; the results are presented in § 3. A model for the development of optical anisotropy is presented in § 4. The comparison of the model and the experimental results is given in § 5. Section 6 contains some final conclusions.

2. Experimental arrangement

The a-$GeSe_2$ films were prepared by vacuum evaporation from a Ta boat at $P = 2 \times 10^{-6}$ Torr (2.7×10^{-4} Pa) onto glass substrates, using polycrystalline $GeSe_2$ ingots

as the evaporation source. The deposition rates were about 20 Å s^{-1} in all cases and the thickness during the evaporation was measured by a quartz-crystal monitor. For the measurements the films were removed from the glass substrates using an ultrasonic bath in order to reduce the effects of multiple light reflections and of the mechanical stresses occurring at the $GeSe_2$–substrate interface.

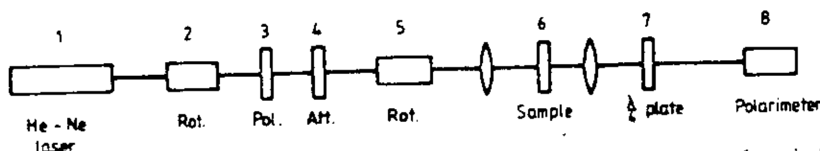

Figure 1. Experimental arrangement for the measurements of light-induced optical anisotropy.

For illumination we used a linearly polarised cw He–Ne laser beam (λ = 6328 Å) which was focused to a Gaussian optical spot, 100–200 μm in diameter. The intensity and the direction of the polarisation of the incident laser beam were regulated with Spectra-Physics polarisation rotators (Model 310-21, nos 2 and 5 in figure 1).

The optical anisotropy was measured with the same laser beam as used for producing the anisotropy but attenuated by a filter (4 in figure 1). The optical characteristics of the outgoing beam were determined by using a polarimeter (8 in figure 1) designed in our institute (Nagy 1978). The polarimeter consists of a Wollaston prism which separates the components of the laser beam polarised parallel and perpendicular to the optical axis of the prism. It measures the intensity ratio of these components. Carrying out measurements with and without a $\lambda/4$ plate (7 in figure 1) and at different directions of polarisation of the incident measuring light beam, the various characteristics of the optical anisotropy of the sample, like rotatory power, birefringence, dichroism and the direction of the principal axes of the index ellipsoid, can be determined. All of the experiments were performed at room temperature.

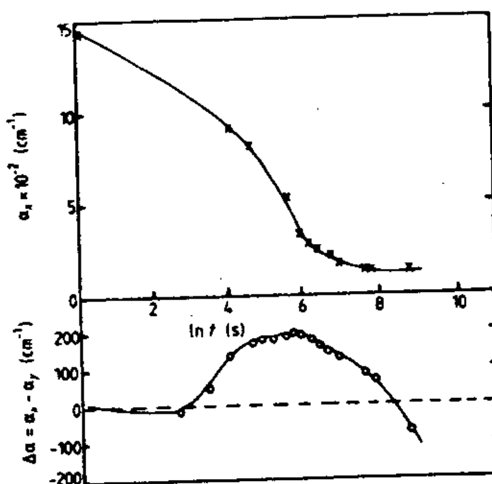

Figure 2. Time dependence of the dichroism and absorption coefficient in a-$GeSe_2$ film. Thickness of the film = 6 μm, incident-laser intensity 50 W cm^{-2}

3. Results

3.1. *Laser-induced dichroism and birefringence in self-supporting $GeSe_2$ films*

In the as-deposited films usually no sign of anisotropy was observed. As a result of laser irradiation both birefringence and dichroism were found systematically. The direction of the principal axes of the index ellipsoid coincided with the direction of the incident-beam polarisation; consequently, no optical activity was induced. Typical curves showing the increase of the laser-induced dichroism and the simultaneous decrease of the absorption coefficient (photobleaching) as a function of time of illumination at a given laser power density are presented in figure 2. As a measure of dichroism we take $\Delta\alpha = \alpha_x - \alpha_y$ where α_x is the absorption coefficient in the x direction (direction of the incident-beam polarisation), α_y is the absorption coefficient in the y direction (perpendicular to x). The dichroism is positive if the absorption coefficient is higher in the direction of incident-beam polarisation. As shown in figure 2, the dichroism is essentially positive for the first period of illumination. This observation is in accordance with the observation of Zhdanov *et al* (1979) where a positive laser-induced dichroism was found in As–Se films. However continuing the laser irradiation for a sufficiently long time we observed that the dichroism reaches a maximum and afterwards decreases again and becomes negative. The time dependence of laser-induced dichroism strongly suggests that at least two distinct processes affecting the absorption should be involved during the illumination. We could not observe any saturation value for the dichroism, while the absorption coefficient approached a stationary value.

As shown in figure 2, during the photobleaching α_x (measured at $\lambda = 6328$ Å) decreases by one order of magnitude. Note that the final equilibrium value of the absorption coefficient is comparable with the laser-induced anisotropy, indicating a very high dichroism.

The details of these processes will be discussed in a separate paper. From now on we concentrate only on the laser-induced birefringence.

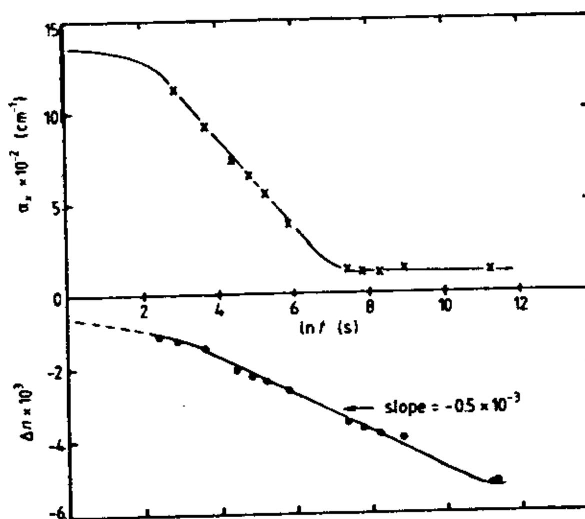

Figure 3. Time dependence of the laser-induced birefringence and absorption coefficient with the same experimental conditions as in figure 2.

The observed birefringence Δn defined as $n_x - n_y$ (the difference in refractive indices measured in the direction of laser polarisation x and perpendicular to it) varies linearly with the logarithm of time of illumination through several orders of magnitude (see figure 3). No change of its sign could be observed in contrast to the case of dichrosim. The logarithmic dependence of birefringence makes it difficult to determine the saturation value. The highest value of the laser-induced birefringence in the self-supporting $GeSe_2$ films observed by us was $\Delta n = 6 \times 10^{-3}$.

It is worth mentioning that the laser-induced anisotropic structure in the amorphous network is stable, at least at room temperature (memory state). No sign of relaxation to the isotropic state was observed keeping the sample in the dark for a few days.

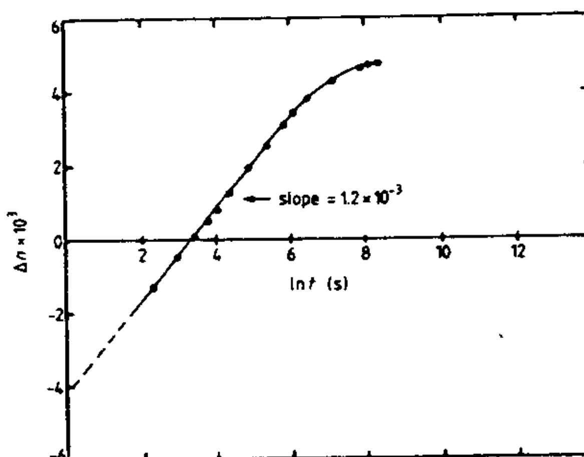

Figure 4. Reorientation of the anisotropy from the x to the y direction on the same spot as used for the measurements in figure 3, with the same experimental conditions.

A remarkable feature of the laser-induced anisotropy is that its principal axis can be reoriented to any direction by changing the direction of incident-beam polarisation. Figure 4 shows an example of reorientation. The experimental results shown in this figure were obtained by continuing the measurement corresponding to figure 3. However the incident-beam polarisation was rotated by 90° with respect to the case shown in figure 3. The initial value of Δn was the same as the final value in figure 3. As a result of irradiation the anisotropy changed its sign and the final absolute value was about the same as in figure 3.

3.2. *Kinetics of reorientation of the laser-induced birefringence*

Most of the reorientation experiments were performed by first orienting the structure in a given direction of polarisation (say the y direction) and then rotating the incident beam by 90° (to the x direction).

We investigated how the direction of the principal axes of the index ellipsoid and the absolute values of the anisotropy of the principal refractive indices vary during the reorientation.

For the two orthogonal principal axes ξ and η (see the inset in figure 5) we have

$$E_\xi^{out} = E_\xi^{in} \exp[i(2\pi/\lambda)n_1 d] \tag{1}$$

$$E_\eta^{out} = E_\eta^{in} \exp[i(2\pi/\lambda)n_2 d] \tag{2}$$

where E^{in} and E^{out} are the electric field vectors of the incoming and outgoing light beams, d is the thickness of the sample, and n_1 and n_2 are the principal refractive indices. To be definite, we consider ξ as the direction to which the smaller principal refractive index belongs (the 'fast axis'; Hartshorne and Stuart (1970)). The birefringence of the sample can be completely described by giving the angle ψ between ξ and x and the value of $n_2 - n_1$. Note that by definition $n_2 - n_1$ is always positive.

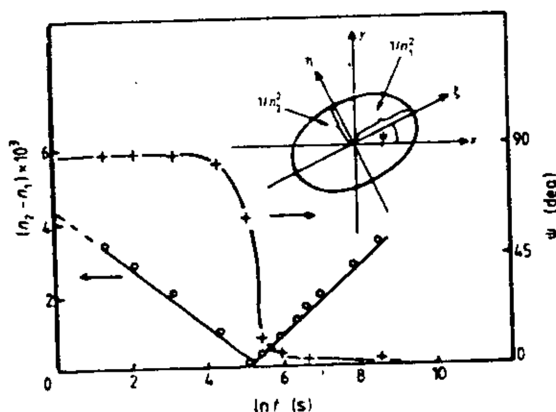

Figure 5. Variation of the 'fast axis' and the difference of the principal refractive indices during the reorientation. The insert shows the index ellipsoid (in W cm^{-2}).

The results are shown in figure 5. As can be seen, at first ψ remains almost constant during the illumination, while $n_2 - n_1$ decreases. At a given time $n_2 - n_1$ becomes practically zero, i.e. the material becomes *isotropic*. On continuing the irradiation the sample again becomes anisotropic ($n_2 - n_1 > 0$) but now ψ is changed by 90°.

It is interesting to note that this type of reorientation, which passes through an isotropic state, is contrary to the laser-induced orientation observed in liquid crystals (Csillag *et al* 1981).

In this latter case $n_2 - n_1$ remains almost constant while ψ changes continuously during the reorientation. The difference arises from the fact that in the case of liquid crystals the reorientation consists of the collective rotation of molecules while in the present case the reorientation takes place through independent atomic events.

As we have seen the x and y axes remain the principal axes during the reorientation process; consequently it is sufficient to use the quantity $\Delta n = n_x - n_y$ for describing the kinetics. $n_x - n_y$ can be positive or negative depending on the orientation of the 'fast axis'.

The time dependence of $n_x - n_y$ in a well defined time interval showed definite logarithmic behaviour (see figure 6) which can be described by the equation

$$n_x - n_y = -A \ln t/t_0. \tag{3}$$

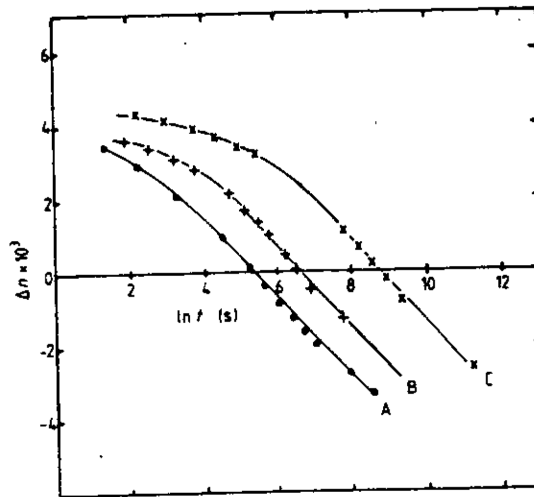

Figure 6. Kinetics of reorientation at different laser intensities, P = (A) 14.6, (B) 7.3, (C) 3.6.

We found this relation empirically in all cases and the slope was independent of the incident-laser power density (see figure 7). This fact indicates that A is determined only by the structure of the amorphous network in $GeSe_2$. However the time at which the sample becomes isotropic (t_0) depends primarily on the incident-laser intensity. As shown in figure 8, t_0 can be written in the form

$$t_0 \sim P^{-s} \quad (4)$$

where P is the laser power density and s is between 2 and 3.

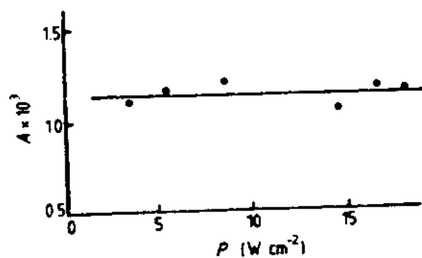

Figure 7. The slope A as a function of laser intensity.

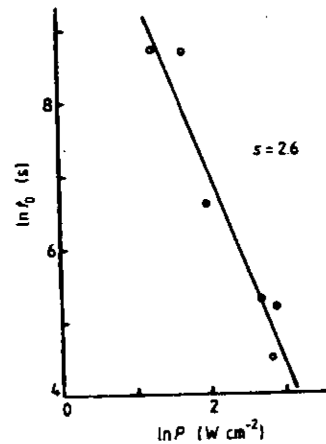

Figure 8. ln t_0 against ln P.

4. Theoretical considerations

4.1. *Considerations about the nature of light-induced anisotropy*

Our experimental results showed that optical anisotropy can be induced by a polarised

laser beam although the structure of $GeSe_2$ remained amorphous; no sign of microcrystallites was observed by simultaneous electron diffraction measurements (Hajtó *et al* 1981). This fact indicates that the phenomenon of optical anisotropy is principally connected to the peculiar structure of the amorphous $GeSe_2$.

It was shown by Phillips *et al* (1980) that the molecular structure of chalcogenide glasses is not an isotropic one on a scale of medium range (30–1000 atoms). There is evidence from x-ray and Raman data (Phillips 1981) that amorphous $GeSe_2$ is built up of large structurally anisotropic units, the so-called 'outrigger rafts', polymerised along one direction. Without any applied external field the directions of the polymerised rafts are distributed randomly on a macroscopic scale; thus the sample is optically isotropic.

We propose a mechanism by which the plane-polarised light can produce optical anistropy on a macroscopic scale. This model is analogous to some extent to the model proposed by Zhdanov *et al* (1979) for the light-induced anisotropy in amorphous As–Se films.

It is assumed theoretically (Mott and Davis 1979) that light can create electron–hole pairs by bond excitation and during the electron–hole recombination an atomic displacement may occur in the amorphous system. As a consequence, a new atomic configuration might be established. We suggest that the 'outrigger rafts' in $GeSe_2$ can continuously rearrange under the influence of laser irradiation in this manner. To explain the development of the optical anisotropy we assume that the cross section for producing an electron–hole pair depends strongly on the angle between the incident-beam polarisation and the excited bond. Thus the stability of a given raft depends on its orientation with respect to the direction of incident-beam polarisation. As a final result of the laser irradiation we obtain an amorphous structure in which there are more polymerised rafts oriented into the more stable direction (determined by the direction of the laser field; see figure 9). This could be the origin of the observed optical anisotropy.

At the present time it is not clear whether the rafts are oriented perpendicular to E (where E is the electric field of the light) as we assumed in figure 9, or oriented parallel to it. Polarised Raman spectroscopy experiments could help in solving this problem.

The whole process would not necessarily be a one-photon reaction. Grigorovici and Vancu (1981) have shown the possibility of a two-phonon reaction for the light-induced polimerisation (photodarkening) in amorphous As–Se films. Our experimental results also suggest (see § 3.2) that reactions involving at least two photons are involved in the displacement of an atom.

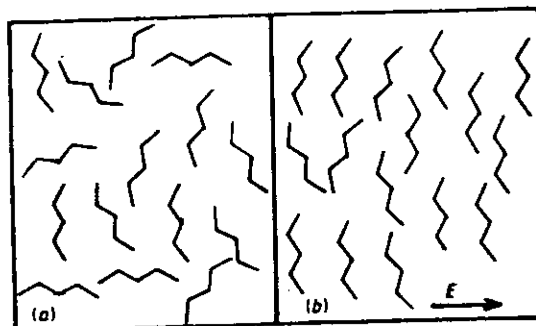

Figure 9. Polymerised rafts in a-GeSe$_2$: (*a*) as-deposited state; (*b*) laser-oriented state

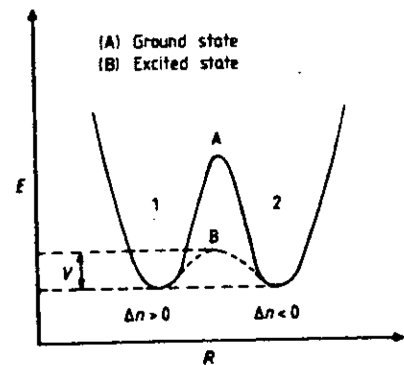

Figure 10. Double-well potential applied to our model

4.2. Model for the light-induced anisotropy

In the following we make the considerations given in the previous section more quantitative.

Let us assume that in the amorphous network there are N sites per unit volume where atoms can displace as a result of laser irradiation. We suppose that in the environment of these sites there are two equilibrium atomic configurations. These configurations will be represented simply by a double-well potential, whose two minima correspond to the two equilibrium positions of the atoms (figure 10). Such a double-well potential model was originally presented for the linear temperature dependence of the specific heat in an amorphous system (Anderson *et al* 1971) and applied by Tanaka (1980) to the photo-structural changes in chalcogenide glasses. Here we consider, for simplicity, symmetric wells.

The two equilibrium configurations correspond to two different contributions to the anisotropy of the refractive indices. We denote by index 1 the minima that correspond to a positive contribution to $\Delta n = n_x - n_y$ (see figure 10). The observed anisotropy according to this model is due to the fact that the atoms are unequally distributed in the two minima. It may be assumed that Δn is proportional to $N_1 - N_2$ where N_1 and N_2 denote the number of atoms per unit volume in the first and second minima respectively ($N_1 + N_2 = N$).

In the ground state the two wells are separated by a barrier whose height is large enough to prevent transitions between the two minima (no thermal relaxation was observed when the sample was kept in dark; see § 3.1). We assume that the laser beam can transfer atoms from one of the minima to the other one in the following way. First the light creates, for example, a metastable electron–hole pair; in this excited state the barrier height is reduced to V (see figure 10) and the displacement of the atoms becomes possible. The probability per unit time of the excitation can be written in the form $\gamma_1 f(P)$ and $\gamma_2 f(P)$ for the first and second minimum respectively; P is the laser power density, and γ_1 and γ_2 are chosen such that $\gamma_1 + \gamma_2 = 1$. The difference, $\gamma_2 - \gamma_1$ reflects the fact that the polarised light beam excites the two configurations with different probabilities. The probability per unit time of a transition between the two minima in the excited state is connected to the barrier height V via $(1/\tau_0)e^{-V/kT}$ (Gilroy and Phillips 1981).

If the barrier height V and the other parameters involved were the same for all sites, the time development of $\Delta N = N_1 - N_2$ would be governed by the simple relaxation equation

$$\tau \mathrm{d}\Delta N(t)/\mathrm{d}t + \Delta N(t) = \Delta N_{eq} \tag{5}$$

with

$$\Delta N_{eq} = (\gamma_2 - \gamma_1) N \qquad \tau = (\tau_0/f(P))\, e^{V/kT}$$

the solution of which is

$$\Delta N(t) = \Delta N(0) + (\Delta N_{eq} - \Delta N(0))(1 - e^{-t/\tau}). \tag{6}$$

However as the effect takes place in an amorphous system it is reasonable to assume that V has a probability distribution (Anderson *et al* 1971). Hence equation (6) should be replaced by

$$\Delta N(t) = \int [\Delta c_0(V) + (\Delta c_{eq}(V) - \Delta c_0(V))(1 - e^{-t/\tau(V)})]\, \mathrm{d}V \tag{7}$$

with $$\Delta c_{eq} = c(V)(\gamma_2 - \gamma_1).$$

Here $c(V)\,dV$ gives the number of sites per unit volume with barrier height between V and $V + dV$; $\Delta c_0(V)\,dV$ is the difference between the number of atoms in the first and second minima at these sites at $t = 0$.

As the sites are not too different from each other, we may imagine that $c(V)$ has a rather sharp maximum at some V_0 and its value is only significant between the energies V_1 and V_2. Let us take for $c(V)$ the simplest possible form that reflects this property:

$$c(V) = \begin{cases} N/(V_2 - V_1) & \text{if } V_1 < V < V_2 \\ 0 & \text{otherwise.} \end{cases} \tag{8}$$

In an as-deposited film we have $c_0 \approx 0$. In this case, differentiating (7) with respect to t and performing the integral over V using the form of $c(V)$ given above we get

$$d\Delta N/dt = \Delta N_{eq}[kT/(V_2 - V_1)]\,(e^{-t/\tau_2} - e^{-t/\tau_1})/t \tag{9}$$

with $\tau_1 = \tau(V_1)$ and $\tau_2 = \tau(V_2)$.

The observed logarithmic time dependence of the birefringence can be explained by assuming that $V_2 - V_1 \gg kT$. In this case a long time interval exists where the inequalities

$$\tau_1 \ll t \ll \tau_2 \tag{10}$$

are satisfied. In this interval $e^{-t/\tau_1} \approx 0$, $e^{-t/\tau_2} \approx 1$, and the solution of (9) is

$$\Delta N(t) \approx \Delta N_{eq}[kT/(V_2 - V_1)]\ln t + C. \tag{11}$$

For the birefringence we have for this time interval

$$\Delta n(t) = -A \ln t/t_0 \tag{12}$$

with

$$A = -g\Delta N_{eq}kT/(V_2 - V_1) \qquad \ln t_0 = gC/A$$

where g is the factor connecting ΔN and Δn.

The reorientation process can be treated similarly. In this case the initial condition can be written as $\Delta c_0 = -\Delta c_{eq}$ (provided that saturation has been reached by the irradiation with the y-polarised light beam). By considerations similar to the above we get

$$\Delta N(t) = 2\Delta N_{eq}[kT/(V_2 - V_1)]\ln t + C \qquad \text{for } \tau_1 \ll t \ll \tau_2. \tag{13}$$

$n(t)$ has the same form as given in (12), but A is now given by

$$A = -2g\Delta N_{eq}[kT/(V_2 - V_1)]. \tag{14}$$

Our model also allows us to treat the influence of an unpolarised or circularly polarised light beam on an area where previously anisotropy had been induced. For an unpolarised light beam $\gamma_1 = \gamma_2$. As can be seen from (5), in this case ΔN decreases in time and its equilibrium value is 0. In other words the unpolarised light beam erases the anisotropy.

5. Comparison of the model with experiment

The model presented in the previous section gives the following results.

(i) The saturation value of the induced birefringence should be independent of the intensity of the light beam. As mentioned, it was hard to determine precise saturation values in our experiments. Nevertheless we found that the increase of the birefringence (measured on a logarithmic time scale) slowed down at $\Delta n = (4\text{–}5) \times 10^{-3}$. This slowing down was observed at somewhat different values of Δn in different measurements, but no definite correlation was found between this value and the laser intensity. The uncertainty in the Δn values at the slowing down could be explained by the assumption that the number of sites per unit volume, N, varies within the sample.

(ii) The model provides an explanation for the observed logarithmic time dependence (see (11) and (12)). The conditions for this kind of dependence can be written as $\tau_1 \ll t \ll \tau_2$. We note that τ_1 and τ_2 can also be estimated from the experiments by regarding the deviations from the logarithmic dependence (see, for example, curve C in figure 6 and the curve in figure 4). This allows us to estimate the value of $V_2 - V_1$, i.e. the spread of the barrier height in the excited state. For this estimation see point (v) below.

(iii) According to (12) and (14) the slope A of $\Delta n(t)$ plotted on a logarithmic time scale should be independent of the light intensity. The experimental verification of this prediction for the reorientation process is given in figure 7.

(iv) The comparison of (12) and (14) shows that the slope A should be twice as large for the reorientation process as for the orientation process in an as-deposited area. This prediction is in a rather good agreement with the experimental results (see figures 3 and 4). We emphasise that the kinetics presented in figures 3 and 4 were measured subsequently on the same spot using the same laser intensity.

(v) The constant C, or equivalently t_0 in (12), depends on the form of the function $f(P)$. Assuming that $f(P) \sim P^s$ (s-photon reaction) the model predicts

$$t_0 \sim P^{-s}.$$

This relation was verified experimentally in § 3.2, the actual value of s was found to be 2.6.

Using this form of $f(P)$ we have

$$\tau_1 \sim P^{-s}\, e^{V_1/kT} \qquad \tau_2 \sim P^{-s}\, e^{V_2/kT}. \tag{15}$$

Estimating, for example, τ_1 from curve C in figure 6 and τ_2 from figure 4, we find, with the help of (15), that $V_2 - V_1$ is of the order of magnitude of 0.1 eV.

(vi) It is evident that anisotropy cannot be induced using unpolarised light. Our model predicts, in addition, that circularly polarised light should erase the previously induced anisotropy. This was indeed found in the experiments.

6. Conclusions

We have presented a comprehensive study of the light-induced anisotropy in $GeSe_2$ films. As shown, both birefringence and dichroism are induced by linearly polarised laser beams. The direction of the principal axis is determined by the direction of the laser polarisation. By changing this latter direction, the previously induced anisotropic structure can be reoriented.

The development of the anisotropic structure can be explained by assuming that anisotropic units, which already exist before the laser irradiation (the 'outrigger rafts' in Phillips' model), become oriented under the influence of the polarised light beam.

Our studies showed clearly that this orientation process cannot consist of collective rotation of these units; it takes place through independent atomic events as a result of which the rafts rearrange. The rather unusual logarithmic time dependence of the orientation and reorientation processes can be explained by the plausible assumption that the heights of the barriers hindering the atomic displacements have an energy distribution whose spread is much larger than kT.

We emphasise once more that these studies were carried out at relatively low power densities ($\simeq 10\ \mathrm{W\ cm^{-2}}$). Studies at higher power densities, where strongly non-linear optical phenomena occur, are under way.

Acknowledgments

We benefitted from useful discussions with Drs N Kroó and L Csillag. One of us (GF) is indebted to W L McMillan for very useful conversations on the theory of amorphous systems.

References

Anderson P W, Halperin B I and Varma C M 1971 *Phil. Mag.* **25** 1
Csillag L, Jánossy I, Kitaeva V F, Kroó N, Sobolev N N and Zolotko A S 1981 *Mol. Cryst. Liq. Cryst.* **78** 173
Gilroy K S and Phillips W A 1981 *Phil. Mag.* B **43** 735
Grigorovici R and Vancu A 1981 *J. Physique* **42** C4 391
Hajtó J 1980 *J. Physique* **41** C4 63
Hajtó J and Ewen P J S 1979 *Phys. Status Solidi a* **54** 385
Hajtó, Radnóczi G, Pogány L and Hajtó E 1981 *Rep. Central Res. Inst. Phys., Budapest* **81** 96
Hartshorne N and Stuart A 1970 *Crystals and the Polarising Microscope* (London: Edward Arnold)
Mott N F and Davis E A 1979 *Electronic Processes in Non-Crystalline Materials* (Oxford: Clarendon)
Nagy Gy 1978 *Rep. Central Res. Int. Phys., Budapest* **78** 789
de Neufville J P 1976 *Optical Properties of Solids, New Developments* ed. B O Seraphin (Amsterdam: North-Holland) p 437
Phillips J C 1981 *J. Non-Cryst. Solids* **43** 37
Phillips J C, Arnold Beevers C and Gould S E B 1980 *Phys. Rev.* B **21** 5724
Tanaka K 1980 *J. Non-Cryst. Solids* **35–36** 1023
Zhdanov V G, Kolomiets B T, Lyubin V M and Malinovskii V K 1979 *Phys. Status Solidi* a **52** 621

J. Physique — LETTRES 43 (1982) L-97 - L-102

1er FÉVRIER 1982, PAGE L-97

Classification
Physics Abstracts
61.40 — 61.50C

Laser induced crystallization of a-Si : H thin films

J. Hajtó, J. Gazsó, G. Zentai and I. Kósa Somogyi

Central Research Institute for Physics, H-1525 Budapest, P.O. Box 49, Hungary

(Reçu le 7 septembre 1981, révisé le 23 novembre, accepté le 4 décembre 1981)

Résumé. — La cristallisation des films amorphes de a-Si : H peut être induite par un faisceau Ar-ion laser continu. La comparaison des résultats de l'expérience avec la résolution de l'équation de la densité de flux thermique montre que le maximum de température au cours de la cristallisation est voisin de 770 °C, considérablement plus bas que le point de fusion du silicium amorphe.

Abstract. — Crystallization in amorphous silicon thin films can be induced by irradiation from a continuous Ar-ion laser. Comparison with the solution of the heat-flow equation shows that the maximum temperature during the crystallization is about 770 °C, well below the melting temperature of the material.

1. **Introduction.** — There is a widespread current interest in laser annealing of silicon thin films and other semiconductor thin films [1-2]. The overwhelming majority of this kind of research is, however, connected with crystalline substances, and laser annealing experiments on originally amorphous films are scarcely mentioned [3]. Dangling bonds present both in the amorphous and in the crystalline states are thought to have detrimental effects on device performance. These dangling bonds arise out of disorder, i.e. throughout the volume of the amorphous phase and at the grain boundaries of the polycrystalline material. It has been realized for some time that hydrogen is efficient in passivating these dangling bonds [4-5].

Preparation of polycrystalline Si films with passivated dangling bonds may be performed through crystallization of hydrogenated amorphous films. It was reported that heat treatment of evaporated a-Si above 600 °C resulted in crystallization [6]. Local heating of the a-Si : H film by appropriate laser irradiation could lead to crystallization, too. The Q-switched laser pulse technique is favoured just because it may be then argued that the crystallization process takes place on a time scale short compared with typical hydrogen diffusion times. We thought that quasi-stationary crystallization (i.e. on a time scale of seconds) induced by a continuous laser though not as efficient as the Q-switched pulse technique still might have advantages over the rather slow conventional heat treatment, where even the much thicker substrate had to be heated up. In our experiments we were able to observe the induced crystal growth under steady state conditions, and to demonstrate convincingly that melting necessitates higher power densities. In addition, we could estimate the maximum temperature during the respective processes from the solution of the heat-flow equation.

2. **Experimentals.** — Amorphous hydrogenated silicon (a-Si : H) films were deposited on fused silica substrates of thickness $d_s = 1.5$ mm using the now familiar glow discharge decomposition of SiH_4 in a capacitively coupled reaction chamber similar to those described in the literature [7]. The amorphous films referred to in this study were grown to thickness $d = 200$ nm at substrate temperature $T_s = 250$ °C. The chamber atmosphere consisted of 0.5 torr (0.67 mbar) Ar and 0.33 torr (0.44 mbar) SiH_4, and the rate of the film growth was kept at 0.5 nm/s. Measurements on the optical and the electrical properties indicated parameters comparable to those reported by other laboratories using similar deposition techniques. Figure 1, curve 2 shows the dependence of the absorption coefficient α on the photon energy $h\nu$ in the amorphous state. (The measurements were carried out on a CARY-17D Spectrophotometer.) Curve 3 in figure 1

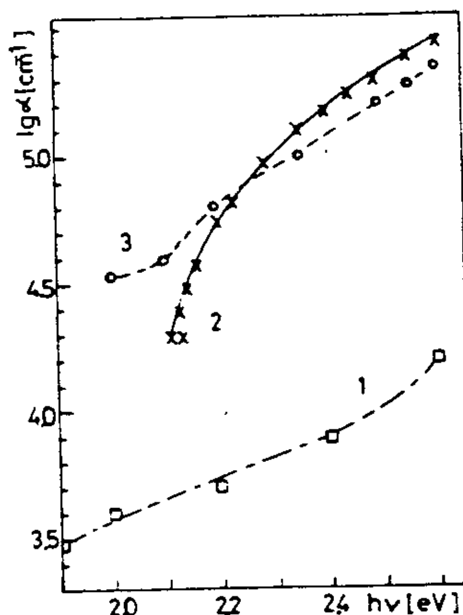

Fig. 1. — The logarithm of the absorption coefficient α in Si *versus* photon energy $h\nu$. Curve 1 : single crystal [7]; 2 : amorphous film; 3 : polycrystalline layer obtained by laser irradiation.

shows the corresponding function for layers crystallized by continuous laser irradiation, the shape of which being very similar to that of curve 1, obtained for single crystal [8]. The one order of magnitude shift upwards is by all probability caused by internal losses on the grain boundaries within the films.

To obtain permanent phase changes induced by irradiation, a cw Ar-ion laser was applied which could provide four wavelengths : λ = 514.5, 496.5, 488.0 and 476.5 nanometers, respectively. We were searching for threshold values in the irradiating power densities at which the desired phase transition (crystallization or melting) just started to take place in the duration of sufficiently long times (tens of seconds) after the irradiation had been focussed onto the investigated volume element. The parallel laser beam was focussed into a converging conical beam with the help of a lens of 5 cm focal length. We assume that the radial distribution of the laser beam intensity is of the Gaussian form :

$$I(r) \sim \exp(-r^2/s^2) . \quad (1)$$

Hence s will be called the « radius » of the laser beam. In order to facilitate observation a magni-

fying system of lenses was mounted behind the sample, and it projected the enlarged picture of the irradiated spot onto a screen. Thus the resolution power of the system was of the order of 1 μ (i.e. the features of the projected picture which could be distinguished by the naked eye corresponded to actual sizes of the order of 1 μ). The irradiated spot diameter could be altered easily by displacing the focussing lens relative to the sample.

The first effect to observe was permanent photodarkening, which is supposed to be connected with the exodiffusion of hydrogen (see e.g. [9]). Typical values for the power density are 75 mW on a spot of 40 microns in diameter. Photodarkening accompanied the crystallization experiments.

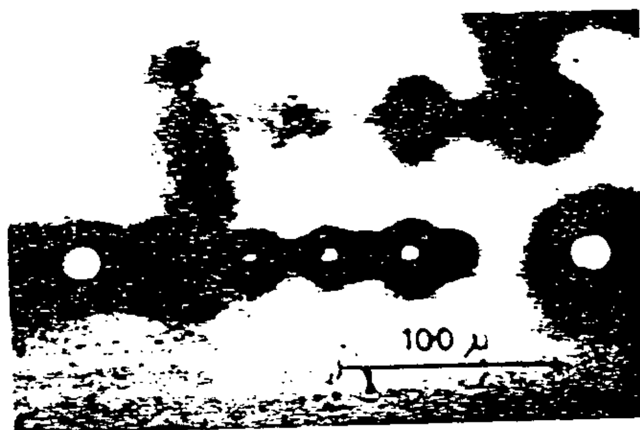

Fig. 2. — Photodarkening and crystallization in a-Si : H films

Figure 2 shows a picture where besides the spots photodarkened only are others which contain crystals in their centre (i.e. the cornered light spots). The typical power density necessary for induced crystallization was found to be about 150 mW on spots of 40 μ in diameter. It was informative to learn that a definite threshold did exist in each case, to a fairly good degree of reproducibility. We think it important to note that we could not find any sign of the so-called « explosive crystallization » [10]. This effect, if present, would appear spectacularly : as soon as a tiny piece of the amorphous film had been transformed into crystalline state with the help

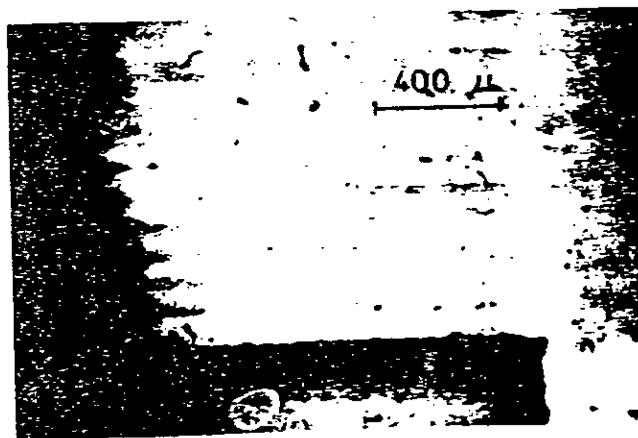

Fig. 3. — Crystallized strips in Si by the cw laser technique λ = 514.5 nm : spot diameter = 120 μ ; incident power = 300 mW ; lateral speed = 26 μ/s.

of the external forces (i.e. with the laser irradiation in our case) then the crystallization front would propagate radially outward spontaneously the driving force being the latent heat of crystallization. In our case we found, on the contrary, that the final size of the crystal depended on the incident power distribution. Relatively large crystals (~ 25 μ) could be produced by broader spots (Fig. 2). Even extended areas could be transformed into crystalline state by the slow movement of the Si film in its plane. For details, see figure 3.

Next we tried to establish the threshold necessary for melting the crystal already present in the middle of the irradiated spot. It can be achieved by either increasing the incident power or by reducing the diameter of the irradiated spot or by a combination of both. When melting eventually occurs, it must be then the melting point of the crystalline Si which is known to be 1 410 °C. We found that the input power had to be sufficiently increased if the spot diameter was kept the same (40 μ) : 285 mW was needed for melting as contrasted with the 150 mW for crystallization.

3. **Considerations based on solution of the heat-flow equation.** — Owing to the stationary nature and the cylindrical symmetry of the problem, in our case the general heat-flow equation reduces to the steady state form

$$\kappa_i \, \Delta T(r, z) = - \rho_i(r, z) . \tag{2}$$

Here Δ represents the Laplace-operator in cylindrical coordinates, the index i specifies the medium ($i = 1$ for the amorphous film and $i = 2$ for the substrate), κ_i stands for the thermal conductivity, and ρ_i is the absorbed power density. Since the substrate is transparent,

$$\rho_2 = 0 . \tag{3}$$

It is of great importance that ρ_1 can be factorized :

$$\rho_1(r, z) = \alpha I_0 . \exp(- \alpha z) . \exp(- r^2/s^2) . (1 - R)/\pi s^2 \tag{4}$$

where I_0 is the incident beam power and R is the reflectivity of the semiconductor surface. It can be shown that the contribution of the infinitesimal layer at $(z', z' + dz')$ to the particular solution of the inhomogeneous equation $T_{IH}^{(1)}$ is of the form [11] :

$$\varphi(r, z, z') \, dz' = \int_0^\infty k . J_0(kr) . f(k) . e^{-k|z-z'|} \, dk . dz' \tag{5}$$

where $J_0(kr)$ is the Bessel function of order zero, and

$$f(k) = \frac{\alpha I_0 (1 - R)}{2 \kappa_1 s^2} \int_0^\infty r' . e^{-r'^2/s^2} . J_0(kr') . dr' \tag{6}$$

which, in turn simplifies to :

$$f(k) = \frac{\alpha I_0 (1 - R)}{4 \pi \kappa_1} \exp(- s^2 k^2/4) . \tag{7}$$

Then

$$T_{IH}^{(1)}(r, z) = \int_0^d \varphi(r, z, z') \, e^{-\alpha z'} \, dz' \tag{8}$$

while the general solution to the homogeneous equation is of the form :

$$T_{H}^{(i)}(r, z) = \int_{0}^{\infty} f(k).J_0(kr).[a_i\, e^{kz} + b_i\, e^{-kz}]\, dk . \tag{9}$$

The expansion coefficients a_i, b_i are to be found from the appropriate boundary conditions :

$$\frac{\partial}{\partial z} T_{H}^{(2)}(z = \infty) = 0 \tag{10}$$

$$T_{IH}^{(1)} + T_{H}^{(1)} = T_{H}^{(2)} \qquad \text{at } z = d \tag{11}$$

$$\kappa_1 \cdot \frac{\partial}{\partial z}[T_{IH}^{(1)} + T_{H}^{(1)}] = \kappa_2 \frac{\partial}{\partial z} T_{H}^{(2)} \quad \text{at } z = d \tag{12}$$

and

$$\frac{\partial}{\partial z}[T_{IH}^{(1)} + T_{H}^{(1)}] = 0 \qquad \text{at } z = 0 . \tag{13}$$

The neglect in (10) and in (13) of heat-flow by radiation or by the thermal conductance of the ambient air can be justified by their much less magnitude compared to the typical values of κ_1 and κ_2. In this context we must admit that while there are data published for crystalline silicon, we could not find any for amorphous Si. On the other hand, κ_2 for the fused silica is well studied [12], and there are general arguments [13] that the thermal conductivities of the amorphous substances may not differ too much. Therefore we chose for simplicity

$$\kappa_1 = \kappa_2 = 4 \times 10^{-3} \text{ cal. cm s} .$$

The reflectivity was regarded as independent of temperature ($R = 0.39$).

Figure 4 shows the maximum temperature increase ΔT_{max} as function of the absorption coefficient computed along these lines, for the particular case of $s = 20\ \mu$ and $I_0 = 100$ mW.

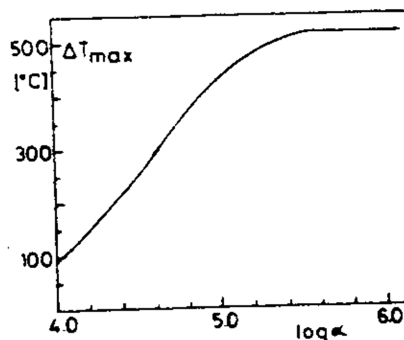

Fig. 4. — Computed values of the maximum temperature increase in a-Si : H films *versus* logarithm of α. (Thickness $d = 200$ nm, spot radius $s = 20\ \mu$, input power $I_0 = 100$ mW, reflectance $R = 0.39$.)

It is apparent that above $\alpha = 10^5\ \text{cm}^{-1}$ the peak temperature is insensitive to the exact value of α. This corresponds to our experimental findings. It turns out that the maximum temperature in the spot when crystallization sets in is about 770 °C. The corresponding values for darkening and for melting are 400 °C and 1 450 °C, respectively. This latter agrees well with $T_m = 1\ 410$ °C.

4. **Summary.** — The cw laser annealing can locally produce (i.e. the crystallization remains localized) hydrogenated polycrystalline Si from a-Si : H layers obtained by glow discharge method. Our experimental findings and numerical calculations show that no melting occurs during the cw laser induced crystallization in good accordance with the previous measurements [6, 15].

The average size of grains is not less than 2 µm and strongly depends on the experimental conditions. There are indications that the grain size can exceed 100 µm as verified by polarized microscope measurements which seems to be promising in view of better photovoltaic conversion efficiency [14] in solar cell applications. It may be noted that, in contrast to the observations on cw laser annealing of rf sputtered a-Si [15], there was no sign of surface deterioration in our samples caused by explosive hydrogen release.

Acknowledgments. — The authors are indebted to Mr. G. Pesti and Mr. L. Takács for their kind assistance.

References

[1] *Laser and electron beam processing of materials*, edited by C. W. White and P. S. Peercy (Academic Press, New York) 1980.
[2] ANDREW, R., BANFAY, L., LAUDE, L. D., LOVATO, M. and WAUTELET, M., *J. Physique Colloq.* **41** (1980) C4-71.
[3] SUSSMAN, R. S., HARRIS, A. J. and OGDEN, R., *J. Non-Cryst. Solids* **35-36** (1980) 249.
[4] PANKOVE, J. I., LAMPERT, M. A. and TARNG, M. L., *Appl. Phys. Lett.* **32** (1978) 439.
[5] SEAGER, C. H. and GINLEY, D. S., *Appl. Phys. Lett.* **34** (1979) 337.
[6] THOMAS, B. A., BRODSKY, M. H., KAPLAN, D. and LEPINE, D., *Phys. Rev. B* **18** (1978) 3059.
[7] CHITTICK, R. C., ALEXANDER, J. H. and STERLING, H. F., *J. Electrochem. Soc.* **116** (1969) 77.
[8] DASH, W. C. and NEWMAN, R., *Phys. Rev.* **99** (1955) 1151.
[9] ZELLEMA, K., GERMAIN, P., SQUELARD, S. and MONGE, J., *J. Non-Cryst. Solids* **35-36** (1980) 225.
[10] MINEO, A., MATSUDA, A., KUROSU, T. and KIKUCHI, M., *Solid State Commun.* **13** (1973) 329.
[11] IVANENKO, D. and SOKOLOV, A., *Classical theory of fields* (Moscow) 1951, p. 45.
[12] *Handbook of thermophysical properties of solid materials*, vol. **3**, p. 895, editors : Goldsmith, A., Waterman, T. E. and Hirschhorn, H. J. (Pergamon, Oxford) 1961.
[13] STEVELS, J. M., *Handbuch der Physik*, Editor : S. Flügge (Springer, Berlin) Vol. **13**, 1962, p. 576.
[14] HOVEL, H. J., *Solar cells (Semiconductor and semimetals)* (Academic Press, N. Y.) 1975, p. 103-109.
[15] THOMAS, J. P. and FALLAVIER, M., *J. Appl. Phys.* **52(1)** (1981) 476.

Commission paritaire N° 59.024

Editions de Physique 1982 — Directrice de la Publication : Jeanne BERGER

Imprimé en France. — Imprimerie JOUVE, 18, rue Saint-Denis, 75001 PARIS
Dépôt légal : Janvier 1982

Photostimulated processes in glassy arsenic and germanium chalcogenides

A. V. Kolobov, B. T. Kolomiets, V. M. Lyubin, N. Sebastian,[1)] M. A. Tagirdzhanov, and J. Hajto[2)]

A. F. Ioffe Physicotechnical Institute, Academy of Sciences of the USSR, Leningrad

(Submitted October 27, 1981)

Fiz. Tverd. Tela (Leningrad) 24, 1062–1067 (April 1982)

A parallel investigation was made of photostimulated processes in glassy chalcogenide semiconductors of the As–Se and Ge–Se systems. In both systems the processes have irreversible and reversible componets. It is shown that the main features of the reversible components are the same for both systems, whereas the irreversible component is manifested in different ways for the two systems. The configurational model proposed earlier is generalized to both systems of glassy chalcogenide semiconductors.

PACS numbers: 61.40.Df, 79.20.Ds, 78.20.Dj, 71.25.Tn

Photostimulated changes in the properties of glassy chalcogenide semiconductors have been the subject of numerous investigations.[1–4] Illumination alters many properties (band gap, refractive index, microhardness, rates of dissolution in various etchants, etc.), whereas annealing restores the original properties. These properties are manifested most clearly by glassy chalcogenide semiconductors belonging to the As–Se system, for which the changes in the parameters are the largest observed.[4] More recently there has been increasing interest in photostimulated processes in glassy chalcogenide semiconductors belonging to the Ge–Se system,[5] but up to now the system has not been investigated sufficiently thoroughly. The data obtained by different authors are contradictory. For example, illumination of freshly prepared samples of this system has been observed to induce both darkening and an increase in the transparency of these materials.[5,6] Comparisons of the photostimulated processes in the As–Se and Ge–Se systems have revealed differences between them,[5] but certain general features, such as the parallel changes in the optical properties and solubility,[7] support the hypothesis that the photostimulated processes in different systems of glassy chalcogenide semiconductors have the same origin.

This makes it desirable to carry out a parallel study of the photostimulated processes in both the above systems in order to establish the common features as well as the differences between the photoinduced changes in the parameters of glassy chalcogenide semiconductors belonging to different groups.

1. EXPERIMENTAL METHOD

We investigated materials with the stoichiometric compositions As_2Se_3 and $GeSe_2$. Samples were prepared by thermal evaporation of a compound on oxide glass substrates in 10^{-5} torr vacuum. The substrate temperature during such evaporation was 300°K. The film thickness ranged from 0.5 to 2.0 μ.

The basic measurement system had the form shown in Fig. 1. A sample was placed in a combined heater and cryostat, where temperature could be varied from 77 to 500°K, and it was illuminated with light from an He–Ne (λ = 633 nm) or Ar (λ = 488 nm) laser causing photostimulated processes. The transmission spectra were recorded with the aid of an MDR-3 monochromator.

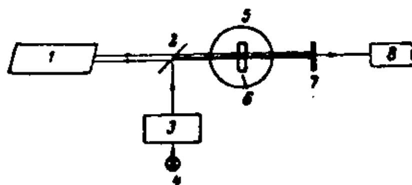

FIG. 1. Schematic diagram of the apparatus: 1) laser; 2) mirror; 3) MDR-3 monochromator; 4) lamp; 5) combined heater and cryostat; 6) sample; 7) selective filter; 8) recording system.

2. EXPERIMENTAL RESULTS

Figures 2 and 2b show the transmission spectra of As_2Se_3 and $GeSe_2$ films. In both cases curve 1 represents the position of the transmission edge of a freshly prepared film. Illumination of such films at room and liquid nitrogen temperatures shifted the transmission edge to the positions represented by curves 2 and 3, respectively.

The position of the transmission edge of the annealed films is represented by curve 4. Illumination of such annealed films (at room temperature) shifted the transmission edge to the position of curve 2 and subsequent annealing displaced the edge back to the position 4.

The results in Fig. 2 thus demonstrate the effects of illumination and temperature on the position of the transmission edge of freshly prepared and annealed As_2Se_3 and $GeSe_2$ samples. We shall now consider the results in greater detail.

a) Annealed Samples

We can see that illumination shifts the transmission

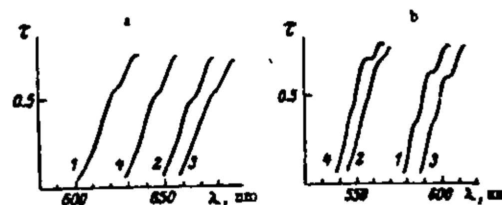

FIG. 2. Transmission spectra of As_2Se_3 and $GeSe_2$ films.

0038-5654/82/04 0603-03 $02.40
© 1982 American Institute of Physics

edge of the annealed films of both systems in the same direction of longer wavelengths, i.e., photoinduced darkening (4 → 2) is observed. Annealing restores the optical transmission (2 → 4). It is worth noting the difference between As_2Se_3 and $GeSe_2$. In the case of As_2Se_3 a complete recovery of the properties occurs at a temperature $T_r \sim 430$°K, which is of the order of the softening temperature $T_g \sim 470$°K, whereas in the case of $GeSe_2$ a complete recovery occurs at $T_r \sim 480$°K, which is considerably less than the softening temperature $T_g \sim 650$°K. We are regarding a temperature as the recovery temperature if the original parameters are restored in 3-5 min.

b) Freshly Prepared Samples

Illumination of freshly prepared As_2Se_3 and $GeSe_2$ samples has different effects on their properties. For example, at room temperature the transmission edge of As_2Se_3 shifts toward longer wavelengths (photoinduced darkening 1 → 2, Fig. 2a); on the other hand, $GeSe_2$ exhibits a shift of the transmission edge toward shorter wavelengths (photoinduced increase in the transmission 1 → 2, Fig. 2b). It is important to note also that the shift of the transmission edge caused by illumination is in the same direction as that caused by annealing: An increase in the transmission occurs in the case of annealing of $GeSe_2$ (1 → 4) and darkening in the case of As_2Se_3 (1 → 4, Fig. 2b). Moreover, the changes in the transmission of the illuminated samples as a result of subsequent annealing are also different. In the case of As_2Se_3 a partial recovery of the initial transmission (2 → 4) takes place whereas annealing of $GeSe_2$ enhances the shift of the transmission edge toward shorter wavelengths (2 → 4, Fig. 2b), i.e., it does not restore the initial transmission but enhances the illumination-induced change.

A study of the dependence of the photostimulated shift on the temperature during illumination shows that in the case of As_2Se_3 the photoinduced darkening increases as a result of cooling (interval 1−3 is longer than 1−2, Fig. 2a), but the photodarkening time then increases; on the other hand, an enhancement of the transmission in the case of $GeSe_2$ decreases as a result of cooling and at 77°K it disappears[3)] being replaced by photodarkening (1−3). This low-temperature photodarkening of $GeSe_2$ is fully reversible: at room temperature after ~3 min the initial transmission is recovered completely (3 → 1). [We recall that in previously annealed $GeSe_2$ samples the recovery process (2−4) occurs at a much higher temperature.]

It is worth noting another feature of unannealed $GeSe_2$ revealed in a study of the kinetics of the photostimulated

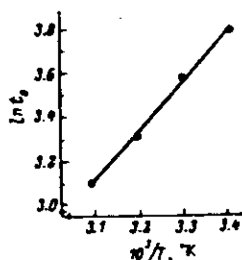

FIG. 3. Temperature dependence of the time constant of the process of increase in the transmission of freshly prepared $GeSe_2$ films.

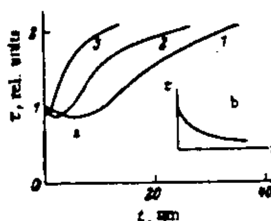

FIG. 4. Kinetics of changes in the transmission of freshly prepared $GeSe_2$. The results for As_2Se_3 are shown in the inset. I (mW/cm²): 1) 50; 2) 150; 3) 500.

processes. Figure 4a shows the changes in the transmission of such samples with time; at room temperature the transmission first decreases and this is followed by an increase in the transmission only after a certain time interval has passed. As the illumination intensity is increased, the process becomes accelerated and the initial stage (darkening) ceases to be significant.

In the case of As_2Se_3 samples the transmission varies monotonically (Fig. 4b).

3. DISCUSSION OF RESULTS

a) Annealed Samples

The process of reversible photodarkening in both systems occurs in qualitatively the same manner and can be discussed using the configurational model (for details see, for example, Refs. 4, 8, and 9) of two stable structural states of the atomic sites in glassy chalcogenide semiconductors between which thermal and optical transitions take place (Fig. 5). Curve 1−1 describes an atomic site in the ground state. Under the influence of light we can expect a transition to a metastable state described by curve 2−2. The ratio of the atomic sites in the ground and metastable states determines, as in a solid solution, the structure of matter and its physicochemical parameters. Heating results in a reverse transition to the ground state accompanied by a recovery of the initial properties of glassy chalcogenide semiconductors. The parameters of the configurational curves are different for different materials, but they are governed by the chemical nature of the atoms of a given substance.[4,8,9]

b) Freshly Prepared Samples

As pointed out above, illumination of freshly prepared As_2Se_3 and $GeSe_2$ films produces opposite changes in the transmission and the shifts are in the same direction as those produced by the annealing of films. This last observation suggests that both annealing and illumination of freshly prepared films have the same result: composition ordering of the films. It is known[10] that in the case of freshly prepared films there is a sufficient number of "irregular" bonds: As−As and Se−Se in the case of As_2Se_3 films, and Ge−Ge and Se−Se in the case of $GeSe_2$

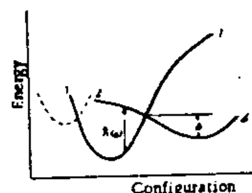

FIG. 5. Configurational diagram.

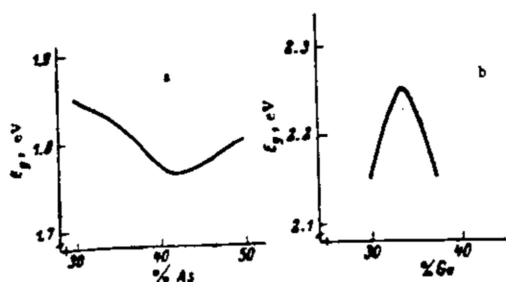

FIG. 6. Composition dependences of the band gaps of the As–Se (a) and Ge–Se (b) systems.[11]

films. Such local deviations from stoichiometry may alter the band gap of the material.

The composition dependences of the band gaps of the As–Se and Ge–Se systems taken from Ref. 11 are plotted in Fig. 6. We can see that in the case of the Ge–Se system such deviations from stoichiometry reduce the band gap, whereas in the case of As–Se they increase this gap. Consequently, composition ordering under the influence of light results either in darkening (As_2Se_3) or in an increase in the transmission ($GeSe_2$) of the films. A similar mechanism has been considered earlier in the case of annealing.[11]

A structural transition under the influence of light from a state representing a freshly prepared sample can also be included in the configurational model (dashed curve in Fig. 5). This approach has been used in Ref. 12 in discussing irreversible structural changes in the As–S system.

The fact that the recovery temperature of $GeSe_2$ depends on the previous thermal history of a sample may also be due to the presence of "incorrect" Ge–Ge and Se–Se bonds, if we assume that the reversible photodarkening is due to the Se–Se bonds. Such an assumption follows from a comparison of the recovery processes in freshly prepared $GeSe_2$ and in elemental glassy selenium[4]: in both materials the recovery at room temperature occurs in the same time of a few minutes. In the case of freshly prepared samples the local deviations from stoichiometry are stronger. Annealing of the structure makes it more ordered, the number of the Se–Se bonds decreases, and consequently the lattice becomes more "rigid." In the configurational model this circumstance increases the parameter Δ (Fig. 5) responsible for the thermal erasure (Ref. 4).

The characteristics of the kinetics of changes in the transmission of freshly prepared $GeSe_2$ samples (darkening is observed during the initial stage) may be due to the opposite directions of the reversible and irreversible components of the photostimulated process. In the case of As_2Se_3 both components cause structural changes which reduce the transmission and, therefore, illumination results in a monotonic reduction in the transmission. It should be noted that when glassy chalcogenide semiconductors containing arsenic are prepared by a special technology, they also exhibit nonmonotonic changes in the absorption coefficient.[13]

It follows that both glassy chalcogenide systems exhibit the reversible and irreversible components of the photostimulated processes. The reversible component is basically the same for both systems and it is described well by the configurational model which allows for transitions of atomic sites between various structural states. The irreversible component, which is very different for the two systems, may be due to compositional ordering of the material under the influence of illumination.

It follows from the results obtained that in the case of different systems of glassy chalcogenide semiconductors the photostimulated changes in the optical properties are due to the same mechanism of photostructural transitions. This conclusion is also confirmed by the fact that, in the case of the Ge–Se as well as the As–Se and As–S systems, the photostimulated changes in the optical properties are accompanied by changes in the physicochemical properties, particularly in the solubility,[14] which are attributed to changes in the polymer structural matter.[15] Consequently, in the case of the photostimulated processes in the Ge–Se system we can use the approach developed earlier for glassy chalcogenide semiconductors containing arsenic. Materials of the Ge–Se system have on important advantage: they do not contain arsenic, which is a toxic material.

We recall that all the results obtained apply to stoichiometric materials. It is very likely that in the case of nonstoichiometric samples of both systems, in which there are considerable changes (compared with the stoichiometric materials) in the ratio of the reversible and irreversible components,[14] the differences may be much greater. This requires separate study.

[1)]Technical University, Dresden, West Germany.
[2)]Central Physics Research Institute, Budapest, Hungary.
[3)]A study of the temperature dependence of the rate of increase in the transmission induced by illumination with light of the 633 nm wavelength makes it possible to estimate the activation energy: $w \sim 0.2$ eV (Fig. 3).

[1]B. T. Kolomiets and V. M. Lyubin, Mater. Res. Bull. 13, 1343 (1978).
[2]K. Tanaka, J. Non-Cryst. Solids 35–36, 1023 (1980).
[3]P. Suptitz, Proc. Second Intern. Symposium on Model Investigation of Photographic Processes and New Photoregistering Systems, Varna, 1980, Part 2, p. 6.
[4]V. L. Averianov, A. V. Kolobov, B. T. Kolomiets, and V. M. Lyubin, Phys. Status Solidi A 57, 81 (1981).
[5]L. Toth, J. Hajto, and G. Zentai, Solid State Commun. 23, 185 (1977).
[6]V. Zieber, P. Suptitz, G. Liebmann, and N. Sebastian, Pis'ma Zh. Tekh. Fiz. 6, 250 (1980) [Sov. Tech. Phys. Lett. 6, 109 (1980)].
[7]P. Suptitz and N. Sebastian, Defects in Insulating Materials [in Russian], Riga (1981), p. 360.
[8]A. V. Kolobov, B. T. Kolomiets, O. V. Konstantinov, and V. M. Lyubin, J. Non-Cryst. Solids 45, 335 (1981).
[9]V. L. Averyanov, A. V. Kolobov, B. T. Kolomiets, and V. M. Lyubin, J. Non-Cryst. Solids 45, 343 (1981).
[10]R. J. Nemanich, G. A. N. Connell, T. M. Hayes, and R. A. Street, Phys. Rev. B 18, 6900 (1978).
[11]R. A. Street, R. J. Nemanich, and G. A. N. Connell, Phys. Rev. B 18, 6915 (1978).
[12]V. Strom and T. P. Martin, Solid State Commun. 29, 527 (1979).
[13]B. T. Kolomiets, V. M. Lyubin, and V. A. Fedorov, Pis'ma Zh. Tekh. Fiz. 5, 3 (1979) [Sov. Tech. Phys. Lett. 5, 1 (1979)].
[14]S. B. Gurevich, N. N. Ilyashenko, B. T. Kolomiets, V. M. Lyubin, and V. P. Shilo, Phys. Status Solidi A 26, K127 (1974).
[15]V. M. Lyubin, Structure and Properties of Noncrystalline Semiconductors (ed. by B. T. Kolomiets) [in Russian], Nauka, Moscow (1976), p. 415.

Translated by A. Tybulewicz

PHILOSOPHICAL MAGAZINE B, 1983, VOL. 47, NO. 4, 347-366

Optical bistability observed in amorphous semiconductor films

By J. HAJTÓ† and I. JÁNOSSY
Central Research Institute for Physics, H-1525 Budapest, P.O. Box 49, Hungary

[Received 28 June 1982 and accepted 30 November 1982]

ABSTRACT

The optical properties of amorphous self-supporting $GeSe_2$ films show strong non-linear behaviour under the influence of relatively low-intensity c.w. laser irradiation. Discontinuities, bistability and, in special circumstances, oscillation in the optical properties have been found. The importance of thermal effects is experimentally proved. A theoretical model is constructed which explains some of the experimental findings. Evidence is presented, however, that, as well as thermal effects, photostructural changes also play an important role in the bistability and oscillatory phenomena.

§ 1. INTRODUCTION

In recent years there has been great interest in optical bistability, which may have potential applications in integrated optics. The effect was first discussed by Szöke, Daneu, Goldhar and Kurnit (1969), and first observed in vapour by Gibbs, McCall and Venkatesan (1976). More recently optical bistability has been found in different crystalline semiconductors (Gibbs, McCall, Venkatesan, Gossard, Passner and Wiegmann 1979, Miller, Smith and Johnston 1979). A review of the present experimental and theoretical situation is given by Abraham and Smith (1982).

Recently we reported that transmission oscillations occur in amorphous semiconductors under the influence of a c.w. laser beam of fixed intensity. This phenomenon was observed both in a-$GeSe_2$ films (Hajtó, Zentai and Kósa Somogyi 1977) and in bulk samples of As_2S_3 (Hajtó and Ewen 1978). The aim in this paper is to report a comprehensive study of non-linear optical phenomena in amorphous *self-supporting* $GeSe_2$ films. The oscillation of the optical properties in self-supporting films occurs only in very restricted circumstances. On the other hand, optical bistability and hysteresis was found. The experiments summarized in this paper help to clarify the underlying mechanism which causes non-linear optical phenomena.

Previously suggested mechanisms for crystalline semiconductors (Gibbs *et al.* 1979, Miller, Seaton, Prise and Smith 1981) cannot operate in our case. This is evident from the fact that if the film is crystallized (e.g. by an intense

† Present address: University of Edinburgh, Department of Electrical Engineering, The King's Buildings, Edinburgh EH9 3JL, Scotland.

laser beam) the observed non-linearities disappear. Therefore we confine our attention to other types of non-linear interaction between the laser field and the amorphous material.

Recently Fazekas (1981) has proposed a theoretical model in order to explain this peculiar non-linear behaviour of semiconductor films. The model is based on the cooperative mechanism of charge disproportionation of defect centres in an amorphous network. In this model electronic processes are dominant and thermal effects are neglected.

In the present paper we consider an alternative explanation in which laser heating produces the observed optical anomalies. In our model the laser beam is considered as a source of local heating only, and the direct non-linear coupling between the laser field and the electronic and atomic structure of the medium is neglected. This is the opposite limit to that considered by Fazekas (1981) but, as we shall demonstrate, our model is also able to explain the observed anomalies in the optical properties of the films.

We emphasize, however, that we do not think that thermal effects are the only source of the observed phenomena. We present in this paper experimental evidence that another effect, namely laser-induced photostructural changes, also plays an important role. It is probable that all three of the effects described above (electronic, thermal and photostructural) are acting simultaneously under the influence of illumination.

The paper is organized as follows: in § 2 we describe the experimental arrangement, § 3 contains the experimental results on self-supporting $GeSe_2$ films, the theoretical considerations are presented in § 4, and § 5 contains some final conclusions.

§ 2. Experimental arrangement

The a-$GeSe_2$ films were prepared by vacuum evaporation from a Ta boat at a pressure of 2×10^{-6} Torr ($2{\cdot}7 \times 10^{-4}$ Pa) onto glass substrates using polycrystalline $GeSe_2$ ingots as an evaporation source. For the measurements the films were removed from the glass substrates using an ultrasonic bath in order to reduce the effects of multiple light reflections and of mechanical stresses occurring at the $GeSe_2$–substrate interface.

For the measurements the films were placed in a sample holder, as shown in the inset of fig. 1. This arrangement allowed us to carry out optical measurements and regulate the temperature of the films. In the following, by the 'film temperature', T_F, we mean the temperature of the sample holder. We note that, because of absorption of the laser light, the temperature of the illuminated spot (spot temperature T_S) may differ from the 'film temperature' T_F.

For illumination we used a linearly polarized c.w. He–Ne laser beam which was focused on a Gaussian optical spot between 35 and 200 μm in diameter. The intensity of the incident laser beam was regulated using a combination of a Spectra-Physics polarization rotator (Model 310-21) and a sheet polarizer plane (2 and 3 in fig. 1).

The intensity of the incident, reflected and transmitted light was measured using Si photodetectors (4, 5 and 7 in fig. 1) and their signals were displayed on a Hewlett-Packard (Model 7046-A) X–Y recorder.

Fig. 1

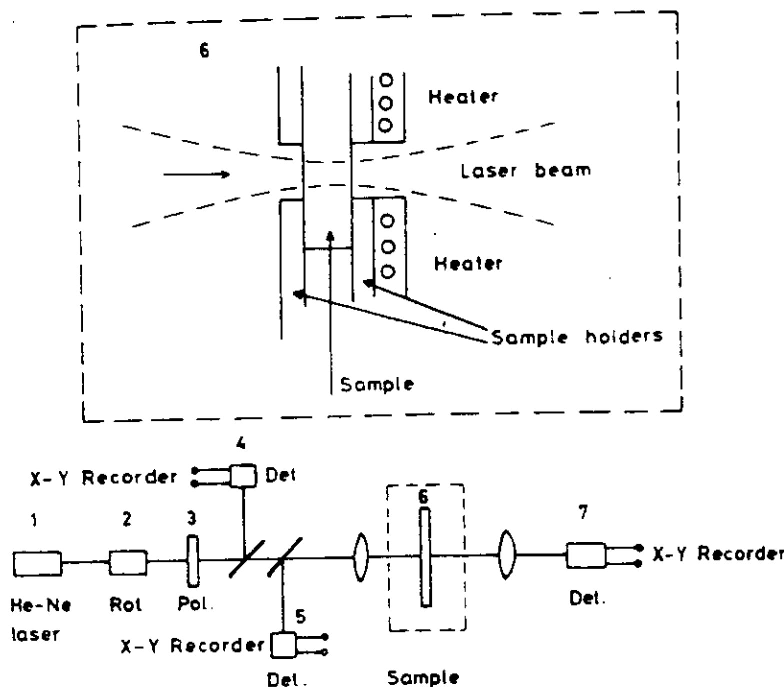

Experimental arrangement. The inset shows the specimen in the sample holder.

§ 3. Results

3.1. *Temperature dependence of absorption coefficient α of amorphous $GeSe_2$ films*

In this section we present measurements of the temperature dependence of the optical properties carried out at a low measuring light intensity where non-linear effects are negligible. The absorption coefficient α was determined from the reflected and transmitted intensity of a He–Ne laser beam ($\lambda_0 = 6328$ Å) at a power density of 10^{-1} W cm^{-2}.

The photon energy of the He–Ne laser light ($h\nu = 1{\cdot}96$ eV at $\lambda_0 = 6328$ Å) used to induce the non-linear optical phenomena is less than the value of the optical energy gap of $GeSe_2$ films ($E_g = 2{\cdot}1$ eV; Hajtó and Füstöss-Wégner 1980). In this energy range (below the band-gap energy) the optical absorption coefficient (10^2 cm^{-1} < α < 10^4 cm^{-1}) varies exponentially with the photon energy (Hajtó 1980), which is the typical Urbach behaviour of chalcogenide glasses (Mott and Davis 1979). At a fixed wavelength in the Urbach region, α is strongly temperature-dependent above room temperature (Mott and Davis 1979). In this temperature region α can be described by the Urbach rule,

$$\alpha = \alpha_0 \exp\left(-\frac{E_g - h\nu}{k_B T}\right); \tag{1 a}$$

Fig. 2

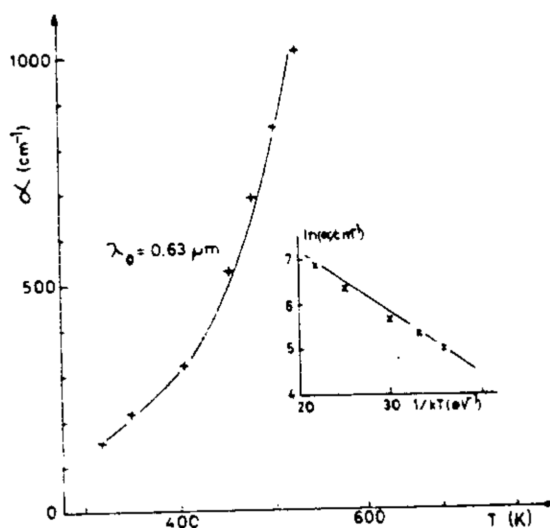

The temperature dependence of the absorption coefficient α.

this rule was also obeyed in our experiments. A 6 μm thick amorphous $GeSe_2$ film was used for measuring α. Figure 2 shows that α is a strongly non-linear function of temperature. As shown in the inset, the Urbach rule is satisfied with $\alpha_0 = 2 \times 10^4$ cm^{-1} (at $\lambda_0 = 6328$ Å) and $E_g - h\nu = 0{\cdot}138$ eV in the temperature range 300–500 K. From the measurements the refractive index n could also be determined. We found, for temperatures of 300–500 K, that

$$n = n_0 + \beta T, \tag{1 b}$$

with $n_0 = 2{\cdot}50$ and $\beta = 2{\cdot}56 \times 10^{-4}$ K^{-1}, i.e. the refractive index is a linear function of temperature. This is in accordance with other experimental results (Kastner 1973). We emphasize that both α and n are *continuous* functions of temperature and that no discontinuity was found in the optical constants when the measuring light intensity was kept at a very low value. However, on increasing the incident light intensity, other types of optical effect started to develop ; these are described in the sections below.

3.2. *Laser-induced optical discontinuity and optical bistability in amorphous $GeSe_2$ films*

We have measured the actual transmission of a c.w. He–Ne laser beam focused onto a self supporting amorphous $GeSe_2$ film as a function of the incident laser intensity. Our optical system (air–sample–air configuration) is a very simple one, no external mirrors being used to form a Fabry–Perot system.

In this section we present the experimental results on the transmitted light intensity to demonstrate the non-linear nature of the optical phenomena. The simultaneous transmission and reflection measurements (necessary for calculating the optical constants) will be presented in § 4.3, where the experimental results are compared with our model. All measurements presented in this section were carried out by changing the incident laser intensity at a constant rate ($\sim 0{\cdot}1$ mW s^{-1}). The recorded values of the transmitted light intensity (I_{Tr}) as a function of the incident laser intensity are shown in fig. 3 for $T_F = 298$ K.

Fig. 3

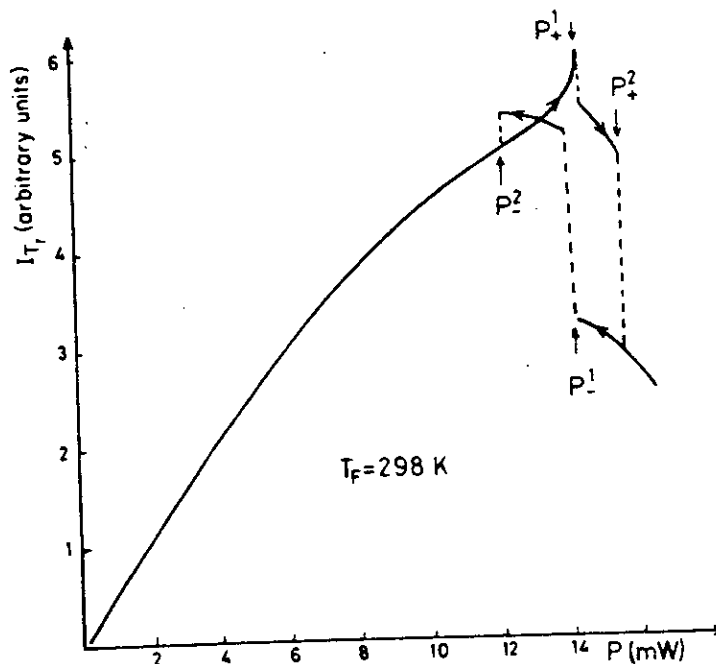

Transmitted light intensity as a function of the incident laser intensity in a-$GeSe_2$ film ($L = 6$ μm, laser spot diameter = 207 μm).

A first discontinuity was observed at 14·4 mW incident laser power (P_-^1), characterized by a sharp increase and subsequent discontinuous decrease in the transmitted signal. On increasing further the incident laser power, a switch to the dark state was observed, i.e. a large decrease in the transmitted signal at 15·6 mW (P_+^2).

Starting from the dark state and decreasing the laser power, the transmitted light showed a hysteresis, e.g. the transition to the bright state (higher transmitted values) occurs at 14·2 mW (P_-^1), which is lower than P_-^2. As a consequence the transmitted light intensity has two different stable values at a fixed laser power between P_-^2 and P_-^1, i.e. optical bistability was found. On further decreasing the laser power, a second discontinuity was observed at 12·3 mW (P_-^2), where the hysteresis disappeared.

Fig. 4

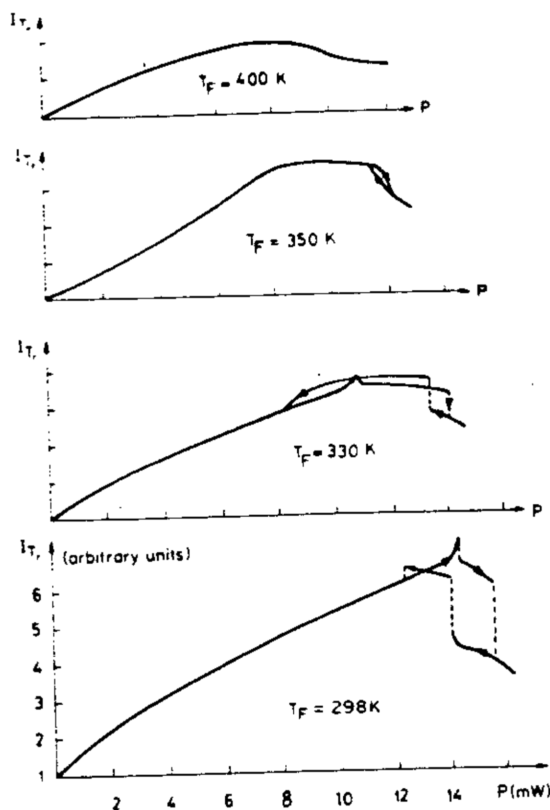

Transmitted light intensity as a function of the laser intensity at different film temperatures T_F.

We found that the shape of the recorded curves varied somewhat with experimental conditions such as the temperature of the films, laser spot diameter and the rate of increase of the intensity. The last of these effects is discussed in § 3.3. The effect of the film temperature is shown in fig. 4. Increasing the film temperature T_F by using the sample heater, as described in § 2, the critical laser powers for producing the optical discontinuities decreased. Similarly, the amplitudes of the optical discontinuities decreased with increasing film temperature. A decrease in the hysteresis $(P_\perp^2 - P_\perp^1)$ with increasing film temperature was also observed. The optical discontinuities and the optical bistability disappeared when the film temperature was increased above 500 K.

We have measured the critical laser power $P_\perp^1$ (at which the first switching from the dark to the bright state occurs) as a function of the incident laser beam diameter. We chose this discontinuity $(P_\perp^1)$ because it seemed to be the most reproducible one ; i.e. it does not depend strongly on the rate of decrease of the intensity. The critical laser flux density ($P_\perp^1$ divided by the area of the laser spot) as a function of the laser spot diameter is shown in fig. 5.

Fig. 5

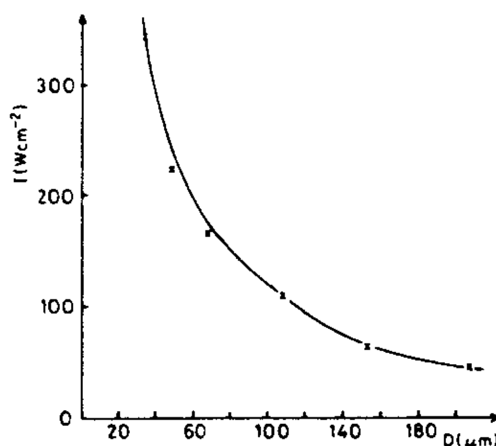

Critical laser flux density as a function of incident laser beam diameter.

Assuming a pure electronic excitation effect for producing optical bistability (Fazekas 1981), one would expect the switch to the dark state to occur at a constant electric field produced by the laser, i.e. at constant laser flux density independent of the laser beam diameter. Figure 5 shows that this is not the case for the a-$GeSe_2$ films. The laser flux density necessary for producing the optical switching effect increases with decreasing laser beam diameter. This experimental observation indicates the importance of thermal effects in connection with the laser-induced non-linear phenomena in a-$GeSe_2$ films. The increase in the spot temperature T_S at a given laser flux density is less when the beam diameter is decreased because of greater heat conduction. Consequently, the laser flux density must be higher to produce a given spot temperature.

3.3. *Photostructural changes*

As mentioned in the previous section, the shape of the transmission curves depends on the rate of increase of the intensity. We established that this dependence can be traced back to another effect, namely that the transmission changes, even under the influence of a *constant* laser power. The details of this effect are shown in fig. 6. In this experiment we recorded the transmitted light intensity at a fixed laser power, which was lower than the critical intensity at which the optical switching occurs to the dark state. In the first period of illumination a continuous decrease in the transmission was observed. This decrease cannot be attributed simply to the increase in the spot temperature, because it possesses a 'memory' behaviour. Switching off the light (points 2 and 4 in fig. 6) and keeping the sample in the dark for a while does not restore the initial transmission value. On switching the light on again (points 3 and 5 in fig. 6), the transmission continues to decrease from the same value as before. This is a memory state, which must be connected with photostructural changes

Fig. 6

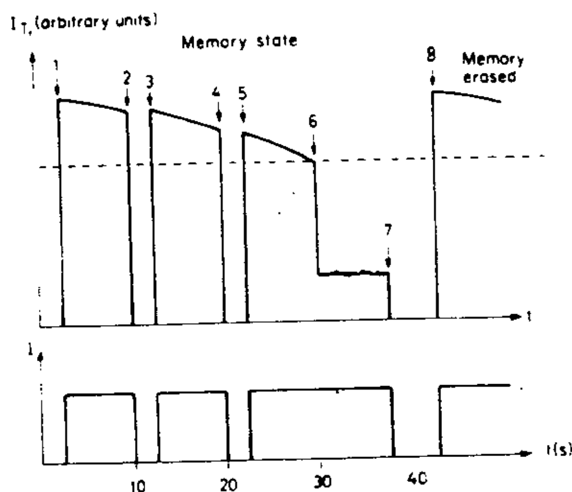

Time dependence of the transmitted light intensity at a fixed laser power ($P = 11$ mW, laser beam diameter $= 207$ μm).

(de Neufville 1976). Different aspects of the laser-induced structural changes in a-$GeSe_2$ were studied recently by Griffiths, Espinosa, Remeika and Phillips (1982) and by Hajtó, Jánossy and Forgács (1982).

When the transmission decreases to a critical value (point 6 in fig. 6), a discontinuous switching to the dark state occurs. We observed that switching off the light in the dark state (point 7 in fig. 6) causes the 'memory' to be erased; the initial transmission value is restored (point 8 in fig. 6) and the whole cycle recommences. This fact indicates that in the dark state a different type of photostructural change takes place which erases the structure of the amorphous network developed in the bright period (above the dashed line in fig. 6).

3.4. *Laser-induced oscillatory phenomena*

We found experimentally that, for an appropriate laser power, the dark state is unstable and it switches back spontaneously to the bright one. In this case periodic oscillation of the optical properties occurs (see fig. 7). Such oscillations had already been found and reported (Hajtó *et al.* 1977) in $GeSe_2$ films on a silica substrate. The differences between self-supporting samples and samples on a substrate are the following. In the latter case a much higher laser intensity (~ 2 kW cm^{-2}) was necessary to produce oscillations, but above a critical laser field oscillations always occur. In the present case oscillation was found only in a rather narrow intensity range which corresponds more or less to the observed hysteresis (see fig. 3). In this range the intensity is of the order of 40 W cm^{-2}, i.e. smaller by a factor of 50 than the intensity for samples on a substrate. As can be seen from fig. 7, the frequency of the oscillation is of the order of few seconds, while for samples on a substrate it is of the order of hundredths of a second (Hajtó 1980).

Fig. 7

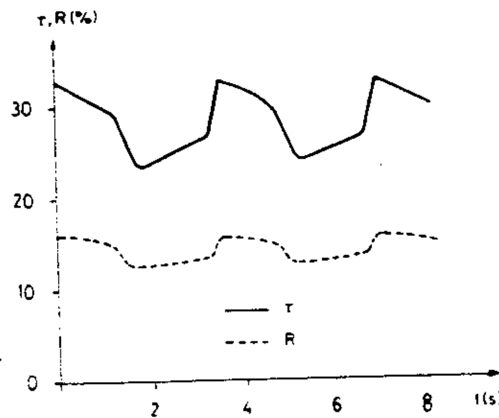

Oscillation of the transmitted and reflected light intensity at a fixed laser power ($P = 14{\cdot}5$ mW, laser beam diameter $= 207$ μm).

§ 4. Theoretical considerations

4.1. *General remarks*

To explain the experimental observations described in the previous section, one has to consider the possible non-linear interactions between the laser field and the amorphous film. We suggest that there are three types of such interactions that may play an important role in the present phenomena.

Thermal effects

As the chalcogenide glasses are poor thermal conductors, the laser beam may produce a significant local temperature rise in the illuminated spot. In turn, the absorption coefficient α, the value of which determines the dissipation of the light field in the sample—and thus the temperature rise, is strongly temperature-dependent (see § 3.1). A simple quantitative treatment of the thermal effects is given in § 4.2, where it is shown that this feedback between the value of α and the temperature rise can give rise to a highly non-linear behaviour of the optical characteristics of the film and may produce discontinuities and bistability in the transmitted light intensity. The dependence of the critical laser intensities as a function of the spot size (see § 3.2) suggests the importance of thermal effects.

Photostructural changes

As is well known from the literature (de Neufville 1976, Tanaka 1980), and also as shown by our observations, laser irradiation causes structural changes in the amorphous network (see § 3.3). These structural changes, which are connected with displacements of atoms, modify the optical constants of the substance. As a result, the absorption coefficient at a given spot depends not only on the local temperature, but also on the history of the amorphous network within that spot.

The ' memory effect ' described in § 3.3 indicates that the photostructural changes in a-$GeSe_2$ are not restricted to a short initial period of the illumination. The observations can be interpreted by assuming that the stationary configuration of the structure is a function of the illuminating laser intensity and the temperature. The stationary configuration, obtained by a long illumination at a fixed laser intensity and at a *fixed* spot temperature, can be altered by changing one or both of these parameters. We note that in the experiments the spot temperature is *not* fixed. In this case it is not necessary, at a constant laser intensity, for a stationary state to be established, i.e. oscillation can occur. This point is discussed further in § 4.4.

' Conventional ' non-linearity

There may also be a ' conventional ' non-linearity in the system, arising from the interaction of the laser field with the electronic structure of the amorphous material. Such an interaction was investigated by Fazekas (1981), who considered the effect to be due to charged and neutral defect centres and demonstrated that the interaction between these centres may lead to a discontinuous change in the electronic structure at a critical laser intensity.

Even if this laser-induced ' phase transition ' was not the origin of the observed discontinuities, one has to consider the possibility that the absorption coefficient may depend explicitly (i.e. not through thermal effects) on the laser intensity.

In our opinion all three effects described above are important in the observed phenomena. However, the measurements carried out up to now are not sufficient to enable their relative importance to be properly estimated. In the following section we consider quantitatively the effect of the thermal component only. This is the opposite limit to that considered by Fazekas (1981) but, as we shall demonstrate, our model is also able to explain some of the observed optical anomalies.

4.2. *Quantitative treatment of the thermal effects*

Let us consider a plane parallel, self-supporting film of thickness L of a given substance. The substance can be characterized by a complex refractive index $\hat{n} = n + i\kappa$, where κ is related to the absorption coefficient by $\alpha = (4\pi/\lambda_0)\kappa$. In this treatment n and α are considered to be single-valued, continuous functions of the temperature. We investigate the case of normal incidence of the light beam and, for simplicity, replace the Gaussian intensity profile of the laser beam by a uniform intensity, I, which is cut off at a radius r_0.

The transmission and reflection coefficients of the film can be calculated by Abelès' method (Born and Wolf 1968). In the limit $\kappa \ll n$, the transmission and reflection coefficients are respectively

$$\tau = 1/(n_1^2 \Gamma + n_2^2/\Gamma - 2n_1 n_2 \cos 2\delta), \quad (2)$$

$$R = n_1 n_2 (\Gamma + 1/\Gamma - 2 \cos 2\delta)\tau, \quad (3)$$

where

$$n_1 = (n+1)^2/4n, \quad n_2 = (n-1)^2/4n$$

$$\Gamma = \exp(\alpha L), \qquad \delta = \frac{2\pi}{\lambda_0} nL.$$

The energy dissipated per unit time and unit area, W, can be determined from the energy conservation law:

$$W = ID, \quad D = 1 - (R + \tau). \tag{4}$$

To determine the temperature distribution in the sample, it is necessary to know how the dissipated heat is conducted away from the spot. We consider two limiting cases.

(1) The heat is conducted away in the direction normal to the surfaces by the surrounding air. The heat flow can be taken to be proportional to $T_S - T_F$. The time dependence of the spot temperature T_S is then governed by the equation

$$\frac{\partial T_S}{\partial t} = \frac{I}{cL} D(T_S) - k(T_S - T_F), \tag{5}$$

where c is the specific heat of the substance and k is a constant.

(2) In the opposite limit we assume that heat conduction takes place only in the plane of the sample. The temperature is assumed to be fixed (T_F) at a radius R. The heat conduction equation in this case is

$$\frac{\partial T}{\partial t} = \begin{cases} \dfrac{I}{cL} D(T(r)) - \lambda \left(\dfrac{\partial^2 T}{\partial r^2} + \dfrac{1}{r} \dfrac{\partial T}{\partial r} \right), & r < r_0 \\[2ex] -\lambda \left(\dfrac{\partial^2 T}{\partial r^2} + \dfrac{1}{r} \dfrac{\partial T}{\partial r} \right), & r > r_0, \end{cases} \tag{6}$$

where r_0 is the radius of the laser beam and λ the heat conductivity. At $r = r_0$ we require T and $\partial T / \partial r$ to be continuous.

For $r > r_0$ the solution can be written as

$$T = A \ln (R/r) + T_F. \tag{7}$$

For $r < r_0$, eqn. (6) can be solved, for example by expanding T and D in powers of r. This gives

$$\left. \begin{aligned} T(r) &= T_0 - Br^2 + \cdots \\ D(T(r)) &= D(T_0) + \left.\frac{\partial D}{\partial T}\right|_{T=T_0} (T - T_0) + \cdots \\ &= D(T_0) - B \left.\frac{\partial D}{\partial T}\right|_{T=T_0} r^2 + \cdots \end{aligned} \right\} \tag{8}$$

where $T_0 = T(0)$. Taking into account that $R \gg r_0$, it can be assumed that the temperature drop within the spot is not too large, so that fourth-and higher-order terms in r can be neglected. In this case

$$T(r_0) \approx T_0 - Br_0^2, \quad T'(r_0) \approx -2Br_0$$

and the continuity conditions give

$$B = \frac{T_0 - T_F}{r_0^2[1 + 2 \ln (R/r_0)]}.$$

Equations (6) and (8) yield

$$\frac{\partial T_0}{\partial t}=\frac{I}{cL}D(T_0)-\frac{\lambda}{r_0^2[1+2\ln(R/r_0)]}(T_0-T_F).$$

Identifying T_0 with the 'spot temperature' T_S, we have the same equation as in case (1), eqn. (5), with

$$k=\frac{\lambda}{r_0^2[1+2\ln(R/r_0)]}. \tag{9}$$

In a real experiment both types of heat conduction occur simultaneously. However, as we have seen, in both limits the same mathematical equation describes the problem. We now investigate the properties of this equation, writing it in the form

$$\tau_0\frac{\partial T}{\partial t}=\eta I D(T)-(T-T_F) \tag{10}$$

(from now on we omit the subscript S from T_S). η is a constant determined by the geometry.

We are interested in stationary solutions, when

$$\eta I D(T)=T-T_F. \tag{11}$$

To solve eqn. (11) explicitly, the temperature dependences of α and n have to be known. As discussed in § 3.1, for amorphous semiconductors these can be given as (see eqns. (1 *a*) and (1 *b*))

$$\alpha(T)=\alpha_0\exp(-(E_g-h\nu)/k_BT],$$
$$n(T)=n_0+\beta T.$$

To demonstrate how discontinuities and bistability can occur, let us first neglect the temperature dependence of the refractive index. A schematic curve representing $D(T)$ for this case is given in fig. 8. At low temperatures, where $\exp(\alpha L)-1\ll 1$, $D(T)$ is proportional to $\alpha(T)$. At high temperatures where $\exp(\alpha L)\gg 1$, $D(T)$ tends to a saturation value, $1-[(n-1)/(n+1)]^2$ (i.e. all light entering the sample is absorbed). Equation (11) can be solved graphically by determining the intercepts of $D(T)$ and the straight line $(T-T_F)/\eta I$. As can be seen from fig. 8, if $I<I_-$ or $I>I_-$, there is only one solution for T. However, in the range $I_-<I<I_-$ there are three solutions.

To decide whether a given solution is stable or not, one has to consider what happens if the temperature deviates slightly from its equilibrium value. If the sign of $\partial T/\partial t$ is such that the temperature approaches the equilibrium value, the solution is stable; in the opposite case it is unstable. From eqn. (10) we deduce the condition of stability to be

$$\frac{\partial}{\partial T}\left(D(T)-\frac{T-T_F}{\eta I}\right)<0. \tag{12}$$

This inequality is satisfied for the solutions denoted by T_1 and T_3 in fig. 8. Consequently, in the intensity range $I_-<I<I_-$ there are two stable solutions. The first solution, T_1, corresponds to a cold and transparent state of the film: this happens when the laser intensity is increased from 0. The state becomes unstable at $I=I_-$, where a discontinuous transition takes place to a warm and

Fig. 8

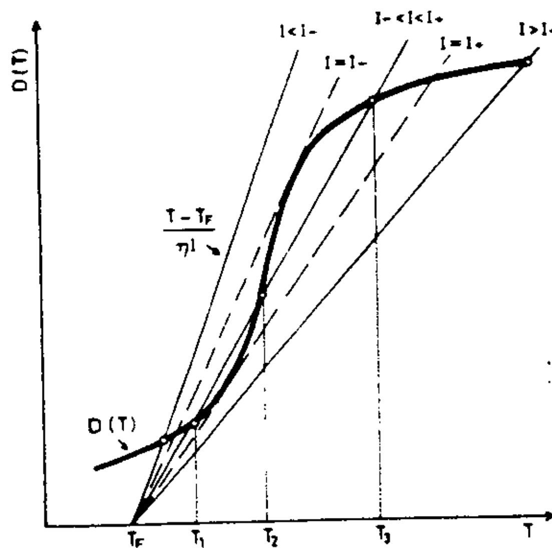

Determination of the spot temperature at different laser intensities: n is considered to be constant.

strongly absorbing state. When the intensity is decreased from a value larger than I_+, the film remains in this 'warm' state down to a second critical intensity, I_- ($I_- < I_+$). At this intensity the film transforms back to the 'cold' state.

The behaviour described above is typical of optical bistability (Abraham and Smith 1982). Note, however, that in the present mechanism the reflection at the boundaries does not play an important role, and that the switching is from the transparent to the dark state when the intensity is increased. These features are the opposite of what is found in conventional optical bistability.

In the above considerations the variation of the refractive index with temperature has been neglected. In fig. 9 we demonstrate that this variation, although weak, may itself also lead to bistability. Keeping α a non-zero constant, D oscillates with increasing T because of the temperature dependence of the term $\cos 2\delta$ in eqns. (2) and (3). As shown in fig. 9, in this case there is again an intensity range in which two stable spot temperatures belong to a given I. (At higher intensities further bistable ranges exist.) In this second mechanism of bistability the reflections of the light beam at the boundaries play an important role. However, we emphasize that the bistability is again caused by the feedback between the temperature rise of the spot and the temperature dependence of the optical constants.

In fig. 10 we present schematically the transmission coefficient τ as a function of laser intensity when only α (fig. 10 (a)) and only n (fig. 10 (b)) depends on the temperature. In both cases the 'dynamical transmission coefficient',

defined as $\partial\tau/\partial I$, becomes infinite at the critical intensities. It can be shown that near the critical intensities

$$\frac{\partial\tau}{\partial I} \sim (I - I_c)^{-1/2}. \tag{13}$$

However, the direction of the jump of τ in one case is the opposite of that in the other.

Fig. 9

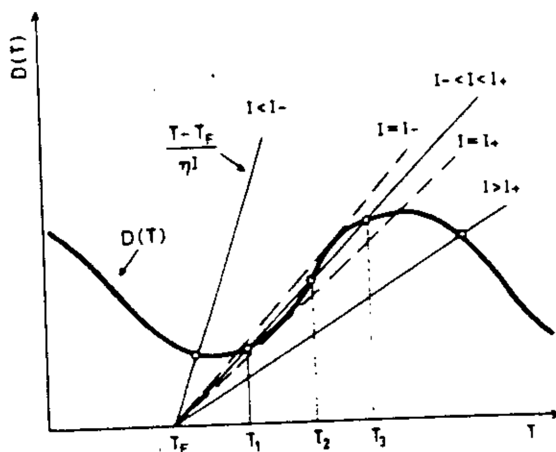

Determination of the spot temperature at different laser intensities: α is considered to be constant.

Fig. 10

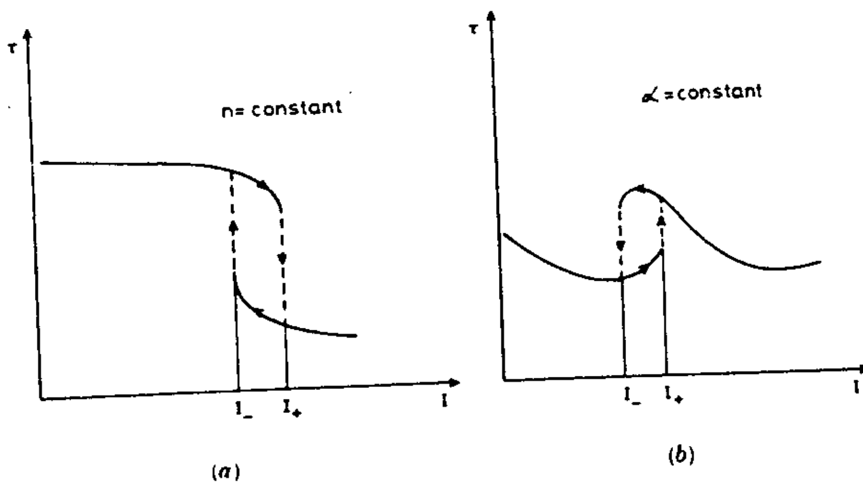

(a) (b)

Transmission coefficient as a function of laser intensity: (a) n = constant. (b) α = constant.

In a real situation, when both α and n are temperature dependent, interference between the two effects leads to different complicated shapes and singularities in the curves of transmission versus incident intensity (see the next section).

4.3. *Application of the model to a-GeSe$_2$ films*

In this section we present some calculated transmission and reflection curves as a function of light intensity in which we utilized the experimentally determined $\alpha(T)$ and $n(T)$ values of a-GeSe$_2$ films (see § 3.1). The shape of the curves also depends on the thickness of the films. The problem arises that the term $\cos 2\delta$ (see eqns. (2) and (3) in § 4.2) is very sensitive to the exact value of the thickness. Therefore in the calculation we used the relation $\delta = \delta_0 + 2(\pi/\lambda_0)L\beta T$ and δ_0 was considered to be an independent parameter. The calculation showed that the shape of the curves is very sensitive to the value of δ_0. This may explain the experimental finding that in samples with slightly different thicknesses the detailed shapes of the curves of transmission versus intensity were rather diverse.

In fig. 11 the experimentally determined transmission (τ) and reflection (R) coefficients are plotted against incident laser power. For comparison, the curves of τ and R versus laser power calculated according to the thermal model (see § 4.2) are shown in fig. 12. The value of δ_0 was chosen such that the calculated and measured τ and R should be the same at zero intensity. Although there is no quantitative agreement between the curves in figs. 11 and 12, the model reflects the non-linear behaviour and, in particular, the discontinuities both in transmission and reflection.

In fig. 13 the experimentally determined values of the absorption coefficient α are compared with the theoretically calculated values. There are two sharp increases in α at the observed optical discontinuities, both in the experimental

Fig. 11

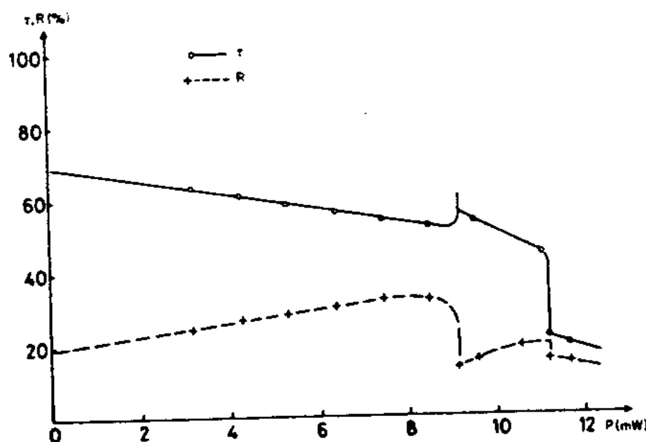

Experimentally determined τ and R values as a function of laser power for a laser beam diameter of 160 μm.

Fig. 12

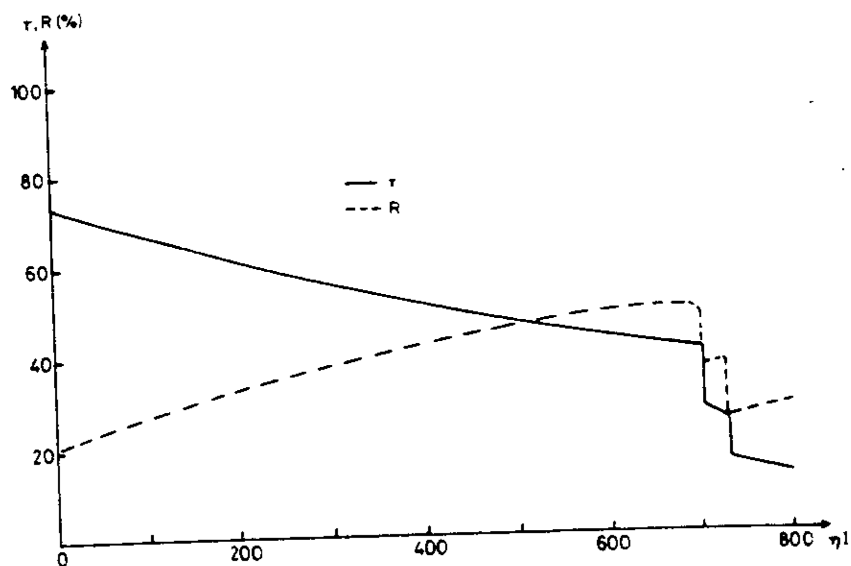

Calculated τ and R values as a function of laser intensity using $\delta_0 = 2{\cdot}21$. (ηI are given in degrees Kelvin.)

Fig. 13

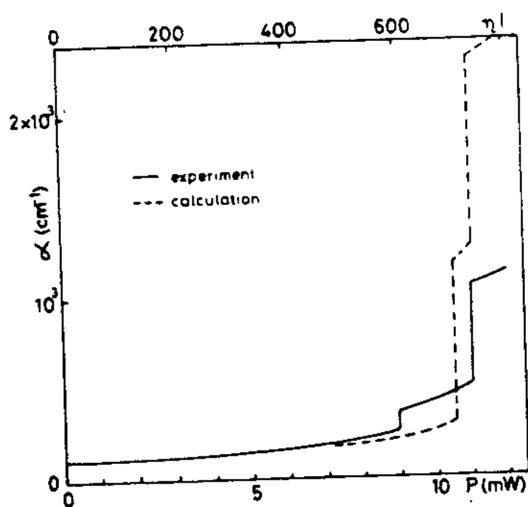

Absorption coefficient α as a function of laser power.

and theoretical curves. However, the model predicts a higher increase in α than was found experimentally.

The model predicts that the critical laser intensity I_c at which the optical switching occurs depends strongly on the spot size. Considering heat conduction to occur only in the plane of the film (see § 4.2, case (2)), we would expect from eqn. (9) that $I_c \sim 1/r_0^2[1 + 2 \ln (R/r_0)]$. This is in accordance with the experimental observation that I_c increases with decreasing laser spot size (see § 3.2).

The model allows us also to investigate the influence of the film temperature. Figure 14 shows the calculated transmitted light intensity I_{Tr} as a function of laser intensity at different film temperatures T_F. In these calculations δ_0 was chosen such that the room-temperature curve should resemble the experimental curve presented in fig. 3. One can see the same tendencies in

Fig. 14

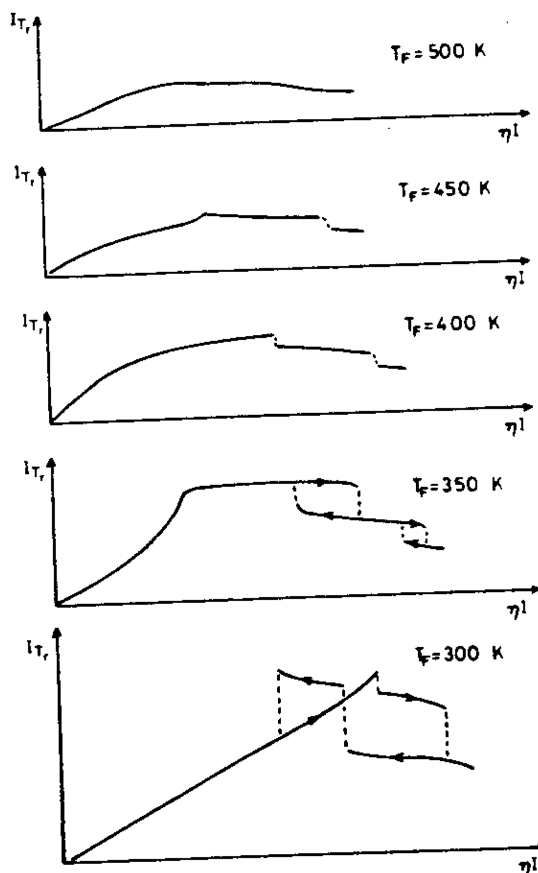

Calculated transmitted light intensity as a function of film temperature using $\delta_0 = 2{\cdot}85$.

fig. 14 as in the experimentally recorded curves (fig. 4): that both the amplitude of the discontinuities and the hysteresis decrease with increasing film temperature. We made no attempt to determine the absolute value of the incident laser intensity in the theoretical calculations described above; this would require knowledge of the value of the term η introduced in eqn. (10).

Considering only the thermal effect, the model is able to reproduce the general trends of the observed phenomena. However, the influence of the increase in film temperature is more pronounced in the experiments than is predicted by our thermal model.

It is clear that we cannot obtain quantitative agreement between experiment and theory without taking into account other effects produced by the irradiation (see, for example, points (2) and (3) in § 4.1). This is particularly true for oscillatory phenomena (see § 3.4) which could not be explained by a purely thermal model.

4.4. *Considerations concerning the oscillatory phenomena*

We suggest that the occurrence of oscillation under certain experimental conditions (see § 3.4) at a fixed laser intensity can be explained by a combination of thermal effects and photostructural changes. To see more precisely how the oscillation occurs, we calculated the oscillation of the absorption coefficient α from the recorded transmission and reflection curves in fig. 7. The result is shown in fig. 15. In the bright state of oscillation (lower α values), α is increasing. The phenomenon has already been discussed (see § 3.3) and has turned out to be connected with photostructural changes. As α increases due to the photostructural change, the spot temperature also increases due to the higher dissipation. This can lead to a discontinuity in the same way as for increasing laser intensity.

In the dark state (higher α values), where the spot temperature is supposed to be higher, the laser irradiation causes a continuous *decrease* in the absorption

Fig. 15

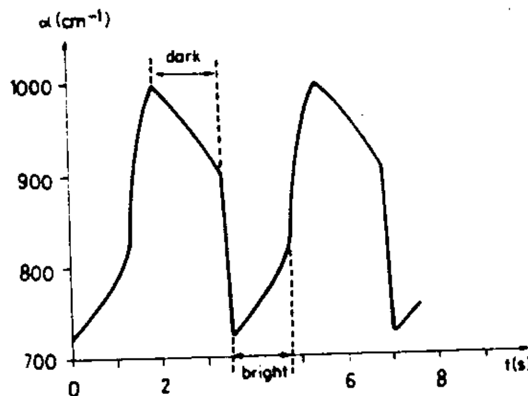

Calculated oscillation of the absorption coefficient using the experimental data presented in fig. 7.

coefficient. At the elevated temperature the direction of the slow photostructural change is reversed, and the spot temperature decreases continuously. This decrease can lead to a discontinuous switch to the bright state (lower α values).

A model for photostructural changes in chalcogenide glasses was presented by Kolobov, Kolomiets, Konstantinov and Lyubin (1981), based on the double well potential description proposed by Tanaka (1980). The model predicts that, on raising the spot temperature, the direction of the photostructural change may reverse. A quantitative treatment of this problem will be given by us in a forthcoming paper.

As mentioned above, there are marked differences in the oscillatory phenomena in samples with and without substrates (self-supporting). The role of the substrate may be that it enables the heat produced by the laser to be conducted away more efficiently. Consequently, thermal effects are reduced and the material can tolerate a much higher laser field without crystallizing. The higher laser field enhances the photostructural effects rather than the thermal effects.

§ 5. Conclusion

We have shown that amorphous semiconductor films display a rich variety of non-linear optical phenomena. We have observed a new type of optical bistability in amorphous $GeSe_2$ films which cannot be explained by the same mechanism (Miller *et al.* 1981, Gibbs *et al.* 1979) used for crystalline semiconductors.

The non-linear behaviour in the present case may be attributed to at least three different mechanisms, namely thermal effects, photostructural changes and electronic non-linearity. Considering only electronic non-linearity, as did Fazekas (1981), one can explain the discontinuity in the optical properties but cannot account for the memory effect and hysteresis. The purely thermal model presented in this paper explains the discontinuity, the hysteresis and the fact that the critical laser power densities depend on the laser beam diameter. On the other hand, the memory effect and the corresponding oscillations cannot be explained.

In order to explain quantitatively all the observations, a model is needed which combines the three mechanisms (thermal, photostructural andelectronic) acting simultaneously during the illumination. In view of this, further optical measurements are planned in order to separate the photostructural changes and electronic non-linearity from the thermal effect.

Finally, we emphasize that amorphous semiconductor films could provide simple and easily accessible elements in some optical applications. Because of the optical singularities (see, for example, fig. 3 and eqn. (13)), the films can be used as a new type of optical transistor.

Acknowledgment

The authors are indebted to Dr. N. Kroó for valuable discussions and continuous encouragement connected with this work and to Mr. G. Pesti for his kind assistance.

REFERENCES

ABRAHAM, E., and SMITH, S. D., 1982, *Rep. Prog. Phys.*, **45**, 815.
BORN, M., and WOLF, E., 1968, *Principles of Optics*, fourth edition (Oxford: Pergamon Press), Chap. 1.
DE NEUFVILLE, J. P., 1976, *Optical Properties of Solids: New Developments*, edited by B. O. Seraphin (Amsterdam: North-Holland), p. 437.
FAZEKAS, P., 1981, *Phil. Mag.* B, **44**, 435.
GIBBS, H. M., MCCALL, S. L., and VENKATESAN, T. N. C., 1976, *Phys. Rev. Lett.*, **36**, 1135.
GIBBS, H. M., MCCALL, S. L., VENKATESAN, T. N. C., GOSSARD, A. C., PASSNER, A., and WIEGMANN, W., 1979, *Appl. Phys. Lett.*, **35**, 451.
GRIFFITHS, J. E., ESPINOSA, G. P., REMEIKA, J. P., and PHILLIPS, J. C., 1982, *Phys. Rev.* B, **25**, 1272.
HAJTÓ, J., 1980, *J. Phys.*, **41**, C4–63.
HAJTÓ, J., and EWEN, P. J. S., 1979, *Phys. Stat. Sol.* (a), **54**, 385.
HAJTÓ, J., and FÜSTÖSS-WÉGNER, M., 1980, Proceedings of the Conference Amorphous Semiconductors '80, Kishinev, U.S.S.R., p. 189.
HAJTÓ, J., JÁNOSSY, I., and FORGÁCS, G., 1982, *J. Phys.* C **15**, 6293.
HAJTÓ, J., ZENTAI, G., and KÓSA SOMOGYI, I., 1977, *Solid St. Commun.*, **23**, 401.
KASTNER, M., 1973, *Phys. Rev.* B, **7**, 5237.
KOLOBOV, A. V., KOLOMIETS, B. T., KONSTANTINOV, O. V., and LYUBIN, V. M., 1981, *J. non-crystalline Solids*, **45**, 335.
MILLER, D. A. B., SEATON, C. T., PRISE, M. E., and SMITH, S. D., 1981, *Phys. Rev. Lett.*, **47**, 197.
MILLER, D. A. B., SMITH, S. D., and JOHNSTON, A., 1979, *Appl. Phys. Lett.*, **35**, 658.
MOTT, N. F., and DAVIS, E. A., 1979, *Electronic Processes in Non-crystalline Materials*, second edition (Oxford: Clarendon Press), Chap. 6.
SZÖKE, A., DANEU, V., GOLDHAR, J., and KURNIT, N. A., 1969, *Appl. Phys. Lett.*, **15**, 376.
TANAKA, K., 1980, *J. non-crystalline Solids*, **35–36**, 1023.

PHILOSOPHICAL MAGAZINE B, 1983, VOL. 48, NO. 4, 311–321

Explanation of the laser-induced oscillatory phenomenon in amorphous semiconductor films

By J. HAJTÓ† and J. JÁNOSSY
Central Research Institute of Physics, Budapest, Hungary

and A. FIRTH
Department of Electrical Engineering, University of Edinburgh, Scotland

[Received 4 February 1983 and accepted 30 May 1983]

ABSTRACT

A new model is presented which explains the recently observed oscillatory phenomena in self-supporting a-$GeSe_2$ films.

The model is based on a combination of thermal and photoinduced effects. It can also be used for predicting the experimental conditions for observing light-induced bistability and oscillatory phenomena in other amorphous semiconductor films.

§ 1. INTRODUCTION

In recent years considerable interest has developed in connection with non-linear optical properties of condensed matter. Of special interest are the non-linear optical phenomena that occur at relatively low levels of light intensity, as these effects may find applications in integrated optics. Perhaps the most promising effect is the intrinsic optical bistability in crystalline semiconductors observed by Gibbs, McCall, Venkatesan, Gossard, Passner and Wiegmann (1979) and Miller, Smith and Johnston (1979) (see also Abraham and Smith 1982).

In the past few years it has been reported that strongly non-linear optical phenomena occur in amorphous evaporated $GeSe_2$ films. The first observations were made on a-$GeSe_2$ films on silica substrates. It was found that under the influence of a continuous focused He–Ne laser beam, the transmission and reflection coefficients of the film show periodic oscillations in time, above a threshold ~ 2 kW cm^{-2} (Hajtó, Zentai and Kósa Somogyi 1977, Hajtó and Apai 1980, Hajtó 1980).

More recently, the optical behaviour of self-supporting a-$GeSe_2$ films has been studied (Hajtó, Jánossy and Forgács 1982). In this case non-linearity occurs at much lower intensity levels (~ 50 W cm^{-2}). Oscillation of the optical properties occurs only in a narrow intensity range. Bistability and hysteresis were also found, without placing the sample in an optical resonator.

Different mechanisms have been suggested to explain this peculiar optical behaviour. Fazekas (1981) proposed that the observed anomalies are due to a

† Present address: Department of Electrical Engineering, University of Edinburgh, Scotland.

collective phenomenon of the charged and neutral defects present in evaporated a-$GeSe_2$ films. Recently Phillips (1982) suggested that the oscillatory behaviour is closely connected to the laser-induced reversible microcrystallization, which was observed in a-$GeSe_2$ with the help of Raman spectroscopy (Griffiths, Espinosa, Remeika and Phillips 1982).

Recently (Hajtó and Jánossy 1983) an alternative interpretation has been considered in which laser heating produces the optical anomalies. This model gives a natural explanation of the differences in the behaviour of self-supporting samples and those on substrates. In the latter case the heat is conducted away much more efficiently from the illuminated spot and consequently in this case a much higher laser field is necessary to produce the same thermal effect. The pure thermal model explains the optical bistability, in terms of a mixture of 'absorptive' and 'dispersive' types of bistability (Abraham and Smith 1982). Furthermore it accounts for the observation that the critical laser power densities depend on the beam diameter. On the other hand it does not explain the oscillatory behaviour.

It was suggested by us that the oscillations can be explained by taking into account the photostructural changes induced by the laser beam in chalcogenide glasses (see, for example, Tanaka 1980). The aim of the present paper is to treat the combined effect of the laser heating and photostructural changes quantitatively and to show how these effects can produce oscillations. We confine ourselves to *reversible* photostructural changes (Tanaka 1980).

The photostructural changes are usually much slower than the thermal effects. Thus the pure thermal model (Hajtó and Jánossy 1983) is relevant for experiments in which the intensity is scanned fast enough to prevent significant photostructural changes. In the present paper we discuss the opposite limit, i.e. what happens at *fixed* intensity. In the theoretical description, presented in § 2, we consider for the sake of simplicity only the changes of the absorption coefficient. In reality the refractive index is also temperature dependent and shows photo-induced changes (Tanaka 1980, Hajtó *et al.* 1982). This fact adds a number of complications to the phenomenon. We think however that our simplified description reflects the main features of the underlying mechanism. Also we show in the discussion (§ 3) this mechanism should also lead to oscillations in other chalcogenide amorphous semiconductors, provided that the relevant parameters (wavelength of light, temperature and thickness of the film) are properly chosen.

§ 2. Theoretical considerations

2.1. *Thermal effects*

A previous treatment of thermal effects was based on the strong temperature dependence of the absorption coefficient α (at fixed wavelength) which is observed in most amorphous semiconductors above room temperature (Mott and Davis 1979). This dependence can be described by Urbach's rule,

$$\alpha = \alpha_0 \exp\left[-\left(\frac{E_g - h\nu}{kT}\right)\right]. \tag{1}$$

The central problem (discussed by Hajtó and Jánossy (1983)) was to determine temperature rise in the illuminated spot due to the dissipation of the laser

beam. This was calculated by assuming that the heat loss is due to the difference in temperature between the illuminated spot and that of the film (the 'spot temperature' T and the 'film temperature' T_F). Thus the spot temperature was determined from the equation

$$\tau_0 \frac{\partial T}{\partial t} = \eta J D(T) - (T - T_F). \tag{2}$$

where η and τ_0 are constants determined by the thermal constants of the material and geometry, J is the incident laser flux, D is the dissipation coefficient (= dissipation/incident flux) which depends on α and thus on T. D is simply related to the transmission and reflection coefficients (Q and R respectively) as

$$D = 1 - Q - R. \tag{3}$$

For self-supporting samples,

$$\left.\begin{aligned} Q &= 1/[n_1^2\,\Gamma + (n_2^2/\Gamma) - 2n_1 n_2 \cos 2\delta], \\ R &= n_1 n_2[\Gamma + (1/\Gamma) - 2 \cos 2\delta]Q, \end{aligned}\right\} \tag{4}$$

where $n_1 = (n+1)^2/4n$, $n_2 = (n-1)^2/4n$ and

$$\Gamma = \exp(\alpha L), \quad \delta = \frac{2\pi}{\lambda_0} nL,$$

where L is the sample thickness and n the refractive index.

The stationary value of the spot temperature can be determined from the equation

$$\eta J D(T) = T - T_F, \tag{5}$$

together with the stability condition

$$\frac{\partial}{\partial T}\left(D(T) - \frac{(T - T_F)}{\eta J}\right) < 0. \tag{6}$$

Discussion of the solutions of the above equations can be found in Hajtó and Jánossy (1983). It is shown there that, at certain critical intensities, 'thermal run-away' occurs. This is the origin of the discontinuities observed when the intensity is scanned.

To describe what happens at fixed intensity, the *photoinduced* processes must also be considered. In order to make the description quantitative, we use the theory of photostructural changes presented by Kolobov, Kolomiets, Konstantinov and Lyubin (1981). In § 2.2 we briefly summarize this theory.

2.2. *Photostructural changes*

A detailed description of photostructural changes in amorphous chalcogenide semiconductors has been given by Tanaka (1980). According to Tanaka (1980) these structural changes are due to photoinduced displacements of chalcogen atoms. A fraction of these atoms can sit in two different equilibrium positions. On a configurational coordinate diagram these positions correspond to the minima of the double-well potential. One of the minima represents the ground state and the other can be considered as a metastable excited state. Transitions from one configuration to the other occur through photoinduced

and—near the glass transition temperature—pure thermal processes. According to Kolobov et al. (1981), the photoinduced transitions consist of two steps: a thermally activated small displacement of the atom and an electronic excitation by the incoming photons, which is followed by a relaxation to the new equilibrium position.

Kolobov et al. (1981) found the population kinetics are governed by the equation

$$\frac{dN}{dt} = -\left[\frac{1}{\tau} + J(\sigma_1 + \sigma_2)\right] N + J\sigma_1, \tag{7}$$

where N is the number of units in the metastable state divided by the total number of sites, and σ_1 and σ_2 are the cross-sections of the transitions from the ground state to the metastable state and for the inverse transitions, respectively. The temperature dependence of the cross-sections can be expressed as

$$\sigma_i = K_i \exp(-E_i/kT), \quad i = 1, 2, \tag{8}$$

where $K_i \sim 1/T$. The activation energies E_i are of the order of tenths of electron-volts.

In eqn. (7), τ is the relaxation time to the ground state via pure thermal transitions. This relaxation is usually very slow, except near the glass-transition temperature T_g, and it can often be neglected.

The stationary solution of eqn. (7) is

$$\bar{N} = \frac{\sigma_1}{1/J\tau + (\sigma_1 + \sigma_2)} = \frac{1}{1/q + 1 + f\exp(-\Delta E/kT)}$$

with $f = K_2/K_1$, $\Delta E = E_2 - E_1$ and $q = J\tau K_1 \exp(-E_1/kT)$. Equation (7) can be rewritten as

$$\frac{dN}{dt} = \frac{\bar{N} - N}{\tau_s}, \quad \text{with} \quad \frac{1}{\tau_s} = J(\sigma_1 + \sigma_2) + \frac{1}{\tau}. \tag{9}$$

The next problem to be considered is the connection between the value of N and the optical parameters of the substance. For the sake of simplicity we assume that the photoinduced processes influence only the value of α_0, otherwise the Urbach rule (eqn. (1)) remains valid. Furthermore we take α_0 proportional to N. With this assumption we derive from eqn. (9) an equation describing the kinetics of photostructural changes:

$$\frac{d\alpha_0}{dt} = \frac{\bar{\alpha}_0 - \alpha_0}{\tau_s}, \tag{10}$$

where $\bar{\alpha}_0$ is the stationary value of α_0:

$$\bar{\alpha}_0(T, J) = \frac{A}{1/q + 1 + f\exp(-\Delta E/kT)}. \tag{11}$$

To sum up, we have the following picture of photostructural change in amorphous semiconductors. The atomic configuration in amorphous materials is not so strictly determined as in crystalline solids, and a large number of metastable configurations can exist in them. In amorphous chalcogenide materials interaction with light quanta can cause certain atoms to move from one equilibrium position to another, thus altering the structure.

In our description, the instantaneous structure of the amorphous network is characterized from the optical point of view by the value of α_0; α_0 represents the fraction of atoms in the metastable state. Under the influence of laser irradiation the network approaches an equilibrium structure in which the number of transitions from the ground state to the metastable state equals the number of inverse transitions. This is characterized by the equilibrium value of α_0, $\overline{\alpha}_0(T, J)$.

We note that the simplifications made in deriving the exact form of $\overline{\alpha}_0(T, J)$ (eqn. (11)) are not essential in describing the oscillatory phenomenon. The important point is that there exists an equilibrium value of α_0 ($\overline{\alpha}_0$) which is determined by the temperature, and in some cases by the light intensity also. However, $\overline{\alpha}_0$ does not depend on the previous history of the illuminated spot, but the value of α_0 itself does depend on the previous history, and at a given moment it can be larger or smaller than the equilibrium value at a given temperature and intensity. In the first case, ($\alpha_0 > \overline{\alpha}_0$), α_0 decreases (photobleaching), in the second ($\alpha_0 < \overline{\alpha}_0$) α_0 increases (photodarkening). Thus whether darkening or bleaching occurs under the influence of the laser beam depends on the history of the given spot. This fact was proved experimentally by Averyanov, Kolobov, Kolomiets and Lyubin (1981).

Finally we estimate the energy change of the system associated with photostructural changes. Tanaka (1980) deduced from volume change measurements that during photostructural processes $N = 10^{19}$–10^{20} cm^{-3} atoms are moved. Furthermore, according to experiments, in a-$GeSe_2$ a typical relaxation time for photostructural changes at room temperature and an intensity level of ~ 50 W cm^{-2} is a few seconds. Suppose that the energy released or absorbed in one atomic event is not more than 1 eV. The energy change per second per cm^3 due to photostructural changes under these conditions does not exceed 1 W cm^{-3}. However, the energy production due to normal absorption $J\alpha$, under the same conditions, is $\sim 5 \times 10^3$ W cm^{-3}, where we have taken $\alpha = 10^2$ cm^{-1}. Consequently, when determining the laser-induced heating, the energy change associated with photostructural changes can be neglected.

2.3. *Determination of the stationary state and its stability*

According to the considerations presented in §§ 2.1 and 2.2, the spot temperature T and α_0 can be considered as independent variables which satisfy the equations

$$\tau_e \frac{\partial T}{\partial t} = \eta J D(\alpha_0, T) - (T - T_F), \tag{12}$$

$$\frac{\partial \alpha_0}{\partial t} = \frac{\overline{\alpha}_0 - \alpha_0}{\tau_s}. \tag{13}$$

The stationary solutions (i.e. at $\partial T/\partial t = \partial \alpha_0/\partial t = 0$) of eqns. (12) and (13) are

$$\eta J D(\alpha_0, T) = T - T_F, \tag{14}$$

$$\alpha_0 = \overline{\alpha}_0(T, J). \tag{15}$$

For the present analysis it is very important to note that under the present experimental conditions the thermal relaxation time τ_e is much smaller than the

structural relaxation time τ_s (this was inferred from experimental observations). As already mentioned, we found τ_s to be a few seconds at $J \sim 50$ W cm^{-2}. However, measurements with a chopped laser beam showed another relaxation process with a time constant of a few milliseconds. A rough estimation of the parameters involved in eqn. (12) showed that this latter process can be identified with the establishment of a pseudo-thermal equilibrium, associated with the actual value of α_0.

As a consequence of the large difference between τ_0 and τ_s, we can assume that after switching on the laser, a pseudo-thermal equilibrium is first quickly established which corresponds to the actual value of α_0. As α_0 is changed by the laser beam, the spot temperature follows 'adiabatically' the pseudo-equilibrium value corresponding to the actual structure. The main point, however, is that this pseudo-equilibrium is not necessarily stable against thermal fluctuations (with fixed α_0).

To derive the condition of thermal stability let us denote by $T^{(s)}$ the temperature of the pseudo-equilibrium with a given α_0 (i.e. $T^{(s)}$ is a solution of eqn. (14), while eqn. (15) is not necessarily satisfied). If by a thermal fluctuation T is changed to $T^{(s)}+\delta T$, from eqn. (12) we obtain

$$\tau_0 \frac{\partial \delta T}{\partial t} = \frac{\partial}{\partial T}[\eta J D - (T^{(s)} - T_F)]\delta T.$$

As τ_0 is positive, δT relaxes to zero if

$$\frac{\partial}{\partial T}[\eta J D - (T^{(s)} - T_F)] < 0. \tag{16}$$

This condition can also be expressed in a more convenient form. Let us examine how $T^{(s)}$ changes if α_0 changes to $\alpha_0 + \delta\alpha_0$. From eqn. (14),

$$\delta[\eta J D(\alpha_0, T^{(s)}) - (T^{(s)} - T_F)] = \eta J \frac{\partial D}{\partial \alpha_0}\delta\alpha_0 - \frac{\partial}{\partial T} \times [\eta J D - (T^{(s)} - T_F)]\delta T^{(s)} = 0.$$

As can be seen from eqns. (3) and (4), $\partial D/\partial\alpha_0 > 0$ (i.e. for a higher absorption coefficient, there is a higher dissipation if all other parameters are fixed). Consequently the stability condition (16) can be written in the form

$$\frac{\delta\alpha_0}{\sigma T^{(s)}} > 0. \tag{17}$$

In fig. 1 α_0 is plotted against $T^{(s)}$ for different laser intensities (different values of ηJ). The parameters used were $L = 6\ \mu$m, $E_g - h\nu = 0{\cdot}138$ eV, $T_F = 300$ K, $n = 2{\cdot}50$, $\cos 2\delta = 0$ (the temperature dependence of n is neglected). These parameters correspond to the data of a-$GeSe_2$ self-supporting films (Hajtó and Jánossy 1983). The dotted lines, where $\delta\alpha_0/T^{(s)} < 0$, correspond to unstable solutions. It can be seen from fig. 1 that there is a region on the α_0, T diagram where stable solutions do not exist. The unstable region separates solutions which correspond to the 'illuminated' and 'dark' states, respectively.

The stationary solution can be found by plotting $\bar{\alpha}_s(T)$ on the same diagram as the $\alpha_0(T)$ curves. As a given intensity the intercept of $\alpha_0(T)$ and $\bar{\alpha}_s(T)$ determines the stationary solution. If $\bar{\alpha}_s(T)$ crosses the unstable region there

Fig. 1

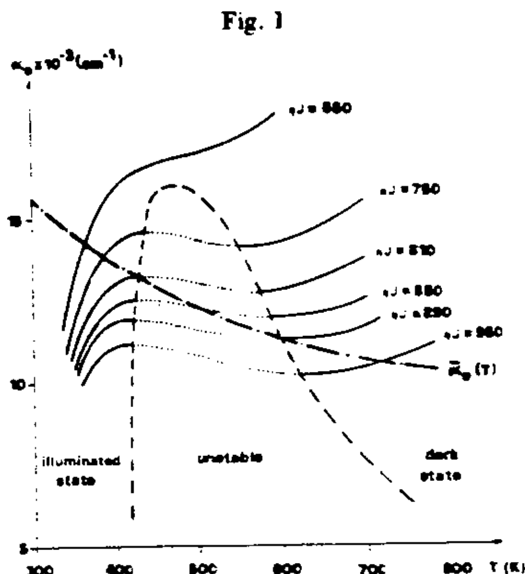

Graphical determination of the stationary state. The continuous and dotted lines represent the stable and unstable parts of the $\alpha_0(T)$ curves. The dashed line marks the boundary between the stable and unstable regions. The stationary state corresponds to the intercept of $\alpha_0(T)$ and $\bar{\alpha}_0(T)$. Oscillation occurs when the intercept is in the unstable region.

is an intensity interval where the intercept corresponds to an unstable solution ; in this case oscillation occurs.

To illustrate this we chose the parameters involved in Kolobov's theory in an arbitrary manner ($\bar{\alpha}_0(0) = 2 \times 10^4$ cm^{-1}, $E_1 = 0{\cdot}15$ eV, $E_2 = 0{\cdot}2$ eV, $f = 2$), and pure thermal relaxation is neglected ($1/\tau = 0$). As shown in fig. 1, with these parameters oscillation occurs in the intensity range $810 < \eta J < 890$.

In § 2.4 we analyse in detail the behaviour of the film in different intensity ranges, assuming that the film was previously annealed.

2.4. *Mechanism of oscillation*

According to our considerations, three different intensity ranges can be distinguished.

(1) The intensity is smaller than the lower threshold for oscillation. In this case only photodarkening takes place and a stationary state is established in the illuminated side.

(2) When no stable stationary solution exists, we use the time-dependent equations (12) and (13) to calculate the time variation of α_0 and T. Because the pseudo-thermal equilibrium is established much faster than the structural equilibrium, we can regard the α_0, T point (characterizing the state of the spot) as moving along the α_0 $(T^{(s)})$ curve corresponding to fixed intensity. It always moves in the direction in which the absolute value of $\bar{\alpha}_0 - \alpha_0$ decreases. The different stages of the oscillation are illustrated in fig. 2. Let us start with a

Fig. 2

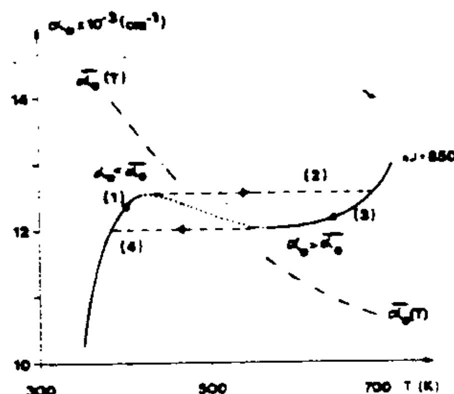

Different stages of oscillation: (1) photodarkening, (2) switch to the dark state, (3) photobleaching, (4) switch to the illuminated state.

sample for which at the beginning α_0 is small. The α_0, T point is on the illuminated branch of the curve. As α_0 is smaller than $\bar{\alpha}_0$, photodarkening occurs and the point moves towards the unstable region. When it reaches the boundary of the unstable region a discontinuous switch takes place. According to our analysis this switch is fast, and there is no time for photostructural changes to take place, i.e. α_0 remains the same. Graphically this means that the spot 'moves' horizontally until it reaches a stable pseudo-equilibrium temperature on the dark side. Along the dark branch of the curve α_0 is larger than $\bar{\alpha}_0$, so photobleaching occurs and the α_0, T point again moves towards the unstable region. At the boundary the next switch takes place to the illuminated state, again fast enough to avoid any significant change in α_0. Thus α_0 again becomes smaller than α_0 and the whole cycle recommences.

The variations in α_0, $\bar{\alpha}_0$ and T during the cycle are presented in fig. 3 for $\eta J = 850$. The corresponding oscillation in the transmission and reflection coefficients are shown in fig. 4, where for comparison experimentally recorded curves are also shown. Considering the simplifications we have made in our model, quantitative agreement of the experimental curves with the calculated ones cannot be expected, but the similarity in the general features of the curves is obvious.

(3) If the intensity is higher than the upper limit for oscillation, photodarkening occurs first, followed by a switch to the dark state. In the dark state photobleaching occurs but is not sufficient to switch the spot back to the illuminated state; a stationary state is established. We note that if the laser beam is switched off and after some time is turned on again, the thermal equilibrium corresponding to the illuminated state is first established (because before switching on the laser, $T = T_F$). The stationary state is reached again through photodarkening, discontinuity and photobleaching. This effect has been observed in a-$GeSe_2$ films (Hajtó and Jánossy 1983, § 3.3, fig. 6).

Fig. 3

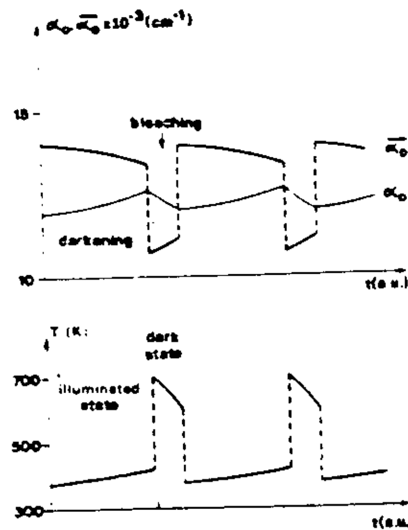

Variations of α_0, $\overline{\alpha_0}$ and T during oscillation for $\eta J = 850$.

Fig. 4

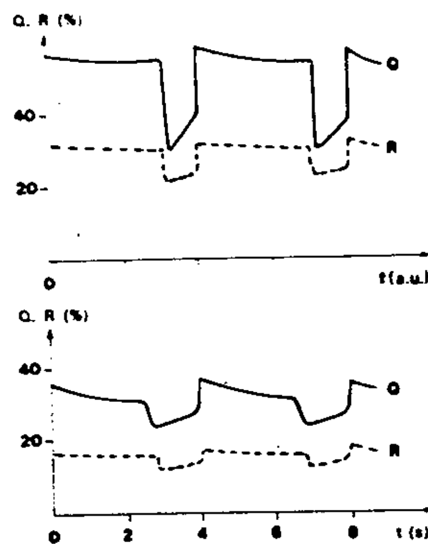

(*a*) Calculated transmission and reflection oscillations for $\eta J = 850$. (*b*) Experimentally registered curves for 6 μm thick self-supporting $GeSe_2$ films. Laser power 13·5 mW, spot diameter 207 μm.

§ 3. Discussion

In § 2 we showed that a combination of thermal and photostructural effects leads to highly non-linear behaviour and to oscillatory phenomenon in chalcogenide amorphous semiconductor films. Our theory explains the main features of observations made of self-supporting a-$GeSe_2$ films (Hajtó *et al.* 1982), namely that oscillations occur in a narrow intensity range; the oscillations consist of four different steps: at lower intensities 'memory effect' photodarkening is observed, at higher intensities the stationary state is reached through photodarkening and discontinuity, and this process is repeated every time the light is switched off. We believe that more detailed agreement could be obtained by taking into account the changes in the refractive index. A further improvement may also be obtained if the thermal relaxation of α_0 could be taken into account, which may have some significance in the dark (high-temperature) phase of the oscillation.

In principal the same theory should hold for $GeSe_2$ samples adhering to a substrate, the main difference being that higher intensities are needed, and as a consequence the oscillations are faster. Indeed, the recorded transmission and reflection oscillations show similar features of self-supporting samples (Hajtó 1980, Hajtó and Apai 1980). A remarkable difference, however, is that the curves obtained with $GeSe_2$ films on substrates are very noisy, especially in the dark state.

In some cases the noise becomes so strong that it is hard to distinguish it from the oscillations. This makes it difficult to carry out systematic measurements with such samples.

As an explanation of this fact we suggest, following Phillips (1982), that the noise is due to laser-induced reversible microcrystallization, and it 'simply reflects the noise of $N \geqslant 10^8$ microcrystallites randomly switching from the ordered crystalline to disordered glassy configurations' (Phillips 1982). The same effect is much weaker in self-supporting films because of the much smaller light intensity.

Finally, we note that according to our model oscillation should occur in any amorphous semiconductor film provided that

(1) the sample thickness, wavelength of the light and film temperature are properly chosen, and
(2) $\bar{\alpha}_s(T)$ is a decreasing function of T.

To show this, consider any material for which Urbach's rule is valid. As a first step the boundary curve between the stable and unstable regions has to be determined. This curve depends only on the thickness L, the film temperature, T_F and $E_g - h\nu$. Thus if L, T_F and (by choosing the wavelength properly) $E_g - h\nu$ are chosen to have the same value as for the curves presented in fig. 1, the same boundary curve is obtained.

The condition for oscillation is that $\bar{\alpha}_s(T)$ should pass through the unstable region. This condition is, of course, not automatically satisfied for a given thickness. However, as $\alpha_0(T)$ at fixed T is inversely proportional to L (D depends only on $\alpha_0 L$, see eqns. (1), (3) and (4)), $\alpha_0(T)$ should necessarily intersect the boundary curve if the thickness is small enough (see fig. 5). Thus if the film is thinner than a critical value of L, oscillation should occur. The above consideration may serve as a guide to finding oscillatory phenomenon in other chalcogenide materials.

Fig. 5

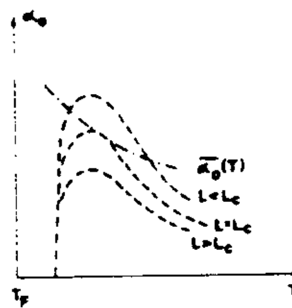

Boundary curves between stable and unstable regions for different thicknesses. If $L < L_c$ the $\bar{x}_0(T)$ curve passes through the unstable region and oscillation occurs.

ACKNOWLEDGMENT

The authors are indebted to Dr. N. Kroó for valuable discussions and continuous encouragement connected with this work, and to Drs. A. E. Owen and M. Frumar for useful conversations on the structure of amorphous systems and for correcting the manuscript.

REFERENCES

ABRAHAM, E., and SMITH, S. D., 1982, *Rep. Prog. Phys.*, **45**, 815.
AVERYANOV, V. L., KOLOBOV, A. V., KOLOMIETS, B. T., and LYUBIN, V. M., 1981, *J. non-crystalline Solids*, **45**, 343.
FAZEKAS, P., 1981, *Phil. Mag.* B, **44**, 435.
GIBBS, H. M., McCALL, S. L., VENKATESAN, T. N. C., GOSSARD, A. C., PASSNER, A., and WIEGMANN, W., 1979, *Appl. Phys. Lett.*, **35**, 451.
GRIFFITHS, J. E., ESPINOSA, G. P., REMEIKA, J. P., and PHILLIPS, J. C., 1982, *Phys. Rev.* B, **25**, 1272.
HAJTÓ, J., 1980, *J. Phys., Paris*, **41**, C4, 63.
HAJTÓ, J., and APAI, P., 1980, *J. non-crystalline Solids*, **35–36**, 1085.
HAJTÓ, J., and JÁNOSSY, J., 1983, *Phil. Mag.* B, **47**, 347.
HAJTÓ, J., JÁNOSSY, J., and FORGÁCS, G., 1982, *J. Phys.* C, **15**, 6293.
HAJTÓ, J., ZENTAI, G., and KÓSA SOMOGYI, J., 1977, *Solid St. Commun.*, **23**, 401.
KOLOBOV, A. V., KOLOMIETS, B. T., KONSTANTINOV, O. V., and LYUBIN, V. M., 1981, *J. non-crystalline Solids*, **45**, 335.
MILLER, D. A. B., SMITH, S. D., and JOHNSTON, A., 1979, *Appl. Phys. Lett.*, **35**, 658.
MOTT, N. F., and DAVIS, E. A., 1979, *Electronic Processes in Non-Crystalline Materials*, second edition (Oxford : Clarendon Press), p. 273.
PHILLIPS, J. C., 1982, *Comments Solid St. Phys.*, **10**, 165.
TANAKA, K., 1980, *J. non-crystalline Solids*, **35–36**, 1023.

Journal of Non-Crystalline Solids 59 & 60 (1983) 1273-1280
North-Holland Publishing Company

MEMORY SWITCHING IN AMORPHOUS SILICON DEVICES

A.E. OWEN*, P.G. LE COMBER+, W.E. SPEAR- and J. HAJTO*

* Department of Electrical Engineering, University of Edinburgh, King's Buildings, Edinburgh EH9 3JL, Scotland, U.K.
+ Carnegie Laboratory of Physics, University of Dundee, Dundee DD1 4HN, Scotland, U.K.

Recent experimental observations on high-speed memory switching in p^+-n-i structures of amorphous silicon are described. Particular emphasis is given to the first switching operation of a virgin device which is effectively a unique forming process for all subsequent operations. There is a characteristic delay for forming, varying over ten orders of magnitude from ~ 10^2 to ~ 10^{-8} s. Evidence is presented to show that forming is a charge controlled process which occurs at a constant field across the n-layer, but details of the switching mechanisms in the a-Si p^+-n-i devices remain obscure.

1. INTRODUCTION

Widespread interest in the phenomena of threshold (monostable or volatile) and memory (bistable or non-volatile) electrical switching in chalcogenide glasses provided the impetus for much of the poineering research in the field of amorphous semiconductors in the late 1960s and early 1970s.[1,2] There are still some controversial features but by and large generally acceptable models for both threshold and memory switching in chalcogenide glasses are now reasonably well established.[3,4]

By contrast, and despite the almost unprecedented growth of research and development on amorphous silicon (a-Si) since the mid-1970s, practically nothing has been reported on electrical switching in that material. Some cursory observations of threshold switching in homogeneous films of evaporated a-Si, with very tentative evidence for memory behaviour, were described by Feldman and Moorjani contemporaneously with some of the early literature on switching in chalcogenide glasses.[5] There seems to have been no further activity until the work of Dey and Fong who observed threshold switching in homogeneous films of evaporated a-Si with titanium contacts.[6,7] Much more recently, den Boer has also reported threshold switching in a-Si, but specifically in <u>hydrogenated</u> n^+-i-n^+ structures (i stands for "intrinsic").[8] To the authors' knowledge, the only other relevant paper, again on hydrogenated a-Si, is the slightly prior publication of Gabriel and Adler[9] who searched unsuccessfully for switching in homogeneous films with molybdenum contacts. They concluded that unlike the chalcogenide glasses, hydrogenated

0022-3093/83/0000-0000/$03.00 © 1983 North-Holland/Physical Society of Japan

a-Si does not have the fundamentally requisite properties for reversible switching behaviour.

The present paper is concerned with studies of the electrical switching behaviour of heterogeneous structures of a-Si which evolved from a collaborative project between the amorphous semiconductor groups at the Universities of Dundee and Edinburgh in the U.K. A preliminary description of this work has already been published[10] and in the following sections a more detailed account of experimental observations will be presented with emphasis on the initial switching operation of freshly prepared (and previously unswitched) devices. It is believed, on the basis of the present evidence, that the first operation is a charge controlled process. The research is still in its early stages however and the switching mechanisms remain obscure.

2. DEVICE STRUCTURE AND FABRICATION

A variety of configurations has been investigated but the majority of the observations to date, and all of the results reported in this paper, have been obtained on devices having a-Si doped and intrinsic (i) layers in the sequence p^+-n-i. The a-Si was deposited by the glow discharge technique, with gas phase doping, as described by Spear.[11] Stainless steel substrates were generally used and the total thickness of the deposited a-Si layers was between 0.5 and 1.0 μm. After completion of the a-Si deposition a series of gold (Au), aluminium (Al) or nichrome (NiCr) dots (up to approximately 1 mm in diameter) was evaporated onto the surface of the samples and the top contact was completed either by a probe or by a thin-wire attached to the metal dots with conducting silver paste.

3. STATIC CURRENT-VOLTAGE CHARACTERISTICS OF VIRGIN DEVICES

Typical current-voltage (I-V) characteristics for a freshly prepared (unswitched) device are illustrated in figure 1(a) in both the forward and reverse directions (the forward direction is defined such that the substrate, and hence the p^+-region, is positively biased). It must be emphasised here that these measurements were taken "by hand", point-by-point, in a manner which required a few seconds for each point to be measured. The significance of this remark will become apparent in the next section. In the forward direction there is a region of ohmic behaviour over an appreciable voltage followed by an abrupt change to a markedly non-ohmic region until, at the point indicated by the arrow, the device was unstable and it was impossible to continue with point-by-point measurements. The change from ohmic to non-ohmic behaviour is more clearly apparent in the conductivity vs. field plot of

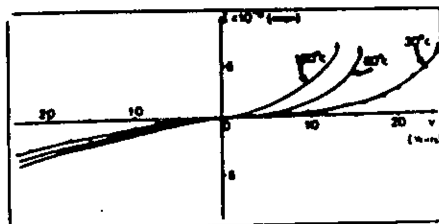

FIGURE 1(a)
Static current-voltage characteristics of a virgin (unformed) device. The positive quadrant corresponds to the p^+-layer positively biased.

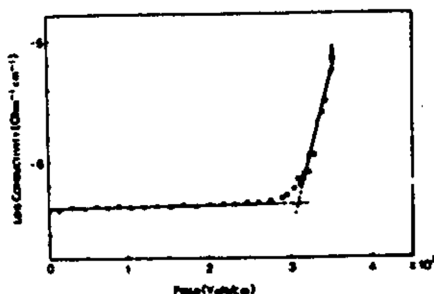

FIGURE 1(b)
The data for 30°C in figure 1(a) plotted in the form log.conductivity vs. field, and illustrating the change from ohmic to non-ohmic behaviour.

of figure 1(b). As ambient temperature increases the onset of non-ohmic behaviour moves to lower voltages. In the reverse direction there is also an initial ohmic region (and this part of the I-V curve is symmetrical) but the change to non-ohmic behaviour is much more gradual and eventually the device breaks down.

4. FORMING - STATIC CHARACTERISTICS

As noted in the previous section, during point-by-point measurements under forward bias, at room temperature, the a-Si p^+-n-i device tends to become unstable when the applied bias is about 25 V. At higher temperatures the instability occurs at lower voltages, as indicated by the arrows in figure 1. On attempting to increase the voltage still further the device switches into a low resistance ON-state. Typical I-V characteristics for both polarities in the ON-state are shown in figure 2; the I-V curve is ohmic, it extrapolates through the origin (i.e. the ON-state is permanent) and it is slightly asymmetrical. Note that the current is now measured in milliamps and the voltages across the device are small. On increasing the voltage in the forward direction the ON-state current continues to increase apparently indefinitely, subject only to any current limiting resistor, and the device is eventually destroyed, presumably by Joule heating. In the reverse

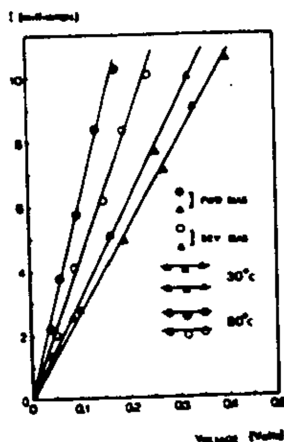

FIGURE 2
Current-voltage characteristics of a device in the ON-state, at different temperatures, in the forward (FWD) and reverse (REV) directions. The forward direction corresponds to the p+-layer positively biased.

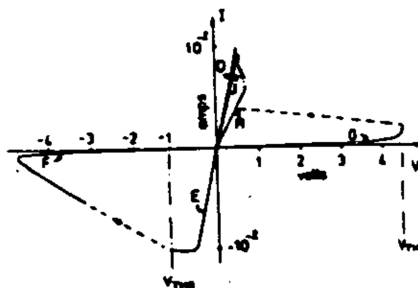

FIGURE 3
Complete static current-voltage characteristics of a formed a-Si p^+-n-i device, showing the forward and reverse threshold voltages, V_{ThF} and V_{ThR} respectively.

direction however another instability is observed and at about -1 V (typically) the device switches back into a high resistance OFF-state. The OFF→ON transition may now be repeated by biasing in the forward direction but on the second and all subsequent switching operations the forward threshold voltage V_{ThF} occurs at a much lower voltage than the first operation e.g. at ~ 5 V compared with the 25 V observed under the conditions obtaining for the measurements shown in figure 1. The first OFF-ON transition, occurring at a relatively high voltage, seems therefore to be unique and by analogy with the usage of switching in chalcogenide glasses, it is referred to as "forming".

The formed a-Si p^+-n-i device may be cycled through ON and OFF states by a sequence of biasing in forward and reverse directions with critical points at V_{ThF} and, in the reverse direction, V_{ThR}. A complete and typical characteristic obtained on a curve tracer is illustrated in figure 3. On occasions the device appears to go through a number of intermediate ON-states during the OFF→ON transition and this is indicated in figure 3. In addition, there is often an observable and appreciable region of negative resistance in the reverse biased OFF-state characteristic of a formed device (also indicated in figure 3).

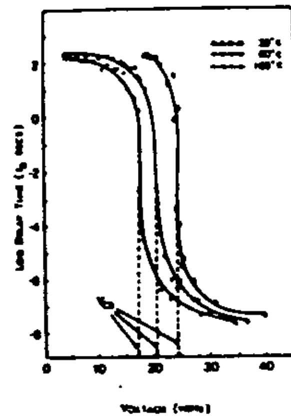

FIGURE 4
The delay time for forming, t_D, as a function of applied voltage, at three different temperatures. See text for details.

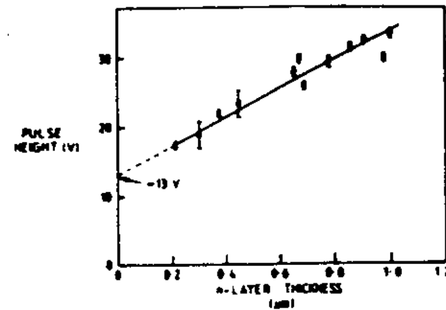

FIGURE 5
Illustrating the variation of the forming voltage, V_F, on applying a voltage pulse, with the thickness of the n-layer.

5. FORMING - DYNAMIC CHARACTERISTICS

The forming process, i.e. the first OFF→ON transition, does not occur instantaneously when a voltage step or pulse is applied to the a-Si p^+-n-i device. Initially there is a delay time, t_D, during which the device current remains essentially constant at the OFF-state value appropriate to the voltage across the device. Only after this delay does the current begin to increase and it then rises essentially instantaneously to its ON-state value. The forming delay time is an extremely sensitive function of the applied voltage and typical data, obtained at three temperatures, are illustrated in figure 4. The forming delay time varies over nearly ten orders of magnitude from a few hundred seconds at low forming voltages to about 10 ns at high voltages. In particular, at a temperature dependent critical voltage V_{CR} there is virtually a discontinuous change in t_D as a function of bias. The voltages V_{CR} indicated in figure 4 are roughly coincident with the voltages at the points of instability marked by the arrows in figure 1; V_{CR} also corresponds to the forming voltage which would be obtained in an experiment on a virgin device with a curve tracer. Note in figure 4 that above and below V_{CR} the delay time tends to a value which seems to be approximately independent of both voltage and temperature; for the particular results illustrated t_D is in the range 10^2-10^3 s for $V < V_{CR}$ and in the range 10-100 ns for $V > V_{CR}$.

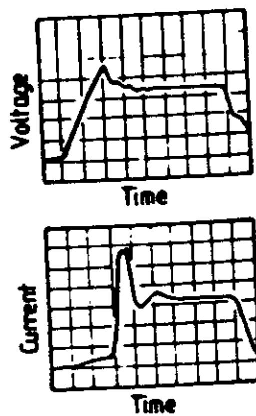

FIGURE 6
The OFF→ON switching transient of a formed device, drawn from an oscilloscope trace. TOP: Applied bias; vertical scale 2 V per division, horizontal scale 20 ns per division. BOTTOM: Device current; vertical scale approximately 6 mA per division, horizontal scale 20 ns per division

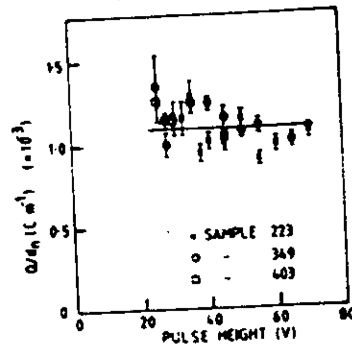

FIGURE 7
The ratio of charge to n-layer thickness (Q/d_n) as a function of forming potential.

The results plotted in figure 4 for $V < V_{CR}$ correspond of course to voltages less than the point of instability indicated in figure 1. There does appear to be a lower limit to the forming voltage however and present results indicate that the limiting voltage coincides with the bias at which the I-V characteristics change from their ohmic to non-ohmic behaviour (see figure 1 and section 3). Several experiments have shown that virgin devices fail to switch (form) even if held for many hours at a forward bias only just below the non-ohmic region. In other words, forming occurs at any forward bias within the non-ohmic region of the I-V characteristics but at voltages below the point of instability t_D is comparatively long. It must also be emphasised again that the device current remains constant at its OFF-state magnitude during the delay time, even when t_D is 100 s or more.

Preliminary experiments have been carried out to determine the effect of device geometry on the forming voltage V_F. It was found that V_F increases linearly with the thickness of the n-layer and data for typical p^+-n-i devices are plotted in figure 5; V_F in this case was measured by a curve tracer and as already mentioned therefore it coincides with the voltage V_{CR} indicated in figure 4. Note that the results do not extrapolate to zero voltage for zero n-layer thickness.

6. DYNAMIC SWITCHING OF FORMED DEVICES

The principal experimental features of the pulsed operation of formed a-Si p^+-n-i devices have already been described.[10] A representative diagram drawn from an oscilloscope trace of the OFF-ON transition on applying a fast voltage ramp is shown in figure 6. The main points to note are as follows:

(i) When biased with a pulse in the forward direction the device switches ON provided the pulse height exceeds the static threshold voltage V_{ThF} as defined in figure 3.

(ii) On the time scale of 1 ns or less, there is no observable delay time in the response of a formed device. The device current follows the applied voltage instantaneously on this timescale.

(iii) Provided the pulse is long enough the ON-state is permanent and the pulse duration required for switching to a memory state increases as the pulse height decreases towards V_{ThF}. In typical cases a permanent ON-state is obtained with pulse durations of a few tens of nanoseconds and magnitude ~ 5 V in excess of V_{ThF}.

(iv) Similarly, on biasing in the reverse direction with a pulse of height V_{ThR} the device switches from OFF-ON and again there is no observable delay in response.

(v) The ON-state appears to be truly permanent. No detectable changes have been observed in devices stored in their ON-state for a year or more.

7. DISCUSSION

The authors' earlier paper on the new a-Si p^+-n-i device focusses mainly on the properties of the formed switch, particularly its dynamic response, and the operational characteristics were compared with those of other switching devices.[10] The switching mechanisms in the new device remain obscure and much more detailed research needs to be done. At this stage therefore there is little to add to the problem of memory switching in formed devices but recent results do provide some insight into the forming process.

It should be noted first that the charge which flows through or into the device during the delay time (i.e. during forming) is an approximately constant function of pulse height for voltages $\geq V_{CR}$. In fact, as illustrated in figure 7, the ratio of charge to n-layer thickness (Q/d_n) seems to be roughly independent of both pulse height and the thickness of the n-layer (sample 403 in figure 7 has an n-layer thickness of 215 nm, sample 349 of 445 nm and 223 of 780 nm). By contrast both the current and the power vary markedly with the pulsing conditions.

These observations suggest very strongly that forming is an electronic process associated with a critical charge density in the n-layer. In terms

of electrons the critical charge is ~ 1.2×10^{19} electrons cm^{-3}. Moreover, the results in figure 5 imply that forming occurs at a constant field across the n-layer. For the particular devices shown the field is 2×10^{5} V cm^{-1}, corresponding to a geometric charge which is rather less than the critical charge. Typically, the ratio of the critical charge to geometric charge varies from about 30 in sample 403 (d_n = 215 nm) to about 100 in sample 223 (d_n = 780 nm). Finally, assuming a carrier mobility of 10^{-1} cm^2 V^{-1} s^{-1}, the transit times across the n-layers are in the range of 1-4 ns for the samples shown. This is not inconsistent with the delay times for $V \;\; V_{CR}$ (see figure 4).

ACKNOWLEDGEMENTS

The authors are grateful to the Venture Research Unit of British Petroleum International Ltd. for a grant supporting the research described in this paper. We also thank Dr. F.F. Carasco, Mr. M.C. Holland (both of Dundee University) and Mr. W.K. Choi for assistance with the experimental work and for enthusiastic help in preparing this paper.

REFERENCES

1) S.R. Ovshinsky. Phys. Rev. Lett. 21, (1968), 1450.

2) A.E. Owen and J.M. Robertson. IEEE Trans. ED-20, (1973), 105.

3) D. Adler, K.H. Hemisch and N.F. Mott. Rev. Mod. Phys., 50, (1978), 209.

4) A.E. Owen, J.M. Robertson and C.M. Main. J. Non-Cryst. Sol., 32, (1979), 29.

5) C. Feldman and K. Moorjani. J. Non-Cryst. Sol., 2, (1970), 82.

6) S.K. Dey and W.T.J. Fong. J. Vac. Sci. and Technol., 16, (1979), 240.

7) S.K. Dey. J. Vac. Sci. and Technol., 17, (1980), 445.

8) M.C. Gabriel and D. Adler. J. Non-Cryst. Sol., 48, (1982), 297.

9) W. den Boer Appl. Phys. Lett. 40, (1982), 812.

10) A.E. Owen, P.G. Le Comber, G. Sarrabayrouse and W.E. Spear. IEE Proc. (Part I, Solid-State Electron Dev.), 129, (1982), 51.

11) W.E. Spear. Adv. in Phys., 26, (1977), 811.

SEMICONDUCTORS AND SEMIMETALS, VOL. 21, PART D

CHAPTER 15

Electronic Switching in Amorphous Silicon Junction Devices

P. G. LeComber

CARNEGIE LABORATORY OF PHYSICS
UNIVERSITY OF DUNDEE
DUNDEE, SCOTLAND

A. E. Owen

DEPARTMENT OF ELECTRICAL ENGINEERING
UNIVERSITY OF EDINBURGH
EDINBURGH, SCOTLAND

W. E. Spear

CARNEGIE LABORATORY OF PHYSICS
UNIVERSITY OF DUNDEE
DUNDEE, SCOTLAND

J. Hajto

DEPARTMENT OF ELECTRICAL ENGINEERING
UNIVERSITY OF EDINBURGH
EDINBURGH, SCOTLAND

W. K. Choi

DEPARTMENT OF ELECTRICAL ENGINEERING
UNIVERSITY OF EDINBURGH
EDINBURGH, SCOTLAND

I. INTRODUCTION 275
II. PREVIOUS WORK ON ELECTRICAL SWITCHING IN AMORPHOUS SILICON 277
III. DEVICE STRUCTURE AND FABRICATION 279
IV. STATIC CURRENT-VOLTAGE CHARACTERISTICS OF VIRGIN DEVICES 279
V. FORMING: STATIC CHARACTERISTICS 281
VI. FORMING: DYNAMIC CHARACTERISTICS 282
VII. DYNAMIC SWITCHING OF FORMED DEVICES 284
VIII. DISCUSSION OF POSSIBLE SWITCHING MECHANISMS 286
REFERENCES 288

I. Introduction

Electronic switches are solid-state devices that can be changed from a nonconducting OFF state to a conducting ON state by an appropriate electrical signal. The importance of such devices in the development of solid-state digital electronics has been enormous and is likely to remain so in the foreseeable future, especially with the increasing demand for memory elements.

Copyright © 1984 by Academic Press, Inc.
All rights of reproduction in any form reserved.
ISBN 0-12-752150-X

The present article is concerned with two-terminal switching devices. Generally, these have one or the other of the two types of current-voltage ($I-V$) characteristics shown schematically in Fig. 1a,b. In Fig. 1a the device switches from its OFF to its ON state at a critical threshold voltage V_{Th}, but if the ON state conditions fall below a critical holding point (I_h, V_h), the device reverts spontaneously to its OFF state. Devices of this kind are called *threshold* switches; they are nonpermanent, or "volatile," and they always revert to the OFF state in the absence of an appropriate bias. In Fig. 1b there is again a critical switching voltage for the OFF to ON transition, but both ON- and OFF-state characteristics extrapolate through the $I-V$ origin. Devices of this kind are therefore permanent, or nonvolatile, and they are called *memory* switches. Memory devices can remain in either the ON or OFF state more or less indefinitely, whether or not a bias is applied and the ON to OFF transition is usually triggered by a current pulse.

By the early 1970s many examples of threshold and memory switching had been reported in *homogeneous* thin films of a variety of amorphous materials, including simple oxides, transition-metal oxides, elemental selenium, and boron. By far the most important materials, however, were the chalcogenide glasses in which, depending on composition, reproducible characteristics of the kind illustrated in Fig. 1a (threshold switching) or Fig. 1b (memory switching) may be obtained (Ovshinsky, 1968; Owen and Robertson, 1973). A substantial specialist literature on electrical switching

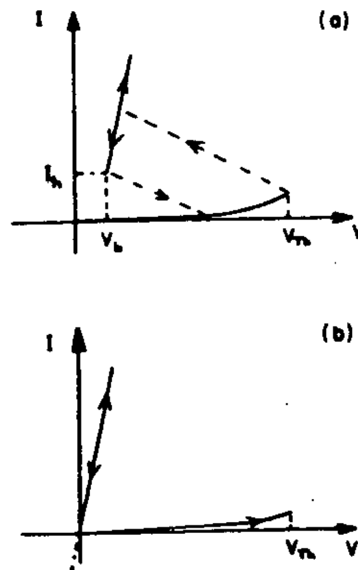

FIG. 1. Current-voltage characteristics for (a) threshold switching and (b) memory switching.

in the chalcogenide glasses has developed, and although there are still some controversial features, generally accepted models of at least a semiquantitative kind are now reasonably well established for both types of switching (Adler *et al.*, 1978; Owen *et al.*, 1979).

This article is concerned with recent studies of a rather different switching behavior in *heterogeneous* structures of amorphous hydrogenated silicon, which evolved from a collaborative project between the authors' groups at the Universities of Dundee and Edinburgh in the United Kingdom. A preliminary account of the work has already been published (Owen *et al.*, 1982), and in the following sections a more detailed description of the experimental observations will be presented.

Before proceeding, however, it is worth noting that, by contrast with the chalcogenide glasses and despite the almost unprecedented growth in research and development on amorphous silicon (a-Si) since the mid-1970s, very little has been reported on electrical switching in the latter material. To put the recent observations in context it is pertinent therefore to review briefly the relatively few previous reports of switching in a-Si.

II. Previous Work on Electrical Switching in Amorphous Silicon

Some cursory observations of threshold switching in homogeneous films of a-Si, with very tentative evidence for memory behavior, were described by Feldman and Moorjani (1970) and Moorjani and Feldman (1970) contemporaneously with some of the early literature switching in chalcogenide glasses. More detailed experiments on the same structures were reported later (Feldman and Charles, 1974; Charles and Feldman, 1975). The authors studied vacuum-evaporated films of a-Si in the range 0.3–2.0 μm thick, fitted with titanium electrodes. They also, incidentally, made similar observations on evaporated films of germanium, boron, and boron plus carbon. As threshold switches these a-Si structures had threshold voltages V_{Th} of 5–10 V, OFF resistances in the range 1–30 kΩ, and an ON resistance of about 100 Ω. In common with the chalcogenide glasses, there was a delay time before switching of 20–50 μsec or more (at room temperature) and the actual switching time was at least several microseconds. Feldman *et al.* did not, however, report any initial "forming" process, unlike the situation in chalcogenide glass switches (see also Part V). As already noted, there was some tentative indication of memory switching, but that feature was apparently not substantiated. Feldman and Charles (1974) interpreted the results in terms of a simple and qualitative electrothermal model involving the formation of a conducting filament; a similar, more quantitative model has been developed for switching in chalcogenide glasses (Owen *et al.*, 1979).

The work of Feldman and his colleagues, which originated in the early

1970s, seems to be the only investigation of switching in a-Si until the later studies of Dey and Fong (1977, 1979) and Dey (1980). These authors report results very similar to those of Feldman *et al.* They studied thin films of a-Si in the range 0.3 - 1.5 μm thick, deposited by electron-beam heating in a vacuum evaporator. Titanium contacts were again used, either in the form of evaporated films or as probes. Dey and Fong reported only threshold switching, with $I-V$ characteristics similar to those in Fig. 1a; they did not mention any evidence for memory behavior. In contrast to Feldman *et al.*, however, Dey and Fong did observe forming effects; that is, the initial threshold voltage was relatively large but it decreased to a more or less constant value after a number of switching cycles. In Dey and Fong's devices the threshold voltage varied systematically from about 6 V for the thinner films (≈ 0.3 μm) to about 9 V for the thicker films (≈ 1.2 μm). The delay time before switching was in the range 2 - 60 μsec, varying in a systematic way with pulse height, pulse duration, and repetition rate, again in a manner very similar to switching in calcogenide glasses (Adler *et al.*, 1978; Owen *et al.*, 1979). Dey and Fong also interpreted their results in terms of a simple one-dimensional electrothermal model, but one developed a little more quantitatively than that by Feldman *et al.*

It should be noted that both Feldman *et al.* and Dey and Fong used a-Si films deposited by vacuum evaporation. This probably accounts for the relatively low OFF-state resistances which they both found (100 - 100 kΩ). It is now well established that vacuum-evaporated a-Si is a very different material from the hydrogenated form of a-Si obtained, for example, by the carefully controlled glow-discharge decomposition of silane (e.g., Spear, 1977).

Three papers concerned specifically with switching in hydrogenated amorphous silicon by Gabriel and Adler (1982), den Boer (1982), and Owen *et al.* (1982) appeared almost concurrently early in 1982, each reporting very different effects observed in different a-Si structures. Our own work (Owen *et al.*, 1982), including recent results, is described in detail in the following sections.

Den Boer studied n^+-i-n^+ structures of a-Si prepared by the glow-discharge decomposition of SiH_4 ("i" stands for "intrinsic" or undoped material). The n^+ layers were 50 nm thick and prepared by adding 1% PH_3 to the SiH_4 gas flow; the i layer in different devices ranged in thickness from 2.5 to 5 μm. Den Boer found that the n^+-i-n^+ devices functioned as threshold switching devices with nonpolar characteristics similar to those sketched in Fig. 1a. For the *first* switching cycle the threshold voltage was in the range 40 - 100 V, but for *all* subsequent operations it was only 10 - 35 V, depending on the i layer thickness (as the i layer thickness increased the threshold voltage also increased). The OFF-state resistance of the n^+-i-n^+ switches

was about 1 MΩ, and the ON-state resistance about 1 kΩ. There was again an observable delay time before switching, ranging from a few microseconds when the applied voltage was about 8 V greater than V_{Th} to about a millisecond for voltages within 1 V of V_{Th}. The n^+-i-n^+ threshold switches could be cycled through at least 10^9 stable switching operations. Den Boer also compared structures with chromium or a combination of chromium and n^+ contacts (i.e., $Cr-n^+-i-Cr$ and $Cr-i-Cr$). The former had rectifying characteristics while the latter switched but were very unstable.

Gabriel and Adler (1982) prepared their a-Si films by sputtering from a polycrystalline silicon target in an argon-hydrogen plasma. In all cases their devices were notionally homogeneous thin films of intrinsic a-Si:H with molybdenum contacts. The samples were fabricated under a wide range of deposition conditions in two sputtering systems, and although results from some of the devices were rendered rather doubtful because of contamination problems, in no case did Gabriel and Adler observe any evidence of reversible switching. They concluded that, in contrast to the chalcogenide glasses, a-Si does not have the electronic and structural properties required for reversible switching.

III. Device Structure and Fabrication

We turn now to the work on electronic switching carried out in the authors' laboratories. Although a number of different a-Si multilayer structures have been investigated, all the results discussed in the following refer to p^+-n-i devices deposited in this sequence by the glow-discharge technique, with gas-phase doping. Stainless steel substrates were generally used and the total thickness of the deposited a-Si layers was between 0.5 and 1.0 μm. After completion of the a-Si deposition a series of gold (Au), aluminum (Al), or nichrome (NiCr) dots (up to approximately 1 mm in diameter) was evaporated onto the surface of the samples, and the top contact was completed either by a probe or by a thin wire attached to the metal dots with conducting silver paste.

IV. Static Current-Voltage Characteristics of Virgin Devices

Typical current-voltage ($I-V$) characteristics for a freshly prepared (unswitched) device are illustrated in Fig. 2a in both the forward and reverse directions. (The forward direction is defined such that the substrate, and hence the p^+ region, is positively biased.) It must be emphasized here that these measurements were taken "by hand," point by point, in a manner that required a few seconds for each point to be measured. (The significance of

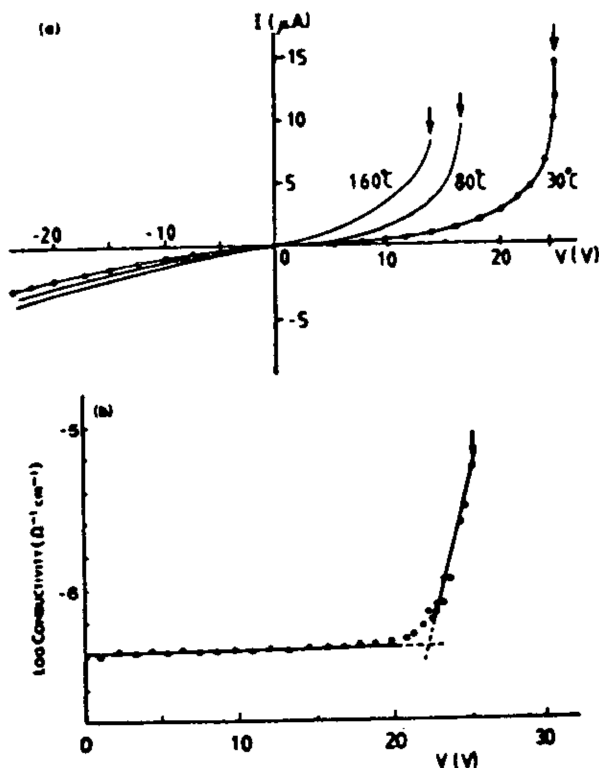

FIG. 2. (a) Static current - voltage characteristics of a virgin (unformed) p^+-n-i device. The positive quadrant corresponds to a positive bias applied to the p^+ layer. (b) The data for 30°C in (a) plotted in the form of log conductivity versus voltage and illustrating the change from ohmic to nonohmic behavior.

this remark will become apparent in the next sections.) In the forward direction there is a region of ohmic behavior over a limited voltage range followed by an abrupt change to a markedly nonohmic region until, at the point indicated by the arrow, the device is unstable and it is impossible to continue with point-by-point measurements. The change from ohmic to nonohmic behavior is more clearly apparent in the effective conductivity versus applied voltage plot of Fig. 2b. As the ambient temperature increases, the onset of nonohmic behavior moves to lower voltages. In the reverse direction, corresponding to a negative potential applied to the p^+ side, there is an initial ohmic region which is symmetrical for positive and negative voltages. However, the change to nonohmic behavior is much more gradual in the reverse direction, leading to the eventual breakdown of the device.

V. Forming: Static Characteristics

As noted in the previous section, during point-by-point measurements under forward bias, the a-Si p^+-n-i device tends to become unstable when the applied bias is about 24 V at room temperature. At higher temperatures the instability occurs at lower voltages, as indicated by the arrows in Fig. 2a. On attempting to increase the voltage still further, the device switches into a low-resistance ON state. Typical $I-V$ characteristics for both polarities in the ON state are shown in Fig. 3; the $I-V$ curve is ohmic, it extrapolates through the origin (i.e., the ON state is permanent), and it is slightly asymmetrical. Note that the current is now measured in milliamperes and that the voltages across the device are small. On increasing the voltage in the forward direction the ON state current continues to increase apparently indefinitely, subject only to any current-limiting resistor, and the device is eventually destroyed, presumably by Joule heating. In the reverse direction, however, another instability is observed, and at about -1 V (typically) the

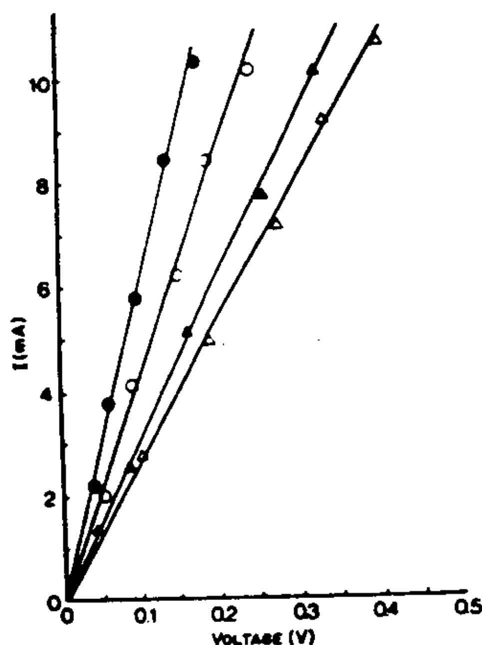

FIG. 3. Current-voltage characteristics of a device in the ON state, at different temperatures, in the forward and reverse directions. The forward direction corresponds to p^+ layer positively biased. (●) forward bias, 80°C; (▲) forward bias, 30°C; (O) reverse bias, 80°C; (△) reverse bias, 30°C.

device switches back into a high-resistance OFF state. The OFF-ON transition may now be repeated by biasing in the forward direction, but on the second and all subsequent switching operations the forward threshold voltage V_{ThF} occurs at a much lower voltage than the first operation, e.g., at ≈ 5 V compared with the 25 V *observed under the conditions obtaining for the measurements shown in Fig. 2.* The first OFF-ON transition, occurring at a relatively high voltage, seems therefore to be unique and by analogy with the usage of switching in chalcogenide glasses, it is referred to as "forming."

The formed a-Si p^+-n-i device may be cycled through ON and OFF states by a sequence of biasing in forward and reverse directions with critical points at V_{ThF} and, in the reverse direction, V_{ThR}. A complete and typical characteristic obtained on a curve tracer is illustrated in Fig. 4. On occasions the device appears to go through a number of intermediate ON states during the OFF-ON transition, and this is indicated in the figure. In addition, there is often an observable and appreciable region of negative resistance in the reverse-biased OFF state characteristic of a formed device, denoted by N in Fig. 4.

VI. Forming: Dynamic Characteristics

The forming process (i.e., the first OFF-ON transition) does not occur instantaneously when a voltage step or pulse is applied to the a-Si p^+-n-i device. Initially there is a delay time t_D during which the device current *remains essentially constant at the OFF-state value appropriate to the voltage across the device.* Only after this delay does the current begin to increase, and it then rises almost instantaneously to its ON-state value. The forming delay time is an extremely sensitive function of the applied forming

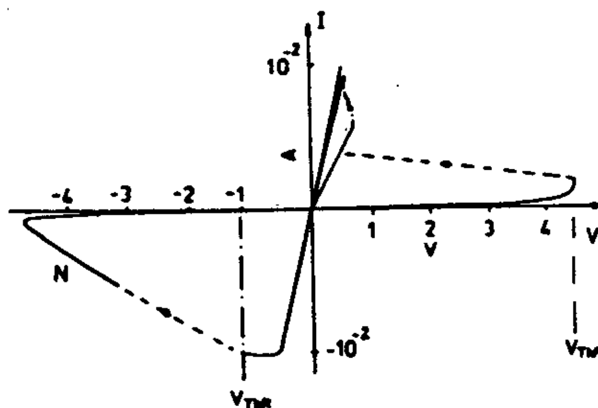

FIG. 4. Complete static current-voltage characteristics of a formed a-Si p^+-n-i device, showing the forward and reverse threshold voltages, V_{ThF} and V_{ThR}, respectively.

voltage V_F, and typical data, obtained at three temperatures, are given in Fig. 5. The forming delay time varies over nearly 10 orders of magnitude, from a few hundred seconds at low forming voltages to about 10 nsec at high V_F. In particular, at a temperature-dependent critical forming voltage V_{CR} there occurs virtually a discontinuous change in t_D. The forming voltages V_{CR} indicated in Fig. 5 are approximately the same as the voltages at the points of instability marked by the arrows in Fig. 2a; V_{CR} also corresponds to the forming voltage obtained in experiment with a curve tracer, operated in ac mode at a frequency of 50 Hz. It can also be seen in Fig. 5 that above and below V_{CR} the delay time tends to a value that seems to be approximately independent of both voltage and temperature; for the particular results illustrated, t_D is in the range 10^2-10^3 sec for $V < V_{CR}$ and lies between 10 and 100 nsec for $V > V_{CR}$.

The results plotted in Fig. 5 for $V < V_{CR}$ correspond of course to voltages less than the point of instability indicated in Fig. 2a. There does appear to be a lower limit to the forming voltage, however, and present results indicate that the limiting voltage coincides with the bias at which the $I-V$ characteristics change from their ohmic to nonohmic behavior (see Fig. 2b). Several

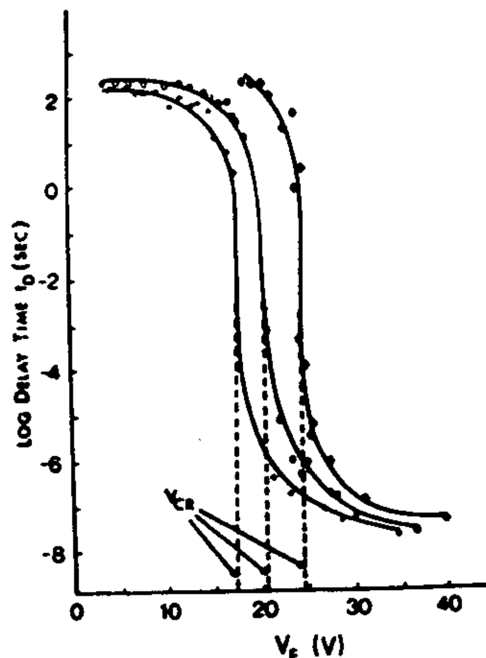

FIG. 5. The delay time for forming t_D as a function of applied forming voltage at three different temperatures: (◆) 30°C, (O) 80°C, (+) 160°C.

experiments have shown that virgin devices fail to switch (form) even if held for many hours at a forward bias only just below the nonohmic region. In other words, forming occurs at any forward bias within the nonohmic region of the $I-V$ characteristics, but at voltages below the point of instability t_D is comparatively long. It must also be emphasized again that the device current remains constant at its OFF-state magnitude during the delay time, even when t_D is 100 sec or more.

Preliminary experiments have been carried out to determine the effects of device geometry on the forming voltage V_F. It was found that V_F increases linearly with the thickness d_n of the n layer. Data for typical p^+-n-i devices are plotted in Fig. 6. In this case V_F was measured by applying a voltage ramp and its value coincides with the voltage V_{CR} indicated in Fig. 5. It can be seen that the results do not extrapolate to zero voltage for zero n layer thickness.

The charge $Q = \int_0^{t_D} I\,dt$, which flows through or into the device during the forming delay time, has been determined for $V_F > V_{CR}$. Figure 7 shows that in this range of V_F the ratio Q/d_n is approximately independent of V_F and d_n for n layer thicknesses between 215 and 780 nm. This could mean that forming occurs when a critical volume charge has accumulated in the n region.

VII. Dynamic Switching of Formed Devices

The principal experimental features of the pulsed operation of formed a-Si p^+-n-i devices have already been described by Owen *et al.* (1982). A representative diagram drawn from an oscilloscope trace of the OFF → ON

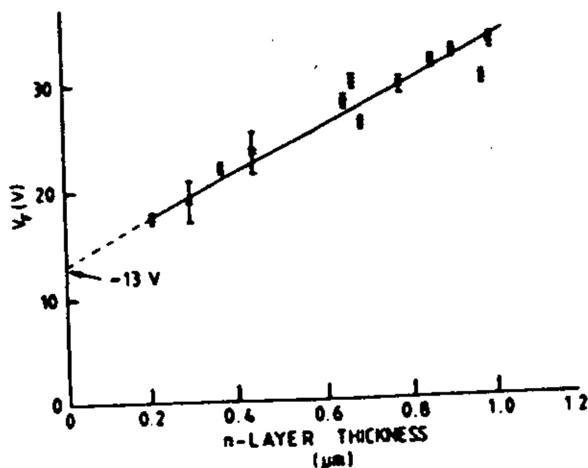

FIG. 6. The dependence of the forming voltage V_F on the thickness of the n layer.

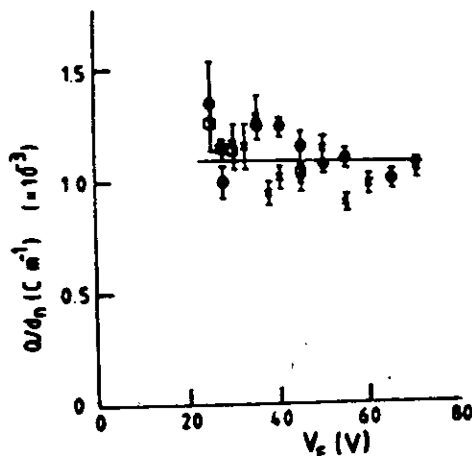

FIG. 7. The ratio of charge to n layer thickness (Q/d_n) as a function of forming potential. d_n = 215 nm (x), 445 nm (O), 780 nm (□).

transition on applying a fast voltage ramp is shown in Fig. 8. The main points to note are as follows:

(i) When biased with a pulse in the forward direction, the device switches ON, provided the pulse height exceeds the static threshold voltage V_{THF} as defined in Fig. 4.

(ii) On the time scale of ~1 nsec or less, there is no observable delay time in the response of a formed device. The device current follows the applied voltage instantaneously on this time scale.

(iii) Provided the pulse is long enough, the ON state is permanent and the pulse duration required for switching to a memory state increases as the

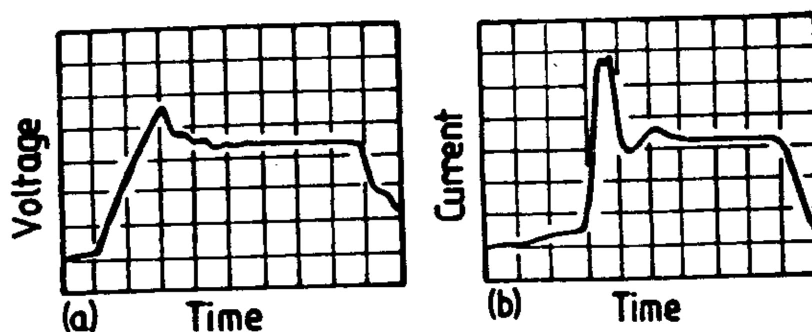

FIG. 8. The OFF-ON switching transient of a formed device, drawn from an oscilloscope trace: (a) applied bias, vertical scale: 2 V per division, horizontal scale: 20 nsec per division; (b) device current, vertical scale: approximately 6 mA per division, horizontal scale: 20 nsec per division.

pulse height decreases toward V_{ThF}. In typical cases a permanent ON state is obtained with pulse durations of a few tens of nanoseconds and magnitude ~5 V in excess of V_{ThF}.

(iv) Similarly, on biasing in the reverse direction with a pulse of height $> V_{ThR}$ the device switches from ON → OFF and again there is no observable delay in response.

(v) The ON-state appears to be truly permanent. No detectable changes have been observed in devices stored in their ON state for a year or more.

VIII. Discussion of Possible Switching Mechanisms

The mechanisms underlying the switching phenomena in the a-Si devices are not understood at present; clearly, more data will be required to explain these exceptional properties. In the following we therefore draw some comparisons with other related switching devices and only briefly speculate on possible mechanisms.

Although there is no observation of memory switching in analogous crystalline Si (c-Si) devices, *threshold* switching is well known in c-Si p^+-n-i, n^+-p-i, and related structures (Yamamoto and Morimoto 1972, Yamamoto *et al.*, 1976; Buxo *et al.*, 1978; Sarrabayrouse *et al.*, 1980; Simmons and El-Badry, 1978; Kroger and Wegener, 1973, 1975). The i-layer in these devices is usually a SiO_2 film (≤ 40 Å), thin enough to pass appreciable tunneling currents, but it may be significant that these metal-insulator-semiconductor-semiconductor (MISS) devices can also be fabricated in an "all-Si" form using polycrystalline Si as the i-layer (Kroger and Wegener, 1975). These devices switch to a nonpermanent ON state when the p^+-n (or n^+-p) junction is forward biased, which is the same polarity producing the memory ON state in the a-Si structures. In the MISS device the switching action is associated with minority-carrier injection from the $p-n$ junction and accumulation at the interface of the i layer, normally leading to punchthrough to the injecting contact, which causes the device to switch ON. The values of the threshold voltage are similar to those observed in the a-Si forming process, and it is conceivable that for this operation the processes are similar. The experimental results described in Part VI, which suggest that the forming process is likely to be charge controlled, would not be inconsistent with this model.

For the c-Si MISS p^+-n-i threshold device the values of threshold voltage are predicted (Simmons and El-Badry, 1978) to depend on $(d_n - W)^2$, where d_n is the thickness of the n layer and W is the width of the depletion region, and for low donor concentrations this dependence is supported experimentally. In contrast, the results in Fig. 6 show that in the a-Si devices the forming voltage varies linearly with d_n. It is difficult to decide at present

whether this disagreement suggests a different mechanism or whether it arises from our attempt to extrapolate from a model developed for a crystalline threshold device to an amorphous memory junction.

An alternative model, based on a regenerative process, has also been suggested for the c-Si MISS devices (Sarrabayrouse *et al.*, 1980), taking into account a carrier multiplication mechanism at the "inverted" Si-SiO_2 interface. The model correctly accounts for a number of MISS properties; for example, it predicts a threshold independent of d_n, which agrees with the observations on p^+-n-i MISS structures when the n layer is more heavily doped. But this model is also in disagreement with the data for the a-Si devices shown in Fig. 6, and just as for the "punchthrough" model, it is therefore difficult at the present stage to decide whether the regenerative model could be relevant to the understanding of a-Si memory switching.

In the field of amorphous semiconductors much attention has been given over the past 10-15 years to memory switching devices fabricated from multicomponent chalcogenide glasses in which the reversible memory action is associated with the growth and destruction of a crystalline filament (Ovshinsky, 1968; Cohen *et al.*, 1972; Steventon, 1974; Owen and Robertson, 1973; Owen *et al.*, 1979). Although it is very likely that in the a-Si devices some form of filament formation (not necessarily crystalline) is taking place in the OFF-ON transition, the switching phenomena are clearly very different from those in the chalcogenides, at least operationally. The most obvious difference is the completely nonpolar character of switching in chalcogenide glass devices, in contrast to the marked polarity dependence of the a-Si memory switches. More important, perhaps, the switching and setting times for the a-Si device are much faster (~ 10 nsec for either the OFF-ON or ON-OFF transition, compared with at least several milliseconds in chalcogenide devices) and the energy involved in the switching process is considerably lower (1 μJ or less, compared with 1 mJ or more). Also chalcogenide glass devices require voltage pulses of magnitude 25-30 V (for a device ≈ 1 μm thick) to establish the ON state, and very often they need 100 or more "forming" cycles before reasonably stable operation is achieved. This again contrasts with the operation of the a-Si memory switch, in which (for a total device thickness of ≈ 1 μm) there is a single forming step with a threshold voltage of about 30 V, and for all subsequent operations the forward threshold (V_{ThF}) is 4-6 V.

The closest parallel to the a-Si devices described in this paper seems to be the observation of memory switching in heterojunctions of n-type ZnSe grown epitaxially on p-type (single-crystal) Ge substrates, reported by Hovel (1970) and by Hovel and Urgell (1971). The ZnSe-Ge heterojunction devices are polar and the transition times for the OFF-ON and ON-OFF operation are both in the region of 100 nsec or less. Similar, but not so

well-substantiated, memory switching characteristics have also been briefly reported in devices fabricated by forming Schottky contacts on *n*-type GaAs and Si (single crystal) (Moser, 1972). Hovel and Urgell (1971), have tentatively and qualitatively explained switching in the heterojunction by a model involving the filling and emptying of traps in the ZnSe, with the formation of a current filament in the ON state. However, even in this case of superficially similar characteristics, there are notable differences. Most significantly, the polarity required for switching in the ZnSe–Ge heterojunction is the opposite to that found in the a-Si devices, and the OFF–ON threshold voltage for the ZnSe–Ge switch decreases substantially with temperature (from about 1 V at 200°K to less than 0.1 V at 400°K), whereas V_{THF} for the a-Si devices investigated so far is at the most only weakly temperature dependent. In addition, the memory state of the ZnSe–Ge heterojunctions is generally lost within a few weeks, whereas no change in the characteristics of the a-Si memory devices has been observed after storage over a period of 18 months.

To conclude this chapter it is perhaps worthwhile to note that the switching phenomena observed in the a-Si memories are not the only nanosecond processes known for this material. Drift mobility studies, which show that electron transit times across about 1-μm-thick films are of the order of 10 nsec or so, have been known for over a decade (LeComber and Spear, 1970; Spear, 1983). More recently, it has been demonstrated that hydrogenated amorphous silicon can be used to modulate light at subnanosecond speeds (Phelan *et al.*, 1981; see also Chapter 13 by Phelan of this volume). In pulsed laser annealing of a-Si it has been suggested that the electron–hole plasma generated by the laser could produce rapid second-order phase transitions (van Vechten *et al.*, 1979). The challenge and excitement in understanding the a-Si memories lies in discovering whether the origins of the fast switching processes are electronic, structural, or both.

ACKNOWLEDGMENT

The authors are grateful to the Venture Research Unit of British Petroleum International PLC for a grant supporting the research described in this paper.

REFERENCES

Adler, D., Henisch, K. H., and Mott, N. F. (1978). *Rev. Mod. Phys.* **50**, 209.
✓ Buxo, J., Owen, A. E., Sarrabayrouse, G., and Sebaa, J. P. (1978). *Rev. Phys. Appl.* **17**, 767.
Charles, H. K., and Feldman, C. (1975). *J. Appl. Phys.* **46**, 819.
✓ den Boer, W. (1982). *Appl. Phys. Lett.* **40**, 812.
✓ den Boer, W. (1983). "Interference Effects and Space-Charge-Limited Conduction in Amorphous Silicon Devices." D. Tech. Thesis, Technische Hogeschool, Delft, The Netherlands, September 1983.

Cohen, M. H., Neale, R. G., and Paskin, A. (1972). *J. Non-Cryst. Solids* **8/10**, 885.
Dey, S. K. (1980). *J. Vac. Sci. Technol.* 17, 445.
Dey, S. K., and Fong, W. T. J. (1977). *Proc. Int. Vacuum Congress. 7th, and Int. Conf. Solid Surfaces, 3rd, Vienna, 1977.* Vol. 3.
Dey, S. K., and Fong, W. T. J. (1979). *J. Vac. Sci. Technol.* **16**, 240.
Feldman, C., and Charles, H. K. (1974). *Solid State Common.* **15**, 551.
Feldman, C., and Moorjani, K. (1970). *J. Non-Cryst. Solids* **2**, 82.
Gabriel, M. C., and Adler, D. (1982). *J. Non-Cryst. Solids* **48**, 297.
Hovel, H. J. (1970). *Appl. Phys. Lett.* **17**, 141.
Hovel, H. J., and Urgell, J. J. (1971). *J. Appl. Phys.* **42**, 5076.
Kroger, H., and Wegener, H. A. R. (1973). *Appl. Phys. Lett.* **23**, 397.
Kroger, H., and Wegener, H. A. R. (1975). *Appl. Phys. Lett.* **27**, 303.
LeComber, P. G., and Spear, W. E. (1970). *Phys. Rev. Lett.* **25**, 509.
Moorjani, K., and Feldman, C. (1970). *J. Non-Cryst. Solids* **4**, 248.
Moser, A. (1972). *Appl. Phys. Lett.* **20**, 244.
Ovshinsky, S. R. (1968). *Phys. Rev. Lett.* **21**, 1450.
Owen, A. E., LeComber P. G., Sarrabayrouse, G., and Spear, W. E. (1982). *IEE Proc. (Part I Solid State Electron Devices)* **129**, 51.
Owen, A. E., and Robertson, J. M. (1973). *IEEE Trans. Electron Devices.* **ED-20**, 105.
Owen, A. E., Robertson, J. M., and Main, C. (1979). *J. Non-Cryst. Solids* **32**, 29.
Phelan, R. J. Jr., Larson, D. R., and Werner, P. E. (1981). *Appl. Phys. Lett.* **38**, 596.
Sarrabayrouse, G., Buxo, J., Owen, A. E., Munoz-Yague, A., and Seboa, J.-P. (1980). *IEE Proc. (Part I. Solid State & Electron Devices)* **127**, (3), 119.
Simmons, J. G., and El-Badry, A. A. (1978). *Radio and Electron. Eng.* **48**, 215.
Spear, W. E. (1977). *Adv. Phys.* **26**, 811C.
Spear, W. E. (1983). *J. Non-Cryst. Solids* **59/60**, 1.
Steventon, A. G. (1974) in Stuke, J., and Brenig, W. eds. "Amorphous and Liquid Semiconductors." Vol. 1, p. 675. Taylor and Francis, London.
Van Vechten, J. A., Tsu, R., and Saris, F. W. (1979). *Phys. Lett.* **74A**, 422.
Yamomoto, T., Kawamura, K., and Shimizu, H. (1976). *Solid State Electron.* **19**, 701.
Yamomoto, T., and Morimoto, H. (1972). *Appl. Phys. Lett.* **20**, 269.

Solid State Communications, Vol.51,No.10, pp.761-764, 1984.
Printed in Great Britain.

0038-1098/84 $3.00 + .00
Pergamon Press Ltd.

PHOTODARKENING AND LIGHT INDUCED ANISOTROPY IN CHALCOGENIDE GLASSES

I. Jánossy, A. Jákli and J. Hajtó*

Central Research Institute for Physics, H-1525 Budapest 114, P.O.B.49, Hungary

(Received May 15, 1984 by A. Zawadowski)

A unified description of photodarkening and light induced anisotropy in chalcogenide glasses is presented in terms of bistable atomic configurations

It is a well established fact, that certain amorphous chalcogenide semiconductors show structural changes under light illumination[1]. There is an irreversible part of the structural changes which occurs in vapour deposited films, prior to any heat treatment[2,3]. On the other hand in melt-quenched glasses or in well-annealed evaporated films so-called reversible structural changes occur. Light illumination, well below the glass transition temperature leads to changes of a number of physical parameters within the illuminated spot, such as optical constants, density etc. Heat treatment near the glass transition temperature restores the initial structure and all parameters become the same as before the illumination. This cycle can be repeated a lot of times.

Photostructural changes are most easily observed through the variation of the absorption coefficient, α.During reversible photostructural changes light irradiation always leads to an increase in α (photodarkening). Furthermore it is observed, that when the illumination is carried out with polarized light, the irradiated spot becomes anisotropic[4,5,6]. The optical axis of the anisotropic structure is determined by the direction of the polarization of the illuminating light beam. The optical axis can be reoriented a lot of times into any direction by rotation of the direction of the polarization. The induced anisotropy can be erased by unpolarized or circularly polarized light[6].

To illustrate the effects mentioned above, in Fig.1 we present experimental results obtained for an annealed $GeSe_2$ film. The absorption coefficients were determined from reflection and transmission measurements, using a dye laser. The film thickness was chosen to be large enough to avoide interference effects. (The dichroism data presented in Ref.(6) may be influenced by interference effects). The anisotropy of the absorption coefficient (dichroism) defined as $\alpha_{\parallel}-\alpha_{\perp}$, is negative and is around 10% of the photodarkening ($\alpha_{\parallel}$ and $\alpha_{\perp}$ are the absorption coefficients for a light beam with polarization parallel and perpendicular to the polarization of the illuminating light beam, resp.).

Photodarkening has been explained by assuming that in chalcogenide glasses local bistable atomic configurations are present[1,7].A similar assumption was made by us to account for the light induced anisotropy[6]. The aim of the present letter is to provide a unified description of photodarkening and induced

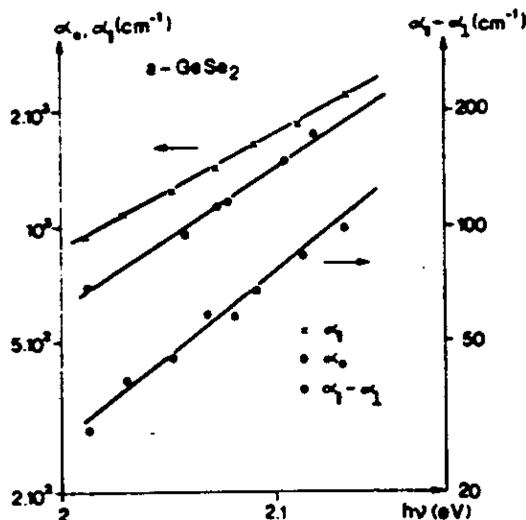

Fig.1 Experimental results for a-$GeSe_2$. Film thickness 20 μm. α_0:absorption coefficient after annealing. $\alpha_{\parallel}$ and $\alpha_{\perp}$: absorption coefficients after illumination at λ=600 nm, for 4h, at power density 12W/cm^2.

* present adress: University of Edinburgh Department of Electrical Engineering Edinburgh, EH9 3JL U.K.

anisotropy by generalizing the previous models.

The existence of bistable configurations (or double-well potentials) is assumed in a number of glasses in order to explain the linear heat capacity and related phenomena observed at low temperatures[6]. We emphasize however that the bistable configurations which are responsible for photostructural changes should differ from those which cause e.g. the linear heat capacity in the following respect. In the latter case there is a continous distribution of the heigth of the potential barriers separating the two minima, thus tunneling transitions occur even at very low temperatures. In case of photostructural changes we assume, that the potential barriers have a more or less well-defined heigth, and this is large enough to prevent thermal transitions even at room temperatures. Such transitions can occur only near the glass transition temperature.

The concept of bistable centres was applied to describe photodarkening quantitatively by Kolobov et.al.[7]. In this model it is assumed that after heat treatment all the bistable atoms sit in the deeper energy minimum. Light irradiation at room temperature makes possible transitions from the ground state to the metastable configuration of the given centre. The transition consists of two steps: an incoming photon excites an electron and this induces the relaxation of the surrounding atoms to a new (metastable) equilibrium position. Of course the invers process, i.e. transition from the metastable state to the ground state can also occur in a similar way. After a long illumination an equilibrium establishes, i.e. the rate of transitions from the ground state equals to that of the invers transitions. Denoting by w_{12} the probability of the first transition and by w_{21} that of the invers one, the equilibrium fraction of the atoms in the metastable state (n_2) is

$$n_2 = \frac{w_{12}}{w_{12}+w_{21}} \qquad /1/$$

The probabilities w_{12} and w_{21} are proportional to $(\mu_1 E)^2$ and $(\mu_2 E)^2$ where $\underline{\mu}_1$ and $\underline{\mu}_2$ are the dipole matrix elements for the electronic excitations in the stable and metastable configurations resp.; $\underline{E}$ is the field strength of the irradiating light beam. Denoting the proportionality factors by A_1 and A_2 we can write.

$$w_{12}=A_1(\underline{\mu}_1\underline{E})^2 \; ; \quad w_{21}=A_2(\underline{\mu}_2\underline{E})^2 \qquad /2/$$

It is reasonable to assume that not only the magnitude of $\underline{\mu}_1$ and $\underline{\mu}_2$ differs but their directions too. We shall show that this circumstance leads to light induced anisotropy.

Although for the time being there is no generally accepted microscopic model of bistable atomic configurations, it is evident that these should be anisotropic. We found convinient to ascribe an "orientation" to the bistable centres in the following way. Let us choose as "reference" centres those bistable configurations for which $\underline{\mu}_1$ and $\underline{\mu}_2$ lie in the XY plane and the bisector of $\underline{\mu}_1$ and $\underline{\mu}_2$ coincides with the X axis. The orientation of a given bistable centre can be characterized by the orthogonal transformation, $\underline{\Omega}$ which transforms a reference centre to the given one. $\underline{\Omega}$ can be expressed with the help of 3 independent parameters, e.g. by the Euler angles[9]. Assuming a uniform distribution of orientations, the number of bistable centres with orientation between $\underline{\Omega}$ and $\underline{\Omega}+d\underline{\Omega}$ in unit volume is $N/8\pi^2 \cdot d\underline{\Omega}$, where N is the total number of the centres per unit volume. /In terms of the Euler angles $d\underline{\Omega} = \sin\theta d\theta d\varphi d\gamma$/.

In the present paper we assume for simplicity that all bistable centres are identical, apart from their orientations. In a reference centre the dipole matrix elements are $\underline{\mu}_1^{(o)}$ and $\underline{\mu}_2^{(o)}$; in a centre with orientation $\underline{\Omega}$ these are $\mu_1=\underline{\Omega}\mu_1^{(o)}$ and $\mu_2=\underline{\Omega}\mu_2^{(o)}$.

The isotropy of the amorphous film after annealing originates from the uniform distribution of the orientations. However after illumination, n_2 depends on the orientation of the bistable centre with respect to the polarization direction of the light beam. From Eqs./1/ and /2/

$$n_2(\underline{\Omega})=A_1(\underline{\mu}_1 E)^2/(A_1(\underline{\mu}_1 E)^2+A_2(\underline{\mu}_2 E)^2) \qquad /3/$$

The dependence of n_2 on the orientation implies macroscopic anisotropy of the illuminated spot.

If the density of the bistable centres is small enough, it can be assumed that these give independent contributions to the change of any physical parameter. In this case the dielectric tensor is

$$\underline{\varepsilon}=\varepsilon_o\underline{1}+\frac{N}{8\pi^2}\int n_2(\underline{\Omega})\underline{\Omega}\underline{v}_o\underline{\Omega}^{-1}d\underline{\Omega} \qquad /4/$$

where ε_o is the dielectric permittivity of the annealed sample.

v_o is a symmetric tensor, which gives the change of $\underline{\varepsilon}$ during a transition from the stable state to the metastable one in a reference centre. $\hat{v}_o$ contains 6 independent parameters, which could be determined only on the basis of a microscopic model. As we shall see below, in fact only 3 parameters enter in the expression for $\underline{\varepsilon}$, wich we shall consider here as phenomenological coefficients.

The imaginary part of $\underline{\varepsilon}$ at optical frequencies determines the absorption coefficients. For symmetry reasons the illuminated spot becomes optically un-

iaxial, so the equilibrium form of $\underline{\epsilon}$ can be written as

$$\epsilon_{ij}=\epsilon_{\perp}\delta_{ij}+(\epsilon_{\parallel}-\epsilon_{\perp})e_i e_j \qquad /5/$$

where $\epsilon_{\perp}$ and $\epsilon_{\parallel}$ denote the dielectric permittivity perpendicular and parallel to the unit vector $\underline{e}$; $\underline{e}$ lies in the direction of the polarization of the irradiating light beam. Evaluating the integral in Eq. /4/ we get

$$Tr\underline{\epsilon}= \epsilon_{\parallel}+2\epsilon_{\perp}=3\epsilon_o+NTr\,\underline{u}_o\, f_o(\beta,M) \qquad /6.a/$$

$$\epsilon_{\parallel}-\epsilon_{\perp}=N\,(u_o^{xx}-u_o^{yy})f_1(\beta,M)+u_o^{xy}f_2(\beta,M) \qquad /6.b/$$

Here β is the angle between $\underline{\mu}_1$ and $\underline{\mu}_2$; $M^2=A_1\mu_1^2/(A_2\mu_2^2)$; the f functions are given in Figs.2 and 3. Eq./6.a/ describes photodarkening, while Eq./6.b/ gives the induced anisotropy.

We note that while $\underline{u}_o$ is a function of the wavelength at which the optical constants are measured, the f functions depend on the wavelength at which the illumination is carried out. According to our model, the dependence of photodarkening and induced anisotropy on the wavelength of illumination/measured atfixed wavelength/ gives information on the wavelength dependence of the parameter $M=(A_1\mu_1^2/(A_2\mu_2^2))^{1/2}$. As f_o is more or less linear in M, from photodarkening measurements the relative variation of M with wavelength can be estimated. On the contrary f_1 and f_2 are far from linear, so anisotropy measurements /in conjuction with photodarkening measurements/ provide information on the absolute value of M.

To demonstrate this possibility, we compared the photoinduced changes

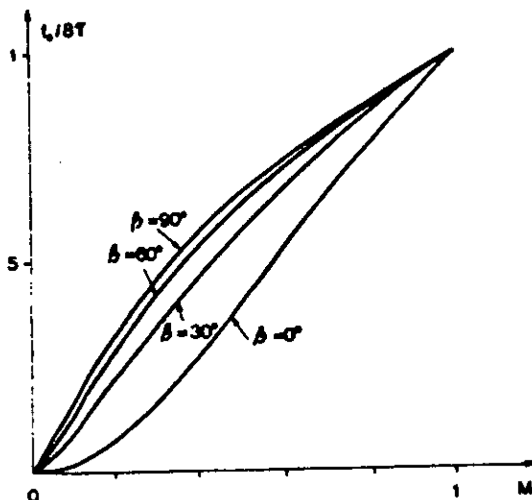

Fig.2 f_o as a function of M and β.

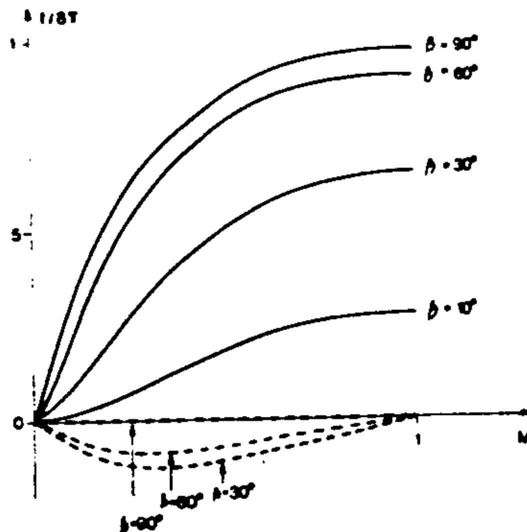

Fig.3 solid line: $f_2(M,\beta)$; dashed line $f_1(M,\beta)$.

in $GeSe_2$ at the wavelengths λ_1=632 nm and λ_2=488 nm (the optical constants were always measured at 488 nm). The first wavelength corresponds to a photon energy which is smaller than the optical gap, while for λ_2 the photon energy exceeds the gap. We found that photodarkening induced by λ_2 is approximately 40% larger than that for λ_1. On the other hand we found that the two wavelengths induce approximately the same anisotropy, although the error of measuerments in this case was rather large /10-15%/. In any case, the difference between the anisotropies seems to be considerably smaller than that of the photodarkening. The results described above are consistent with the assumption that $M(\lambda_2)\gtrsim 1$ and $M(\lambda_1)\lesssim 0.5$. /We assume that $u_o^{xx}-u_o^{yy}$ is not considerably larger than u_o^{xy}. In this case the anisotropy is determined essentially by f_2 /Fig.3//.

The description of photostructural changes presented above implies that to every wavelength and state of polarization of the illuminating light there belongs an equilibrium (usually anisotropic) structure, which is determined by the n /$\underline{\Omega}$/ distribution. Whatever is the initial structure, light irradation establishes the equilibrium configuration belonging to the given wavelength and polarization. This fact makes possible to switch the amorphous film revemibily between different structures by changing the polarization / see reorientation experiments[6]/ or the wavelength. In accordance with this consideration, we

found in GeSe that if a spot was first illuminated at the wavelength $\lambda_{\perp}$, subsequent irradiation at $\lambda_{\parallel}$ bleached the spot, i.e. α decreased by 40%.

As a summary, we think that the description of photosturctural changes in terms of bistable atomic configurations explains the main features of the phenomena. There is of course a number of way to improve the present model. E.g. it may be assumed that two electrons per centre can be excited to induce atomic rearrengments. These electrons may be the two bonding electrons between a Se atom and the two neighbourning Ge atoms. A calculation, where we assumed that the magnitudes of the dipole matrix elements are equal for the two bonding electrons and that these are perpendicular to each other, gave very similar results to those presented in Fig. 2. Furthermore it seems likely that there is a distribution not only for the orientation of the bistable centers, but for other parameters like M and B too. This circumstance is important for the kinetics of photoinduced changes [6].

REFERENCES

1 K. TANAKA, Journ.of Non Cryst.Solids 35-36, 1023 (1980)
2 J.P. de NEUFVILLE in B.O. SERAPHIN (ed), Optical properties of Solids (North-Holland, Amsterdam, 1975/p.437
3 S.RAJOGOPALAN, K.S. HARSHAVARDHAN, L.K. MALHOTRA and K.L. CHOPRA, Journal of Non-Cryst. Solids 50, 29 (1982)
4 V. G. ZHDANOV, B.T. KOLOMIETS, V.M. LYUBIN and V.K. MALINOVSKI, Phys. Stat. Sol. (a) 52, 621 (1979)
5 J. HAJTO and P.J.S. EWEN, Phys.Stat.Sol. (a) 54, 385 (1979)
6 J. HAJTO, I. JANOSSY and G. FORGACS, J.Phys. 15, 6293 (1982)
7 A.V. KOLOBOV, B.T. KOLOMIETS, B.T. KONSTANTINOV and V.M. LYUBIN, Journ. of Non-Cryst. Solids 45, 335 (1981)
8 W.A. PHILLIPS (ed), Amorphous Solids, Low-Temperature Properties (Topics in Current Physics Vol. 24, Springer-Verlag Berlin, 1981).
9 G.A. KORN and T.M. KORN Mathematical Handbook for Scientists and Engineers (MC.Graw-Hill. New York, 1961) p.413

Applications of Amorphous Semiconductor Materials in Electronics

J. HAJTO and A. E. OWEN *Department of Electrical Engineering, University of Edinburgh, Edinburgh EH9 3JL*

Abstract

A brief summary of the present state of the art of amorphous semiconductors and their applications in modern electronics is presented in this paper. The recent developments in chalcogenide glass thin film devices and in amorphous silicon electronic devices are reviewed. A potentially interesting application of a-Si (p^+-n-i) thin film structures as fast non-volatile electronic memory elements is also discussed.

Introduction

The purpose of this paper is to provide a brief summary of the present state of the art of amorphous semiconductor materials and their applications in modern electronics. In certain applications amorphous semiconductors can compete with crystalline semiconductors as active and passive elements in electronics and optoelectronics. The physical properties of amorphous semiconductors are now better understood, leading the way to a wider range of new applications in electronics. Their preparation usually does not require carefully controlled growth techniques and this can be an important economic advantage in some applications. Amorphous semiconductors are often easily prepared in the form of glasses by fast cooling the material from its liquid phase. The freedom from the constraint of atomic periodicity means that an even wider range of compositions can be formed as thin films by deposition from the vapour phase onto any suitable substrate, forming non-epitaxial heterostructure junctions.

The main difference between crystalline and amorphous semiconductors lies in their structure. In crystalline materials the constituent atoms or molecules are aligned in regular three dimensional arrays that exhibit a long range periodicity. In the amorphous materials there is no long-range periodicity, although there is a well defined short range order of atoms or molecules since the distance between the closest neighbouring atoms is well established, as illustrated in Figure 1.

Amorphous materials, like their crystalline counterparts can be insulators, semiconductors or metals, and in some cases superconductors. This is possible because, as suggested first by A.F. Ioffe and A.R. Regel in 1960, the electronic properties of amorphous solids are determined by their short range order (i.e. the chemical nature of their constituent atoms) and not by their long range order.

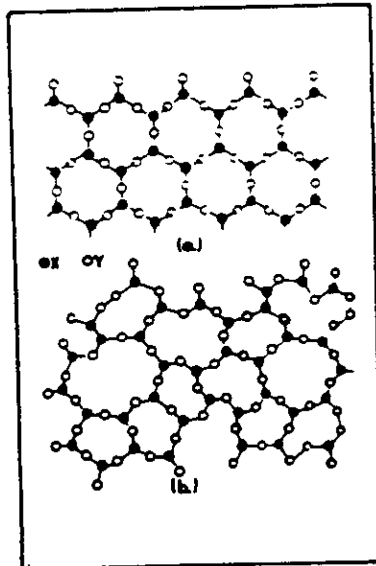

Fig. 1 A two dimensional representation of the structure of a hypothetical compound of stoichiometry X_2Y_3 in the crystalline (a) and amorphous form (b).

There are two main classes of amorphous semiconductors, insofar as practical applications are concerned, viz. The chalcogenide glasses: glasses containing a large percentage of one or more of the "chalcogen" elements (sulfur, selenium and tellurium). Due to the elasticity of the chemical bonding configuration (lone-pair bonding structure), the chalcogenide glasses possess a high degree of structural and electrical flexibility. As a consequence, many new physical phenomena such as reversible phase transition, electrical switching and memory effects, photostructural changes and photodoping have been observed in these materials.

The second important group of amorphous semiconductors is represented by the tetrahedrally bonded amorphous solids such as a-Si and a-Ge whose physical properties are not radically different from those of the corresponding crystals. They can be doped with chemical impurities i.e. they can be made into solid state p-n structures (diodes, transistors etc.). In contrast to chalcogenide glasses, the tetrahedrally bonded amorphous semiconductors show more structural rigidity.

Both classes of amorphous semiconductors can be used for a wide variety of potential applications. In the Table 1 the observed physical or chemical effects and the applications of the amorphous semiconductors are summarised.

A detailed account of all the possible applications of amorphous semiconductors is not possible in this paper. For

example, amorphous selenium a (conventional photoconductive material) was used in a Zerox 914 copier that was the first automatic photocopying machine in the world. We have selected what we felt to be the most promising topics in the technology developed recently. Our emphasis has been placed on some of the newest applications connected to chalcogenide glasses and to the tetrahedrally bonded amorphous silicon structures.

In part 1 the various electronic and structural properties of amorphous chalcogenide glasses are described in relation to the photostructural and photodoping effects which have important application aspects in micro-lithography.

In part 2 the device physics and fabrication technologies of amorphous silicon structures are described. The amorphous silicon solar cells are also discussed here. The structure and application of thin film field effect transistors are also demonstrated. A potentially interesting application of a-Si (p^+-n-i) thin film structures as fast non-volatile electronic memory elements is also shown in this section.

Conclusion

The amorphous semiconductor materials reviewed here will have an important impact on modern electronics in the near future. These materials have characteristics similar to plastic and metallic compounds, namely wide controllability and flexibility of their physical and chemical properties.

Being free from the constraints of periodicity in the atomic network, amorphous semiconductors promise relatively low cost fabrication of large area thin film elements (basic elements for almost all of the practical electronic devices) with good mass producibility.

The recent discovery of valency controllability in tetrahedrally bonded amorphous semiconductors (a-Si, a-Ge) promises a wide variety of potential applications in electronics and opto-electronics. These materials also have excellent photoconductivity and high absorption coefficient for visible light as well as thin film large area feasibility which is a necessity in low cost

BASIC PROCESS	PERTURBATION	CONTROLLABLE PROPERTY	APPLICATIONS
Low field conductivity	Temperature	Conductivity	Thermistor
Double injection Impact ionization Filamentary breakdown	Electric field	Conductivity	Threshold switch Triode analog device (4 tots)
Thermal instability Negative resistance	Electric energy (V x I x t)	Conductivity	Thermistor Bistable switch
Interface effect Valency control	Bias voltage	Potential, interface potential and current across the barrier	Polarized switch Amorphous transistor FET
	Light (Optical image)	Photoconductivity (Surface charge)	Electrostatic printing Electro-photographic printing (Xerox)
		Photoconductivity Photovoltaic effect	Photosensor Solar cell (a-Si:H:F) Image convertor Image pick-up (Saticon)
Photoelectron emission	Light	Secondary electron emission rate	Electron beam memory
Reversible phase transition	Pulse current	Conductivity	Memory switch
Photoinduced crystallization	Light pulse (Laser scanning)	Reflectance Transmittance	Optical mass memory Holography
Photoinduced nucleation	Light pulse (Optical image)	Reflectance	Photography Microfiche
Photodarkening	Light (Optical image)	Reflectance Transmittance	Super microfiche Optical memory
Photochemical effect	Light (Optical image)	Etching rate	Mask processor Photo-lithography
Photostopping effect	Light (Laser beam)	Absorption coefficient	Light switch Optical modulator
Electro-optical effect	Acoustic wave	Refractive index	Light switch Beam deflector Optical modulator

TABLE 1 Physics and applications of amorphous semiconductors (after Hamakawa 23)

solar photovoltaic systems and in the field of optoelectronic image sensing elements.

By intensive research in device technology and preparation techniques large area high packing density a-Si devices will be in practical use in the near future.

PART 1

Chalcogenide Glasses and their applications in electronics and optoelectronics

We want to emphasise that their differences, rather than their similarities make the subject of the application of the chalcogenide glasses interesting. One fundamental difference is that the structure and the chemical bonding configurations of chalcogenide glasses are not determined and fixed by thermodynamic equilibrium conditions but can be altered, sometimes reversibly, by an electric field or by illumination. In this part we discuss mainly the structural changes caused by illumination (light).

Effect of light

At least seven distinct photo-induced structural of physico-chemical changes can be observed in amorphous chalcogenides when they are exposed to light:

1. Light induced changes in local atomic configuration including photo-darkening and photo-bleaching effect.
2. Photo-decomposition (in compounds).
3. Photo-crystallization.
4. Photo-polymerisation.
5. Photo-induced morphological changes
6. Photo-dissolution of metals.
7. Photo-vaporization.

The effects may be reversible i.e. annealing at Tg (softening temperature) will restore the original structure and properties, or irreversible. The above mentioned effects seem to be a feature of the amorphous structure and are not observed in the corresponding crystalline material.

Much attention has been focused on the basic physical processes in order to understand these new phenomena [1] as well as on applications for photographic imaging [2], holography [3-4], optical memories [5] and particularly microlithography [6]. Broadly speaking, all of the photo-induced phenomena in chalcogenide glasses can basically be characterised as changes in the amorphous structure caused by irradiation. The resulting new amorphous structure is different not only in optical but also in electrical, mechanical and chemical properties. The photo-induced changes in the chemical properties promise one of the most important applications for chalcogenide glasses in microfabrication technology and lithographic printing.

Photocrystallization

The photocrystallization effect is an amorphous-crystalline phase transformation under the influence of the laser irradiation. The effect can be used for optical mass memory applications because the optical density is altered by several orders of magnitude for light near the absorption edge. The structural state of the illuminated area can be read out in reflection, for example. The reflectivity of tellurium-rich amorphous chalcogenide films changes by a factor of 2 as a result of amorphous-crystalline phase transition [7]. For practical applications the amorphous chalcogenide film is deposited on a transparent disk rotated by a motor. The same laser beam can be used for dot writing, erasing and for reading the binary information (amorphous or crystalline state). The stability, reversibility and the speed of the photocrystallization ($1\ \mu m/10^{-6}$ sec at 10^{-8} Joule laser energy) makes this system promising for high density and fast optical memories.

Video-Disk Based on Photo-induced morphological changes

Tellurium based amorphous chalcogenide films such as As-Te and As-Se-Te systems provide optical video recording material of excellent quality [8]. The amorphous chalcogenide films are evaporated on a glass or PMMA (polymethyl-methacrylate) disks with diameter of 33 cm. The thickness of the active material is about 400 A. The optical recording is realised by creating holes in the chalcogenide layer using focused pulsed argon-ion laser beam (λ = 4800 A). The thermal effect of the laser beam causes the central part of the irradiation spot to be either evaporated or pulled away toward the edge of the softened area by surface tension. The pulse duration of the Ar-ion laser is about 22 nanoseconds. These effects result in clean shaped holes in the thin film, suitable for optical video recording. The prototype of a high speed random access colour video disk was developed using As-Te-Se thin film as a recording medium [8] with the estimated signal to noise ratio about 45 dB.

Photodoping and Microlithography

The photodoping effect is probably the most promising for applications. Relatively large amounts of metals, especially silver, can diffuse into chalcogenide glass films under the influence of irradiation. The effect can be observed at room temperature at illumination levels as low as 10^{-4} J/cm^2.

As a result of Ag-photodoping, a drastic change takes place in the chemical solubility of chalcogenide glasses. Normally these glasses dissolve easily in alkaline solutions but after photodoping with silver they become almost insoluble in alkaline solutions. The Ag-(As_2S_3) and Ag-(Ge-Se) systems have been investigated most intensively.

Structural studies by Raman spectroscopy [9] suggest that the photodoping process is a two-stage solid state reaction. Initially Ag_2S is formed and after a prolonged exposure there is a further photo-induced effect towards the formation of a glassy Ag-As-S phase. X-ray diffraction studies [10] also reveal the formation of Ag_2SS and As_2S_2 crystallites during the photodoping process.

For practical application the Ag-Se-Ge system is often chosen because it does not contain arsenic (a typical donor impurity in silicon). In this system both the photodoping and the photostructural changes can be effectively used in such a way that both negative and positive type photo-resists can be realised. However the photodoping effect has the advantage of the bigger sensitivity to light. So far organic polymers have been used as photoresists for manufacturing silicon integrated circuits. The Ag-Ge-Se system can be used as a new inorganic photoresist. The typical etching characteristics of amorphous $Ge_{75}Ge_{25}$ thin films are shown in Figure 2. The etch rate of the exposed area is about 15% higher than that of the unexposed area [11]. The etch rate ratio between exposed and unexposed area was about constant. This effect

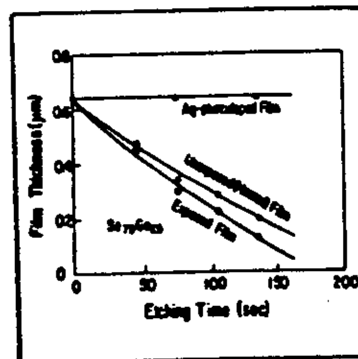

Fig. 2 Etching characteristics of $Se_{75}Ge_{25}$ glass thin film in an aqueous solution of NH_3 (after A. Yoshikawa et al [11]).

yields a positive type photoresist. On the other hand, the Ag photodoped Se-Ge film does not dissolve into alkaline solutions. This suggests a negative type photoresist application. The typical photoetching process steps are shown in Figure 3. After the deposition of the Ge-Se film, the process is divided into positive and negative cases. The positive process is simpler because no additional Ag deposition is necessary. The positive process is attributed to the photo-structural changes. The negative process is based on the Ag-photodoping effect. A precise etching control is not necessary for the negative process because the decrease in film thickness of the exposed area during the complete etching off process of the unexposed area is negligible. This permits use of a fairly thin starting film which is advantageous for fine patterning. The experimental results indicate that the negative type application is superior to the positive one considering the sensitivity, contrast and remaining final thickness.

On the other hand amorphous Se-Ge films showed a strong resistivity to acid solutions, such as HF, HF-NF-NH_4F, H_3PO_4, HCl and H_2SO_4 which are conventionally used in silicon device fabrication. This fact is important because the etch-resistant capability is a fundamental requirement for a photoresist-film.

The Se-Ge films also have a very good "dry development" capability (using plasma etching) which is an advantageous feature of this new type of inorganic photoresist [12]. Also the electron beam exposure characteristics [13] in the low accelerating range are comparable to that of the polymethyl methacrylate (a conventional organic photoresist).

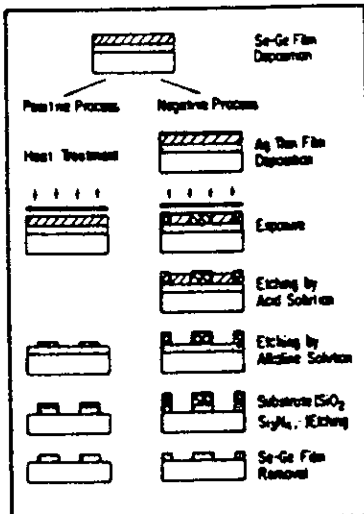

Fig. 3 Photoetching process for a-Se-Ge thin films (after A. Yoshikawa et al [11]).

The attractive feature of the chalcogenide glass photoresists is their high resolution. Fine patterns less than 1 μm wide can be easily obtained by normal contact printing. Grating patterns under 1000 Å, produced by holographic exposure, have also been reported [14]. The intrinsic resolving limit expected from the nature of the amorphous structure is probably less than 100 Å. It has been demonstrated experimentally, by use of transmission electron microscopy, that the spatial resolution for the Ag-photodoping effect is at least as fine as 10 Å [15].

This new inorganic photoresist material is the subject of intense research and development because of its high resolution capacity and dry processing nature. One of the most important applications of chalcogenide glasses is believed to be in this microlithography technology.

PART 2

Application of Amorphous Silicon in Electronics

With the recent developments in the crystalline silicon VLSI (Very Large Scale Integration) technology there has been a fascinating achievement in chip sizes and integrated functions.

However there is always a potential need for new types of materials because of the present disadvantages of the devices based on the crystalline materials. We should mention here for example that due to the high temperature and slow crystal growth process the energy requirements in the manufacture of crystalline silicon devices are high. Furthermore, it is difficult to produce large area devices to control display or sensing elements. A liquid crystal real time TV display has been demonstrated recently that uses integrated multiplex switching arrays (240 x 240) on a single crystal Si wafer. The display area (44 x 56) mm^2 has been limited by the wafer size.

Another problem arises in the field of the electronic memory devices, namely that there is a lack of an economic low power, fast read/write non-volatile memory (i.e. the data are stored if the power is removed) based on crystalline silicon technology.

The amorphous silicon (a-Si:H) produced by glow discharge decomposition of silane (SiH_4) seems to be one of the most promising new semiconductor materials. It possesses several new features as compared to the crystalline silicon:

- (a) large area device feasibility;
- (b) ease of preparation and chemical stability;
- (c) lower cost in manufacture;
- (d) high optical absorption and high photoconductivity;
- (e) new type physical effects attributed to the amorphous structure only.

In 1975 Spear and Le Comber demonstrated that the electronic properties of the hydrogenated amorphous silicon (a-Si:H) films prepared by the glow discharge decomposition of silane (SiH_4) could be controlled by a substitutional doping in the gas phase [16]. The doping effects on electrical conductivity is shown in Figure 4.

It is apparent from Figure 4 that relatively small concentrations of diborane and phosphine in the silane gas during the deposition can change the room temperature conductivity of a-Si:H films by more than six orders of magnitude. The ability to control the doping of a-Si:H films (n-type and p-type) has opened up a wide variety of potential applications for amorphous silicon films in the field of electronics and optoelectronics. Applications as electronic devices such as diodes [17], transistors [18] as well as optoelectronic devices such as solar cells [19], xerographic printers [20], image pick-up tubes [21] and image sensing array [22] have been investigated. In this section we will discuss the application of amorphous silicon films in solar cells, field effect transistors and image sensors. A new non-volatile electronic

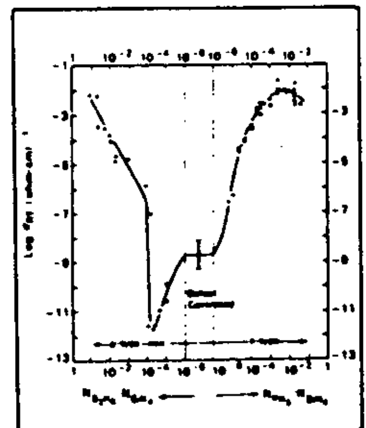

Fig. 4 Dark electrical conductivity at room temperature for a-Si:H films as a function of doping gas ratio (after W.E. Spear and P.G. Le Comber [16]).

memory device based on amorphous silicon p⁺-n-i structure is also described.

Amorphous Silicon Solar Cells

Photovoltaic energy conversion is based on three processes: (a) light absorption through the interband optical transition, (b) free carrier generation by dissociation of photo-excited electron-hole pairs, (c) free carrier transport by drift and/or diffusion. There is a clear difference between photovoltaic generation in single crystalline silicon p-n junctions and amorphous silicon p-i-n junctions (i stands for the intrinsic layer). The collection efficiency in the latter is presently limited by the low value of the minority carrier diffusion length. The hole mobility value in the n-region is below 1 $cm^2/V/sec$, therefore the corresponding diffusion length is about 0.3 μm. As a consequence the collection of electron-hole pairs is restricted to the space-charge region which is about 0.3 μm thick and this is not enough to absorb the sunlight fully. Another limitation is that the optical energy gap of the material (E_g - 1.7 eV) is too large to absorb the whole solar spectrum for high efficiency solar cells.

Theoretical estimates of the photovoltaic conversion efficiency give a highest possible value of 15% [23], assuming 100% collection efficiency in a 1 μm thick film. The conversion efficiency achievable using the present p-i-n type structures is about 10% assuming a fill factor of 0.75 for an amorphous silicon solar cell with a minimum localised state density of 10^{17} $cm^{-3} eV^{-1}$. The progress in improving the efficiency of a-Si solar cells and the possible improvement in the near future are summarized in Figure 5 (after Y. Hamakawa [23]).

The first commercial a-Si solar cells for calculators were developed and marketed by Fuji Electric and Sanyo in 1980. Also a power generation system consisting of a-Si solar cell modules was built in Japan in 1981.

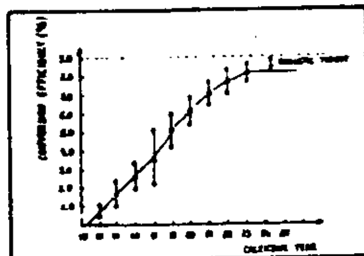

Fig. 5 Technological progress in the efficiency of a-Si solar cells and the possible improvements for the near future (after Y. Hamakawa [23]).

Further improvement in cell performance requires the quality of the intrinsic region to be improved by reducing the density of localised defect states in the bandgap. Nevertheless, amorphous silicon solar cells have good prospects, and the following are important practical advantages:

(a) The energy requirement in manufacturing an a-Si solar cell is much less than that for a single crystal Si solar cell because of the much lower temperatures involved in the preparation of a-Si (200-400°C), and because it does not require the very lengthy high temperature crystal growth.

(b) Solar cells of a-Si can be constructed with a thin film structure of about 1 μm in thickness, because of the large absorption coefficient of the material ($\alpha > 10^4$ cm^{-1}) in the visible region of the solar spectrum.

(c) The preparation of a-Si films by the glow discharge decomposition of silane on inexpensive substrates such as stainless steel or glass plate is ideally suited to the development of large area solar cells. For example a-Si cells with 49 cm^2 and 100 cm^2 area were developed by Fuji Electric and Sanyo.

Amorphous Silicon Field Effect Transistors

In 1972 Spear and Le Comber investigated the density of states distribution in a-Si by the field effect method [24]. They demonstrated that the conductivity of the a-Si:H films can be altered by several orders of magnitude by applying moderate gate voltages. The cross-sectional structures of a-Si FETs (field effect transistors) investigated so far are summarized in Figure 6 [23].

For the active layer, non-doped or slightly doped a-Si:H layers are used. Doped low resistive single crystal Si wafers are used for substrates. Glass or vitreous quartz can also be used for integrated devices. In the first a-Si FET (type (c) in Figure 6) plasma continuous vapour discharge (CVD) Si_3N_4 was used as the gate insulator and glow discharge deposited a-Si:H was employed for the active layer [25]. The drain current increases three orders of magnitude with 20 V on the gate. An improved FET was also developed by Snell et al which was applied to a 5 x 7 element liquid crystal driver [26]. In this device the drain current in the OFF state (zero gate voltage) is below 10 pA and the current increases five orders of magnitude with 15 V on the gate.

The non-doped a-Si insulated gate FET should operate in both n- and p-channel modes [27]. Generally an OFF-ON drain current ratio of more than 10^4 can be achieved using different structures. This is sufficient for matrix switching applications in liquid crystal display devices [26].

The switching speed of the a-Si FET is limited by the carrier mobility of the amorphous silicon which is lower than in the case of the crystalline material. However in the experimental a-Si FET structures the rise time of the drain current can be reduced to 1 μ sec or les by optimizing the geometry of the device and applying large transient pulses on the gate.

Due to the large area device feasibility (the size is not limited by the single crystal wafer) the a-Si FETs have a clear advantage over the crystalline ones when the switching speed is not a limiting factor. Hence the application of a-Si FETs is favourable in the

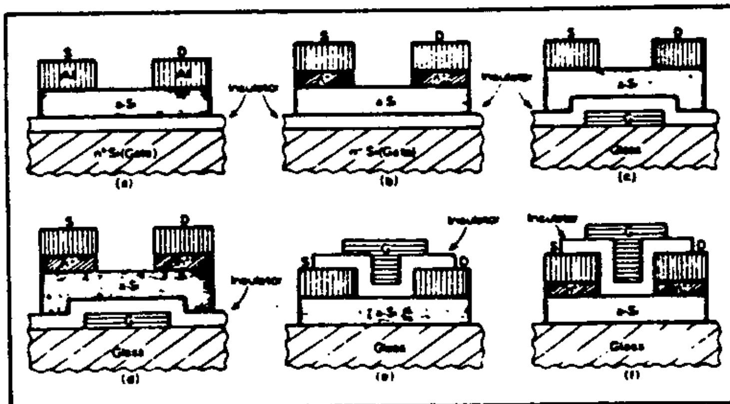

Fig. 6 The cross-sectional structures of a.Si FETs investigated.

field of integrated image sensors.

Integrated Image Sensors

In 1982 the Microelectronics Research Laboratories (Nippon Electric Co.) developed a 960 element a-Si:H contact linear image sensor using Si_3N_4 as a hole blocking layer and a p-type a-Si:H (p-a-Si:H) as an electron blocking layer [22]. The structure of the photosensing element is shown in Figure 7. The I-Si(H) layer refers to the intrinsic amorphous silicon and the ITO electrode refers to Indium Tin Oxide transparent electrode. The photosensing elements were connected to standard 8 elements/chip MOSFET (Metal Oxide Semiconductor) switches using flexible printed circuit sheets and 120 MOS ICs (integrated circuits) were used for driving the 960 photosensing elements. Figure 8 shows the detection and suppression circuit. The signal light irradiates the photosensing element and generates a photocurrent.

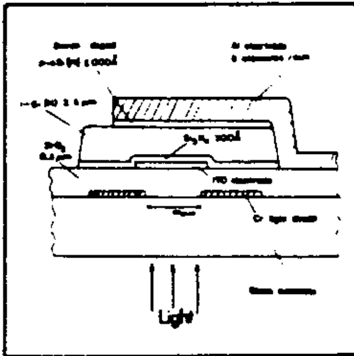

Fig. 7 The structure of a photosensing element (after S. Kaneko et al [22]).

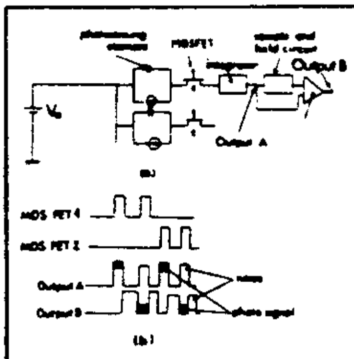

Fig. 8(a) Detection and noise suppression unit.
(b) MOSFET gate pulse and output signal timing diagram (after S. Kaneko et al [22]).

During an integration period, charge in the photosensing element is discharged by the photocurrent. When the MOSFET is turned on, the photosensing element is charged and this charging current is used as a signal current. Signal per noise ratios as high as 32 dB are obtained at 0.7 lux-sec exposure using a new noise suppression method.

The amorphous silicon is an attractive material for this compact and high speed structure because of its short photoresponse time and simplicity of fabrication [28]. In this device the good performance of the a-Si FET is combined with the a-Si high photoconductivity and the high dark resistivity.

Non-Volatile Amorphous Silicon Memory Device

The phenomenon of memory switching in glow discharge deposited a-Si p^+-n-i thin film structures was first demonstrated by Owen et al [29].

The structure of the memory device is depicted in Figure 9. Here i stands for the intrinsic a-Si layer, and n, p are the PH_3 (n-type) and B_2H_6 (p-type) doped a-Si layers respectively (see Figure 4 for doping of the amorphous silicon).

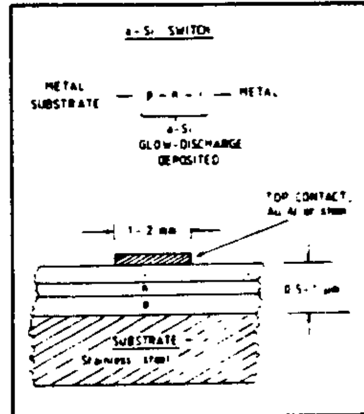

Fig. 9
The structure of the memory element.

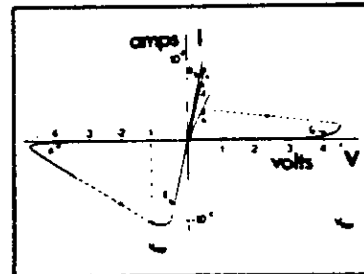

Fig. 10 Complete static current-voltage characteristics of a formed a-Si$^+$-n-i device showing the forward and reverse threshold voltage. V_{ThF} and V_{ThR} respectively (after A.E. Owen et al [30]).

The complete and typical current-voltage characteristics of a formed a-Si (p^+-n-i) memory device is illustrated in Figure 10 [30]. The device switches from its OFF to ON state at a critical voltage V_{ThF} ($\sim$4.5 V) following a non-ohmic region (represented by G) at forward bias. (Forward bias is defined in such a way that the p^+-layer is positively biased.)

In the ON state, the I-V curve is ohmic and it extrapolates through the origin (i.e. the ON state is permanent) and slightly assymetrical (D and E for forward and reverse direction respectively). Increase in the voltage in the forward direction causes the ON-state current to continue to increase apparently indefinitely, subject only to any current limiting resistor, the device is eventually destroyed by Joule heating. In the reverse direction however, another instability is observed: at about -1 V (typically) the device switches back into a high resistance OFF state (see the negative resistance region F which is a precursor to erasing). The OFF-ON transition may be repeated by biasing again in the forward direction.

The switching and setting times for the a-Si device are very short ($\sim$10 nsec) for either the OFF-ON or ON-OFF transition and the energy involved in the switching is low ($\sim$1 μJ).

All of the semiconductor switching devices currently used in computer memories and other digital electronics are *volatile* three terminal switches of the BJT (Bipolar Junction Transistor) and MOSFET (Metal-Oxide-Semiconductor-FET) type. The shaded area in Figure 11 indicates roughly the power-time characteristics of that group of devices.

Also indicated in Figure 11 are areas corresponding to the *non-volatile* (i.e. the data are retained after the power is switched off) type of MOSFET switches, namely MNOS and FAMOS devices.

The MNOS cell is a transistor with a gate consisting of Metal over Nitride over Oxide over the Silicon substrate. The FAMOS devices refer to the Floating gate Avalanche injection MOS. The storage mechanism in these devices is based on the accumulated capacitive charge. From Figure 11 it can be seen that the MNOS and FAMOS devices are considerably slower and consume more power than the a-Si p^+-n-i memory structures.

The area corresponding to the *non-*

volatile amorphous chalcogenide memory devices is also shown in Figure 11. In the chalcogenide glasses the reversible memory action is associated with the growth and destruction of a crystalline filamen [31], therefore this device is also considerably slower than that of the a-Si p⁺-n-i memory structures.

It is clear from Figure 11 that the performance of the new type of a-Si p⁺-n-i memory devices (high speed, low power requirement, non-volatile) indicates a great potential for practical applications in electronics.

References

1. K. Tanaka: Fundamental Physics of Amorphous Semiconductors ed. by F. Yonezawa (Springer Verlag, 1980), 104.
2. S.R. Ovshinsky and P.H. Klose: Journal Of Non Crystalline Solids 8-10 (1972), 892.
3. A.D. Pearson: 8th Int. Congr. on Glass, London, July 1968.
4. S Zembutsu, Y Toyoshima, T. Tgo and H. Nagai: Applied Optics, 14, (1975), 3073
5. P. Chaudhari, S.R. Herd, D. Ast, H.H. Brodsky and R.J. von Gutfeld Journal of Non-Crystalline Solids 8-10, (1972), 900.
6. Y. Mizushima and A. Yoshikawa in Amorphous Semiconductor Technologies and Device ed. by Y. Hamanakawa, North Holland Amsterdam, 1982, p.277.
7. J. Feinleib and S.R. Ovshinsky: J. Non Cryst. Solids, 4, (1970), 564
8. M. Terao, K. Shigematsu, H. Ojima, K. Taniguchi, S. Horigome and S. Yonezawa: Proceedings of the 11th Conference on Solid State Devices, TRokyo 1979, Japan J Appl Phys 19, (1980), Suppl 19-1, 579
9. A P Firth, P S Ewen and A.E. Owen The Structure of Non Crystalline Materials, ed. by P H Gaskell, J N Parker and E.A Davis, Taylor and Francis Ltd., London and New York, 1982, p 286
10. A. Matsuda and H. Kikuchi. Proc. Fourth Conf Solid State Devices, Tokyo 1972
11. A. Yoshikawa, O Ochi, H. Nagai and Y Hizushima: Appl. Phys. Letters, 29, (1976), 677
12. A. Yoshikawa, O. Ochi and Y. Hizushima: Appl. Phys Lett., 36, (1980), 107.
13. A. Yoshikawa, O. Ochi, H. Nagai and Y Hizushima: Appl. Phys. Letters 31, (1977), 161
14. K.L. Tai, L.F. Johnson, D.W. Murphy and M.S.C. Chung: The Electrochem. Soc. Spring Meet. Boston, (1979), Abstracts No.94, p.244.
15. A. Yoshikawa, S. Hirota, O. Ochi, A. Takeda and Y. Hizushima: Japan J. Appl. Phys. 20, (1981), L.81.

Part 2

16. W.E. Spear and P.G. Le Comber: Solid State Commun. 17 (1975), 1193.
17. C.R. Wronski, D.E. Carlson and D.E. Daniel: Appl. Phys. Lett., 29, (1976), 602.
18. W.E. Spear, P.G. Le Comber, S. Kinmond and M.H. Brodsky: Appl. Phys. Lett. 29, (1976), 105.
19. D.E. Carlson: Solar Energy Materials, 3 (1980), 503.
20. N. Yamamoto, Y. Nakayama, K. Wakita, H. Nakano and T. Kawamura: Jpn. J. Appl Phys Suppl. 20-1, (1981), 305
21. I Shimizu, T Komatsu, K Saito and E Inone J Non Crystalline Solids, 35-36, (1980), 773
22. S Kaneko, M Sakamoto, F Okumura, T Itano, H Kataniwa, Y Kajimara, M Kanamori, M. Yasumoto, T. Saito and T Ohkubo: Reprint of the International Electron Device Meeting, 328-IEDH 82, Japan.
23. Y Hamakawa: In Amorphous Semiconductor Technologies and Devices Ed. by Y. Hamakawa, North Holland Amsterdam, 1982.
24. W E. Spear and P.G. Le Comber: J. Non Cryst. Solids 8-10 (1972), 727.
25. P.G Le Comber, W E. Spear and A Ghaith: Electron Lett., 15, (1979), 179
26. A.J. Snell, K.D. Mackenzie, W.E Spear, P.G. Le Comber and A.J. Hughes: ESSDERC'80 Europhysics Conf. Abstracts, (1980), 99, see also: Appl. Phys. 24 (1981), 357.
27. M. Matsumura and Y. Nara: J. Appl. Phys. 51 (1980), 6443.
28. T. Ozawa, M. Takenouchi, T. Hamano, H. Ito, M. Iuse and T. Nakamura: Proc. of 1982 IMC (Tokyo), p.132, May 1982.
29. A.E. Owen, P.G. Le Comber, G. Sarrabayrouse and W. Spear: IEE Proc. (Part I Solid State Electron. Dev.) 129, (1982), 51.
30. P.G. Le Comber, A.E. Owen, W.E. Spear, J. Hajto and W.K. Choi: in Hydrogenated Amorphous Silicon, ed. by I. Panhore, Academic Press, New York (to be published).
31. C.H. Sie, M.P. Dugan and C. Moss: Journal of Non Crystalline Solids, 8-10, (1972), 877.

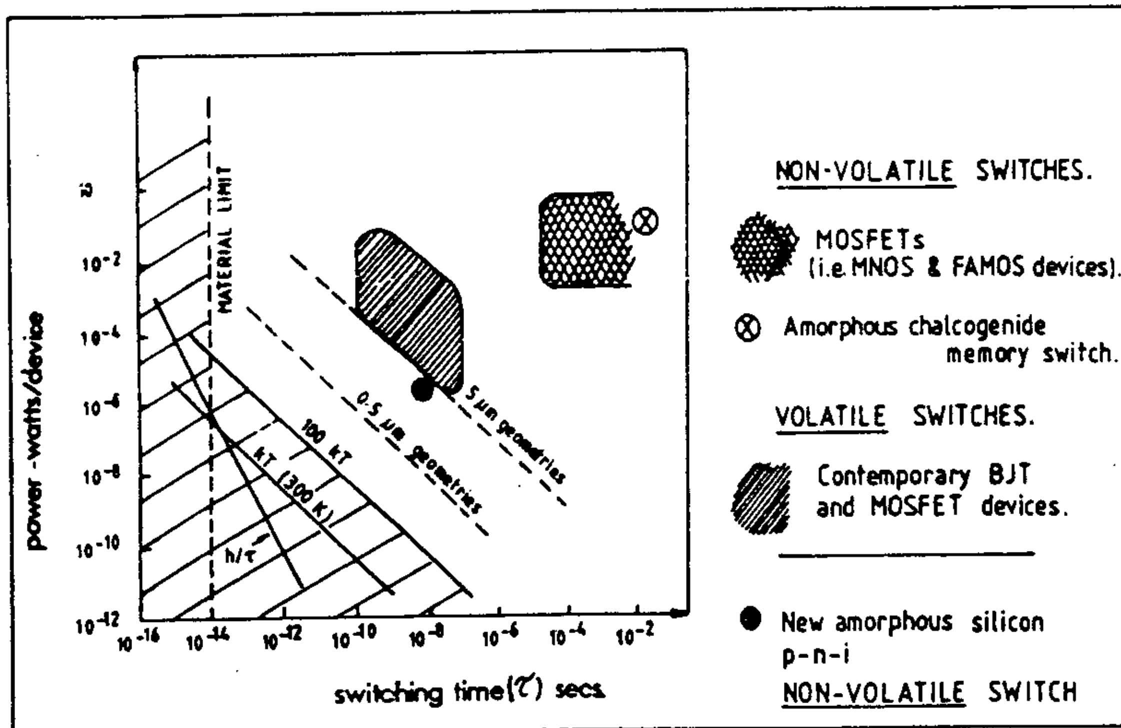

Fig. 11 The power requirement versus the switching time for different memory structures.

Journal of Non-Crystalline Solids 77 & 78 (1985) 1273-1276
North-Holland, Amsterdam

OPTICAL BISTABILITY AND OSCILLATORY PHENOMENA IN AMORPHOUS SEMICONDUCTORS

J. HAJTO, I. JANOSSY*, W.K. CHOI

Department of Electrical Engineering, University of Edinburgh, U.K.
*Department of Physics, Heriot-Watt University, Edinburgh, U.K.

New experimental results are presented on the laser induced optical bistability and oscillatory behaviour in amorphous $GeSe_2$ vacuum evaporated films. The amplitude and the frequency of the oscillation changes linearly on a logarithmic time scale at a fixed intensity, i.e. logarithmic time dependence was found. A double-well potential model is proposed to explain the new observations.

1. INTRODUCTION

The optical properties of amorphous semiconductor films show strong non-linear behaviour under the influence of c.w. irradiation. Recently discontinuities, bistability[1] and in special circumstances oscillation in the optical properties have been found[2]. Several mechanisms were proposed to explain this peculiar optical behaviour. Fazekas[3] proposed that the observed anomalies are due to a collective phenomena of charged and neutral defects present in the evaporated amorphous semiconductor films. Recently Phillips[4] suggested that the oscillatory behaviour is closely connected to the laser induced reversible microcrystallization, which was observed in a-$GeSe_2$ films by means of Raman Spectroscopy[5]. It was also suggested by us[6] that the oscillation can be explained by taking into account the combination of the laser heating (thermal effect) and the photostructural changes (optical effect)[7,8] induced by the c.w. laser irradiation in amorphous chalcogenide films. The pure thermal model explains the optical bistability, in terms of a mixture of 'absorptive' and 'dispersive' types of bistability[9]. Furthermore the combination of the thermal and photostructural effects leads to oscillatory behaviour in amorphous semiconductors[6]. In the theoretical description we considered (for the sake of simplicity) only the changes of the absorption coefficient. The theory predicts monotonic oscillation provided the laser intensity is constant. In this paper we present new experimental evidence for the non-monotonic oscillation which might occur under the influence of fixed laser intensity.

2. EXPERIMENTAL RESULTS

The details of the optical arrangement and the preparation of the a-$GeSe_2$

0022-3093/85/$03.30 © Elsevier Science Publishers B.V.
(North-Holland Physics Publishing Division)

films are described in reference 1. Oscillation of the optical properties can be observed at a relatively narrow intensity range (I_0 = 50-70 W/cm^2) in the case of ~ 6 µm thick a-$GeSe_2$ self supporting films. Monitoring the oscillation of the optical properties for a longer time interval revealed that at least three different types of oscillation can be distinguished which may occur consecutively at a fixed laser intensity within the above mentioned intensity range:

(a) 'Monotonic' oscillation when the frequency and the amplitude do not change noticeably for a limited time interval (usually in the range of 0-600 seconds). These oscillations are described in reference 6.

(b) The frequency and the amplitude change within a longer time interval (usually in the range of 600-3000 seconds). A typical observation is depicted in Figure 1.

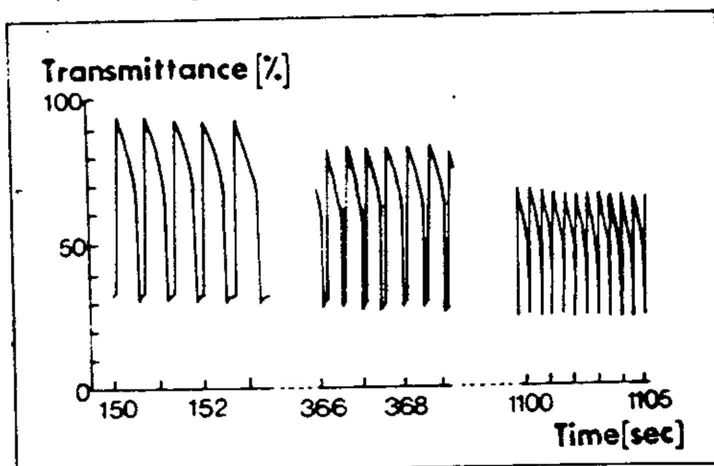

FIGURE 1
Experimentally recorded oscillation of transmittance

The frequency of the oscillation (Figure 2(a) increases linearly on the logarithmic time scale, i.e. logarithmic time dependence was found. A similar, but decreasing logarithmic time dependence of the amplitude can be observed simultaneously (Figure 2(b)).

(c) Optical 'stopping' effect, i.e. the oscillation stops for 10-200 seconds and then starts again. We should emphasize again that this effect happens at fixed laser intensity. A typical recording is depicted in Figure 3.

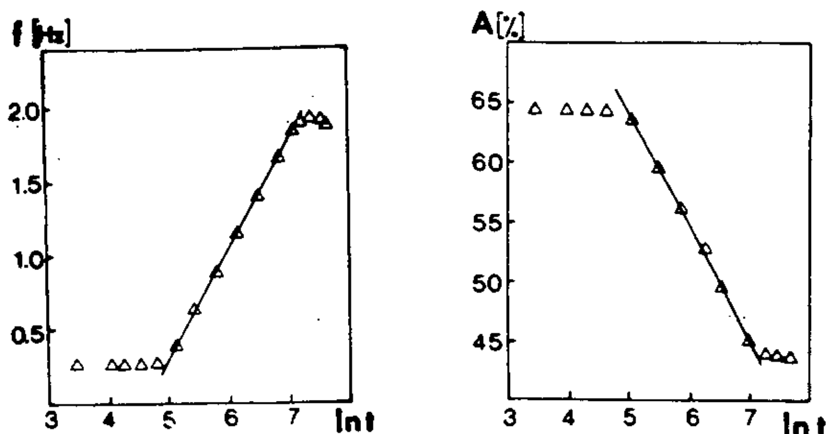

FIGURE 2
Frequency (a) and amplitude (b) of transmittance oscillations. Time measured in seconds

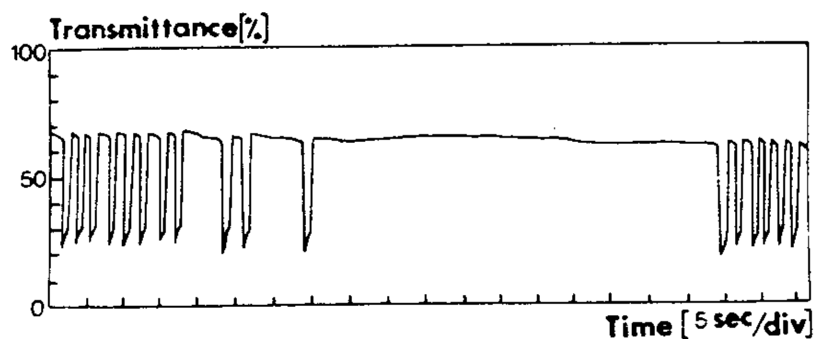

FIGURE 3
'Stopping' of transmittance oscillations

3. DISCUSSION

The observed logarithmic behaviour of the time dependance of the amplitude and the frequency is similar to the previously reported logarithmic time dependence of the laser induced anisotropy in amorphous semiconductors[10]. Therefore we suggest that the underlying mechanism determining the time development of these phenomena is the same. According to the model in reference 10, the photostructural changes are associated with the bistable.

atomic configurations which can be described by a double well potential. The observed logarithmic time dependence can be explained by assuming that the energy barriers separating the two minima have a distribution width ΔE much larger than kT (ΔE = 0.1-0.2 eV). In the previous model of oscillation yielding monotonic oscillation the momentary state of the amorphous network was characterized by a single parameter α_0[6]. In the forthcoming paper[11] we take into account quantitatively the effect of the distribution and show that this would lead to a non-monotonic oscillation in a better agreement with the new observations described above.

REFERENCES

1) J. Hajto and I. Janossy, 1983, Phil. Mag. B, 47, 347.

2) J. Hajto, G. Zentai and I. Kosa Somogyi, 1977, Solid St. Commun., 23, 401.

3) P. Fazekas, Phil. Mag. B, 1981, 44, 435.

4) J.C. Phillips, 1982, Comments Solid St. Phys., 10, 165.

5) J.E. Griffiths, G.P. Espinosa, J.P. Remeika and J.C. Phillips, 1982, Phys. Rev. B, 25, 1272.

6) J. Hajto, I. Janossy and A. Firth, 1983, Phil. Mag. B, 48, 311.

7) K. Tanaka, J. Non-Cryst. Solids, 35-36, 1023.

8) A.V. Kolobov, B.T. Kolomiets, O.V. Konstantinov and V.M. Lyubin, 1981, J. Non-Cryst. Solids, 45, 335.

9) E. Abraham and S.D. Smith, Rep. Prog. Phys., 45, 815.

10) J. Hajto, I. Janossy and G. Forgacs, 1982, J. Phys. C: Solid State Phys., 15, 6293.

11) Manuscript in preparation.

Journal of Non-Crystalline Solids 77 & 78 (1985) 1373-1382
North-Holland, Amsterdam

THE SWITCHING MECHANISM IN AMORPHOUS SILICON JUNCTIONS

P.G. LECOMBER*, A.E. OWEN+, W.E. SPEAR*, J. HAJTO+, A.J. SNELL*, W.K. CHOI+, M.J. ROSE* and S. REYNOLDS+

*Carnegie Laboratory of Physics, University of Dundee, Scotland.
+Department of Electrical Engineering, University of Edinburgh, Scotland.

Extensive new results have been obtained on memory switching in a-Si p+ni junctions. It is shown that the ON-state has its origins in a highly conducting filament less than 1μm in diameter. The physical mechanisms that could play a role in the switching operations are discussed.

1. INTRODUCTION

Threshold and memory switching in the chalcogenide glasses greatly stimulated research on these materials in the late 1960s and early 1970s[1,2]. In spite of the wide-ranging work on amorphous Si (a-Si) in recent years, memory switching phenomena were not observed and this led to a general belief that *homogeneous* films of this and other tetrahedrally bonded amorphous materials do not possess the physical properties required for switching behaviour[3]. However, some three years ago we demonstrated that *heterogeneous* junction layers of a-Si could be made to exhibit reliable, fast, polarity dependent memory switching[4-6]. The present paper is concerned with recent results on these specimens.

As prepared, the a-Si layers, generally with a p+ni structure, require one forming operation after which they are in a non-volatile low resistance ON-state. They can be switched back (ERASED) to a non-volatile high resistance OFF-state by the application of a negative potential to the p+ layer and switched ON again (WRITE operation) by a positive voltage. This cycle can be repeated many times[4-6]. The particular exciting aspect of these devices is their remarkable switching speed. Pulses of a few volts in height and a few tens of nsecs duration[5,6] are sufficient for both the WRITE and ERASE operations.

In the first part of this paper our latest results, mainly for formed devices, will be presented. This will be followed by a discussion of possible physical mechanisms that could be playing a role in the switching operation.

2. SPECIMEN PREPARATION

The samples were prepared by the RF glow discharge decomposition of silane or appropriate silane gas mixtures. The majority of the results have been obtained on specimens having a p+ni structure where i denotes an undoped layer. We have also observed similar results for n+pi and related structures and recently

0022-3093/85/$03.30 © Elsevier Science Publishers B.V.
(North-Holland Physics Publishing Division)

Gangopadhyay et al[7] have reported memory switching in p^+in^+ samples. The samples were deposited onto Corning 7059 glass substrates at 300°C and generally prepared with Cr bottom electrodes and Al or Cr top contacts, although a number of other metals have been investigated. The active area of the samples, defined by photolithographic techniques, ranged from about $10^{-7}cm^2$ to $10^{-3}cm^2$. The work has also been extended to specimens in which the a-Si i-layer was replaced by an insulator. The results for these samples showed the same general features as those reported for the p^+ni layers and will be described in subsequent publications.

3. STATIC EXPERIMENTAL RESULTS

A number of dc experiments have been carried out on formed devices in an attempt to provide additional information primarily about the nature of the ON-state. The current-voltage characteristics of recent p^+ni specimens had the same general features as those reported previously[4-6], although by carefully controlling the forming process their ON-state resistances were generally kept at a somewhat higher level (~1kΩ).

3.1. Area Dependence of ON- and OFF-state Resistances

Fig. 1 shows the area dependence of the OFF-state resistance, R_{OFF}, for samples of different area fabricated from a single p^+ni deposition run. These results were obtained on specimens that had been previously switched many times. Within the experimental scatter, R_{OFF} clearly scales with the reciprocal of the area A demonstrating that in the OFF-state the current flows throughout the whole area of the specimen.

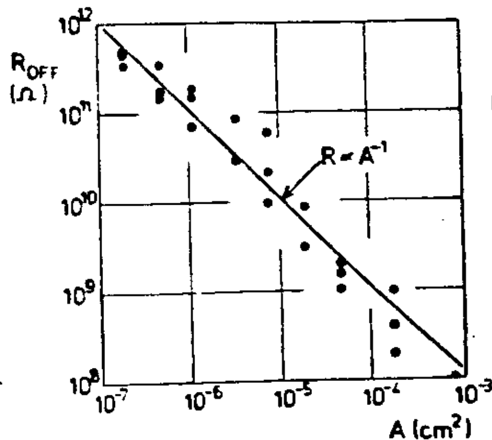

FIGURE 1
Area dependence of R_{OFF}.

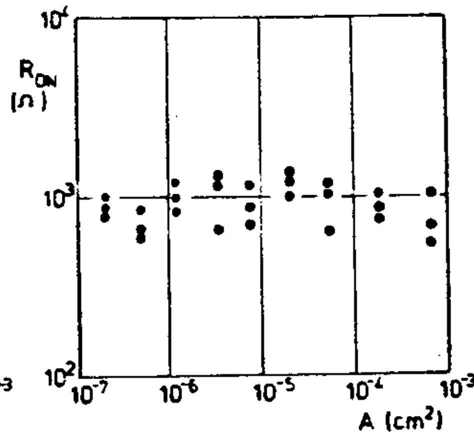

FIGURE 2
Area dependence of R_{ON}.

In complete contrast, the values of the ON-state resistances, R_{ON}, for the same specimens show no area dependence at all as can be seen from fig. 2. This result can be understood only if the ON-state has its origin in a highly conducting filament, less than a few μm in diameter, that extends at least part of the way through the specimen thickness. This result, although not entirely unexpected[4], will obviously be of central importance in developing a model for the switching process. A direct proof of the existence of a filamentary ON-state is provided by the results in section 4.

3.2. Temperature Dependence of the ON- and OFF-states

The temperature dependence of both the ON- and OFF-state conductance has been measured over the temperature range from about 230K to 400K. Results for a typical p^+ni specimen are shown in fig. 3. The OFF-state conductance G_{OFF} varied slowly with temperature, increasing by less than a factor of three between 230K and 360K. The ON-state conductance was even less temperature dependent, increasing by only 10% over this temperature range. The insensitivity of these device parameters to temperature is also observed in other properties. For example, the magnitudes of the WRITE and the ERASE voltage, measured under pulsed conditions, both increase by only a factor of 2.5 as the temperature is decreased from 400K to 200K. Clearly the general insensitivity of the switching parameters must also be a feature of any model proposed to explain the switching behaviour.

3.3. Magnetoresistance Measurements of the ON-state

Transverse magnetoresistance measurements of the ON-state of a number of specimens have been carried out at room temperature up to fields of 0.5T. Within the experimental error, $\Delta\rho/\rho$ was proportional to B^2 and found to be positive. The values of $\Delta\rho/(\rho B^2)$ ranged from $(0.5 \text{ to } 2.0) \times 10^{-4} T^{-2}$. Experiments on phosphorus doped a-Si after thermal crystallisation also gave a positive magnetoresistance with the same $\Delta\rho/(\rho B^2)$ dependence. Unfortunately, no results on homogeneous undoped glow discharge a-Si films have been reported.

It is therefore difficult to draw any definite conclusions about the amorphous or crystalline

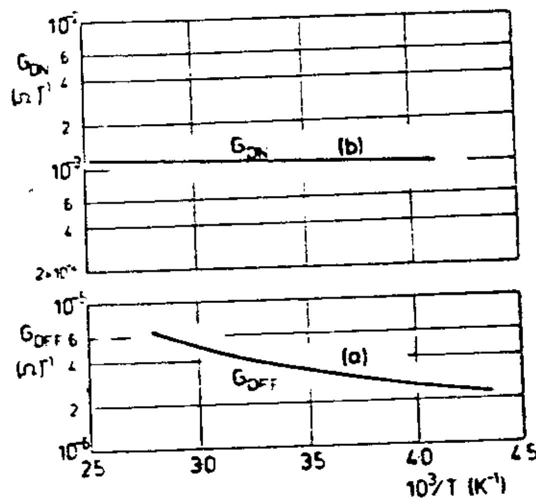

FIGURE 3
Temperature dependence of
(a) OFF- and (b) ON-state conductances

nature of the ON-state filament from the present results. However, it is probably correct to associate the B^2 dependence of the memory ON-state with a longer mean free path than is normal in amorphous solids. Using conventional crystalline theory[8] the magnitude of the measured $\Delta\rho/(\rho B^2)$ would lead to an *effective* mobility ~ $100cm^2V^{-1}s^{-1}$ in support of this suggestion.

4. OBSERVATION OF ON-STATE FILAMENT

In order to learn more about the ON-state a series of experiments have been carried out in which the surface of the a-Si device was covered with a thin layer of thermochromic liquid crystal. By passing current through the device in the ON-state it is possible to observe the current path from the changes produced by Joule heating in the reflected colour of the liquid crystal (LC). The results for two 20μm diameter structures, viewed through a high power optical microscope, are given in fig. 4. Fig. 4(a) shows the LC surface in the absence of any current flow through the specimen and fig. 4(b) shows a sample with current flowing in the ON-state. The change in the LC appearance produced by Joule heating within the filament can be clearly seen. Fig. 4(c) represents another device in which the filament has been made more visible by passing a larger current through it. We estimate from a number of measurements that the ON-state is associated with a filament of maximum diameter 0.5μm. The result therefore has interesting implications for the understanding of the switching process. The visual observation of the current filament has also enabled us to establish that switching a device OFF and ON again produces the current filament in the same place and this implies that the switching processes are not destructive.

In another series of experiments the specimens were covered by a thin layer of a liquid crystal, 4-cyano-4 altylbiphenyl, which undergoes a nematic-liquid phase transition at 35.3°C. The phase boundary may be observed quite easily in cross-polarised light and the transition was found to be fast and without

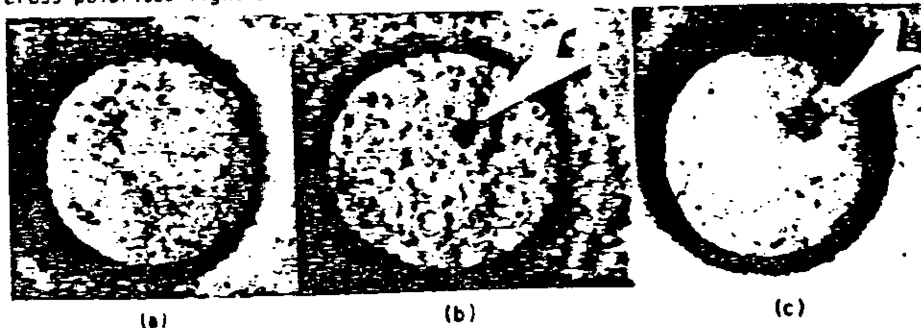

FIGURE 4
Photographs of LC surface covering 20μm diameter memories.
The arrows in (b) and (c) denote the positions of the current filaments.

hysteresis. If the sample temperature is fixed using a thermostatically controlled stage, the difference in temperature between a region of local heating (at a temperature T_h) and the surrounding film (at T_f) may be determined. The results indicate that no observable temperature rise occurred as a result of applying electrical power to the pore in either the unformed stage just prior to forming, or in the formed OFF-state just prior to switching. However, as described above, in the ON-state local heating which results on applying continuous power could be clearly seen. The effect of changing the RMS power applied to a 50μm diameter pore was studied using a continuous train of 300ns pulses. The stage was maintained at 21°C, thus the phase boundary represented the locus of points (35.3-21) = 14.3°C above the film temperature. These isotherms were circular and in the particular case studied were symmetric about the centre of the pore.

A plot of the phase boundary diameter d_i vs. RMS power P is shown in fig. 5. Although there is considerable scatter it can be seen that the relationship between d_i and P is substantially linear for $d_i \gtrsim 2\mu m$. Below this the accuracy of the measurements is limited by the resolution of the microscope used. A linear dependence of d_i on P is obtained as a solution of the heat conductivity equation for an idealised system of this kind, in which the source of local heating is assumed to be much smaller than d_i. Thus this data indicates that the diameter of the ON-state filament must be much less than 2μm, in agreement with the above experiments.

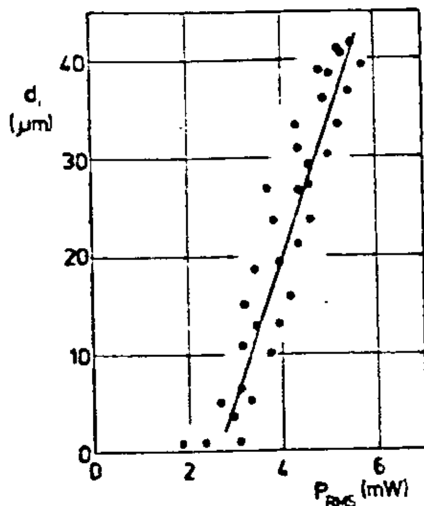

FIGURE 5
Diameter of 35°C isotherm as a function of RMS power.

5. DYNAMIC BEHAVIOUR

In an earlier publication[5] the existence of a voltage dependent delay time had been established for the forming operation. In the course of our recent work we have observed a number of other time dependent effects and these will be described in the following.

5.1. Current Instabilities in Unformed Structures

Current instability phenomena have been observed at voltages *below those required for forming*, in *unformed a-Si p⁺ni structures* with thin i-layers. Typical results obtained under pulsed operation are shown in fig. 6 for three pulse heights decreasing in amplitude from (i) to (iii).

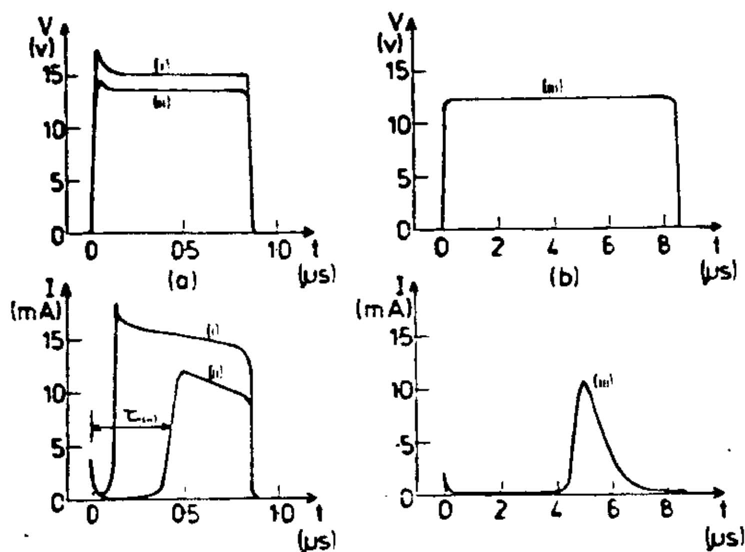

FIGURE 6
Voltage and current responses of an a-Si memory prior to forming.

It can be seen that the current increases after a delay time such as $\tau_{(ii)}$. At first sight the results in fig. 6(a) for the unformed a-Si memories appear to be similar to those observed in crystalline Si MISS devices[9]. However, the a-Si p+ni device does not remain in a high conductivity state whilst the voltage is maintained, as is the case for the MISS. The current increases fairly rapidly and then decays over a somewhat longer time-scale, resulting in an asymmetric current pulse as shown in fig. 6(b). However, it is worth emphasising that these current instabilities were observed at voltages just below those required for forming. If the voltage pulse was left on for many tens of microseconds then, some time after the first, a second current pulse would propagate through the sample, and then a third, etc. As the applied voltage V approached the forming voltage V_F these current pulses appeared to merge until at $V = V_F$ the current level remained high as the device formed. These current instabilities therefore appear to be an important precursor to the forming process.

5.2. WRITE and ERASE Delay Times

We have recently observed a delay in the WRITE operation which is a strong function of the WRITE pulse magnitude as shown in fig. 7. Note that these delay times t_d are significantly faster than the forming delay times reported previously[5,6]. If the results in fig. 7 are expressed in the form $t_d = t_0 \exp(-V/V_0)$ then t_0 = 335ns and V_0 = 4.5V. Similar results have been obtained for all the specimens investigated although the V_0 values ranged from about 0.5V to 13V.

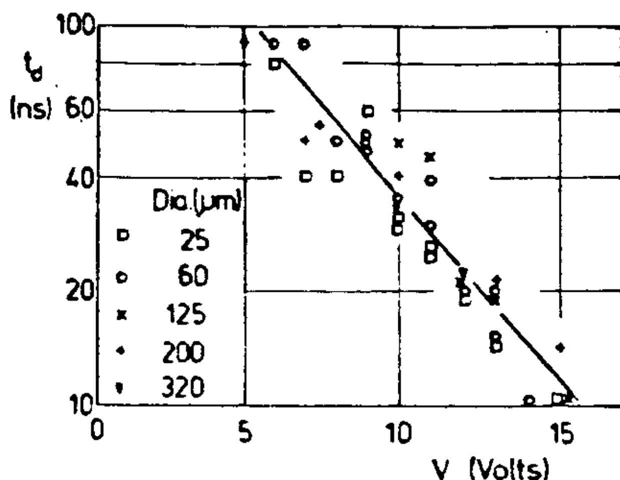

Experiments to measure any ERASE delay time were unsuccessful implying that any delay was less than the rise time of the measuring circuit, i.e. typically less than 5ns.

FIGURE 7
Dependence of WRITE delay time on forward bias pulse height.

6. DISCUSSION OF POSSIBLE SWITCHING MECHANISMS

The work described above contained a number of important new results. Probably the most crucial of these to an understanding of the physical processes underlying the switching mechanism, was the proof of the existence of a filament in the memory ON-state. Filamentary conduction has been observed previously in a wide range of materials. These include single crystal silicon, gallium arsenide, zinc telluride, gallium arsenide phosphide and polycrystalline silicon, all of which can show current-voltage characteristics associated with threshold switching[10]. This applies as well to the amorphous chalcogenide glasses[1,2] in which both threshold and memory behaviour can be observed. In the following we shall begin by discussing the filament formation and then describe some of the models that have been used for these materials and discuss their relevance to the switching in a-Si.

6.1. Filament formation

During the forming process which, as has been demonstrated, leads to a current filament, the metal-insulator barrier of the device will be under reverse bias. This suggests that the forming is likely to be associated with extremely high local fields across the thin a-Si i-layer which may approach $10^6 Vcm^{-1}$. Under these conditions tunnelling of field emitted electrons from the top of the electron distribution in the metal electrode becomes the dominant transport mechanism, injecting appreciable electron densities into the semiconductor. The current instabilities described in section 5.1 would certainly be consistent with such a model.

How is the reproducible filament produced during the forming process? A possible answer is suggested by the extensive work on thin film composite

materials in which small isolated metallic particles are dispersed in a dielectric medium[11]. This work has given a great deal of insight into the tunnelling process between isolated metal particles and its dependence on average particle size and separation, applied fields, etc. It is feasible that the high fields and current densities developing locally during forming could lead to enhanced diffusion of metallic particles from the electrode into the thin insulator. Such a region would become the preferred current path carrying the electron current in the ON-state. Further experimental work is required to confirm such a model; the observed field and temperature dependence in the ON-state is certainly consistent with results established in the previous work on these systems.

6.2. Possible Mechanisms for Memory Switching

The above considerations refer to the initial formation of the filament but cannot as such explain the subsequent memory switching. We should now like to critically discuss a number of possible mechanisms to explain this behaviour.

6.2.1. Thermal models

At first sight this model[12], used to explain the behaviour of the amorphous chalcogenide memories, might appear to offer a basis for explaining the a-Si switching processes. In the chalcogenides the ON-state is associated with a filament of crystalline material which is formed after sufficient power has been applied to the layer to melt a small area of the material. Switching OFF is achieved by burning out this filament using a number of relatively short high-power pulses and allowing rapid quenching to reform the highly resistive amorphous phase. However, there are a number of important differences between the a-Si and the chalcogenide memories: (a) it has been established that the a-Si memories do not form or WRITE at constant power; in general forming occurs at much lower powers ($< 10^{-8}$J) than in the chalcogenides (10^{-4} - 10^{-3}J); (b) the forming, WRITE and ERASE operations for the a-Si memories are generally polarity dependent; (c) no rise in the temperature of the a-Si specimens can be observed immediately prior to switching; and (d) the a-Si WRITE and ERASE times are many orders of magnitude faster than those for the chalcogenides e.g. for the WRITE operation 10^{-8}s compared with 10^{-3}s.[2] For all these reasons we do not believe that the crystalline/amorphous thermal model is applicable to a-Si.

6.2.2. Models based on Trapped Space Charge

In many respects the behaviour of the amorphous Si layers appears to be closely related to that of crystalline Si MISS structures in that both show fast polarity dependent switching, both show current instabilities during some stage of the forming processes and both have high conductance states associated with current filaments. The major difference of course is that the MISS structures are threshold switches which always revert to the OFF-state when the power is

removed, whereas the a-Si layers have the additional advantage (and complexity) of non-volatile memory behaviour.

It is nonetheless possible that the memory switching in the a-Si devices is closely related to the mechanisms proposed for the MISS layers. Essentially two models have been used to explain the MISS behaviour[13]. These are generally referred to as "punch-through" and the "avalanche-mode" and both rely for switching on establishing high fields across space charge barriers in the films. In addition, in both models the low impedance state is produced by injected charge causing inversion of the Si at the Si/insulator interface. It is tempting to suggest that the "permanent" memory of the a-Si layers may be produced by a similar mechanism in which the charge is trapped in deep gap states at the insulator-semiconductor interface for which the probability of release is very small. However, the a-Si layers retain their memory without any observable change in their properties for as long as we have measured them, namely, for over one year at room temperature and 24 hours at 95°C.

Using the thermal release time from deep mid-gap states as a measure of the persistence of the trapped space charge, then from the well-known expression for the average thermal release time we estimate that the capture cross-section of these centres should be less than $10^{-18} cm^2$. Although extremely small, such values would be consistent with Coulomb repulsive centres identified in crystalline materials[14]. However, the problem is that recombination of the trapped distribution through tunnelling or diffusion may well invalidate the above estimate by leading to a much faster decay of any trapped space charge distribution. All one can say at present is that a model in which the observed memory is associated with a trapped space charge cannot be excluded but, in view of the remarkable non-volatility of the memory states, may not be the correct explanation.

6.2.3. Other suggestions

It should be remembered that in the random network of the a-Si layers significant amounts of hydrogen are incorporated. The possibility therefore exists that memory switching may be associated with some atomic motion of hydrogen in the material. For instance, it has been reported that in ambient sensors containing Pd/a-Si Schottky barriers, hydrogen plays an important role in lowering the barrier[15]. Also the polarity dependence of the threshold voltages for the a-Si memories could be understood on the basis of field assisted hydrogen diffusion. Like all the possibilities mentioned above, this remains at present somewhat speculative and further work is required to identify the most likely memory switching mechanism.

7. CONCLUSIONS

A number of new results, including the observation of a filamentary ON-state,

are reported in this paper. These provide important information relating to the physical processes underlying the operation of the a-Si memories.

At present we believe that the initial stages of memory formation are likely to be associated with high fields and/or trapped charges in a manner analogous to that responsible for the threshold switching in crystalline Si MISS devices. However, neither the nature of the ON-state current filament nor the physical mechanisms responsible for the permanent memory of the a-Si layers, have been established with any certainty at the present time.

ACKNOWLEDGEMENTS

We should like to thank S. Kinmond and A. Carrie for their help with the specimen preparation. The financial support of the B.P. Venture Research Unit for some of the work described in this paper is gratefully acknowledged.

REFERENCES

1) S.R. Ovshinsky, Phys. Rev. Lett. 21 (1968) 1450.

2) A.E. Owen and J.M. Robertson, IEEE Trans. ED-20 (1973) 105.

3) M.C. Gabriel and D. Adler, J. Non-Crystal. Sol. 48 (1982) 297.

4) A.E. Owen, P.G. LeComber, G. Sarrabayrouse and W.E. Spear, Proc. IEE 129 (1982) 51.

5) A.E. Owen, P.G. LeComber, W.E. Spear and J. Hajto, J. Non-Crystal. Sol. 59 and 60 (1983) 1273.

6) P.G. LeComber, A.E. Owen, W.E. Spear and J. Hajto, in: Semiconductors and Semimetals, Vol. 21D, eds. R.K. Willardson & A.C. Beer (Academic Press, 1984) pp 275 - 289.

7) S. Gangopadhyay, J. Geiger, B. Schröder, H. Rübel and S. Iselborn, in print.

8) E.H. Putley, The Hall Effect and Related Phenomena (Butterworths, London, 1960)

9) J. Buxo, A.E. Owen, G. Sarrabayrouse and J.P. Sebaa, Revue de Physique Appl. 13 (1978) 767.

10) A.M. Barnett, in: Semiconductors and Semimetals, Vol. 6 eds. R.K. Willardson and A.C. Beer (Academic Press, 1970) pp 141 - 200.

11) e.g. B. Abeles, Ping Sheng, M.D. Coutts and Y. Arie, Adv. Phys. 24 (1975) 407.

12) A.E. Owen, J.M. Robertson and C. Main, J. Non-Crystal. Sol. 32 (1979) 29.

13) J.G. Simmons and A.A. El-Badry, Radio and Electronic Engineer 48 (1978) 215.

14) A. Rose, Concepts in Photoconductivity and Allied Problems (Krieger, N.Y., 1978)

15) A. D'Amico and G. Fortunato, in: Semiconductors and Semimetals, Vol. 21D, eds. R.K. Willardson and A.C. Beer (Academic Press, 1984) pp 209 - 237.

Journal of Non-Crystalline Solids 90 (1987) 529 - 532
North-Holland, Amsterdam

MECHANISM OF LASER-INDUCED OPTICAL ANISOTROPY IN CHALCOGENIDE GLASSES

I. Jánossy[+], J. Hajtó[§] and W.K. Choi[§]

[+]Central Research Institute for Physics
H-1525 Budapest P.O.B. 49, Hungary

[§]University of Edinburgh, Department of Electrical
Engineering, The King's Buildings, Edinburgh EH9 3JL Scotland

1. INTRODUCTION

It has been reported in several papers[1-5], that chalcogenide glasses which show photodarkening also become anisotropic under the influence of plane polarized laser beam. The resulting anisotropic structure does not relax at room temperature but it can be reoriented by changing the input polarization and similarly to photodarkening, it can be erased by annealing near the glass-transition temperature.

Kolobov et al.[6] proposed a phenomenological description of the photodarkening process in terms of bistable atomic configurations. In a recent publication[4] we demonstrated that by an extension of the Kolobov model photodarkening and photo-induced anisotropy can be treated within the framework of a unified theory.

Very recently Elliott[7] presented a comprehensive description of atomic models of photostructural changes. According to these models the photoinduced processes consist of two steps. At the first stage an electron-hole pair is created by the laser beam and certain bonds are weakened. This leads to the displacement of the atoms near the excited pair. Hence the recombination of the electron-hole pair takes place in a different atomic configuration as compared to its excitation. As a consequence at certain atomic sites the final equilibrium state might be different from the initial one.

The basic assumption of our considerations is that under the influence of laser illumination a dynamical equilibrium is established between the two atomic configurations. The population in the metastable configuration depends, amongst other factors on the probability of the electronic excitation in the ground state rela-

0022-3093/87/$03.50 © Elsevier Science Publishers B.V.
(North-Holland Physics Publishing Division)

tive to that in the metastable state. The origin of the anisotropy is that this relative probability depends on the orientation of the bistable centre with respect to the laser polarization.

In the following we first investigate the orientational dependence of the first stage in the case of the excitation of a two-fold coordinated chalcogen atom. In Sec. 3 we apply the results to a specific type of atomic rearrangement.

2. ORIENTATIONAL DEPENDENCE OF OPTICAL EXCITATION

Chalcogen atoms have 6 outer electrons two of which are in the s state and do not contribute significantly to chemical bonding. Two p electrons form σ bonds with the first neighbours in the network. The remaining two electrons occupy the third p orbital forming a lone-pair. The lone-pair electrons are situated at the top of the valence band while the bottom of the conduction band corresponds to antibonding σ^* states. Therefore at the optical edge absorption is caused by transitions of lone-pair electrons to antibonding states.

The probability of such a transition is proportional to the quantity $(\underline{p}\,\underline{\mu})^2$. $\underline{p}$ is a unit vector in the direction of the polarization of the light beam and $\underline{\mu}$ is the dipole-matrix element:

$$\underline{\mu} \sim \int \psi^*_{in}\, \underline{r}\, \psi_{fin} d\underline{r}$$

where ψ_{in} is the wavefunction of the initial state (lone-pair orbital), ψ_{fin} is that of the final state (σ^* orbital). Let us suppose that the p orbitals of the chalcogen atom are unperturbed by the bond-formation, i.e. we neglect sp_3 hybridization and the interactions with other atoms. In this case it follows from symmetry considerations that the matrix element $\underline{\mu}$ is parallel to the radius vector joining the chalcogen atom and its neighbour ($\underline{\mu} \parallel \underline{r}$, see Fig.1). The probability, P_1, of exciting one of the lone-pair electrons to the C-A_1 σ^* orbital is $\sim \cos^2\theta_1$; similarly the probability P_2 for the C-A_2 σ^* orbital is $\sim \cos^2\theta_2$ where θ_1 and θ_2 are the angles between the direction of polarization, p, and the corresponding radius vectors. The total probability of exciting the chalcogen atom (C) is the sum of P_1 and P_2:

$$P = P_1 + P_2 \sim \cos^2\theta_1 + \cos^2\theta_2 = \sin^2\theta\ .$$

θ is the angle between $\underline{p}$ and $\underline{n}$, the normal of the plane given by the three atoms C,A_1,A_2 ("bonding plane", see Fig.1).

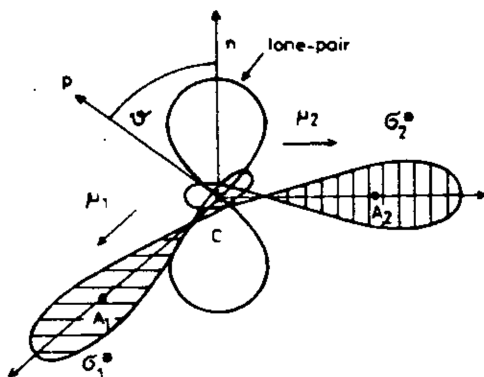

FIGURE 1
Electron orbitals involved in the excitation process

The above considerations although simplified, shows that if the polarization direction is parallel to n the chalcogen atom (C) is much less vulnarable to optical excitation than if p is parallel to the bonding plane.

3. APPLICATION TO A SPECIFIC MODEL OF PHOTOINDUCED CHANGES

The simplest atomic model of photostructural changes was proposed by Tanaka[8]. According to this model all of the chemical bonds are unchanged but a chalcogen atom is displaced from its original position to a new one (Fig.2). A more detailed version is given by Elliott[7] who considers the relatively strong interaction between the chalcogen and its nearest non-bonding neighbour ("back-bonding")

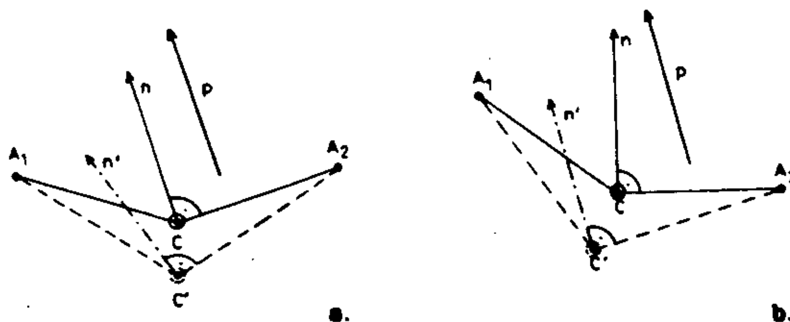

FIGURE 2
Two bistable centres according to the Tanaka-Elliott model.
a.) n ∥ p ; b.) n' ∥ p

As shown in Fig.2. the normal vectors n and n' of the bonding planes in the ground state (A_1CA_2) and the metastable state ($A_1C'A_2$) resp. are not parallel to each other. Let us first examine a bistable centre where n is parallel to p (Fig.2a). From the considerations presented in Sec.2. it follows that in this case the probability of excitation in the ground state is much lower than the corresponding probability in the metastable state. Hence the probability of the C → C' transition is much lower than that of the C' → C transition and the population in the metastable state will be low.

Consider next a bistable centre which is identical to the first one apart from being rotated so that now n' is parallel to the laser polarization (Fig.2b). In this case the C → C' transition has a much higher probability than the C'→C transition. Therefore the population in the metastable state at this bistable centre will be much higher than at the previous one.

The above arguments demonstrates that the population in the metastable state is a function of the bistable centre. To observe macroscopic anisotropy it is necessary that the bistable centres should have an anisotropic structure.

In conclusion our model shows clearly that photodarkening and photo-induced anisotropy are the consequence of the same atomic processes hence these are inherently connected.

REFERENCES

1) V.G. Zhdanov et.al. Phys. Stat. Sol. (a) 52 (1979) 621.

2) J. Hajtó, I. Jánossy and G. Forgács, J.Phys. C 15 (1982) 6293.

3) R. Grigorovici, A. Vancu and L. Chita, J.Non-Cryst. Solids 59-60 (1983) 909

4) I. Jánossy, A. Jákli and J. Hajtó, Solid State Comm. 51 (1984) 761.

5) K. Kimura et.al., J. Non-Cryst. Solids 77-78 (1985) 1203.

6) A.V. Kolobov et.al. J. Non-Cryst. Solids 45 (1981) 335.

7) S.R. Elliott, J. Non-Cryst. Solids 81 (1986) 71.

8) K. Tanaka, J. Non-Cryst Solids 35-36 (1980) 1023.

Journal of Non-Crystalline Solids 97&98 (1987) 1207-1210
North-Holland, Amsterdam

MODEL FOR THE NON-LINEAR INTENSITY DEPENDENCE OF PHOTOSTRUCTURAL CHANGES IN AMORPHOUS SEMICONDUCTORS

J. HAJTO and I. JANOSSY*

Department of Electrical Engineering, Kings Buildings, University of Edinburgh, Edinburgh
*Department of Physics, Heriot-Watt University, Edinburgh

In this paper a model of the photostructural changes is presented, with emphasis on the non-linear intensity dependence. The quantitative analysis of the model predicts non-linear intensity dependence for the kinetics of the photostructural changes as well as for the light induced optical anisotropy in accordance with experiments.

1. INTRODUCTION

The experimental evidence obtained for photostructural changes[1-8] shows that rearrangements of atomic configurations cannot be described by a single-photon process. It is observed that the rate of the photostructural change (v) depends on the illuminating intensity (I) as $v \sim I^{\delta}$ with the exponent δ varying between 1.26 and 2.4.[1-5] A common feature of all data is that δ is larger than 1. The primary process could involve the absorption of two photons within a short time interval. Such processes are well known in photochemistry.[9] A specific model for a-$GeSe_2$ assuming successive absorption of two photons has been described by Vancu and Grigorovici.[7], which predicts $\delta = 2$ for moderate intensities. Explanation of the observed wide range of non-integer processes requires a further assumption, namely that the photostructural changes are caused by the superposition of one and two-photon processes, and in the case of $\delta > 2$, even three-photon processes must be considered. Instinctively the experimentally observed non-integer power-law behaviour appears to be related to the similar well-known behaviour of the intensity dependence of the photocurrent.[10] It is frequently observed, in insulators and semiconductors, that the photocurrent σ depends on the illuminating intensity as $\sigma \sim I^{\gamma}$ where γ is usually between 0.5 and 1, but under certain conditions $\gamma > 1$ can occur (supralinearity). Sublinearity and supralinearity can be observed in the same material depending on the preparation conditions[11]. This relationship reflects the intensity dependence of the density of photogenerated free carriers[10], and therefore it seems plausible to suggest that the photostructural changes are also associated with free carriers. For a-Si:H, this idea has been taken up by a number of authors.[2,4,12] Stutzmann et al[4] propose a model where the "only" role of the light is to generate free carriers, and transitions from the ground state to the metastable state occur during the recombination of free electrons and holes. This assumption is supported by the observation that degradation of solar cells takes place in p-i-n layers under double injection, without any illumination.[13]

The fact that polarized light induces optical anisotropy[5-8] shows, in contrast, that at least in chalcogenides the role of light is not merely to generate free carriers. Free carriers (once generated) would move independently of the properties of the exciting light, which precludes anisotropy.

0022-3093/87/$03.50 ©Elsevier Science Publishers B.V.
(North-Holland Physics Publishing Division)

However, illumination of chalcogenide glasses by polarized light induces optical anisotropy at the irradiated spot, with the optical axis parallel to the electric vector of the exciting beam. The anisotropic structure may be reoriented by changing the polarization direction of the illuminating beam, or erased by circularly-polarized light. It has been shown that these effects follow naturally from the concept of bistable centres, provided that the anisotropy of the individual centres is taken into account.[5,8] The reorientation process gives an excellent means of studying the intensity dependence of the kinetics of the photostructural phenomena. Reorientation may be repeated several times, and there is no need to anneal between successive runs. It is found that the reorientation curves measured at different intensities are identical, within experimental error, on the reduced time scale t/t_0, where t_0 denotes the time elapsed from the start of the reorientation until the anisotropy becames zero.[5] We should emphasise that $1/t_0$ is proportional to the transition rate between the two states of the bistable centres.[5,8] The experimental data[5,14] indicate a power-law relation

$$1/t_0 \sim I^{\delta} \tag{1}$$

with $\delta = 2.4$ and $\delta = 1.26$-1.37. In this paper a model is proposed which explains both the nonlinear intensity dependence of photostructural changes and the kinetics of the light induced anisotropy.

2. MODEL

Photostructural changes are associated with the rearrangement of atomic positions near certain centres.[1,5] At these centres, two distinct equilibrium atomic configurations exist; one being the ground state, the other being metastable. We suggest that the primary excitation process is the same for both the photostructural changes and the light-induced optical anisotropy, as illustrated in Figure 1 a-c. The first step in the rearrangement of a bistable centre is the capture of a free electron by a trap located in energy near the bottom of the conduction band (Fig.1a). In most cases this electron is either thermally reactivated into the conduction band or recombines with a free hole. We assume that at the bistable centres, rearrangement takes place if during the time while the trap is filled, a photon removes a valence electron from a neighbouring atom (Fig.1b-c).

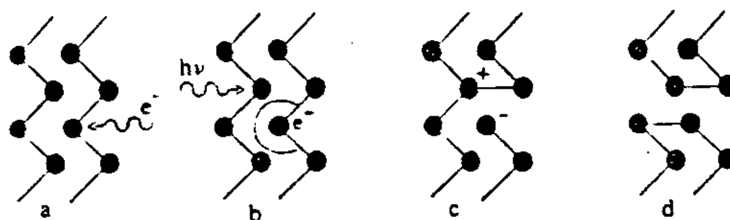

Figure 1. Rearrangement of chalcogen atoms (S or Se) leading to photostructural change and optical anisotropy

For pure chalcogen elements, the suggested rearrangement leads to the formation of a D^+ D^- defect pair ("self-trapped exciton"). In Street's model of photostructural changes [15], this pair corresponds to the metastable configuration. The creation of a D^+ D^- pair may, however, be only

an intermediate step which is followed by the rearrangement of chemical bonds as shown in Figure 1d. This second step was proposed by Elliott[16] for chalcogenide alloys. Raman spectroscopy[17,18] provides evidence for this mechanism of homopolar bond formation in certain alloys.

In the following we analyse in a simple way the nonlinear behaviour connected with the proposed mechanism of photostructural changes. The "bottleneck" of the transition process from the ground state to the metastable state is the second step shown in Figure 1 b-c i.e. the ionization of an atom while the neighbouring trap is filled. This determines the overall transition rate ($\sim 1/t_o$), hence

$$1/t_o \sim n_i I \tag{2}$$

where n_i is the number of the centres per unit volume at which the trap is filled by an electron. As discussed in several papers[10,11] the density of occupied traps with energy E_i can be expressed as;

$$n_i = N_i \frac{b_{in} n}{b_{in} n + b_{ip} p} \left[1 + e^{(E_i - E_{mi})/kT}\right]^{-1} \tag{3}$$

Here N_i is the total number of traps, n and p are the free electron and hole densities, and b_{in} and b_{ip} are the electron and hole capture cross-sections respectively. E_{mi} is the "trap Fermi level" for electrons;

$$E_{mi} = E_F + kT \ln\left[(b_{in} n + b_{ip} p)/b_{in} n_o\right] \tag{4}$$

E_F and n_o denote the Fermi level energy and free electron density in the absence of illumination. For our purposes it is more convenient to express n_i in a different form;

$$n_i = N_i \frac{b_{in} n}{b_{in} n + b_{ip} p + b_{in} N e^{-(E_c - E_i)/kT}} \tag{5}$$

where N is the "effective density of states in the conduction band", which is of order 10^{19} cm^{-3} at room temperature.[10] For small levels of excitation;

$$n, p << N e^{-(E_c - E_i)/kT} \tag{6}$$

In this case, the terms proportional to n and p can be neglected in the denominator, yielding

$$n_i \sim n \tag{7}$$

Taking into account the proportionality between n and the photocurrent σ, Eqns 2 and 7 give

$$1/t_o \sim n_i I \sim I^{1+\gamma} \tag{8}$$

or compared with Eqn. 1

$$\delta = 1 + \gamma \tag{9}$$

For very high levels of excitation inequality (6) is reversed and n_i becomes intensity independent. In this limit $\delta = 1$, i.e. the reciprocity law should hold. The crossover from "low" to "high" excitation levels takes place in the intensity range where n and $N e^{-(E_c - E_i)/kT}$ are comparable. (It is assumed that $n\, b_{in}$ and $p b_{ip}$ are similar). In this context it is important to note that E_i has a distribution over a certain energy range rather than a definite value. This fact has been brought out in

the study of the kinetics of the reorientation.[5] The distribution E_i may extend considerably over the crossover range because of the exponential dependence of n on E_i. These circumstances can reduce the measured exponent from $1 + \gamma$ to a value $1 < \delta < 1+\gamma$ over a wide intensity range. The above considerations show that the photoinduced changes increases more than linearly with increasing intensity. In the case of a supralinear dependence of the photocurrent on intensity ($\gamma > 1$), an exponent larger than 2 is expected. For the sublinear case ($0.5 < \gamma < 1$) an exponent between 1.5 and 2 is predicted for low intensity levels. It is furthermore predicted that on increasing the intensity the exponent should gradually decrease to 1. Thus the observed values of δ smaller than 1.5 may correspond to the extended crossover range, in which the exponent changes from $1+\gamma$ to 1 (i.e. the linear region)

3. CONCLUSION

The model presented in this paper explains the light induced optical anisotropy in the same way as discussed in the earlier papers,[5-8] but here we point out that the excitation probability depends on the orientation of the bistable centre with respect to the direction of the light polarisation. Reorientation of the anisotropic structure when the polarisation of the writing beam has changed implies that, under illumination there exists a dynamical equilibrium between the two states i.e. transitions from the metastable to the ground state may also be induced by light.

REFERENCES

1) K.Tanaka, Journal of Non.-Cryst. Solids 35-36 (1980) 1023
2) S.Guha, in: Physical Properties of Amorphous Materials, Plenum Press New York (1985) p.423
3) S.Guha, Appl.Phys.Lett. 45 (1984) 569
4) M.Stutzmann, W.B.Jackson and C.C.Tsai, in: Optical Effects in Amorphous Semiconductors AIP Conference Proceedings No 120(1984) p.213
5) J.Hajto, I.Janossy and G.Forgacs, Journ.Phys.C. 15 (1982) 6293
6) V.G.Zhdanov, B.T.Kolomiets, V.M.Lyubin and V.K.Malinovskii, Phys.Stat.Sol. 52 (1979) 621
7) R.Grigorovici, A.Vancu and L.Chita, Journal of Non-Cryst.Solids 59-60 (1983) 909
8) I.Janossy, A.Jakli and J.Hajto, Solid State Comm. 51 (1984) 761
9) R.Wayne, in: Photochemistry, Butterworth London (1970) Chapter 5
10) A.Rose, in: Concepts in Photoconductivity and Allied Problems, John Wiley & Sons New York
11) B.Gu, D.Han, C.Li and S.Zhao, Phil.Mag.B 321 (1986)
12) D.Adler, in: Physical Properties of Amorphous Materials, Plenum Press, New york (1985) p.72
13) D.L.Staebler, R.Crandall and R.Williams, Appl.Phys.Lett. 39 (1981) 733
14) I.Janossy, J.Hajto, To be published in Journal of Non-Cryst.Solids
15) R.A.Street, Solid State Comm. 24 (1977) 363
16) S.R.Elliott, Journal of Non.-Cryst. Solids 81 (1986) 71
17) M.Frumar, A.P.Firth and A.E.Owen, Phil.Mag.B 50 (1984) 463
18) J.C.Phillips, C.A.Beevers and S.E.B.Gould, Phys.Rev.B 21 (1980) 572

Journal of Non-Crystalline Solids 97&98 (1987) 1331-1334
North-Holland, Amsterdam

PRE-FORMED J-V AND C-V CHARACTERISTICS OF a-Si:H p^+ ni JUNCTIONS

W.K. CHOI, S. REYNOLDS, J. HAJTO, S.M. GAGE, A.E. OWEN, A.J. SNELL and I.M. FLANAGAN

Department of Electrical Engineering, University of Edinburgh, Scotland

M.J. ROSE, F.J. DJAMDJI, P.G. LeCOMBER and W.E. SPEAR

Department of Applied Physics and Electronic & Manufacturing Engineering, University of Dundee, Scotland

Static and dynamic J-V, and static C-V characteristics of a-Si:H p^+ni structures in the unformed state are presented and discussed. Certain aspects of their behaviour may be qualitatively explained in terms of models developed for analogous crystalline semiconductor structures when differences in their electronic and structural properties are taken into account.

1. INTRODUCTION

Some years ago, we reported the existence of memory and threshold switching in a-Si:H p^+ni structures following conditioning by means of a high applied voltage ('forming'). Subsequent work[1] has concentrated on characterising aspects of device behaviour concerned with memory switching, but since no memory switching has yet been observed in unformed ('virgin') structures they have received somewhat less attention.

The virgin a-Si:H p^+ni device is notionally analogous to the metal-insulator-semiconductor-semiconductor (MISS) threshold switch, a Minp$^+$ (or Mipn$^+$) structure usually comprising crystalline Si p and n regions and a thin Si oxide, oxynitride, or thick polycrystalline Si layer[2]. The operation of the MISS device is quite well understood[2-4]. In this paper we compare and contrast the static I-V and C-V and pulsed I-V characteristics[5] of both types of devices and show how certain aspects of MISS switching theory may be applied qualitatively to the amorphous device.

2. RESULTS AND DISCUSSION

Samples were prepared in layer sequence p^+, n, i by the RF glow discharge decomposition of silane gas mixtures onto glass/Cr or stainless steel substrates held at about 300°C. The p^+ layer was deposited from a mixture containing 10^4 vppm B_2H_6 and was 0.08-0.15μm thick. Details of the n and i layers used in particular experimental structures are given in the text; Al was used for top electrode metallisation throughout.

0022-3093/87/$03.50 ©Elsevier Science Publishers B.V.
(North-Holland Physics Publishing Division)

2.1 Static J-V and C-V characteristics

Room temperature J-V and C-V (1 MHz) characteristics[6] for a-Si:H p^+ni samples with similar i-layer thickness (70 nm) and n-layer doping (30 vppm PH_3) but differing n-layer thickness d_n are shown below. The J-V characteristics obtained with the p^+ layer biased negative were found to be similar in all cases.

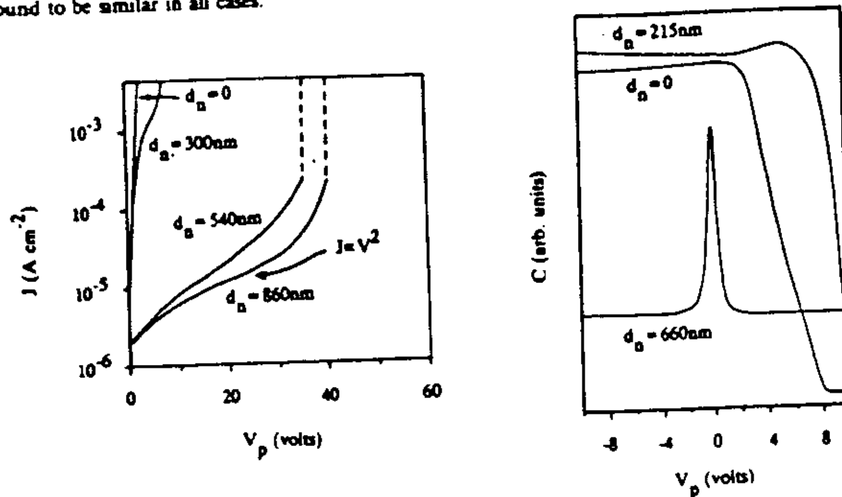

The dependence of the J-V characteristics on d_n can be qualitatively explained as follows. In a-Si:H p^+n junctions with the doping levels used here, the depletion layer extends predominantly into the n-layer, to perhaps 100nm, and the space-charge depletion layer due to the Schottky barrier may also be of the order of 200nm[7]. Thus for d_n<300nm, a p^+ni junction might be expected to behave in much the same way as a p^+i junction. If the region where $J \propto V^2$ is ascribed to a space-charge-limited current in the n-layer, then it should be better developed for large d_n, and as this is a bulk effect J should scale approximately with the n-layer thickness. As V is further increased, J begins to rise more rapidly and becomes almost discontinuous prior to forming. This transition from low to high conductivity is not associated with threshold switching; it persists as the bias is reduced to zero and no stable negative resistance phenomena are observed.

The C-V characteristics also show a marked dependence on d_n in accord with the foregoing remarks. When d_n<300 nm, they resemble those of the p^+i structure, although there are discrepancies in absolute values which are not understood. Similar general features are exhibited by crystalline MOS junctions[8] in the high-frequency limit. However, the peaked shape of the C-V

plots for p^+ni samples where d_n>600nm resemble those obtained for MISS structures in the off-state, which Yamamoto et al[4] explain in terms of the bias-dependent series capacitances associated with the insulator, the n-i surface depletion layer and the p^+n junction.

2.2 Pulsed I-V characteristics

In a-Si:H p^+ni devices where the i-layer is thin (<10nm), or lightly n-doped, current instabilities[5] can be observed in pulsed operation at voltages just below those required for forming. The behaviour of the delay time t_d as a function of applied voltage pulse height is similar to that exhibited by an MISS device prior to switching[3], as shown below:

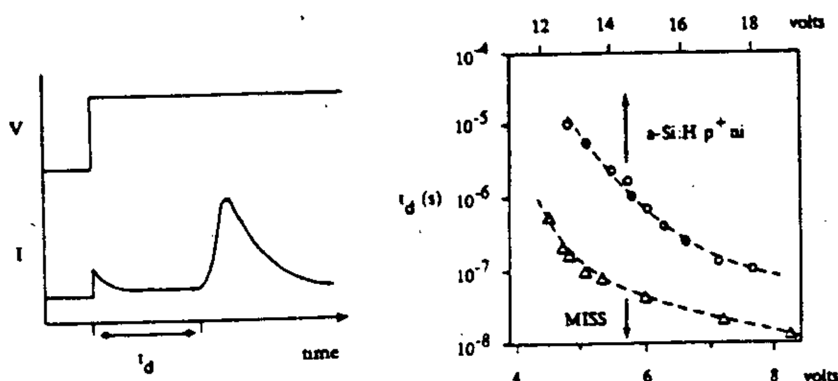

In the case of the MISS device, it is believed that the current rise occurs following inversion of the n-layer at the n-i interface due to hole injection from the forward-biased p^+n junction. The time taken for this to occur corresponds to t_d. The high electric field across the insulator is augmented by the positive space charge, causing a large electron tunnel current to flow through the insulator into the n-layer conduction band, or into the valence band in the inverted layer. In the MISS device, this on-state is maintained even when V is reduced provided it exceeds a 'holding' level. A regenerative process, which maintains the supply of holes necessary for inversion must therefore operate; the mechanism(s) by which this takes place is not fully understood. Although a similar model may be applicable to the amorphous device, it appears that, by analogy, the supply of holes in this case is insufficient to maintain the on-state. This may be due to an increased likelihood of hole recombination, possibly with electrons that have tunnelled through the insulator, leading to current collapse shortly after the onset.

Several other differences between the two are observed[5]. The current instability maximum at constant V increases only slightly with increasing contact area, indicating that current flow is largely filamentary and confined to a region of perhaps 100 μm^2. Repeated operation of the amorphous device at high bias causes progressive changes in characteristics which culminate in forming. This is perhaps not surprising, as the filament current density may exceed 10^6 A cm^{-2}, well in excess of values sustained in other a-Si:H devices. It also suggests that the conduction mechanism differs from that in the on-state MISS device and may perhaps be due to avalanche processes.

3. CONCLUSIONS

Certain similarities in the electrical properties of notionally analogous crystalline MISS and amorphous p^+ni structures can be qualitatively explained in terms of models developed for the crystalline device. However, one important feature, namely threshold switching, is not observed in the amorphous structure. This could be because the inversion layer established at the point of switching cannot be maintained due to the rate of hole recombination exceeding the supply rate. The predominantly filamentary conduction during the current instability gives rise to high local current densities which lead to changes in the electrical characteristics.

REFERENCES

1) P.G. LeComber, A.E. Owen, W.E. Spear, J. Hajto, A.J. Snell, W.K. Choi, M. Rose and S. Reynolds, J. Non-Crystal. Sol. 77 and 78 (1985) 1373 (and references therein).

2) H. Kroger and H.A.R. Wegener, Sol. St. Electron. 21 (1978) 643.

3) J. Buxo, A.E. Owen, G. Sarrabayrouse and J. Sebaa, Rev. Phys. Appl. 13 (1978) 767.

4) T. Yamamoto, K. Kawamura and H. Shimizu, Sol. St. Electron. 19 (1976) 701.

5) W.K. Choi, S. Reynolds, J. Hajto, A.E. Owen, A.J. Snell, M.J. Rose, P.G. LeComber and W.E. Spear, Proc. IEE 134 (1987) 1.

6) W.K. Choi, Ph.D Thesis, University of Edinburgh, U.K.

7) W.E. Spear, P.G. LeComber and A.J. Snell, Phil. Mag. B 38 (1978) 381.

8) S.M. Sze, Physics of Semiconductor Devices (Wiley Interscience, New York, 1981).

Journal of Non-Crystalline Solids 97&98 (1987) 1191-1194
North-Holland, Amsterdam

OPTICAL PROPERTIES OF SPIN-COATED AMORPHOUS CHALCOGENIDE THIN FILMS

E. HAJTO, P.J.S. EWEN, R. BELFORD, J. HAJTO and A.E. OWEN

Department of Electrical Engineering, Kings Buildings, University of Edinburgh, Edinburgh

Optical spectra of spin-coated amorphous As-S thin films are given. These indicate different bondind structure compared to the vacuum evaporated thin films.

1. INTRODUCTION

Recent studies have shown that a broad range of chalcogenide thin films can be prepared from organic solutions using spin deposition techniques[1]. Some of the materials have been demonstrated to be potentially useful for high resolution microlithography.[2] For this application it is required that the thin film of chalcogenide material should be sensitive to the photodiffusion of metals such as silver and should also have a uniform thickness in the range of 0.02 to 2μm. It is also important that the material should have a large absorption coefficient for the irradiation commonly used in standard microlithographic techniques.

The present paper is concerned with the optical properties of thin films prepared by spin coating from solutions of As-S chalcogenide glasses dissolved in n-propylamine.

2. EXPERIMENTAL

The bulk materials (As_xS_{100-x}) were prepared by direct synthesis from 5N purity elements in evacuated quartz ampoules at 800 °C for 12 hr. After synthesis the ampoules were air quenched. Solutions of the chalcogenides were made by dissolving the powdered glass in anhydrous n-propylamine. The solution was filtered, using a 0.5 μm pore size filter on deposition, this ensured that the solution was free from solid material. The resulting film thickness varies with the concentration of the solution, the spinning time and speed. It was found for example that 2gms $As_{40}S_{60}$ dissolved in 10 ml n-propylamine (i.e. 0.81M solution) and spin-deposited onto a glass substrate (3000rpm for 20sec) resulted in a uniform film of ~ 1μm thickness. The spin coated chalcogenide films were annealed for ~ 1 hour at 90 °C in order to remove the remains of the solvent.

The optical transmittance and reflectance of thin films for a broad range of As_x-S_{100-x} compositions were measured in the spectral region of 0.2 to 2.5 μm using an UV-VIS-NIR spectrophotometer (Perkin-Elmer Lambda 9). The optical constants, refractive index n and absorption coefficient α, were calculated from the transmittance and the reflectance data using the methods suggested by Swanepoel[3] and Abeles[4].

3. RESULTS

The compositional dependence of the refractive index (measured at photon energy $\hbar\omega$ = 1.23 eV) for spin-coated As_x-S_{100-x} films is depicted in Figure 1.

0022-3093/87/$03.50 ©Elsevier Science Publishers B.V.
(North-Holland Physics Publishing Division)

It can be seen that the value of refractive index gradually increases towards the composition $As_{40}S_{60}$ (i.e. the molecular composition As_2S_3.) Similar compositional dependence was observed for vacuum evaporated As-S films[5].

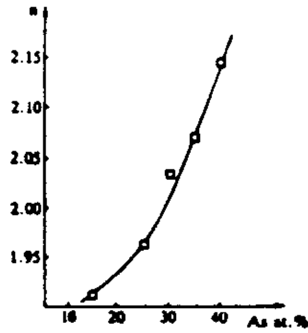

Figure 1. Compositional dependence of n for spin coated As-S films

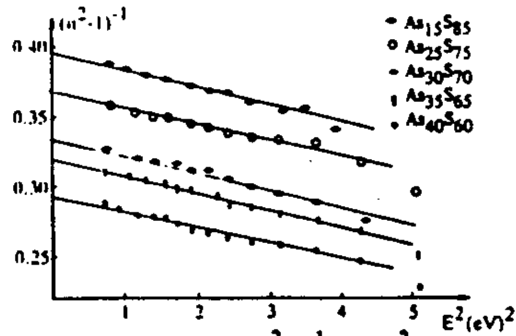

Figure 2. Plot of $(n^2-1)^{-1}$ vs $(\hbar\omega)^2$ for spin coated As-S films

The energy dependence of the refractive index n(E) can be fitted by the Wemple-Di Domenico [6] dispersion relationship;

$$\epsilon_1(\omega) = n^2(\omega) = 1 + E_0E_d/[E_0^2 - (\hbar\omega)^2] \tag{1}$$

where $\hbar\omega$ is the photon energy, E_0 is the single oscillator energy and E_d is the dispersion energy. By plotting $(n^2-1)^{-1}$ versus $(\hbar\omega)^2$ (see Figure 2.) and fitting the data with a straight line, E_d and E_0 can be directly determined from the intercept (E_0/E_d) and the slope $(-1/E_0E_d)$. The negative curvature deviation which is observed in the higher energy portion in Figure 2 is due to the onset of interband optical absorption. The dependences of the single oscillator energy E_0 and its dispersion energy E_d on composition are plotted in Figure 3.a,b. Also plotted are data for vacuum evaporated As-S films obtained by various authors[7].

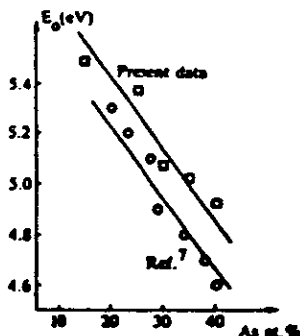

Figure 3.a. Compositional dependence of the single oscillator energy E_0

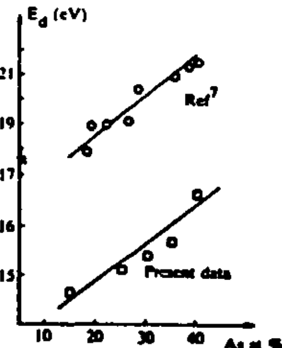

Figure 3.b. compositional dependence of dispersion energy E_d

The common features of these data are the maximum in E_d and the minimum in E_o at the stoichiometric composition ($As_{40}S_{60}$). However the values of the oscillator dispersion energy E_d for spin-coated films are considerably lower than those obtained for vacuum evaporated films. It was demonstrated[6] that E_d obeys a simple empirical relationship $E_d = \beta N_c Z_a N_e$, where β is a constant, N_c is the number of the nearest neighbour cations to the anion, Z_a is the formal chemical valency of the anion and N_e is the effective number of valence electrons per anion. Therefore the smaller E_d suggest a different bonding structure for those films prepared by spin-coating compared to those prepared by vacuum evaporation. The optical absorption spectra for spin coated As-S films are depicted in Figure 4. It is a salient feature that films of identical composition give different absorption spectra solely depending on their mode of deposition i.e. spun or vacuum evaporated. In the case of vacuum evaporated As-S films the absorption coefficient rises exponentially with photon energy over the region 1.5 to 2.7 eV according to the Urbach rule;

$$\alpha = \alpha_o \exp[B(\hbar\omega - \hbar\omega_o)] \tag{2}$$

where B and α_o are constants. This exponential absorption edge is typical for vacuum evaporated amorphous chalcogenide films[8]. In the case of spin coated As_xS_{100-x} films the exponential region is restricted to a smaller energy region (2.4 to 2.6 eV) and the slopes are smaller (B is ranging from 5 to 9 eV^{-1}) than the slopes measured for the vacuum evaporated films[8] (B ~ 19 eV^{-1}). Also a broad absorption band is present for $\alpha \le 10^3$ cm^{-1} and in the photon energy range 1.2 to 2.3 eV. This band is not present in the vacuum evaporated films.

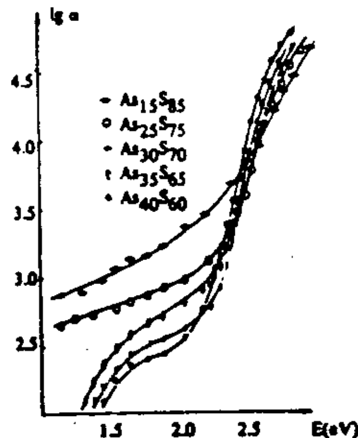

Figure 4. α vs photon energy for spin coated As-S films

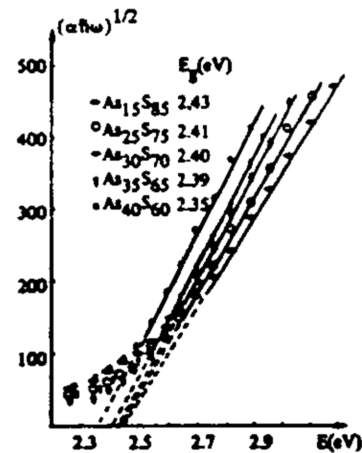

Figure 5. $(\alpha\hbar\omega)^{1/2}$ vs photon energy for spin coated As-S films

The broad absorption band might be associated with light scattering from inhomogeneities of the order of hundreds of angstroms in diameter[9]. At higher values of the optical absorption coefficient, its exponential dependence on photon energy ceases to hold and the absorption coefficient rises less steeply. Figure 5 shows that for this region the α values can be linearised as;

$$\alpha^{1/2} \sim (\alpha\hbar\omega)^{1/2} = C(\hbar\omega - E_g)^2 \qquad (3)$$

Such spectral dependence of the absorption coefficient can be attributed to interband electronic transitions since one can write[8].

$$\alpha = \text{const}\,\frac{M^2}{\hbar\omega} \int_0^{\hbar\omega - E_g} g_v(E)\,g_c(\hbar\omega - E_g - E)\,dE \qquad (4)$$

where g_v and g_c are the densities of states in valence and conduction bands. Assuming that $g(E) \sim E^{1/2}$ and that the transition matrix element M is constant in the energy range under consideration, equation (4) takes on the form expressed by equation (3). The value of the optical energy gap E_g can be obtained by extrapolating $\alpha^{1/2}$ towards zero (see Figure 5.). The value of the optical energy gap E_g decreases with the As content. The slope C on the other hand increases towards the stoichiometric composition indicating a narrowing of the conduction band and the valence band (i.e. increasing order in the chemical bond statistics). Similar compositional dependences were found for vacuum evaporated As-S films[7].

4.CONCLUSION

Varying the composition of spin coated As-S films induces changes in E_g through modifications of the average bonding energy (i.e. by varying the chemical bond statistics.) This is consistent with changes in E_g observed in vacuum evaporated As-S films[7]. As the composition became increasingly sulphur rich, the trends shown in E_d, E_o, B and C are attributed to either an increasing disorder or to chemical changes resulting in a redistribution of the density of states within a certain energy gap. Furthermore, the broad absorption band and the fact that E_d, B and C are smaller than the corresponding parameters for vacuum evaporated films[7], indicate a different bonding structure in the amorphous network for the films prepared by spin-coating and vacuum evaporation. Measurements are currently underway to study the photodissolution of metals in spin-coated films.

REFERENCES

1) G.C.Chern, I.Lauks, J.Appl.Phys. 53(10) Oct. (1982) 6979
2) A.P.Firth, P.J.S.Ewen, A.E.Owen, C.M.Huntley, Advances in Resist Technology and Processing II. Vol.539. (1985) 160
3) R.Swanepoel, J.Phys. E: Sci Instrum., 16 (1983) 1214
4) F. Abeles, Optical Properties of Solids, Amsterdam North-Holland Publ. Co. (New York American Elsevier 1972)
5) Z.U.Borisova, Glassy Semiconductors, (Plenum Press New York 1981) p.136
6) S.H.Wemple, Jr. DiDomenico, Phys Rew.B3 (1971) 1338
7) K.Tanaka, Thin Solid Films, 66 (1980) 271
8) N.F.Mott, E.A. Davis, Electronic Processes in Non Cryst. Materials (Clarendon Press Oxford 1979) p.273
9) A.Vancu, St.Sladaru and R.Grigorovici, in Proc. of 5th Int.Conf. on Am. and Liquid Semiconductors, (Taylor and Francis London 1974) p.631

Transient current instabilities in a-Si : H p^+ni structures

W.K. Choi
S. Reynolds
J. Hajto
Prof. A.E. Owen
A.J. Snell
M.J. Rose
Prof. P.G. LeComber
Prof. W.E. Spear

Indexing terms: Semiconductor devices and materials, Transients, Switches and switching theory

Abstract: It has been demonstrated that amorphous silicon p^+ni junctions exhibit nonvolatile polarity dependent memory switching after initial conditioning by means of a high applied potential ('forming'). The memory on-state is due to the presence of a highly conducting filament, whose physical properties are not well understood. Recent work has shown that in junctions where the i-layer is either thin or lightly n-doped the forming process may be preceded by a transient current instability, which decays even when the voltage across the device is maintained. Unlike the forming process, the occurrence of a current instability does not necessarily modify the device, although progressive changes may result after repeated operation. The magnitude of the current maximum shows only a weak dependence on device area, which suggests that conduction during the current instability is localised within an incipient filament. In certain respects this behaviour resembles the off to on transition observed in notionally analogous crystalline threshold switches, although in our case the high conducting on-state cannot be maintained by a holding voltage. A qualitative model which accounts for most of the observed features is presented and discussed.

1 Introduction

Threshold and memory switching phenomena in amorphous materials were first observed in various chalcogenide glasses [1, 2] and metal oxides [3]. Feldman and Moorjani [4] reported that similar effects could be induced in thin films of amorphous silicon (a-Si), germanium and boron prepared by electron bombardment. More recently, den Boer [5] has shown that n^+in^+ sandwich structures of a-Si : H prepared by RF decomposition of silane and appropriate dopant gas exhibit threshold switching after an initial 'forming' process, which consists in conditioning the structure by means of a high applied potential. Also, some of the present authors have recently shown that p^+ni structures of glow-discharge deposited a-Si : H have the properties of fast nonvolatile memories [6–9] and these devices are the subject of a patent [10]. This nonvolatile switch also requires a forming process. It should be noted that after forming the same p^+ni structures can function as a threshold switch [11], rather similar to that reported by den Boer, but with a switching time one or two orders of magnitude faster than that reported for the n^+in^+ structure.

This paper is concerned entirely with the properties of p^+ni a-Si : H structures in their unformed virgin state, and in particular with unusual transient electrical properties. These transient phenomena have been observed only in p^+ni configurations in which the i-layer is either much thinner than used in previous devices (i.e. < 10 nm), or in which the i-layer is slightly n-doped (i.e. a ν-layer). Under pulsed operation, with the p^+-layer positively biased, a rapid increase in current is observed some time after the bias voltage is applied. The onset time is of the order of microseconds. However, contrary to the usual behaviour of threshold switches, the current decays over a similar time scale even though the voltage pulse is maintained. The device also exhibits a recovery effect, i.e. a certain time must elapse between consecutive voltage pulses for the second pulse to give rise to a current instability. This recovery time can be of the order of milliseconds. We present results showing how the onset time, recovery time and peak current vary with voltage pulse height, temperature and contact area, and discuss possible physical origins of these effects.

2 Sample preparation and electrical measurements

All the devices reported here were prepared by the glow-discharge decomposition of silane (SiH_4). Amorphous silicon layers (a-Si : H) were deposited in the sequence p^+ni onto glass substrates with metal contacts, as described in previous papers [7–9]. The metal contact used in this work was usually chromium (Cr).

Pulsed electrical measurements were taken primarily using a Hewlett-Packard pulse generator (Model 8160A) and digital storage oscilloscope (Model 54200A). In cases where a long delay (> 100 μs) between consecutive short voltage pulses was required, an additional pulse generator was used as a trigger source and a Tektronix oscilloscope (Model 7633) monitored the current corresponding to the second pulse. The trigger signal for this instrument was conditioned by means of a divide by two circuit, and the time between pulses determined using an interval timer.

Paper 5104I (E3), received 14th August 1986

Dr. Choi, Dr. Reynolds, Dr. Hajto, Dr. Snell and Prof. Owen are with the Department of Electrical Engineering, University of Edinburgh, Kings Buildings, Edinburgh EH9 3JL, United Kingdom

Mr. Rose, Prof. LeComber and Prof. Spear are with the Carnegie Laboratory of Physics, University of Dundee, Dundee DD1 4HN, United Kingdom

Electrical contacts were made to the electrodes by spring loaded probes. Measurements at temperatures other than ambient were taken with the sample mounted on a metal block held at the appropriate temperature, under vacuum in most of the experiments.

3 Experimental results

3.1 Principal features

The principal features associated with the current instabilities are shown in Fig. 1. To facilitate description, the

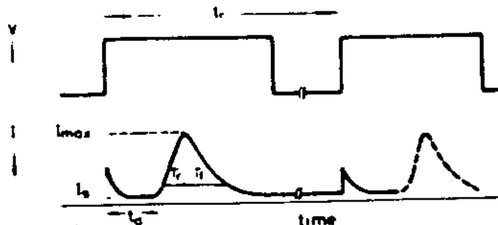

Fig. 1 *Schematic illustration of the various parameters in the transient current instability in a virgin a-Si : H p⁺ni device with thin i-layer (~10 nm)*

following nomenclature will be used. A voltage pulse V, greater than a minimum threshold V_c but less than the voltage required to produce a memory device [9], is applied such that the p^+-layer is positively biased. A displacement current occurs, which decays to a steady current I_s. Some time t_d after the voltage pulse has been applied the current rises abruptly, with characteristic time τ_r. After reaching a maximum value I_{max}, the current decays with characteristic time τ_f. A second voltage pulse is applied at a time t_r after the first. This pulse may or may not give rise to a current instability depending upon the values of V and t_r.

3.2 Voltage and temperature dependence of onset time t_d

The dependence of the onset time t_d on pulse height V and temperature T for a typical sample is shown in Fig. 2. It can be seen that the onset times above the critical

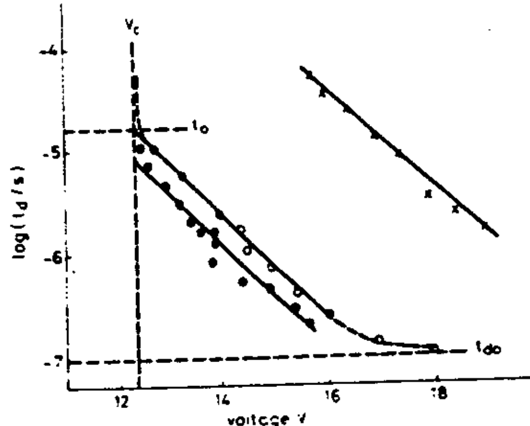

Fig. 2 *Dependence of the onset time t_d with pulse height V and temperature T for a typical a-Si : H p⁺ni structure*

●–● 366 K
○–○ 295 K
×–× 210 K

voltage V_c show a dependence on V of the following empirical form:

$$t_d = t_{d0} + t_c \exp\left[\frac{-(V - V_c)}{V_0}\right]$$

where V_0 is usually in the range 0.6–0.8 V and, for a given sample, appears independent of T. Our present measurements are insufficiently detailed to permit the separation of the possible temperature dependence of t_{d0}, t_c and V_c, but it seems likely that decreasing T results in an increase in V_c, with t_{d0} being relatively unaffected. V_c, t_c and t_{d0} are found to lie in the ranges 10–15 V, 10–50 μs and 0.1–0.3 μs, respectively, at 295 K.

The detailed behaviour of t_d with V at the extremes of the voltage range is difficult to establish. At $V = V_c$ there is a tendency for t_d to become erratic, but no current instabilities have yet been recorded with $t_d > 100$ μs. Thus we conclude that either t_d increases almost discontinuously at $V \sim V_c$, or the effect simply does not occur under these conditions. As V is increased several volts above V_c, the curve flattens i.e. $t_d \to t_{d0}$. Increasing V further ultimately causes an irreversible change in the device characteristics. There is an abrupt increase in current, and the device remains in a permanent low resistance state (10^2–10^4 Ω) when the voltage pulse is removed [8, 9].

3.3 Voltage dependence of rise- and falltimes

The rise- and falltimes of the current instability decrease exponentially as a function of increasing V, as shown in Fig. 3 for a typical sample. The current decay is essen-

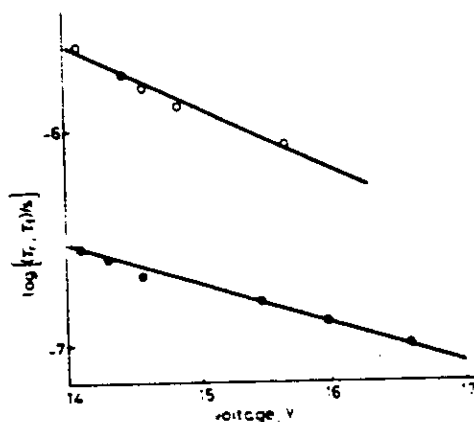

Fig. 3 *Rise (τ_r) and fall (τ_f) times of the current instability as a function of V for a-Si : H p⁺ni structure*

○–○ τ_f
●–● τ_r

tially exponential, as illustrated in Fig. 4, and thus τ_f is the time constant of this decay. The form of the current rise is less clear, and in this case τ_r denotes the time taken for the current to increase from 10% to 90% of I_{max}.

3.4 Variation of current maximum with voltage pulse height and device area

The variation of the current maximum I_{max} with pulse height V for three identically prepared samples with differing areas is shown in Fig. 5. It can be seen that in each case I_{max} scales linearly with V ($V > V_c$), but is not correlated with sample area. Measurements on a large number of samples with areas varying by three orders of magni-

tude failed to reveal a direct proportionality between I_{max} (measured at a constant t_d) and contact area. The current I_{max} ranges over an order of magnitude in the various samples, but it seems to be primarily a random variation with a small but systematic increase in I_{max} as the contact area increases. It should also be mentioned that the threshold voltage V_c shows a tendency to decrease with increasing area.

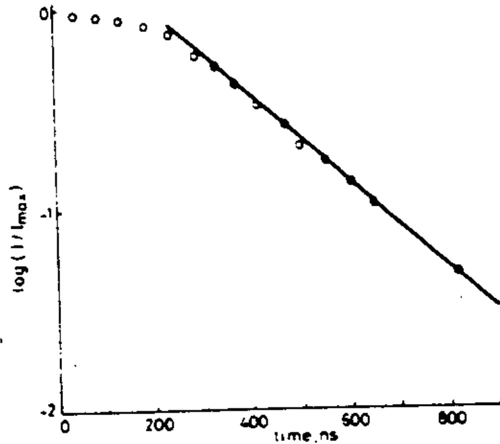

Fig. 4 *Current decay of the instability of a typical a-Si : H p⁺ni structure*

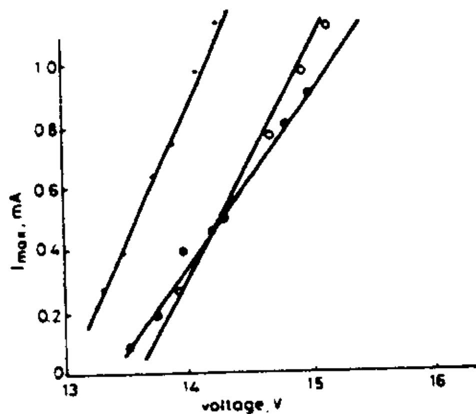

Fig. 5 *Variation of I_{max} with V for three identically prepared samples with differing contact areas A*

●—● $A = 5 \times 10^{-7}$ cm²
○—○ $A = 1.1 \times 10^{-6}$ cm²
+—+ $A = 7 \times 10^{-6}$ cm²

3.5 'Recovery' effects

Our initial observations indicated that at voltages slightly above V_c, only a single current instability would propagate through the sample even if the voltage pulse was maintained for orders of magnitude longer than the onset time t_d. However, during the course of these measurements, a sustained voltage pulse was often found to cause an abrupt change to a permanent low resistance state. To minimise the risk of this occurring during a series of measurements, two voltage pulses of equal height and width were used to determine the recovery time t_r which must elapse for the second pulse to give rise to a current instability with similar t_d and I_{max} to the first. The variation of t_r with pulse height V is shown in Fig. 6.

At voltages substantially above V_c, i.e. where t_d approaches t_{do}, the current decay associated with the first voltage pulse was frequently observed to behave erratically, contrary to the trend shown in Fig. 3. Under these conditions t_r was found to be commensurate with t_d, and local maxima could occasionally be seen shortly after the initial current rise. However, no well defined oscillations have yet been observed.

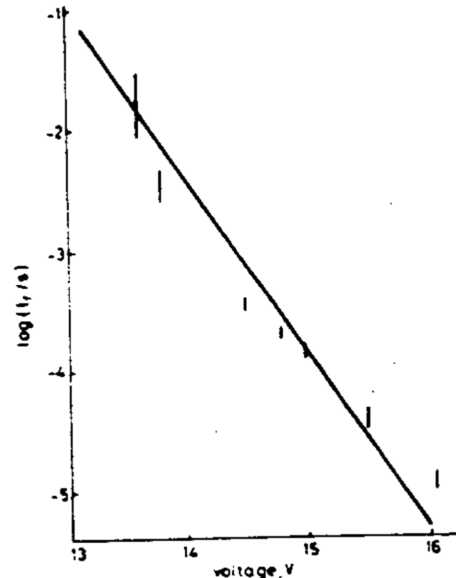

Fig. 6 *Variation of the recovery time (t_r) with pulse height V for a-Si : H p⁺ni structures*

3.6 Progressive irreversible changes in the sample characteristics

In addition to the abrupt changes in the electrical properties of samples which have been mentioned above, less obvious irreversible changes were also found. These effects occur particularly in the period prior to the onset of the current instability, taking the form of a progressive increase in the current with successive constant amplitude voltage pulses. This increase is more pronounced when voltage pulses substantially above V_c are applied. Prior to the point at which this becomes noticeable, the pre-instability current I_s is approximately exponentially dependent on the applied voltage and scales linearly with sample area.

Typical static I/V characteristics of a sample which has undergone progressive changes are shown in Fig. 7. It can be seen that the forward biased (p^+ positive) characteristic is substantially modified but the reverse biased (p^+ negative) characteristic is essentially unaltered.

4 Discussion

4.1 Evidence for filamentary conduction

The absence of a pronounced dependence of I_{max} on device area suggests that the current instability occurs in a localised region. As the smallest device examined in the present study is of the order of 10 μm in diameter, it appears that the majority of the current during the instability is transported through a region of these dimensions or less.

When an abrupt permanent change in the sample conductivity occurs ('forming') the subsequent sample resistance is found to be entirely uncorrelated with area, in accord with previous results obtained for similar samples

[9]. Imaging of the surface of the formed sample, by observing the temperature rise due to Joule heating using

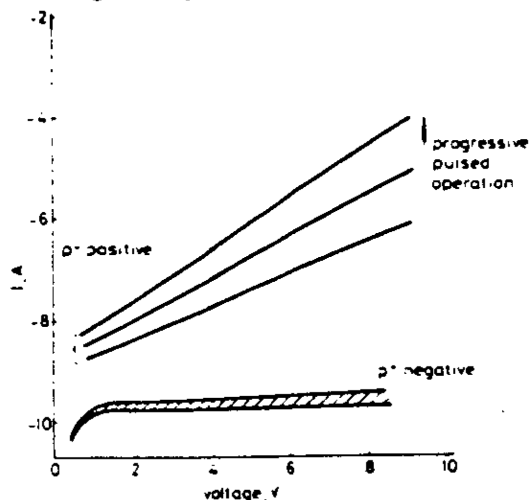

Fig. 7 *Typical static I/V characteristics of a-Si : H p⁺ni structure which has undergone progressive changes*

Note that the forward biased characteristic has increased while reverse biased characteristic is essentially unaltered

a thin film of liquid crystal, has confirmed [9] that conduction after forming is filamentary, with a transverse dimension of 1 μm or less. Furthermore, the shape of the forming delay time against voltage curve (Fig. 5 of Reference 8) at high applied bias is similar to the t_d against V results presented here. On this basis it seems reasonable to suppose that the current instability is a precursor to forming, although there is no direct evidence to support this. Indeed there are certain indications that these events may be only indirectly related, as current instabilities are not always observed prior to forming in the samples described above, and very seldom in samples with thicker *i*-layers.

The observation of one or more current filaments has been reported in many materials, both amorphous [4, 12] and crystalline [13], and very often voltage- and/or current-controlled negative resistance phenomena are associated with these filaments. In our samples, however, we have not observed these latter effects under static DC conditions prior to forming, and it would appear that our structures cannot support high local current densities (and consequent Joule heating) for more than a short time before a permanent change in the material properties of this region occurs. The progressive changes in the static I/V characteristics shown in Fig. 7 tend to substantiate this view. The increase in the rectification properties suggest that the *i*-layer, or the metal/*i*-layer interface becomes less blocking to holes and a larger proportion of the applied forward voltage appears across the p^+n junction.

4.2 Origin of current rise and onset time

The t_d against V data at several temperatures, shown in Fig. 2, are of similar form to the corresponding results obtained for the crystalline silicon metal-insulator-semiconductor structure (*c*-MISS) [14, 15], which suggests that the principles on which the theory of the latter device are based may be applicable to our structures. Although the theories put forward [15, 16] differ somewhat in detail, the central concept is the creation of an 'inversion' layer due to holes injected by the forward-biased *pn* junction accumulating at the *ni* interface. Sarrabayrouse *et al.* [15] have shown that a theoretical expression for the t_d against V relationship based on the establishment of an inversion layer is in good agreement with experiment.

Tentative band diagrams for the *a*-Si : H p^+ni structure at zero, moderate and high applied bias are shown in Fig. 8. Under zero bias (Fig. 8*a*), the M_1-*i* interface

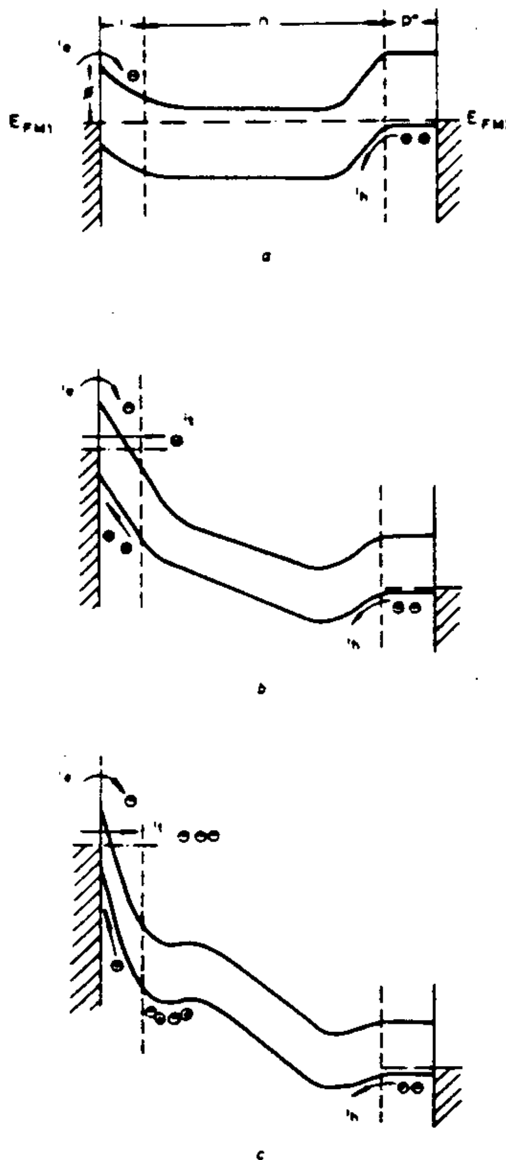

Fig. 8 *Schematic band diagrams for a-Si : H p⁺ni structures*

a Zero bias
b Moderate bias
c High bias

represents a Schottky barrier in which the *i*-layer is totally depleted [17]. The equilibrium currents i_e and i_h originate from thermionic emission over the Schottky barrier and hole diffusion from the p^+-layer, respectively. If a moderate bias is applied (Fig. 8*b*), the effective M_1-*i* barrier width is decreased and electrons near E_{FM1} can tunnel into the conduction band, adding to the thermionic current. However, the *pn* junction is not substan-

tially forward biased and the hole current will be comparable to the electron tunnel current. As the field in the n-region is small the holes will gradually diffuse towards M_1. Under high bias conditions (Fig. 8c) the electron tunnel current will be substantial, as the effective barrier width is further reduced. In addition, hole injection will increase as a result of a larger forward bias on the pn junction. It is possible that the increased hole injection gives rise to a positive space charge in the vicinity of the M_1-i interface which will further reduce the effective tunnelling barrier by its electrostatic effect. This would account for an abrupt increase in the measured current after a delay time if it is considered that the positive space charge takes approximately t_d to build up to some critical level.

The rapid rise in current after the onset time may be a consequence of the high energy tunnelling electrons causing impact ionisation, and leading to an avalanche breakdown. Such effects are known to occur widely in dielectric films and reverse biased pn junctions [2]. Furthermore, avalanche breakdown in pn junctions occur in local high-field regions which is in accord with our observations of a weak dependence of I_{max} on sample area. It has been pointed out [2] that the onset of avalanche breakdown is a statistical process, and thus if this were to be the primary origin of the observed onset time, one would expect little correlation between this parameter and the applied voltage. This does not appear to be the case here and therefore we suggest that the onset time is governed by the more predictable mechanisms of hole accumulation.

The observed relationships between t_d and V, and V_c and T can be explained qualitatively in our case by assuming that prior to the onset a critical charge density Q_c must be obtained in the vicinity of the i-layer. Below V_c, the pn junction cannot supply sufficient holes to offset conduction and recombination, and Q_c is never reached. Above V_c, the supply of holes is increased by virtue of a larger forward bias appearing across the pn junction and after a certain time, corresponding to the onset time t_d, Q_c is reached and a large electron current occurs. As the hole injection current is exponentially dependent on the junction bias, it is reasonable that the time taken for Q_c to develop should behave as $\exp(-(V - V_c)/V_0)$, assuming a fixed proportion of the total applied bias with $V > V_c$ appears across the pn junction. The existence of a minimum value of t_d, i.e. t_{d0}, can be explained by estimating the time taken for a large hole current, sufficient to result in Q_c, to diffuse through the n-layer. Taking a representative n-layer thickness and applied field, and a typical value of t_{d0} of 0.1 µs, we obtain a value of 10^{-3} cm^2 V^{-1} s^{-1} for the hole mobility, which is not unreasonable [18]. Increasing the temperature will increase the hole saturation current, and consequently a smaller forward bias will provide sufficient hole injection for Q_c to be reached at a lower V_c, provided that recombination in the n and i regions is not manifestly altered.

4.3 Origin of current decay

Once the c-MISS device is in the high conducting state, it will remain in this state indefinitely provided that a holding voltage is maintained. Although our device exhibits similar t_d against V behaviour, only a transient high conducting state is usually observed, and thus a modification of the c-MISS theory of operation must be made to account for this. One possible mechanism is outlined below.

As the current increases abruptly a large number of electrons are injected into the ni region, and consequently the possibility exists that the holes constituting the positive space charge will recombine with these injected electrons. If this were to occur, it is to be expected that the measured current will decrease as the barrier will then become less transparent to electrons. However, once the original potential distribution has been reached the current should again rise after an appropriate delay time. In practice this effect is not observed on a time scale of the order of t_d.

If avalanche breakdown occurs during the current rise, then, in the absence of a positive feedback mechanism [19], the current will reach a steady value. However, if the initial stimulus, i.e. the electrons tunnelling through the Schottky barrier, is diminished on account of the recombination effects described above, the avalanche process would not be sustained, and the measured current would decrease.

4.4 Origin of recovery time

There appear to be at least two possible explanations for the existence of a recovery time. These are discussed, in turn, below.

4.4.1 Charge storage: Adan and Zolomy [20] have reported that the threshold voltage for c-MISS samples decreases as the frequency of applied voltage pulses is increased. They attribute this effect to a residual charge being stored at the ni interface and a diffusion charge extending through the n-layer from the pn junction to the interface. This stored charge is released on a time scale of microseconds, and thus if the period of the applied pulse train is of this order, the effective threshold voltage will be reduced. Unfortunately we could not perform measurements in this way as our device undergoes rapid changes in the low bias I/V characteristic and will very often 'form' when a continuous train of pulses is applied. However, the 2-pulse technique we have used leads to essentially identical results inasmuch as any charge storage effect of this kind should be apparent from the current response to the second voltage pulse; one would expect t_d to decrease as a result. From our data it would appear that t_d actually increases after the first instability, and it follows that an equivalent charge storage model is inappropriate. However, as there will be substantial electron injection from the metal at the onset of conduction, it is possible that a residual electronic charge will remain trapped close to the metal-i interface after hole recombination (which results in the current decay) is complete. The electrostatic effect of this negative charge could then increase the barrier width and inhibit subsequent conduction. Vardeny [21] has investigated photoluminescence decay in intrinsic a-Si : H, and concludes that under these conditions bimolecular diffusion-limited recombination processes of characteristic time 10^{-6}–10^{-2} s can occur. Such a time scale is in accord with our observations of the recovery time, although any comparisons must be treated as highly speculative because of the uncertainty in what is being measured by our experiment and the relative complexity of our sample.

4.4.2 Structural changes: In addition to the electrostatic effects associated with the trapped electronic charge, it is also possible that atomic displacements may result, giving rise to a new atomic configuration which persists until the charge is released. The properties of the new

configuration could be sufficiently different from the original to inhibit the onset of the current instability under the same external conditions.

As mentioned earlier, previous experiments on formed samples have shown that once a permanent low resistance state has been established, conduction is localised to within an area of the order of 1 μm^2. If a similar area is involved in conduction in the case of the current instability, high peak current densities ($\sim 10^5$ A/cm^2) and powers ($\sim 10^6$ W cm^2) will occur. The resulting Joule heating may give rise to high transient local temperatures. Simple estimates, where the Joule heat is considered as a point source impulse [22], indicate that under these conditions temperatures of the order of 100 K above ambient can occur for a few microseconds within the filamentary volume of the a-Si : H. Although it is apparent that, in general, such heating effects are insufficient to bring about permanent changes, it is possible that the recovery time corresponds to the time taken for a thermally excited state to revert to the pre-instability state.

5 Conclusions

It has been shown that certain a-Si : H p^+ni sandwich structures exhibit transient current instabilities when a bias in excess of some temperature dependent critical value is applied. The onset time is found to be exponentially dependent on bias voltage, and in this respect the behaviour is qualitatively similar to that observed in analogous crystalline structures. However, the subsequent decay in the current and the existence of recovery effects appear unique to the amorphous device. It is suggested that charge trapping, recombination, and possibly structural changes can account for this behaviour. The absence of a pronounced area dependence of the current maximum indicates that conduction during the instability is localised within a filamentary volume, and as a similar result is obtained in the memory on-state it is possible that the current instability is a precursor to the 'forming' process necessary to elicit memory switching.

6 Acknowledgments

We would like to thank the Venture Research Unit of BP Company Ltd. for financial assistance, and S. Kinmond and A. Carrie of the Carnegie Laboratory of Physics, University of Dundee for their help in preparing samples.

7 References

1 OVSHINSKY, S.R.: 'Reversible electrical switching phenomena in disordered structures', *Phys. Rev. Lett.*, 1968, **21**, pp. 1450–1453

2 OWEN, A.E., and ROBERTSON, J.M.: 'Electronic conduction and switching in chalcogenide glasses', *IEEE Trans.*, 1973, **ED-20**, pp. 105–122

3 DEARNLEY, G., STONEHAM, A.M., and MORGAN, D.V.: 'Electrical phenomena in amorphous oxide films', *Rep. Prog. Phys.*, 1970, **33**, pp. 1129–1191

4 FELDMAN, C., and MOORJANI, K.: 'Switching in elemental amorphous semiconductors', *J. Non-Cryst. Solids*, 1970, **2**, pp. 82–90

5 DEN BOER, W.: 'Threshold switching in hydrogenated amorphous silicon', *Appl. Phys. Lett.*, 1982, **40**, (9), pp. 812–813

6 OWEN, A.E., LECOMBER, P.G., SARRABAYROUSE, G., and SPEAR, W.E.: 'New amorphous-silicon electrically programmable nonvolatile switching device', *IEE Proc. I, Solid-State & Electron Dev.*, 1982, **129**, (2), pp. 51–54

7 OWEN, A.E., LECOMBER, P.G., SPEAR, W.E., and HAJTO, J.: 'Memory switching in amorphous silicon devices', *J. Non-Cryst. Solids*, 1983, (59/60), pp. 1272–1280

8 LECOMBER, P.G., OWEN, A.E., SPEAR, W.E., HAJTO, J., and CHOI, W.K.: 'Electronic switching in amorphous silicon junction devices', in PANKOVE, J.I. (Ed.): 'Semiconductors and semimetals, Vol. 21, Part D' (Academic Press, New York, 1984), pp. 275–289

9 LECOMBER, P.G., OWEN, A.E., SPEAR, W.E., HAJTO, J., SNELL, A.J., CHOI, W.K., ROSE, M., and REYNOLDS, S.: 'The switching mechanism in amorphous silicon junctions', *J. Non-Cryst. Solids*, 1985, (77/78), pp. 1373–1382

10 OWEN, A.E., SPEAR, W.E., SARRABAYROUSE, G., and LECOMBER, P.G.: 'Improved semiconductor device'. British Patent Application 8124248, 7th Aug. 1981

11 CHOI, W.K., HAJTO, J., LECOMBER, P.G., OWEN, A.E., and SPEAR, W.E.: 'Threshold switch'. British Patent Application 2153147A, 14th Aug. 1985

12 FRITZSCHE, H.: 'Switching and memory in amorphous semiconductors', in TAUC, J. (Ed.): 'Amorphous and liquid semiconductors' (Plenum Press, 1974), pp. 313–319

13 BARNETT, A.M.: 'Current filaments in semiconductors', *IBM J. Res. & Dev.*, 1969, **13**, (5), pp. 522–528

14 BUXO, J., OWEN, A.E., SARRABAYROUSE, G., and SEBAA, J.-P.: 'The characteristics of metal-thin insulator-n-p^+ silicon switching devices', *Rev. Phys. Appl.*, 1978, **17**, pp. 767–770

15 SARRABAYROUSE, G., BUXO, J., MUNOZ-YAGUE, A., OWEN, A.E., and SEBAA, J.-P.: 'Dynamic properties of switching in MISS structures and applications to charge transfer devices', *Inst. Phys. Conf. Ser. 50*, 1979, pp. 179–185

16 SIMMONS, J.G., and EL-BADRY, A.A.: 'Switching phenomena in metal-insulator-n-p^+ structures: theory, experiment and applications', *Radio & Electron. Eng.*, 1978, **48**, pp. 215–226

17 SPEAR, W.E., LECOMBER, P.G., and SNELL, A.J.: 'An investigation of the amorphous-silicon barrier and pn junction', *Philos. Mag. B*, 1978, **38**, (3), pp. 303–317

18 ALLAN, D.: 'Hole drift mobility in amorphous silicon', *ibid.*, 1978, **38**, (4), pp. 381–392

19 CRANDALL, R.S.: 'Current controlled negative resistance in semiconductors', *J. Phys. & Chem. Solids*, 1970, **31**, pp. 2069–2077

20 ADAN, A., and ZOLOMY, I.: 'Charge storage effects in MIS diodes', *Phys. Status Solidi a*, 1980, **57**, pp. 113–116

21 VARDENY, Z.: 'Transient induced absorption in amorphous semiconductors for picoseconds to milliseconds', *J. Non-Cryst. Solids*, 1983, (59/60), pp. 317–324

22 LUIKOV, A.V.: 'Analytical heat diffusion theory' (Academic Press, 1968), pp. 381–384

304

Journal of Non-Crystalline Solids 114 (1989) 304-306
North-Holland

MODEL OF LASER INDUCED REGULAR AND CHAOTIC OSCILLATIONS IN AMORPHOUS $GeSe_2$ FILMS

J. HAJTO,[†] L. JANOSSY,[§] W.K. CHOI[†] and A.E. OWEN[†]

† Department of Electrical Engineering, University of Edinburgh, Edinburgh EH9 3JL, Scotland
§ Central Research Institute of Physics, Budapest, PO Box 49, Hungary

An improvement of the model of the laser induced oscillatory phenomena is suggested. The different types of oscillatory phenomena can be explained by assuming that both absorption coefficient α and refractive index n fluctuate during oscillations.

1. INTRODUCTION

The optical properties of amorphous $GeSe_2$ films show strong non-linear optical behaviour under the influence of relatively low intensity ($1-10^3$ Wcm^{-2}) c.w. laser irradiation[1]. Discontinuities, bistability and in special circumstances oscillation in the optical properties were observed[2]. The experimental results show[3] that at least three different types of oscillation can be distinguished which may occur at fixed c.w. laser intensity, a) monotonic oscillation, b) logarithmic time dependence in the oscillation amplitude and frequency, c) chaotic oscillations. The discovery of non-linear optical effects in amorphous $GeSe_2$ films generated a considerable interest and several models were suggested to explain the oscillatory phenomena[4-9]. It was also suggested by us that oscillation can be explained by combination of photostructural changes (optical effect) and laser heating (thermal effect)[1-2]. In the previous model we considered (for the sake of simplicity) only the changes of the absorption coefficient (α). That theory predicted monotonic oscillation at constant laser intensity. The aim of this paper is to demonstrate that a more detailed agreement with the experimental results can be obtained by taking into account the changes in the refractive index (n) together with the changes of the absorption coefficient (α).

2. RESULTS & DISCUSSION

According to our previous model[1-2], the oscillation can be described as a combination of 'fast' thermal effects (associated with the 'thermal runaway' phenomenon) and 'slow' photostructural changes under the influence of c.w. irradiation. The thermal effects are described[2] by the dissipation coefficient D,

$$D = 1 - Q - R \qquad (1)$$

where Q and R are the transmission and reflection coefficients respectively. The photostructural changes are described[2] by the instantaneous absorption coefficient α_o and the equilibrium value of the absorption coefficient $\bar{\alpha}_o$.

$$\frac{\partial \alpha_o}{\partial t} = \frac{\bar{\alpha}_o - \alpha_o}{\tau_s} \qquad (2)$$

$$\bar{\alpha}_o(T,J) = \frac{A}{1/q + f\exp(-\Delta E/kT)} \qquad (3)$$

where τ_s is the structural relaxation time, $f = K_1/K_2$ is the ratio of the constants determined by the transitions from the ground state to the metastable state and for the inverse transitions respectively. $\Delta E = E_2 - E_1$ and $q = J/K_1\exp(-E_1/kT)$. The mathematical solutions of these equations can be found in Ref 2. The stationary solution can be obtained by plotting $\bar{\alpha}_o(T)$ on the same diagram as the $\alpha_o(T)$ curves. At a given intensity the intercept of $\alpha_o(T)$ and $\bar{\alpha}_o(T)$ determines the stationary solution. The essence of the stability condition is $\partial\alpha_o/\partial T > 0$. If $\bar{\alpha}_o(T)$ crosses the unstable region there is an intensity interval where the intercept corresponds to an unstable solution; in this case oscillation occurs. In that previous model the refractive index of the film

0022-3093/89/$03.50 © Elsevier Science Publishers B.V.
(North-Holland)

(n) was considered constant i.e. the temperature dependence of the refractive index was ignored. The model is now further developed by taking into account the refractive index changes as well. Due to the shortage of space available, the mathematical description will be published elsewhere[7]. However, some important conclusions are briefly summarised below. The calculations showed that the dissipated energy (and the corresponding oscillatory phenomena) are rather sensitive to the actual value of the phase angle (δ). Therefore we introduced the relation

$$\delta = \delta_o + 2(\pi/\lambda_o)\,L\beta T \tag{4}$$

where β is the temperature coefficient of the refractive index

$$n = n_o + \beta T \tag{5}$$

and δ_o is considered to be a variable which is determined by photostructural changes i.e. by the concentration of light induced metastable states in the material[10]. δ_o is described by

$$\delta_o = 2(\pi/\lambda)_o L n_o \tag{6}$$

It is important to recognize that the value of the phase angle δ can change for two different reasons. Firstly because of the temperature dependence of the refractive index (see eqs. 4-5) and secondly because the value of δ_o (see eq. 6) might be different (due to photostructural changes). These possibilities are demonstrated in Figures 1 and 2.

In Figure 1 the value of δ_o is fixed (180°), but because T is increasing, the value of δ continuously changes (thermal effect). There exist three unstable regions (labelled with I, II and III) where oscillations can be found. Region III is the most interesting for us because the equilibrium value of α, $\bar{\alpha}_o$ (see Ref 2) crosses that region. Figure 2 shows the region III with different values of δ_o. In this case both the thermal effects (δ-T) and the photostructural changes (different δ_o) are included. The equilibrium value of α_o, $\bar{\alpha}_o$, is also plotted in this Figure.

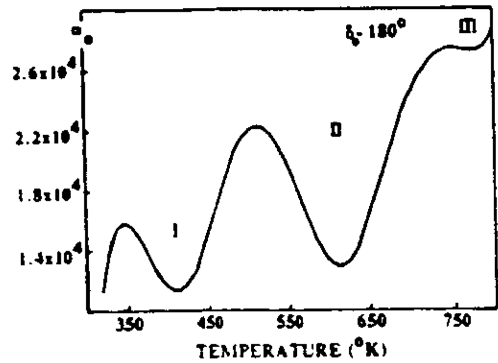

FIGURE 1
α_o – T plot for a 6 μm a-$GeSe_2$ film

The condition for oscillatory behaviour is that $\bar{\alpha}_o - T$ should cross $\alpha_o - T$ in the unstable region. This condition is satisfied at δ_o = 179 – 183°.

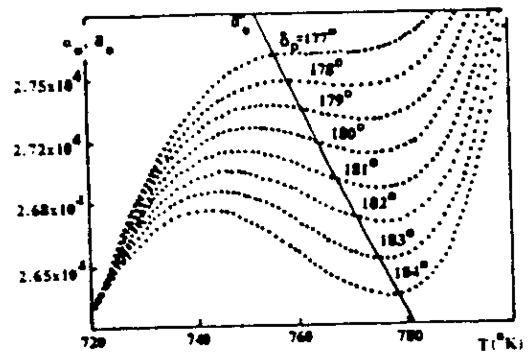

FIGURE 2
α_o–T and $\bar{\alpha}_o$–T for a 6μm a-$GeSe_2$ film with different values of δ_o

It is important to emphasize that the magnitude of the 'negative absorbance' region and its temperature range increase significantly with small changes in δ_o. Figure 3 shows the calculated oscillations at fixed laser intensity but different δ_o. The amplitude of the oscillations increases and at the same time the frequency of the oscillations decreases with increasing δ_o.

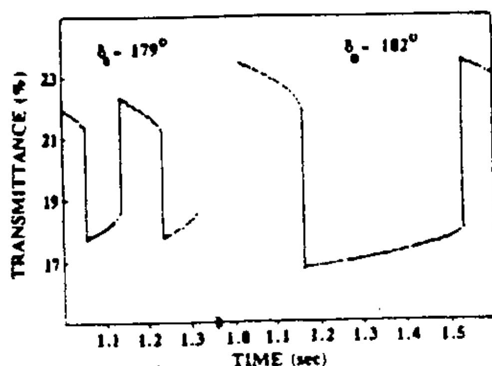

FIGURE 3
Laser induced oscillations (at fixed light intensity) using different values of δ_o.

These oscillations are in good agreement with the previous experimental results (see fig. 1 of Ref 3). The time dependence of δ_o is modelled under the assumption that there exists a number (N) of uniformly distributed metastable states in the amorphous system. Each is characterized by an energy level U_i, and each contributes to the change in δ_o. The energy level of each metastable state is determined by.

$$U_i = U_o + U_T/N \tag{7}$$

where U_o is a constant and U_T is the total energy difference between the highest and the lowest energy levels The time dependence of δ_o can be expressed as,

$$\delta_o = \delta_o' - \log(t)\ 1/B \sum_{i=1}^{i=N} kT/U_i \tag{8}$$

where δ_o, B are constants related to the amorphous system, t is the time elapsed. Assuming logarithmic time dependence for δ_o (i.e. logarithmic time dependence for the refractive index of the film), the oscillation amplitude and frequency change logarithmically. This is in good agreement with the previous experimental results (see Ref 3). In the case of δ_o ~ 179°, the oscillation stops (the negative absorbance disappears). This prediction is in a good agreement with the observed 'optical stopping effect' reported in Ref 3. However, oscillation will start again after a certain time elapsed because the refractive index is included in a cosine function (phase angle, see eq 4 in Ref 2).

4. CONCLUSION

The analysis of the improved model shows that oscillation can be stable if the refractive index of the film has the same value at the beginning of each oscillating cycle. On the other hand, small changes in the refractive index (associated with photostructural changes) can significantly change the oscillation frequency and amplitude in good agreement with the experimental results. The condition of the chaotic behaviour is that n should change randomly at the beginning of each oscillating cycle. At the moment the physical mechanism responsible for this is not known, but it is possible that under the influence of the laser beam 'random crystallisation' occurs[6] which might account for the chaotic behaviour. This possibility will be further investigated.

REFERENCES

1. J. Hajto and I. Janossy, Phil. Mag. B 47 (1983) 347.
2. J. Hajto, I. Janossy and A. Firth, Phil. Mag. B 48 (1983) 311.
3. J. Hajto, I. Janossy and W.K. Choi, J. Non-Cryst. Sol. 77-78 (1985) 1273.
4. M. Noga, Phys. Lett. 80A (1980) 91.
5. P. Fazekas, Phil. Mag. B 44 (1981) 435.
6. J.C. Phillips, Comments Solid State Physics 10 (1982) 165.
7. J. Hajto and I. Janossy, Phil. Mag. (1989) in print.
8. I. Janossy, phys. stat. sol. (b) 150 (1988) 783.
9. Lun-Biao Xu, Shou-Fu Cai and Guo-Xin Xie, phys. stat. sol. (b) 150 (1988) 797.
10. I. Janossy, A. Jakli and J. Hajto, Sol. St. Commun. 51 (1984) 761.

168

Journal of Non-Crystalline Solids 115 (1989) 168–170
North-Holland

AMORPHOUS SILICON ANALOGUE MEMORY DEVICES

M. J. ROSE,‡ J. HAJTO,† P. G. LECOMBER,‡ S. M. GAGE,† W. K. CHOI,† A. J. SNELL† and A. E. OWEN†

‡ Department of Applied Physics and Electronic & Manufacturing Engineering, University of Dundee, Dundee DD1 4HN, Scotland
† Department of Electrical Engineering, University of Edinburgh, Edinburgh EH9 3JL, Scotland

Amorphous silicon M-p^+ni-M and M-p^+-M memory devices have been prepared. The characteristics are critically dependent on the metal used for the top contact. Devices with Cr top contacts exhibit the fast digital behaviour reported previously, whereas those using V exhibit fast analogue switching. The paper reports results for these and other metals.

1. INTRODUCTION

The past decade has seen the commercialisation of a large number of amorphous silicon (a-Si) devices, with many other devices and applications under development. In this latter category is an electrically programmable non-volatile digital memory [1-2]. These heterogeneous a-Si devices are two-terminal structures with p^+ni and related configurations, and have been shown to be filamentary in nature [2]. The present paper describes results for a new device which, rather than exhibiting a two-state digital operation, has a continuum of stable states which are non-volatile and fully programmable by single 10ns voltage pulses. In effect, it is a 'programmable variable resistor' which may have applications in artificial neural networks.

We have investigated many structures in an attempt to elucidate the switching mechanism reported previously. Different combinations of p^+-, n- and i-layers have been tried, along with double and single layer devices of intrinsic and doped a-Si. All have been found to exhibit some form of memory action. However, only two configurations have shown consistently reliable memory action over 10^6 cycles viz. M-p^+ni-M and M-p^+-M, where M denotes a metal contact. M-p^+-M structures when formed resemble p^+ni devices in every respect of speed and non-volatility etc. Both the p^+ni and p^+ structures show differences in operation depending on the metal used for the top contact.

0022-3093/89/$03.50 © Elsevier Science Publishers B.V.
(North-Holland)

2. DEVICE FABRICATION

The p^+ a-Si samples have been prepared by the r.f. glow discharge decomposition of SiH_4 containing 10^4 vppm of B_2H_6. Films 1000A thick were deposited on Corning 7059 glass substrates with patterned metal (generally Cr) bottom contacts. The a-Si was then patterned, and an insulator used to delineate an active area of 10^{-6} cm^2. The metals used for the top contact were generally Cr or V and the choice of this contact is crucial to the device characteristics.

3. FORMING CHARACTERISTICS

In accordance with p^+ni digital memories, the analogue device exhibits a forming step. However, whereas M-p^+ni-Cr structures show a sudden, discontinuous change in resistance from $10^{10}\,\Omega$ to $10^3\,\Omega$, the M-p^+-V device exhibits a less catastrophic event. Biasing the top electrode with progressively increasing 300ns pulses leads to a resistance change of nearly three orders of magnitude (Figure 1). This control of the device resistance may have applications in artificial neural networks as weak synapses.

On reaching a critical voltage, the device switched into an ON-state of 10^3 to $10^4\,\Omega$. Subsequent switching characteristics were dependent on the top metal contact. Previous devices using Al as a top contact showed the OFF-state resistance equal to the pre-formed value and scaling with area. However, our new work, using Cr electrodes, showed R_{OFF} significantly

less than the pre-formed value and independent of area.

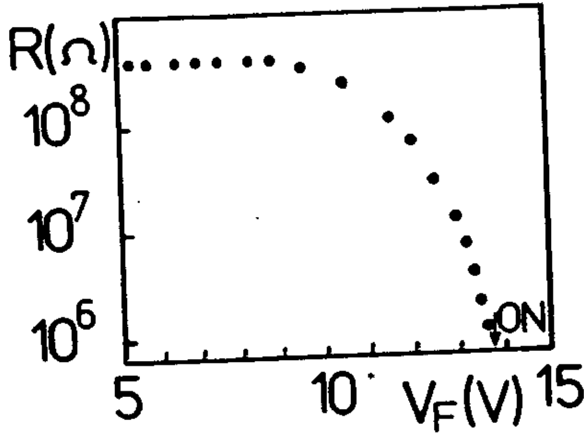

FIGURE 1
Resistance R of a Cr-p^+-V device as a function of forming pulse voltage V_F.

4. RESULTS AND DISCUSSION

Once the device had reached its first non-volatile ON-state all subsequent switching operations were performed with 10-100ns pulses 1-5 volts in magnitude. The ERASE operation was now obtained with a negative going pulse applied to the bottom electrode.

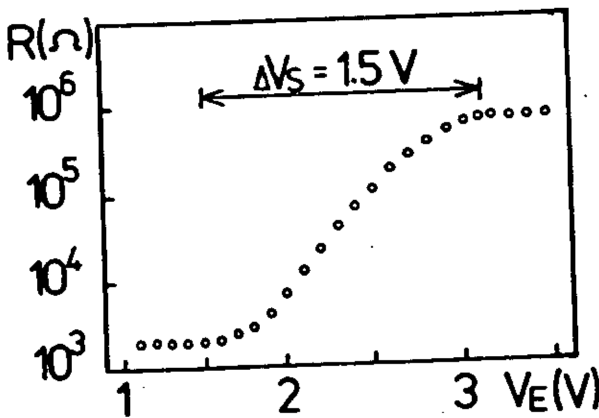

FIGURE 2
Resistance R of a Cr-p^+-V device as a function of ERASE pulse voltage V_E.

The magnitude of the new 'OFF'-state resistance was determined by the magnitude of the ERASE voltage. As shown in figure 2, a voltage range ΔV_S of 1.5V gave a change in resistance from $\sim 10^6\,\Omega$ to $10^3\,\Omega$. The WRITE operation was now achieved by positive pulses applied to the bottom contact, and again the resultant 'ON'-state resistance was determined by the magnitude of the WRITE voltage. The device will switch between any two resistance states by selecting the correct magnitude of WRITE and ERASE pulses. For example, in one experiment the ERASE pulses were maintained at a constant value of 3.5V while the WRITE pulse amplitude was incremented from 1V to 3.5V. Figure 3 shows that in this case the value of the OFF-state resistance remained at approximately $10^6\,\Omega$, while the ON-state resistance decreased through a continuum of intermediate states.

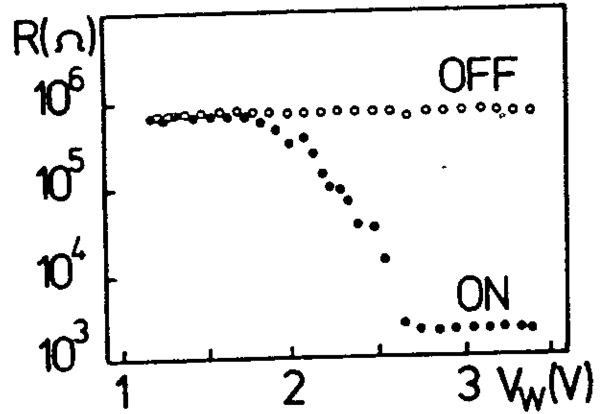

FIGURE 3
Resistance R of a Cr-p^+-V device as a function of WRITE pulse voltage for a constant ERASE pulse of 3.5V.

Similarly, with the WRITE pulses kept at a constant level of 3.5V, the ON-state remained at $10^3\,\Omega$, while the device was progressively switched between this and new stable intermediate states, until a final OFF-state resistance of $\sim 10^6\,\Omega$ was achieved. At this point the device characteristics resembled those of a digital memory device. It should be stressed that the device will switch between any two programmed resistance levels (depending on the magnitude of the WRITE and

ERASE pulses) for up to 10^6 cycles with 100% efficiency. Furthermore, any of the programmed states were found to be non-volatile on the time scale investigated (i.e. several months).

We have repeated the above experiments on p^+ devices with Cr as the top metal and observe similar forming characteristics. However, in subsequent WRITE and ERASE experiments, intermediate states were only found to exist over a narrow ΔV_S of 0.2V as shown in figure 4. These devices are useful only as digital devices.

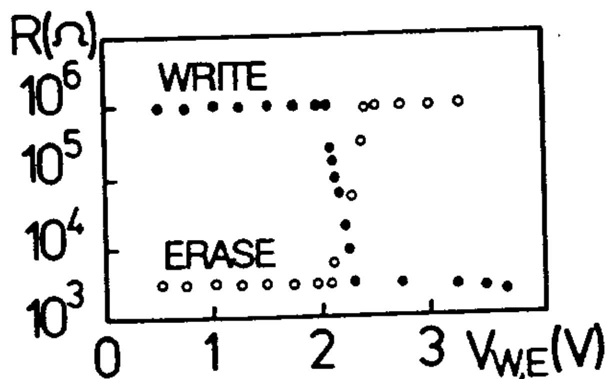

FIGURE 4
Resistance R of a Cr-p^+-Cr device as a function of the WRITE and ERASE voltages.

Further evidence for the role of the top metal contact has been found by fabricating devices with V-p^+-Cr and Cr-p^+-V structures, where, as before, the layers are listed in the order of deposition. Using the analogue switching voltage window, ΔV_S, as a guide, it is found that its value is entierly dependent on the top contact, and completely independent of the bottom metallisation, i.e. Cr top electrode devices are always digital and V top electrode devices are always analogue irrespective of the bottom electrode. Furthermore, if an analogue device has its top V metal removed after the forming step and replaced with Cr, the device still behaves as a V device, indicating that the type of the device is determined during the forming operation.

X-ray microanalysis studies of the devices [3] have been carried out, and the top electrode material has been found embedded in a filamentary region of the a-Si. This suggests that the top metal becomes distributed in the filament, and may play a role in the mechanism of switching. However, it is difficult to determine if the metal incorporation is a cause or a consequence of switching these devices.

The results reported above were for devices with Cr or V top contacts showing digital or analogue behaviour respectively. However, we have investigated a much larger range of top metal contacts. The values of ΔV_S range from about 0.1V to 2.0V, but at present there appears no obvious correlation between the properties of the metal and the value of ΔV_S.

5. CONCLUSIONS

Analogue devices can be programmed by single 10ns pulses of 1.5V to 3V, with a minimum requirement of 1.5V providing an inbuilt noise immunity. A READ pulse of 0.5V in the input line enables the state of the device to be determined without changing the value of the programmed state. With the potential of large packing densities of these two terminal devices, they appear to be ideally suited to new parallel computing methods.

ACKNOWLEDGEMENTS

The authors would like to thank Stewart Kinmond and Arch Carrie for their technical assistance, and BP Research International for their financial support in this work.

REFERENCES

1) A.E. Owen, P.G. LeComber, G. Sarrabayrouse and W.E. Spear, IEE Proc. I. Solid State & Electron Dev. 129 Pt.1 (1982) 51

2) P.G. LeComber, A.E. Owen, W.E. Spear, J. Hajto, A.J. Snell, W.K. Choi, M.J. Rose and S. Reynolds, J. Non-Cryst. Solids 77 & 78 (1985) 1373

3) A.G. Fitzgerald, Private Communication

Journal of Non-Crystalline Solids 115 (1989) 171-173
North-Holland

ANOMALOUS HIGH ZERO BIAS RESISTANCE IN METAL - AMORPHOUS SILICON - METAL STRUCTURES

S. M. GAGE,[†] J. HAJTO,[†] S. REYNOLDS,[†] W. K. CHOI,[†] M. J. ROSE,[‡] P. G. LECOMBER,[‡] A. J. SNELL[†] and A. E. OWEN[†]

† Department of Electrical Engineering, University of Edinburgh, Edinburgh EH9 3JL, Scotland
‡ Department of Applied Physics and Electronic & Manufacturing Engineering, University of Dundee, Dundee DD1 4HN, Scotland

It has been demonstrated previously that metal-amorphous silicon-metal thin film structures exhibit non-volatile polarity dependent memory switching after initial conditioning, or 'forming', by means of a high applied potential. Under certain circumstances conduction in the formed device is associated with a highly conducting filament. The physical nature of the filament is, however, largely unknown. This paper describes the low temperature conductivity behaviour of such formed memory structures, and analyses this in terms of possible metal incorporation in the filamentary region.

1. INTRODUCTION

Memory switching in a-Si was first reported by Owen et al. in p-n and p-n-i structures using metal contacts[1]. In a subsequent paper on such devices[2] it was shown that conduction in the low resistance ON state at room temperature was associated with a highly conductive filament of modified material with a diameter of $<0.5\mu m$. These early devices could be switched to an extremely resistive OFF state in which the current was found to scale with device area. More recent device configurations show a somewhat lower OFF resistance that is independent of area. In this paper we shall report results from an investigation of the conduction mechanisms in the device structure at temperatures down to 4.2K. This work gives some insight into the composition and structure of the filament, and indicates that the filament contains metal from the electrodes.

2. SPECIMEN PREPARATION

The samples used for this work were p-n-i structures with a total layer thickness of $0.3\mu m$ and an active area of $8\times10^{-7}cm^2$. The bottom contact was chromium and the top contact was either Cr, gold, iron or aluminium. Full details of the sample preparation and structure can be found in reference 2. Each device was 'formed' by the application of a voltage pulse of 10-15 volt amplitude for a period of between 100ns and $5\mu s$, and was then switched between memory ON and OFF states for a number of cycles to confirm that an operational device was being measured.

3. CONDUCTIVITY RESULTS

The conductivity of samples in both ON and OFF states has been investigated as a function of temperature and bias. The measurements were made using phase sensitive detection of a small 1kHz a.c. signal ($<1mV$) superimposed on a d.c. bias.

3.1. Cr, Au and Fe contacts

The conductivity of the samples in both ON and OFF states at an applied bias of 100mV was found to decrease as the temperature decreased in the range 100K to 4K. The averaged temperature coefficient of resistance (TCR) over this temperature range was around $10^{-3}/K$, the OFF states showing a tendency towards somewhat higher values. Measurements of the dynamic resistance, dV/dI, at biases less than 100mV for both ON and OFF states revealed, for all three contact materials, a resistance peak centred about zero volts. This is illustrated by the data in figure 1, which is for a sample with a Cr top contact in a low resistance state of $2k\Omega$ as measured at room temperature. It can be seen that dV/dI increases as both the magnitude of the bias and the temperature are decreased. Devices in higher resistance states of a few hundred $k\Omega$ showed

0022-3093/89/$03.50 © Elsevier Science Publishers B.V. (North-Holland)

results of the same form, with resistance maxima similar to those seen in figure 1. The relative size of these peaks, as measured by the percentage increase in dV/dI when moving from a bias of ±100mV to 0V along the 4.2K isotherm, was found to vary from sample to sample, and ranged from a few percent to over 100%.

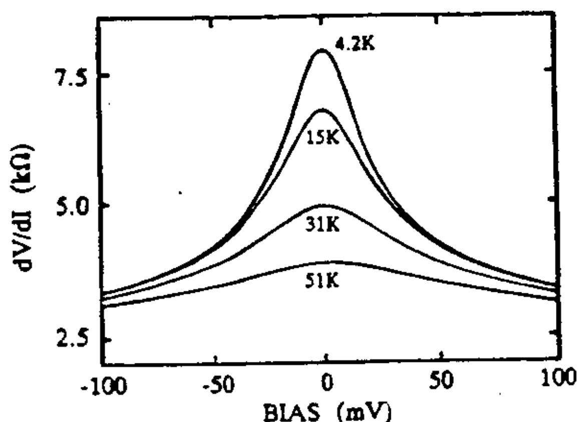

FIGURE 1
dV/dI versus temperature and bias for a formed sample with Cr top contacts in a memory ON state, showing a resistance maximum.

Conductance variations of this type have been shown to be characteristic of conduction in materials consisting of small metal particles embedded in a dielectric medium and in which carrier transport is predominantly by electron tunnelling between these particles[3]. In such a system the creation of free carriers is an activated process - this relates to the increase in the electrostatic potential of a particle when a free electron is added to it[3]. This activation energy can be provided entirely by thermal energy or, in the presence of an applied field, part or all of it can be provided by the the field itself. Thus the electrical conductance increases with increasing field and temperature in a fashion similar to that seen in figure 1. If, as we suggest, this conduction mechanism is responsible for the data presented in figure 1 it appears to imply that the filament contains small metal islands embedded, presumably, in a matrix of amorphous silicon.

3.2. Aluminium contacts

Only the low resistance ON state of these samples was investigated which, with a typical value of a few hundred Ohms, was somewhat lower than those of samples with Cr, Au and Fe contacts. Their resistance measured away from zero bias (±20mV) increased with decreasing temperature with a TCR of 10^{-4}/K.

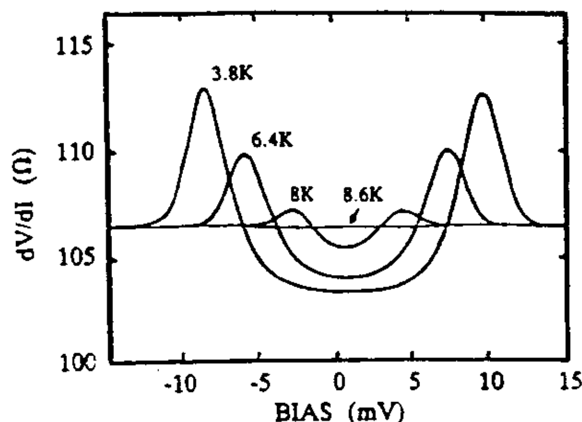

FIGURE 2
dV/dI versus temperature and bias for a formed sample with Al top contacts in a memory ON state, showing a resistance minimum.

Close to zero bias these samples showed a decrease in dV/dI of a few percent at 4.2K as shown in figure 2 which, in contrast to the Cr, Au and Fe top contact samples, indicates a resistance minimum at zero bias. This resistance minimum could be largely removed by the application of a transverse magnetic field of 0.2 Tesla suggesting that this effect could be the result of a normal to superconducting transition in part of the filament. The variation in zero bias resistance with temperature for a similar sample is shown in figure 3. From the point at which this curve levels off it would appear that an upper limit for the critical temperature, T_C, of the superconducting material is 8 - 9K. This is in excess of the T_C for aluminium (1.15K) and Cr and Si are not known to superconduct at this temperature. However, it has been shown that Al:Si alloys have a T_C as high as 8.3K when the Al content is around 65%[4]. For mixtures with either higher or lower concentrations of Al the T_C decreases - it may be

reasonable to suggest, therefore, that the broad transition from low to high resistance seen in figure 3 reflects a range of Al:Si compositions. The indication from these observations of superconductivity is that Al from the top electrode has mixed with the a-Si. The fact that the resistance minimum amounts to no more than a few percent of the overall device resistance may indicate that this mixing is occurring only on a small scale.

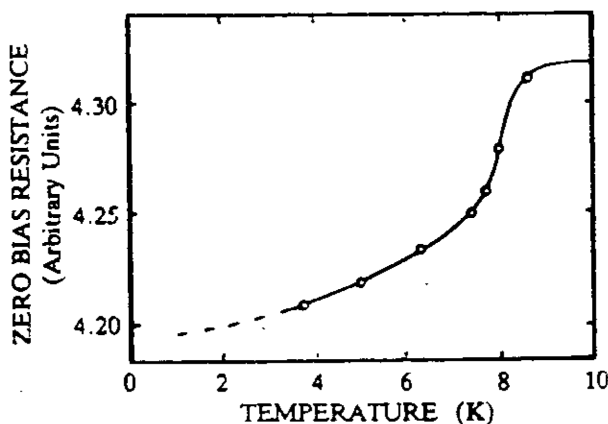

FIGURE 3
Zero bias resistance versus temperature showing the transition from a low resistance to a high resistance.

4. DISCUSSION

The relatively high level of conductance of all four sample types (i.e. those with Al, Cr, Au or Fe top contacts) at 4.2K and the insensitivity of the device resistance to decreasing temperature suggests that the filament of modified material extends continuously between the top and bottom contacts i.e. conduction can not be taking place to any large degree through unmodified a-Si as this would show up as a much stronger temperature dependence of resistance. If we assume a uniform filament diameter of 0.5μm and a device thickness of 1μm the resistivity of the filament material must lie between 10^{-4} and $5\times10^{-3}\,\Omega$.cm. This suggests the filament material is made either of heavily doped crystalline Si[5] (possibly from the p- and n- layers) or from a Si:metal mixture[4]. Although these experiments have not permitted us to say anything conclusive about the presence of crystallised Si, there are strong indications from the features in the zero bias resistance data that metal is present in the filament. In the case of samples with Al top contacts the mixing of the Al with the Si has been suggested by the possible presence of a superconducting Al:Si mixture. In the samples with Cr, Fe and Au contacts the presence of metals has been inferred from the observation at 4.2K of resistance peaks at zero bias which are characteristic of a conduction mechanism involving tunnelling between isolated metal particles in a dielectric matrix. If metal is present in the filament it seems probable that its migration from the electrodes takes place during the forming process. The field strengths associated with forming are high[2], possibly up to 10^6 Vcm^{-1}, and large localised temperature increases are possible. Both of these effects could conspire to encourage the injection of metal in to the a-Si layer. The role of this injected metal in the switching mechanism is, at present, unclear. It is hoped, however, that further comparison of the low temperature conduction mechanisms in samples in ON and OFF states may reveal something of the changes occurring during switching.

ACKNOWLEDGEMENTS

The authors would like to thank Stewart Kinmond and Arch Carrie for their technical help, and gratefully acknowledge the financial support of BP Research International for this work.

REFERENCES

1) A.E. Owen, P.G. LeComber, G. Sarrabayrouse and W.E. Spear, IEE Proc. I. Solid State & Electron Dev. 129 Pt.1 (1982) 51

2) P.G. LeComber, A.E. Owen, W.E. Spear, J. Hajto, A.J. Snell, W.K. Choi, M.J. Rose and S. Reynolds, J. Non-Cryst. Solids 77 & 78 (1985) 1373

3) I. Giaever and H.R. Zeller, Phys. Rev. Let. 20 (1968) 1504

4) F. Meunier, P. Pfeuty, A.M. Lamoise, J. Chaumont, H. Bernas and C. Cohen, J. de Physique-Let. 38 (1977) L-435.

5) M. Takeshima, Phys. Rev. B 36 (1987) 1186.

MATERIALS RESEARCH SOCIETY SYMPOSIUM PROCEEDINGS VOLUME 192

Amorphous Silicon Technology - 1990

Symposium held April 17-20, 1990, San Francisco, California, U.S.A.

EDITORS:

P. C. Taylor
University of Utah, Salt Lake City, Utah, U.S.A.

M. J. Thompson
Xerox PARC, Palo Alto, California, U.S.A.

P. G. LeComber
University of Dundee, Dundee, United Kingdom

Y. Hamakawa
Osaka University, Osaka, Japan

Arun Madan
SERI, Golden, Colorado, U.S.A.

MATERIALS RESEARCH SOCIETY
Pittsburgh, Pennsylvania

405

THE PROGRAMMABILITY OF AMORPHOUS SILICON ANALOGUE MEMORY ELEMENTS

J. HAJTO *, M.J. ROSE †, A.J. SNELL *, P.G. LECOMBER † and A.E. OWEN *

* Department of Electrical Engineering, University of Edinburgh, EH9 3JL, Scotland

† Department of Applied Physics and Electronic & Manufacturing Engineering, University of Dundee, DD1 4HN, Scotland

ABSTRACT

This paper outlines recent results from work on non-volatile, analogue switching effects in amorphous silicon devices. The implication for the switching mechanism of these results and also the technological applications of such analogue devices are discussed. Particular reference is made to their use as re-programmable, non-volatile weighting elements in neural network synapses.

INTRODUCTION

We have previously shown that amorphous silicon metal-p^+-n-i-metal and metal-p^+-metal junctions exhibit non-volatile, polarity dependent digital and analogue memory switching phenomena [1-2] after initial conditioning by means of a moderately high applied potential ("forming"). This paper summarizes some new results on non-volatile analogue switching effects in amorphous silicon metal-p^+-metal devices.

EXPERIMENTAL

The samples used for this work were amorphous silicon Cr-p^+-V thin film structures. The p^+ layer was prepared by r.f. glow discharge decomposition of SiH_4 containing 10^4 vppm of B_2H_6. Films of 1000 Å thickness were deposited on Corning 7059 glass substrates previously patterned with chromium bottom contacts. The p^+ amorphous silicon was then patterned and an insulating layer was used to define an active device area of 10^{-6} cm^2. The metal used for the top contact was vanadium. In accordance with our previous results [2], memory devices prepared in this way require an initial forming process. After forming the resistance of the unformed device is lowered from $R \sim 10^9\,\Omega$ to $R \sim 10^3 - 10^4\,\Omega$ (i.e. the typical value of an ON state). This can be achieved by biasing the sample with a single voltage pulse (duration 300 nsec, magnitude ~12 V) with positive polarity applied to the top V contact. Details of the subsequent memory operation are described in [2]. The devices exhibit fast analogue switching at room temperature i.e. they have a continuum of stable (non-volatile) states between $R_{ON} = 10^3\,\Omega$ and $R_{OFF} = 10^6\,\Omega$. In this work we have studied the programmability of these analogue memory devices.

RESULTS

An example of the programmability of the analog memory device is shown in Fig. 1. where the sample resistance is plotted as a function of the applied alternating WRITE and ERASE pulses (100 nsec pulse duration each). It is important to

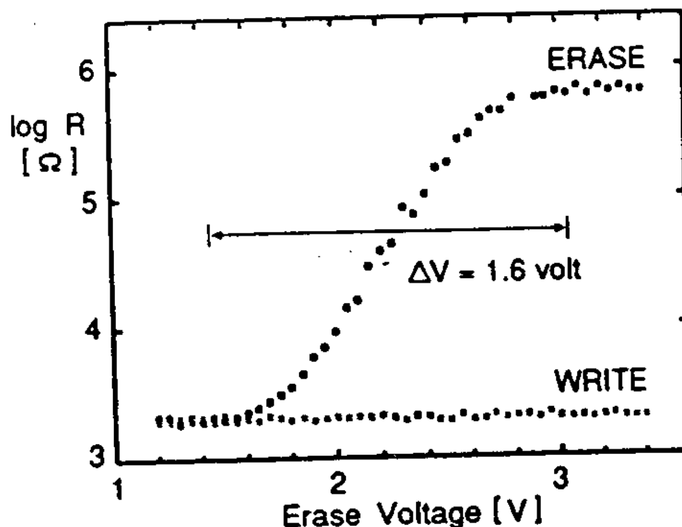

FIG. 1 Memory resistance as a function of ERASE voltage.

emphasize the polarity dependence of the analogue memory behaviour. In the case of the WRITE pulses, positive polarity is applied to the Cr track (bottom contact) while ERASE pulses have opposite polarity. The sample was first switched to an ON state ($R_{ON} = 2x10^3\,\Omega$) and then a series of alternating WRITE and ERASE pulses were applied. WRITE pulses were kept at a constant magnitude of 3.4 V, but ERASE pulses were incremented by 0.05 V steps from 1.2 to 3.4 V after each WRITE pulse. It can be seen from Fig. 1. that the sample resistance changes in an analogue manner as the magnitude of the ERASE pulse increases i.e. the difference between R_{ON} and R_{OFF} is a function of the magnitude of the ERASE pulses. A voltage range of ΔV (ERASE) = 1.6 V resulted in a change in resistance from $R \sim 2x10^3\,\Omega$ to $R \sim 6x10^5\,\Omega$. The shaded area in Fig. 1. indicates the reproducibility of the analogue memory switching i.e. the scattering in the resistance during repeated experiments (data from 100 cycles are included). Fig. 2. shows another case where the ERASE pulses were maintained at a constant value of V = 3.4 V but the WRITE pulses were incremented from 1.2 V to 3.4 V in 0.05 V steps. The value of the OFF state resistance remained constant at $\sim 6x10^5\,\Omega$ (i.e. it changed back to this constant level from every ON state) while the ON state resistance decreased through a continuum of intermediate states. The shaded area in Fig. 2. again represents the reproducibility of the analogue switching for 100 complete cycles. It is emphasized that the device will switch between any two resistance states by selecting the correct polarity and magnitude of the WRITE and ERASE pulses.

Fig. 3. shows another series of ERASE experiments where the resistance of the sample is plotted against the number of pulses applied. In this case the sample was switched to an $R_{ON} = 3x10^3\,\Omega$ state and 70 single pulses (1.8 V magnitude, 100 nsec pulse length) with positive polarity to the V top contact (i.e. ERASE pulses) were applied (see curve *a* in Fig. 3.). This caused little effect on the sample resistance as seen on curve *a*. This observation is in accordance with Fig. 1. where the 1.8 V ERASE pulse

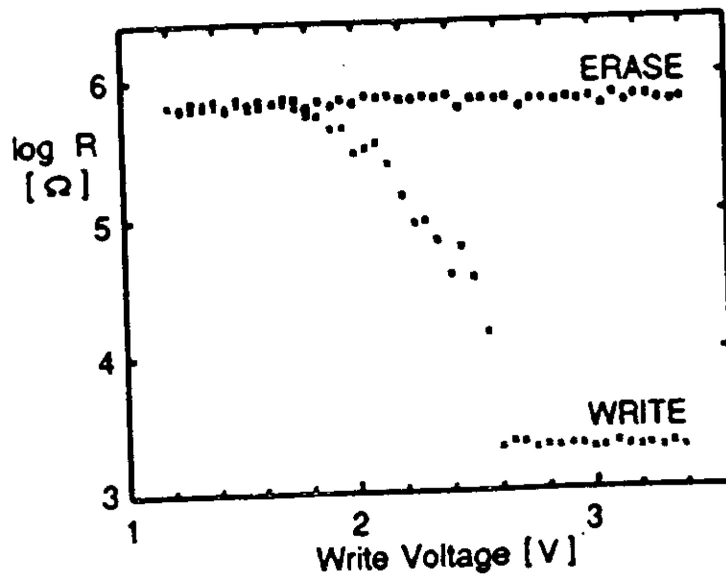

FIG.2 Memory resistance as a function of WRITE voltage.

magnitude will only slightly increase the sample resistance. It is emphasized that in this particular experiment no WRITE pulses were applied between the ERASE pulses. After the first series of pulses the sample resistance was switched back to $3x10^3$ Ω and another 70 ERASE pulses of magnitude 1.92V were applied. The sample resistance increased to $6.6x10^3$ Ω after the first pulse was applied but remained constant within 20% as 70 pulses were applied with the same magnitude. Curves *c-f* in Fig. 3. show similar ERASE experiments, where in each case the sample resistance was switched back to $3x10^3$ Ω at the beginning of the set of measurements. The magnitude of the pulses was kept constant within each series of ERASE pulses but increased at the beginning of each cycle (i.e. at the beginning of each curve). The magnitudes of ERASE pulses were 1.8, 1.92, 2.02, 2.40 2.56 and 3.52V for curves *a-f* respectively. It can be seen that the first ERASE pulse at the beginning of each cycle causes a sudden change in the device resistance, but after this change the resistance remains constant usually to better than 20% i.e. no gradual ERASE is observed after the first pulse has set the resistance.

Fig. 4. depicts the resistance of the device after applying a number of pulses with either the WRITE or ERASE polarity. In this experiment the initial sample resistance was $1.2x10^5$ Ω and a series of WRITE pulses were applied (denoted by A, B, C, D, E, F and G). The magnitude of the voltage was kept constant for 20 pulses (i.e. within A, B, etc.) and then increased to the next voltage level. The magnitude of the voltage levels were 1.29, 1.84, 2.0, 2.29, 2.40, 2.45 and 2.55 for A, B, C, D, E, F, G pulses respectively. It can be seen that when the sample was in the $1.2x10^5$ Ω OFF state, corresponding to an "intermediate" state of the analogue memory (as seen in Fig. 1. or Fig. 2.), the WRITE voltage levels of 1.29-2.29V (ranges A-D in Fig. 5.) did not change the memory resistance even with up to 20 pulses applied in each case. On the other hand, if V=2.4V (range E) was applied, the value of resistance changed from after the first pulse but remained constant for another

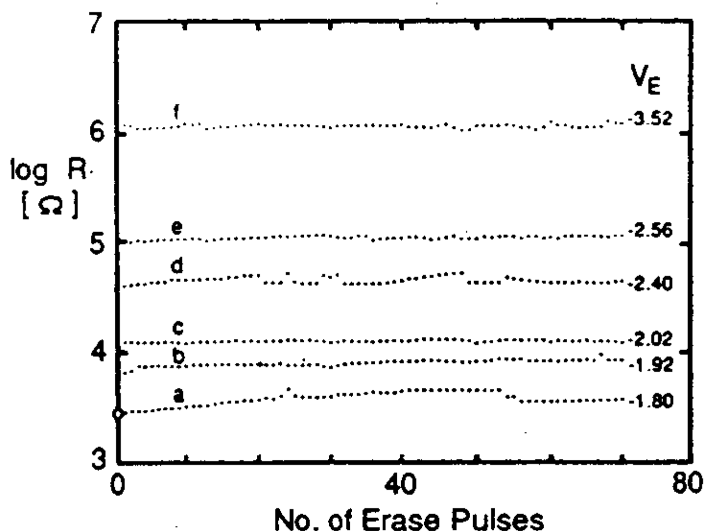

FIG. 3 Memory resistance as a function of applied pulses.

19 pulses. Range F shows a similar behaviour. Under the influence of V=2.45 V WRITE pulses the device resistance changed from $R = 7.6 \times 10^4\,\Omega$ (as left in range E) to $R = 6.6 \times 10^4\,\Omega$ after the first pulse was applied and remained constant for another 19 pulses. Range G also shows similar behaviour with the resistance changing from $6.6 \times 10^4\,\Omega$ to $1.5 \times 10^4\,\Omega$ on applying the first pulse. It is emphasized that nc ERASE pulses are applied between any of the WRITE pulses during this experiment.

Having reached a resistance of $R = 1.5 \times 10^4\,\Omega$ resistance (range G), a series of ERASE pulses (positive polarity to the V top contact) were applied (ranges H, I and J). On applying a 2.42V ERASE pulse (range H), the resistance changed from $R = 1.5 \times 10^4\,\Omega$ to $R = 7.6 \times 10^4\,\Omega$ i.e. an analogue ERASE occurred after the first pulse was applied, and no further change occured after the subsequent 19 pulses. Ranges I and J show a similar trend, namely analogue ERASE occured (i.e. the value of resistance changed in accordance with Figs. 1. and 2.) after the first pulse applied and no further change was experienced after the subsequent 19 pulses of the same magnitude.

Summarizing the results on the analogue switching, the device resistance appears to be uniquely determined by the magnitude and polarity of the applied voltage. Repeatedly applying pulses of the same magnitude does not appear to have any cumulative effect during either ERASE or WRITE operations. This may imply that there is, in the switching part of the device, a distribution of "active centres" each with its own fixed voltage threshold and by applying a pulse of a particular voltage value we "switch" only those centres with thresholds below or equal to this value. This idea would concur with the observations of Figs. 1. and 2.

We suggest that the Cr-p^+-V structures can be used as non-volatile and reprogrammable memory elements in analogue neural networks. The basic operating

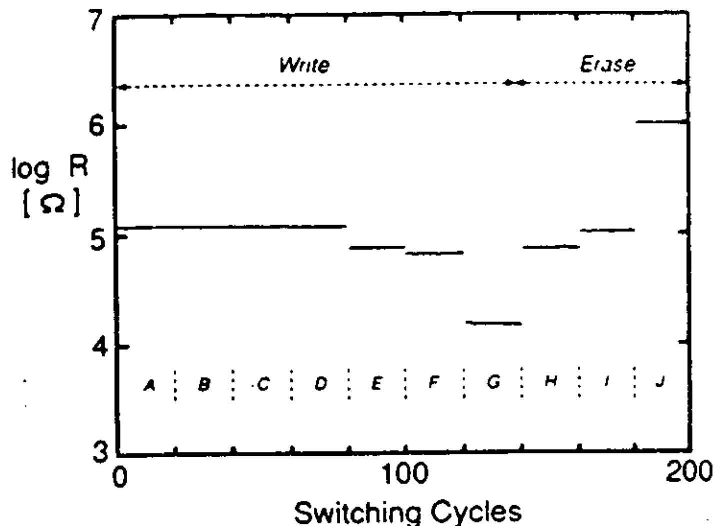

FIG. 4 Memory resistance as a function of WRITE and ERASE voltage.

unit in a neural network has to perform some sort of weighted summation of at least two inputs i.e.

$$\sum T_{ij} V_j \qquad (1)$$

where V_j is the "neural state" eg the value of a voltage level or a pulse width, and T_{ij} is a synaptic weighting factor. The electronic implementation of this function requires an element that will weight each of the input signals and then perform a summation.

Present day circuits are rather complicated involving numerous components and are not particularly well suited to VLSI. For example one of the "simplest" circuits suggested by Murray et al [3] using pulse stream arithmetic techniques requires the use of 5 MOS transistors plus two capacitors for a single neuron element. Furthermore, the weighting function, T_{ij}, must be continually refreshed using D to A conversion of the weighting values which in turn are held in a DRAM; this process calls on large amounts of circuitry and is time consuming.

A different and apparently much simpler approach to the problem of weighting the input signals would be to employ a non-volatile electrically programmable analogue memory. The properties of the Cr-p^+-V analogue memory device reported described in this paper are potentially very well suited to this purpose. To appreciate how a programmable variable resistor might be used in a weighting element of a neural network consider Fig. 5. Here, the output voltage is effectively "weighted" by the value of the variable resistor with the output signal linearly dependent on the value of R. By reprogramming the value of R the weighting for the output signal will be changed. For a two terminal device the "programming" signals (V_P) and the "READ" signals (V_R) must necessarily appear along the same line and should therefore be separated to

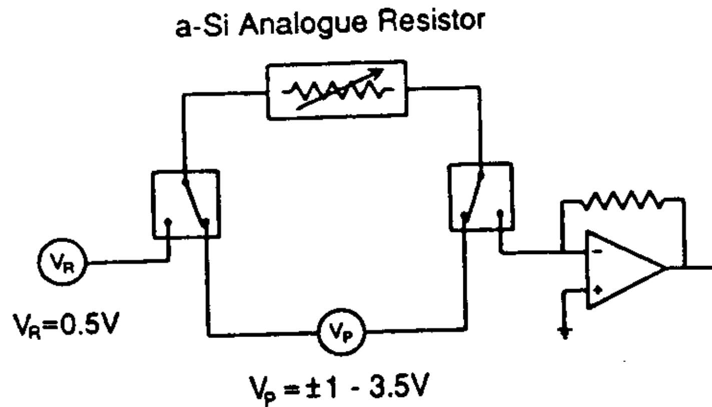

FIG. 5 Suggested application of analogue memory device in neural networks.

avoid confusion. An important feature of a suitable variable resistance element is that the READ pulses should not be confused as programming pulses by the device i.e. the element must be able to pass read signals without changing its resistance state. Turning now to the Cr-p$^+$-V devices, it can be seen from our results that resistances in the range of $10^3\,\Omega$ to $10^6\,\Omega$ can be attained using strings of programming pulses of ~1.2 V to ~3.4 V. These resistance states are non-volatile. Furthermore a READ voltage of up to 0.5 V does not appear to cause a change in the device resistance.

In conclusion, the characteristics of the Cr-p$^+$-V device described here seem to match very well those necessary for applications to neural networks.

REFERENCES

1. S.M. Gage, J. Hajto, S. Reynolds, W.K. Choi, M.J. Rose, P.G. LeComber, A.J. Snell and A.E. Owen, J. Non-Cryst. Sol., 77/78 1373 (1985)

2. M.J. Rose, J. Hajto, P.G. LeComber, S.M. Gage, W.K. Choi, A.J. Snell, and A.E. Owen, J. Non-Cryst. Sol., 115 168 (1989)

3. A.F. Murray et al., Int'l Symp. Circuits and Systems, IEEE Press. 1210-1212 (1989)

MATERIALS RESEARCH SOCIETY SYMPOSIUM PROCEEDINGS VOLUME 192

Amorphous Silicon Technology - 1990

Symposium held April 17-20, 1990, San Francisco, California, U.S.A.

EDITORS:

P. C. Taylor
University of Utah, Salt Lake City, Utah, U.S.A.

M. J. Thompson
Xerox PARC, Palo Alto, California, U.S.A.

P. G. LeComber
University of Dundee, Dundee, United Kingdom

Y. Hamakawa
Osaka University, Osaka, Japan

Arun Madan
SERI, Golden, Colorado, U.S.A.

MATERIALS RESEARCH SOCIETY
Pittsburgh, Pennsylvania

OBSERVATION OF QUANTISED BALLISTIC TRANSPORT IN AMORPHOUS SILICON MEMORY STRUCTURES

J. HAJTO [*], M.J. ROSE [†], P.G. LECOMBER [†], A.E. OWEN [*], and A.J. SNELL [*]

* Department of Electrical Engineering, University of Edinburgh, EH9 3JL, Scotland
† Department of Applied Physics and Electronic & Manufacturing Engineering, University of Dundee, DD1 4HN, Scotland

ABSTRACT

We present experimental results showing that the ON state of amorphous silicon memory structures exhibits ballistic electron transport associated with a quantised resistance, $h/2ie^2$, where i is the number of occupied one dimensional conducting channels (sub-bands) and the spin degeneracy is two (in the case when no magnetic field is applied). Conduction in the memory ON state is restricted to a narrow conducting channel through which the electrons can travel ballistically i.e. no collisions occur. As the applied voltage is increased, the width of the conducting channel is broadened. This results in additional conducting channels (sub-bands) passing through the Fermi energy and consequently the resistance drops by quantised values. In the presence of a magnetic field additional steps occur corresponding to the split levels at values of $h/2(i+½)e^2$. A particular feature of this quantised resistance is that the effect can be observed at relatively high temperatures (from 4.2 K up to ~190 K).

INTRODUCTION

We have previously shown[1-3] that amorphous silicon metal-p^+-n-i-metal and metal-p^+-metal junctions exhibit non-volatile, polarity dependent digital and analogue memory switching phenomena after initial conditioning by means of a moderately high applied potential ("forming"). An essential feature of the forming process is the creation of a filamentary region of highly conductive material.

Recent studies[4-6] have also shown that the resistance of a short narrow channel in which one-dimensional conduction occurs should have a quantised value. This behaviour is associated with ballistic electron transport, where electrons have an elastic mean free path much greater than the channel length. The aim of the present work is to show that amorphous silicon memory structures exhibit quantised resistance, indicative of ballistic transport of electrons in a one-dimensional conduction channel.

EXPERIMENTAL

The samples used for this work were amorphous silicon Cr-p^+-V sandwich structures. The p^+ amorphous silicon layers were prepared by r.f. glow discharge decomposition of SiH_4 containing 10^4 vppm of B_2H_6. Films of 1000 A thickness were deposited on Corning 7059 glass substrates with previously patterned chromium bottom contacts. The p^+ amorphous silicon was then patterned and an insulating layer was used to define an active device area of 10^{-6} cm^2. The metal used for the top contact was vanadium. The details of the subsequent memory operation are described in Ref 2. The devices exhibit fast analogue switching at room temperature i.e. they have a continuum

of stable states (between $R_{ON} = 10^3\ \Omega$ and $R_{OFF} = 10^6\ \Omega$) which are non-volatile and fully programmable by single 10 nsec voltage pulses. In the present work we have studied the low temperature conductivity behaviour of a range of analogue memory states.

RESULTS

Typical current-voltage characteristics of a formed memory ON state are shown in Fig.1. In the voltage region from 0 to 0.36 V, the current around zero bias is of the order of $\sim 10^{-9}$ A but increases to $\sim 10^{-6}$ A at voltages approaching 0.36 V i.e. a strong non-linear behaviour is found. The observed large increase in the resistance around zero bias (see Fig.2.) is an consistent with tunnelling conduction between metallic particles embedded in an insulating matrix[7].

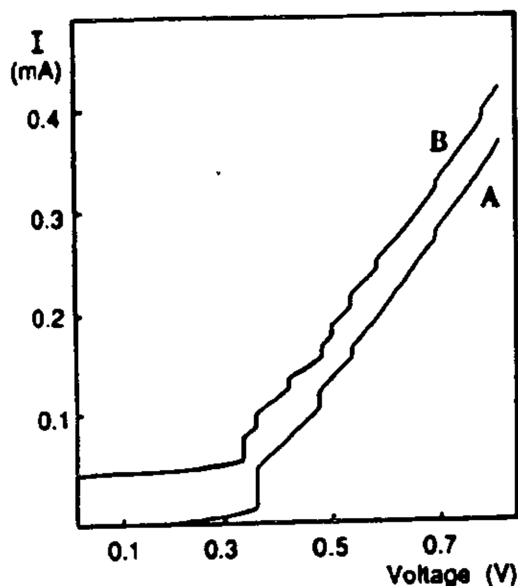

FIG. 1. I-V curves at 4.2K with (B) and without (A) magnetic field (Curve B is displaced vertically for clarity.)

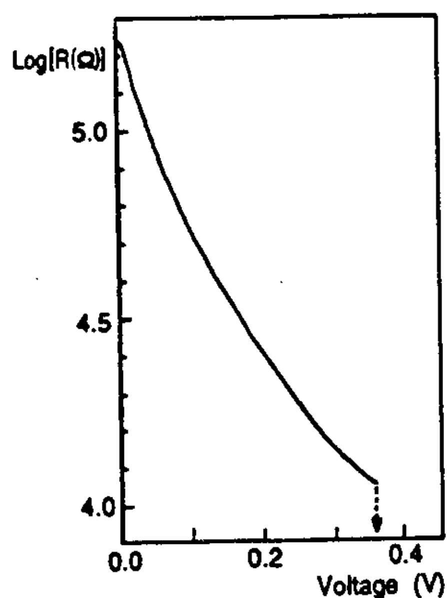

FIG. 2. R-V curve at 4.2K below the critical voltage V_{cr}

At 0.36 V, a current jump occurs and the resistance of the sample is lowered to the order of a few kΩ. After the first current jump at 0.36 V, further current steps can be observed at 0.47, 0.53 and 0.70 V (curve A in Fig.1.). At 0.36 V (henceforth called the critical voltage V_{cr}) there is a dramatic change in the behaviour of the sample. At voltages lower than V_{cr}, no discontinuities are observed but at voltages higher than V_{cr}, the resistance is lowered and the current increases in discrete steps. The current-voltage characteristics are symmetrical i.e. the same behaviour is observed for the opposite polarity. Curve B in Fig.1. depicts the current-voltage characteristics of the same sample under the influence of a 0.2 T magnetic field. The curve has been displaced by 50 μA in the current scale for clarity. The direction of the magnetic field is 30° with respect to the conducting channel (i.e. the filament). Additional steps can be observed at 0.34, 0.42, 0.5 0.59 and 0.79 V together with the steps observed in the zero magnetic field

case (curve A). The effect of the magnetic field is reversible, i.e. if the magnetic field is removed the current-voltage characteristics revert to the zero magnetic field case. A number of I-V characteristics have been obtained in which sharp and well defined steps can be observed at 4.2 K. The critical voltage V_{cr} at which the first current jump is observed and the magnitude of the first current jump are dependent on the resistance of the memory ON state investigated. Fig.3. shows the effect of increased memory ON state resistance on the observed current steps. The curves have been displaced by 100μA on the current scale for clarity. The critical voltage and the magnitude of the first current jump increase with increasing resistance (i.e. $R_C > R_B > R_A$), but after the first jump the characteristics are rather similar suggesting a similar conduction mechanism at higher voltages. The first current jump would appear to be associated with the formation of a highly conducting path within the structure whose characteristics are independent of the low bias behaviour (i.e. the different memory states).

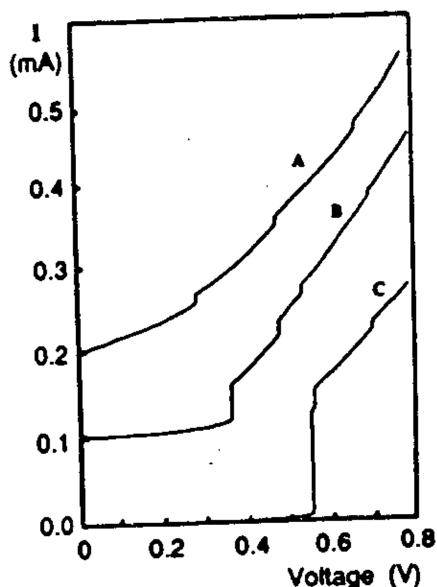

FIG. 3. I-V curves of different memory ON states at 4.2K. $R_A < R_B < R_C$ (Curves displaced vertically for clarity)

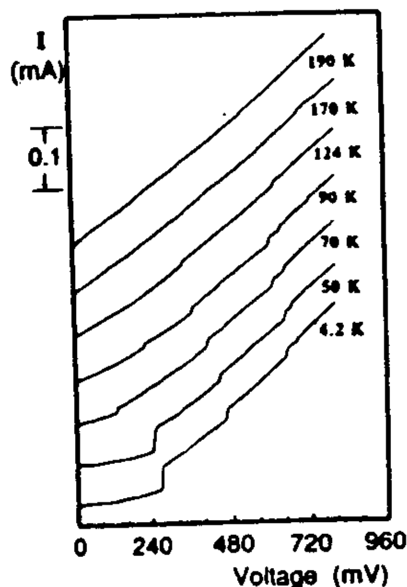

FIG. 4. I-V curves as a function of temperature

Fig.4. shows the effect of temperature on the I-V curves. The curves have been shifted along the current axis for clarity, with 100 μA magnitude indicated. The current steps decrease gradually in size with increasing temperature and the effect is no longer observable at ~190 K. Fig.5. shows the resistance of a memory state (corresponding to curve A in Fig.1.) as a function of applied voltage. The first large step (at 0.36 V) is associated with the formation of a narrow, highly conducting channel which significantly lowers the resistance of the sample. With further increase in the applied voltage, the resistance is lowered in steps, corresponding to quantised resistance values $R=h/2ie^2$ where i is an integer. In the voltage range from 0.36 to 0.8 V, there are four steps (corresponding to the observed current rises in curve A, Fig.1.) with i being 2, 3, 4 and 5. Higher voltages have not been applied to the sample because this could change the resistance of the particular memory state. If a magnetic field is now applied to the sample, further quantisation of resistance is observed at values $R=h/2(i+½)e^2$. This is

illustrated in Fig.6 (the data correspond to curve B in Fig.1.). It can be seen that extra steps in the resistance occur at i = 2.5, 3.5, 4.5 and 5.5.

DISCUSSION

The experimental data show that we have observed quantised resistance in the ON state of amorphous silicon Cr-p^+-V structures. A possible mechanism which might explain this behaviour is outlined below. The current-voltage characteristics (see Fig.1 and 2) suggest that the filament has a relatively large resistance around zero bias i.e. a barrier for the electron flow exists. The current-voltage characteristics from 0 to 0.36 V show a continuous, but strongly non-linear behaviour due to the creation of free carriers by the high electric field across the small tunnelling distance.

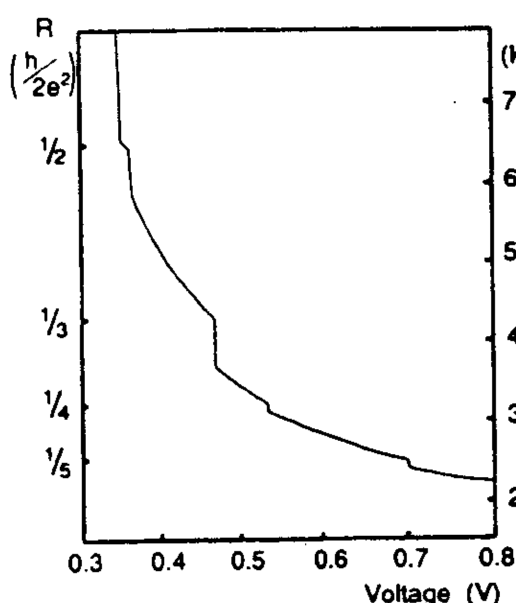

FIG. 5. Resistance versus voltage at 4.2K with no magnetic field

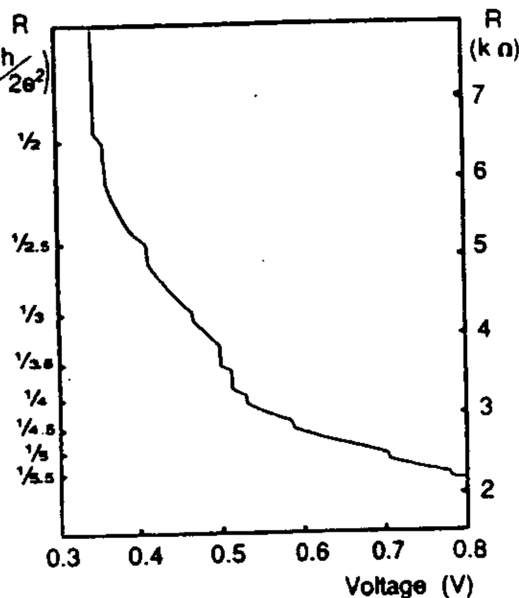

FIG. 6. Resistance versus voltage with a 0.2 T magnetic field

At the critical voltage V_{cr} the tunnelling barrier "breaks down" and much larger current flow can be observed. The barrier breakdown within the filament occurs locally i.e. over a very small area. So the first jump at V_{cr} corresponds to the formation of a narrow conductive channel where the electrons "punch" through. Because of the short length of the conductive channel and the high field present, scattering phenomena are negligible. The large electron reservoir in the metal ($\sim 10^{22}\,cm^{-3}$) should provide an adequate supply of electrons through the channel. The amorphous silicon memory device operates in the following way. As the voltage reaches the critical level V_{cr}, the one-dimensional conducting channel is established. A further increase in voltage in this regime results in an increase in the width of the conducting channel. The effect can be explained by assuming that the filament edge has a curved shape i.e. the tunnelling barrier will "break down" at larger areas under the influence of higher voltages. The larger voltage applied will produce the same critical electric field at larger distances between the filament and the metal electrode, therefore the area of the one-dimensional

channel increases. The criteria for ballistic conductivity is that the electron mean free path should be much longer than the one-dimensional channel length (L_x). The electrons are confined by the applied potential in the conducting channel. Its cross section is approximated by a rectangle (in a manner analagous to the "electron in a box" problem), whose dimensions L_y and L_z are comparable to an electron wavelength. The energy of electrons E in the lowest quantum level of the one-dimensional channel are given by

$$E = \frac{\hbar^2}{2m^*}k^2 + \frac{\hbar^2}{2m^*}\left[\left(\frac{\pi}{L_y}\right)^2 + \left(\frac{\pi}{L_z}\right)^2\right] \qquad (1)$$

The first term in (1) describes the kinetic energy of a ballistic electron in motion along the channel. The second term represents the quantum energy level which is uniquely determined by the dimensions L_y and L_z. It is important to emphasize that the electron can accelerate freely along the channel, due to the collision free nature of the motion i.e. its momentum can increase continuously as the applied voltage increases. On the other hand the electron momentum is quantised in the direction across the channel (defined by L_y and L_z). Therefore as the voltage increases, two opposite effects can be observed; one is characterised by the increase of the electron kinetic energy along the channel and the other is associated with the increase of the cross section of the conducting channel (i.e. with increase of L_y and L_z). According to (1) this latter effect will decrease the quantised energy levels until the nearest higher energy level (nearest sub-band) becomes lower in energy than the Fermi level and will be occupied by the "more energetic" electrons. Consequently a new sub-band is created at higher voltage (i.e. at larger values of L_y and L_z) which in turn will lower the resistance in a quantised manner. This physical scenario was first suggested by Sharvin [8] as a possible method for studying Fermi surfaces of metals. According to the theoretical predictions [6,9], the resistance a of one-dimensional channel (in which the electrons punch through ballistically) should have a quantised value which can be given by:

$$R_x = h/g_s e^2 = h/2e^2 \qquad (2)$$

where R_x is the sub-band resistance and g_s is the spin degeneracy ($g_s = 2$) in the non-magnetic field case. However, the value of $R_x = h/2e^2$ applies only to one sub-band. If a new sub-band is created at higher voltage (i.e. by changing the cross section of the channel), the total resistance becomes $h/(2ie^2)$ (i=integer defining the number of sub-bands) in the same manner as in the case of parallel resistors. This is possible because there is no scattering in the conducting sub-bands i.e. they do not interact with each other. Consequently the resistance drops in a quantised manner with i=2, 3, 4 and 5 (as seen in Fig.5.). When a magnetic field is applied additional steps occur. This is due to the Zeeman splitting of electron energy levels i.e. lifting the spin degeneracy. Each sub-band splits into two and therefore extra steps can be observed at $R=h/2(i+½)e^2$ resistance levels as seen in Fig.6. The plateaux of the individual quantum steps are not flat but they have a slope i.e. the resistance decreases at higher voltages between the individual plateaux. This is possibly due to the increase in mobility indicating that some scattering effects are present in the channel.

The most important feature of the observed ballistic behaviour is that it can be observed up to ~190 K i.e. much higher temperatures than previously observed. We suggest that this might be due to the very small size of the ballistic channel. The temperature dependence (see Fig.4.) suggests an energy separation of kT ~ ΔE

$\sim 1.6 \times 10^{-2}$ eV. This is the temperature where the differences between the quantised electron levels are smeared out. This indicates ~ 40 Å change in L_y and L_z dimensions (as follows from (1)) between the subsequent steps which correspond to the energy separation of the observed quantum steps. Finally we emphasize that the effect has been observed in what is initially a metal-amorphous semiconductor structure. The "classical mobility" of the amorphous silicon is many orders of magnitude lower than is expected for ballistic behaviour. It is not known with any certainty what effect the forming process has on the structure of the conducting channel but the observed behaviour suggests the importance of the dimension of the conduction channel rather than other material parameters. The significance of using amorphous silicon sandwich structures lies in the forming process i.e. the process which allows the fabrication of such small structures.

REFERENCES

1. A.E. Owen, P.G. LeComber, G Sarrabayuse and W.E. Spear, IEE Proc. I. Solid State & Electron Devices, 129 Pt.1 (1982) 51

2. M.J. Rose, J. Hajto, P.G. LeComber, S.M. Gage, W.K. Choi, A.J. Snell and A.E. Owen, Journal of Non-Crystalline Solids 115 (1989) 168

3. S.M. Gage, J. Hajto, S. Reynolds, W.K. Choi, M.J. Rose, P.G. LeComber, A.J. Snell and A.E. Owen, Journal of Non-Crystalline Solids, 115 (1989) 171

4. R. Landauer, 1985, Localisation Interactions and Transport Phenomena, Ed. by B. Kramer, G. Bergmann and Y. Bruyserade (Heidelberg: Springer) p.38

5. B.J. van Wees, H. van Houten, C.W.J. Beenakker, J.G. Williamson, L.P. Kouwenhoven, D. van der Marel and C.T. Foxon, Physical Review Letters, Vol. 60, No 9, (1988) 848

6. D.A. Wharam, M. Pepper, H. Ahmed, J.E.F. Frost, D.G. Hasko, D.C. Peacock, D.A. Ritchie and G.A.C. Jones, J.Phys. C: Solid State Physics 21 (1988) L887

7 I. Giaver and H.R. Zeller, Physical Review Letters, Vol 20 (1968) 1504

8. Y.V. Sharvin, JETP Letters 1 (1965) 152

9. Y. Imry, 1986 Directions in Condensed Matter Physics, ed. by G. Grinstein and G. Mazenko (Singapore: World Scientific) p. 101

PHILOSOPHICAL MAGAZINE B, 1991, VOL. 63, NO. 1, 349–369

Analogue memory and ballistic electron effects in metal–amorphous silicon structures

By J. HAJTO, A. E. OWEN and A. J. SNELL

Department of Electrical Engineering, University of Edinburgh, Edinburgh EH9 3JL, Scotland

and P. G. LE COMBER and M. J. ROSE

Department of Applied Physics and Electronic and Manufacturing Engineering, University of Dundee, Dundee, DD1 4HN, Scotland

[*Received 11 June 1990 and accepted 15 June 1990*]

ABSTRACT

We present experimental results showing that p^+ amorphous silicon memory structures exhibit polarity-dependent analogue memory switching. The effect is non-volatile and we propose that it is associated with changes in a tunnelling barrier within the structure. It is also observed that conduction in the memory ON state is restricted to a narrow conducting channel through which the electrons can, under certain conditions, travel ballistically. As a consequence, quantized resistance levels associated with ballistic electron transport are observed under certain circumstances. In the presence of a magnetic field, additional steps in the quantized resistance levels occur. A particular feature of this quantized resistance is that the effect can be observed at relatively high temperatures (up to about 190 K).

§ 1. INTRODUCTION

Results on metal–p^+–n–i–metal amorphous silicon devices have provided experimental evidence that such structures exhibit extremely fast non-volatile polarity-dependent digital memory switching phenomena (Le Comber *et al.* 1985) after initial conditioning by means of a moderately high applied potential ('forming'). The most important result to emerge on formed devices is that in the ON state the currrent is carried by a highly conducting filament which is less than 1 μm in diameter. Filamentation has been demonstrated by experiments on the ON state resistance as a function of area (R_{ON} is independent of area), by thermal imaging techniques with liquid crystals and by direct observation with a scanning electron microscope combined with microanalysis. The latter indicated that the formation of the current filament may be associated with diffusion of the top metal contact into the amorphous silicon resulting in a region of intermingled metal and silicon. More recent experimental results (Rose *et al.* 1989) have demonstrated a new metal–p^+–metal amorphous silicon device which, rather than exhibiting a two-state digital operation, has a continuum of stable states which are non-volatile and fully programmable by single 10 ns voltage pulses. It has also been suggested that the new analogue memory devices can be used as non-volatile and reprogrammable memory elements in analogue neural networks (Hajto, Rose, Snell, Le Comber and Owen 1990).

In this paper we present a summary of the new results obtained on non-volatile analogue switching effects in amorphous silicon metal–p^+–metal devices and discuss the possible physical mechanisms responsible for the phenomena.

0141-8637/91 $3.00 © 1991 Taylor & Francis Ltd.

§2. Experimental

The samples used for this work were amorphous silicon Cr–p^+–V thin-film structures. The p^+ layer was prepared by r.f. glow-discharge decomposition of SiH_4 containing 10^4 vol. p.p.m. of B_2H_6. Films of 1000 Å thickness were deposited on Corning glass substrates previously patterned with chromium bottom contacts. The p^+ amorphous silicon was then patterned and an insulating layer was used to define an active device area of 10^{-6} cm^2. The metal used for the top contact was normally vanadium. However, a number of different metals were also used and their influence on the memory operation will also be described.

In accordance with our previous results (Le Comber *et al.* 1985), memory devices prepared in this way require an initial forming process. This means that the resistance of the as-deposited (unformed) device has to be lowered from $R \approx 10^9\,\Omega$ to $R \approx 10^3$–$10^4\,\Omega$ (i.e. the typical value of an ON state). The forming can be achieved by biasing the sample with a single voltage pulse (duration 300 ns; magnitude about 12 V) with positive polarity applied to the top vanadium contact.

The formed samples were mounted in a 24-pin chip carrier and wire bonded. The carrier was then inserted into a standard socket in an Oxford Instruments cryostat in order to investigate the low-temperature characteristics. The current–voltage characteristics were measured using an HP 4145B semiconductor parameter analyser.

§3. Results

The metal–p^+–metal memory structures exhibit a forming step which is different from the previously investigated metal–p^+–n–i–metal structures (Le Comber *et al.* 1985). The differences are demonstrated in figs. 1 and 2. In the case of metal–p^+–n–i–metal structures, the resistance suddenly drops from about $10^{10}\,\Omega$ (virgin state) to about $10^3\,\Omega$, after the critical voltage (forming voltage V_F) has been applied. No change in the virgin resistance occurs when the sample is biased with voltages less than V_F. This type of forming is termed *hard forming*. In contrast with this, the resistance of the unformed metal–p^+–metal structures can be lowered gradually by applying voltage levels with progressively increasing magnitudes. In this case no sudden change in the current or voltage signal can be detected when the sample is biased with a voltage pulse, as seen in fig. 2. This process is called *soft forming*. Figure 3 shows the device resistance as a function of the soft-forming voltage (pulse duration, 300 ns). On reaching a critical voltage (about 14 V in fig. 3) the device resistance suddenly drops from about 10^6 to about 10^4–$10^3\,\Omega$. This is the memory ON state of the device. Once the memory device had reached its first (non-volatile) ON state all subsequent switching operations were performed with 10–100 ns pulses 1–5 V in magnitude.

An example of the analogue switching effect is shown in fig. 4, where the sample resistance is plotted as a function of applied alternating WRITE and ERASE pulses (100 ns pulse duration each). It is important to emphasize the polarity dependence of the analogue memory behaviour. In the case of the WRITE pulses, positive polarity is applied to the chromium (bottom contact) while ERASE pulses have opposite polarity. The sample was first switched to an ON state ($R_{ON} = 2 \times 10^3\,\Omega$) and then a series of alternating WRITE and ERASE pulses were applied. The WRITE pulses were kept at a constant magnitude of 3·4 V but the ERASE pulses were incremented by 0·05 V steps from 1·2 to 3·4 V after each WRITE pulse. It can be seen from fig. 4 that the sample resistance changes in an analogue manner as the magnitude of the ERASE pulse increases, that is the difference between R_{ON} and R_{OFF} is a function of the magnitude of the ERASE pulses. A voltage range ΔV(ERASE) of 1·6 V resulted in a change in

Fig. 1

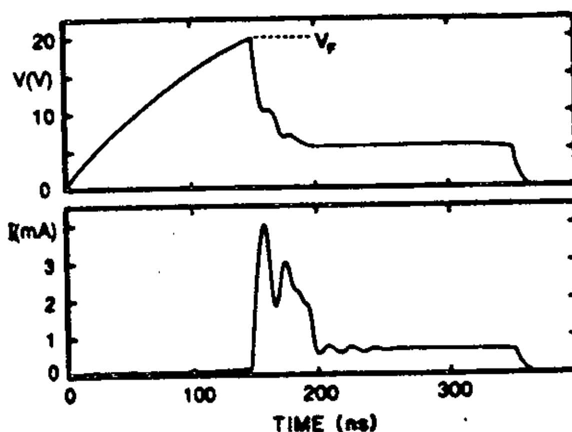

Waveforms of a single forming pulse applied to an amorphous silicon Cr–p$^+$–n–i–Al structure showing 'hard forming'. V and I represent the voltage across the device and the corresponding device current respectively.

Fig. 2

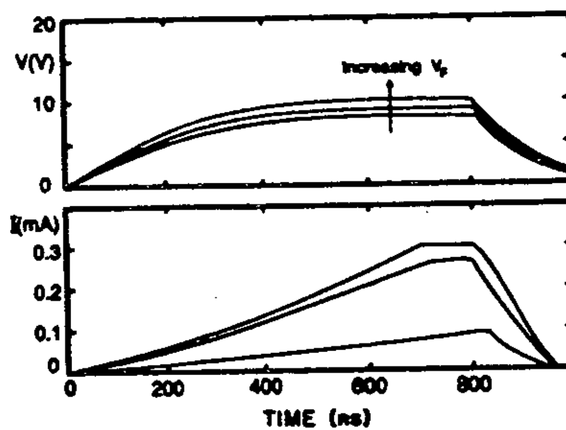

Waveforms of single pulses of increasing magnitude applied to an amorphous silicon Cr–p$^+$–V structure showing 'soft forming'. V and I represent the voltage across the device and the corresponding device current respectively.

Fig. 3

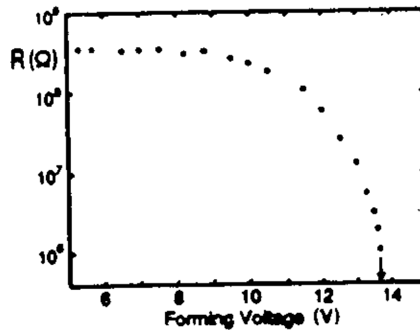

Resistance of an amorphous silicon Cr–p$^+$–V memory structure as a function of forming voltage.

Fig. 4

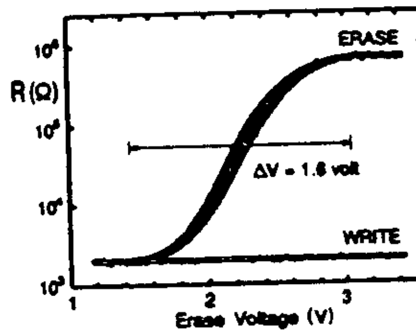

Memory resistance as a function of ERASE voltage in a Cr–p$^+$–V structure.

resistance from $R \approx 2 \times 10^3\,\Omega$ to $R \approx 6 \times 10^5\,\Omega$. The shaded area in fig. 4 indicates the reproducibility of the analogue memory switching by showing the scattering in the resistance during repeated experiments (data from 100 cycles are included). Figure 5 shows another case where the ERASE pulses were maintained at a constant value of $V = 3{\cdot}4$ V but the WRITE pulses were incremented from 1·2 V to 3·4 V in 0·05 V steps. The value of the OFF state resistance remained constant at about $6 \times 10^5\,\Omega$ (i.e. it changed back to this constant level from every ON state) whilst the ON state resistance decreased through a continuum of intermediate states over a similar ΔV to the ERASE operation. The shaded area in fig. 5 again represents the reproducibility of the analogue switching for 100 complete cycles. It is emphasized that the device will switch between any two resistance states within the range from about 1 kΩ to 1 MΩ by selecting the correct polarity and the magnitude of the WRITE and ERASE pulses. For all devices with a vandium top contact, the values of ΔV range from 1·5 to 2·0 V for both the WRITE and the ERASE operations.

We have repeated the above experiments on metal–p$^+$–metal devices with chromium as top metal and observed similar polarity-dependent changes in the memory state resistance. However, in the WRITE and ERASE experiments, intermediate states were found to exist only over a narrow ΔV of about 0·2 V as shown in fig. 6. Therefore these devices are considered as 'digital' devices. It is important to

Fig. 5

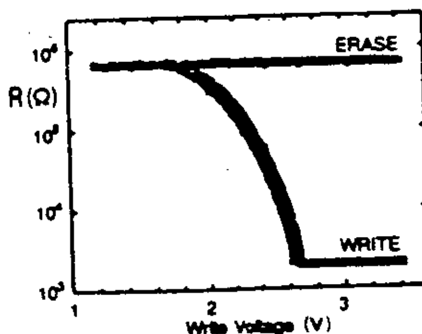

Memory resistance as a function of WRITE voltage in a Cr–p$^+$–V structure.

Fig. 6

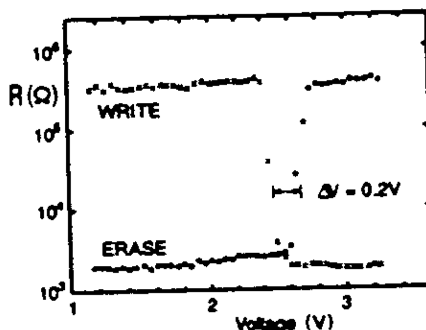

Memory resistance as a function of WRITE and ERASE voltages in a Cr–p$^+$–Cr structure.

emphasize that both the analogue (seen in figs. 4 and 5) and the 'digital' (seen in fig. 6) memory switching effects are non-volatile. Devices set to ON or OFF states have been monitored over 2 years without any significant change in their resistance. Also, operation at temperatures up to 160°C shows little change in the threshold voltages or in the device stability. However, it is also found that devices with certain top metal contacts such as molybdenum and palladium show a volatile memory switching effect. This is illustrated in fig. 7 where the signal through the device is continuously monitored at a low voltage level (at 0·5 V) that is below the voltage level of the programming pulses. The current decays rapidly after the end of the programming pulse, that is the memory state is volatile. The role of the top metal contact has been investigated by fabricating devices with a range of different top metals but with otherwise identical physical parameters (i.e. about 1000 Å thickness of the p$^+$ layer, and a chromium bottom electrode). Using the analogue switching voltage window ΔV as a guide, it is found that its value is significantly dependent on the top metallization contact. This is illustrated in the table. It can also be seen that the definition of 'analogue' ($\Delta V \geq 1\,V$) or 'digital' (0·5 V or less) memory switching is somewhat arbitrary, because there is no sharp boundary between the two types of operation, and they are almost certainly associated with the same underlying physical phenomena. However, in the cases of molybdenum and palladium top contacts, a new type of volatile

Fig. 7

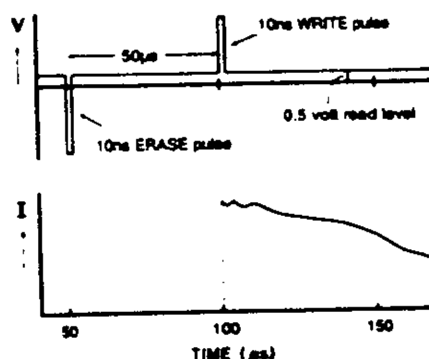

Volatile memory effect in a Cr–p^+–Mo structure.

Effect of top metallization on the switching behaviour.

Metal	ΔV (V)	Switching characteristics
Ag	>0·1	Digital, non-volatile
Al	>0·1	Digital, non-volatile
Cr	0·2	Digital, non-volatile
Mn	≈0·5	Digital, non-volatile
Fe	≈0·5	Digital, non-volatile
Ti	—	Unstable switching
Au	—	No switching
Cu	—	No switching
W	≈1·0	Analogue, non-volatile
V	1·8	Analogue, non-volatile
Ni	2·0	Analogue, non-volatile
Co	2·0	Analogue, non-volatile
Mo	2·0	Analogue, volatile
Pd	2·0	Analogue, volatile

switching effect is observed and in the cases of titanium, gold and copper no reproducible switching effects can be observed. These results suggest that the top metal contact plays a crucial role in determining the type of memory switching phenomena observed in these devices. In this paper we shall concentrate on the p^+ memory devices with vanadium top contact because these show typical non-volatile analogue memory switching.

The current–voltage characteristics of analogue memory resistance states have been systematically investigated at both room temperature and lower temperatures and the following results obtained. It is found that all the room-temperature current–voltage characteristics show a 'linear-plus-power-law' behaviour in the various analogue memory resistance states (seen in fig. 8). The I–V curves can be described by a simple nonlinear relationship

$$I = C_1 V + C_2 V^n, \qquad (1)$$

Fig. 8

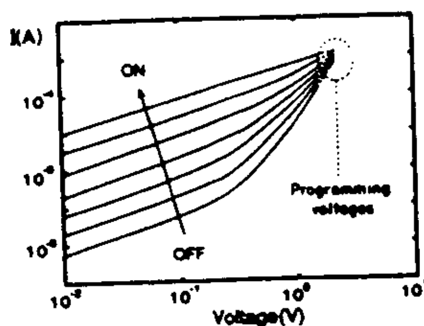

Current–voltage characteristics of analogue memory states plotted on a log–log scale. The characteristics are symmetric about the origin.

where C_1 and C_2 are constants and the exponent n increases with increasing low-bias (linear region) resistance according to the relationship $n = A + B \log R$. The observed power-law behaviour could indicate the possibility of space-charge-limited conduction at higher biases, although investigation of the thickness dependence has shown this to be unlikely. In accordance with the pulsed analogue memory switching results, a continuous transition of states can be found between the low-bias ON (about $10^3\,\Omega$) and OFF (about $10^6\,\Omega$) states. The terms ON and OFF seem to be somewhat arbitrary therefore, and are only used in this paper for practical reasons. If the curves in fig. 8 are extrapolated above 1 V, they meet in the region of about 3–4 V, that is at typical programming levels (see figs. 4 and 5). It is also found that the exponent n does not depend on the thickness or the active device diameter but it is primarily determined by the low-bias (linear region) resistance of the analogue memory state. This indicates that the nature of the electrical conduction is quite similar in all memory states. However, repeatedly switching the device into the same resistance state need not always result in an identical value of the exponent. This appears to indicate that the 'same' resistance state can be achieved through different conduction paths within the same device. This is in accordance with the suggestion that the conduction path (filament) might have a structure similar to that of granular metals embedded in an insulating matrix and this structure may provide a variety of conduction paths (Giaver and Zeller 1968).

It is possible to extend the range of the I–V characteristics (up to the critical field where switching occurs) using very short single voltage pulses of varying polarities and pulse heights. Figure 9 shows the room-temperature 'pulsed' current–voltage characteristics of the analogue Cr–p^+–V memory device. These characteristics are obtained using 400 ns pulses of progressively increasing magnitude and of both polarities. The 400 ns pulse length is long enough to observe a plateau in the pulse signal, that is RC effects are avoided. Positive polarity refers to (positive) voltages applied to the chromium bottom contact. Starting from a $9{\cdot}5 \times 10^5\,\Omega$ OFF state (measured at 0·5 V (fig. 9 (a))), the onset of the strong nonlinear rise in the current occurs at about + 1·1 V. Figure 9 (a) is reproducible (i.e. it can be repeated many times without a change in the device resistance) up to a voltage level of about + 1·7 V. Further increase in the voltage height will result in a permanent decrease in the device resistance and consequently a change in fig. 9 (a). The decrease in resistance is determined by the magnitude of the maximum voltage applied.

Fig. 9

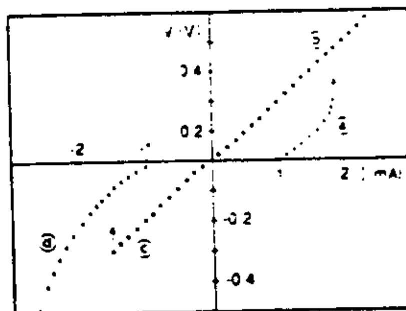

'Pulsed' current–voltage characteristics of a Cr–p⁺–V analogue structure.

Figure 9(*b*) represents a memory ON state ($R = 5{\cdot}6 \times 10^3\ \Omega$ at 0·5 V) of the device and is reproducible up to a voltage level of about 5 V if positive polarity is applied. Further increase in voltage might destroy the device. However, if a negative voltage is applied to the same ON state (fig. 9(*c*), an ERASE process is observed at voltage levels of magnitude greater than about 1·7 V. On the other hand, if an OFF state ($R = 9 \times 10^5\ \Omega$) is negatively biased fig. 9(*d*), no change in the OFF state resistance can be observed up to a voltage of about −5 V. The apparent polarity dependence suggests that the analogue memory switching is not determined simply by the magnitude of the applied power or energy. This is further supported by the comparison of individual switching transients with opposite polarity. Figure 10(*a*) shows the waveform of a single WRITE pulse from OFF ($R = 2 \times 10^5\ \Omega$) to ON ($R = 3{\cdot}8 \times 10^3\ \Omega$) and of an ERASE pulse from OFF ($R = 2 \times 10^5\ \Omega$) to a slightly higher OFF state ($R = 2{\cdot}4 \times 10^5\ \Omega$). In the second case a large change in the memory state resistance does not occur although similar voltage and current levels are measured. The calculated total charge (flowing through the sample) is also rather similar: $Q_W = 8{\cdot}5 \times 10^{-11}$ C for the WRITE and $Q_E = 7{\cdot}2 \times 10^{-11}$ C for the ERASE pulse. The rather high level of 'ringing' oscillations on these transients was caused by poorly matched cable impedances.

These measurements suggest that the memory state resistance is determined by a combination of applied voltage level and the appropriate polarity. On the other hand, the memory resistance not being determined uniquely by the applied power or energy suggests that the memory switching does not depend significantly on the internal temperature of the device. Figure 11 (*a*) shows a switching transient of an ERASE pulse at 300 K where the device resistance is changed from $R_{ON} = 3 \times 10^3\ \Omega$ to $R_{OFF} = 6 \times 10^5\ \Omega$. Figure 11(*b*) shows a similar ERASE transient at much lower temperature (4·2 K) where the device resistance has also changed from $R_{ON} = 3 \times 10^3\ \Omega$ to $R_{OFF} = 6 \times 10^5\ \Omega$. It can be seen that, despite the large temperature difference (more than two orders of magnitude), the current level and the threshold voltage (for achieving the same ERASE process as at room temperature) increase by a factor of less than two. It should also be emphasized that the device continues to operate even at liquid-helium temperature. The analogue switching effect is still observed at 4·2 K without large changes in either the threshold voltage or the current level. This suggests that the electrical conduction and the memory phenomena are possibly connected to a temperature-independent physical process which we propose may be associated with tunnelling.

Fig. 10

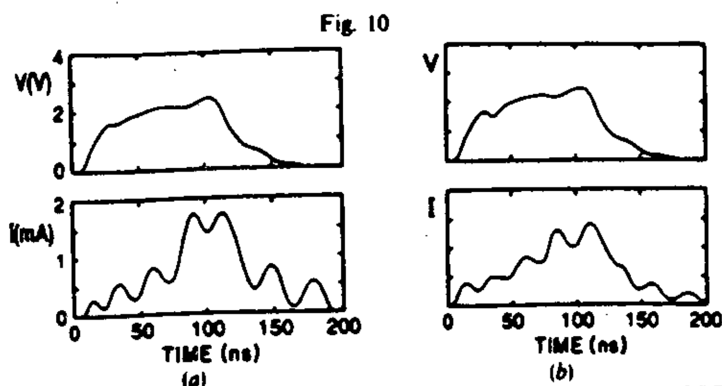

Waveforms of single-pulse memory switching: (*a*) OFF→ON transient; (*b*) OFF→OFF transient.

Fig. 11

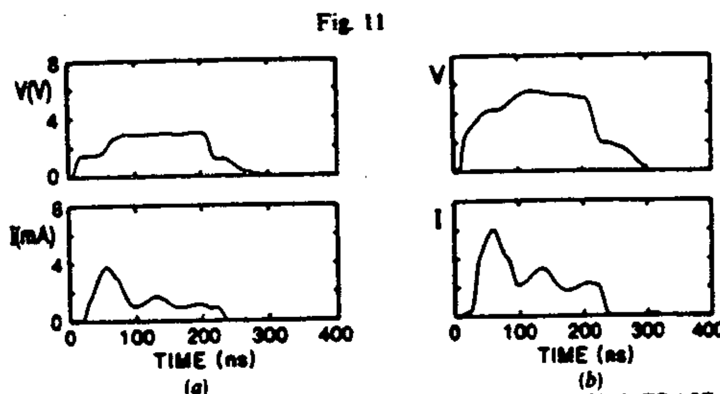

Waveforms of single pulse memory switching: (*a*) ERASE transient at 300 K; (*b*) ERASE transient at 4·2 K.

The above suggestion is supported by recent results obtained during investigation of the low-temperature conductivity of the analogue memory states (Hajto *et al.* 1990). Typical current–voltage characteristics of a formed memory ON state at 4·2 K are shown in fig. 12. In the voltage region from 0 to 0·36 V, the current around zero bias is of the order of 10^{-9} A but increases to about 10^{-6} A at voltages approaching 0·36 V, that is a strong nonlinear behaviour is found. It is important to emphasize that the room-temperature current–voltage characteristics of the memory ON state are linear. The observed large increase in the resistance around zero bias (fig. 13) is consistent with tunnelling conduction between metallic particles embedded in an insulating matrix (Giaver and Zeller 1968). Further experimental evidence for the tunnelling conduction comes from the temperature dependence of the device current. Figure 14 shows the current at a fixed voltage (0·2 V) plotted against T^2. The linear plot indicates a T^2 dependence of the current at a constant V which is in accordance with tunnelling conduction.

At 0·36 V, a current jump occurs and the resistance of the sample is lowered to the order of a few kilohms. After the first current jump at 0·36 V, further current steps can be observed at 0·47, 0·53 and 0·70 V (fig. 12(*a*)). At 0·36 V (henceforth called the critical voltage V_{cr}) there is a dramatic change in the behaviour of the sample. At voltages lower than V_{cr}, no discontinuities are observed but, at voltages higher than V_{cr}, the resistance

Fig. 12

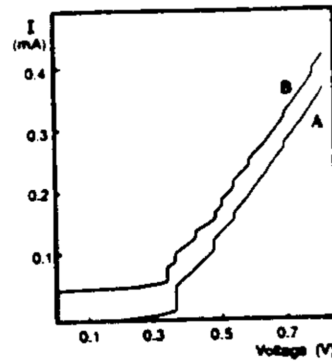

Current-voltage characteristics at 4·2 K (B) with and (A) without magnetic field. (B) is displaced vertically for clarity.

Fig. 13

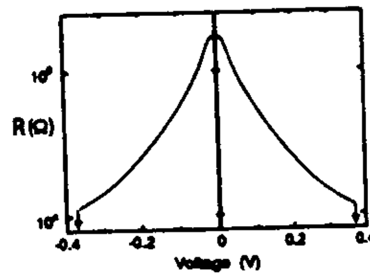

Resistance as a function of applied bias at 4·2 K.

Fig. 14

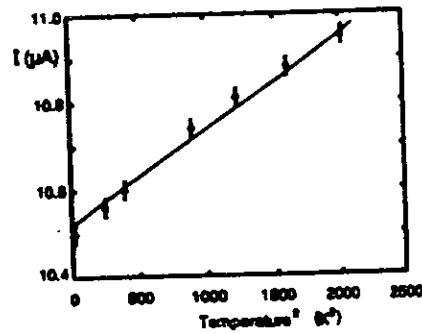

Current (at fixed voltage of 0·2 V) as a function of T^2.

is lowered and the current increases in discrete steps. The current-voltage characteristics are symmetrical, that is the same behaviour is observed for the opposite polarity. Figure 12(B) depicts the current–voltage characteristics of the same sample under the influence of a 0·2 T magnetic field. The curve has been displaced by 50 μA in the current scale for clarity. The direction of the magnetic field is 30° with respect to the conducting channel (i.e. the filament). Additional steps can be observed at 0·34, 0·42, 0·5, 0·59 and 0·79 V together with the steps observed in the zero magnetic field case (fig. 12(B)). The effect of the magnetic field is reversible, that is, if the magnetic field is removed, the current–voltage characeristics revert to the zero-magnetic-field case. A number of $I-V$ more characteristics have been obtained in which sharp and well defined steps can be observed at 4·2 K.

The critical voltage V_{cr} at which the first current jump is observed and the magnitude of the first current jump are dependent on the resistance of the memory ON state investigated. Figure 15 shows the effect of changing the memory ON state resistance on the observed current steps. The curves have been displaced by 100 μA on the current scale for clarity. The critical voltage and the magnitude of the first current jump increase with increasing resistance (i.e. $R_c > R_b > R_a$), but after the first jump the characteristics are rather similar, suggesting a similar conduction mechanism at higher voltages. The first current jump appears to be associated with the formation of a highly conducting path within the structure whose characteristics are independent of the low-bias behaviour (i.e. the different memory states). On the other hand, the position of the current steps is dependent on the direction of the voltage sweep, that is some hysteresis is observed as illustrated in fig. 16.

Further information can be obtained if the resistance of a memory state (corresponding to fig. 12(A)) is plotted as a function of applied voltage as illustrated in fig. 17. We propose that the first large current step (at 0·36 V) is associated with the formation of a narrow, highly conducting channel which significantly lowers the resistance of the sample. With further increase in the applied voltage, the resistance is lowered in steps, corresponding to quantized resistance values $R = h/2ie^2$ where i is an integer. In the voltage range from 0·36 to 0·8 V, there are four steps (corresponding to the observed current rises in fig. 12(A)) with i being 2, 3, 4 and 5. Higher voltages have not been applied to the sample because this could change the resistance of the particular memory state. If a magnetic field is now applied to the sample, further quantization of resistance is observed at values $R = h/2(i+\frac{1}{2})e^2$. This is illustrated in fig. 18 (the data correspond to fig. 12(B)). It can be seen that extra steps in the resistance occur at $i = 2·5$, 3·5, 4·5 and 5·5. The effect of temperature is illustrated in fig. 19. The curves have been shifted along the current axis for clarity. The observed current steps gradually decrease with increasing temperature until the effect is no longer observable at about 190 K. The results summarized in figs. 15–19 are indicative of ballistic electron transport (Hajto *et al.* 1990).

§4. Discussion

In analysing the main results of this work, two important facts should be emphasized. Firstly the observation of ballistic electron transport provides a vital clue to the structure of the analogue memory element. Secondly, the programmability of the analogue memory provides information about the possible mechanism of the switching process itself.

The starting point of our discussion is that the analogue memory effect in amorphous silicon metal–p⁺–metal structures can only be observed if the sample is

Fig. 15

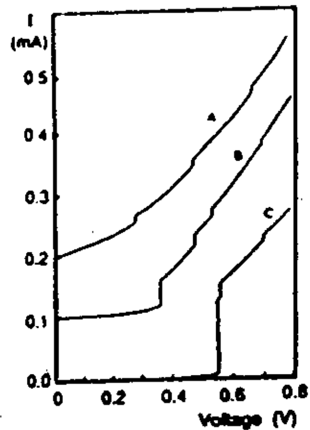

Current–voltage characteristics of different memory states at 4·2 K. $R_C > R_B > R_A$ (curves displaced for clarity).

Fig. 16

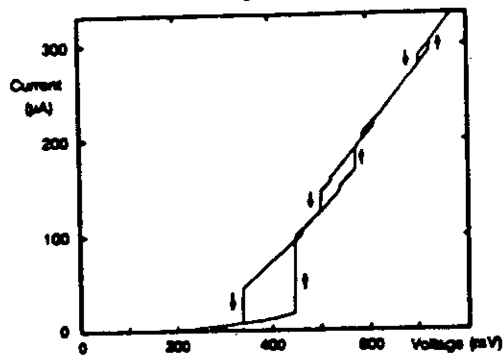

Current–voltage characteristics at 4·2 K showing the hysteresis observed on first increasing and then decreasing the voltage.

Fig. 17

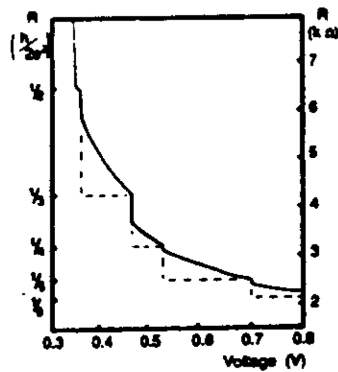

Resistance against voltage at 4·2 K with no magnetic field: (– – –) indicates the idealized contribution from the ballistic transport channel.

Fig. 18

Resistance against voltage at 4·2 K with a 0·2 T magnetic field.

Fig. 19

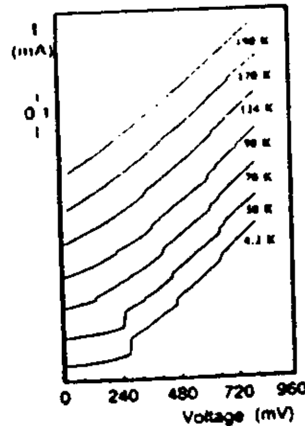

Current–voltage characteristics as a function of temperature. The curves are displaced vertically for clarity.

subjected to an initial forming process. The forming process is characterized not only by the breakdown of the high-resistance state of the structure but, more importantly, also by presence of a positive feedback mechanism which provides a low-resistance ON state so that the breakdown is non-destructive and repetitive switching is possible. Furthermore, the experimental results suggest a strong influence of the choice of the top metal contacts (summarized in the table) on the type of memory switching observed (i.e. digital or analogue switching) and on the success of obtaining stable and reproducible switching. These results are in good accordance with the previous observation (Gage *et al.* 1989) that the first switching event (i.e. the forming) causes a local structural modification of the p^+ amorphous silicon layer, producing a highly conducting filament which does not revert to the original amorphous material when the device is switched OFF. After the forming process the p^+ devices usually exhibit a lower OFF resistance than the unformed device in contrast with our original data for p^+–n–i devices (Le Comber *et al.* 1985). The temperature dependence of the conductivity is also greatly reduced by the forming process. The area independence of R_{ON} (Le Comber

et al. 1985) suggests localized electrical conduction after forming. These results, together with the newly observed ballistic electron transport phenomena (see figs. 12–18), provide strong experimental evidence that the forming process creates a filamentary region consisting of a new material whose properties have changed significantly compared with those of the unformed original material. It is feasible that the high fields and current densities present during forming result in the development of high temperatures locally, which could lead to enhanced diffusion of metallic particles from the electrode into the thin amorphous film. Such a region would become the preferred current path carrying the electron current in the ON state. The current–voltage characteristics in the ON state at room temperature (see fig. 8) suggest that any material rearrangement within the filament occurs so as to destroy the rectifying properties of the original metal–p^+ Schottky contact, and it should also be noted that this is the case even in a typical OFF state.

Lowering the temperature of the memory device reveals further information about the possible structure. The low-temperature current–voltage characteristics (see figs. 12 and 13) show that we have observed a zero-bias high-resistance anomaly and quantized resistance steps (associated with ballistic electron transport) in the ON state of amorphous silicon Cr–p^+–V structures. The phenomenon of ballistic transport is observed in the case when the mean free path λ of the electrons is larger than the length of the conducting channel. The usual approach to the fabrication of devices based on ballistic conduction is to use a very high mobility material (usually high-purity GaAs), where the mobility can reach values of the order of 10^5 cm^2 V^{-1} s^{-1}, leading to values of the electron mean free path of the order of 1 μm. The value of $\lambda \approx 1$ μm is certainly longer than the device dimensions which can be achieved by modern submicrometre technology. The structure in which ballistic transport is most widely investigated is a GaAs–$Al_xGa_{1-x}As$ heterojunction with a split-gate field-effect transistor configuration, usually less than 0·5 μm in length, with a gap of about 0·7 μm (Wharam *et al.* 1988, Van Wees *et al.* 1988). As the voltage on the gate is made increasingly negative, the depletion region increases, narrowing the effective gap and hence the width of the conducting channel decreases. As a consequence, the (one-dimensional) channel width becomes comparable with the electron wavelength, that is becomes sufficiently small that quantization occurs. On the other hand, the channel length is sufficiently short that electrons pass through ballistically (i.e. without appreciable scattering). Our structure is quite different and a possible mechanism which explains the ballistic transport in amorphous silicon structures is outlined below.

The current–voltage characteristics (see fig. 13) suggest that the filament has relatively large resistance around zero bias, that is a barrier for the current flow exists. The observed zero-bias anomaly is consistent with tunnelling conduction between metallic particles embedded in an insulating matrix (Giaver and Zeller 1968). The current–voltage characteristics from 0 to 0·36 V show a continuous, but strongly non-linear behaviour owing to the the high electric field across the small tunnelling distance. In such a system the injection of free carriers is an activated process related to the increase in the electrostatic potential of a particle when a free electron is added to it. The activation energy can be provided entirely by thermal energy (hence the effect diminishes at higher temperatures) or, in the presence of an applied field, part or all of it can be provided by the field itself. The experimental observation of an approximate T^2 dependence of the current at a constant voltage observation of *less than* V_{cr} (see fig. 14) is also in agreement with the assumption that the electron transport is dominated by field-activated tunnelling processes in this region.

These results can be partially explained by assuming that the conducting filament is composed of two parts: small-scale inclusions of permanently changed material connected by conducting channels which are formed, broken, dimensionally changed, re-formed, etc, during switching. Figure 20 illustrates an idealized model, having a single permanent inclusion extending from the top contact, with a narrow channel connecting it to the bottom contact. The evidence is (Le Comber *et al.* 1985) that the overall diameter of the filament at the top contact is less than 0·5 μm. The length of the channel must be consistent with tunnelling.

With increasing applied voltage, the tunnelling current increases exponentially. This implies that at the critical voltage V_{cr} the tunnelling barrier effectively 'breaks down' and a very large current flow occurs. This is not a destructive effect as the process is completely reversible and no material changes ensue. Because of the curved shape of the metallic inclusion illustrated in fig. 20, the current flow is restricted to a very localized area. Thus the channel can be considered to be an electron waveguide with confinement being brought about by the combination of the applied field and the geometry of the metallic inclusion. The observation of ballistic transport shown in figs. 15–19 can only be explained by assuming that the carrier transit time across the channel must be less than a scattering time, that is $t_t < \tau$. This leads to the condition

$$\mu^2 > \frac{ed^2}{m^* V}, \tag{2}$$

where m^* is the effective mass, μ is the mobility and d is the channel length. With $d \approx 50$ Å and $V \approx V_{cr} = 0{\cdot}4$ V this leads to $\mu \geqslant 100\,\mathrm{cm^2\,V^{-1}\,s^{-1}}$. The question remains, however, of whether it is feasible to have such a mobility in the material of the conducting channel. Assuming that the channel length is about 50 Å (typical tunnelling length), the potential gradient along the channel is about 0·36 V/50 Å, that is $E \approx 7 \times 10^5\,\mathrm{V\,cm^{-1}}$. The low-field value of mobility in amorphous silicon is about $10\,\mathrm{cm^2\,V^{-1}\,s^{-1}}$, but this might be increased by the presence of high local fields, when the more energetic carriers might have a larger mean free path because of the reduced scattering cross-section. There is also a possibility that, because of the presence of the metal, alloys could be formed, yielding still higher mobility values. In this connection it is worth noting that we have previously estimated a carrier mobility of $100\,\mathrm{cm^2\,V^{-1}\,s^{-1}}$ in similar devices from magneto-resistance measurements (Le Comber *et al.* 1985). Therefore, although there is considerable uncertainty regarding the structure of the channel and the mobility value there, it looks quite certain that it is

Fig. 20

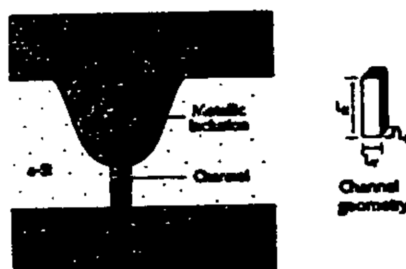

Schematic description of the filament showing the proposed metallic inclusion and the one-dimensional conducting channel.

the small channel *length* which makes ballistic conduction possible at much lower values of mobilities than in the previous 'conventional' cases (Wharam *et al.* 1988). It is important to emphasize, however, that in our case the electron mobility does not need to have the same very high value as in the case of GaAs–$Al_xGa_{1-x}As$ heterostructures (Wharam *et al.* 1988). In our case the one-dimensional conducting channel is established by the dramatic increase in the tunnelling current at voltage V_{cr}. A further increase in voltage in the ballistic regime results in an increase in the cross-section of the conducting channel. This effect can be explained by assuming that the edge of the permanent inclusion has a curved shape as illustrated in fig. 20, that is the tunnelling barrier will break down at larger areas under the influence of higher voltages. The larger voltage applied will produce the same critical electric field at larger distances between the inclusion and the metal electrode; therefore the area of the one-dimensional channel increases. It should be noted that the voltage has an opposite effect on the cross-section of the conduction channel in the case of split-gate structures where the increased voltage level 'squeezes' the channel width. In our case the electrons are confined by the applied potential in the conducting channel whose cross-section increases with increased voltage levels.

This cross-section can be approximated by a rectangle (in a manner analogous to the 'electron-in-a-box' problem), whose dimensions L_y and L_z are comparable with an electron wavelength (fig. 20). The wavefunction Ψ and the energy of the electrons in the lowest quantum level of the one-dimensional channel are given by

$$\Psi = L_x^{-1/2} \exp(ik\kappa)\, g_y(y) g_z(z), \tag{3}$$

$$E = \frac{\hbar^2}{2m^*}k^2 + \frac{\hbar}{2m^*}\left[\left(\frac{\pi}{L_y}\right)^2 + \left(\frac{\pi}{L_z}\right)^2\right], \tag{4}$$

where g_y and g_z are the normalized standing-wave functions of the forms $2^{1/2}\cos(\pi y/L_y)$ and $2^{1/2}\cos(\pi z/L_z)$ respectively. L_x is the length of the conducting channel; L_y and L_z are the cross-section dimensions of the channel (fig. 20). The first term in eqn. (4) describes the kinetic energy of a ballistic electron in motion along the channel. The second term represents the quantum energy level which is uniquely determined by the dimensions L_y and L_z. It is important to emphasize that the electron can accelerate freely along the channel, owing to the collision-free nature of the motion, that is its momentum can increase continuously as the applied voltage increases. On the other hand the electron momentum is quantized in the direction across the channel (defined by L_y and L_z). Therefore, as the voltage increases, two opposite effects can be observed; one is characterized by the increase in the electron kinetic energy along the channel and the other is associated with the increase in the cross-section of the conducting channel (i.e. with increase in L_y and L_z). According to eqn. (4) this latter effect will decrease the quantized energy levels until the nearest higher energy level (termed sub-band (Landauer 1985)) becomes lower in energy than the Fermi level and will be occupied by the 'more energetic' electrons. Consequently a new sub-band is created at higher voltage (i.e. at larger values of L_y and L_z) which in turn will lower the resistance in a quantized manner. This physical scenario was first suggested by Sharvin (1965) as a possible method for studying the Fermi surfaces of metals. It is thus a necessary consequence of the observation of quantized resistance values that the quasi-Fermi level must be within the sub-bands. This we believe to be a direct result of the extremely high current density in the channel, estimated to be of the order of 10^8 A cm^2.

According to the theoretical predictions (Landauer 1985, Imry 1986, Wharam *et al.* 1988), the resistance of a one-dimensional channel (in which the electrons punch through ballistically) should have a quantized value. This is because, in the absence of scattering, the change of electron kinetic energy is determined directly by the applied field across the one-dimensional channel. The current flow is given by

$$I = ne\,\delta v, \tag{5}$$

where n is half the number of carriers per unit length within one particular electron energy level (sub-band) and δv is the increase in the electron velocity acquired on transit through the one-dimensional channel. The number of carriers can be obtained by integrating the density of states in one dimension:

$$n = \int_0^{E_F} N(E)\,\mathrm{d}E = \frac{g_s}{2\pi\hbar}\left(\frac{m^* E_F}{2}\right)^{1/2} = \frac{g_s m^* v_F}{2\pi\hbar}, \tag{6}$$

where E_F is the Fermi energy and v_F is the Fermi velocity. It is assumed that the applied voltage is sufficiently small that the velocity acquired by the electrons during the transit in the channel is small compared with the Fermi velocity. In this case the increase in velocity is given by

$$\delta v = eV/m^* v_F. \tag{7}$$

Substituting eqns. (6) and (7) into eqn. (5) yields

$$I_s = \frac{g_s e^2 V}{2\pi\hbar} \tag{8}$$

for the current and

$$R_s = \frac{h}{g_s e^2} = \frac{h}{2e^2} \tag{9}$$

where R_s is the sub-band resistance and g_s is the spin degeneracy ($g_s = 2$) in the non-magnetic field case. However, the value of $R_s = h/2e^2$ applies to only one sub-band. If a new sub-band is created at a higher voltage (i.e. by changing the cross-section of the channel), the total resistance becomes $h/2ie^2$ (i is an integer defining the number of sub-bands below E_F) in the same manner as in the case of parallel resistors. This is possible because there is no scattering in the conducting sub-bands, that is they do not interact with each other. Consequently the resistance drops in a quantized manner with $i = 2, 3, 4$ and 5 (as seen in fig. 17). In the case of our results, the plateaux of the individual quantum steps are not flat but they have a finite slope, that is the resistance decreases at higher voltages between the individual plateaux. This could be caused by the presence of additional non-ballistic conduction mechanisms. The broken line in fig. 17 indicates the resistance–voltage characteristics expected from the idealised ballistic component. We emphasize that the data presented in figs. 15–19 are raw data, and no attempt has been made in the present work to distinguish between the various contributions to the conductivity. In the above model we have considered the effect of moving the sub-bands through the quasi-Fermi level by changing the dimensions of the channel. In principle, we believe it would be equally possible to explain the data with a model in which the sub-bands are fixed in energy and the quasi-Fermi level is varied by the changing concentration of injected charge in the channel as a function of applied voltage.

When a magnetic field is applied, additional steps occur. This is probably due to the Zeeman splitting of electron energy levels, that is a lifting of the spin degeneracy splits each level into two. Therefore extra steps will be observed at $R = h/2(i + \frac{1}{2})e^2$ resistance levels as seen in fig. 18. The magnitude of the effect seen is rather surprising for a temperature of 4·2 K and a magnetic field of 0·2 T. However, this could be explained by assuming an anomalously high value for g_v.

The most important feature of the observed ballistic behaviour is that it can be observed up to about 190 K namely, much higher temperatures than previously observed. We suggest that this might be due to the very small size of the ballistic channel.

The model suggested above describes the possible mechanism for the ballistic transport and provides important information about the structure of the filament but, as it stands, it does not explain the memory switching. The most important difference between the two phenomena lies in the fact that ballistic transport is observed at applied voltage levels lower than about 1 V, that is at voltage levels where no memory switching occurs. The observed quantized jumps in the device resistance are of the type associated with threshold switching; if the voltage is lowered, the sample resistance reverts to the original low-bias case, that is there is no permanent change in the current–voltage characteristics of the device. On the other hand, memory switching occurs at voltage levels from about 1·5 V to about 4 V, resulting in a permanent change in the current–voltage characteristics of the device, that is a different resistance state of the memory. In order to explain the different and permanent resistance states a model for memory switching should embody one or more of the following features:

(*a*) changes in the conductivity of the whole filament;
(*b*) local changes in conductivity at a certain point(s) in the filament;
(*c*) changes in the filament geometry.

Model (*a*) would presumably require an average energy for switching of a similar order to that established for forming, but it has been found that ON→OFF→ON switching can be achieved using single pulse energies of about 10^{-10} J (see fig. 10). In addition, if it is assumed that the filament is homogeneous, there is no obvious way of introducing a polarity dependence. However, if there are inhomogeneities in the filament, it may be possible to increase substantially the local energy density and field strength. Consider for example, the simple one-dimensional arrangement shown in fig. 21. The regions A consist of a high-conductivity material separated by regions of lower-conductivity material B. The observed resistance of the filament will depend

Fig. 21

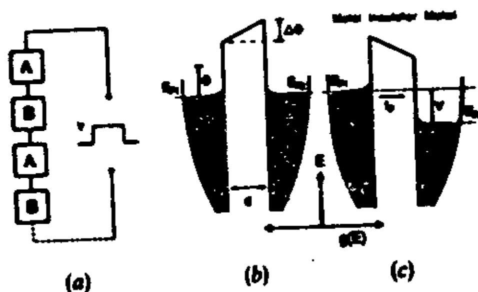

(*a*) Possible one-dimensional arrangement of the conducting filament; (*b*), (*c*), schematic energy diagrams for the tunnelling region.

upon the proportions of A and B and hence the relative contributions to the filament resistance of regions A and B. If $R_B < R_A$, the properties of the type A material will be observed and, if $R_A < R_B$, the properties of the type B material will be observed. If the 'gaps' between the highly conducting regions are small, then it is also necessary to consider the possibility of inter-island tunnelling. In order to establish such a model, a more detailed description of regions A and B must be included, for example, as follows.

(1) A is metallic or a degenerately doped material whose contribution to the filament is fixed and $\sigma_A \neq f(V)$ where V is the applied voltage and σ is the conductivity.
(2) B is a 'gap' between type A material which is sufficiently small to allow significant tunnelling to occur; consequently σ_B is some function of the voltage.

One possible explanation is that, in the ON state, $R_B < R_A$ and the measured conduction properties of the filament are those corresponding to material A, that is Ohmic current–voltage characteristics, and a small thermal activation. In the OFF state, $R_A < R_B$ and the conduction properties are governed by the behaviour of the tunnelling regions. For the purpose of the model the tunnelling region can be represented in a simplified way, as shown in fig. 21. The current density in such a simplified system is governed by the following factors:

(1) the applied bias V;
(2) the average tunnelling distance d;
(3) the average barrier height Φ and asymmetry $\Delta\Phi$;
(4) the density of states $g(E)$ in the metallic regions;
(5) the occupation of $g(E)$, that is the temperature dependence.

The functional form $J(V, T)$ of the current density J against voltage V at different temperatures can be obtained under limiting conditions.

(*a*) $V \ll \Phi$, and $\Delta\Phi \ll \Phi$, constant T. In this case the transmission probability $P = c\exp(-d\Phi^{1/2})$ may be treated as a constant for electrons near the Fermi energy F_F and provided that $g(E)$ variations near E_F are small, J will increase *linearly* with V as more empty states become accessible in metallic region A. Conduction is then approximately *Ohmic* and *symmetric* (Giaver and Zeller 1968) in good accordance with fig. 8.

(*b*) $V < \Phi$, and the temperature is varied. In this case, P is not very dependent on T as usually $kT \approx 10^{-2}$ eV. Thus only a few electrons are promoted thermally to levels where P is significantly larger than at E_F. The approximate form of the current density–voltage characteristics can be obtained as

$$J(V, T) = J(V, 0)\left(1 + \frac{3 \times 10^{-9} d^2 T^2}{\Phi}\right), \tag{10}$$

with d in Ångström units, Φ in electronvolts and T in kelvins (Giaver and Zeller 1968). The T^2 dependence of J at a constant V has been observed (see fig. 14) and the slope correlated with $d = 50$ Å and $\Phi = 1$ eV.

How might switching be achieved in terms of the tunnelling model? The low-bias isothermal resistance of 'region-B-like' parts of the filament can be expressed as

$$R = c\exp(d\Phi^{1/2}), \tag{11}$$

where the constant c is determined by geometric factors and the transmission probability. This expression gives R directly in ohms if d is in Ångström units and Φ is in electronvolts (with c as a small correction factor). Taking $d = 50$ Å and $\Phi = 1$ eV, then $R_1 = c\exp(50)$ and increasing d by 5 Å gives $R_2 = \exp(55)$, that is R has increased by about a factor of 150. An equivalent increase in resistance is obtained by keeping d constant and increasing Φ from 1 to 1·2 eV. Therefore dimensional changes in the tunnel barrier on an atomic scale, or small (20%) changes in barrier height, could account for the presence of switching. A change in the particle size and/or their spatial distribution as a result of localized heating or high field effects could explain the differences between high- and low-resistance states. The high switching speeds (about 10 ns) and the insensitivity of switching to temperature suggest that large-scale structural changes are unlikely. The observation of the quantized jumps in resistance and especially the magnetic field dependence of the quantized resistance levels at values of $R = h/2(i + \frac{1}{2})e^2$ provide an important experimental proof that the electron transport is ballistic in the formed Cr–p$^+$–V memory structures. The most important feature of the observed ballistic behaviour is that it can be observed up to about 190 K, namely much higher temperatures than previously observed (Wharam *et al.* 1988). This temperature dependence (see fig. 19) suggests that the states responsible for the quantized resistance levels are separated in energy by $\Delta E \approx 1{\cdot}6 \times 10^{-2}$ eV which is about kT, T being the temperature at which the differences between the quantized electron levels are smeared out. This energy indicates a change of about 40 Å in the L_y and L_z dimensions (as follows from eqn. (4)) between the subsequent steps which correspond to the energy separation of the observed quantum steps. Finally we emphasize that the effect has been observed in what is initially a metal–amorphous semiconductor structure. The 'classical mobility' of the amorphous silicon is many orders of magnitude lower than is expected for ballistic behaviour. It is not known with any certainty what effect the forming process has on the structure of the conducting channel but the observed behaviour suggests the importance of the very small dimensions of the conducting channel rather than other physical parameters. The significance of using amorphous silicon sandwich structures lies in the forming process which allows the fabrication of such small structures. The strong influence of the metal contact on the observed memory switching behaviour indicates the importance of 'alloying' during the forming process. It has been reported for example that solid-phase amorphization or glass formation occurs in V–Si reactions induced by rapid thermal annealing (i.e. at conditions similar to forming) but do not occur in Co–Si and Cr–Si (Nathan 1988). Therefore the presence of a very small tunnelling conduction path in amorphous silicon Cr–p$^+$–V structures might be due to a new type of solid-phase reaction (induced by forming) which creates a homogeneous (possibly amorphous) V–Si silicide.

§5. Conclusions

The experimental results presented in this paper show that Cr–p$^+$–V amorphous silicon structures exhibit polarity-dependent analogue memory switching. The analogue resistance values are stable after removing the programming voltages and up to temperatures of about 160°C, that is the effect is non-volatile. The temperature dependence of the current–voltage characteristics and of the memory switching transients suggest that the effect can be explained by either dimensional changes in a tunnelling barrier present in the structure on an atomic scale or small changes in barrier height.

Perhaps the most important observation is that the conduction in the memory ON state is restricted to a narrow conducting channel through which the electrons can, under certain conditions, travel ballistically. As a consequence, quantized resistance levels at $R = h/2ie^2$ values are observed where i is the number of occupied one-dimensional conducting channels (sub-bands) and the spin degeneracy is two (in the case when no magnetic field is applied). As the applied voltage is increased, the cross-section of the conducting channel in increased. This results in additional conducting channels (sub-bands) passing through the Fermi energy and consequently the resistance drops by quantized values.

In the presence of a magnetic field, additional steps occur corresponding to the split levels at values of $R = h/2(i + \frac{1}{2})e^2$. The quantized resistance effect can be observed at relatively high temperatures (up to about 190 K), suggesting an energy separation of $kT \approx \Delta E \approx 1{\cdot}6 \times 10^{-2}$ eV. This indicates a change of about 40 Å in the dimensions of the cross-section of the conducting channel between the subsequent steps of the quantized resistance.

Acknowledgments

It is a great pleasure to contribute to this *Festschrift* in honour of Professor Walter Spear on the occasion of his seventieth birthday. His contribution to the subject of amorphous materials has been outstanding and we are delighted to participate in this acknowledgment of his achievements. We have also had the privilege of collaborating with Professor Spear in the early stages of our work on amorphous silicon memory devices and we are grateful for his valuable contributions and for his continued interest.

References

Gage, S. M., Hajto, J., Reynolds, S., Choi, W. K., Rose, M. J., Le Comber, P. G., Snell, A. J., and Owen, A. E., 1989, *J. non-crystalline Solids*, **115**, 171.

Giaver, I., Zeller, H. R., 1968, *Phys. Rev. Lett.*, **20**, 1504.

Hajto, J., Owen, A. E., Gage, S. M., Snell, A. J., Le Comber, P. G., and Rose, M. J., 1990, *Phys. Rev. Lett.* (submitted).

Hajto, J., Rose, M. J., Snell, A. J., Le Comber, P. G., and Owen, A. E., 1990, *Mater. Res. Soc. Symp. Proc.*, **192**, 347.

Imry, Y., 1986, *Directions in Condensed Matter Physics*, edited by G. Grinstein and G. Mazenko (Singapore: World Scientific), p. 101.

Landauer, R., 1985, *Localisation Interactions and Transport Phenomena*, edited by B. Kramer, G. Bergmann and Y. Bruyserade (Berlin: Springer), p. 38.

Le Comber, P. G., Owen, A. E., Spear, W. E., Hajto, J., Snell, A. J., Choi, W. K., Rose, M. J., and Reynolds, S., 1985, *J. non-crystalline Solids*, **77 & 78**, 1373.

Nathan, M., 1988, *J. appl. Phys.*, **63**, 5534.

Owen, A. E., Le Comber, P. G., Sarrabayrouse, G., and Spear, W. E., 1982, *Proc. Inst. elect. Engrs*, Part I, **129**, 51.

Rose, M. J., Hajto, J., Le Comber, P. G., Gage, S. M., Choi, W. K., Snell, A. J., and Owen, A. E., 1989, *J. non-crystalline Solids*, **115**, 168.

Sharvin, Y. V., 1965, *JETP Lett.*, **1**, 152.

Van Wees, B. J., Van Houten, H., Beenakker, C. W. J., Williamson, J. G., Kouwenhoven, L. P., Van der Marel, D., and Foxon, C. T., 1988, *Phys. Rev. Lett.*, **60**, 848.

Wharam, D. A., Pepper, M., Ahmed, H., Frost, J. E. F., Hasko, D. G., Peacock, D. C., Ritchie, D. A., and Jones, G. A. C., 1988, *J. Phys. C*, **21**, L887.

VOLUME 66, NUMBER 14 PHYSICAL REVIEW LETTERS 8 APRIL 1991

Quantized Electron Transport in Amorphous-Silicon Memory Structures

J. Hajto, A. E. Owen, S. M. Gage, and A. J. Snell
Department of Electrical Engineering, University of Edinburgh, Edinburgh EH9 3JL, Scotland

P. G. LeComber and M. J. Rose
Department of Applied Physics and Electronic and Manufacturing Engineering, University of Dundee, Dundee DD1 4HN, Scotland

(Received 26 March 1990)

Conduction in the ON state of amorphous-silicon memory devices is constrained to a narrow conducting filament. We present experimental evidence to show that the memory ON state is associated with quantized electron transport which is presumably related to quantum confinement effects in the small conducting filament. Current-voltage characteristics of typical ON states exhibit discrete steps which correspond to quantized resistance states and the steps split appropriately in a magnetic field. An especially notable feature is that the quantization can be observed at relatively high temperatures (up to ~190 K).

PACS numbers: 73.40.Sx, 72.80.Ng

We have previously shown that amorphous-silicon metal-p^+-n-i-metal and metal-p^+-metal junctions exhibit nonvolatile, polarity-dependent digital and analog memory-switching phenomena after initial conditioning by means of a moderately high applied potential ("forming").[1-4] An essential feature of this forming process is the creation of a filamentary region of highly conducting material. In the ON state the current is carried primarily through this region, which is much less than 1 μm in diameter. Experimental evidence for filamentation comes from studies of the ON-state resistance, which show R_{ON} to be independent of area, by thermal imaging with liquid crystals, and by direct observation with a scanning electron microscope combined with microanalysis. The latter technique indicated that the formation of the current filament is associated with local diffusion of the top metal contact into the amorphous silicon, resulting in a region of mixed or "alloyed" metal and silicon. More recent experimental work has resulted in a new metal-p^+-metal amorphous-silicon device which, rather than exhibiting two-state digital operation, has a continuum of stable conductance states which are nonvolatile and fully programmable by single 10-ns voltage pulses.[4] These new analog memory devices have applications as nonvolatile, reprogrammable memory elements in analog neural networks. In this paper we present new results showing that the current-voltage characteristics of such structures at low temperatures exhibit steplike features associated with quantized transport.

The samples used for this work were amorphous-silicon Cr-p^+-V sandwich structures configured as shown in Fig. 1. The 1000-Å-thick p^+ amorphous-silicon layer was prepared by rf-glow-discharge decomposition of SiH_4 containing 10^4 ppm by volume of B_2H_6, with the contact area defined by a 10-μm-diam pore in an insulating layer. The top and bottom metal electrodes were prepared by vacuum evaporation. By applying 300-ns voltage pulses of progressively increasing magnitude, the resistance of the as-prepared device can be gradually lowered from 10^9 Ω to $\sim 10^3$-10^4 Ω. After this initial forming step, all subsequent memory-switching operations can be performed with 10-100-ns pulses, 1.5-5 V in magnitude. Under these conditions the devices exhibit fast analog switching;[4] i.e., they show a continuum of nonvolatile states with resistances ranging from $R_{ON}=10^3$ Ω to $R_{OFF}=10^6$ Ω. In the present work we have studied the low-temperature conductivity behavior of the devices in a range of such analog memory states.

Typical current-voltage characteristics of a formed memory ON state measured at 4.2 K are shown in Fig. 2. In the voltage region from 0 to 0.37 V, the current in-

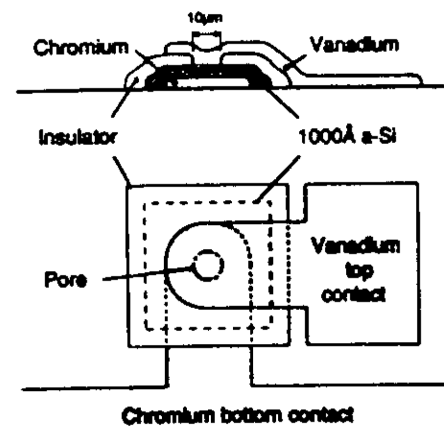

FIG. 1. Structure of the amorphous-silicon device.

© 1991 The American Physical Society

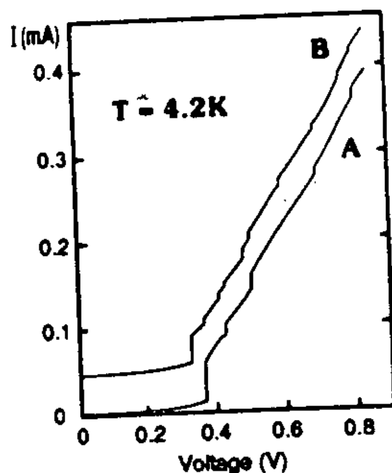

FIG. 2. I-V curves at 4.2 K with and without magnetic field. Curve B has been offset by 50 μA on the current scale for clarity.

creases continuously in a non-Ohmic manner. At a critical voltage V_{cr}, in this instance at 0.37 V, there is a distinct change in the behavior of the sample. A sudden current jump occurs at this point and the resistance of the sample is lowered to the order of a few kΩ. After the first current jump at 0.37 V, further current steps can be observed at 0.43, 0.51, 0.70, and 0.81 V (curve A in Fig. 2). The current-voltage characteristics are symmetrical about the origin.

Curve B in Fig. 2 depicts the current-voltage characteristics of the same sample under the influence of a 0.2-T magnetic field. The curve has been displaced by 50 μA on the current scale for clarity. The direction of the magnetic field is 30° with respect to the filament. Further steps can now be observed at 0.33, 0.41, 0.49, 0.60, and 0.78 V in addition to those observed in the zero-magnetic-field case (curve A). The effect of the magnetic field is completely reversible. Similar I-V characteristics have been obtained for a range of samples with varying initial resistance states. The critical voltage V_{cr} at which the first current jump occurs and the amplitude of this first current jump are dependent on the resistance of the memory ON state investigated. After the first jump, however, the characteristics for each sample investigated lie on a similar curve, suggesting a similar conduction mechanism at voltages above V_{cr}.

Figure 3 shows the effect of temperature on the current-voltage characteristics of a different sample from the one shown in Fig. 2. The curves have been shifted along the current axis for clarity. The magnitude of the current steps gradually decreases with increasing temperature until the effect is no longer observable at ~190 K. Figure 4 shows the data for curve A in Fig. 2 replotted to show resistance as a function of applied voltage. The steps in the current are clearly seen to be associated

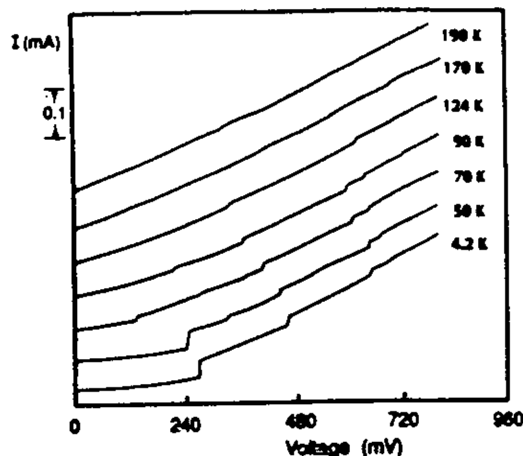

FIG. 3. I-V curves as a function of temperature. The curves have been offset on the current scale for clarity.

with a quantized resistance $R = h/2ie^2$, where i is an integer. In the voltage range from 0.3 to 0.8 V, there are five steps in the current in curve A, Fig. 2, corresponding to values for i of 2, 3, 4, 5, and 6. Higher voltages have not been applied to the sample because these could change the resistance of the particular memory state. With a magnetic field applied to the same sample further quantization of resistance is observed at values $R = h/2(i+\frac{1}{2})e^2$. Theoretical considerations predict that the steps should be flat, as shown by the dashed lines in Fig. 4. That they are not flat in the present results is thought to be due to the presence of a parallel conduction path through the bulk of the amorphous silicon around the filament. Figure 5 shows that a sample in a given resistance state exhibits reproducible behavior at low temperatures even after thermal cycling. Curves a and b show

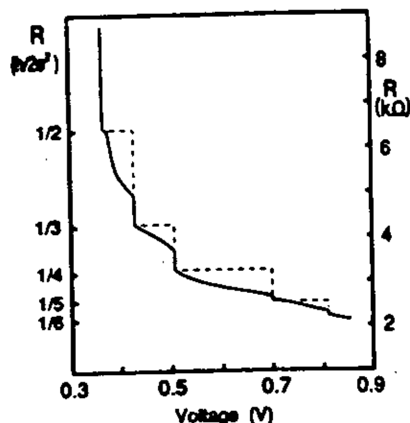

FIG. 4. Resistance vs voltage at 4.2 K with no magnetic field. The dashed line indicates the behavior predicted by theory.

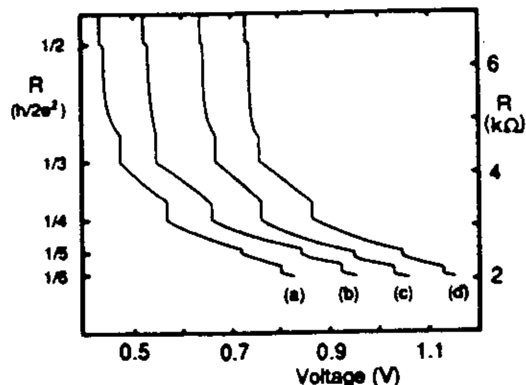

FIG. 5. Reproducibility of resistance characteristics before and after thermal cycling. Curves are offset by 0.1 V on the voltage scale for clarity.

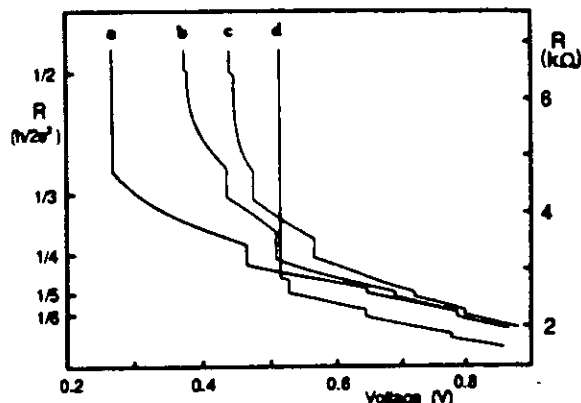

FIG. 6. Reproducibility of the resistance-voltage characteristics obtained on different samples.

the electrical characteristics of a sample at 4.2 K with a delay of several hours between measurements. Curves c and d show measurements on the same sample after temperature cycling between room temperature and 4.2 K.

Figure 6 shows the reproducibility of the observed quantized resistance jumps for four different samples (denoted by a, b, c, and d). (Curve a was obtained by replotting the current-voltage characteristics in Fig. 3 at 4.2 K.) These curves represent the largest deviation among the samples measured—the resistance-voltage curves of all of the other samples measured lay within these values. It is important to note that in this case there is no offset between the curves; i.e., they are directly replotted from the measured current-voltage characteristics. The critical voltage V_{cr} and the voltage values at which the quantized resistance jumps occur are different for the different samples but the quantized jumps are always very close to the values of the quantized resistance $R=h/2ie^2$. The typical deviations are $\pm 2\%$ at $i=2$, $\pm 2.5\%$ at $i=3$, $\pm 6\%$ at $i=4$, $\pm 4\%$ at $i=5$, and $\pm 4\%$ at $i=6$. The first jump, however, occurs from $R=15\,200\ \Omega$ to $4820\ \Omega$ in curve a, which is apparently a 12% deviation from the quantized resistance value of $R=4291\ \Omega$ (at $i=3$). Also, in the case of curve d, the resistance jumps first to $R=4820\ \Omega$ at $V_{cr}=0.51$ V followed by another closely spaced jump (at $V=0.525$ V) to $R=2550\ \Omega$, which is very close to the quantized value of $R=2575\ \Omega$ (at $i=5$). These relatively large discrepancies are always associated with the *first* current jump in the I-V characteristics at V_{cr}, and hence with a change in the conduction mechanism. This first transition at V_{cr} might not be expected to occur therefore at a voltage corresponding to a change in quantized resistance value.

The experimental data presented above show that we have observed discrete steps in the I-V characteristics for the ON state of amorphous-silicon Cr-p^+-V structures which are associated with a quantized resistance. The current-voltage characteristics (see Fig. 2) indicate that the filament has a relatively large resistance around zero bias. Such an anomalously high zero-bias resistance in metal/amorphous-silicon/metal structures was recently shown to be consistent with the assumption that electron transport in the filament at low bias is dominated by tunneling between small metallic particles embedded in a dielectric medium (presumably amorphous silicon).[3] We assume that the conducting filament is composed of two parts—small-scale inclusions of permanently changed material connected by conducting channels which are formed, broken, dimensionally changed, reformed, etc., during switching. The evidence is that the overall diameter of the filament at the top contact is $\ll 0.5\ \mu m^2$. The length of the channels must be consistent with tunneling. With increasing applied voltage, the tunneling current increases exponentially. This implies that at the critical voltage V_{cr}, the tunneling barrier effectively "breaks down" and a much larger current flow occurs. This is not a destructive effect as the process is completely reversible and no material changes ensue. Assuming that the metallic inclusion has a curved shape, the current flow would be restricted to a *very localized area*. The observation of quantized resistance suggests that the channel can be considered to be an electron waveguide with confinement being brought about by the combination of the applied field and the geometry and constitution of the conducting filament.

There is a wide range of experimental and theoretical work on electrical transport through quantum point contacts.[5] These are short and narrow constrictions in a two-dimensional electron gas, with a width of the order of the Fermi wavelength λ_F. Because of the high mobility, elastic impurity scattering and inelastic scattering are negligible and therefore the mean free path of the electrons is longer than the length of the conduction channel. In this case ballistic transport takes place and the resistance of such quantum point contacts is quantized in

units of $h/2e^2$. The notion of a very small conducting filament in the amorphous silicon devices being made up of metallic inclusions has similarities to the idea of quantum point contacts and it is possible, therefore, that the quantized resistance states described here are a result of the same sort of mechanism. The crucial question is whether ballistic transport is possible in the amorphous-silicon device. Carrier mobilities in amorphous silicon are normally trap limited and are orders of magnitude lower than expected for ballistic behavior (e.g., $\sim 10^{-2}$ $cm^2 V^{-1} sec^{-1}$). It is worth noting, however, that we have previously estimated a carrier mobility as high as 100 $cm^2 V^{-1} sec^{-1}$ from magnetoresistance measurements on devices similar to those used in the present experiments and that mobility is certainly related to the conducting filament rather than the "bulk" amorphous silicon.[4] On the other hand, it is entirely unexpected that quantized resistance states associated with ballistic transport should be observed when, as in the present case, the applied voltage is greater than kT (or greater than the spacing between subbands).[6,7] At the moment, therefore, the issue is unresolved and it is not realistic to speculate further about mechanisms except to note that the observed quantized transport effects suggest the importance of the dimensions of the conducting channel rather than material parameters. The significance of using amorphous-silicon devices lies in the forming process which promotes the formation of very small features which then dominate conduction.

[1] A. E. Owen, P. G. LeComber, G. Sarrabayrouse, and W. E. Spear, IEE Proc. Part I: Solid State Electron Devices **129**, 51–54 (1982).

[2] M. J. Rose, J. Hajto, P. G. LeComber, S. M. Gage, W. K. Choi, A. J. Snell, and A. E. Owen, J. Non-Cryst. Solids **115**, 168 (1989).

[3] S. M. Gage, J. Hajto, S. Reynolds, W. K. Choi, M. J. Rose, P. G. LeComber, A. J. Snell, and A. E. Owen, J. Non-Cryst. Solids **115**, 171 (1989).

[4] P. G. LeComber, A. E. Owen, W. E. Spear, J. Hajto, A. J. Snell, W. K. Choi, M. J. Rose, and S. Reynolds, J. Non-Cryst. Solids **77/78**, 1373 (1985).

[5] H. van Houten, C. W. J. Beenakker, and B. J. van Wees (to be published); in *Semiconductors and Semimetals*, edited by M. A. Reed (Academic, New York, 1990).

[6] B. J. van Wees, H. van Houten, C. W. J. Beenakker, J. G. Williamson, L. P. Kouwenhoven, D. van der Marel, and C. T. Foxon, Phys. Rev. Lett. **60**, 848 (1988).

[7] D. A. Wharam, M. Pepper, H. Ahmed, J. E. F. Frost, D. G. Hasko, D. C. Peacock, D. A. Ritchie, and G. A. C. Jones, J. Phys. C **21**, L887 (1988).

Journal of Non-Crystalline Solids 137&138 (1991) 499–502
North-Holland

NON-CRYSTALLINE SOLIDS

QUANTISED ELECTRON EFFECTS IN METAL/a-Si:H/METAL THIN FILM STRUCTURES

J. HAJTO,[†] M.J. ROSE,[‡] A.J. SNELL,[†] I.S. OSBORNE,[‡] A.E. OWEN,[†] and P.G. LECOMBER.[‡]

† Department of Electrical Engineering, University of Edinburgh, Edinburgh EH9 3JL, Scotland
‡ Department of Applied Physics and Electronic & Manufacturing Engineering, University of Dundee, Dundee DD1 4HN, Scotland

We present experimental results showing that metal/p⁺/metal amorphous silicon (a-Si:H) memory structures exhibit room temperature quantised electron transport associated with quantised resistance. The quantisation of resistance is observed at values of $R = h/2ie^2$, where i is an integer or a half integer.

1. INTRODUCTION

We have previously shown that a-Si:H metal/p^+/metal structures exhibit non-volatile, polarity dependent analogue memory phenomena after initial conditioning by means of a moderately high applied potential [1,2]. An essential feature of this 'forming' process is the creation of a filamentary region of highly conducting material. The filament is associated with local diffusion of the top metal contact into the a-Si:H, resulting in a region of mixed metal and silicon of unknown composition. More recent experiments [3] have shown that, at low temperatures, the ON states of such memories exhibit quantised resistance values of $R=h/2ie^2$, where h is Planck's constant, e is the electron charge and i is an integer or half integer. We now present new experimental observations showing that such structures exhibit *room temperature* quantised resistance, and will discuss possible physical mechanisms responsible for this phenomena.

2. RESULTS

The samples used for this work were a-Si:H Cr/p^+/V sandwich structures, the preparation and geometry of which have been described elsewhere [3]. The structures have an initial low voltage resistance of ~10^9 Ω which is lowered to ~ 10^3-10^4 Ω by applying 300 nsec voltage pulses of increasing magnitude up to ~ 14 V. The positive polarity is applied to the vanadium top contact. After this forming step the devices exhibit fast analogue switching at room temperature i.e. they show a continuum of non-volatile states between $R_{ON} = 10^3$ Ω and $R_{OFF} = 10^6$ Ω. At low temperatures the ON states of these devices exhibit discrete steps in the current-voltage characteristics associated with quantised resistance [3]. The effect is most readily observed at 4 K and disappears gradually as the temperature of the sample is increased to ~ 190 K.

Room temperature quantisation is observed generally, but not exclusively, after further treatment of the sample. In this 'conditioning' step, a device in a 10^3 Ω ON state is modified by applying a relatively slow voltage ramp (0 to 5 V, 1V sec^{-1}, 50mV steps) with the positive polarity applied to the top contact. Fig. 1 shows a typical I-V characteristic of a Cr/p^+/V

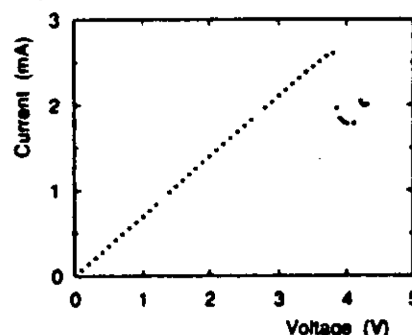

FIG. 1. Current versus voltage at 300 K taken during the conditioning step of a Cr/p^+/V structure.

0022-3093/91/$03.50 © 1991 – Elsevier Science Publishers B.V. All rights reserved.

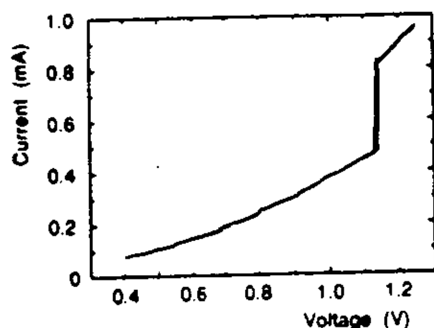

FIG. 2. Current versus voltage at 300 K of a conditioned Cr/p⁺/V structure.

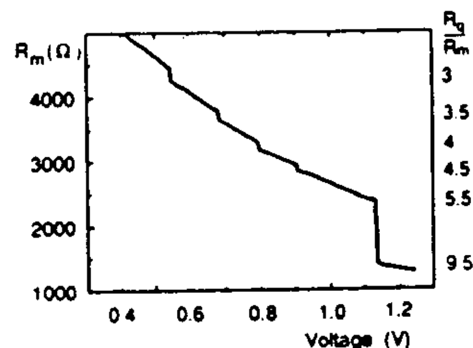

FIG. 3. Resistance versus voltage at 300 K for the sample shown in Fig. 2.

device measured at room temperature during the conditioning step. The I-V characteristic is slightly non-ohmic and, at V = 4 V (the conditioning voltage, V_{co}), the resistance increases suddenly. After conditioning, the characteristic has completely changed, with the current now increasing in sudden steps as the voltage is increased.

Fig.2 shows a typical I-V characteristic of a conditioned device measured at 300 K, obtained by using a HP Parameter Analyzer in voltage source mode with applied voltage steps of 2mV. In the voltage region up to a critical voltage V_{cr} = 0.55 V, the current increases monotonically in a non-ohmic manner. At 0.55 V, a small jump in current occurs, indicating a drop in resistance. After this first jump further small current steps are observed at 0.69, 0.80 and 0.91, with a larger jump at 1.14 V. The current-voltage characteristic is symmetrical. Fig. 3 shows the static resistance of the same sample as a function of applied voltage. The measured resistance changes at values of $R_m = R_q/i$, where $R_q = h/2e^2 = 12906\ \Omega$ and i is an integer or a half integer. In the voltage range from 0.55 to 1.14 V there are five such steps, with i being 3, 3.5, 4, 4.5, and 9.5. The accuracy of the quantised resistance is defined as $i\Delta R/R_q$, where ΔR is the deviation between the measured resistance R_m and the predicted quantised resistance R_q/i. Table I summarizes the accuracy of the quantisation shown in Figs. 2 and 3. The rated accuracy of the Semiconductor Parameter Analyzer is 0.15% for voltage and 0.4% for current measurements. It can be seen that ΔR is less than 2% for all of the quantised levels observed. The stability and reproducibility of the observed quantisation has been investigated in a number of samples and for a duration of 10 hours at room temperature. Typical accuracies obtained remained within ±2%. Fig. 4 illustrates this reproducibility in the form of a histogram for a quantised resistance value, corresponding to $R_q/4$, measured at room temperature. The plot contains 180 values collected over a period of three hours. The calculated mean value (using a Gaussian fit) is $R_m = 3.2\times10^3\ \Omega$, which differs by 0.82% from the quantised value of R/4 = 3226 Ω. The standard deviation is σ = 32 Ω. All devices which have been formed and conditioned in this way show quantised behaviour similar to that in Figs. 2 and 3. Fig. 5

Table I. Characteristic values of room temperature quantisation described in Figs. 2 and 3.

V [V]	R_m [Ω]	R_q/i [Ω]	ΔR [Ω]	$i\Delta R/R_q$ [%]
0.55	4243	R/3=4302	-59	-1.37
0.69	3760	R/3.5=3687	-31	-0.84
0.80	3199	R/4=3226	-27	-0.84
0.91	2849	R/4.5=2868	-19	-0.66
1.14	1377	R/9.5=1358	+18	+1.36

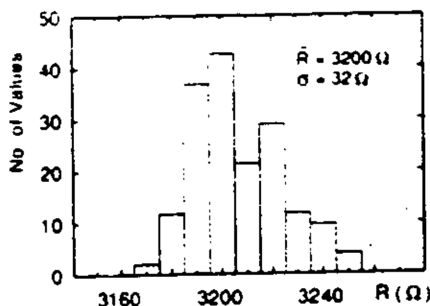

FIG. 4. Histogram of a room temperature quantised resistance value in a $Cr/p^+/V$ conditioned structure.

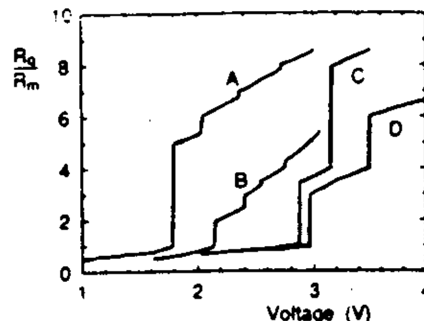

FIG. 5. Normalized room temperature resistance versus voltage for four different samples.

shows representative normalized resistance-voltage curves for four different samples, as calculated from the measured I-V characteristics. Note that in different samples, V_{th} and the magnitude of the steps are different but the resistance values are always quantised.

The resistance values are expressed in terms of a resistance function R_q/R_m where $R_q = h/2e^2 = 12906\,\Omega$ as before and R_m is the resistance measured from the I-V characteristics. If the measured resistance was quantised, this function would give integer or half integer values. In all cases the first instability occurs at a value of R_q/R_m close to 1 i.e. $R_m = 12906\,\Omega$. However, the range of the first resistance jump varies: from i = 1 to 5, from 1 to 2, from 1 to 3.5, and from 1 to 3 in samples A, B, C, and D respectively. Subsequent jumps are also different - in the case of sample A the second jump occurs from i = 5.5 to 6 and smaller jumps can be seen at i = 7 and 8. In sample B the second jump occurs from i = 2.5 to 3, followed by a small jump at i = 3.5 and another jump from i = 4 to 4.5. In sample C the second jump occurs between i = 4 and 8 and in sample D the second jump occurs between i = 4 and 6. In all cases the accuracy of the quantised values remains within ±2%.

The experiments described above refer to I-V characteristics measured under voltage source conditions. Under current source conditions the devices exhibit S-shaped I-V characteristics. This type of characteristic is typical of filamentary conduction, showing two regimes separated by a relatively large region of current controlled negative differential resistance. The limits of the negative resistance region seen in Fig.6 correspond accurately to quantised values of resistance. The discontinuity is equivalent to a change in resistance from $R_m = 6.47\times10^3\,\Omega$ to $R_m = 4.27\times10^3\,\Omega$, corresponding to a change in quantisation from $R_q/R_m = 1$ to 3.

At present we have no firm explanation for these results. Experiments on other one and two-dimensional systems show electrical properties that are associated with quantised resistance, but are only observed at very low temperatures. In a two-dimensional electron gas [3] the quantum Hall effect is related to e^2/h and in a one-dimensional electron gas [4] in the ballistic regime resistance is quantised in terms of $h/2e^2$. However, it is not expected that quantised resistance states associated with ballistic transport should be observed when, as in the present case, the applied voltage is much greater than kT - if, for example, all the applied voltage were to appear across the critical part of the structure, the equivalent 'temperature' would be in excess of 1000 K.

We have suggested previously [2] that the quantised phenomena might be related to electrical transport through a quantum point contact. Assuming that the inclusion of modifed material created during forming

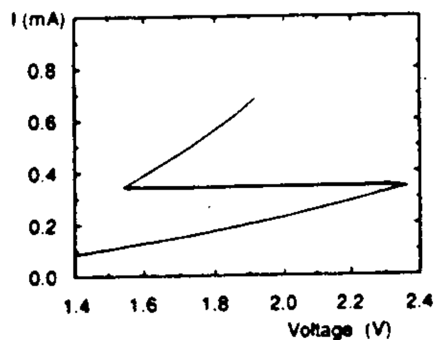

Fig. 6 Room temperature I-V characteristics of a conditioned device under constant current conditions

has a tapered shape, the resulting current flow could be restricted to a very localised area. The device resistance could thus be determined by the contact area where the 'tip' of the modified region and the lower metal electrode are in close proximity. At such distances the resistance might be associated with either a single or a small number of contact atoms [5]. It has been shown theoretically [6] that the resistance associated with a single contact atom reaches saturation with a minimum value given by $R = h/2e^2$ provided that no elastic deformation occurs. This is the 'constriction' resistance ($\approx 12906\,\Omega$) associated with an ideal conduction channel. It should be noted that this quantised resistance value is predicted assuming current flow through a single atomic orbital only. If more orbitals (conduction paths) are available, these would reduce the quantised resistance value. Recent experimental results from Gimzewski and Moller [7] showed a resistance jump in a Scanning Tunnelling Microscope using an Ir tip at a value $R \sim 4\times10^4\,\Omega$, rather larger than that predicted theoretically. In this experiment the tunnelling current is recorded as a function of distance Δz from the conducting surface. The jump occurs at the transition from the tunnelling to the one-atom point contact regime in the STM.

3. CONCLUSIONS

Our measurements show that the resistance of conditioned a-Si:H sandwich structures can be quantised under some circumstances. The voltages at which this occurs correspond to energies that are greatly in excess of the thermal energy kT. Furthermore, the quantised resistance values reflected in the I-V characteristics do not involve *all* possible integer or half integer values. For example in sample C of Fig. 4, the quantisation integer changes from i=4 to i=8, and in sample D the from i=4 to i=6. For these reasons we believe that existing theories [5,6] of quantised resistance associated with ballistic transport are not applicable to our structure. However, the results obtained so far do not appear incompatible with current flow through atomic scale point contacts [5,6,7], and it is possible that this could explain the room temperature quantisation observed.

ACKNOWLEDGMENTS

Financial support from British Telecom plc for some of the work described in this paper is gratefully acknowledged.

REFERENCES

1. M.J. Rose, J. Hajto, P.G. LeComber, S.M. Gage, W.K. Choi, A.J. Snell and A.E. Owen, J. Non-Cryst. Sol., 115, 168 (1989)

2. J. Hajto, A.E. Owen, S.M. Gage, A.J. Snell, P.G. LeComber, and M.J. Rose, Phys. Rev. Lett. 66, 1918 (1991)

3. K.von Klitzing, Rev. Mod. Phys. 58, 519 (1986)

4. D.A. Wharam, M. Pepper, H. Ahmed, J.E.F. Frost, D.G. Hasko, D.C. Peacock, D.A. Ritchie and G.A.C. Jones, J. Phys. C: Sol. St. Phys. 21, L887 (1988)

5. N.D. Lang, Phys.Rev.B, 36, 8173 (1987)

6. A. Martin-Rodero, J.Ferrer and F.Flores, Journ. of Microscopy, 152, 317 (1988) J.Phys.C, 4, 916 (1971)

7. J.K. Gimzewski and R. Moller, Phys.Rev.B, 36, 1284 (1987)

Journal of Non-Crystalline Solids 137&138 (1991) 1257-1262
North-Holland

NON-CRYSTALLINE SOLIDS

Section 25. Memory devices, light emitting, and special diodes

ANALOGUE MEMORY EFFECTS IN METAL/a-Si:H/METAL MEMORY DEVICES

A.J. SNELL,† P.G. LECOMBER,‡ J. HAJTO,† M.J. ROSE,‡ A.E. OWEN† and I.S. OSBORNE‡

‡ Department of Applied Physics and Electronic & Manufacturing Engineering, University of Dundee, Dundee DD1 4HN, Scotland

† Department of Electrical Engineering, University of Edinburgh, Edinburgh EH9 3JL, Scotland

In this paper we present experimental data for Metal/a-Si:H/Metal structures which demonstrate that they can be programmed into a range of non-volatile resistance states between 1 kΩ and 1 MΩ with nanosecond pulses of less than 5 V magnitude. A number of results are presented which show the importance of the top metal in the device operation.

1. INTRODUCTION

Thin homogeneous layers of boron doped (p^+) a-Si:H deposited by plasma enhanced chemical vapour deposition (PECVD) from silane and diborane mixtures at substrate surface temperatures of 250°C, and sandwiched between two metal (M) electrodes, have been shown to exhibit fast electrically programmable digital and analogue memory switching after an initial forming process by means of a moderately high bias [1]. In a recent paper we demonstrated that the top metal plays an important role in determining the memory characteristics of the device [2]. In particular, the resulting switching behaviour is found to be essentially digital for some metals (e.g., Ag, Al, Cr, Mn, Fe) and analogue for others (e.g. W, V, Ni, Co). The forming process has been associated with the creation of a filamentary region of modified material. Imaging with thermochromic liquid crystals and direct observation with an SEM has shown that the diameter of this filamentary region is less than 0.5 μm and X-ray microanalysis has shown that the top metal diffuses into the p^+ layer during the forming process [3]. This paper reviews the basic characteristics of the analogue behaviour - its dependence on the metal contacts and on the test parameters such as pulse height and length. Particular attention is given to the initial forming process, the WRITE and ERASE parameters, and the resistance changes.

2. RESULTS AND DISCUSSION

2.1. Memory Switching

The $M/p^+/M$ memory structures generally exhibit a forming step which is different from the previously investigated M/p^+-n-i/M structures [4]. In the case of M/p^+-n-i/M structures, the resistance suddenly drops from $\sim 10^{10}\,\Omega$ (virgin state) to $\sim 10^3\,\Omega$, after the critical voltage (forming voltage V_F) has been applied. No change in the virgin resistance occurs when the sample is biased with voltages less than V_F. This type of forming is termed *hard forming*. In contrast, the resistance of the unformed $M/p^+/M$ structures can be lowered gradually by applying voltage pulses of progressively increasing magnitude. In this case no sudden change of the current or voltage signal can be detected when the sample is

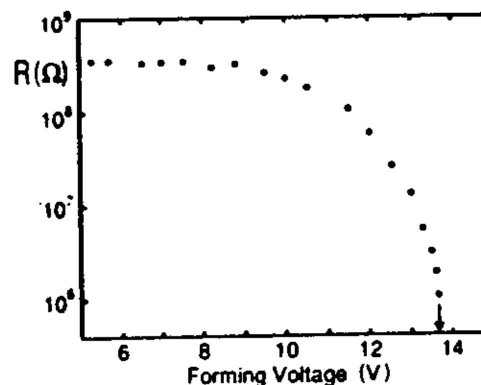

FIG. 1 Resistance of an a-Si:H $Cr/p^+/V$ memory structure as a function of forming voltage

0022-3093/91/$03.50 © 1991 - Elsevier Science Publishers B.V. All rights reserved.

biased with a voltage pulse. This process is called *soft forming*. Fig 1 shows the device resistance as a function of the soft forming voltage (pulse duration =300 nsec). On reaching a critical voltage (~14 V in Fig. 1) the device resistance suddenly drops from ~10^6 Ω to ~10^4 - 10^3 Ω, the memory ON state of the device. Once the device has reached this first (non-volatile) ON state all subsequent switching operations were performed with 10-100 ns pulses 1-5 Volts in magnitude. One striking feature of the devices after forming is the remarkably non-volatile nature of the memory resistance states [5]. For example, the measured ON (1.6 kΩ) and OFF (1.0 MΩ) resistance states of a Cr/p⁺-n-i/Cr device changed by less than 5% over a period of four years. The more recently studied analogue states in Cr/p⁺/V devices appear to be equally stable although to date these have only been measured over a six month period. The devices are also stable with respect to temperature [5]. Devices in the ON- or OFF- state retain their memory state at 180°C for up to 120 hours, and subsequently still show switching at room temperature. With regard to the actual switching operations themselves, these are known to occur at temperatures down to 4 K and up to 430 K without large changes in the WRITE and ERASE voltages [3,5]. A further example of the non-volatile nature of these devices come from radiation experiments [5]. A total of 180 devices were exposed to a flux of 0.508 rad/hour γ-radiation for ten hours. There was no evidence of any resistance changes for this 5 Mrad dose, and the values of the WRITE and ERASE voltages were unchanged to within 7%. CMOS ICs irradiated during the same experiment were completely inoperable. Also, about 30 characterised devices were irradiated by a Cf^{252} source simulating an outer space environment. They received an integrated flux of $2.7x10^5$ cm^{-2} fission particles, $1x10^6$ cm^{-2} neutrons and $3x10^6$ cm^{-2} α-particles. The linear energy transfer for these particles is 43 MeV mg^{-1} cm^{-2}, amounting to 2 MeV cm^{-1} for the a-Si:H devices which were irradiated for 17 hours. Again no resistance changes were found, while a 4k CMOS RAM showed 1500 errors. The extreme non-volatility makes any interpretation of the memory action in terms of charge storage mechanisms or changes in the density of metastable defects extremely unlikely [5].

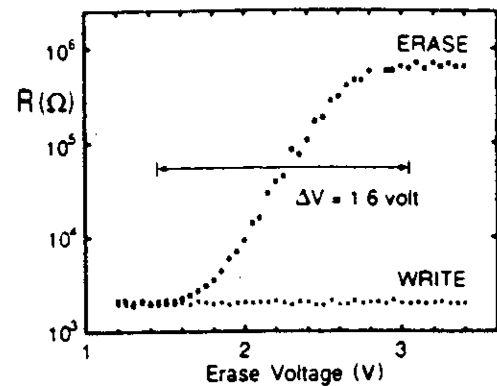

FIG. 2 Memory resistance as a function of ERASE voltage in a Cr/p⁺/V structure

An example of the analogue switching effect is shown in Fig. 2. It is important to emphasize the polarity dependence of the analogue memory behaviour. In the case of the WRITE pulses, positive polarity is applied to the Cr bottom contact while ERASE pulses have opposite polarity. The sample was first switched to an ON state (R_{ON} = $2x10^3$ Ω) and then a series of alternating 100 ns ERASE and WRITE pulses were applied. The WRITE pulses were kept at a constant magnitude of 3.4 V but the ERASE pulses were incremented by 50 mV steps from 1.2 to 3.4 V after each WRITE pulse. It can be seen from Fig. 2 that the sample resistance changes in an analogue manner as the magnitude of the ERASE pulse increases. The sample resistance changes from R~$2x10^3$ Ω to R~$6x10^5$ Ω over a voltage range of ΔV (ERASE) = 1.6 V. The shaded area in Fig. 2 indicates the scatter in the resistance over 100 cycles. Fig. 3 shows another case where the ERASE pulses were maintained at a constant value of V = 3.4 V but the WRITE pulses were incremented from 1.2 V to 3.4 V in 50 mV steps. The value of the OFF state resistance remained constant at ~$6x10^5$ Ω whilst the ON state resistance decreased through a continuum of intermediate states over a similar ΔV to the ERASE

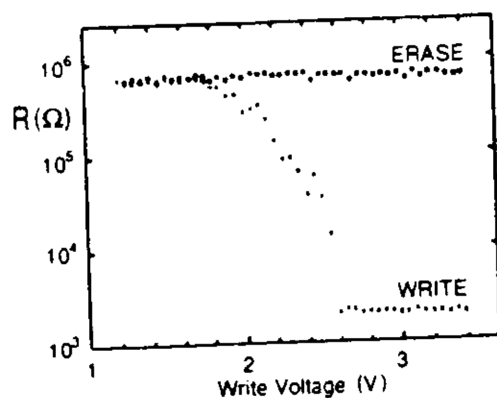

FIG. 3 Memory resistance as a function of WRITE voltage in a Cr/p⁺/V structure

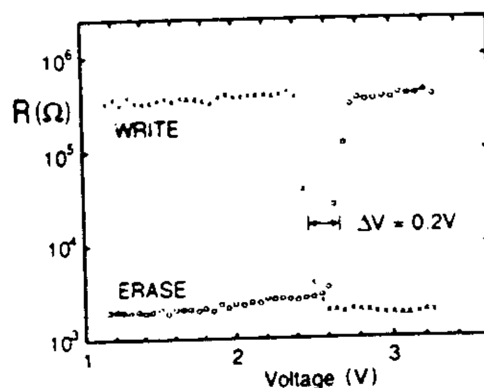

FIG. 4 Memory resistance as a function of WRITE and ERASE voltages in a Cr/p⁺/Cr structure

operation. The shaded area in Fig. 3 again represents the reproducibility of the analogue switching for 100 complete cycles. The device will switch between any two resistance states within the range from about 1 kΩ to 1 MΩ by selecting the correct polarity and the magnitude of the WRITE and ERASE pulses. For all devices with a V top contact, the values of ΔV range from 1.5 V to 2.0 V for both the WRITE and ERASE operations.

We have repeated the above experiments on M/p⁺/M devices with Cr as top metal and observed similar polarity dependent changes in the memory state resistance. However in the WRITE and ERASE experiments intermediate states were found to exist only over a narrow ΔV of about 0.2 V as shown in Fig. 4. Therefore these devices are considered as 'digital' devices. It is important to emphasize that both the analogue (Figs. 2 & 3) and the 'digital' (Fig. 4) memory switching effects are non-volatile. New results also give more evidence for the importance of the top metal. If the top metal, i.e. the vanadium, is removed from an analogue device after forming and replaced with a metal known to give digital behaviour, e.g. chromium, then analogue switching is still observed. To exhibit the central role played by the top metal contact, we fabricated devices with μc-Si:H as the top contact. The I-V characteristics of these are found to be similar to those of the M/a-Si:H/M devices, suggesting good contact is made. However, no forming is observed for the μc-Si:H contact devices, even though currents far in excess of those normally sustained by a-Si:H are measured. This suggests that the filamentary breakdown is initiated at the reverse bias Schottky barrier top contact, presumably by a high-field enhanced migration of metal in the form of atoms or ions. However, if devices are integrated with c-Si FETs, with the FET source contact becoming the bottom contact of the a-Si:H device, then providing metal is used as the top contact switching is again observed, which demonstrates the insensitivity of the device to the type of bottom contact.

The role of the top metal contact has also been investigated by fabricating devices with a range of different top metals but with otherwise identical physical parameters (i.e. ~1000 Å layer of p⁺ a-Si:H, Cr bottom electrode). Using the analogue switching voltage window, ΔV, as a guide, it is found that its value is significantly dependent on the top metal. This is illustrated in Table I. It can be also seen that the definition of 'analogue' (ΔV ≥ 1 V) or 'digital' (≤ 0.5 V) memory switching is somewhat arbitrary, because there is no sharp boundary between the two types of operation. In the cases of Mo and Pd top contacts, volatile switching is observed, whereas for Ti, Au and Cu no reproducible switching can be observed. These results show that the top metal contact plays a crucial role in determining the type of

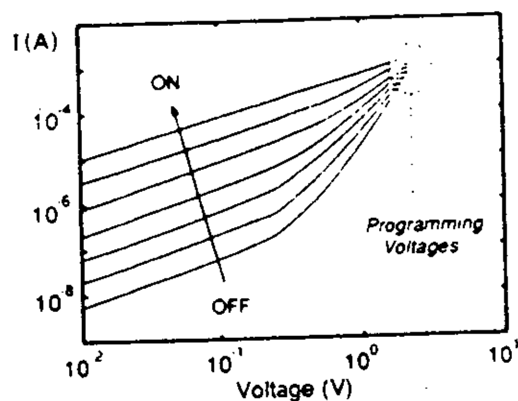

FIG. 5 Current-voltage characteristics of analogue memory states plotted on a log-log scale.

memory switching phenomena observed.

We have demonstrated that a-Si:H memory devices have great sensitivity to the top contact metal, but what of the a-Si:H layer itself? Experiments have been carried out on a range of layers with different doping configurations from SiH_4/B_2H_6 ratios of 0 to 5×10^4 vppm, each 1000Å thick with vanadium top contacts[7]. A systematic decrease in the range of resistances over which soft forming occurs is found on decreasing the doping concentration. The voltage at which the device forms with a discontinuous jump to $3\times10^3\,\Omega$, decreases to a minimum of 8 V for 10^3 vppm, rising to 13 V for 10^4 vppm. The analogue switching range ΔV is also affected by the dopant concentration, systematically decreasing from about 2 V for 10^4 vppm to about 1 V for intrinsic silicon.

In this paper we concentrate on the p^+ memory devices with V top contacts because these show typical non-volatile, analogue memory switching.

2.2. I-V Charcteristics

The current-voltage characteristics of analogue memory resistance states have been investigated both at room temperature and at lower temperatures. It is generally found that the room temperature current-voltage characteristics show a 'linear plus power law' behaviour in the various analogue memory resistance states (seen in Fig. 5). However, a study of the Cr/p^+/V analogue memory device I-V characteristics at low temperatures has shown discontinuities in the current in the form of discrete steps[9]. These occur at values of resistance $R = h/2ie^2$ where i is an integer, i.e. the value of R is quantised. Our most recent results appear to indicate room temperature quantisation, and are discussed in another paper presented at this conference[8].

The I-V curves normally obtained at room temperature can be described by a simple non-linear relationship $I = C_1V + C_2V^n$ where C_1 and C_2 are constants and the exponent n increases with the low bias (linear region) resistance according to the relationship $n = A + B\log R$. In accordance with the pulsed analogue memory switching results, a continuous range of states can be found between the low bias ON ($\sim10^3\,\Omega$) and OFF ($\sim10^8\,\Omega$) states. The terms ON and OFF are somewhat arbitrary therefore, and are used in this paper for practical reasons only. If the curves in Fig. 5 are extrapolated above 1 V, they meet in the region of ~3 - 4 V i.e. at typical programming levels (see Figs. 2,3). It is also found that the exponent n does not depend on the device geometry but it is primarily determined by the low bias (linear region) resistance of the analogue memory state. This indicates that the nature of the electrical conduction is similar in all memory states. However, repeatedly switching the device into the same resistance state does not always result in an

TABLE I. Effect of top metal on switching behaviour

Metal	ΔV (V)	Switching characteristics
Ag, Al	>0.1	digital, non-volatile
Cr	0.2	digital, non-volatile
Mn, Fe	~0.5	digital, non-volatile
Ti	-	unstable switching
Au, Cu	-	no switching
W	~1.0	analogue, non-volatile
V	1.8	analogue, non-volatile
Ni, Co	2.0	analogue, non-volatile
Mo, Pd	2.0	analogue, volatile

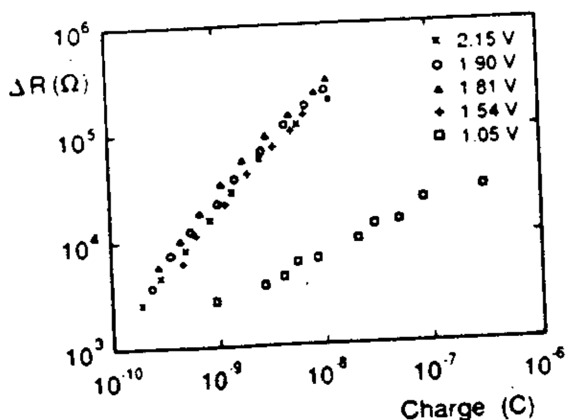

FIG. 6 Resistance change against applied charge

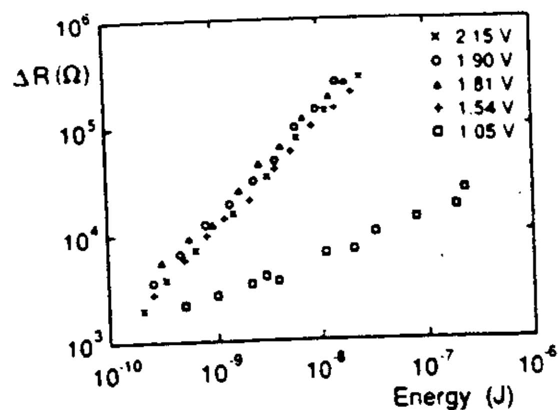

FIG. 7 Resistance change against applied energy

identical value of the exponent. This suggests that the 'same' resistance state can be achieved through different conduction paths within the same device, in accordance with the proposal that the conduction path (filament) might have a structure similar to that of granular metal embedded in an insulating matrix[3].

2.3. The Switching Operation

The switching operations can be analysed in terms of the power, energy and charge required to produce the corresponding resistance changes. To this end, the memory devices were first programmed into a consistent memory ON state ($R_{ON} = 3\times10^3\ \Omega$) then erased using voltage pulses of a range of magnitude and length. Fig. 6 shows the change of resistance ΔR of $Cr/p^+/V$ memory structures as a function of the charge passing through the device during the switching operation. Essentially the same functional dependence is obtained if ΔR is plotted against the energy involved in switching, as in Fig.7. It would appear that except for the lowest voltage investigated, ΔR is approximately proportional to the charge or the switching energy. Furthermore ΔR does not seem to depend strongly on voltage in the range from 1.5 V to 2.2 V, whilst going from 1.0 V to 1.5 V causes a rather dramatic change. Fig. 8 shows ΔR vs. applied power for a number of devices. Comparison of Figs. 6, 7 and 8 suggests a better correlation of ΔR with charge or energy than with power.

The switching transients for the memory operation can be further investigated with emphasis on the polarity dependence. It is found that both WRITE and ERASE operations have a clearly defined polarity dependence, as shown earlier in Figs. 2 and 3. The comparison of single switching transients at the same voltage levels but with opposite polarity reveals interesting features about the resistance changes. Comparing a single switching transient from $R_{OFF} = 2\times10^5\ \Omega$ to $R_{ON} = 3.8\times10^3\ \Omega$ state using a WRITE pulse with a transient from $R_{OFF} = 2\times10^5\ \Omega$ using an pulse of opposite polarity shows no change in the memory resistance in the latter case although similar voltage and current levels are applied. The calculated total charge flowing through the device during these transients is also very similar: $Q_W = 8.5\times10^{-11}$ C for WRITE and $Q_E = 7.3\times10^{-11}$ C for the other polarity. These measurements suggest that the memory switching is not simply controlled by the applied power or energy because these quantities are independent of the polarity.

2.4. Temperature Dependence

The temperature dependence of the device conductance has been investigated for a range of memory states. $Cr/p^+/Cr$ devices were programmed to various resistance states, and the resistance measured as a function of temperature from 298 K to 435 K. The resistance follows the functional form $R = R_0 \exp(E_{act}/kT)$ where it is possible to identify a single activation energy E_{act} for each state. Values of

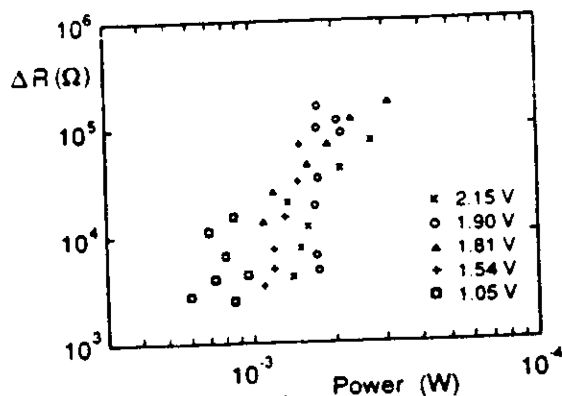

FIG. 8 Resistance change against applied power

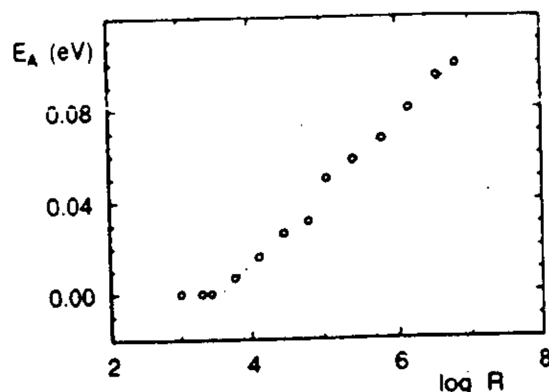

FIG. 9 Activation energy vs. memory state resistance

E_A are plotted against the room temperature resistance for each state in Fig. 9. The activation energy increases continuously from a notional value of ~ kT to ~0.1 eV. Similar values are also found for Cr/p⁺/V devices. This behaviour is consistent with conduction between metallic particles dispersed in an insulating matrix, with the current transport governed primarily by a variable activation energy [9]. Such an interpretation would also be consistent with EDX data on M/p⁺/M films where, after removal of the top contact, a peak corresponding to the top metal is found only in the filamentary region of the pore [3]. Similar results for metal incorporation are found for devices with Cr top contacts.

3. CONCLUSIONS

M/p⁺/M structures can be used as electrically programmable non-volatile memory devices, with a range of voltage addressable intermediate resistance states. In this paper we have presented a range of results which clearly demonstrate the importance of the top metal in determining the detailed behaviour of such devices. Further work aimed at elucidating the precise role of the incorporated metal in the memory operation is in progress.

ACKNOWLEDGEMENTS

The financial support of British Telecom plc for some of the work described in this paper is gratefully acknowledged.

REFERENCES

1. M.J. Rose, J. Hajto, P.G. LeComber, S.M. Gage, W.K. Choi, A.J. Snell and A.E. Owen, J. Non-Cryst. Sol. 115 (1989) 168

2. J. Hajto, A.E. Owen, A.J. Snell, P.G. LeComber and M.J. Rose, Phil. Mag. 63 (1991) 349

3. M.J. Rose, J. Hajto, P.G. LeComber, A.J. Snell, A.E. Owen and I.S. Osborne, Proc. MRS Symp. (1991) 219

4. P.G. LeComber, A.E. Owen, W.E. Spear, J. Hajto, A.J. Snell, W.K. Choi, M.J. Rose and S. Reynolds, J.Non-Cryst. Sol. 77-78 (1985) 1373

5. M.J. Rose, A.J. Snell, P.G. LeComber, A.E. Owen, J. Hajto and J.H. Steven, to be published.

6. J. Hajto, A.E. Owen, S.M. Gage, A.J. Snell, P.G. LeComber and M.J. Rose, Phys. Rev. Lett. 66 (1991) 1918

7. I.S. Osborne, A.E. Owen, M.J. Rose, A.J. Snell, P.G. LeComber and J.Hajto, to be published.

8. J. Hajto, M.J. Rose, A.J. Snell, I.S. Osborne, A.E. Owen and P.G. LeComber, this conference.

9. Moser A. and Rohrer H. Sol. State Comm. 17 (1975) 939

AMORPHOUS SILICON ANALOGUE MEMORY ELEMENTS

M.J. ROSE*, J. HAJTO+, P.G. LeCOMBER*, A.J. SNELL+, A.E. OWEN+ and J.S. OSBORNE*
*University of Dundee, Dundee, Scotland, U.K.
+University of Edinburgh, Edinburgh, Scotland, U.K.

ABSTRACT

Both $Cr/p^+/V$ and $Cr/p^+/Cr$ devices exhibit fast electrically programmable memory switching with a programmable voltage range, ΔV_s, which depends only on the choice of the top metal. Despite a difference in ΔV_s, both types of device have very similar electrical properties, but show one major difference in room temperature I-V characteristics, where under certain conditions, discontinuities are observed.

INTRODUCTION

In a previous paper [1] we reported that metal/p^+-a-Si:H/metal ($M/p^+/M$) structures show a polarity dependent programmable analogue memory effect. A range of stable intermediate resistance states is found and the voltage range, ΔV_s, over which the device is programmable, is determined by the nature of the top metal contact. If the configuration is $Cr/p^+/V$, the voltage range for programming these addressable resistance states ΔV_s is ~2V. If $Cr/p^+/Cr$ devices are used, ΔV_s is found to be ~0.5V. The devices are first formed by a high field pulse and subsequent conduction is by a current filament [2], with metal from the top contact dispersed in the filamentary region. In this paper we report new measurements on $Cr/p^+/V$ and $Cr/p^+/Cr$ devices showing them to have many similarities and one major difference.

$Cr/p^+/V$ devices, when programmed to an ON-state and measured at temperatures between 4K and 190K, exhibit I-V characteristics with a step-like structure in the current which is associated with quantised resistance values of $R = h/2ie^2$, where i is an integer (h is Planck's constant and the e elementary electronic charge), suggesting quantum confinement for the electron flow [3]. These jumps subsequently split to $(i + \frac{1}{2})$ values in the presence of a magnetic field. Further measurements on quantum transport in these devices have been made and we find that there may be evidence for quantised resistance even at room temperature, with the room temperature I-V characteristics showing structure similar to those measured at low temperature. These are implicitly associated with a current-controlled negative-differential resistance (CCNDR), the type associated with filaments and threshold type switching. In contrast, $Cr/p^+/Cr$ devices do not exhibit these step-like characteristics.

EXPERIMENTAL METHODS

The devices used in this work were $Cr/p^+/Cr$ or $Cr/p^+/V$ structures. The a-Si:H for these was prepared from the gas phase by the R.F. glow discharge decomposition of SiH_4 with 10^4 vppm of B_2H_6 at 300°C, to a thickness of

1000Å. From these layers 10 μm "pore" structures were prepared as described previously [3]. Devices were electrically formed by the application to the top contact of 300 ns pulses whose magnitude was gradually increased up to 12V, inducing a gradual change in resistance from the initial $10^9\Omega$ to a $10^3\Omega$ ON-state. The formed samples were bonded into chip carriers. Devices are subsequently switched using 10 ns or 100 ns pulses, +ve to the bottom contact to WRITE, and -ve to the bottom contact to ERASE. I-V measurements were taken using an HP 4145B semiconductor parameter analyser.

RESULTS AND DISCUSSION

(i) Analogue Behaviour

Both $Cr/p^+/Cr$ and $Cr/p^+/V$ devices operate as electrically programmable non-volatile memory devices, with a range of voltage addressable intermediate states, but of these two, only $Cr/p^+/V$ devices have a useful programmable range ΔV_s of ~2V. As in previous experiments, a range of top metal contacts were tried giving values of ΔV_s of 0.5 - 2V, but there is no obvious correlation between the properties of the metal and the subsequent programmable range. However, despite the difference in the programmable range ΔV_s, there are many similarities between the devices in switching and I-V characteristics, in their non-volatility and in the effects of temperature and the mechanism of switching must be largely the same in each case.

Temperature dependence

A number of $Cr/p^+/Cr$ devices were programmed to various resistance states and the change in resistance with increasing temperature measured in the range from 298K to 435K. The results for a typical sample are shown in Fig.1. The states near the $10^3\Omega$ ON-state show little sensitivity to

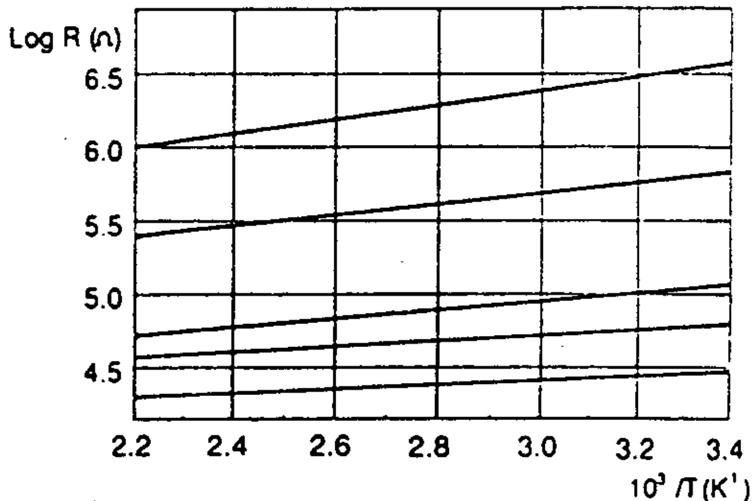

Fig.1 Log resistance state vs. 1/T for different memory states

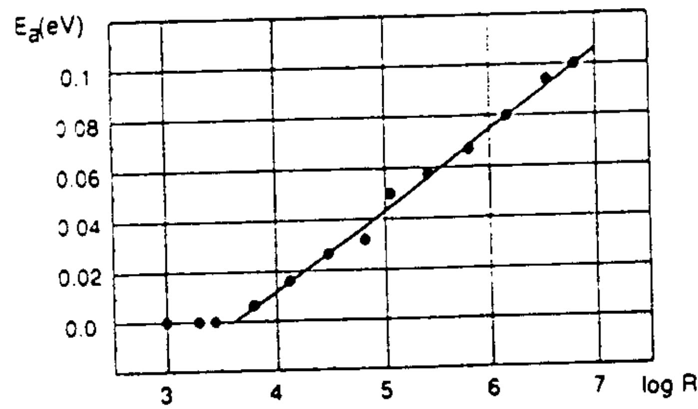

Fig.2 Activation energy vs. memory state resistance

temperature, but become increasingly more activated as the resistance state is increased towards the $10^6\Omega$ OFF-state. Each stable state follows the functional form

$$R = R_o \exp\left[\varepsilon_{act}/kT \right]$$

where it is possible to identify a single activation energy ε_{act} for each state, and this value, plotted against the room temperature resistance for each state, is shown in Fig.2. It is found that the activation energy increases continuously from a notional activation energy $\leq$ kT to the unformed device value.

Similar results are also found for $Cr/p^+/V$ devices. This behaviour is consistent with conduction between metallic-like particles dispersed in an insulating matrix with the current transport governed by a variable activation energy [4]. Such an interpretation would also be consistent with EDX data on $M/p^+/M$ films where (in accordance with published data [2] for M/p^+-n-i/M devices) a peak corresponding to top metal material is found in the filamentary region of the pore, after removal of the top contact, and nowhere else in the device. This is shown in Figs.3(a) and (b) for a $Cr/p^+/V$ device. Similar results for metal incorporation are found for devices with Cr top contacts.

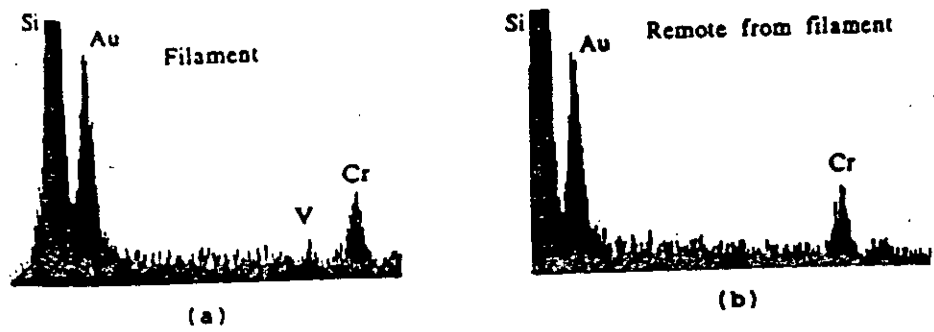

Fig.3(a) EDX data from filament, and (b) remote from filament

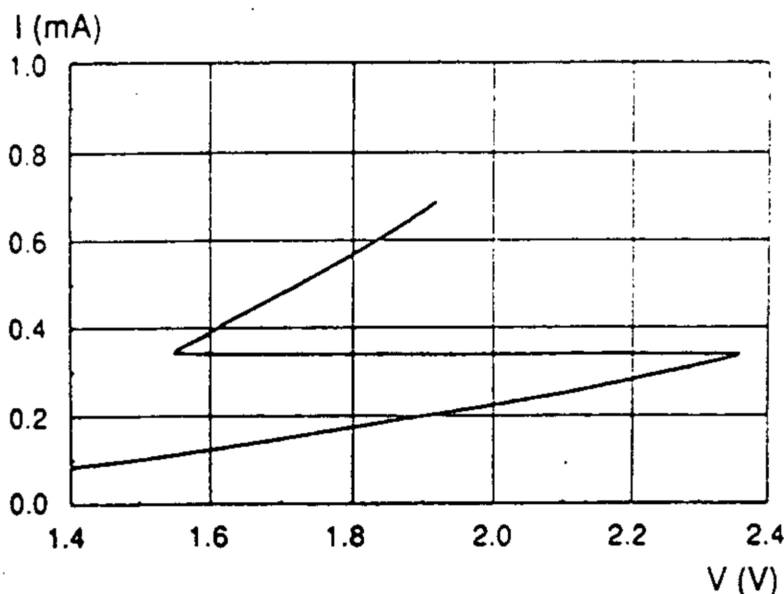

Fig. 4 Room temperature I-V characteristic of a formed $Cr/p^+/V$ device under constant current conditions

(ii) Quantised Behaviour

A study of the analogue device I-V characteristics in the temperature range from 4.2K to 190K has shown discontinuities or jumps in the current in the form of discrete steps. These jumps in current occur at values of resistance $R = h/2ie^2$, where i is an integer, i.e. the value of R is quantised. Furthermore, the values of R take on $(i + \frac{1}{2})$ values in the presence of a 0.2 Tesla magnetic field orientated, somewhat arbitrarily, at 30° with respect to the current direction.

These effects have been attributed to the breakdown of a tunnel barrier and subsequent transport in one dimensional (1-D) channels or subbands, where the transit time is small compared to the scattering time [5]. The subbands move through the Fermi level (or vice versa) in response to dimensional changes in the channel or by changes in the injected electron density induced by the applied voltage.

In a number of recent experiments we have extended these measurements to higher temperatures. Fig.4 shows a room temperature I-V characteristic of a formed $Cr/p^+/V$ device under forward bias and measured under conditions of constant current. This is a characteristic typical of filamentary conduction showing two regimes separated by a large region of current controlled negative differential resistance. This is a threshold switching characteristic typical of many different types of devices, for example, forward biased MISS type devices which operate by a "punch through" or avalanche mechanism [6], or chalcogenide thin film devices which have a trap limited mobility in the OFF state, and an enhanced mobility in the ON state after field-induced carrier generation neutralises the trapping centres [7]. Some vanadium oxide thin film compounds also show this behaviour [8].

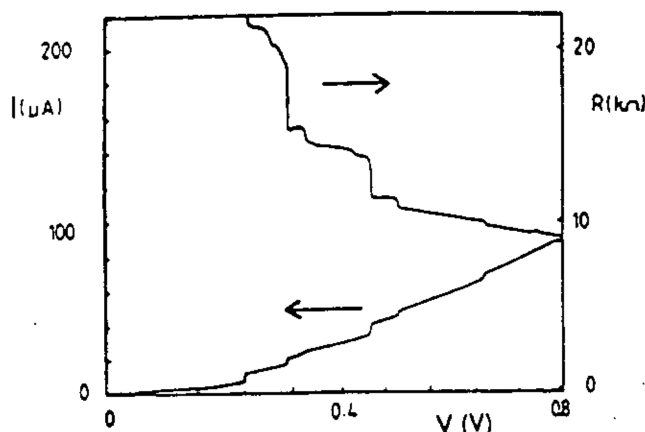

Fig.5 Room temperature I-V, R-V characteristics under constant voltage conditions

However, consider now the room temperature I-V and R-V characteristic measured under constant voltage conditions and shown in Fig.5 for a device in a 10kΩ (at 0.5V) "ON"-state. In agreement with the low temperature observations, the device has a relatively large resistance at low bias. The barrier to current flow breaks down, in this case at 0.242V. Increasing the applied voltage above this value leads to further structure in the I-V and R-V plots. These occur at 0.311V, 0.454V, 0.504V and 0.656V. After subtraction of a series resistance of 6.7 kΩ, the start or bottom of these jumps in the I-V characteristics has a value of resistance $R = h/2ie^2$ for i = 1, 2, 3 and 4, which would imply that the resistance may be quantised at room temperature! Observations of this behaviour can be consistently made with jumps in the I-V characteristics corresponding to $R = h/2ie^2$ to within 1% in each case.

Consider again the threshold-like instability of Fig.4. The jump in current occurs at R = 6.47 kΩ to R = 4.27 kΩ. This would correspond to a jump from i = 2 to i = 3.

It should be noted that these effects are only observed for $Cr/p^+/V$ devices and have never been seen in $Cr/p^+/Cr$ devices at any temperature. This again indicates the influence of the top contact metal on device operation. Both types of device show filamentary conduction with current transport which may be interpreted as being associated with tunnelling, and both show a range of analogue resistance states with similar properties. To find structure in low temperature I-V characteristics related to a quantised resistance in a film that is originally amorphous is somewhat surprising. However, to see such effects at room temperature is even more extraordinary. We cannot exclude the possibility that the effect is not quantisation and that the close agreement between the R values and those given by $R = h/2ie^2$ are mere coincidence, and may for example be related to multiple filament formation However, in the devices measured to date, the values of R obtained agree with the predicted quantised values usually within 1 or 2%. Also the room temperature I-V characteristics bear a remarkably close resemblance to those measured at low temperature where the action of a magnetic field in producing steps corresponding to $(i + \frac{1}{2})$ is further evidence for quantisation. The effects described above may be associated with the small dimensions of the filament and intergrain distances but clearly the choice of metal for the top contact plays a significant role in determining the presence or otherwise of quantisation. It seems likely that the choice of V

for the top contact produces during forming a filament of significantly smaller dimension than that obtained with a Cr top electrode device. Although both subsequently show analogue memory switching, only the V filament is sufficiently small to exhibit one-dimensional quantised behaviour.

CONCLUSIONS

Further measurements on $Cr/p^+/V$ and $Cr/p^+/Cr$ devices have been made and many similarities are found in their switching characteristics, implying similar current transport processes. The major difference is that jumps in the I-V characteristics occur at resistance values corresponding to $h/2ie^2$, for the $Cr/p^+/V$ devices, even at room temperature, whereas no such behaviour has been seen for $Cr/p^+/Cr$ devices. It is proposed that this is a consequence of the different sizes of the current filaments produced during the forming process. Further work is in progress to establish the exact nature of the I-V steps, and the role of the metal contact.

ACKNOWLEDGEMENTS

We would like to thank Mr S. Anthony and Mr D. Williams for their technical assistance, and Dr A.G. Fitzgerald for EDX analysis. The financial support of British Petroleum for some of the work described in this paper is gratefully acknowledged.

REFERENCES

1. M.J. Rose, J. Hajto, P.G. LeComber, S.M. Gage, W.K. Choi, A.J.Snell and A.E. Owen, J. Non-Cryst. Solids 115, 168 (1989).

2. P.G. LeComber, A.E. Owen, W.E. Spear, J. Hajto, A.J. Snell, W.K. Choi, M.J. Rose and S. Reynolds, J. Non-Cryst. Solids 77/78, 1378 (1985).

3. J. Hajto, A.E. Owen, S.M. Gage, A.J. Snell, P.G. LeComber and M.J. Rose, Phys. Rev. Lett. 66, No. 14, 1918 (1991).

4. A. Moser and H. Rohrer, Solid State Comm. 17, 939-943 (1975).

5. J. Hajto, A.E. Owen, A.J. Snell, P.G. LeComber and M.J. Rose, Phil. Mag. B. 61, No. 1, 349-369 (1991).

6. J.G. Simmons and A. El-Badry, Solid State Electronics, Pergamon Press, Vol. 20, pp.954-961 (1977).

7. D. Adler, M.K. Henish and N.F. Mott, Rev. Mod. Phys. 50, 209 (1978).

8. J.K. Higgins, B.K. Temple and J.E. Lewis, J. Non-Cryst. Solids 23, 187-215 (1977).

INT. J. ELECTRONICS, 1992, VOL. 73, NO. 5, 897-906

Switching in amorphous devices

A. E. OWEN†, P. G. LE COMBER‡, J. HAJTO†, M. J. ROSE‡ and A. J. SNELL†

Electrical switching of a kind can be observed in a great variety of materials in many different forms and structures. Much the most reproducible switching is observed, however, in small and geometrically well-defined devices fabricated from thin films of certain amorphous semiconductors. This paper is concerned with such devices. The general features of electrical switching are first reviewed, followed by a more detailed account of recent work in the authors' own laboratories on digital and analogue switching in hydrogenated amorphous silicon.

1. Introduction

Electronic switching in amorphous thin films can be divided into two general categories:

(*a*) threshold switching; in which continuous electrical power is required to maintain the highly conducting ON state; and
(*b*) memory switching; in which both ON and OFF states can be maintained without electrical power.

It is common to describe the switching phenomena in terms of ON and OFF states, but as we will show in § 5.2, switching devices are not always rigidly bistable in their operation, i.e. they are not always 'digital' devices. In some cases, a continuous range of intermediate states is observed between the ON and OFF states, giving an 'analogue' memory effect.

The speed of switching transients varies from device to device and covers a range from <10 ns to >1 ms. The actual switching is usually extremely fast (nanoseconds), but is preceded near the threshold, by a delay time typically of the order of microseconds to milliseconds.

2. The forming process: a precursor to memory switching

Newly fabricated devices rarely show threshold or memory switching effects without an initial modification of their 'as-deposited' structure, a process which is usually called 'forming'. Forming is achieved by the application of suitable voltage pulses which are always higher in magnitude than the subsequent 'programming' pulses. This invariably produces an irreversible change in the characteristics of a device, often with a substantial decrease in the overall terminal resistance.

The processes involved in forming depend on the nature and quality of the thin film, the geometrical structure of the device and, in some cases, the electrode material. The changes can be either structural, involving a movement of material from one part of the device to another, or they can be electronic, wherein a quasi-

† Department of Electrical Engineering, University of Edinburgh, Edinburgh EH9 3JL, U.K.

‡ Department of Applied Physics and Electronic & Manufacturing Engineering, University of Dundee, Dundee DD1 4HN, U.K.

0020-7217/92 $3.00 © 1992 Taylor & Francis Ltd.

permanent change in the occupancy of some electronic states takes place. The changes can occur throughout the bulk of the film or in a localized region. The most common localized effect is the formation of a filament of highly conducting material that extends completely or part way through the device. Such permanent filament formation is a consequence of temporary filamentary breakdown, often observed in metal-insulator-metal and metal-semiconductor-metal sandwich structures under double injection conditions (Ridley 1963), Barnett and Milnes (1966).

In the case of amorphous thin film structures, however, the development of the filament during the forming process is usually accompanied by an irreversible modification of the original structure. This means that the filament, or part of the filament, is permanently 'written in' to the original uniform amorphous structure. Permanent filament formation can occur via crystallization of an amorphous film (Ovshinsky and Fitzsche 1973), stoichiometric changes (Manhart 1973), diffusion of the electrode material into the film (Gibbons and Beadle 1964), or ionization of deep traps (Simhony and Williams 1969). All of these changes usually refer to a localized modification of the structure in the area of the filament. Reports of bulk forming effects are much rarer, one example being bulk diffusion of electrode material into the film (Madams *et al.* 1974).

The modification of the initial structure during the forming process is the most important factor determining the subsequent switching operation. This is because, in most cases, forming creates a 'new device' within the original structure, the characteristics of which determine the ensuing threshold or memory switching operation. For example, a permanent filament may have a cross-sectional area many times less than the original device area, but its effective conductance is often so much higher than that of the surrounding uniform material that it becomes the dominant conducting path.

It is important to emphasize that in both threshold- and memory-type devices, the initial switching mechanism appears to be the same (Owen and Robertson 1973). It is initiated by field-dependent non-ohmic conductivity and a consequent instability. Whether what follows is threshold switching, memory switching or, in some cases, destructive electrical breakdown depends upon the properties of the material and on the presence or absence of suitable feedback in the system.

3. The mechanism of threshold switching

The detailed current-voltage characteristics of chalcogenide glass threshold switching devices have been widely investigated since the original publication by Ovshinsky (1968) and a general survey of the most significant results has been provided by Adler *et al.* (1978). The suggested physical models can be divided into two categories; the first assumes that the threshold switching is due to thermal processes (Warren 1973), and the second regards it as purely an electronic phenomenon (Henisch *et al.* 1970, Lucas 1971). The thermal, or more generally, a combined thermal and electrical mechanism, dependent only on the thermal and electrical bulk properties of the amorphous semiconducting material, is sufficient to explain most aspects of threshold switching.

Several authors have proposed alternative non-thermal, electronic models for creating conditions of instability leading to switching. One of the most frequently used models is based on double injection with recombination in which, in the ON state, carriers are injected at both electrodes giving rise to a high density of carriers

in the valence and conduction bands. In this case the energy input is either stored in the dielectric as injected charge Q_{inj} or is lost through recombination. A qualitative explanation along the above lines was suggested first by Henisch *et al.* (1971). Similar, more quantitative models have also been proposed by Lucas (1971) and Mott (1971).

There is no doubt, in fact, that there are significant non-thermal (isothermal) electronic effects causing non-ohmic conduction in the pre-switching region of chalcogenide glass switches. A comparative study of their relative importance has been given by Owen and Robertson (1973) and Adler *et al.* (1978). The main point of discussion has been to what extent switching can be attributed to thermal or electronic processes and that depends on a variety of factors including, crucially, the film thickness. For example, Kolomiets *et al.* (1969) have shown, experimentally, that in relatively thick films ($>8\,\mu m$) of chalcogenide glasses, the breakdown field is proportional to the inverse of thickness and has a strong temperature dependence. Stocker *et al.* (1970) have developed a quantitative model for threshold switching based on a thermal consideration only (i.e. no field dependence of conductivity) and they show that the switching behaviour of such thick films, as observed by Kolomiets *et al.*, can be adequately described by the simplest thermal model involving ohmic conduction and Joule heating. In thinner chalcogenide films however ($<8\,\mu m$) Kolomiets *et al.* found that the breakdown field is independent of thickness and only weakly dependent on temperature. These features cannot be explained by simple thermal models and it is necessary to invoke electronic processes. Even so, it is likely that electrothermal models in which pre-breakdown non-ohmic conduction processes increase the rate at which energy is delivered to the device can still describe most aspects of threshold switching, at least semi-quantitatively (Owen *et al.* 1979).

4. Mechanisms for memory switching

For memory switching the active material must be capable of changing in some way (e.g. an overall or localized change in the electronic, atomic or microscopic structure) into a permanent conducting state, but one that can be reversed to the OFF state by a suitable current (energy) pulse. Obviously, the system must also be able to absorb the reversing pulse without destructive breakdown. The suggested models for memory switching can therefore be divided into two broad categories; electronic or structural. The former is based on the long term storage of charge (i.e. without any major structural modification) to account for the non-volatile nature of the switch.

The most commonly proposed charge storage sites are traps, either in the bulk or at an interface between two dissimilar materials. The necessary characteristics of such traps is that they have a release time comparable to the retention time of the memory which may range from a few hours to many years.

On the other hand, memory switching in chalcogenide glass devices depends upon a structural rearrangement. During the initial forming pulses a filament of material crystallizes in the amorphous structure (Ovshinsky and Fritzsche 1973); this normally happens near the centre of the device where the highest temperatures are attained. This modified material has a higher conductivity than the bulk and therefore becomes the preferred current path during subsequent voltage pulses. In the erase operation (i.e. to switch from the ON to OFF state) large voltage pulses

with steep trailing edges are applied, melting the crystalline filament and causing it to solidify in an amorphous form. To write in again (i.e. to switch from the OFF to ON state) pulses with more gradual trailing edges are used, also melting the filament but allowing the material to solidify in a crystalline form.

5. Electrical switching in amorphous silicon structures

5.1. *Background*

The earliest reports of switching in amorphous silicon (a-Si) were published in 1970 by Feldman and Moorjani (1970) and Moorjani and Feldman (1970), contemporaneously with some of the early literature on switching in chalcogenide glasses. More detailed experiments on the same structures were reported later by Feldman and Charles (1974) and Charles and Feldman (1975). These authors studied vacuum evaporated films of a-Si in the range of 0·3–2·0 μm thick, fitted with titanium electrodes. As threshold devices, these a-Si structures had threshold voltages V_{th} of 5–10 V, OFF state resistances in the range of 1–30 kΩ, an ON resistance of about 100 Ω, and there was also some tentative indication of memory switching but that feature was not substantiated.

The work of Feldman and his colleagues was the only investigation of switching in a-Si until the later studies of Dey and Fong (1979) and Dey (1980). These authors report results very similar to those of Feldman *et al.* (1970). They studied thin films of a-Si in the range 0·3–1·5 μm thick, deposited by electron-beam heating in a vacuum evaporator. Titanium contacts were again used, either in the form of evaporated films or as probes. Dey and Fong (1979) reported only threshold switching; they did not mention any evidence for memory behaviour. In contrast to Feldman *et al.* however, Dey and Fong did observe forming effects; that is, the initial threshold voltage was relatively large but it decreased to a more or less constant value after a number of switching cycles. It should be noted that both Feldman and Charles (1974) and Dey and Fong used a-Si films deposited by vacuum evaporation. This probably accounts for the relatively low OFF state resistances which they both found ($\approx$ 100 kΩ). It is now well established that vacuum-evaporated a-Si is a very different material from the hydrogenated form of a-Si obtained, for example, by glow-discharge deposition of silane (e.g. Spear and Le Comber 1976).

Three papers concerned specifically with switching in *hydrogenated* amorphous silicon (a-Si:H), by Gabriel and Adler (1982), den Boer (1982) and Owen *et al.* (1982), appeared almost concurrently early in 1982, each reporting very different effects observed in different amorphous silicon structures. Our own work (Le Comber *et al.* 1984, Le Comber *et al.* 1985, Choi *et al.* 1987, Rose *et al.* 1989, Hajto *et al.* 1990), including recent results, is described in the following sections.

Den Boer studied n^+-i-n^+ structures of a-Si:H prepared by the glow discharge decomposition of SiH_4 ('i' stands for near-intrinsic or undoped material). The n^+ layers were 0·05 μm thick and prepared by adding 1% PH_3 to the SiH_4 gas flow; the i layer in different devices ranged in thickness from 2·5 to 5 μm. Den Boer found that the n^+-i-n^+ devices functioned as threshold switching devices with non-polar characteristics. For the first switching cycle the threshold voltage was in the range 40–100 V, but for all subsequent operations it was only 10–35 V depending on the i layer thickness (as the i layer thickness increased the threshold voltage also increased). The OFF state resistance of the n^+-i-n^+ devices was about 1 MΩ, and the ON state resistance was about 1 kΩ.

Gabriel and Adler (1982) prepared their films by sputtering from a polycrystalline silicon target in an argon-hydrogen plasma. In all cases their devices were notionally homogeneous thin films of intrinsic a-Si:H with molybdenum contacts. The samples were fabricted under a wide range of deposition conditions in two sputtering systems, and although results from some of the devices were rendered rather doubtful because of contamination problems, in no case did Gabriel and Adler observe any evidence of reversible switching.

5.2. *Digital and analogue memory switching in a-Si:H devices*

Work in the authors' laboratories has concentrated on two basic structures utilizing a-Si:H:

(i) Cr-p^+-n-i-M; and simple

(ii) Cr-p^+-M devices.

In both cases the devices are fabricated in small arrays on Corning 7059 glass substrates in a 'pore' structure with the diameter of the pore varying from $\approx 10\,\mu m$ to $\approx 250\,\mu m$ in individual switches. The Cr bottom contact is immediately adjacent to the substrate and a variety of metals has been used for the top contact M. The total thickness of the a-Si:H layer(s) is $\approx 0{\cdot}1\,\mu m$.

The Cr-p^+-n-i-M amorphous silicon devices exhibit extremely fast, non-volatile, polarity dependent digital memory switching phenomena (Le Comber *et al.* 1985) after initial conditioning by means of a moderately high applied potential ('forming'). The most important result to emerge on formed devices is that in the ON state the current is carried by a highly conducting filament which is less than 1 µm in diameter. Filamentation has been demonstrated by experiments on the ON state resistance as a function of area (R_{ON} is independent of area), by thermal imaging techniques with liquid crystals and by direct observation with a scanning electron microscope combined with microanalysis. The latter indicated that the formation of the current filament may be associated with diffusion of the top metal contact into the amorphous silicon resulting in a region of intermingled metal and silicon.

The Cr-p^+-M memory devices exhibit a forming step which is quite different from the Cr-p^+-n-i-M structures (Le Comber *et al.* 1985) and the differences are demonstrated in Figs 1 and 2. In the case of Cr-p^+-n-i-M structures, the resistance suddenly drops from $\approx 10^{10}\,\Omega$ (virgin state) to $\approx 10^3\,\Omega$, after the critical voltage (forming voltage V_F) has been applied. No change in the virgin resistance occurs when the sample is biased with voltages less than V_F. This type of forming is termed *hard forming*. By contrast, the resistance of the unformed Cr-p^+-M structures can be lowered gradually by applying voltage levels with progressively increasing magnitudes. In this case no sudden change of the current or voltage signal can be detected when the sample is biased with a voltage pulse, as seen in Fig. 2. This process is called *soft forming*. On reaching a critical voltage (≈ 14 V) the device resistance suddenly drops from $\approx 10^6$ to $\approx 10^4$-$10^3\,\Omega$. This is the memory ON state of the device. Once the memory device had reached its first (non-volatile) ON state all subsequent switching operations are performed with 10-100 ns pulses 1-5 V in magnitude.

An example of the analogue switching effect for a device with a vandium (V) top contact is shown in Fig. 3, where the sample resistance is plotted as a function of

applied alternating WRITE and ERASE pulse (100 ns pulse duration each). It is important to emphasize the polarity dependence of the analogue memory behaviour. In the case of the WRITE pulses, positive polarity is applied to the Cr track (bottom contact) while ERASE pulses have opposite polarity. The sample was first switched to an ON state ($R_{ON} = 2 \times 10^3\,\Omega$) and then a series of alternating WRITE and ERASE pulses were applied. The WRITE pulses were kept at a constant magnitude of 3·4 V but the ERASE pulses were incremented by 0·05 V steps from 1·2 to 3·4 V after each WRITE pulse. It can be seen from Fig. 3 that the sample resistance changes in an analogue manner as the magnitude of the ERASE pulse increases. A voltage range of ΔV (ERASE) = 1·6 V resulted in a change in resistance from $R \approx 2 \times 10^3\,\Omega$ to $R \approx 6 \times 15^5\,\Omega$. The reverse operation can also be readily carried out, i.e. maintaining a constant ERASE voltage and increasing the voltage of WRITE pulses to write in an analogue fashion. Typical devices will switch between any two resistance states within the range from about 1 kΩ to 1 MΩ by selecting the correct polarity and the magnitude of the WRITE and ERASE pulses. For all devices with a V top contact, the values of ΔV range from 1·5 V for both the WRITE and ERASE operations.

The above experiments have been repeated on Cr-p$^+$-M devices with Cr as the top metal and similar polarity dependent changes in the memory state resistance were observed. However, in the WRITE and ERASE experiments intermediate states were found to exist only over a narrow ΔV of about 0·2 V. Therefore, these devices are considered as 'digital' devices. It is important to emphasize that both the analogue and the 'digital' memory switching effects are non-volatile. Devices set to ON or OFF states have been monitored over two years without any significant change in their resistance. Also, operation at temperatures up to 160°C shows little change in the threshold voltages or in the device stability. However, it is also found that devices with certain top metal contacts such as Mo and Pd show a volatile memory switching effect; the current signal decays rapidly after the end of the

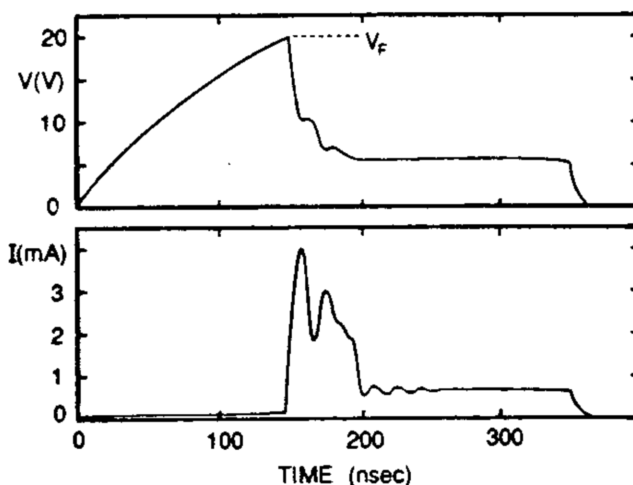

Figure 1. Waveforms of a single forming pulse applied to an amorphous silicon Cr-p$^+$-n-i-Al structure showing 'hard forming'; V and I represent the voltage across the device and the corresponding device current respectively.

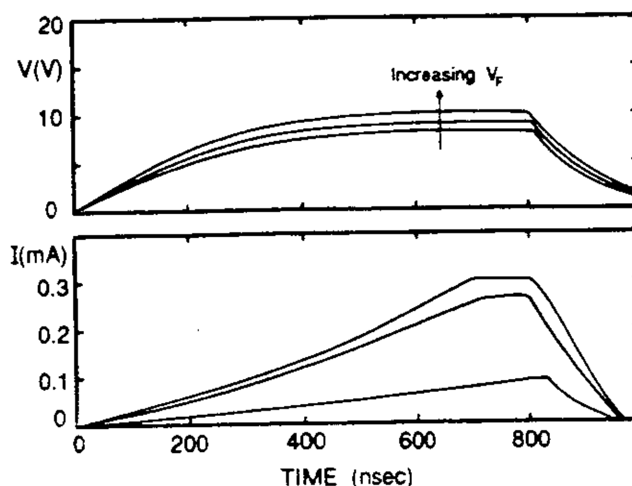

Figure 2. Waveforms of single pulses of increasing magnitude applied to an amorphous silicon Cr-p$^+$-V structure showing 'soft forming'; V and I represent the voltage across the device and the corresponding device current.

programming pulse. The role of the top metal contact has therefore been thoroughly investigated by fabricating devices with a range of different top metals but with otherwise identical physical parameters (i.e. ~1000 Å thickness of p$^+$ layer, Cr bottom electrode). Using the analogue switching voltage window, ΔV, as a guide, it is found that its value is significantly dependent on the top metallization contact, as given in the Table.

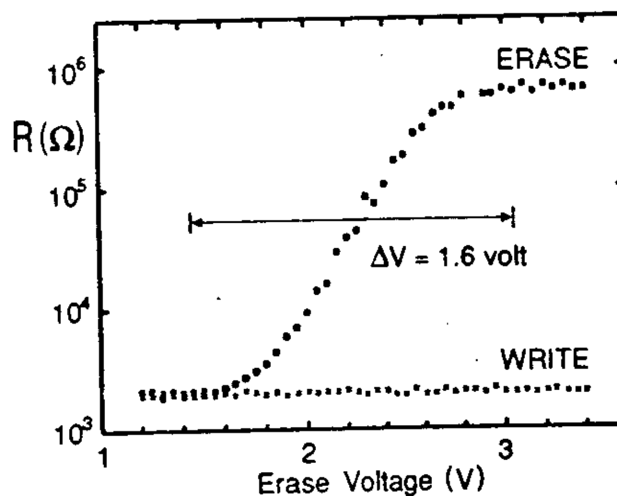

Figure 3. Memory resistance as a function of ERASE voltage in a Cr-p$^+$-V analogue memory switching device. The shading indicates the reproducibility of switching over 100 complete WRITE/ERASE cycles.

Metal	ΔV (V)	Switching characteristics
Ag	>0·1	Digital, non-volatile
Al	>0·1	Digital, non-volatile
Cr	0·2	Digital, non-volatile
Mn	~0·5	Digital, non-volatile
Fe	~0·5	Digital, non-volatile
Ti	—	Unstable switching
Au	—	No switching
Cu	—	No switching
W	~1·0	Analogue, non-volatile
V	1·8	Analogue, non-volatile
Ni	2·0	Analogue, non-volatile
Co	2·0	Analogue, non-volatile
Mo	2·0	Analogue, volatile
Pd	2·0	Analogue, volatile

Effect of top metallization on the switching behaviour.

It can also be seen that the definition of 'analogue' ($\Delta V \geq 1$ V) or 'digital' ($\leq 0{\cdot}5$ V) memory switching is somewhat arbitrary; there is no sharp boundary between the two types of operation and they are possibly associated with the same underlying physical phenomena. However, in the cases of Mo and Pd top contacts volatile switching occurs and in the cases of Ti, Au and Cu no reproducible switching effects can be observed. The top metal contact clearly plays a crucial role in determining the type of memory switching phenomena.

Typical static current-voltage (I-V) characteristics for a *formed* p^+-n-i device, with Al as the top contact, are shown in Fig. 4. Again, notice the polarity

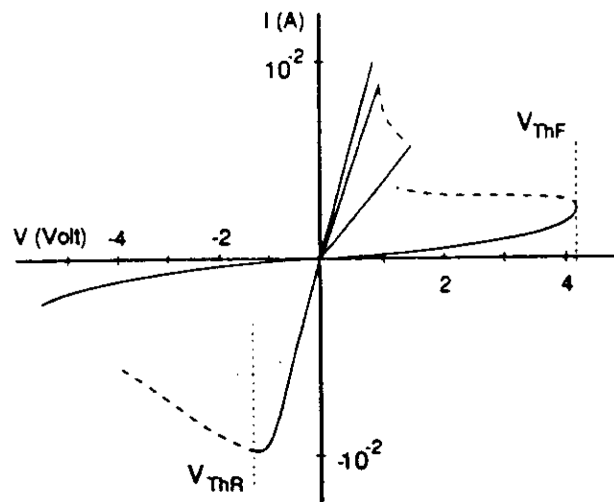

Figure 4. Current-voltage characteristics of a Cr-p^+-n-i-Al digital memory switching device.

dependence; the top right-hand (forward) quadrant corresponds to positive polarity applied to the Cr bottom contact. In the forward direction the device switches from OFF to ON (i.e. the WRITE operation) at a d.c. threshold voltage of just over 4 V. In Fig. 4 there are one or two intermediate states before the final ON-state is reached but the WRITE operation is essentially digital. To ERASE, a negative voltage of $\approx 1{\cdot}5$ V must be applied to the Cr bottom contact and the device reverts to its OFF state. The ERASE operation in p^+-n-i devices has always been observed to be strictly digital.

Under pulse conditions the WRITE and ERASE operations of both types of device (digital p^+-n-i, or analogue p^+) can be achieved with voltage pulses of 100 ns or less.

5.3. *Discussion*

The crucial feature of the amorphous silicon structures is that memory switching, either digital or analogue, can only be observed if the device is subjected to an initial forming process. The forming process is characterized, not only by the breakdown of the high resistance state of the structure but, more importantly, by the presence of a positive feedback mechanism which provides a low resistance ON state so that the breakdown is non-destructive and repetitive switching is possible. Furthermore, the experimental results suggest a strong influence of the choice of the top metal contacts (summarized in the Table) on the type of memory switching observed (i.e. digital or analogue switching) and on the success of obtaining stable and reproducible switching. These results are in good accordance with the previous observations (Gage *et al.* 1989) that the first switching event (i.e. the forming) causes a local structural modification of the p^+ amorphous silicon layer, producing a highly conducting filament which does not revert to the original amorphous material when the device is switched OFF. After the forming process, the p^+ devices usually exhibit a lower OFF resistance than the unformed device, in contrast to our original data for p^+-n-i devices (Le Comber *et al.* 1985). The temperature dependence of the conductivity is also greatly reduced by the forming process. The area independence of R_{ON} (Le Comber *et al.* 19815) suggests localized electrical conduction after forming. These results provide strong experimental evidence that the forming process creates a filamentary region consisting of a new material whose properties have changed significantly compared with those of the unformed original material. It is feasible that the high fields and current densities present during forming result in high temperatures developing locally, which could lead to enhanced diffusion of metallic particles from the electrode into the thin amorphouse film. Such a region would become the preferred current path carrying the electron current in the ON state. The current-voltage characteristics in the ON-state at room temperature suggest that any material re-arrangement within the filament occurs so as to destroy the rectifying properties of the original metal-p^+ Schottky contact, and it should also be noted that this is the case even in a typical OFF state.

Acknowledgments

The financial support of British Petroleum International plc and British Telecom plc for some of the work described in this paper is gratefully acknowledged.

References

Adler, D., Henisch, H. K., and Mott, N. E., 1978, *Review of Modern Physics*, **50**, 209-220.
Barnett, A. M., and Milnes, A. G., 1966, *Journal of Applied Physics*, **37**, 4215-4223.
Charles, H. K., and Feldman, C., 1975, *Journal of Applied Physics*, **46**, 819-830.
Choi, W. K., Reynolds, S., Hajto, J., Gage, S. M., Owen, A. E., Snell, A. J., Flanagan, I. M., Rose, M. J., Djamdji, F. J., Le Comber, P. G., and Spear, W. E., 1987, *Journal of Non-Crystalline Solids*, **97-98**, 1330-1334.
den Boer, W., 1982, *Applied Physics Letters*, **40**, 812-813.
Dey, S. K., 1980, *Journal of Vacuum Science Technology*, **17**, 445-448.
Dey, S. K., and Fong, W. J. T.,1979, *Journal of Vacuum Science Technology*, **16**, 240-243.
Feldman, C., and Charles, H. K., 1974, *Solid State Communications*, **15**, 551-554.
Feldman, C., and Moorjani, K., 1970, *Thin Solid Films*, **5**, R1-R4.
Gabriel, M. C., and Adler, D., 1982, *Journal of Non-Crystalline Solids*, **48**, 297-305.
Gage, S. M., Hajto, J., Reynolds, S., Choi, W. K., Rose, M. J., Comber, P. G., Snell, A. J., and Owen, A. E., 1989, *Journal of Non-Crystalline Solids*, **115**, 171-173.
Gibbons, J. F., and Beadle, W. E., 1964, *Solid State Electronics*, **7**, 785-797.
Hajto, J. M., Rose, M. J., Le Comber, P. G., Owen, A. E., and Snell, A. J., 1990, *Proceedings of the Material Research Society*, **192**, 347-352.
Henisch, H. K., Fagen, E. A., and Ovshinsky, S. R., 1970, *Journal of Non-Crystalline Solids*, **4**, 538-547.
Kolomiets, B. T., Lebedev, E. A., and Taksami, I. A., 1969, *Soviet Physics of Semiconductors*, **3**, 267-272.
Le Comber, P. G., Owen, A. E., Spear, W. E., Hajto, J., and Choi, W. K., 1984, *Semiconductors and Semimetals*, **21**; *Hydrogenated Amorphous Silicon*, Part D, J. I. Pankove (ed.), 275-289.
Le Comber, P. G., Owen, A. E., Spear, W. E., Hajto, J., Snell, A. J., Choi, W. K., Rose, M. J., and Reynolds, S. 1985, *Non-Crystalline Solids*, **77-78**, 1383-1388.
Lucas, I., 1971, *Journal of Non-Crystalline Solids*, **6**, 136-144.
Madams, C. I., Morgan, D. V., and Howes, M. I., 1974, *Journal of Applied Physics*, **45**, 5088-5090.
Manhart, S., 1973, *Journal of Physics D: Applied Physics*, **6**, 82-86.
Moorjani, K., and Feldman, C., 1970, *Journal of Non-Crystalline Solids*, **14**, 248-255.
Mott, N. F., 1971, *Philosophical Magazine*, **24**, 911-958.
Owen, A. E., Le Comber, P. G., Sarrabayrouse, G., and Spear, W. E., 1982, *Proceedings of the Institution of Electrical Engineers*, Pt I, **129**, No. 2, 51-54.
Owen, A. E., and Robertson, J., 1973, *I.E.E.E. Transactions on Electronic Devices*, **20**, 105-122.
Owen, A. E., Robertson, J., and Main, C., 1979, *Journal of Non-Crystalline Solids*, **32**, 29-52.
Ovshinsky, S. R., 1968, *Physics Review Letters*, **21**, 1450-1453.
Ovshinsky, S. R., and Fritzsche, H., 1973, *I.E.E.E. Transactions on Electronic Devices*, **20**, 91-104.
Ridley, B. K., 1963, *Proceedings at the Royal Society A*, **82**, 954-960.
Rose, M. J., Hajto, J., Le Comber, P. G., Gage, S. M., Choi, W. K., Snell, A. J., Owen, A. E., 1989, *Journal of Non-Crystalline Solids*, **115**, 168-170.
Simhony, M., and Williams, R., 1969, *Journal of Applied Physics*, **40**, 691-696.
Spear, W. E., and Le Comber, P. G., 1976, *Philosophical Magazine*, **33**, 935-949.
Stocker, H. J., Barlow, C. A., and Weirauch, D. F., 1970, *Journal of Non-Crystalline Solids*, **4**, 523-535.
Warren, A. C., 1973, *I.E.E.E. Transactions on Electronic Devices*, **20**, 123-130.

INT. J. ELECTRONICS, 1992, VOL. 73, NO. 5, 911-913

Quantization effects in metal/a-Si:H/metal devices

J. HAJTO†, M. J. ROSE‡, I. S. OSBORNE‡, A. J. SNELL†, P. G. LE COMBER‡ and A. E. OWEN†

We present experimental results showing that metal/p⁺/metal amorphous silicon (a-Si:H) memory structures exhibit room temperature quantized electron transport associated with quantized resistance. The quantization of resistance is observed at values of $R = h/2ie^2$, where i is an integer or a half integer.

1. Introduction

We have previously shown that a-Si:H metal/p^+/metal structures exhibit non-volatile, polarity dependent analogue memory phenomena after initial conditioning by means of a moderately high applied potential (Rose *et al.* 1989). An essential feature of this 'forming' process is the creation of a filamentary region of highly conducting material. The filament is associated with local diffusion of the top metal contact into the a-Si:H, resulting in a region of mixed metal and silicon of unknown composition. More recent experiments (Hajto *et al.* 1991) have shown that, at low temperatures, the on-states of such memories exhibit quantized resistance values of $R = h/2ie^2$, where h is Planck's constant, e is the electron charge and i is an integer or a half integer. We now present new experimental observations showing that such structures exhibit room temperature quantized resistance, and will discuss possible physical mechanisms responsible for this phenomena.

2. Results

The samples used for this work were a-Si:H Cr/p^+/V sandwich structures, the preparation and geometry of which have been described elsewhere (Hajto *et al.* 1991). The structures have an initial low voltage resistance of $\sim 10^9\,\Omega$ which is lowered to $\sim 10^3\,\Omega$ by applying 300 nsec voltage pulses of increasing magnitude up to ~ 14 V. After this forming step the devices exhibit fast analogue switching at room temperature. At low temperatures the on-states of these devices exhibit discrete steps in the current-voltage characteristics associated with quantized resistance (Hajto *et al.* 1991). The effect is most readily observed at 4 K and disappears gradually as the temperature of the sample is increased to ~ 190 K.

Room temperature quantization is observed generally, but not exclusively, after further treatment of the sample. In this 'conditioning' step, a device in a $10^3\,\Omega$ on-state is modified by applying a relatively slow voltage ramp (0 to 5 V, 1 V sec^{-1}, 50 mV steps) with the positive polarity applied to the top contact. After conditioning the I-V characteristic has completley changed, with the current now increasing in sudden steps as the voltage is increased. The figure shows the static resistance of such a sample as a function of applied voltage. The measured resistance changes at

†Department of Electrical Engineering, University of Edinburgh, Edinburgh EH9 3JL, U.K.

‡Department of Applied Physics, and Electronic & Manufacturing Engineering, University of Dundee, Dundee DD1 4HN, U.K.

0020-7217/92 $3.00 © 1992 Taylor & Francis Ltd.

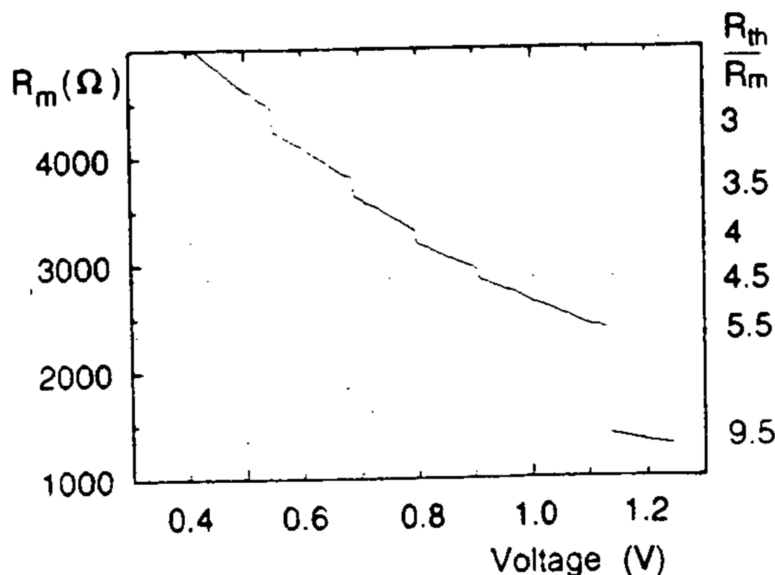

Resistance versus voltage at 300 K of a conditioned Cr/p$^+$/Cr structure.

values of $R_m = R_q/i$, where $R_q = h/2e^2 = 12906\,\Omega$ and i is an integer or a half integer. The acccuracy of the quantized resistance is defined as $i\Delta R/R_q$, where ΔR is the deviation between the mesured resistance R_m and the predicted quantized resistance R_q/i. ΔR is less than 2% for all of the quantized levels observed. The stability and reproducibility of the observed quantization has been investigated in a number of samples and for a duration of 10 hours at room temperature. Typical accuracies obtained remained within $\pm 2\%$. All devices which have been formed and conditioned in this way show quantized behaviour, although in different samples V_{cr} and the magnitude of the steps may vary. In all cases the first instability occurs at a value of R_q/R_m close to 1 i.e. $R_m = 12906\,\Omega$. However, the range of the first resistance jump varies: from $i = 1$ to 5, from 1 to 2, from 1 to 3·5, and from 1 to 3, for example. In all cases the accuracy of the quantized values remains within $\pm 2\%$.

At present we have no firm explanation for these results. Experiments on other one- and two-dimensional systems show electrical properties that are associated with quantized resistance, but are only observed at very low tempertures. In a one-dimensional electron gas (Wharam *et al.* 1988) in the ballistic regime resistance is quantized in terms of $h/2e^2$. However, it is not expected that quantized resistance states associated with ballistic transport should be observed when, as in the present case, the applied voltage is much greater than kT—if, for example, all the applied voltage were to appear across the critical part of the structure, the equivalent 'temperature' would be in excess of 1000 K.

We have suggested previously (Hajto *et al.* 1991) that the quantized phenomena might be related to electrical transport through a quantum point contact. Assuming that the inclusion of modified material created during forming has a tapered shape, the resulting current flow could be restricted to a very localized area. The device resistance could thus be determined by the contact area where the 'tip' of the modified region and the lower metal electrode are in close proximity. At such

distances the resistance might be associated with either a single or a small number of contact atoms. It has been shown theoretically (Martin-Rodero *et al.* 1988) that the resistance associated with a single contact atom reaches saturation with a minimum value given by $R = h/2e^2$ provided that no elastic deformation occurs. This is the 'constriction' resistance ($= 12906\,\Omega$) associated with an ideal conduction channel. It should be noted that this quantized resistance value is predicted assuming current flow through a single atomic orbital only. If more orbitals (conduction paths) are available, these would reduce the quantized resistance value.

3. Conclusions

Our measurements show that the resistance of conditioned a-Si:H sandwich structures can be quantized under some circumstances. The voltages at which this occurs correspond to energies that are greatly in excess of the thermal energy kT. Furthermore, the quantized resistance values reflected in the I–V characteristics do not involve all possible integer or half integer values. For these reasons we believe that existing theories of quantized resistance associated with ballistic transport are not applicable to our structure. However, the results obtained so far do not appear incompatible with current flow through atomic scale point contacts and it is possible that this could explain the room temperature quantization observed.

ACKNOWLEDGMENTS

Financial support from British Telecom PLC for some of the work described in this paper is gratefully acknowledged.

REFERENCES

HAJTO, J., OWEN, A. E., GAGE, S. M., SNELL, A. J., LECOMBER, P. G., and ROSE, M. J., 1991, *Physics Review Letters*, **66**, 1918.

MARTIN-RODERO, A., FERRER, J., and FLORES, F., 1988, *Journal of Microscopy*, **152**, 317; 1971, *Journal of Physics C*, **4**, 916.

ROSE, M. J., HAJTO, J., LECOMBER, P. G., GAGE, S. M., CHOI, W. K., SNELL, A. J., and OWEN, A. E., 1989, *Journal of Non-Crystalline Solids*, **115**, 168.

WHARAM, D. A., PEPPER, M., AHMED, H., FROST, J. E. F., HASKO, D. G., PEACOCK, D. C., RITCHIE, D. A., and JONES, G. A. C., 1988, *Journal of Physics C: Solid State Physics*, **21**, L887.

Chapter 14

Electronic Switching in Amorphous-Semiconductor Thin Films

J. Hajto, A. E. Owen, and A. J. Snell
Department of Electrical Engineering, University of Edinburgh, Scotland, U. K.

P. G. LeComber and M. J. Rose
Department of Applied Physics and Electronic & Manufacturing Engineering, University of Dundee, Scotland, U. K.

The aim of this chapter is to summarize experimental and theoretical work on electrical instabilities such as electronic switching and memory phenomena in amorphous thin films and particularly in amorphous silicon thin-film structures. Section 14.1 is a general survey of the field, comparing and contrasting experimental observations and theoretical models of switching in a variety of amorphous thin films, including a brief review of the early work on amorphous silicon. In Section 14.2 recent work in the authors' own laboratories on digital and analog amorphous silicon switching devices is described and discussed in more detail.

For the present purposes, electronic switches are two-terminal solid-state devices that can be changed from a nonconducting OFF state to a conducting ON state by an appropriate electric signal. Electronic switching is associated, explicitly or implicitly, with *negative differential resistance* (NDR). Two types of NDR exist: *current-controlled* NDR (CCNDR) [1] shown in Figure 14.1(a) and *voltage-controlled* NDR (VCNDR) [2] shown in Figure 14.1(b). Conduction in CCNDR involves the creation of conducting filaments in which the current density differs from that of the surrounding material [3] or circuit-controlled oscillations [4]. VCNDR is associated with stationary [2] or steady-travelling high-electric-field domains [5], or with sustained circuit-controlled oscillations [6]. Both CCNDR and VCNDR can give rise to a range of switching phenomena.

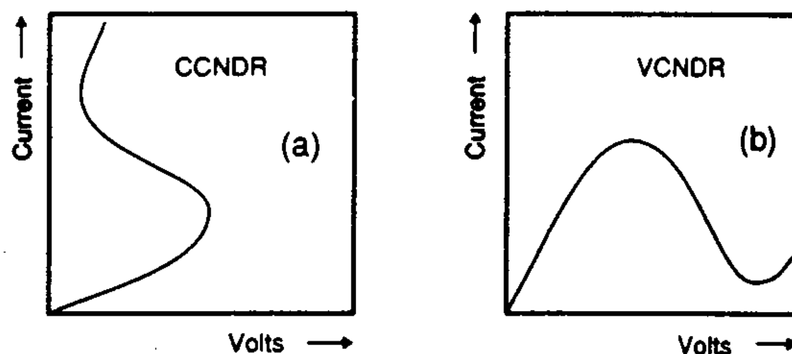

Figure 14.1 Schematic forms of (a) CCNDR and (b) VCNDR.

14.1 GENERAL SWITCHING PHENOMENA IN AMORPHOUS SEMICONDUCTORS

14.1.1 Threshold and Memory Switching

Many examples of threshold and memory switching have been reported in initially homogeneous thin films of a variety of materials including simple oxides [7], transition-metal-oxides [8]; elemental boron [9], metal-semiconductor-metal structures [10], and Langmuir-Blodgett films [11]. Interest in amorphous semiconductor films was stimulated by the discovery of reversible switching in certain amorphous semiconductors [12]. From 1968 onward, interest concentrated primarily on a class of covalently bonded alloys of group IV, V, and VI elements called the chalcogenide glasses. These materials, with appropriate electrodes, exhibit a transition from a low conductance (OFF) to a high conductance (ON) state under the influence of sufficiently high fields.

To illustrate the switching characteristics that are often observed, we shall first describe some typical results for the chalcogenide glasses. A typical switching device consists of a thin film of chalcogenide glass (thickness approximately 0.1–10 μm) sandwiched between two electrodes of refractory metals. Conduction is ohmic up to fields of about 10^4 Vcm^{-1}. At higher fields, nonohmic processes become evident and the current rises exponentially with applied voltage. Switching occurs at fields of about 10^5 Vcm^{-1} and schematic *current-voltage* (*I-V*) characteristics are shown in Figure 14.2(a). Upon switching (at the threshold voltage V_{TH}), the voltage across the device drops sharply along the load line until a holding voltage V_H of about 1V is reached. Experimental results show that conduction in the ON state is filamentary in character [13]. The device may be maintained in the ON state as

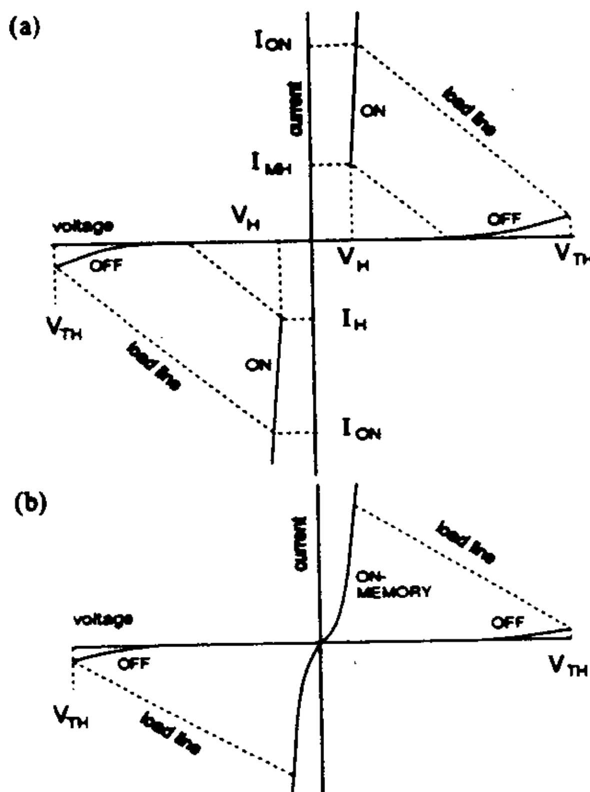

Figure 14.2 Schematic representation of (a) threshold switching and (b) memory switching.

long as the current does not drop below a critical holding current I_H and if that is not maintained the device switches back to the low-conducting OFF state. The switching process is highly reproducible, reversible, and essentially independent of polarity. Devices of this kind are called *threshold* switches; they are nonpermanent, or volatile, and always revert to the OFF state in the absence of an appropriate bias.

The schematic I-V characteristics for a different type of switching are shown in Figure 14.2(b). There is again a critical switching voltage for the OFF to ON transition, but both ON- and OFF-state characteristics extrapolate through the I-V origin. In these devices, if the high ON-state current is maintained for about a millisecond after the OFF to ON switching, the material along the current filament is modified and a high density of crystallites forms, creating a permanent bridge of high-conductivity material between the two electrodes [14]. After this modifi-

cation of the original structure has occurred, the device remains in the low-resistance ON state even after the electric field is removed. It is possible to return the device to its high-resistance OFF state by applying a sufficiently high, short, current pulse. This "erase" pulse melts the high conductivity material in the conducting channel. Subsequent rapid cooling of the melt restores the original amorphous phase. Devices of this kind are permanent (nonvolatile) and hence are known as *memory* switches. The amorphous-to-crystalline transition outlined above is, of course, only one possible mechanism by which memory switching can be implemented. In general, memory switching refers to any mechanism that results in the ON and OFF states persisting more or less indefinitely in the absence of any bias.

To summarize, switching phenomena can be characterized into two main categories:

1. Threshold switching, in which continuous electrical power is required to maintain the highly conducting ON state;
2. Memory switching, in which both ON and OFF states can be maintained without electrical power.

It is common to describe switching phenomena in terms of ON and OFF states, but as we will show in Section 14.2.2, switching devices are not always rigidly bistable in their operation, that is, they are not always digital devices. In some cases, a continuous range of intermediate states is observed between the ON and OFF states, giving an analog memory effect.

The speed of the switching transients varies from device to device and covers a range from <10 ns to >1 ms. The actual switching is extremely fast (nanoseconds) but is preceded by a delay time of the order of microseconds near the threshold. The delay time decreases exponentially with the overvoltage, that is, with the voltage above the threshold. Figure 14.3(a) shows a simple circuit that can be used to measure the voltage and current waveforms during a single switching pulse to obtain the speed of the switching transient, and Figure 14.3(b) shows schematic waveforms of the measured voltage V_S and current I_S across the device during an OFF to ON transition (associated with either threshold switching or a memory "write-in" operation). There is a sudden rise in the voltage across the device at time t_0 but the current remains low (i.e., the sample is in its low-conducting OFF state) for a certain time termed the "delay time" (t_{DW}), equivalent to $t_1 - t_0$. At t_1 there is a sudden rise in the current and at the same time a similarly fast decrease in the voltage associated with the OFF to ON transition (i.e., a sudden increase in the device conductivity). The duration of the ON to OFF transition ($t_2 - t_1$) is called the "switching time," and it is usually much faster than the delay time t_{DW}. Figure 14.3(c) refers to the erase operation for a memory device. This situation obviously does not arise in a volatile threshold device. When the voltage pulse is applied at time t_0, the current is high at first, as the sample is in its ON state. After

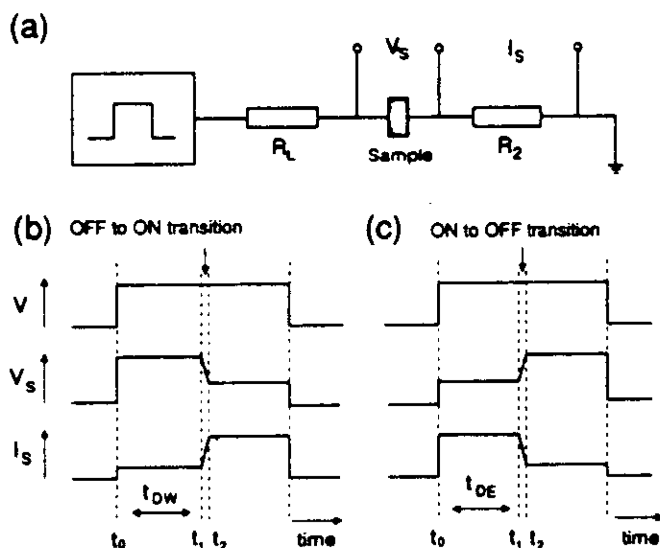

Figure 14.3 (a) Experimental arrangement of the switching circuitry, (b) waveforms of WRITE transient; and (c) waveforms of ERASE transient.

a delay time t_{DE}, the sample conductance decreases rapidly during the erase switching time $(t_2 - t_1)$, and at the same time the voltage across the device increases.

Most chalcogenide devices, whether threshold or memory, can sustain many hundreds of cycles of ON→OFF→ON transitions. The best threshold devices can switch up to 10^9 times before they fail. Good memory devices will operate for at least 10^6 WRITE-ERASE cycles before failure.

14.1.2 The Forming Process: A Precursor to Threshold and Memory Switching

Newly fabricated devices rarely show threshold or memory switching effects without an initial modification of their as-deposited structure, a process usually called *forming*. Forming is achieved by the application of suitable voltage pulses that are always higher in magnitude than the subsequent programming pulses. This invariably produces an irreversible change in the electrical characteristics of a device, often with a substantial decrease in the overall terminal resistance.

The processes involved in forming depend on the type and quality of the thin film, the geometrical structure of the device and in some cases the electrode material. The changes can be either physicochemical, involving a redistribution of the

constituents, or they can be electronic, wherein a quasi-permanent change in the occupancy of some electronic states takes place. The changes can occur throughout the bulk of the film or in a localized region. The most common localized effect is the formation of a filament of highly conducting material that extends completely or a part of the way through the device. Such permanent filament formation is a consequence of temporary filamentary breakdown usually observed in metal-insulator-metal and metal-semiconductor-metal sandwich structures under double-injection conditions [3]. Barnett and Milnes have considered current and voltage instabilities in semiconductors and have shown that with current-controlled negative resistances, such as those expected in double-injection structures, energy considerations imply the formation of a filament. The filament develops first at some device inhomogeneity, is stationary, and grows in size about the nucleation region as the current is increased. This filament should not be confused with the moving transverse wave of a voltage-controlled instability (Gunn effect), which was also considered by Barnett and Milnes. Rather earlier, Ridley [15] had also shown by general thermodynamic arguments that CCNDR implies the formation of current filaments, while field domains are involved in VCNDR.

Filamentary conduction has been experimentally observed in a wide range of materials and sandwich structures. These include single crystal silicon [16], gallium arsenide [17], zinc telluride [18], compensated germanium [19], and polycrystalline silicon [20], all of which show *I-V* characteristics associated with threshold switching of the kind shown in Figure 14.2(a). In these cases the filament collapses and disappears as the voltage is removed, and there is no permanent change in the device structure or in its electrical characteristics.

In the case of amorphous thin-film structures, however, the development of the filament during the forming process is always accompanied by an irreversible modification of the original structure. This means that the filament—or part of the filament—is permanently "written in" to the originally uniform amorphous structure (i.e., it will not disappear after the voltage is removed). Permanent filament formation can occur by crystallization of an amorphous film [14], stoichiometric changes [21], diffusion of the electrode material into the film [7], or ionization of deep traps [22]. All of these changes usually refer to a localized modification of the structure in the area of the filament. Reports of bulk forming effects are much rarer, one example being bulk diffusion of electrode material into the film [23].

The modification of the initial structure during the forming process is the most important factor determining the subsequent switching operation. This is because in most cases forming creates a new device within the originally deposited structure, whose characteristics determine the ensuing threshold-switching or memory-switching operation. For example, a permanent filament may have a cross-sectional area many times less than the device area, but its effective conductance is often so much higher than that of the surrounding material that it becomes the dominant conducting path.

It is important to emphasize that in both the threshold- and memory-type devices, the initial switching mechanism appears to be the same [24]. It is often initiated by field-dependent nonohmic conductivity and consequent instability. Whether what follows is threshold switching, memory switching, or, in some cases, destructive electrical breakdown depends on the properties of the material and the presence or absence of suitable feedback in the system.

14.1.3 The Mechanism of Threshold Switching

The detailed *I-V* characteristics of chalcogenide-based threshold-switching devices have been widely investigated since the original publication by Ovshinsky in 1968 [12], and a general survey of the most significant results has been provided by Adler, Henisch, and Mott [25]. The suggested physical models can be divided into two categories; the first assumes that threshold switching is due to thermal processes [26], and the second considers that it is associated purely with electronic phenomena [27, 28]. Thermal or, more generally, combined thermal and electrical mechanisms are sufficient to explain threshold switching. In the thermal models, the increase in conductivity under the influence of an electric field exceeding the switching threshold V_{th} is controlled only by Joule heating by a "thermal runaway." This is regarded as the principal driving force of the switching mechanism. The explanation of threshold switching in terms of thermal processes involves a feedback loop, illustrating how, in materials with a thermally activated conduction process, thermal runaway can occur and cause a sharp drop in the device resistance. The feedback loop is:

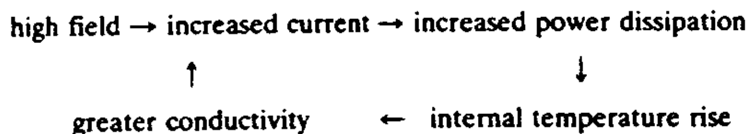

The essential link is the sensitivity of the conductivity to temperature. Whether the final result is threshold switching or memory switching, the conditions leading to the electrical instability can usually be formally described by an energy-balance equation [26]:

$$A(T, E, \alpha) = B(T, \alpha) \tag{14.1}$$

where A is the rate at which energy is gained from the field E at temperature T, and B is the rate at which it is absorbed or dissipated. The parameter α is introduced to denote any other relevant property of the current carriers depending on the particular experimental conditions. The variation of the two sides of this energy-balance equation will be generally as shown in Figure 14.4, in which the abscissa

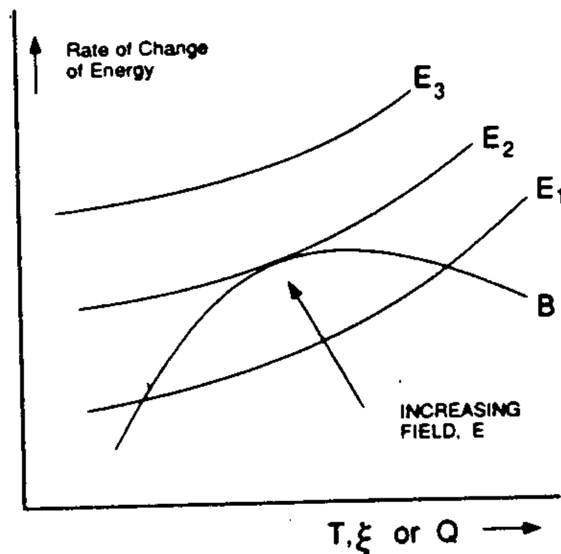

Figure 14.4 Schematic representation of solutions to energy-balance equations.

represents some appropriate parameter such as temperature, energy ξ, or injected charge Q. The rate of gain of energy from the field will normally be given by

$$A = \sigma(T, E)\xi^2 \tag{14.2}$$

or some variant of this. The conductivity $\sigma(T, E)$ is generally a function of temperature and field. With a sufficiently large conductivity that is temperature-dependent, the material will heat up through Joule heating, and, if thermal processes are dominant, then

$$B = \left\{\rho \frac{C}{K}\right\} \frac{\partial T}{\partial t} - \nabla^2 T \tag{14.3}$$

The characteristics of purely thermal threshold switching can be accurately predicted from the solution of (14.2) and (14.3) in a one-dimensional form with conductivity expressed only as a function of temperature, that is, $\sigma = \sigma(T)$. The general solution is shown in Figure 14.4; the abscissa in this case represents temperature and the intersection of B and field E_2 determines the point at which instability sets in. It should also be noted that even in the case when the isothermal conductivity is ohmic, the dynamic conductance will not be constant because of

Joule heating. The most detailed calculations of the thermal, one-dimensional model have been reported by Warren [26]. The general conclusion, summarized more fully at the end of this section, is that such a simple model is not sufficient to explain switching in relatively thin films (e.g., <8 μm), although the evidence shows it is adequate to account for the switching characteristics of thicker films.

Kroll and Owen et al. have provided the most detailed mathematical description of threshold switching phenomenon in amorphous semiconductors based on a combined thermal and electrical model (i.e., $\sigma = \sigma(T, E)$) [29, 30]. In Kroll's calculation, the *I-V* characteristics were obtained from very general mathematical considerations concerning stability and bifurcation of solutions of the nonlinear equations for temperature and field, and he showed that switching occurs by the nucleation and growth of a hot spot approximately in the center of the device interior. The primary results of Kroll's analysis are shown in Figure 14.5. The model predicts the formation of the S-shaped CCNDR associated with high-current filaments (Figure 14.1(a)). The existence of a region of negative differential resistance on the *I-V* characteristics was determined by radially uniform solutions of the thermal balance equation. It was also shown that the dashed portions of seg-

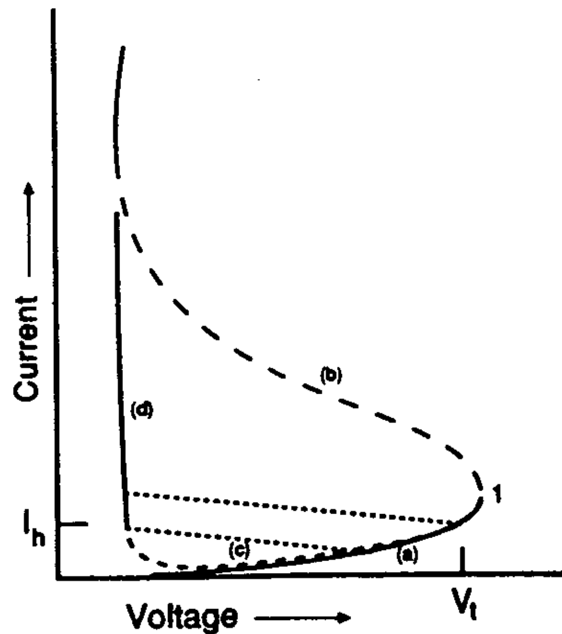

Figure 14.5 *I-V* characteristics: solid curve, stable solutions; dashed curve, unstable solutions; dotted line, load line. From: [29].

ments (b) and (c) are locally unstable against temperature and field perturbations which keep the total current through the device constant, and that branches (a) and (d) are stable with respect to such perturbations. Switching is initiated at some point not too far below turnaround (see point 1 in Figure 14.5) as the result of a macroscopic critical fluctuation. Once the switching is initiated, the device discharges through the embryonic channel and switches along the load line to the stable vertical portion of branch (d). Here all the current flow is carried in a hot channel. The possibility of thermally induced negative differential conductivity was suggested and described in other publications [31, 32]. Experimental evidence of high filamentary temperatures during threshold switching has also been reported [33].

Several authors have put forward alternative nonthermal electrical models for creating conditions of instability leading to switching. One of the most frequently used electrical models is based on double injection with recombination in which, in the ON state, carriers are injected at both electrodes, giving rise to a high density of carriers in the valence and conduction bands. In this case the energy input is either stored in the dielectric as injected charge q_{inj} or is lost through recombination. An energy-balance equation (14.1) could therefore be written as

$$\sigma(T, E)\xi^2 = \frac{q_{inj}}{D\epsilon_0\epsilon_r}\frac{dq_{inj}}{dt} - j_{rec}\psi_{in} \tag{14.4}$$

where ϵ_r is the relative permittivity, D is a suitable geometrical factor, and j_{rec} is the recombination current driven by some appropriate internal potential ψ_{in}. In this case the abscissa of Figure 14.4 would represent q_{inj}. A qualitative explanation along the above lines was suggested first by Henisch [27]. Similar but more quantitative models have also been proposed by Lucas [28] and Mott [34]. The conductive ON state is sustained by double injection, provided the applied voltage exceeds the mobility gap. It is assumed that the tails of localized states (typically present in amorphous semiconductors [35]) extend from the conduction and valence bands and overlap somewhere near the center of the energy gap (or mobility gap). This provides a completely compensated set of positively and negatively charged states above and below the Fermi level pinned at or near the center of the gap. These features are inherent in the *Cohen-Fritsche-Ovshinsky* (CFO) model of the electronic band structure of chalcogenide glasses [36] and are further supported by more recent theoretical interpretations involving the concept of negative-U states [35]. The injected electrons and holes will recombine with and neutralize the positively and negatively charged states, setting up a negative and a positive space charge adjacent to the cathode and anode, respectively. The regions of space charge will limit the current flow in the vicinity of the electrodes, and the field will be redistributed in a way that would be decreasing near the electrodes and increasing

in the center. As the applied voltage is increased, more charge is injected and the space-charge regions grow until eventually they meet and overlap. The physical situation then rapidly becomes unstable. When the space-charge clouds overlap they neutralize each other, causing the field in the interior to collapse and allowing the same or larger current to flow with a lower applied voltage, causing a negative resistance characteristic. The conductivity in the center increases and the field decreases, while the field near the electrodes increases. Electrons and holes are accelerated rapidly across the neutral region and, because of the increased field, injection of carriers at the electrodes increases. Both effects increase the rate at which space-charge overlap occurs (i.e., there is a positive feedback and hence an unstable situation). The stable state, corresponding to the ON state, is achieved when the space charge has spread right across the structure and the bands are practically flat. Schottky-type barriers are established at the electrodes, but because of the high density of traps and because they are thin (about 1 nm), electrons can easily tunnel through from the Fermi level of the metal into the conduction band of the chalcogenide glass and, similarly, holes from the anode tunnel into the valence band. Because the space charge has been neutralized and the traps are filled, the conductivity in the device is now high (i.e., the drift mobility is no longer limited by trapping).

Homma [37] published a systematic and detailed comparison between the threshold switching properties of a chalcogenide material ($Te_{40}As_{35}Ge_7Si_{18}$) and a nonchalcogenide alloy ($Cd_{23}Ge_{12}As_{65}$) of nearly equal forbidden gap but higher conductivity. The results showed that two alloys of rather different resistivities have the same threshold voltage and also that symmetrical threshold voltages may be associated with highly asymmetric threshold currents. Furthermore, in both cases, the threshold current is light-sensitive (both materials are photoconductive) but the threshold voltage is not but remains practically unchanged by illumination despite a power increase by a factor of three or more. This indicates that a critical field is involved in the circumstances and determines the onset of switching. These results provide evidence against thermal interpretations and thereby support electronic models. Microwave noise and *transient ON-characteristics* (TONC) measurements [38] also suggest that the Joule heat is not the main cause of the formation of the current filament. Also, relaxation processes and polarization effects [39] observed at low temperatures show an effect on threshold switching opposite to that expected from the thermal theory. It is found that if, during double-pulse experiments, the first pulse is of insufficient height to cause switching, the magnitude necessary for the second pulse to cause switching is lowered if the pulses are of the same polarity and increased if they are of opposite polarities. It appears that contact, injection, and trapping effects must play some role in explaining certain of the asymmetric effects described above. Therefore, although the electrothermal theory describes well the observed initial switching instabilities, it is also clear that contact, injection, and trapping effects must play some role in explaining certain

of the asymmetric electrode effects and polarization and relaxation phenomena described above.

Many other conditions of electrical instability leading to switching have also been investigated. For intrinsic electronic breakdown in the single-electron approximation, for example, the function A in (14.1) is of the form [24]

$$A = e\mu(\xi)E^2 = \frac{e^2E^2\tau(\xi)}{m} \tag{14.5}$$

where μ, the mobility, and τ the relaxation time, are functions of energy. The electron loses energy to the lattice through phonon interactions, and the value of B (14.1) can be written as

$$B = \frac{h\omega}{\tau_c(\xi)(2N_\omega + 1)}\left\{1 - \frac{kT}{\xi}\right\} \tag{14.6}$$

where τ_c is the mean time between collisions and is a function of energy, and N_ω is the average number of phonons of frequency ω. Thus, in Figure 14.4, the abscissa represents energy ξ, and the field E_2 again corresponds to the onset of instability.

Electron-electron collisions may also lead to electrical instabilities [24]. With a high collision rate and a rate of energy exchange due to electron-phonon interactions, the electron energy-distribution function is Maxwellian with a mean temperature T_d above the ambient temperature T_a or the lattice temperature T. This means that the energy rate of change terms A and B (14.1) can be averaged to $\bar{A}$ and $\bar{B}$, having a similar functional dependence so that the general picture of Figure 14.4 remains valid at least up to energies ξ_m at the maximum of curve B. This collective description has a strong analogy with thermal runaway, and the abscissa corresponds to the electron temperature T_d. In this case, therefore, it is the steady-state electron temperature that rises until, at a critical value, no equilibrium is possible and instability sets in. Near ξ_m, however, the electron-phonon energy transfer increases, implying an increase in the internal temperature of the material, with consequential thermal effects.

Impact ionization and avalanche breakdown can also produce instabilities [22]. If the electron density is low, a high-energy electron may collide with an atom instead of another electron and thus ionize it, producing a hole and two low-energy electrons. The two electrons, in turn, will be accelerated to high energies and ionize more atoms; thus the process can cascade to cause an electron avalanche.

Summarizing these results, there is no doubt that, besides thermal effects, there are significant electronic effects causing nonohmic conduction and CCNDR in the preswitching region of chalcogenide glass switches. A comparative study of their relative importance has been given by Owen and Robertson [24] and Adler

[25]. The main point of discussion has concerned the extent to which switching can be attributed to thermal or electronic processes.

In either case (thermal or electronic), heating may be the initial process, but the critical field E_{cr} at which switching occurs may behave differently with different thicknesses of the films. For thin films ($< \sim 1$ μm) conduction at breakdown is nonohmic. Therefore it is expected in this case that V_S will be independent of the film thickness and will decrease linearly with temperature [34]. The nonohmic field-dependent conductivity implies electronic processes such as double injection or avalanche breakdown, as discussed above. Furthermore, the constant value of the threshold voltage in the presence of illumination [37], the microwave noise and TONC measurements [38], and the polarization effects [39] also provide evidence for electrical mechanisms. Based on these experimental results, there are strong reasons for believing that in chalcogenide thin-film ($d \leq 1$ μm) threshold-switching devices ("Ovonic switches" [12]), thermal considerations do not play a significant role.

However, for thick films (≥ 8 μm) for which current at breakdown is ohmic, E_{cr} should be proportional to the inverse of the thickness and decrease exponentially with increasing temperature [34]. Kolomiets [40] found a dependence on the thickness showing that in thin films (≤ 8 μm), the breakdown field was independent of the thickness and depended only weakly on temperature, suggesting that the switching mechanism in thin films is not associated with simple thermal breakdown. On the other hand, in thick films (≥ 8 μm), the breakdown field is inversely proportional to the thickness and shows strong temperature dependence, confirming the essentially thermal nature of the breakdown in thicker films. Stocker [41] described a quantitative model for threshold switching in semiconducting films ≥ 8 μm thick based on thermal considerations only (i.e., no field dependence of conductivity) and has shown that the switching behavior of these thicker films can be described adequately by a simple thermal model.

The most useful approach seems therefore to be to compare, wherever possible, the functional dependence of parameters such as the threshold voltage and delay time on, for example, temperature, field, and geometry with the predictions of the related models. With several possible mechanisms competing, the dominant process can change drastically as a function of such factors as temperature or the geometry of the specimen.

14.1.4 Mechanisms for Memory Switching

As described in the previous paragraph, the precursor to memory phenomena in thin (~ 1 μm) film is the onset of nonlinear field-dependent conductivity leading to instabilities and threshold switching. For threshold switching, the material must be capable of carrying a much increased current, either uniformly or locally in a

filament, but reversing spontaneously to the original nonconducting OFF state when the holding voltage is removed. For memory switching, the dielectric material must be capable of changing into a permanent conducting state in some way—an overall or localized change in the atomic or microscopic structure for example—but one that can be reversed to the OFF state by a suitable current (energy) pulse. Obviously the system must also be able to absorb the reversing pulse without destructive breakdown. Alternatively, the memory-switching process may be based on charge storage (i.e., without a modification of the structure).

Models for memory switching can therefore be divided into two broad categories: electronic or structural. The first of these is based on the long-term storage of charge, with no major structural modification, to account for the nonvolatile nature of the switch. The most commonly proposed charge storage sites are traps, either in the bulk or at an interface between two dissimilar materials. The necessary characteristic of such traps is that they have a release time comparable to the retention time of the memory, which may range from a few hours to many years. If the charge is stored in the amorphous thin-film sandwich structure, it can affect the conductance in a number of different ways. For example, when stored in the bulk or at interfaces, it can cause band bending, which in turn modifies the conductance. Simmons and Verderber have used an electronic model to explain their observations of memory switching in thin silicon monoxide (SiO) films fitted with gold electrodes [2]. The *I-V* characteristics of their device (Figure 14.6) show a VCNDR, and the device could be switched between several memory states (A, B, C, D) that persisted for a few weeks. The forming process in these devices is due to gold ion injection into the bulk of the silicon monoxide film, the source of the ions being the positively biased gold electrode. The sample cannot be formed at liquid nitrogen temperatures but forms more readily at elevated temperatures, indicating that ion injection with subsequent ion migration is the origin of the forming process. The current-voltage characteristics and the weak temperature dependence of the conduction process suggest that the main factor determining the current flow in this system is tunneling. For a reasonable current flow in the system, adjacent ionic sites must be positioned within ~30Å of each other, which means that the injected ion density must be at least of the order of 10^{19} cm^{-3}. The authors concluded that in these devices the conduction and memory processes are electronic in nature and that the memory effect is due to charge trapping in the bulk of the silicon monoxide, which in turn modifies the conductance of the metal-silicon monoxide barrier.

Hovel and Urgell have also suggested an electrical model to explain their observations of memory switching in epitaxial ZnSe films grown on crystalline Ge [42]. In the OFF state the current flow through the device is limited mainly by the high-resistance ZnSe layer. In the ON state, the barrier at the ZnSe/Ge interface has been narrowed by the ionization of traps at the interface from neutral to positive, thereby permitting easy tunneling through it. The same general type

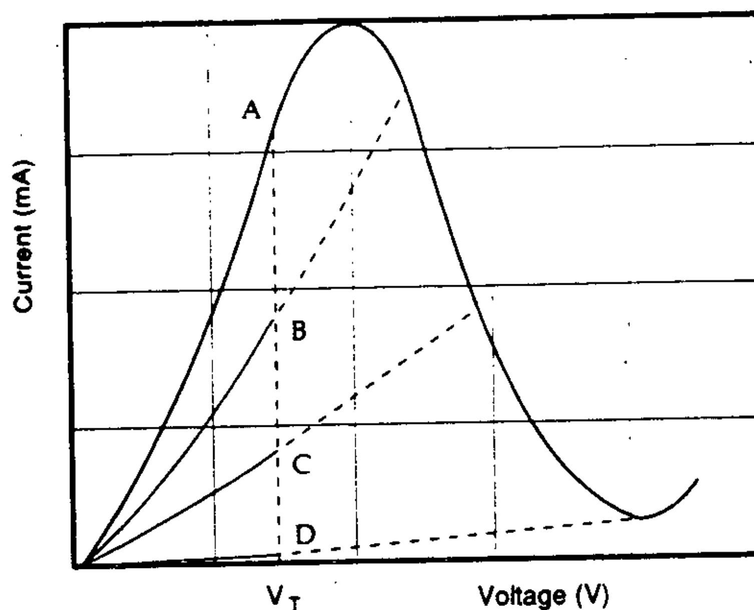

Figure 14.6 Schematic diagram of dynamic I-V characteristics illustrating several memory states (A, B, C, D) and the threshold voltage V_T. From: [2].

of phenomenon has been observed in ZnSe-GaAs [43], GaP-Ge [43], AlN-Si [44], and SbSi-SnO_2 heterojunctions [45].

Switching in chalcogenide glass memory devices is based on a rearrangement of the structure in the ON and OFF states, as seen in Figure 14.7. During initial forming pulses, a filament of material crystallizes in the amorphous structure [14]; this normally happens near the center of the device where the highest temperatures are attained. This modified material has a higher conductivity than the bulk and therefore becomes the preferred current path during subsequent voltage pulses. In the erase operation (i.e., switching from ON to OFF), large voltage pulses with steep trailing edges are applied. These melt the crystalline filament, causing it to solidify in an amorphous form. To write in again, switching from OFF to ON, pulses with more gradual trailing edges are used. These pulses also melt the filament but allow the material to solidify in a crystalline form.

Manhart has also proposed a structural model to explain memory switching in silicon monoxide sandwich structures with silver electrodes [21]. In these structures, a forming pulse was again used to reduce the device resistance from its initial value of $\sim 10^9 \Omega$ to $\sim 300 \Omega$. According to Manhart's model, the forming process gives rise to a temperature increase sufficient to induce silver from the electrodes

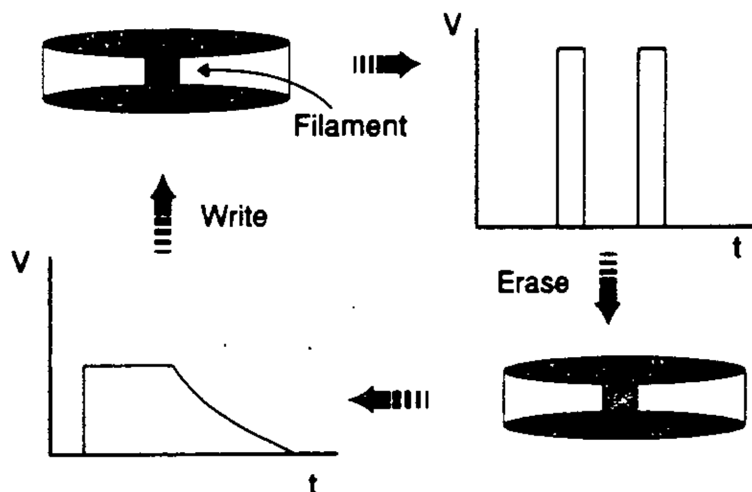

Figure 14.7 Memory-switching process in metal-chalcogenide-metal devices.

to migrate into the silicon monoxide film to produce a metallic filament. This explains the subsequent linear *I-V* characteristics and positive temperature coefficient in the ON state. Two different mechanisms were suggested for the switching. The first assumes that the erase pulse (10V, trailing edge 1000 ns) melts the metal filament only at the narrowest point. The metal disperses into the silicon monoxide, breaking the link. To write in again and hence reconstruct the filament, a write pulse (6–8V, trailing edge >0.1 ms) encourages more metal from the electrodes to enter, that is, a long pulse is able to heat the boundaries sufficiently to cause new diffusion from the electrodes. The second model also suggests that the erase pulse melts the metal filament. After the removal of the pulse, rapid cooling leads to the formation of a high-resistance amorphous mixture of metal and silicon monoxide phases. To write in again, this material is melted again but then cooled more gradually. The difference in the freezing points of the metal and the silicon monoxide cause them to separate, thus restoring the filament.

Memory switching in thermally grown microcrystalline NiO has been reported by Gibbons and Beadle [7]. They too suggest that a metallic filament is formed in their structures, not by the diffusion of metal from the electrodes, but by the collection of nickel atoms at a structural defect in the oxide. This occurs during the forming stage of the device where a filament of material becomes sufficiently hot for this stoichiometric change to take place. The device can have an ON-state resistance of approximately 100Ω and an OFF state resistance of 25 MΩ. In the ON state a nickel filament is formed, which connects the ohmic contacts. Once the device is switched ON, the device can be very rapidly switched OFF by essentially burning out a small section of the conducting filament. Once the filament is

formed, only the section removed or reoxidized during the OFF state need be replaced. The main body of the filament, which remains more or less intact during the OFF-state transient, provides a large nickel reserve for this replacement. This will obviously limit the lifetime of the device.

14.1.5 Electrical Switching in Amorphous-Silicon Structures

The earliest reports of switching in amorphous silicon (a-Si) were published in 1970 [13, 46] contemporaneously with some of the early literature on switching in chalcogenide glasses. More detailed experiments on the same structures were reported later [9, 47]. These investigations studied vacuum-evaporated films of a-Si in the range 0.3–2.0 μm thick, fitted with titanium electrodes. Similar observations were made on evaporated films of germanium, boron, and boron plus carbon. As threshold devices, these a-Si structures had threshold voltages V_{th} of 5–10V, OFF-state resistances in the range of 1–30 kΩ, and an ON resistance of about 100Ω. In common with the chalcogenide glasses, there was a delay time t_r before switching of 20–50 μs or more at room temperature, and the actual switching time was at least several microseconds. Feldman and Charles [9, 47] did not, however, report any initial forming process, unlike the situation in chalcogenide glass switches (Section 14.1.1). There was also some tentative indication of memory switching but this apparently was not substantiated. They interpreted their results in terms of a simple and qualitative electrothermal model involving the formation of a conducting filament.

The work of Feldman and his colleagues [13, 46], which originated in the early 1970s, seems to be the only investigation of switching in a-Si until the rather later studies of Dey and Fong [48, 49]. These authors reported results very similar to those of Feldman. They studied thin films of a-Si in the range 0.3–1.5 μm thick, deposited by electron-beam heating in a vacuum evaporator. Titanium contacts were again used, either in the form of evaporated films or as probes. Dey and Fong reported only threshold switching, with *I-V* characteristics similar to those in Figure 14.3; they did not mention any evidence for memory behavior. In contrast to Feldman, however, Dey and Fong did observe forming effects, that is, the initial threshold voltage was relatively large but decreased to a more or less constant value after a number of switching cycles. In Dey and Fong's devices the threshold voltage varied systematically from about 6V for the thinner films (~0.3 μm) to about 9V for the thicker films (~1.2 μm). The delay time before switching was in the range 2–60 μs, varying in a systematic way with pulse height, pulse duration, and repetition rate, again in a manner very similar to threshold switching in chalcogenide glasses. Dey and Fong also interpreted their results in terms of a simple one-dimensional electrothermal model, although developed a little more quantitatively than that by Feldman and Charles [9, 47]. It should be noted that both teams (Feldman and Charles, and Dey and Fong) used a-Si films deposited by vacuum evaporation, which probably accounts for the relatively low OFF-state

resistances (~100 kΩ) they both found. It is now well established that vacuum-evaporated a-Si is a very different material from the hydrogenated form of a-Si obtained, for example, by glow-discharge deposition of silane [50].

Three papers, concerned specifically with switching in amorphous silicon, by Gabriel and Adler [51], den Boer [52], and Owen [53] appeared almost concurrently early in 1982, each reporting very different effects observed in different amorphous silicon structures. Our own work [54–58], including recent results, will be described in detail in the following sections.

Den Boer studied n^+-i-n^+ structures of a-Si:H prepared by the glow discharge decomposition of SiH_4 (i stands for near-intrinsic, or undoped, material). The n^+ layers were 0.05 μm thick and were prepared by adding 1% PH_3 to the SiH_4 gas flow; the i layer in different devices ranged in thickness from 2.5 to 5 μm. Den Boer found that the n^+-i-n^+ devices functioned as threshold switching devices with nonpolar characteristics similar to those in Figure 14.2(a). For the first switching cycle, the threshold voltage was in the range 40–100V, but for all subsequent operations it was only 10–35V, depending on the i layer thickness. (As the i layer thickness increased, the threshold voltage also increased.) The OFF-state resistance of the n^+-i-n^+ devices was about 1 MΩ, and the ON-state resistance was about 1 kΩ. There was an observable delay time before switching, ranging from a few microseconds when the applied voltage was about 8V greater than V_{th} to about a millisecond for voltages within 1V of V_{th}. The n^+-i-n^+ switches could be cycled through at least 10^9 stable switching operations. Den Boer also compared structures with chromium or a combination of chromium and n^+ contacts (i.e., Cr-n^+-i-Cr and Cr-i-Cr). The Cr-n^+-i-Cr contacts had rectifying characteristics, while the Cr-i-Cr contacts switched but were very unstable.

Gabriel and Adler [51] prepared their films by sputtering from a polycrystalline silicon target in an argon-hydrogen plasma. In all cases their devices were notionally homogeneous thin films of intrinsic a-Si:H with molybdenum contacts. The samples were fabricated under a wide range of deposition conditions in two sputtering systems, and although results from some of the devices were rendered rather doubtful because of contamination problems, in no case did Gabriel and Adler observe any evidence of reversible switching. They concluded that, in contrast to the chalcogenide glasses, amorphous silicon does not have the electronic and structural properties required for reversible switching.

14.2 RECENT DEVELOPMENTS ON AMORPHOUS-SILICON SWITCHES

14.2.1 Digital Switching in a-Si:H p^+-n-i Devices

We now turn to the work on electrical switching carried out in the authors' laboratories. Although a number of different a-Si:H multilayer structures have been investigated, all the earlier results discussed in the following refer to metal-

p^+-n-i-metal devices deposited in that sequence by the glow-discharge technique with gas-phase doping. In the early stages of the work, the a-Si:H layers were deposited onto a stainless-steel substrate. After completion of the a-Si:H deposition, a series of gold (Au), aluminum (Al), or nichrome (NiCr) dots, up to approximately 1 mm in diameter, was evaporated onto the surface of the samples. The top contact was completed by a probe or by a thin wire attached to the metal dots with conducting silver paste.

In order to facilitate the investigation of device properties on a more reproducible basis, a "pore" device structure was designed, with device areas down to a few μm in diameter. A set of photomasks was produced that allowed modern photolithographic technique to be combined with the normal a-Si:H deposition process. Figure 14.8(a) shows a cross section of one of the pore structures produced by photolithographic techniques, and Figure 14.8(b) represents a plan view of the same structure. The a-Si:H films were deposited on Corning glass substrates previously patterned with chromium bottom contacts. The a-Si:H was prepared in a layer sequence of p^+, n, i by the glow-discharge decomposition of silane using gas-phase doping. The p^+-n-i films were then patterned, and an insulating layer was used to define an active device area of 10^{-6} cm^2. The metal used for the top contact was normally chromium but a number of other metals were also used, and their influence on the memory operation was thoroughly investigated.

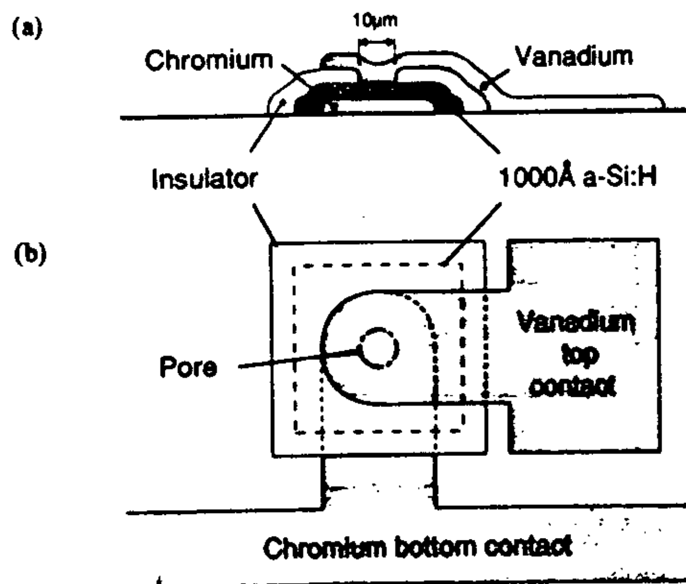

Figure 14.8 Structure of metal-amorphous silicon-metal switch device.

14.2.1.1 Static Current-Voltage Characteristics

Typical *I-V* characteristics for a freshly prepared (unswitched) device are illustrated in Figure 14.9(a) in both the forward and reverse directions; the forward direction is defined so that the substrate (and hence the p^+ region) is positively biased. It must be emphasized here that these measurements were taken "by hand," point by point, in a manner that required a few seconds for each measurement. (The significance of this remark will become apparent in the next sections.) In the forward direction there is a region of ohmic behavior over a limited voltage range followed by an abrupt change to a markedly nonohmic region until, at the point indicated by the arrow, the device is unstable and it becomes impossible to continue with point-by-point measurement. The change from ohmic to nonohmic behavior is more

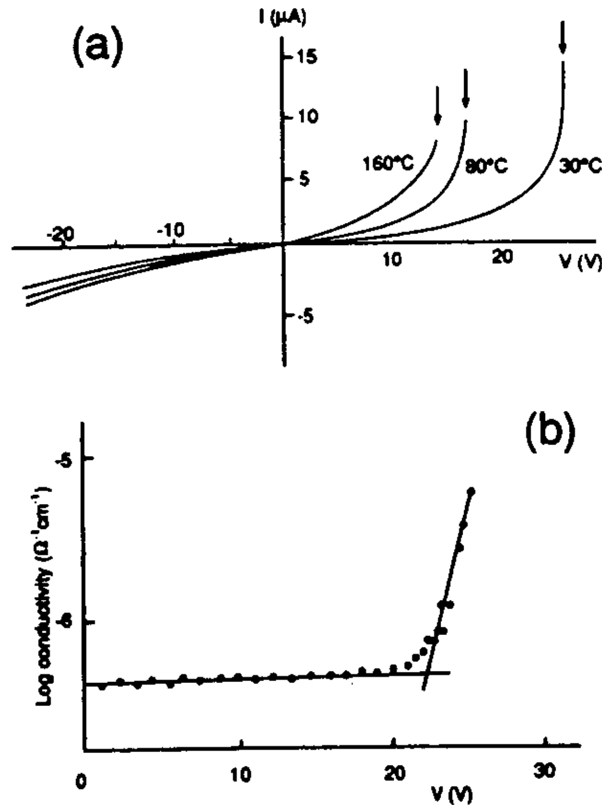

Figure 14.9 (a) *I-V* characteristics of unformed (unswitched) amorphous silicon device; (b) conductivity versus voltage plot.

clearly apparent in the effective-conductivity-versus-applied-voltage plot of Figure 14.9(b). As the temperature increases, the onset of nonohmic behavior moves to lower voltages. In the reverse direction, corresponding to a negative potential applied to the p^+ side, there is an initial ohmic region that is symmetrical for positive and negative voltages. However, the change to nonohmic behavior is much more gradual in the reverse direction, leading to eventual breakdown of the device.

As noted above, during point-by-point measurements under forward bias, the a-Si:H p^+-n-i device tends to become unstable when the applied bias is about 24V at room temperature. At higher temperatures, the instability, indicated by the arrows in Figure 14.9(a), occurs at lower voltages. When we attempt to increase the voltage still further, the device switches into a low-resistance ON state. Typical I-V characteristics for both polarities in the ON state are shown in Figure 14.10. The I-V curve is ohmic; it extrapolates through the origin (i.e., the ON state is a permanent memory state); and it is slightly asymmetrical. Note that the current is now measured in milliamperes and the voltages across the device are small. On increasing the voltage in the forward direction, we find that the ON-state current continues to increase apparently indefinitely, subject only to any current-limiting resistor, and the device is eventually destroyed, presumably by Joule heating. In the reverse direction, however, another instability is observed, and at about -1V (typically) the device switches back into a high-resistance OFF state, as shown in Figure 14.11. The OFF-to-ON transition may now be repeated by biasing in the

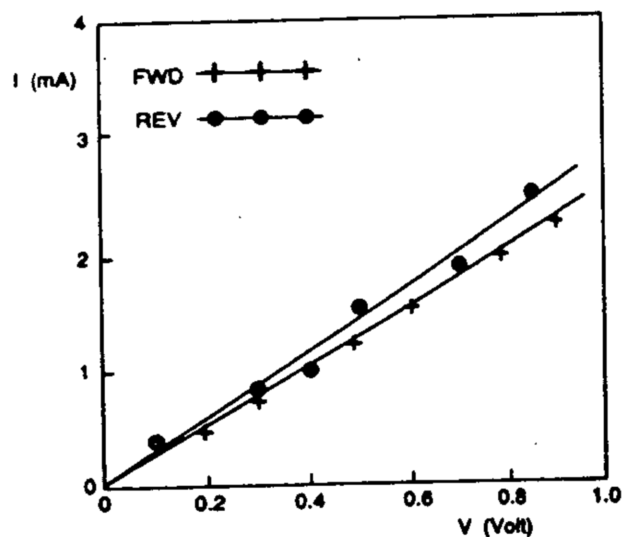

Figure 14.10 I-V characteristics of memory ON states.

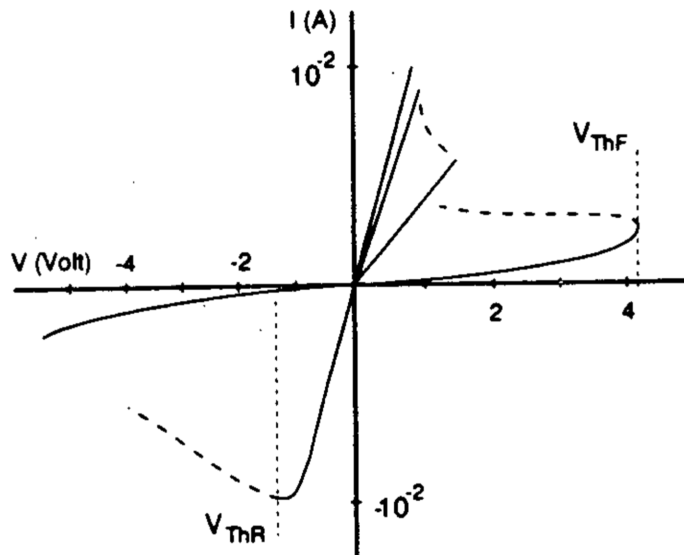

Figure 14.11 *I-V* characteristics of memory switching device for both polarities.

forward direction, but on the second and all subsequent switching operations the forward threshold voltage V_{Thf} occurs at a much lower voltage than the first operation (e.g., at ~5V compared with the 25V observed under the conditions of the measurements shown in Figure 14.9). The first OFF-to-ON transition, occurring at a relatively high voltage, seems unique and by analogy with the terminology in chalcogenide glasses, it is referred to as "forming."

The formed p^+-n-i device may be cycled through ON and OFF states by a biasing in forward and reverse directions with critical points at V_{Thf} and, in the reverse direction, V_{Thr}, as illustrated in Figure 14.11. It is important to emphasize that these devices exhibit not only nonvolatile but polarity-dependent memory switching. On occasions the device appears to go through a number of intermediate states during the OFF to ON transition, and this is indicated in the figure. In addition, there is often an observable and appreciable region of negative resistance in the reverse-biased OFF-state characteristics of the formed device.

A number of other dc experiments have also been carried out on formed devices in an attempt to provide additional information, primarily about the nature of the ON state. Figure 14.12(a) compares the area dependence of the OFF- and ON-state resistances for samples of different area (i.e., different pore sizes with diameters from 5 to 300 μm) from a single p^+-n-i deposition run [54]. These results were obtained on specimens that had previously been switched many times. Within

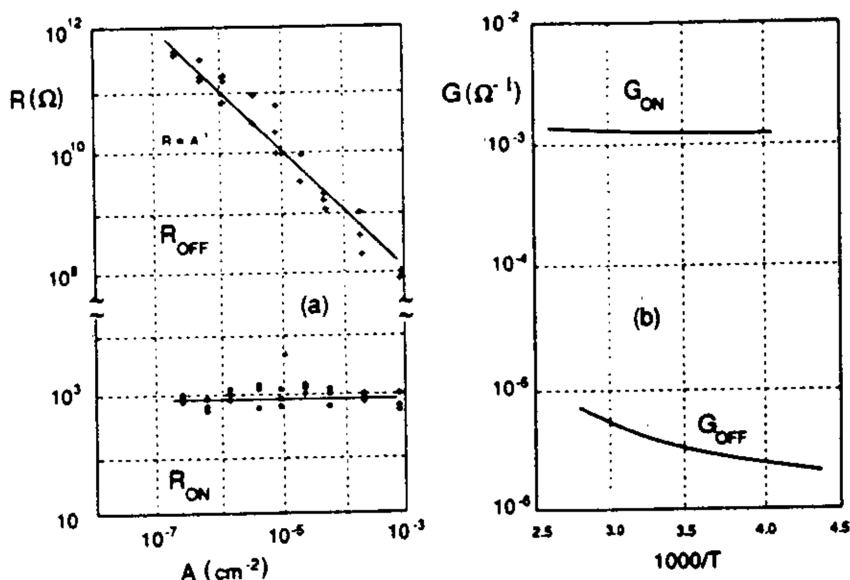

Figure 14.12 (a) Area dependence of ON and OFF state resistances; (b) temperature dependence of ON and OFF state conductances.

the experimental scatter, R_{OFF} clearly scales with the reciprocal of the area A, demonstrating that in the OFF state the current flows throughout the whole area of the specimen. In complete contrast, the values of the ON-state resistances R_{ON} for the same specimens show no area dependence at all. This result can be understood only if the ON state has its origin in a highly conducting filament, less or equal to a few μm in diameter, that extends through at least part of the specimen thickness.

The temperature dependence of both the ON- and OFF-state conductance has also been measured over the temperature range from about 230K to 400K. Results for a typical p^+-n-i specimen are shown in Figure 14.12(b). The OFF-state conductance G_{OFF} varied slowly with temperature, increasing by less than a factor of three between 230K and 360K. The ON-state conductance was even less temperature-dependent, increasing by only 10% over this temperature range. The insensitivity of these device parameters to temperature is also observed in other properties. For example, the magnitudes of the voltages required to switch the device ON and OFF, measured under pulsed conditions, both increase by only a factor of 2.5 as the temperature is decreased from 400K to 200K. Clearly, the general temperature insensitivity of the switching must also be a feature of any theoretical model.

Transverse magnetoresistance $\Delta\rho/\rho$ measurements of the ON state of a number of specimens have also been carried out at room temperature up to magnetic fields of $B = 0.5\ T$ [55]. Within the experimental error, $\Delta\rho/\rho$ was proportional to the square of the magnetic field strength B and was found to be positive. The values of $\Delta\rho/\rho(B^2)$ ranged from 0.5 to $2.0 \times 10^{-4}T^{-2}$. Experiments on phosphorus-doped a-Si:H after thermal crystallization also gave a positive magnetoresistance with the same $\Delta\rho/\rho(B^2)$ dependence. Unfortunately, no results have been reported; on homogeneous undoped glow-discharge a-Si films; it is therefore difficult to draw any definite conclusions about the amorphous or crystalline nature of the filament from the present results. However, it is probably correct to associate the B^2 dependence of the memory ON state with a longer mean free path than is normal in amorphous solids. By conventional crystalline theory [58], the magnitude of the measured $\Delta\rho/\rho(B^2)$ would lead to an effective mobility $\sim 100\ cm^2V^{-1}s^{-1}$ supporting of this suggestion. The importance of this measurement will be further discussed in Section 14.2.2.1 in connection with the very recent observation of electron quantization phenomena observed at low temperatures.

Direct evidence for the existence of a filamentary ON state was obtained from thermal imaging [59]. The a-Si:H p^+-n-i device was covered with a thin layer of thermochromic liquid crystal. By passing current through the device in the ON state, it is possible to observe the current path from the changes produced by Joule heating in the reflected color of the liquid crystal. The resulting features for 20-μm pore diameter structures were viewed through a high-powered optical microscope. The change in the liquid-crystal appearance produced by the filament in the ON state could be seen clearly as a small circular "hot spot" approximately in the center of the pore. The visual observation of the current filament has also enabled us to establish that switching a device OFF and ON again produces the current filament in the same place and this implies that the switching processes are not destructive. In these experiments the specimens were covered by a thin layer of a liquid crystal, 4-cyano-4-alkylbiphenyl, which undergoes a nematic-liquid phase transition at 35.3°C. The phase boundary may be observed quite easily in cross-polarized light, and the transition was found to be fast and without hysteresis. If the sample temperature is fixed using a thermostatically controlled stage, the difference in temperature between a region of local heating (at temperature T_h) and the surrounding film (at T_f) may be determined. The results indicate that no observable temperature rise occurred as a result of applying electrical power to the pore in either the unformed state just prior to forming or in the formed OFF state just prior to switching. However, as described above, in the ON state, local heating (which results from applying continuous power) could be clearly seen. The effect of changing the rms power applied to a 50-μm-diameter pore was studied using a continuous train of 300-ns pulses. The stage was maintained at 21°C; thus the phase boundary represented the locus of points (35.3° − 21° = 14.3°C) above the film

temperature. These isotherms were circular and in the particular case studied were symmetric about the center of the pore.

A plot of the phase boundary diameter d_i versus rms power P_{RMS} is shown in Figure 14.13(a). Although there is considerable scatter, it can be seen that the relationship between d_i and P_{RMS} is substantially linear for $d_i > 2$ μm. Below this the accuracy of the measurements is limited by the resolution of the microscope used; the onset of observable effects occurs at $P_{RMS} = 2$ mW. A linear dependence of d_i on P_{RMS} is obtained as a solution of the heat conductivity equation for an idealized system of this kind, in which the source of local heating is assumed to be much smaller than d_i. Thus these data indicate that the diameter of the ON-state filament d_f must be less than about 2 μm.

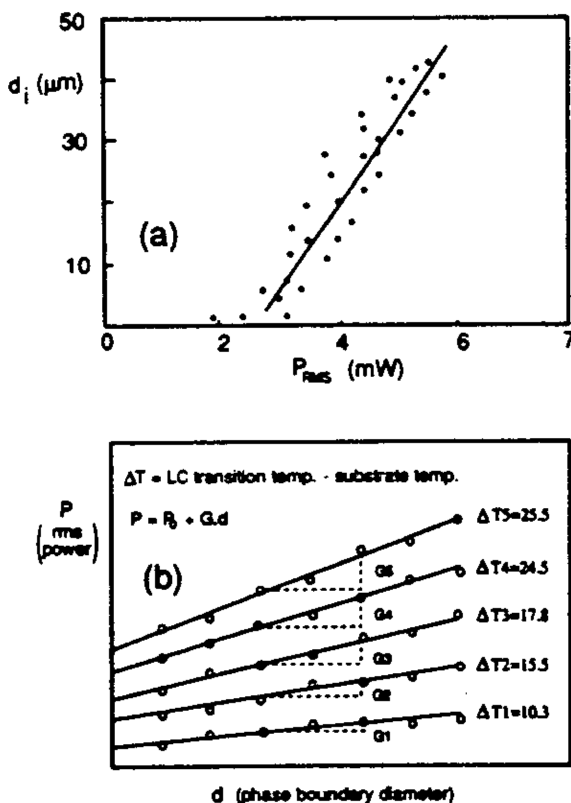

Figure 14.13 (a) Liquid crystal phase boundary diameter versus RMS power; (b) phase boundary diameter versus RMS power at various values of excess temperature ΔT.

The steady-state thermal properties of the 20-μm pore structures with different top electrodes (Al, Cr, Ti) have also been studied, and the results are reprsented in Figure 14.13(b), where rms power is plotted versus the phase boundary diameter for different local temperature increases. It is found that the gradients G_n and intercepts P_{0n} scale linearly with the local temperature rise ΔT, with the constants of proportionality M_G and M_{P_0} depending on the top electrode metal (and possibly its thickness, although this has yet to be established). Therefore, the following relationships can be used to characterize the steady state thermal properties:

$$G = M_G \Delta T \tag{14.7}$$

$$P_0 = M_{P_0} \Delta T \tag{14.8}$$

and therefore

$$P = M_{P_0} \Delta T + M_G \Delta T d \tag{14.9}$$

The values of M_G and M_{P_0} are summarized in Table 14.1. In the case of Al and Cr top electrodes, several different samples have been investigated, with the values obtained being similar to those in the table.

Table 14.1
Summary of Thermal Properties

Top electrode	$M_G (Wm^{-1}K^{-1})$	$M_{P_0} (mWK^{-1})$
Al	3	0.2
Cr	6	0.02
Ti	7	0.007

The physical significance of M_G is that it represents the surface thermal conductivity of the pore, and thus it is not surprising that the values obtained experimentally lie between the bulk values for glass (1 $Wm^{-1}K^{-1}$) and metal (100 $Wm^{-1}K^{-1}$). The significance of M_{P_0} is less clear. In the ideal case of a point heat source located on one thermally insulated surface of an infinite plate, the other surface being isothermal, M_{P_0} should be zero. Thus it may be that the nonzero values in some way reflect the extent of the heat source. If this is the case, it would appear that the filaments in pores with Cr and Ti top electrodes are smaller than in those with Al electrodes.

14.2.1.2 Current Instabilities in Unformed State

Unusual current instability phenomena have been observed in a-Si:H p^+-n-i structures with Al top electrodes in which the i layer is either thin (100Å) or lightly n-doped (1–5 vppm) [56]. The principal features associated with the current instability are shown in Figure 14.14. A voltage pulse V, greater than a minimum threshold V_c (specified later) is applied so the p^+-layer is positively biased. A displacement current occurs, which decays to a steady current I_s. Some time t_d after the voltage pulse is first applied, the current rises abruptly. After reaching a maximum value I_{max}, the current decays. A second pulse may be applied at time t_r after the first pulse, which may or may not give rise to a second instability, depending on the values of V and t_r. The dependence of the onset time t_d on pulse height V

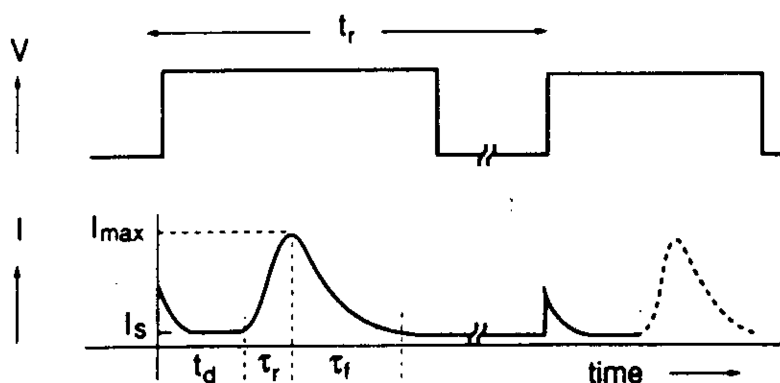

Figure 14.14 Current instability in metal-amorphous silicon structure.

for three different temperatures is shown in Figure 14.15. The experimental data are summarized by the following empirical relation:

$$t_d = t_{d0} + t_0 \exp\left[\frac{-(V - V_c)}{V_0}\right] \qquad (14.10)$$

where $V_0 \sim 0.6$–0.8V, $V_c \sim 10$–15V, $t_0 \sim 10$–100 μs, and $t_{d0} \sim 100$ ns. We note that V_o is temperature independent over the range studied, but some or all of the other parameters clearly show a temperature dependence.

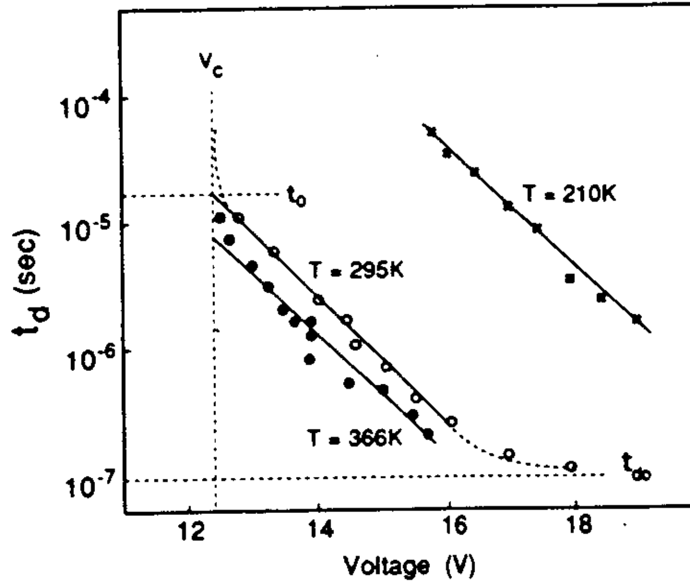

Figure 14.15 Onset time versus pulse height (current instability) at different temperatures.

The above relation applies only to the region where V is somewhat larger than V_c. The detailed relationship between t_d and V at $V \sim V_c$ is difficult to establish; there is a tendency towards erratic behavior, but no current instabilities have yet been recorded with $t_d > 100$ μs. It appears that t_d either increases almost discontinuously at $V = V_c$ or the effect simply does not occur under these conditions. As V is increased, several volts above V_c, $t_d \rightarrow t_{do}$, but further increase in V causes an irreversible change in the device characteristics, culminating in a permanent low-resistance (10^3 – $10^4\Omega$) state when the voltage pulse is removed.

The observed minimum delay time t_{do} may correspond to the transit time of an injected pulse of holes through the n-region. Taking typical values of t_{do}, n-layer thickness, and maximum applied voltage (0.1 μs, 0.1–0.3 μm, and 10–20V, respectively) and assuming that a large proportion of the applied bias under these conditions appears across the n-layer, the hole-mobility values can be estimated to lie in the range 10^{-4} to 10^{-3} cm^{2}V^{-1}s^{-1}, which is not unreasonable. Measurements of the dependence of I_{max} at constant t_d on device areas over the range 10^{-4}–10^{-7} cm^2 have failed to reveal a direct proportionality; I_{max} ranges over an order of magnitude in the various samples, but this seems to be primarily a random variation. As the smallest device examined in this study was about 10 μm in diameter, this suggests that the current during the instability is transported through a region of these dimensions or less. This is an important observation, as it has been established

(Figure 14.13(a)) that conduction in the memory-ON state is localized within a filament of 1-μm diameter or less. Thus it seems that the localized conduction occurring during the current instability may signify the formation of an incipient filament and is therefore a precursor to the memory-forming process. Additional indirect evidence supporting this view is that the forming delay time versus applied voltage relationship can be described by an expression similar to that given in (14.10).

Certain features associated with the current instability are found to occur in the analogous crystalline-silicon *metal/i-n-p⁺/metal* (MISS) devices [10]. In particular, the relationship between t_d and V is similar. This suggests that the principles on which the theory of operation of the crystalline device is based may be applicable here. Although such theories differ somewhat in detail, the central concept is that sufficient holes, injected from the forward-biased *p-n* junction, accumulate to form an inversion region at the *n-i* interface. Buxo [59] demonstrated that the theoretical expression for the t_d-versus-V relationship, based on the establishment of an inversion layer, is in good agreement with experiment. However, the behavior of the amorphous device differs in two important aspects. First, the current decays after reaching a maximum value, even when the voltage is maintained. The crystalline MISS device remains in its high-conductivity state provided a "holding" voltage is present. Second, there exists a voltage-dependent recovery time t_r, as described earlier and shown in Figure 14.14. This effect has no analog in the crystalline MISS device. The current decay may occur as a result of electron-hole recombination close to the *n-i* interface, which will increase the potential barrier to electrons tunneling from the metal into the conduction band in the *n*-layer. This negative feedback will decrease the tunneling contribution to the total current; however, once the initial conditions are reestablished, the current should again rise, and this is not observed experimentally on a time scale of μs. The recovery effect may be the consequence of some longer-term structural change caused by recombination, or by Joule heating, as the local power density will be quite high.

14.2.1.3 Forming

The forming process does not occur instantaneously when a voltage step or pulse is applied to the device. Initially there is a delay time τ_D during which the device current remains essentially constant at the OFF-state value appropriate to the voltage across the device. Only after this delay does the current begin to increase, and it then rises almost instantaneously to its ON-state value. The forming delay time is an extremely sensitive function of the applied forming voltage V_F, and typical data, obtained at three temperatures, are given in Figure 14.16. The forming delay time varies over nearly 10 orders of magnitude, from a few hundred seconds at low forming voltages to about 10 ns at high V_F. In particular, at a temperature-dependent critical forming voltage V_c, there occurs a virtually discontinuous change

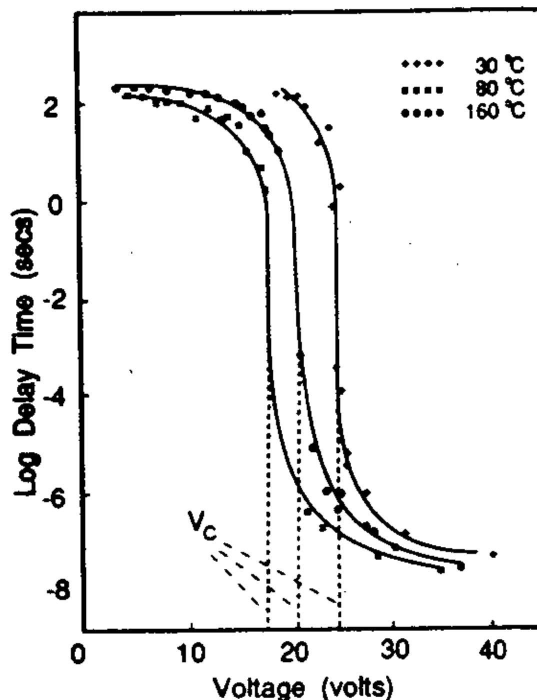

Figure 14.16 Forming delay time versus voltage height.

in τ_D. The critical voltages V_c indicated in Figure 14.16 are approximately the same as the voltages at the points of instability marked by the arrows in Figure 14.9(a); V_c also corresponds to the forming voltage obtained in experiment with a curve tracer operated in ac mode at a frequency of 100 Hz. It can also be seen in Figure 14.16 that above and below V_c the delay time tends to a value that seems to be approximately independent of both voltage and temperature; for the particular results illustrated, τ_D is in the range 10^2–10^3 s for $V < V_c$ and lies between 10 and 100 ns for $V > V_c$.

The results plotted in Figure 14.16 for $V < V_c$ correspond, of course, to voltages less than the point of instability indicated in Figure 14.9(a). There does appear to be a lower limit to the forming voltage, however, and present results indicate that the limiting voltage coincides with the bias at which the I-V characteristics change from their ohmic to nonohmic behavior (Figure 14.9(b)). Several experiments have shown that virgin devices fail to switch (form), even if held for many hours at a forward bias only slightly below the nonohmic region. In other words, forming occurs at any forward bias within the nonohmic region of the I-V

characteristics, but at voltages below the point of instability, τ_D is comparatively long. It must also be reemphasized that the device current remains constant at its preformed magnitude during the delay time, even when τ_D is 100 s or more.

Experiments have also been carried out to determine the effects of p^+-n-i device geometry on the forming voltage V_F. It was found that V_F increases linearly with the thickness d_n of the n-layer [54]. The charge $Q = \int I dt$, which flows through or into the device during the forming delay time, has also been determined for $V_F > V_c$. In this range the ratio (Q/d_n) is approximately independent of V_F and d_n for n-layer thicknesses between 0.2 and 0.8 μm. This could mean that forming occurs when a critical volume charge has accumulated in the n-region.

The current I-V characteristics in the high-field preswitching region are plotted as $\log \sigma$ versus $E^{1/2}$ in Figure 14.17, showing that the logarithm of conductivity prior to forming is proportional to the square root of the applied electrical field. There are at least two conduction mechanisms that can give rise to nonohmic behavior of this kind:

1. The Poole-Frenkel effect, in which the potential barrier for the thermal excitation of trapped electrons into the conduction band is lowered by the applied external field;
2. The Richardson-Schottky effect, which is associated with the lowering of the effective work function (or barrier) for charge-carrier emission from a metal electrode when an electric field is applied. The lowering is due to combined effects of the field and the image force.

Assuming that the conductivity is bulk limited, the high frequency dielectric constant obtained by fitting the experimental data to the Poole-Frenkel model is 48.7, whereas a value of 12.7 is obtained using the Richardson-Schottky model. The dielectric constant for crystalline silicon is about 12, and this value does not change very much with frequency. The dielectric constant for amorphous silicon is probably similar. It is more likely therefore that the current flow in the high-field preswitching region (just prior to forming) is determined by the Richardson-Schottky effect at the metal/i-layer contact. This conclusion is further supported by the observation that the forming voltages are different in devices with different metal electrodes but otherwise identical thicknesses, indicating the importance of the Schottky barrier in the structure. However, it should be kept in mind that the values of E in the above analysis presuppose a uniform field whose magnitude is proportional to applied bias. It was shown in Section 14.1.1 that, under certain circumstances, conduction in p^+-n-i samples in the high-bias regime is spatially nonuniform, which suggests that the assumptions made concerning the field within the conducting region may become less valid as the bias is increased. The rapid rise in conductivity under these conditions, as shown in Figure 14.17, may correspond to the onset of electron tunneling from the metal through the i-layer under a very high field.

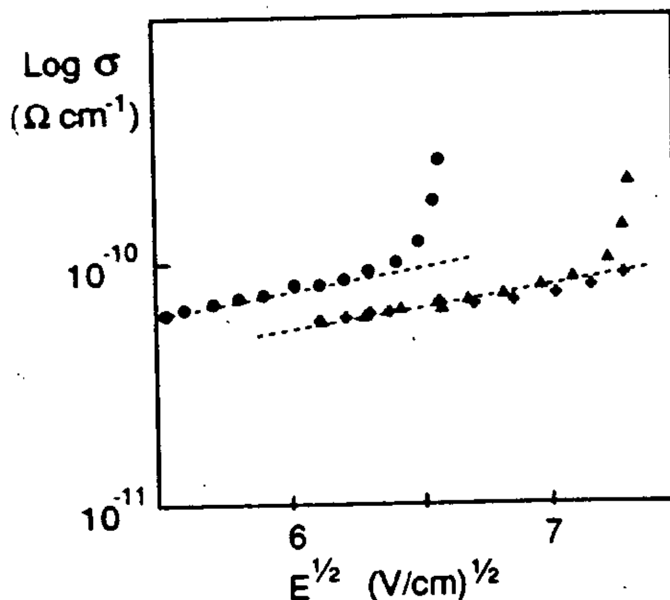

Figure 14.17 Log conductivity versus square root of electric field.

14.2.1.4 Dynamic Switching Behavior

The principal features of the pulsed operation of formed a-Si:H p^+-n-i devices have been described by Owen [53] and LeComber [54]. A representative diagram from an oscilloscope trace of the OFF → ON (WRITE) and the ON → OFF (ERASE) transitions on applying a voltage pulse is shown in Figure 14.18. The oscillations on these traces are caused by ringing effects in the rather poorly matched electrical setup. The main points to note are:

1. When biased with a pulse in the forward direction, the device switches from OFF to ON (WRITE), provided the pulse height exceeds the static threshold voltage V_{TH}, as defined in Figure 14.11.
2. There is a delay time in the WRITE operation (Figure 14.18(a)) which is a strong function of the WRITE pulse magnitude as shown in Figure 14.19. These delay times are significantly faster than the delay times reported for chalcogenide switches (see for example [12, 14]). If the results in Figure 14.19 are expressed in the form $t_d = t_o \exp(-V/V_o)$ then t_o = 335 ns and V_o = 4.5V. Similar results have been obtained for all the specimens investigated although the V_o values ranged from about 0.5 to 13V.

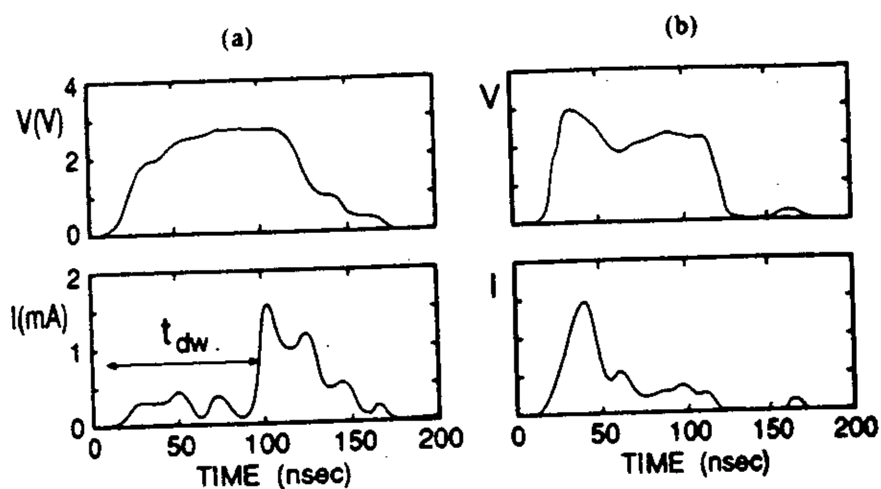

Figure 14.18 (a) WRITE and (b) ERASE switching transient waveforms.

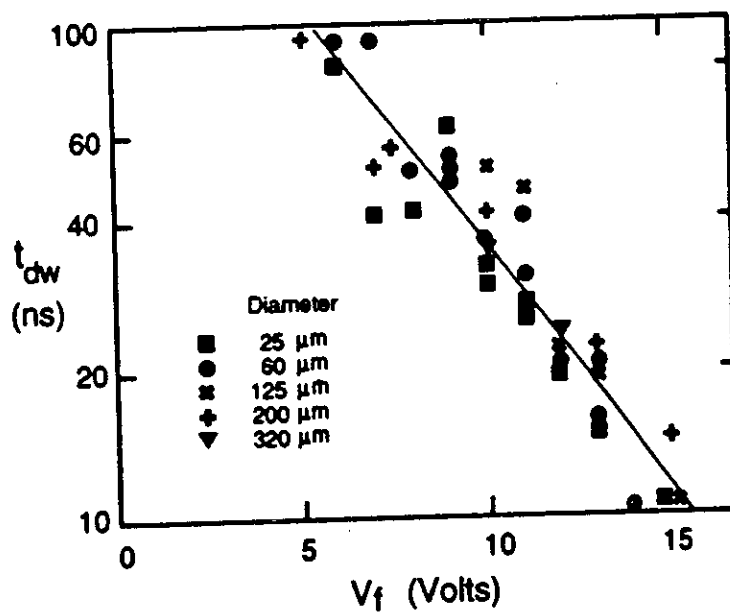

Figure 14.19 WRITE delay time versus voltage height.

3. Provided the pulse is long enough, the ON state is permanent and the pulse duration required for switching to a memory state increases as the pulse height decreases toward V_{Thf}. In typical cases a permanent ON state is obtained with pulse durations of a few tens of nanoseconds and magnitude ~5V in excess of V_{Thf}.
4. Similarly, on biasing in the reverse direction with a pulse of height $>V_{Thr}$ the device switches from ON → OFF (ERASE) and again there is a delay time of the order of nanoseconds in the response (Figure 14.18(b)).
5. Both the OFF and ON states appear to be truly permanent. No detectable changes have been observed in devices stored at room temperature, either in the OFF or ON state, for a number of years.

14.2.2 Analog Memory Effects in a-Si:H Metal-p^+-Metal Structures

More recent experimental results [57, 60] have demonstrated a new metal-p^+-metal amorphous silicon device which, rather than exhibiting a two-state digital operation, has a continuum of stable states that are nonvolatile and fully programmable by single 10-ns voltage pulses. It has also been suggested that the new analog memory devices can be used as nonvolatile and reprogrammable memory elements in analog neural networks [61]. In this section we present a summary of the new results obtained on nonvolatile analog switching effects in amorphous silicon metal-p^+-metal devices and discuss the possible physical mechanisms responsible for the phenomena. The samples used for this work were amorphous silicon Cr-p^+-V thin-film structures. The p^+-layer was prepared by RF glow-discharge decomposition of SiH_4 containing 10^4 vppm of B_2H_6. Films of 1000Å thickness were deposited onto Corning glass substrates previously patterned with chromium bottom contacts. The p^+ amorphous silicon was then patterned, and an insulating layer was used to define an active device area of $10^{-6}cm^2$. The metal used for the top contact was normally vanadium. However, a number of different metals were also used, and their influence on the memory operation will also be described.

In accordance with our previous results [53], memory devices prepared in this way require an initial forming process. This means that the resistance of the as-deposited (unformed) device has to be lowered from $R \sim 10^9 \Omega$ to $R \sim 10^3 - 10^4 \Omega$ (i.e., the typical value of an ON state). The forming can be achieved by biasing the sample with a single voltage pulse (duration 300 ns, magnitude ~12V) with positive polarity applied to the top V contact. The metal-p^+-metal memory structures exhibit a forming step that is different from the previously investigated metal-p^+-n-i-metal structures [55]. The differences are demonstrated in Figure 14.20. In the case of metal-p^+-n-i-metal structures, the resistance suddenly drops from $\sim 10^{10} \Omega$ (virgin state) to $\sim 10^3 \Omega$ after the critical voltage (forming voltage V_F) has been applied. No change in the virgin resistance occurs when the sample is biased

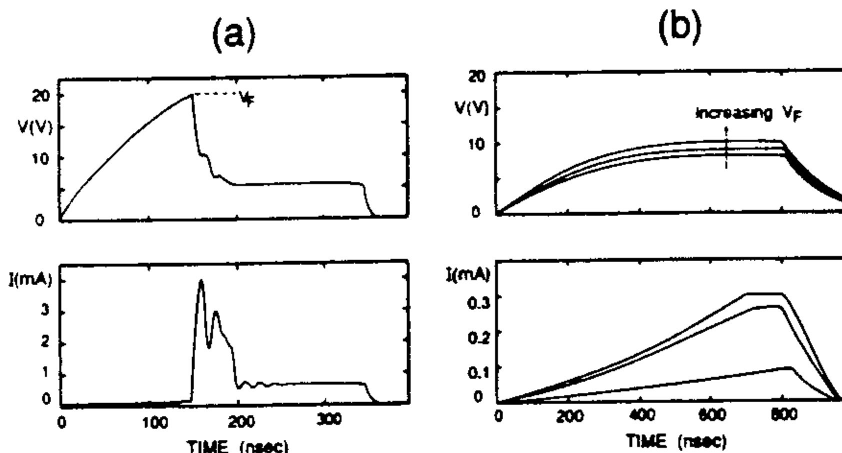

Figure 14.20 (a) Waveforms of a single forming pulse applied to amorphous silicon Cr-p^+-n-i Al structure showing hard forming; (b) waveforms of single pulses of increasing magnitude applied to amorphous silicon Cr-p^+-V structure showing soft forming (V and I represent voltage across device and corresponding device current, respectively).

with voltages less than V_F. This type of forming is termed *hard forming*. In contrast to this, the resistance of the unformed metal-p^+-metal structures can be lowered gradually by applying voltage levels with progressively increasing magnitudes. In this case no sudden change of the current or voltage signal can be detected when the sample is biased with a voltage pulse, as seen in Figure 14.20(b). This process is called *soft forming*. Figure 14.21 shows the device resistance as a function of the soft-forming voltage (pulse duration = 300 ns). On reaching a critical voltage (~14V in Figure 14.21) the device resistance suddenly drops from ~$10^6\Omega$ to ~10^4–$10^3\Omega$. This is the memory-ON state of the device. Once the memory device had reached its first (nonvolatile) ON state, all subsequent switching operations were performed with 10–100-ns pulses of 1–5V.

An example of the analog switching effect is shown in Figure 14.22(a), where the sample resistance is plotted as a function of applied alternating WRITE and ERASE pulses (100 ns pulse duration each). It is important to emphasize the polarity dependence of the analog memory behavior. In the case of the WRITE pulses, positive polarity is applied to the Cr track (bottom contact), whereas ERASE pulses have opposite polarity. The sample was first switched to an ON state (R_{ON} = 2 × $10^3\Omega$) and then a series of alternating WRITE and ERASE pulses were applied. The WRITE pulses were kept at a constant magnitude of 3.4V but the ERASE pulses were incremented by 0.05V steps from 1.2 to 3.4V after each WRITE pulse. It can be seen from Figure 14.22(a) that the sample resistance

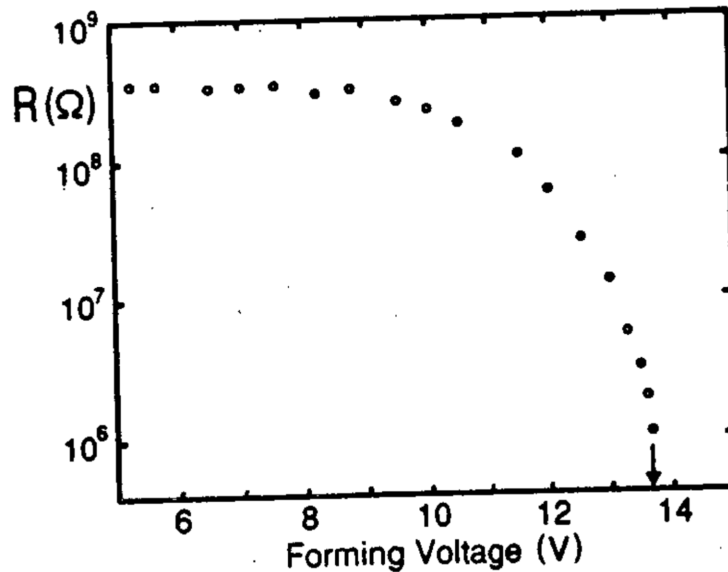

Figure 14.21. Resistance of an amorphous silicon Cr-p^+-V memory structure as a function of forming voltage.

changes in an analog manner as the magnitude of the ERASE pulse increases, that is, the difference between R_{ON} and R_{OFF} is a function of the magnitude of the ERASE pulses. A voltage range of ΔV (ERASE) = 1.6V resulted in a change in resistance from R~2 × $10^3\Omega$ to R~6 × $10^5\Omega$. The shaded-area in Figure 14.22(a) indicates the reproducibility of the analogue memory switching, i.e., the scattering in the resistance during repeated experiments (data from 100 cycles are shown). Figure 14.22(b) shows another case where the ERASE pulses were maintained at a constant value of V = 3.4V, but the WRITE pulses were incremented from 1.2V to 3.4V in 0.05V steps. The value of the OFF-state resistance remained constant at ~6 × $10^5\Omega$ that is, it changed back to this constant level from every ON state, while the ON-state resistance decreased through a continuum of intermediate states over a similar ΔV to the ERASE operation. The shaded area in Figure 14.22(b) again represents the reproducibilty of the analog switching for 100 complete cycles. It is emphasized that the device will switch between any two resistance states within the range from about 1 kΩ to 1 MΩ by selecting the correct polarity and magnitude of the WRITE and ERASE pulses. For all devices with a vanadium top contact, the values of ΔV range from 1.5 to 2.0V for both the WRITE and ERASE operations.

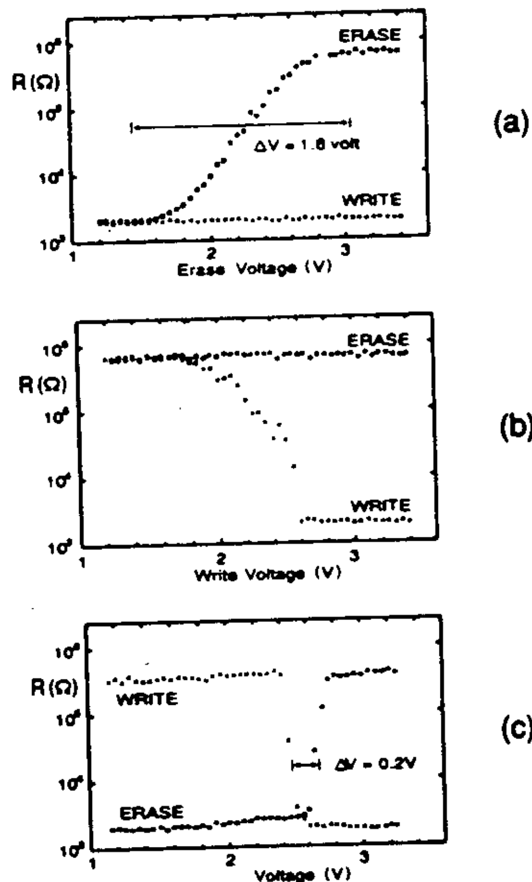

Figure 14.22 (a) Memory resistance as a function of ERASE voltage in a Cr-p^+-V structure; (b) memory resistance as a function of WRITE voltage in a Cr-p^+-V structure; (c) memory resistance as a function of WRITE and ERASE voltages in a Cr-p^+-Cr structure.

We have repeated the above experiments on metal-p^+-metal devices with Cr as top metal and observed similar polarity dependent changes in the memory state resistance. However, in the WRITE and ERASE experiments, intermediate states were found to exist over only a narrow ΔV of about 0.2V, as shown in Figure 14.22(c). Therefore, these devices are considered as digital devices. It is important to emphasize that both the analog (Figures 14.22(a) and (b)) and digital (Figure 14.22(c)) memory switching effects are nonvolatile. Devices set to ON or OFF states have been monitored for more than two years without any significant change

their resistance. Also, operation at temperatures up to 160°C shows little change in the threshold voltages or device stability. However, it is also found that devices with certain top metal contacts, such as Mo and Pd, show a volatile memory-switching effect. This is illustrated in Figure 14.23, where the current signal through the device is continuously monitored at a low voltage level (0.5V), which is below the voltage level of the programming pulses. The current signal decays rapidly after the end of the programming pulse, indicating that the memory state is volatile. The role of the top metal contact, therefore, has been thoroughly investigated by fabricating devices with a range of different top metals but with otherwsie identical physical parameters (i.e., ~1000Å thickness of p^+-layer, Cr bottom electrode). With the analog switching voltage window ΔV as a guide, its value is found significantly dependent on the top metallization contact. This is illustrated in Table 14.2.

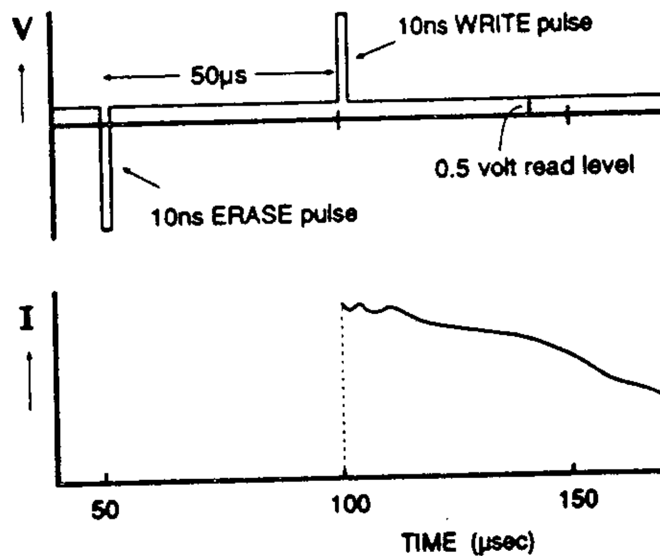

Figure 14.23 Volatile memory effect in a Cr-p^+-Mo structure.

It can also be seen that the definition of analog ($\Delta V \geq 1$V) or digital (≤ 0.5V) memory switching is somewhat arbitrary, because there is no sharp boundary between the two types of operation, that is, they are almost certainly associated with the same underlying physical phenomena. However, in the cases of Mo and Pd top contacts, a new type of volatile switching effect is observed and in the cases

Table 14.2
Effect of Top Metallization on Switching Behavior

Metal	*ΔV(V)*	*Switching Characteristics*
Ag, Al	<0.1	Digital, nonvolatile
Cr	0.2	Digital, nonvolatile
Mn, Fe	~0.5	Digital, nonvolatile
Ti	—	Unstable switching
Au, Cu	—	No switching
W	~1.0	Analog, nonvolatile
V	1.8	Analog, nonvolatile
Ni, Co	2.0	Analog, nonvolatile
Mo, Pd	2.0	Analog, volatile

of Ti, Au, and Cu, no reproducible switching effects can be observed. These results suggest that the top metal contact plays a crucial role in determining the type of memory-switching phenomena observed in these devices. Here we will concentrate on the p^+ memory devices with vanadium top contact, because these show typical nonvolatile analog memory switching.

The *I-V* characteristics of analog memory-resistance states were investigated systematically, both at room temperature and lower temperatures, and the following results were obtained. It was found that all the room temperature current-voltage characteristics show a linear-plus-power-law behavior in the various analog memory resistance states as shown in Figure 14.24. The *I-V* curves can be described by a simple nonlinear relationship:

$$I = C_1V + C_2V^n \tag{14.11}$$

where C_1 and C_2 are constants and the exponent n increases with the low bias (linear region) resistance according to the relationship $n = A + B \log R$. The observed power-law behavior could indicate the possibility of space-charge limited conduction at higher bias, although investigation of the thickness dependence has shown this to be unlikely. In accordance with the pulsed analog memory switching results, a continuous transition of states can be found between the ON ($\sim 10^3 \Omega$) and OFF ($\sim 10^6 \Omega$) states. The terms ON and OFF seem to be somewhat arbitrary, therefore, and are used in this chapter only for practical reasons. If the curves in Figure 14.24 are extrapolated above 1V, they meet in the region of 3 to 4V (i.e., at typical programming levels—see Figures 14.22(a)–14.22(b)). It was also found that the exponent n does not depend on the thickness or the diameter of the active device but it is primarily determined by the low bias (or linear region) resistance of the analog memory state. This indicates that the nature of the electrical conduction is quite similar in all memory states. However, repeatedly switching the device into the same resistance state need not always result in an identical value

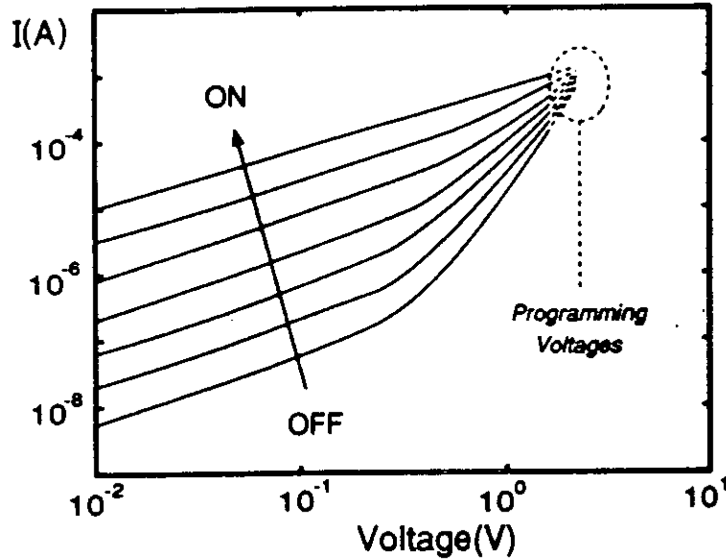

Figure 14.24 *I-V* characteristics of analog memory states plotted on log-log scale; characteristics are symmetrical about origin.

of the exponent. This appears to indicate that the "same" resistance state can be achieved through different conduction paths within the same device. This is consistent with the suggestion that the conduction path (the filament) might have an inhomogeneous structure consisting of a small-scale dispersion of metallic-like particles embedded in an insulating matrix; this structure may provide a variety of conduction paths.

It is possible to extend the range of the *I-V* characteristics up to the critical field where switching occurs using very short, single voltage pulses of varying polarities and pulse heights. Figure 14.25 shows the room-temperature "pulsed" current-voltage characteristics of an analog V-p^+-Cr memory device. These characteristics were obtained using 400-ns pulses of progressively increasing magnitude and of both polarities. The 400-ns pulse length is long enough to observe a plateau in the pulse signal (i.e., RC effects are avoided). Positive polarity means that the Cr bottom contact is more positive than the top contact. Starting from a 9.5×10^5 Ω OFF state (measured at 0.5 V, curve (a) in Figure 14.25), the onset of the strong nonlinear rise in the current occurs at about +1.1V. Curve (a) is reproducible in that it can be repeated many times without a change in the device resistance, up to a voltage level of about +1.7V. Further increase in the voltage height will result in a permanent decrease in the device resistance and, consequently, a change in the characteristics. The decrease of resistance is determined by the magnitude of the maximum voltage applied.

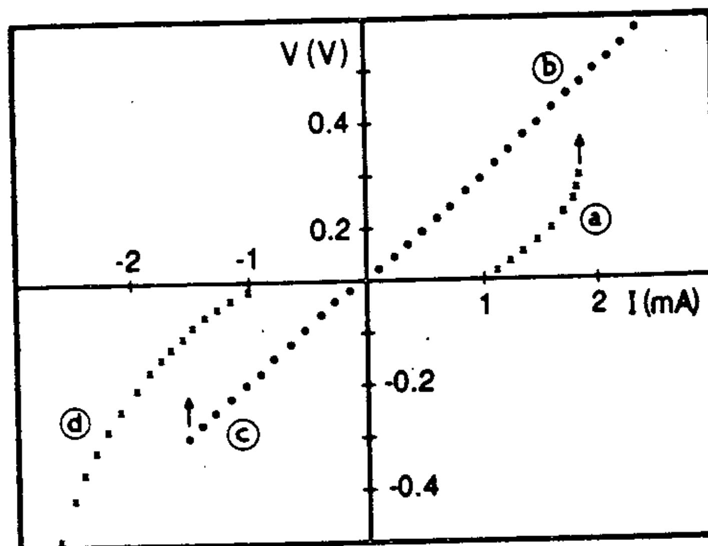

Figure 14.25 Pulsed I-V characteristics of Cr-p^+-V analog structure.

Curve (b) represents a memory-ON state (R = 5.6 × $10^3\Omega$ at 0.5V) of the device. Curve (b) is reproducible up to a voltage level of ~5V if positive polarity is applied. Further increase in voltage might destroy the device. However, if a negative voltage is applied to the same ON state (curve (c)), an ERASE process is observed at voltage levels greater than about 1.7V. On the other hand, if an OFF state (R = 9 × $10^5\Omega$) is negatively biased (curve (d)), no change in the OFF-state resistance can be observed up to a voltage of about −5V. The apparent polarity dependence suggests that the analog memory switching is not determined simply by the magnitude of the applied power or energy. This is further supported by a comparison of individual switching transients with opposite polarity. Figure 14.26 shows the waveforms of a single WRITE pulse (a) from OFF (R = 2 × $10^5\Omega$) to ON (R = 3.8 × $10^3\Omega$) and of an ERASE pulse (b) from OFF (R = 2 × $10^5\Omega$) to a slightly higher OFF state (R = 2.4 × $10^5\Omega$). In the second case there is no change in the memory state resistance although similar voltage and current levels are applied. The calculated total charge flowing through the sample is also similar: Q_W = 8.53 × 10^{-11}C for the WRITE and Q_E = 7.24 × 10^{-11}C for the ERASE pulse.

These measurements suggest that the memory-state resistance is determined by a combination of applied voltage level and appropriate polarity. On the other hand, the fact that the memory resistance is not determined by the applied power or energy suggests that the memory switching does not depend significantly on the internal temperature of the device. Figure 14.27(a) shows a switching transient of

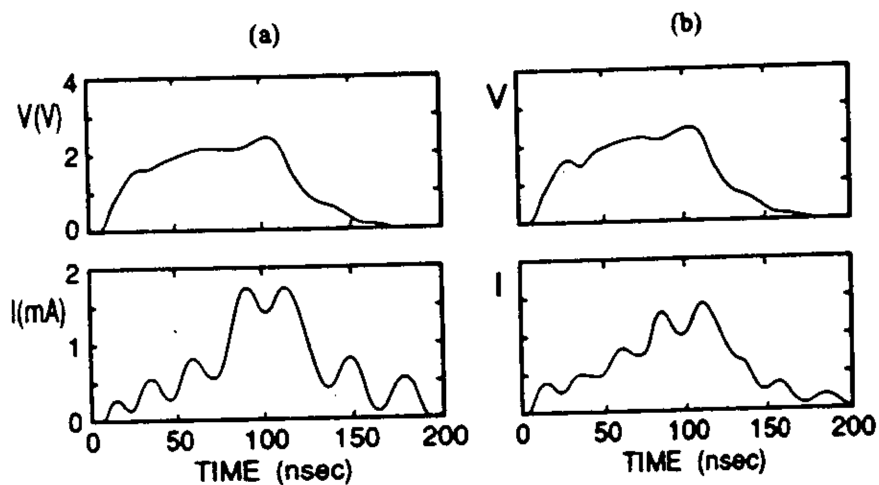

Figure 14.26 Waveforms of single-pulse memory switching: (a) OFF→ON transient; (b) ON→OFF transient.

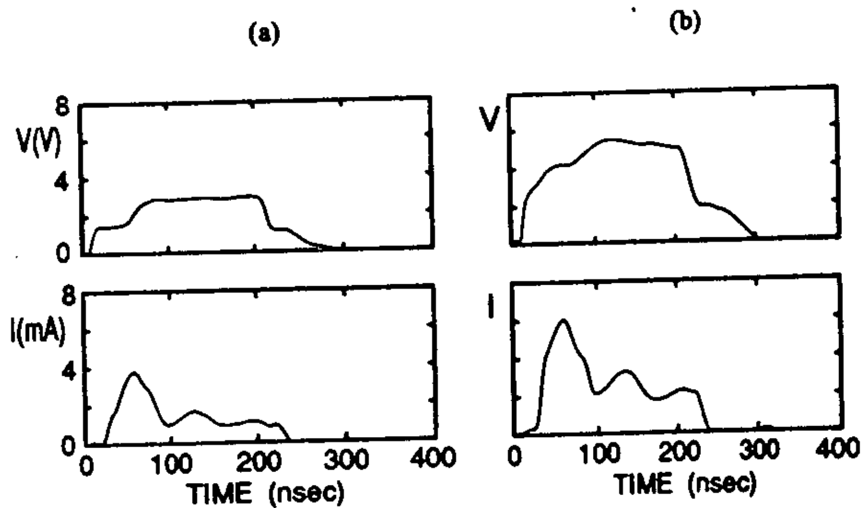

Figure 14.27 Waveforms of single-pulse memory switching: (a) ERASE transient at 300K; (b) ERASE transient at 4.2K.

an ERASE pulse at 300K, where the device resistance is changed from R_{ON} = $3 \times 10^3\Omega$ to $R_{OFF} = 6 \times 10^5\Omega$. Figure 14.27(b) shows a similar ERASE transient at much lower temperature (4.2K) where the device resistance has also changed from $R_{ON} = 3 \times 10^3\Omega$ to $R_{OFF} = 6 \times 10^5\Omega$. It can be seen that despite the large temperature difference, the current level and the threshold voltage required to achieve the same ERASE process as at room temperature increase by less than a factor of two. It should also be emphasized that the device continues to operate even at liquid helium temperatures. The analog switching effect is still observed at 4.2K without significant changes either in the threshold voltage or the current level. This suggests that the electrical conduction and memory phenomena are possibly connected to a temperature-independent physical process, which we propose may be associated with tunneling, for example, or with conduction through a channel of very small dimensions in which metallic-like inhomogeneities are distributed.

14.2.2.1 Low-Temperature Quantization Effects in a-Si:H Structures

The behavior proposed in the previous section is supported by recent results obtained during investigations of the low temperature conductivity of the analog memory states [61], [62]. Typical *I-V* characteristics of a formed memory-ON state at 4.2K are shown in Figure 14.28(a). In the voltage region from 0 to 0.36V, the current around zero bias is of the order of $\sim 10^{-9}$A but increases to $\sim 10^{-6}$A at voltages approaching 0.3V (i.e., a strong nonlinear behavior is found). It is important to emphasize that the room-temperature *I-V* characteristics of the memory-ON state are linear. The observed large increase in the resistance around zero bias is shown in the inset to Figure 14.28(a) and is consistent with tunneling conduction between metallic particles embedded in an insulating matrix [63]. Further experimental evidence for tunneling conduction comes from the temperature dependence of the device current at low bias voltages. In this regime, V is smaller than the tunneling barrier Φ and the conduction is associated with field-assisted tunneling. The approximate form of the current density/voltage characteristics is [63]:

$$J(V, T) = J(V, 0)\left(1 + \frac{3 \times 10^{-9} d^2 T^2}{\phi}\right) \tag{14.12}$$

where d is in Angstrom units, ϕ is in electronvolts and T is in Kelvin. The experimentally observed T^2 dependence is consistent with d = 50Å and ϕ = 1 eV.

At 0.36V, a current jump occurs and the resistance of the sample is lowered to the order of a few kΩ. After the first current jump at 0.36V, further current steps can be observed at 0.47, 0.53, and 0.70V (curve A, Figure 14.28(a)). At 0.36V (henceforth called the critical voltage V_{cr}) there is thus a dramatic change

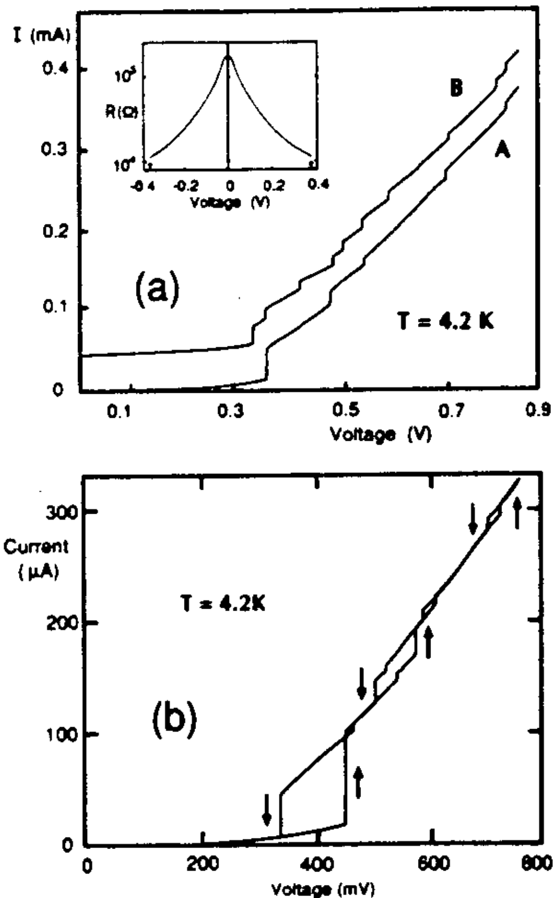

Figure 14.28 (a) *I-V* characteristics at 4.2K with (curve B) and without (curve A) magnetic field (curve B is displaced vertically for clarity, with (inset) resistance-voltage characteristics at 4.2K showing zero bias anomaly); (b) *I-V* characteristics at 4.2K showing hysteresis observed on first increasing, then decreasing voltage.

in the behavior of the sample. At voltages lower than V_{cr}, no discontinuities are observed but at voltages higher than V_{cr} the resistance is lowered and the current increases in discrete steps. The current-voltage characteristics are symmetrical (i.e., the same behavior is observed for the opposite polarity. Curve B in Figure 14.28(a) depicts the *I-V* characteristics of the same sample under the influence of a $B = 0.2\ T$ magnetic field. The curve has been displaced by 50 μA in the current scale for clarity. The direction of the magnetic field is 30° with respect to the conducting channel (the filament). Additional steps can be observed at 0.34, 0.42, 0.5, 0.59,

and 0.79V together with the steps observed in the zero magnetic field case (curve A). The effect of the magnetic field is reversible, and if the field is removed the *I-V* characteristics revert to the zero magnetic field case. A number of *I-V* characteristics have been obtained in which sharp and well-defined steps can be observed at 4.2K. However, it should be pointed out that the position of the observed steps is dependent on the direction of the voltage sweep (i.e., some hysteresis is observed as illustrated in Figure 14.28(b)).

The critical voltage V_{cr} at which the first current jump is observed and the magnitude of the first current jump are dependent on the resistance of the memory-ON-state investigated. Figure 14.29 shows the effect of changing the memory-ON-state resistance on the observed resistance steps. Resistance (in kΩ) is plotted on the right hand vertical axis; on the left, resistance is plotted in the dimensionless quantized units of ($h/2e^2$). The critical voltage and the magnitude of the first jump increase with increasing resistance ($R_d > R_c > R_b > R_a$), but after the first jump the characteristics are rather similar, suggesting a similar conduction mechanism at higher voltages. The first jump appears to be associated with the formation of a highly conducting path within the structure whose characteristics are independent of the low-bias behavior (i.e., of the different memory states). Therefore, we propose that the first large current step (at 0.36V) is associated with the formation of a narrow, highly conducting channel that significantly lowers the resistance of the sample. With further increase in the applied voltage the resistance is lowered

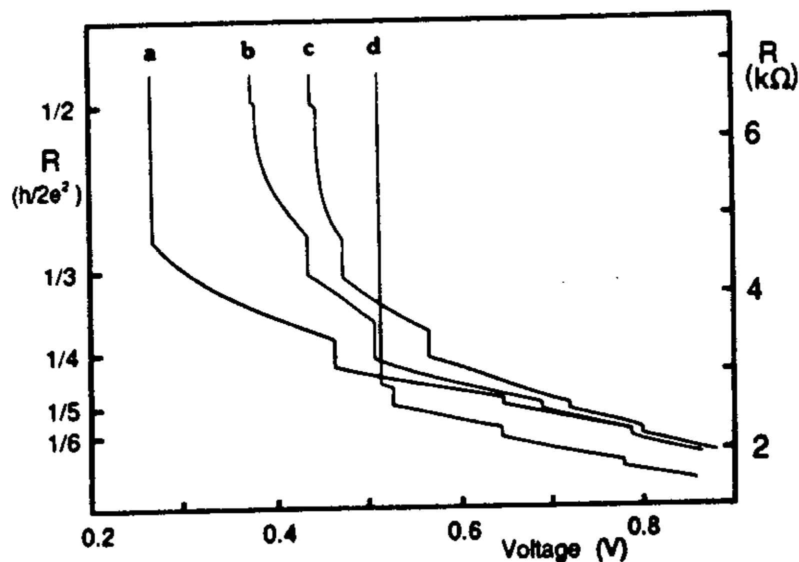

Figure 14.29 *I-V* characteristics of different memory states at 4.2K ($R_c > R_b > R_a$).

in steps, corresponding to quantized resistance values $R = h/2ie^2$ where i is an integer. In the voltage range from 0.36 to 0.8V, there are four steps, with i being 2, 3, 4, and 5. These correspond to the observed current rises in curve A, Figure 14.28(a). Higher voltages have not been applied to the sample because this could change the resistance of the particular memory state. If a magnetic field is now applied to the sample, further quantization of resistance is observed at values $R = h/2(i + 1/2)e^2$. This is illustrated in Figure 14.30(b), in which the data correspond to curve B in Figure 14.28(a). It can be seen that extra steps in the resistance occur at i = 2.5, 3.5, 4.5, and 5.5. The effect of temperature is illustrated in Figure 14.31. The curves have been shifted along the current axis for clarity. The observed current steps gradually decrease with increasing temperature, finally disappearing at the remarkably high temperature of 190K. In our more recent work [64], using samples that have undergone a further conditioning step, similar quantization effects have been observed at temperatures up to 400K.

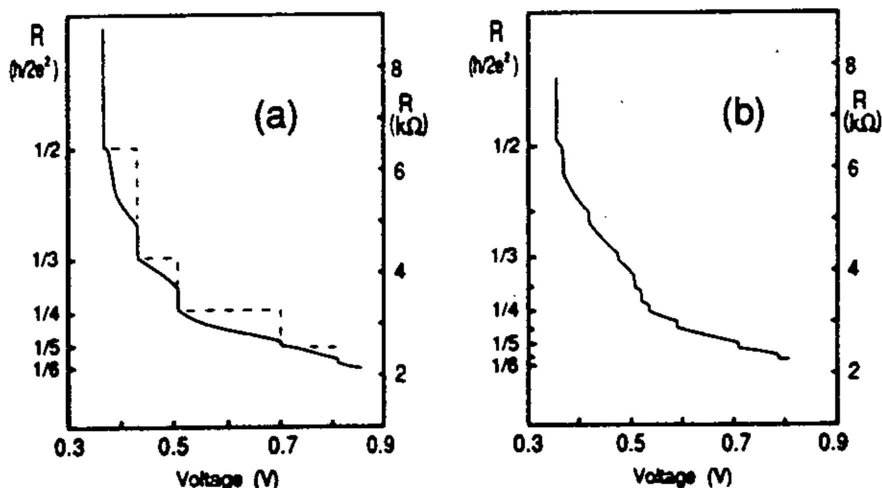

Figure 14.30 (a) Resistance versus voltage at 4.2K with no magnetic field (dashed line indicates idealized contribution from ballistic transport channel); (b) resistance versus voltage at 4.2K with 0.2-T magnetic field.

In analyzing the main results of this work, two important facts should be emphasized. First, the observation of quantized electron transport provides a vital clue to the structure of the analog memory element. Second, the programmability of the analog memory provides information about the possible mechanism of the switching process itself. The analog memory effect in amorphous silicon metal-p^+-metal structures can only be observed if the sample is subjected to an initial forming

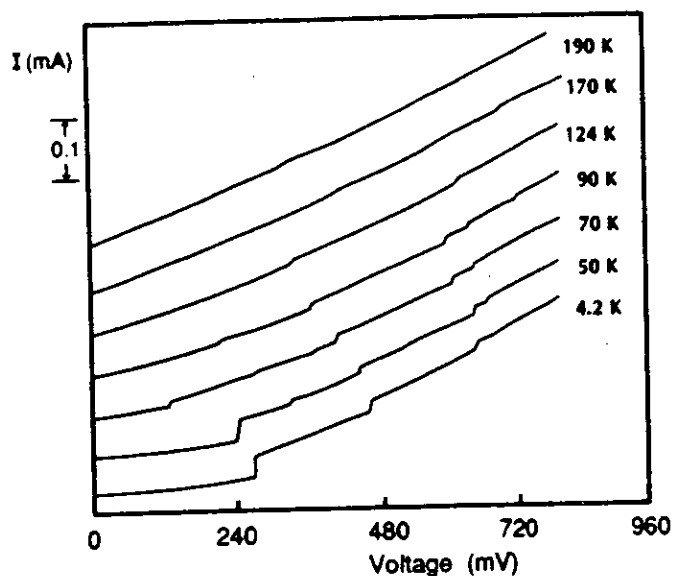

Figure 14.31 *I-V* characteristics as function of temperature (curves displaced vertically for clarity).

process. The forming process is characterized not only by the breakdown of the high-resistance state of the structure but, more importantly, by the presence of a positive feedback mechanism that provides a low-resistance ON state so that the breakdown is nondestructive and repetitive switching is possible. Furthermore, the experimental results suggest a strong influence of the choice of the top metal contacts (summarized in Table 14.2) on the type of memory switching observed (digital or analog switching) and on the success of obtaining stable and reproducible switching. These results are in good accordance with the previous observations [65] that the first switching event (forming) causes a local structural modification of the p^+ amorphous silicon layer, producing a highly conducting filament that does not revert to the original amorphous material when the device is switched OFF. After the forming process, the p^+ devices usually exhibit a lower OFF resistance than the unformed device resistance, in contrast to our original data for p^+-n-i devices [55]. The temperature dependence of the conductivity is also greatly reduced by the forming process. The area independence of R_{ON} (Figure 14.15) suggests localized electrical conduction after forming. These results, together with the newly observed quantized electron transport phenomena (Figures 14.28–14.31), provide strong experimental evidence that the forming process creates a filamentary region consisting of a new material whose properties have changed significantly compared to those of the unformed original material. It is feasible that the high fields and

current densities present during forming result in high temperatures developing locally, which could lead to enhanced diffusion of metallic particles from the electrode into the thin amorphous film. Such a region would become the preferred current path carrying the electron current in the ON state. The *I-V* characteristics in the ON state (Figure 14.10) suggest that any material rearrangement within the filament ocurs so as to destroy the rectifying properties of the original metal-p^+ Schottky contact at room temperature; it should also be noted that this is the case even in a typical OFF state.

Lowering the temperature of the memory device reveals further information about the possible structure. The low-temperature *I-V* characteristics (Figure 14.28(a)) show that we have observed a zero-bias anomaly and quantized resistance in the ON state of amorphous silicon Cr-p^+-V structures. The phenomenon of quantized electron transport is usually observed in the case where the mean free path of the electron λ is larger than the length of the conducting channel, resulting in ballistic conduction [66, 67]. The usual approach to the fabrication of devices based on ballistic conduction is to use a very high mobility material (usually high-purity GaAs), where the mobility can reach values in the order of $\sim 10^5$ $cm^2V^{-1}s^{-1}$ leading to the values of electron mean free path:

$$\lambda \sim \tau v_{th} \sim \frac{\mu}{q}(3kTm^*)^{1/2} \sim 1\ \mu m \qquad (14.13)$$

where τ is the momentum relaxation time, v_{th} is the thermal velocity, T is the lattice temperature, m^* is the effective mass of the electron, q is the electronic charge and k is the Boltzmann's constant. For the above estimate, $m^* \sim 0.068\ m_e$ (m_e is the free electron mass) has been used in the case of GaAs. The value of $\lambda \sim 1\ \mu m$ is certainly longer than the device dimensions that can be achieved by modern submicron technology. The structure in which ballistic transport is most widely investigated is a GaAs-AlGaAs heterojunction with a split gate *field-effect transistor* (FET) configuration, usually less than 0.5 μm in length, with a gap of about 0.7 μm [65, 66]. As the voltage on the gate is made increasingly negative, the width of the conducting channel decreases and becomes sufficiently small that one-dimensional quantization occurs as the channel width becomes comparable to the electron wavelength. This is sufficiently short that electrons may pass through the conducting channel without appreciable scattering. Our structure is quite different and one possible mechanism that would explain the quantized transport in amorphous silicon structures is outlined below. The observed *I-V* characteristics at low temperatures show two distinct regimes, as shown in Figures 14.28–14.31. Below the critical voltage V_{cr}, the curves are nonlinear but there are no discontinuities; however, above V_{cr} sudden jumps in current are observed associated with quantized resistance. These observations suggest that the current flow below and above V_{cr} is determined by different mechanisms.

The I-V characteristics below V_{cr} (see inset, Figure 14.28(a)) suggest that the filament has a relatively large resistance around zero bias (i.e., a barrier for electron flow exists). The observed zero-bias anomaly is consistent with tunneling conduction between metallic particles embedded in an insulating matrix [63]. Below V_{cr} the I-V characteristics show a continuous but strongly nonlinear behavior due to the creation of free carriers by the high electric field across the small tunneling distance. In such a system the creation of free carriers is an activated process related to the increase in the electrostatic potential of a particle when a free electron is added to it. The activation energy can be provided entirely by thermal energy, hence the effect diminishes at higher temperatures; or, in the presence of an applied field, part or all of it can be provided by the field itself. Experimentally, a T^2 dependence of the current at a constant voltage (less than V_{cr}) is observed in good accordance with the assumption that the electron transport is dominated by field-activated tunneling processes in this region. Figure 14.32 illustrates an idealized model having a single permanent inclusion extending from the top contact, with a narrow channel connecting it to the bottom contact. The evidence [55] is that the overall diameter at the top contact is less than 0.5 μm. The length of the channel must be consistent with tunneling. With increasing applied voltage, the tunneling current increases exponentially. The sudden increase in current at V_{cr} implies that the tunneling

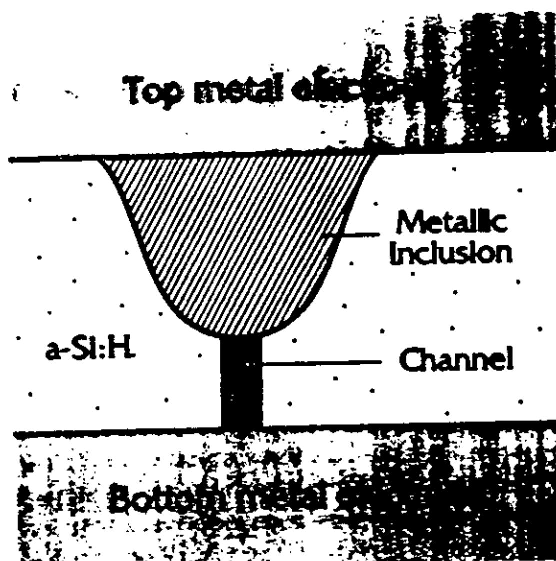

Figure 14.32 Schematic description of filament showing proposed metallic inclusion and one-dimensional conducting channel.

barrier effectively breaks down. This is not a destructive effect, however, as the process is completely reversible and no material changes ensue.

At present we have no firm explanation for the steps in the current above V_{cr}, which we have associated with quantized resistance. Experiments on other one- and two-dimensional systems show electrical properties that are associated with quantized resistance, but these are only observed at very low temperatures. For example, in a two-dimensional electron gas [66], the quantum Hall effect is related to e^2/h, and in a one-dimensional electron gas [67, 68] in the ballistic regime, resistance is quantized in terms of $h/2e^2$. However, it is not expected that quantized resistance states associated with ballistic transport should be observed when, as in the present case, the applied voltage is much greater than kT—if, for example, all the applied voltage were to appear across the critical part of the structure, the equivalent temperature would be in excess of 1000K. We have suggested elsewhere [64] that the quantized phenomena might be related to electrical transport through a quantum point contact. Assuming that the inclusion of modified material created during forming has a tapered shape (Figure 14.32), the resulting current flow could be restricted to a very localized area. The device resistance could thus be determined by the contact area where the tip of the modified region and the lower metal electrode are in close proximity. At such distances the resistance might be associated with either a single atom or a small number of contact atoms [69]. It has been shown theoretically [70] that the resistance associated with a single contact atom reaches saturation with a minimum value given by $R = h/2e^2$, provided that no elastic deformation occurs. This is the constriction resistance ($= 12906\Omega$) associated with an ideal conduction channel. It should be noted that this quantized resistance value is predicted assuming current flow through a single atomic orbital only. If more orbitals (conduction paths) are involved, these would reduce the quantized resistance value in integer steps according to the number of paths involved. Experimental results from a scanning tunneling microscope (STM) using an Ir tip showed a resistance jump to a value $R \sim 4 \times 10^4\Omega$ at close contact, rather larger than was predicted theoretically [71]. In this experiment the tunneling current is recorded as a function of distance D, from the conducting surface. The jump occurs at the transition from the tunneling to the one-atom point contact regime in the STM.

Our measurements show that the resistance of conditioned a-Si:H sandwich structures can be quantized under some circumstances. The voltages at which this occurs correspond to energies that are greatly in excess of the thermal energy kT. Furthermore, the quantized resistance values reflected in the I-V characteristics do not involve all possible integer or half integer values. For these reasons we believe that existing theories of quantized resistance associated with ballistic transport are not applicable to our structure. However, the results obtained so far do not appear incompatible with current flow through atomic scale point contacts, and it is possible that this could explain the room temperature quantization observed. The most important feature of the observed quantized behavior is that it can be observed up to ~400K, much higher than previously reported.

The model outlined above describes one possible mechanism for the quantized electron transport and provides important information about the structure of the filament, but as it stands it does not explain the memory switching. The most important difference between the two phenomena lies in the fact that the quantized electron transport observed in memory devices is seen at applied voltage levels lower than ~1V, that is, at voltage levels where no memory switching would be expected to occur. The observed quantized jumps in the device resistance are threshold-switching type: if the voltage is lowered, the sample resistance reverts to the original low-bias case and there is no permanent change in the *I-V* characteristics of the device. On the other hand, memory switching occurs at voltage levels from ~1.5 to ~4V, resulting in a permanent change in the *I-V* characteristics of the device (i.e., a different resistance state of the memory).

14.2.2.2 Models for Memory Switching

Some of the possible mechanisms that might explain the memory-switching behavior are discussed below.

Thermal Models

The thermal models [26, 29] used to explain the behavior of the amorphous chalcogenide memories might appear to offer a basis for explaining the a-Si:H switching process. In the chalcogenide memories the ON state is associated with a filament of crystalline material that is formed after sufficient power has been applied to the layer to melt a small area of the material. Switching OFF is achieved by burning out this filament using a number of relatively short high-power pulses and allowing rapid quenching to reform the highly resistive amorphous phase. However, there are a number of important differences between the amorphous silicon and the chalcogenide memories:

1. It has been established that the a-Si:H memories do not form or WRITE at constant power; in general, forming occurs at much lower energy ($<10^{-9}$ J) than in the chalcogenides (10^{-3}–10^{-4} J).
2. The forming, WRITE, and ERASE operations for the a-Si:H memories are generally polarity dependent.
3. No rise in the temperature of the a-Si:H specimens can be observed prior to switching.
4. The a-Si:H WRITE and ERASE times are many orders of magnitude shorter than those for the chalcogenides (e.g., 10^{-8} s for the WRITE operation compared with 10^{-3} s).

It is thus unlikely that the crystalline/amorphous thermal model is applicable to a-Si:H memories.

Models Based on Trapped Space Charge

In many respects the behavior of the a-Si:H layers appears to be closely related to that of crystalline-silicon MISS structures in that both show fast polarity-dependent switching, both show current instabilities, and both have high conductance states associated with current filaments. However, the crystalline MISS structures are threshold switches that always revert to the OFF state when the power is removed, whereas the a-Si:H structures have the additional feature (and complexity) of nonvolatile memory behavior. It is nonetheless possible that the initiation of memory switching in the amorphous silicon devices is closely related to the mechanism proposed to explain threshold switching in crystalline MISS structures. Essentially two models have been used to explain MISS behavior [10]. These are generally referred to as the "punch-through" and "avalanche" modes, and both mechanisms require that high fields be developed across space-charge barriers in the films. In addition, in both models the low-impedance (ON) state is produced by injected charge, causing inversion of the Si at the Si/insulator interface. It is tempting to suggest that the "permanent" memory of the a-Si:H layers may be produced by a similar mechanism in which the charge is trapped in deep gap states at the insulator semiconductor interface for which the probability of release is very small. However, the a-Si:H devices retain their ON-state memory conductance without any observable change for at least 1 year at room temperature and at least 24 hours at 95°C.

Using thermal release rates from deep midgap states of energy E_i as a measure of the persistance of the trapped space charge, the average thermal release time ($\propto \exp[-(E_c - E_i)/kT]$) indicates that the capture cross section of these centers would have to be less than 10^{-18} cm^2 in order to agree with the experimental data. Although extremely small, such values would be consistent with Coulomb repulsive centers identified in crystalline materials. However, the problem is that recombination of the trapped charge distribution through tunneling or diffusion may well invalidate the above estimate by leading to a much faster decay of any trapped space charge distribution. All that can be said at present is that a model in which the observed memory is associated with a trapped space charge cannot be excluded, but in view of the remarkable nonvolatility of the memory states, it is unlikely to be the basis of anything more than a partial explanation.

Hydrogen Motion in a-Si:H

It is known that significant amounts of hydrogen are incorporated in the random network of the a-Si:H layer. The possibility exists, therefore, that memory switching may be associated with some atomic motion of hydrogen in the material. For instance, it has been reported that in n-type crystalline-silicon-Cr Schottky barrier

structures, hydrogen plays an important role in lowering the contact barrier [74]. Also, the polarity dependence of the threshold voltages for the a-Si:H memories could be understood on the basis of field-assisted diffusion.

Tunneling Method

One possible explanation for the quantized electron transport and the zero-bias anomaly observed at lower temperatures is that tunneling processes are involved and hence must be taken into account when suggesting a model for memory switching. In order to explain the different and permanent resistance states, the model should embody the following features:

(1) Changes in the conductivity of the whole filament;
(2) Local changes in conductivity at a certain point(s) in the filament;
(3) Changes in the filament geometry.

Thermal models would presumably require an average energy for switching of an order similar to that established for forming, but is has been found that ON → OFF → ON switching can be achieved using single-pulse energies of $\sim 10^{10}$ J (Figure 14.26). In addition, if it is assumed that the filament is homogeneous, there is no obvious way of introducing a polarity dependence. However, if there are inhomogeneities in the filament it may be possible to substantially increase the local energy density and field strength. Consider, for example, a simple one-dimensional filament consisting of alternating regions of material A and B. The observed resistance of the filament will depend on the relative contributions to the filament resistance of A and B type material, that is, if $R_B < R_A$, the properties of the A type will be observed, and if $R_A < R_B$, the properties of the type B material will be observed. If highly conducting regions are separated by small gaps, it is also necessary to consider the possibility of inter-island tunneling. In order to establish such a model, a more detailed description of regions A and B would have to be included, for example:

1. Region A is metallic or a degenerately doped material whose conribution to the filament is fixed and $\sigma_A \neq f(V)$ where V is the applied voltage and σ is the conductivity.
2. Region B is a gap between A-type material that can be sufficiently small to allow significant tunneling to occur; σ_B is some function of the voltage.

In the ON state, $R_B < R_A$ and the measured conduction properties of the filament are those corresponding to material A, namely, ohmic I-V characteristics and small thermal activation. In the OFF state, $R_A < R_B$ and the conduction properties are governed by the behavior of the tunneling regions. The current density in such a one-dimensional system is governed by (1) the applied bias V, (2) the barrier thickness d, (3) the barrier average height Φ and asymmetry $\Delta\Phi$,

(4) the density of states $g(E)$ in the metallic regions, and (5) the occupation of $g(E)$ (i.e., the temperature dependence).

In this case, the functional form of the current density J versus voltage V at different temperatures $J(V, T)$ can be obtained under two limiting conditions. First:

$V \ll \Phi$, and $\Delta\Phi \ll \Phi$, constant T

In this case the transmission probability $P = c \exp(-d\Phi^{1/2})$ may be treated as a constant for electrons near the Fermi energy E_F. Provided that $g(E)$ variations near E_F are small, J will increase *linearly* with V as more empty states become accessible in metallic region A (i.e., conduction is approximately *ohmic* and *symmetric*). This is consistent with the experimental data shown in Figure 14.12. Second:

$V < \Phi$, and the temperature is varied

In this case P is essentially independent of T because usually $kT \sim 10^{-2}$eV. Thus only a few electrons are promoted thermally to levels where P is significantly larger than at E_F. The approximate form of thermal J-V characteristics in this regime is as given in Equation (14.12).

How might switching be achieved in terms of the tunneling model? The low-bias *isothermal* resistance of region B-like parts of the filament is determined by geometric factors (included in constant c) and the transmission probability. Therefore one obtains:

$$J = cV \exp(-d\Phi^{1/2}) \qquad (14.14)$$

or

$$R = c \exp(d\Phi^{1/2}) \qquad (14.15)$$

The exponent is almost numerically correct if d is in Å and Φ is in eV. Taking $d = 50$Å and $\Phi = 1$eV, then $R_1 = c \exp(50)$ and increasing d by 5Å gives $R_2 = \exp(55)$ (i.e., R has increased by about a factor of 150). An equivalent increase in resistance is obtained by keeping d constant and increasing Φ from 1eV to 1.2eV. Changes in the tunnel barrier width on an atomic scale, or small (20%) changes in barrier height, could therefore account for the presence of switching. It is not clear, however, how these could occur in a manner that would explain the systematic dependence of device resistance on the magnitude *and* polarity of the switching voltages as shown, for example, by the data in Figures 14.22(a) and 14.22(b).

Finally we should note that in this model the cross section of the conducting channel is considered to be constant. The possibility exists that memory switching

might be associated with some permanent change to the cross section of the conducting channel (i.e., the high currents involved might cause small-scale material rearrangements).

In summary, we can say that, based on the available experimental evidence, it is possible that memory switching in the amorphous silicon metal-p^+-metal structures might be associated with a tunneling barrier within a permanent filament produced by the forming process. A change in the particle size or spatial distribution as a result of localized heating or high-field effects could explain the differences between high- and low-resistance states. However, the high switching speeds (~10 ns) and the insensitivity of switching to temperature suggest that large-scale structural changes are unlikely. It is possible though, that a structure might arise with small variations at a "weak link" in the filament that could produce the observed changes in a short time. As tunneling is a quantum mechanical effect, the nanosecond time scale for the switching is feasible.

Finally we emphasize that the effect has been observed in what is initially a metal-amorphous semiconductor structure. It is not known with any certainty what effect the forming process has on the structure of the conducting channel, but the observed quantized behavior suggests the importance of the very small dimensions of the conducting channel rather than other physical parameters. The significance of using amorphous silicon sandwich structures lies in the forming process, that is, in the process that allows the fabrication of such small structures. The strong influence of the metal contact on the observed memory switching behavior indicates the importance of alloying during the forming process. It has been reported, for example, that solid-phase amorphization or glass formation occurs in V-Si reactions induced by rapid thermal annealing (i.e., at conditions similar to forming) but does not occur in Co-Si and Cr-Si [75]. Therefore, the presence of a very small tunneling conduction path in amorphous silicon V-p^+-Cr structures might be due to a new type of solid-phase reaction, induced by forming, that creates a homogeneous (possibly amorphous) V-Si silicide.

14.3 CONCLUSION

Research into electronic switching in amorphous semiconductor thin films has a long history, with several distinct stages involved. Early work was concentrated on chalcogenide thin-film devices in which the basic switching took place between highly conducting ON and highly resistive OFF states (that is, an essentially digital mode of operation was involved). Memory switching in chalcogenide glasses is based on a crystalline/amorphous phase transition, whereas threshold switching in these glasses can be described by purely electronic mechanisms for films $\leq 1\ \mu m$ thick or by electrothermal considerations for film thickness from 1 to 10 μm.

More recent observations on amorphous silicon thin-film structures have shown that, in contrast to chalcogenide thin films, these devices can exhibit an

analog behavior under certain conditions. This analog switching mechanism appears to be associated with interatomic processes such as tunneling, and, as a consequence, is significantly faster than switching in chalcogenide glasses.

Finally, our most recent results have demonstrated that in certain a-Si memory structures, quantized electron transport phenomena occur. These results are most surprising considering the magnitude of the effect and the high temperatures involved and appear to be a consequence of the extremely small (atomic scale) dimensions of the structures involved.

REFERENCES

[1] Shaw, M. P., H. L. Grubin, and I. J. Gastman, "Analysis of An Inhomogeneous Bulk S-Shaped Negative Differential Conductivity Element in a Circuit Containing Reactive Elements," *IEEE Trans. Electron Devices*, *Vol. ED-20*, No. 2, February 1973, pp. 169–178.

[2] Simmons, J. G., and R. R. Verderber, "New Conduction and Reversible Memory Phenomena in Thin Insulating Films," *Proc. Royal Society A.*, *Vol. 301*, 1967, pp. 77–102.

[3] Barnett, A. M., and A. G. Milnes, "Filamentary Injection in Semi-insulating Silicon," *J. Appl. Phys.*, *Vol. 37*, No. 11, October 1966, pp. 4215–4223.

[4] Shaw, M. P., and I. J. Gastman, "Circuit Controlled Current Instabilities in S-Shaped Negative Differential Conductivity Elements," *Appl. Phys. Lett.*, *Vol. 19*, 1971, pp. 243–245.

[5] Gunn, J. B., "Instabilities of Current in III-V. Semiconductors," *IBM J. Res. Develop.*, *Vol. 8*, April 1964, pp. 141–159.

[6] Copeland, J. A., "Theoretical Study of a Gunn Diode in a Resonant Circuit," *IEEE Trans. Electron Devices*, *Vol. ED-14*, February 1967, pp. 55–58.

[7] Gibbons, J. F., and W. E. Beadle, "Switching Properties of Thin NiO Films," *Solid State Electronics*, *Vol. 7*, Pergamon Press, 1964, pp. 785–797.

[8] Argall, F., "Switching Phenomena in Titanium Oxide Films," *Solid State Electronics*, *Vol. 11*, 1968, pp. 535–541.

[9] Feldman, C., and H. K. Charles, "Electrothermal Model of Switching in Amorphous Boron and Silicon Thin Films," *Solid State Communications*, *Vol. 15*, 1974, pp. 551–554.

[10] Simmons, J. G., and A. El-Badry, "Theory of Switching Phenomena in Metal-Semiinsulator-n-p^+ Silicon Devices," *Solid State Electronics*, *Vol. 20*, Pergamon Press, 1977, pp. 954–961.

[11] Sakai, K., H. Matsuda, H. Kawada, K. Eguchi, and T. Nagakiri, "Switching and Memory Phenomena in Langmuir-Blodgett Films," *Appl. Phys. Lett.*, *Vol. 14*, No. 3, October 1988, pp. 1274–1276.

[12] Ovshinsky, S. R., "Reversible Electrical Switching Phenomena in Disordered Structures," *Phys. Rev. Lett.*, *Vol. 21*, 1968, pp. 1450–1453.

[13] Feldman, C., and K. Moorjani, "Observation of Filament Formation in Amorphous Films During Switching," *Thin Solid Films*, *Vol. 5*, 1970, pp. R1–R4.

[14] Ovshinsky, S. R., and H. Fritzsche, "Amorphous Semiconductors for Switching, Memory, and Imaging Applications," *IEEE Trans. Electron Devices*, *Vol. ED-20*, No. 2, February 1973, pp. 91–104.

[15] Ridley, B. K., "Specific Negative Resistance in Solids," *Proc. Phys. Soc.*, *Vol. 82*, 1963, pp. 954–966.

[16] Wagener, J. L., and A. G. Milnes, "Post-Breakdown Conduction in Forward Biased *p-i-n* Silicon Diodes," *Appl. Phys. Lett.*, *Vol. 5*, No. 9, November 1964, pp. 186–188.

[17] Moser, A., "Bistable Switching in Metal-Semiconductor Junctions," *Appl. Phys. Lett.*, *Vol. 20*, No. 7, April 1972, pp. 244–245.

[18] Burgelmann, M., "Conduction Mechanisms in the OFF State of Thin ZnTe Films," *Solid State Electronics*, *Vol. 20*, 1977, pp. 523–528.
[19] Melngailis, I., and A. G. Milnes, "Filamentary Impact Ionization in Compensated Germanium at 4.2K," *J. Appl. Phys.*, *Vol. 33*, No. 3, March 1962, pp. 995–1000.
[20] Kroeger, H., and H. A. L. Wegener, "Controlled Inversion Transistors," *Appl. Phys. Lett.*, *Vol. 27*, 1975, pp. 303–304.
[21] Manhart, S., "Memory Switching in SiO films with Ag and Co Electrodes," *J. Phys. D., Appl. Phys.*, *Vol. 6*, 1973, pp. 82–86.
[22] Simhony, M., and R. Williams, "Impact Ionization of Filled Traps in Cadmium Sulfide," *J. Appl. Phys.*, *Vol. 40*, No. 2, February 1969, pp. 691–696.
[23] Madams, C. J., D. V. Morgan, and M. J. Howes, "Migration of Gold Atoms Through Thin Silicon Oxide Films," *J. Appl. Phys.*, *Vol. 45*, No. 11, November 1974, pp. 5088–5090.
[24] Owen, A. E., and J. Robertson, "Electronic Conduction and Switching in Chalcogenide Glasses," *IEEE Trans. Electron Devices*, *Vol. ED-20*, No. 2, February 1973, pp. 105–122.
[25] Adler, D., H. K. Henisch, and N. F. Mott, "The Mechanism of Threshold Switching in Amorphous Alloys," *Rev. Mod. Phys.*, *Vol. 50*, 1978, pp. 209–220.
[26] Warren, A. C., "Reversible Thermal Breakdown as a Switching Mechanism in Chalcogenide Glasses," *IEEE Trans. Electron Devices*, *Vol. ED-20*, No. 2, February 1973, pp. 123–130.
[27] Henisch, H. K., E. A. Fagen, and S. R. Ovshinsky, "A Qualitative Theory of Electrical Switching Processes in Metastable Amorphous Substances," *Journal of Non-Crystalline Solids*, *Vol. 4*, 1970, pp. 538–547.
[28] Lucas, I., "Interpretation of the Switching Effect in Amorphous Semiconductors as a Recombination Instability," *Journal of Non-Crystalline Solids*, *Vol. 6*, 1971, pp. 136–144.
[29] Kroll, D. M., "Theory of Electrical Instabilities of Mixed Electronic and Thermal Origin," *Phys. Rev. B*, *Vol. 9*, No. 4, February 1974, pp. 1669–1706.
[30] Owen, A. E., J. M. Robertson, and C. Main, "The Threshold Characteristics of Chalcogenide Glass Memory Switches," *Journal of Non-Crystalline Solids*, *Vol. 32*, 1979, pp. 29–52.
[31] Popescu, C., "The Thermal Runaway Mechanism of Second Breakdown Phenomenon," *Solid State Electronics*, *Vol. 13*, 1970, pp. 887–901.
[32] Berglund, C. N., and N. Klein, "Thermal Effects on Switching of Solids from an Insulating to a Conducting State," *Proc. IEEE*, July 1971, pp. 1099–1110.
[33] Pontius, D. H., W. B. Smith, and P. P. Budestein, "Filamentation in Silicon on Sapphire Homogeneous Thin Films," *J. Appl. Phys.*, *Vol. 44*, No. 1, January 1973, pp. 331–340.
[34] Mott, N. F., "Conduction in Non-Crystalline Systems VII. Non-Ohmic Behaviour and Switching," *Vol. 24*, December 1971, pp. 911–958.
[35] Mott, N. F., and E. A. Davis, "Electronic Processes in Non-Crystalline Materials," Clarendon Press, Oxford, 1971, pp. 6–10.
[36] Cohen, M. H., H. Fritzsche, and S. R. Ovshinsky, "Simple Model for Amorphous Semiconducting Alloys," *Phys. Rev. Lett.*, *Vol. 22*, No. 20, May 1969, pp. 1065–1068.
[37] Homma, K., H. K. Henisch, and S. R. Ovshinsky, "New Experiments on Threshold Switching in Chalcogenide and Non-Chalcogenide Alloys," *Journal of Non-Crystalline Solids*, *Vols. 35, 36*, 1980, pp. 1105–1110.
[38] Henisch, H. K., R. W. Pryor, and G. J. Vendura, "Characteristics and Mechanism of Threshold Switches," *Journal of Non-Crystalline Solids*, *Vol. 8-10*, 1972, pp. 415–422.
[39] Pryor, R. W., and H. K. Henisch, "Nature of the ON-state in Chalcogenide Glass Switches," *Journal of Non-Crystalline Solids*, *Vol. 7*, 1972, pp. 181–191.
[40] Kolomiets, B. T., E. A. Lebedev, and I. A. Taksami, "Mechanism of the Breakdown in Films of Glassy Chalcogenide Semiconductors," *Sov. Phys. Semicond.*, *Vol. 3*, 1969, pp. 267–272.
[41] Stocker, H. J., C. A. Barlow, and D. F. Weirauch, "Mechanism of threshold switching in semiconductor glasses," *Journal of Non-Crystalline Solids*, *Vol. 4*, 1970, pp. 523–535.

[42] Hovel, H. J., and J. J. Urgell, "Switching and Memory Characteristics of ZnSe-Ge heterojunctions," *J. Appl. Phys.*, *Vol. 42*, No. 12, November 1971, pp. 5077–5083.
[43] Hovel, H. J., "Switching and Memory in ZnSe-Ge Heterojunctions," *Appl. Phys. Lett.*, *Vol. 17*, No. 4, August 1970, pp. 141–143.
[44] Rutz, R. F., private communication.
[45] Hamakawa, Y., and M. Yoshida, *Proc. of the Second Conference on Solid State Devices*, Tokyo, 1970, (unpublished).
[46] Moorjani, K., and C. Feldman, "Electrical Conduction in Amorphous Boron and Silicon," *Journal of Non-Crystalline Solids*, *Vol. 4*, 1970, pp. 248–255.
[47] Charles, H. K., and C. Feldman, Switching Times in Amorphous Boron, Boron Plus Carbon, and Silicon Thin Films," *J. Appl. Phys.*, *Vol. 46*, No. 2, 1975, pp. 819–830.
[48] Dey, S. K., and W. J. T. Fong, "Conduction Processes and Threshold Switching in Amorphous Si Films," *J. Vac. Sci. Technol.*, *Vol. 16*, 1979, pp. 240–243.
[49] Dey, S. K., "Electrothermal Model of Switching in Amorphous Silicon Films," *J. Vac. Sci. Technol.*, *Vol. 17*, 1980, pp. 445–448.
[50] Spear, W. E., and P. G. LeComber, "Electronic Properties of Substitutionally Doped Amorphous Si and Ge," *Phil. Mag.*, *Vol. 33*, No. 6, 1976, pp. 935–949.
[51] Gabriel, M. C., and D. Adler, "Switching in Hydrogenated Amorphous Silicon," *Journal of Non-Crystalline Solids*, *Vol. 48*, 1982, pp. 297–305.
[52] Den Boer, W., "Threshold Switching in Hydrogenated Amorphous Silicon," *Appl. Phys. Lett.*, *Vol. 40*, 1982, pp. 812–813.
[53] Owen, A. E., P. G. LeComber, G. Sarrabayrouse, and W. E. Spear, "New Amorphous Silicon Electrically Programmable Nonvolatile Switching Device," *IEE Proc.*, *Vol. 129*, Pt. I, No. 2, April 1982, pp. 51–54.
[54] LeComber, P. G., A. E. Owen, W. E. Spear, J. Hajto, and W. K. Choi, "Hydrogenated Amorphous Silicon," *Semiconductors and Semimetals*, *Vol. 21*, Part D, J. I. Pankove, ed., 1984, pp. 275–289.
[55] LeComber, P. G., A. E. Owen, W. E. Spear, J. Hajto, A. J. Snell, W. K. Choi, M. J. Rose, and S. Reynolds, "The Switching Mechanism in Amorphous Silicon Junctions," *Journal of Non-Crystalline Solids*, *Vols. 77, 78*, 1985, pp. 1383–1388.
[56] Choi, W. K., S. Reynolds, J. Hajto, S. M. Gage, A. E. Owen, A. J. Snell, I. M. Flanagan, M. J. Rose, F. J. Djamdji, P. G. LeComber, and W. E. Spear, "Preformed J-V and C-V Characteristics of a-Si:H p^+-n-i junctions," *Journal of Non-Crystalline Solids*, *Vols. 97, 98*, 1987, pp. 1331–1334.
[57] Rose, M. J., J. Hajto, P. G. LeComber, S. M. Gage, W. K. Choi, A. J. Snell, and A. E. Owen, "Amorphous Silicon Analogue Memory Devices," *Journal of Non-Crystalline Solids*, *Vol. 115*, 1989, pp. 168–170.
[58] Putley, E. H., *The Hall Effect and Related Phenomena*, Butterwords, London, 1960.
[59] Buxo, J., A. E. Owen, G. Sarrabayrouse, and J. P. Sebaa, "The Characteristics of Metal-Thin Insulator-n-p^+ Silicon Switching Devices," *Revue de Physique Appl.*, *Vol. 17*, 1978, pp. 767–770.
[60] Hajto, J., M. J. Rose, A. J. Snell, P. G. LeComber, and A. E. Owen, "The Programmability of Amorphous Silicon Memory Elements," *Proc. MRS. Soc. Symp.*, *Vol. 192*, San Francisco, 1990, pp. 405–410.
[61] Hajto, J., M. J. Rose, P. B. LeComber, A. E. Owen, and A. J. Snell, "Observation of Quantised Ballistic Transport in Amorphous Silicon Memory Structures," *Proc. MRS. Soc. Symp.*, *Vol. 192*, San Francisco, 1990, pp. 347–352.
[62] Hajto, J., A. E. Owen, A. J. Snell, P. G. LeComber, and M. J. Rose, "Analogue Memory and Ballistic Electron Effects in Metal-Amorphous Silicon Structures," *Phil. Mag. B.*, *Vol. 63*, No. 1, 1991, pp. 349–369.

[63] Giaver, I., and H. R. Zeller, "Superconductivity of Small Tin Particles Measured by Tunnelling," *Phys. Rev. Lett.*, *Vol. 20*, No. 26, 1968, pp. 1504–1507.

[64] Hajto, J., M. J. Rose, A. J. Snell, I. S. Osborne, A. E. Owen, and P. G. LeComber, "Quantised Electron Effects in Metal/a-Si:H/Metal Thin Film Structures," *Journal of Non-Crystalline Solids*, in press.

[65] Gage, S. M., J. Hajto, S. Reynolds, W. K. Choi, M. J. Rose, P. G. LeComber, A. J. Snell, and A. E. Owen, "Anomalous High Zero Bias Resistance in Metal-Amorphous Silicon-Metal Structures," *Journal of Non-Crystalline Solids*, *Vol. 115*, 1989, pp. 171–173.

[66] von Klitzing, K., "The Quantised Hall Effect," *Rev. Mod. Phys.*, *Vol. 58*, 1986, pp. 519–523.

[67] Van Wees, B. J., H. van Houten, C. W. J. Beenakker, J. G. Williamson, L. P. Kouwenhoven, D. van der Marel, and C. T. Foxon, "Quantised Resistance of Point Contacts in a Two Dimensional Electron Gas," *Phys. Rev. Lett.*, *Vol. 60*, 1988, pp. 848–851.

[68] Wharam, D. A., T. J. Thornton, R. Newbury, M. Pepper, H. Ahmed, J. E. F. Frost, D. G. Hasko, D. C. Peacock, D. A. Ritchie, and G. A. C. Jones, "One-Dimensional Transport and the Quantisation of the Ballistic Resistance," *J. Phys. C, Solid State Phys*, *Vol. 21*, 1988, pp. L209–L214.

[69] Lang, N. D., "Resistance of a One-atom Contact in the Scanning Tunneling Microscope," *Phys. Rev. B.*, *Vol. 36*, 1987, pp. 8173–8176.

[70] Martin-Rodero, A., J. Ferrer, and F. Flores, "Contact Resistance and Saturation Effects in the Scanning Tunnelling Microscope," *J. Microscopy*, *Vol. 152*, 1988, pp. 317–323.

[71] Sharvin, Y. V., "A Possible Method for Studying Fermi Surfaces," *J. Exptl. Theoret. Phys. (USSR)*, *Vol. 48*, 1965, pp. 984–985.

[72] Landauer, R., "Localisation Interactions and Transport Phenomena," B. Kramer, G. Bergmann, and Y. Bruyserade, eds., Heidelberg:Springer, 1985, pp. 38–40.

[73] Imry, Y., 1986, *Directions in Condensed Matter Physics*, G. Grinstein and G. Mazenko, eds., Singapore: World Scientific, p. 101.

[74] Szadkowski, A. J., A. Kalnitsky, K. B. Ma, and S. Zukotynski, "Implications of the Change in Work Function of Chromium by the Presence of Hydrogen on the Properties of Electrical Contact Between Chromium and Hydrogenated Amorphous Silicon," *J. Appl. Phys.*, *Vol. 53*, No. 1, January 1982, pp. 557–558.

[75] Nathan, M., "Solid Phase Reactions in Free Standing Layered M-Si (M = Ti, V, Cr, Co) Films," *J. Appl. Phys.*, *Vol. 63*, No. 11, June 1988, pp. 5534–5540.

SYMBOLS

Symbol	*Description*
B	Magnetic field strength
d	Layer thickness
d_n	n-layer thickness
d_i	Phase boundary diameter of phase transition
e	Electronic charge
E	Electric field (Vcm^{-1})
E_{cr}	Critical field for switching
E_F	Fermi energy
ξ	Energy
j_{rec}	Recombination current density

Symbol	Description
J	Current density
k	Boltzmann's constant
$g(E)$	Density of states (DOS)
G_{OFF}	OFF-state conductance
G_n	Gradient of phase boundary diameter
I_H	Critical holding current
I_s	Steady current
I_{max}	Maximum current
m^*	Electron-effective mass
m_n	Free electron mass
N_ω	Average number of phonons of frequency ω
P_{RMS}	RMS power
P	Transmission probability
P_n	Intercept of phase boundary diameter
q_{inj}	Injected charge
Q	Charge
R_{OFF}	OFF-state resistance
R_{ON}	ON-state resistance
t_d	Switching delay time
t_{DW}	WRITE delay time
t_{DE}	ERASE delay time
T	Temperature
T_{el}	Electron temperature
V_c	Critical forming voltage
V_{cr}	Critical voltage
V_F	Forming voltage
V_H	Holding voltage
V_{Th}	Threshold voltage
V_{Thf}	Forward bias threshold voltage
V_{Thr}	Reverse bias threshold voltage
$\Delta\rho/\rho(B)$	Transverse magnetoresistance
ΔV	Voltage window for analogue memory programming
σ	Conductivity
λ	Electron mean free path
μ	Mobility
π	Tunneling barrier height
τ	Relaxation time
τ_D	Forming delay time
τ_c	Mean time between electron-lattice collisions
ω	Frequency
Ω	Resistance

ACRONYMS

CCNDR	Current-controlled NDR
CFO	Cohen-Fritsche-Ovshinsky
FET	Field-effect transistor
I-V	Current-voltage
MISS	Metal/i-n-p^+/metal
NDR	Negative differential resistance
TONC	Transient ON characteristics
VCNDR	Voltage-controlled NDR

Material Research Society Conf. Proc. San Francisco, USA, vol.258 (1992)

ASPECTS OF NON-VOLATILITY IN a-Si:H MEMORY DEVICES.

M.J. ROSE,* A.J. SNELL,** P.G. LeCOMBER,* J. HAJTO,** A.G. FITZGERALD,* and A.E. OWEN.**

* Dept. Applied Physics and Electronic & Manufacturing Engineering, University of Dundee, Dundee, DD1 4HN, Scotland, U.K.

** Department of Electrical Engineering, University of Edinburgh, Edinburgh, EH9 3JL, Scotland, U.K.

ABSTRACT.

a-Si:H p^+-n-i devices, after a once only forming process, switch between two distinct states, both of which are memory states, and are electrically programmable with pulses in the nanosecond range with at least a 1 million cycle endurance. They are known to be non-volatile memory states which persist for long periods. This paper examines the nature of this non-volatility by looking at the effects of time, temperature, bias and radiation. It is found that these digital memory states persist with no change in state for at least four years under zero bias, and that they can withstand high temperatures both under bias and at zero bias. This and a resistance to radiation and a space environment shows that a mechanism of charge storage is unlikely and that they may have applications in hostile environments. The reason for such stability is unclear, but may be associated with the incorporation and distribution of metal in the filamentary region.

1. Introduction.

After a once only 'forming' operation, amorphous silicon (a-Si:H) p^+-n-i memories become fast, polarity dependent two terminal devices that operate by filamentary conduction [1], the current being confined to a small region of the device of a diameter less than 0.5μm. Single layer devices of p^+ a-Si:H also operate in this way, and with particular metallisation can operate as analogue devices [2,3]. A high field pulse of 300 ns duration results in the ON state of ≈3kΩ. This state and the OFF state of ≈1MΩ are retained under zero bias conditions for long periods. The persistance of this retained memory state under different conditions should help elucidate the conduction mechanism in the a-Si:H memories. Many conventional memory devices operate by means of charge storage, and at first sight it is tempting to suggest that this may also be the case in the present devices. Furthermore, because of the metastable nature of a-Si:H, intrinsic defects may also play some role. A number of tests have been carried out to 'stress' the devices in various ways to see if either of these mechanisms may apply. The results indicate that the devices operate under extremes of conditions without loss of performance and that neither trapped charge or known intrinsic defects can account for the memory storage.

2. Experimental methods.

The a-Si:H samples were of either a p^+-n-i or a p^+ configuration and were sandwiched between two metal electrodes. The a-Si:H was deposited by the R.F. glow discharge decomposition of SiH_4 onto pre-patterned chromium (Cr) electrodes on Corning 7059 glass. The p^+ single layers were deposited from a 10^4 vppm B_2H_6 mixture in SiH_4 to a thickness of 0.1μm and fabricated as described in previous work [2] into pore structures with an defined area generally of 10^{-4} mm^2 although for some experiments different size areas were also used. The experimental methods used for each stressing test are described in the text under that heading.

3. Results and discussion.

3.1 Non Volatility of p+-n-i digital devices.

A number of M_1/p^+-n-i/M_2 devices after forming were switched and checked for good memory action, and left in different memory states under zero bias conditions. Devices had either chromium (Cr) or aluminium (Al) top metal (M_2) contacts and were bonded using conducting silver paste. The resistance states were periodically monitored by connecting them into circuit and setting the appropriate READ conditions (0.5V). This READ level is sub-threshold and does not perturb the memory state. To check that the devices still operate after an elapsed time, a number of devices on the same substrate were selected for memory switching tests (threshold values and conductance ratio). Fig. 1 shows the resistance of an ON and OFF state device over a four year period. These are two different devices from one substrate where the resistance values were measured at 0.5 V and recorded. The results are typical of all those devices monitored over a period of four years. There is little deviation from the programmed ON- and OFF-states after four years under zero bias conditions. This long retention time makes these devices attractive for a number of applications.

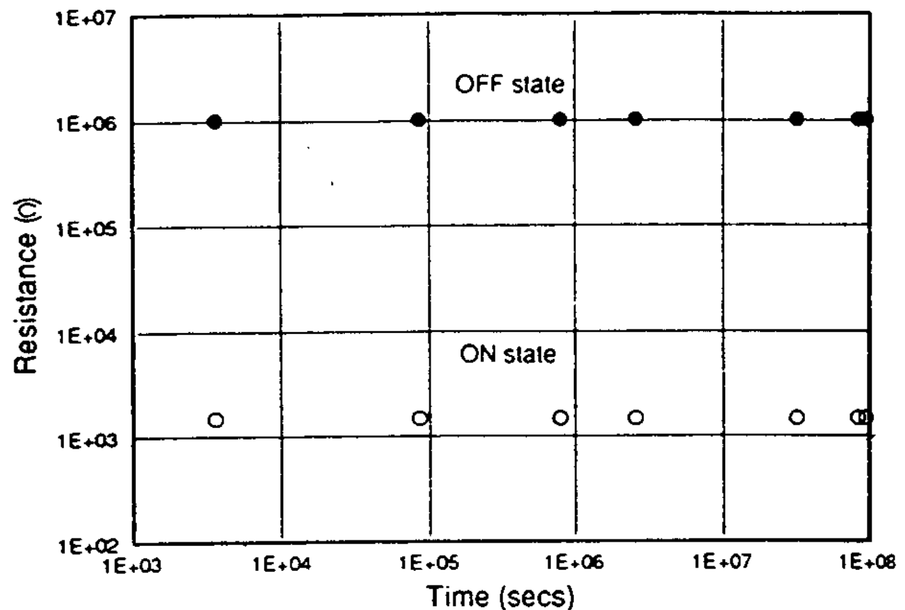

Fig.1 Persistance of memory ON and OFF states.

The characteristics of the a-Si:H devices are dependent largely on the top metal contact. The ON state resistance is independent of device area for all metals and silicon configurations used. However, the OFF state is markedly different for different top metals tried. This is summarised in Fig. 2 for a number of formed and unformed devices of various areas. Only for early devices with Al as the top contact does the OFF state resistance scale inversely with device area, switching back to its unformed value of resistance, indicating that conduction takes place throughout the bulk of the device, and that conduction here is no longer confined to a filamentary region. Devices that have Cr or vanadium (V) as the top contact, switch to an area independent OFF state of about 1MΩ, suggesting that all memory action takes place within the filament. Both types of device (p^+ and p^+-n-i)have a range of intermediate resistance states that are voltage addressable [2].

3.2 Effects of Temperature.

For devices where memory storage is by charge trapping, the effects of temperature can be quite significant and provide information on the nature of the trapping centres. Also it is known [4] that in a-Si:H, biasing and annealing effects can alter the distribution of electronic states leading to changes in conductivity, the values being frozen in by rapid cooling. These defect states are annealed out at characteristic temperatures of 150°C for n-type and 95°C for p-type a-Si:H. If changes in these density of states are responsible for memory action in the a-Si:H devices, then the ON and OFF states of these devices should be sensitive to changes in temperature.

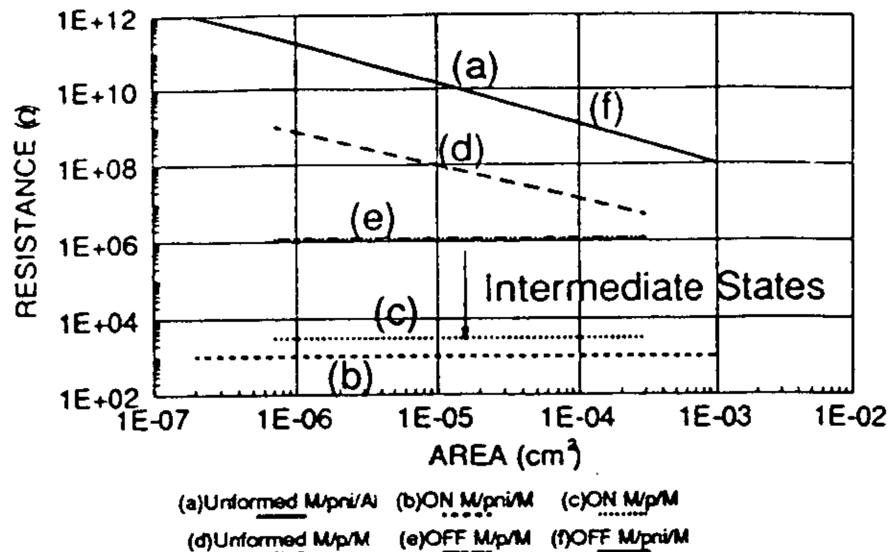

Fig.2 Unformed, OFF and ON state resistance as a function of area.

In addition to this, emission time experiments using DLTS [5] have been used used to study current induced metastable defect annealing and creation in a-Si:H. The charge on the metastable defect (MSD) is determined by the injected charge, and the MSD^+ and MSD^- have a barrier to creation of >1 eV. The activation energy for annealing the hole trap defect is up to 1.8 eV, making this an attractive candidate for memory action. These MSDs have been associated with dangling bond formation (as e.g. D^+,D^0). If the memory action is associated with defects of this type, then holding devices at 160°C under applied bias should show a thermal release time of tens of minutes.

Experiments have been carried out to examine the effects of temperature on the memory devices under different biasing conditions. A number of memory devices (both p^+-n-i and p^+) were bonded and mounted in a vacuum holder and connected to a computerised monitoring system. A temperature controller was used to set the desired temperature and an electrometer was used to measure the current through the device for various sub-threshold bias conditions of ±0.5 V and ±1 V. The devices were heated using a slow temperature ramp to a temperature of 180°C and held at that temperature for 8 hours. The ON state resistance was found to be practically temperature independent from room temperature to 180°C, and after 8 hours at 180°C no change in resistance was observed. Devices in the ON state have retained their memory state for up to 120 hours at 180°C with no significant change in the ON state resistance. If the devices are then switched there is no obvious degredation in memory performance. The OFF state also shows little change in resistance value when heated under bias for similar temperatures and times.

Dynamically, with the devices being switched between a clearly defined ON and OFF state whilst being monitored on an oscilloscope, it is found that they operate up to a temperature of 165°C, where the switching threshold values collapse and the device locks into an ON state. This ON state is maintained on cooling down to room temperature. More significantly, the devices switch down to a temperature of 4K with only a relatively slight increase in switching thresholds (< a factor of 2).

3.3 Effects of Radiation

Conventional memory states can be explained by the presence or absence of charge, and exposure to photons or charged particles can have an adverse effect on device operation. In this work experiments were carried out on a-Si:H memory devices and conventional CMOS structures under gamma-radiation conditions, particle bombardment and radiation resembling

that of outer space. At AERE Harwell a 1 μCurie Californium^{252} source emitting 3.6 x 10^4 α-particles per sec, 10^3 fission fragment particles per sec and 4 x 10^3 neutrons per sec simulate a space environment, and this was used in testing the a-Si:H devices.

A number of characterised a-Si:H devices were irradiated by the ^{252}Cf source for 17 hours, receiving an integrated flux of 2.7 x 10^5/cm^2 fission particles, 10^6/cm^2 of neutrons and 3 x 10^6/cm^2 of α -particles. The linear energy transfer (energy dissipated per cm path length) for these particles is 43MeV/(mg cm)^2. In the a-Si:H devices, this amounts to 2MeV/cm. Fig. 3 shows the effect of this bombardment on the ON state resistance ratio $R_{ON(SE)}$ to $R_{ON(0)}$, that is the resistance after and the resistance before irradiation, for 32 devices. Although there is some scatter, no significant changes in R_{ON} were observed.

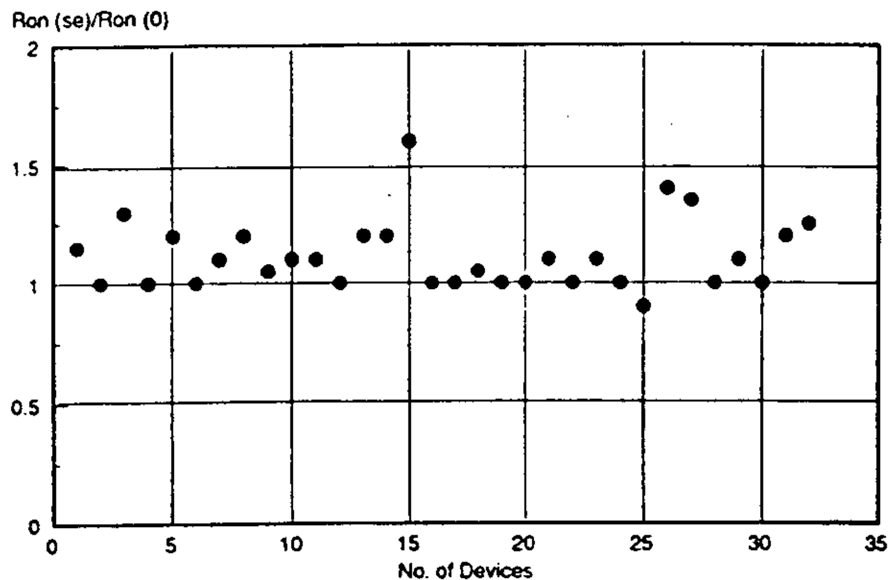

Fig.3 Effect of Space Environment Simulation Conditions on Ron.

The effect of this radiation on the OFF state I-V characteristics was tested for some 20 devices. Only random changes within a few percent were detected.

Experiments carried out on 4k CMOS RAM devices showed that typically the number of changed states (single event upsets) was 150 out of 4096 in 100 minutes using the same source. The a-Si:H devices were irradiated for 17 hours, and under these conditions one would expect the 4k CMOS RAM to show 1500 single event upsets. This gives a cross section for upsets of 10^{-2} cm^2 for the CMOS device, and sets an upper limit of 5 x 10^{-4}cm^2 for the a-Si:H devices.

Devices were also exposed to gamma-radiation. A total of 180 p^+-n-i devices were exposed to a flux of 0.508 Mrad/hour for 10 hours. Fig. 4 shows the ratio $R_{ON(BEFORE)}/R_{ON(AFTER)}$, showing no evidence of single event upsets for a 5MRad dose. All 50 devices in the OFF state also remained unchanged. The values of the OFF to ON threshold, $V_{th(forward)}$ and the ON to OFF threshold $V_{th(reverse)}$, were unchanged to within ±7% and ±6% respectively. The 5Mrad dose was sufficient to discolour the glass substrate, and the CMOS I.C. irradiated during the same experiment was found to be completely inoperable. These results suggest that the a-Si:H memories may have applications in areas where radiation adversely affects existing devices.

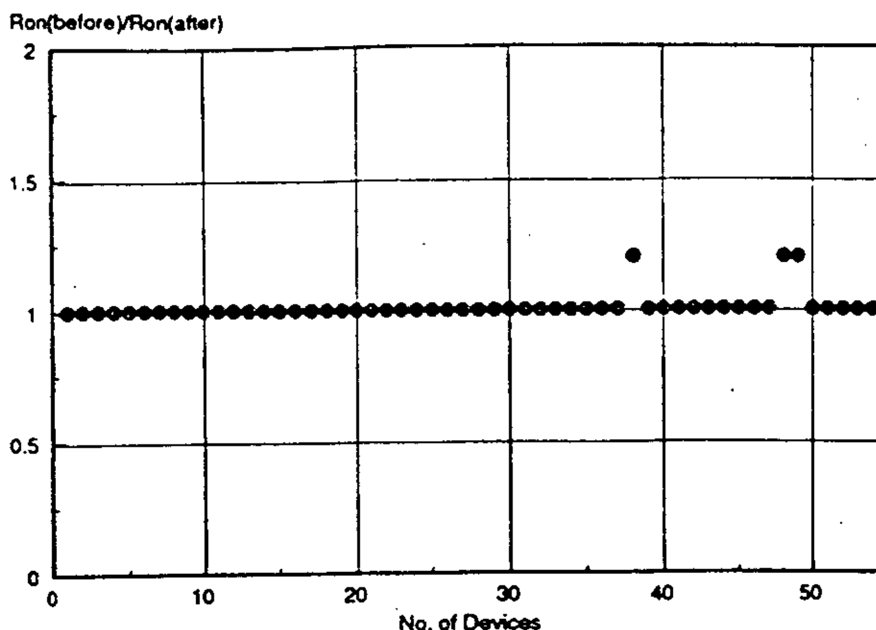

Fig.4 Effect of 5Mrad Radiation on Ron.

3.4 SEM and EDX analysis.

The resistance of the a-Si:H p^+-n-i devices to temperature stressing and radiation suggests a novel mechanism of memory storage and suggests some material change in the a-Si:H. We have previously published EDX data on Cr-p^+-V devices [6] and they showed that some material from the top contact had diffused into the filamentary region. To determine the features of the filamentary region of the p+-n-i devices, these X-ray micro-analysis probes were again used. A JEOL JSM-T330 SEM with a LINK Scientific 5508 detector and DAPPLE spectrum acquisition system was used to obtain the energy dispersive x-ray microanalysis (EDX) spectra. An electron probe of <200Å was used to analyse the filamentary region and to determine whether electrode material could diffuse into this region during forming. The devices used had titanium (Ti) bottom electrodes and Cr top electrodes to separate electrode detection. The devices were switched and subsequently had the top Cr electrode removed by conventional etching techniques before analysis.

Compositional analysis of the altered region reveals a Cr X-ray K_α peak at 5.414keV in the spectrum, suggesting that Cr from the top electrode has diffused into the filamentary region during the forming pulse. Such a region is likely to become the prefered current path (reflected in the area independence of the resistance mentioned above). This has been compared to a region outwith the filamentary region where no peak correlating with Cr K_α is detected. That this mixed phase silicon/metal filament is the prefered current path in the conduction of these devices is also suggested by work done at low temperatures [7] where an anomalous resistance at zero bias is found, consistent with tunneling transport between isolated metal particles.

p^+ analogue devices also operate by filamentary conduction and form area independent ON and OFF states. Metal is found to be incorporated into the filament here also [7]. SIMS analysis of these have been undertaken and are reported elsewhere at this conference [8].

4. Conclusions.

The memory states of a-Si:H devices are remarkably non-volatile. The reason for this stability is not clear, but is likely to be connected with the incorporation of metal into the filamentary region. The possibility of the stable states being caused by some charge trapping mechanism is remote in the light of the thermal release and radiation experiments above. This would cast doubt on the defects intrinsic to a-Si:H playing a role. However, the silicon does play some role in subsequent forming and memory behaviour as reported at this conference [9].

Acknowledgements

Some of this work was supported by British Petroleum RCS. We would like to thank Dr. J. Stevens at AERE Harwell for his kind help. The technical assistance of Mr. S. Kinmond and Mr. S. Anthony is also greatly appreciated. We would also like to thank Mr. I. Osborne and Mr. A. Plöeßl for their help.

REFERENCES.

1. LeComber, P.G., A.E. Owen, W.E. Spear, J. Hajto, A.J.Snell, W.K.Choi, M.J Rose, S. Reynolds. J Non Cryst. Sol. 77-78 1383 (1985).

2. Rose, M.J., J. Hajto, P.G. LeComber, S.M. Gage, W.K. Choi, A.J. Snell, A.E. Owen. J. Non Cryst. Sol. 115 168 (1989).

3. Hajto, J.,M.J. Rose, A.J. Snell, P.G. LeComber, A.E. Owen. MRS Symp. Proc. 192 405 (1990).

4. Street, R.A., J Kakalios. Phil. Mag. B 54 No. 1 L21-L26 (1986).

5. Crandall, R.S., Phys Rev B 36 No.5 2645 (1987).

6. Rose, M.J., J. Hajto, P.G. LeComber, A.J. Snell, A.E. Owen, I.S. Osborne. MRS Symp. Proc. 219 525 (1991).

7. Gage, S.M., J. Hajto, S. Reynolds, W.K. Choi, M.J. Rose, P.G. LeComber, A.J. Snell, A.E. Owen. J. Non Cryst. Sol. 115 171 (1989).

8. Reeder, A.A., I.P. Thomas, C. Smith, J. Wittgreffe, D.J. Godfrey, J. Hajto, A.E. Owen, A.J. Snell, A.F. Murray, M.J. Rose, I.S. Osborne, P.G. LeComber, this conference.

9. Osborne, I.S., J. Hajto, M.J. Rose, A.J. Snell, P.G. LeComber, A.E. Owen, this conference.

APPLICATION OF ANALOGUE AMORPHOUS SILICON MEMORY DEVICES TO RESISTIVE SYNAPSES FOR NEURAL NETWORKS

A A Reeder*, I P Thomas*, C Smith*, J Wittgreffe*, D J Godfrey*, J Hajto**, A E Owen**, A J Snell**, A F Murray**, M J Rose***, I S Osborne*** and P G LeComber***

*British Telecom Laboratories, Martlesham Heath, Suffolk, England

**Department of Electrical Engineering, University of Edinburgh, Edinburgh, Scotland

***Department of Applied Physics, University of Dundee, Dundee, Scotland.

Abstract

The amorphous silicon memory device shows promise as an analogue weight element in neural networks. The device resistance can be programmed to within 5% of any specific value between 1kΩ and 1MΩ using 10ns to 1μs voltage pulses in the range 1-5V. In this paper we describe the physical structure of the element and its electrical characteristics. Finally, a simple example is discussed of a small neural network implementing the EXOR function using amorphous silicon memory elements as a resistive array of weights and external op-amps as the current summing nodes.

1 Introduction

The development of large array size neural networks is hampered by the lack of a device technology which can be used to implement large arrays of programmable analogue synaptic weights in a cost effective manner. Recent approaches have used charge storage on the gate of a MOSFET to displace the threshold[1]. In this paper an alternative technology is described which uses the unique properties of a non-volatile, programmable amorphous silicon (a-Si:H) memory[2,3] (resistor) as synaptic elements in a resistive array. It is shown that a single a-Si:H device can be used to provide a synapse resistor with values between 10^3Ω and 10^6 Ω with a programming accuracy of +/-5%. The typical active area of the resistor is indicated as being less than 2μm x 2μm. The a-Si:H technology is fully compatible with conventional silicon device processes which are required for the formation of the neurons (operational amplifiers) in the network.
In this paper we discuss the physical structure of the a-Si:H memory device and its associated electrical characteristics. An example is given of a network, namely a 2 input XOR, which has been built. Finally, architectures for implementing large arrays are briefly discussed.

2 Physical structure and forming of a-Si:H memory device

The amorphous silicon device discussed in this paper was developed by Dundee University and Edinburgh University and is detailed in References [2,3]. The device consists of a thin (typically 100nm) layer of p-type a-Si:H, deposited by PECVD of

silane and diborane mixtures, which is sandwiched between two metal contacting electrodes (top electrode - vanadium or chromium and bottom electrode - chromium). For the top electrode, the contact to the a-Si:H is made via a small pore (typical diameter 10μm) cut into a photoresist overlayer. After device fabrication, the structure has a resistance of $\sim 10^9\ \Omega$. A pulse (up to 12V for $\sim$300nsec) is then used to form the memory device. It is thought that the forming pulse produces local heating which results in diffusion of the top metal electrode into the a-Si:H layer. A schematic representation of this process is given in Figures 1a and 1b.

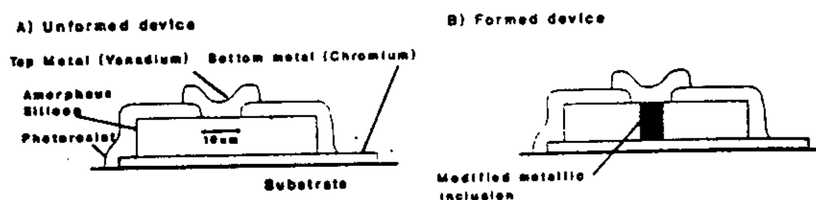

Figure 1a. Schematic cross-section of unformed device.

Figure 1b. Schematic cross-section of formed device.

Evidence for this effect has been obtained from EDX data and from Secondary Ion Mass Spectroscopy (SIMS) surface images of the pore region. As an example of the latter, Figure 2a shows a surface image of an unformed a-Si:H device after removal of the top electrode where no significant amounts of the top metal can be seen in the pore region. In contrast, Figure 2b, which illustrates an equivalent image from a formed device, shows a metallic like inclusion with an apparent diameter of 2μm. However if the broadening caused by the SIMS ion beam is taken into account, the true diameter of the inclusion may be as low as 0.2μm. This figure is in agreement with other experimental measurements of the filament diameter given in reference[2,3]. Experiments have shown that it is possible to produce working devices with a pore size of 2μm.

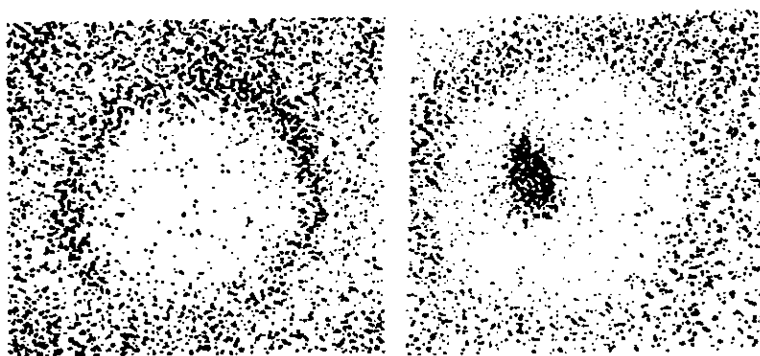

Figure 2. SIMS Measurements on Left) an unformed pore Right) on a formed pore. Regions of high Vanaduim concentration are darker.

The electrical properties of the device are controlled predominantly by the choice of the top electrode metal[3]. If vanadium is used for the top electrode and chromium for the bottom electrode, the resultant formed device has a resistance which can be programmed between an on-state value of ~3kΩ and an OFF-state value of ~10^6Ω using programming voltages of between +/-1V and +/-4V with a pulse length of typically 10-100nsec.

For example, Figure 3 shows that the resistance of a device initially in a low resistance state can be increased in a controllable fashion using an incrementally increasing negative going pulse (conventionally termed an ERASE pulse) to the bottom device electrode[3]. In this example a voltage range of 1.5V gave the full resistance change (see figure 3). Resistance can be programmed in the opposite sense (ie decreasing resistance) by applying a positive going pulse to the bottom contact (conventionally termed a WRITE pulse). As for the ERASE pulse, the final resistance state of the device is defined by the magnitude of the voltage pulse. Thus, the a-Si:H memory device may be made to switch between any two resistance states by selecting the appropriate values of WRITE and ERASE pulses. The accuracy with which a given resistance value can be achieved is discussed in Section 5. Finally, as can be seen from figure 3, the resistance of the programmed device is unaltered by voltages of up to 1.5V for pulse widths of 10-100ns.

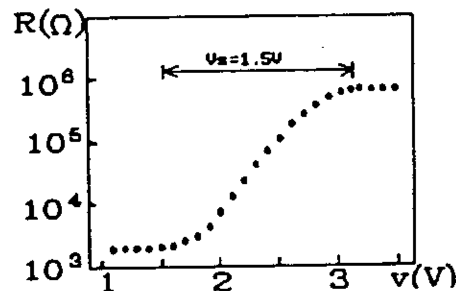

Figure 3. Erase pulse programming

3 Pulse width progamming

In the previous section, it was shown that the resistance of the device was dependent on the amplitude of a pulse of given width. An alternative programming method is to keep the pulse amplitude constant and alter the pulse width. Figure 4 shows the results of such an experiment. Initially, the device was set in the off state and a series of pulses of amplitude 2.5V were applied with the pulse width increasing from 10ns to 1μs. The log-log plot shows the resistance decreased linearly indicating the resistance depends on a low power of the pulse width. By contrast, the resistance shows a near exponential dependence when programmed using pulse amplitude, (figure 3). When the experiment was repeated with pulses of amplitude 3.5V (see figure 4) a similar effect was seen but the characteristic is displaced to shorter pulse widths. Similar effects are obtained for erase cycles, as figure 5 shows. As a result, it may be expected that improved accuracy of programming may be achieved using pulse width rather than amplitude programming.

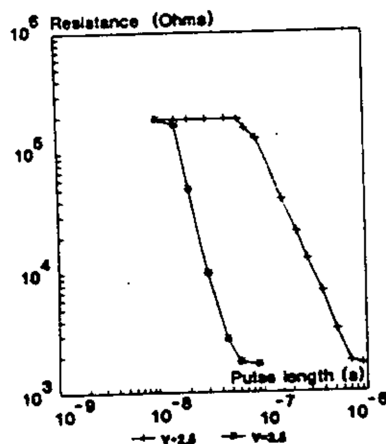

Figure 4. WRITE cycle using pulse width programming

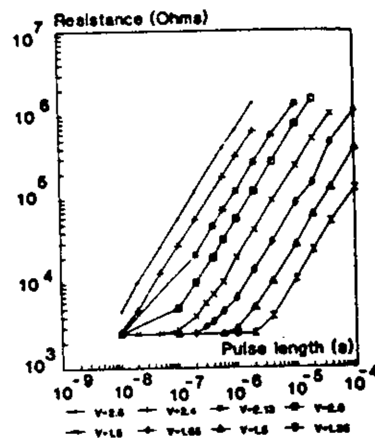

Figure 5. ERASE cycle using pulse width programming

4 Accuracy of programming discrete a-Si:H resistors

In order to study the accuracy with which the resistance of formed discrete devices may be set, the following procedure for programming the devices has been adopted:

a) a target resistance value (R_T) is chosen together with a required accuracy.

b) the initial resistance value of the device is measured (R_M)

c) if R_M is greater than R_T, a WRITE sequence is initiated and if R_M is less than R_T, an ERASE sequence is used (see Section 2 for definitions of WRITE and ERASE procedures).

d) in the WRITE case, the programming pulse of 100 nsec is applied in the voltage range between 0V and 9.99V. The same procedure is used in the ERASE case, except that the polarity of the voltage pulse is reversed.

e) the value of R_M is measured and tested against R_T and either Step c) or Step d) is repeated as required with the necessary increment in the programming voltage.

As an example of this process, a target value of 10kΩ with a required accuracy of +/-5% and a programming voltage step of 0.05V have been chosen. Figure 6 shows the resistance-voltage (R-V) characteristic obtained using this approach for a device with an initial resistance value of $2.32 \times 10^5 \Omega$. The final resistance value obtained was 9.6×10^3 Ω which is within the required accuracy. In contrast, Figure 7 shows a similar programming sequence in which the resistance R_M jumped to 6309Ω, missing the required target value. As a result, an ERASE sequence was initiated. It can be seen that the device reached its target resistance at an ERASE voltage of 1.96V. Similar behaviour has been demonstrated for devices where the initial resistance was below the target value. This procedure has been studied in a large number of samples and it has been shown that a programming accuracy of 5% can be achieved in more than 95% of devices.

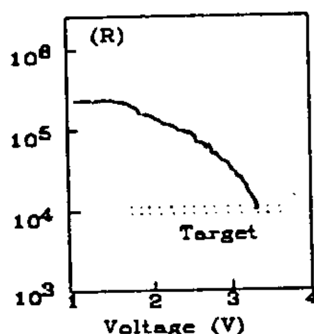

Figure 6. Resistance as a function of voltage amplitude.

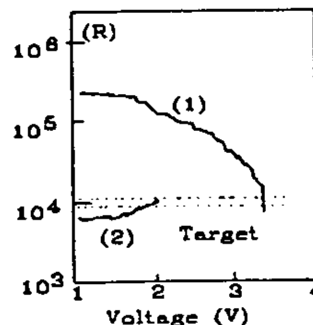

Figure 7. Resistance as a function of voltage amplitude.

It may be concluded that in the case of the present discrete devices, it is possible to readily achieve a programming accuracy of +/-5%. Indeed, it is expected that the degree of accuracy available may be improved by further optimisation of the device fabrication, the device forming process and the control of the voltage pulses used to programme the a-Si:H memory. A similar procedure may be used with the pulse width programming described earlier.

5 Two input EXOR circuit using a-Si:H resistors and external operational amplifiers

In order to provide a simple test for the a-Si:H memory devices, a two input exclusive-OR circuit has been constructed using a 5x4 a-Si:H synapse array and commercial operational amplifiers. The circuit diagram for the exclusive-OR, including the target resistance values, is given in Figure 8. The required accuracy for the resistors in the array in order to maintain the logic function of the circuit was determined using fixed metal oxide resistors and circuit simulation. It was found that an accuracy of typically +/-30% was needed. As can be seen from the previous section, this figure is well within that available for the a-Si:H devices. Figure 9 shows the input and output voltage traces obtained from the exclusive-OR circuit using the a-Si:H devices. It can be seen that the correct logic function has been obtained. The voltage used in the circuit was set at 0.3V to avoid affecting the resistance values of the a-Si:H memories. The speed of operation of the demonstration circuit was limited to ~1MHz by the slew rate of the current summing amplifiers. Thus, this circuit can not be used to estimate the potential speed performance of a-Si:H based neural networks. However, it has been shown that the device may be programmed using 10 nsec pulses (see Section 2). It is likely that the final speed of a neural network using a-Si:H memories will be limited by the performance of the on chip operational amplifiers and a typical cycle time would be a few microseconds.

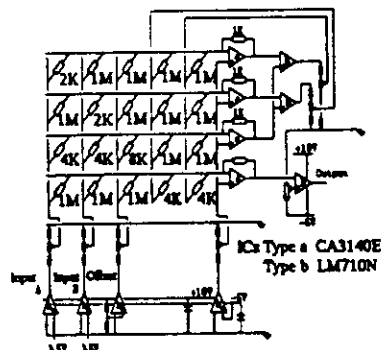

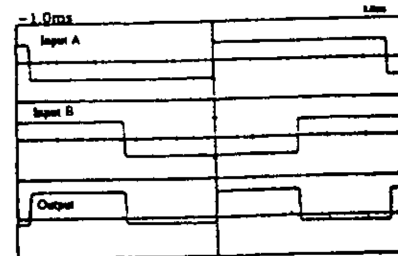

Figure 8. XOR circuit.

Figure 9. XOR input/output

To incorporate the a-Si:H device in an array it is necessary to incorporate an access transistor to provide satisfactory isolation. The transistor must able to supply enough current to form the device (8mA) and withstand the forming voltage (15V). With the resistance range currently available, power considerations limit the resistive array size to approximately 20,000 synapses. Other neural network architectures [5] employing the non volatile a-Si:H device are also under consideration .

6 Conclusions

It has been shown that analogue synaptic weights may be produced using a single non-volatile a-Si:H memory device. The resulting synapse resistance can be set between $10^3\Omega$ and $10^6\Omega$ with a typical accuracy of +/-5%. This technology is fully compatible with conventional silicon technology .

A limitation of the present approach is the requirement to 'down-load' the synaptic resistance values. Future work will include the study of both resistive arrays and pulse stream implementations using a-Si:H devices aimed at providing 'on-chip' learning.

References

1 M Holler,S Tam,H Castro, R Benson,IJCNN International Joint Conference on Neural Networks,1989,191-196

2 P G LeComber, A E Owen , W E Spear, J Hajto, A J Snell, W K Choi, M J Rose and S Reynolds, Journal of Non-Crystalline Solids 77 & 78 (1985) 1373.

3 M J Rose, J Hajto, P G LeComber, S N Gage, W K Choi, A J Snell and A E Owen, Journal of Non-Crystalline Solids,115 (1989) 168-170.

4 M J Rose, J Hajto, P G LeComber, A J Snell, A E Owen and I S Osborne, MRS Proceedings 219, 525-530 (1991)

5 A F Murray, D D Corso, and L Tarassenko, IEEE Transactions On Neural Networks, Vol 2, No 2 (1991) 193.

THE ROLE OF THE a-Si:H LAYER IN METAL / a-Si:H / METAL MEMORY STRUCTURES

I.S.OSBORNE*, J.HAJTO**, M.J.ROSE*, A.J.SNELL**, P.G.LeCOMBER*, and A.E.OWEN**.

* DEPARTMENT OF APPLIED PHYSICS & ELECTRICAL AND MANUFACTURING ENGINEERING, UNIVERSITY OF DUNDEE, DUNDEE, DD1 4HN, SCOTLAND, UK.

** DEPARTMENT OF ELECTRICAL ENGINEERING, UNIVERSITY OF EDINBURGH, EH9 3JL, SCOTLAND, UK

Abstract

In this paper we report the role of the a-Si:H on the electrical behaviour of Metal/ a-Si:H / Metal memory devices. We have investigated layers deposited at 250°C by the glow discharge method with various doping concentrations, from undoped up to 10^4 vppm of either diborane or phosphine in silane. We have found that the a-Si:H layer affects the initial forming process and the subsequent OFF state resistance. The hydrogen contents of the films have been measured and are found to correlate, for the p-type samples, with the forming voltage.

1.Introduction

The structure of the devices used in this study is similar to those reported previously [1], and is shown schematically in Figure 1. The a-Si:H layer, deposited by plasma enhanced chemical vapour deposition of silane, is sandwiched between two metal contacts, the bottom being chromium and the top contact being vanadium. In the earlier devices the a-Si:H layer was doped by the addition of 10^4 vppm of diborane in the SiH_4. A pore 10 microns in diameter is patterned in a layer of insulating photoresist giving a pore area $\approx 10^{-6}$ cm^2 although it is believed that the actual active device area is much less than this, with a diameter <0.5μm. After an initial forming process, whereby the device resistance is reduced from the as-fabricated 10^9 ohms down to several kohms by the application of a voltage pulse of 300ns in duration and around 12V in magnitude, the device exhibits non-volatile, polarity dependent, electrically programmable analogue or digital memory switching [2]. That is, the devices may be programmed over a continuum of resistance states with the application of the appropriate programming pulses. A recent publication [2] reported on the role of the top metal on the switching behaviour of the devices. It was found that the switching behaviour was essentially digital for some metals (eg. Cr, Ag, Al) and analogue for others (eg. V, Ni, Co). We define an analogue device as one in which the range of programming voltages is > 1.0V and a digital device as one in which the range of programming voltages < 1.0V. The forming process is thought to be associated with the creation of a highly conducting filament [3] and it is through this modified region that the current is primarily carried and to which the switching behaviour is most likely attributed. X-ray microanalysis, including EDX and SIMS, indicate that the top metal is incorporated into the a-Si:H layer during the forming process [3,4].

During the course of this work it became evident that the precise role of the a-Si:H layer was unclear. This paper reports on the results obtained on devices where the doping of the a-Si:H layer was varied from undoped up to 10^4 vppm of either diborane or phosphine in the silane used to prepare the films. We have investigated the effect of the a-Si:H layer on : (i) the forming process by measuring the forming voltage, V_F, as a function of the doping concentration; (ii) the subsequent switching states by measuring the range of programmable resistance values, $\Delta \log R$; and (iii) the voltage range, ΔV, over which the device may be programmed as a function of the doping concentration. It should be emphasised here that all the samples reported here have undergone identical processing procedures. Also, since V_F is known to be dependent on the thickness of the a-Si:H layer, all samples were prepared with notionally the same thickness, namely 960Å with a standard deviation of 50Å. The hydrogen content of the samples was measured by thermal evolution.

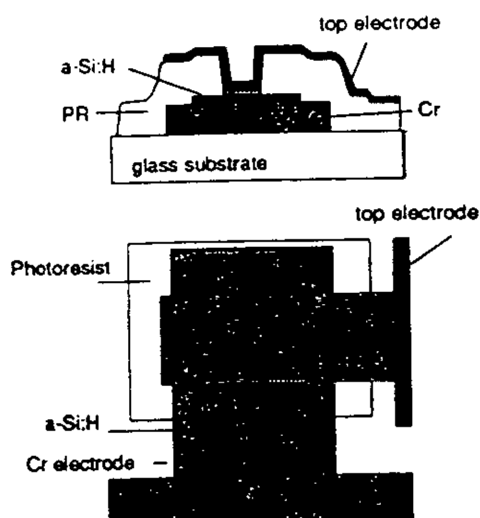

Figure 1. Schematic Device Structure

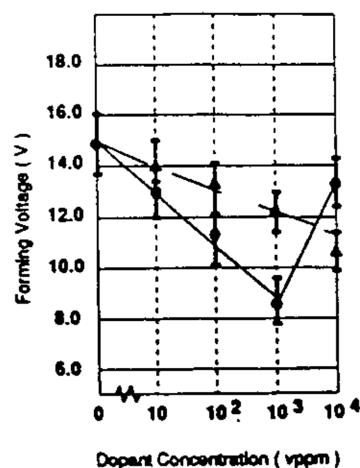

Figure 2. Forming Voltage as a function of dopant gas conc. • B_2H_6 ▲ PH_3

2.Results

The results reported here are the average values taken from a selection of 2 or 3 substrates from a single deposition and with some 40 or so devices tested on each substrate. Each point in the following figures therefore represents the average of some 100 or so measurements. In addition, the measurements have been repeated for several sets of samples prepared in another deposition with the same deposition and fabrication parameters and similar results were obtained. We first look at the effect of the a-Si:H layer on the forming voltage of the devices. The subsequent section deals with the effect on the switching parameters and finally we report on the results from the hydrogen content measurements.

2.1.Forming

The forming process consists of applying successively incremented pulses of 300 ns duration across the device, with positive polarity to the top V electrode, and measuring the resistance at 0.5V, at which the resistance is stable, after each pulse has been applied. At a critical voltage, called the forming voltage, the device resistance decreases to a few kohms and the device may then be switched with significantly lower programming voltages. It was previously reported [2] that for p-type samples doped with 10^4 vppm of diborane in silane, the device exhibited 'soft forming' with the resistance initially being reduced gradually over several orders of magnitude prior to the dramatic decrease to around a kohm for a subsequent increase in the forming voltage. In the present study most samples have only shown the hard forming behaviour, with only the heavier doped samples, prepared from 10^3 and 10^4 vppm of diborane and phosphine in silane, showing soft-forming over about one order of magnitude. The dependence of the forming voltage on the dopant concentration is shown in Figure 2. For the n-type devices the forming voltage decreases monotonically from 14.9V for the undoped samples down to 10.4V for the heaviest doped 10^4 vppm devices. If we now consider the p-type devices we can see that the forming voltage decreases to 8.3V for 10^3 vppm devices and then increases as the doping concentration is increased to 10^4 vppm. We would like to emphasize that each of the points in Figure 2 is an average of some 100 or so measurements with the error bars representing the standard deviation in the measurements.

2.2.Switching

It was observed that the polarity dependence of the switching remained the same for both the n- and p-type samples, i.e. it was found that positive polarity applied to the top erased the device whilst negative polarity to the top electrode wrote to the device, irrespective of the a-Si:H doping.

The range of programmable resistance states over which the devices may be programmed is shown in Figure 3. Here we see the logarithm of the ratio of the OFF to ON state resistance, the ON state being in each case equal to $\approx 10^3\ \Omega$. The range of accessible resistance states is a maximum for the undoped samples which can be programmed over the range from $10^3\ \Omega$ up to $10^8\ \Omega$. The programmable resistance ranges for both the diborane and phosphine doped samples decrease monotonically. For the heaviest doped samples the accessible range extends over two orders of magnitude corresponding to an OFF state of $10^5\ \Omega$. In view of the very different conductivities of n- and p-type films produced from the same concentration of PH_3 and B_2H_6, the agreement of the data for both n- and p-type samples in Figure 3 is very surprising.

The effect of the a-Si:H layer on the range of programming voltages, ΔV, as define in reference [2] is shown in Figure 4. For the n-type devices, ΔV decreases only by a small amount as the phosphine concentration varies from the undoped up to 10^4 vppm devices. In contrast the range of programming voltages increases from 1.0V for the undoped films up to 2.0V for the samples doped with 10^4 vppm of diborane. The standard deviation of the measurements across several substrates from a single deposition in the values shown in this figure are about 0.1 V for each doping level.

The actual values of the threshold voltages at which the device begins to turn ON or OFF did not show any systematic dependence on the a-Si:H parameters and indeed could vary, in the worst case, from device to device across a given substrate by as much as 2V.

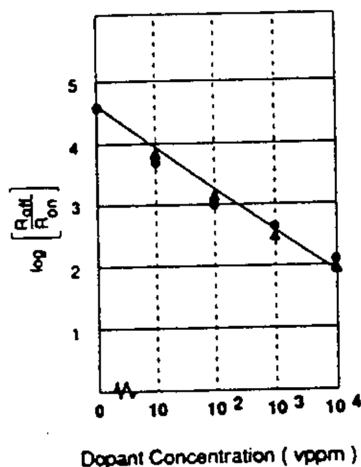

Figure 3. OFF to ON ratio as a function dopant gas conc. in SiH_4

● B_2H_6 ▲ PH_3

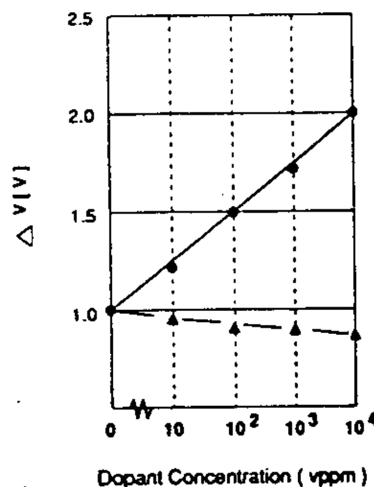

Figure 4. Programmable Voltage Range as a function of doping gas conc.

● B_2H_6 ▲ PH_3

2.3.Hydrogen content

The amount of hydrogen incorporated into the layer was measured on samples deposited in the same run using thermal evolution. The results are shown in Figure 5. If we consider first the n-type samples we see that the atomic hydrogen concentration C_H remains constant at about 5.0% over the entire range of doping concentration. In contrast the concentration of hydrogen for the p-type samples depend strongly on the doping concentration, increasing up to a maximum of 17.3% for the 10^3 vppm samples and then decreasing dramatically to 5.4 at.% as the doping level is further increased to 10^4 vppm of diborane. This trend in the atomic hydrogen content with the doping level for both the n- and p-type films has been observed for three other sets of samples prepared with identical deposition parameters. This maximum in the hydrogen content

at 10^3 vppm of B_2H_6 in SiH_4 coincides with the minimum in the forming voltage at this doping level and suggests that there may be a correlation between the forming voltage and the hydrogen content.

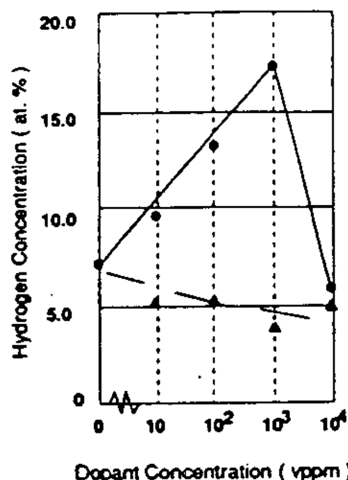

Figure 5. Hydrogen Concentration as a function of doping gas conc.
• B_2H_6 ▲ PH_3

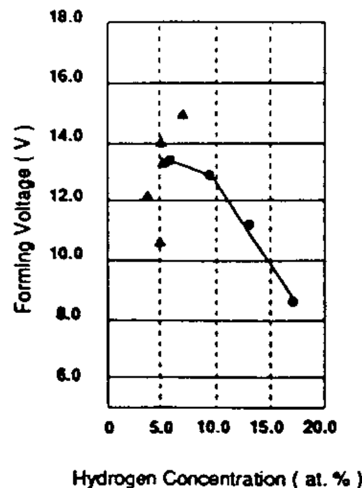

Figure 6. Forming Voltage as a function of Hydrogen content
• B_2H_6 ▲ PH_3

If we now plot the results for the forming voltage as a function of the hydrogen content, as shown in Figure 6, we can see that for the p-type samples the forming voltage decreases as the amount of hydrogen incorporated into the films increases. The n-type samples, however, do not display such a dependency as C_H is constant whereas the forming voltage decreases as the amount of dopant is increased.

3.Discussion

The results presented in this paper indicate that the properties of the a-Si:H films do play a role in determining the behaviour of metal/a-Si:H/metal memory devices. In general, increasing the dopant concentration decreases the forming voltage for both n- and p-type samples and decreases the OFF state resistance, whereas the ON state resistance is essentially independent of the doping level. The voltage range that can be used to programme the devices decreases only slowly with increasing PH_3 but increases by a factor of 2 in going from undoped to 10^4 vppm of B_2H_6. Although there is no correlation between V_F and C_H in the n-type films, there is an interesting correlation between these parameters in the p-type films.

Our earlier work [2] has shown the importance of the top metal in determining the memory characteristics. If, as we believe, the memory behaviour is a direct consequence of the formation of a composite metal/a-Si:H filament, brought about by diffusion of the top metal into the a-Si:H during the forming process, then our new results would indicate that doping, and possibly variations in the hydrogen content, influence both the ease with which the metal diffuses and possibly the way in which it is distributed.

It is now well established [10] that doping increases the defect density in a-Si:H. It is also very likely that the increase in the defect density with increasing doping could enhance the diffusion of the top metal into the a-Si:H layer and thereby lower V_F. However, the results presented in this paper do not always vary monotonically with doping and it is therefore likely that this is not a complete answer. We have also considered the possibility that the behaviour of the forming voltage with doping could be explained by the variation of the metal/a-Si:H barrier height. However, the fact that V_F does not vary monotonically with doping for the p-type films would, at least at first sight, appear to make this unlikely as the sole mechanism. Nevertheless, further work is required before we can definitely exclude this possibility.

The correlation of V_F with C_H shown in Figure 6 for the p-type samples suggests that

hydrogen may also play a role. This result is consistent with the recently published work [5] which reported that hydrogen induces detrapping of transition metals, such as Pd or Cu, in the amorphous silicon layer causing the metal to move further in regions where hydrogen was present. It is fairly well established that the charge state of hydrogen in p-type c-Si:H is positive [6,7] and recent work [8,9] suggests that hydrogen has a negative charged state in n-type c-Si:H. In keeping with this idea and taking the analogy over to the amorphous case, it might be expected that in going from p-type to n-type devices and assuming that hydrogen may play a role in the switching mechanism, the polarity dependence should change for either case. This however is not what we observe, but it should be remembered that the structure of the device is no longer likely to be just a-Si:H once it has been formed and the filament is probably a complex mixture of all the constituent parts used in producing these devices.

4.Conclusion

From the results presented here it is clear that the a-Si:H does play a role in the switching behaviour of the devices, suggesting that it may be possible to fabricate devices with customised switching characteristics necessary for particular applications. The results also suggest that the detailed properties of the amorphous silicon layer play a role determining during forming precisely how the top metal is incorporated into the filamentary region. Further work, particularly with samples deposited at lower deposition temperature, with compensated samples and with sputtered films, is in progress aimed at providing further information on the roles played by defects, dopants and hydrogen in the memory operation.

Acknowledgements

The financial support from SERC and British Telecom plc for some of this work is gratefully acknowledged. The authors would like to thank S.Anthony for the preparation of the a-Si:H films and are very grateful to D.J.Godfrey, A.A Reeder, I.P.Thomas and A.E.Ploessl for many useful discussions.

References

1. M.J.Rose, J.Hajto, P.G.LeComber, S.M.Gage, W.K.Choi, A.J.Snell and A.E.Owen, J.Non.Cryst.Sol., 115, 168, (1989).
2. J.Hajto, A.E.Owen, A.J.Snell, P.G.LeComber and M.J.Rose, Phil.Mag., 63, 349, (1991).
3. M.J.Rose, J.Hajto, P.G.LeComber, A.J.Snell, A.E.Owen, and I.S.Osborne, MRS.Symp.Proc., 219, 525, (1991).
4. A.A.Reeder, I.P.Thomas, C.Smith, J.Wittgreffe, D.J.Godfrey, J.Hajto, A.E.Owen, A.J.Snell, A.F.Murray, M.J.Rose, I.S.Osborne, P.G.LeComber, this conference.
5. S.Coffa, J.M.Poate, App.Phys.Lett., 59, 18, 2296, (1991).
6. C.Sah, J.Y.Sun, J.J.Tzou, App.Phys.Lett., 43, 2, 204, (1983).
7. A.J.Tavendale, P.Alexiev, A.A.Williams, App.Phys.Lett., 47, 3, 316, (1985).
8. A.J.Tavendale, S.J.Pearton, A.A.Williams, App.Phys.Lett., 56, 10, 949, (1990).
9. J.Zhu, N.M.Johnson, C.Herring, Phys.Rev.B., 41, 17, 12354, (1990).
10. See, e.g., R.A.Street, "Hydrogenated Amorphous Silicon", Cambridge University Press, 1991, and references therein.